NONLINEAR BEHAVIOUR

OF

PANEL BUILDINGS

by

© MANI M. NAVABI, B.Sc., M.Sc.

A Thesis

Submitted to the School of Graduate Studies

in Partial Fulfilment of the Requirements

for the Degree

Doctor of Philosophy

McMaster University

June, 1979

DOCTOR OF PHILOPSOPHY (1979) McMASTER UNIVERSITY

(Civil Engineering) Hamilton, Ontario.

TITLE: Nonlinear Behaviour of Panel Buildings

AUTHOR: Mani M. Navabi, B.Sc. (Queen's University)
M.Sc. (University of Surrey)

SUPERVISORS: Dr. R. G. Drysdale
Dr. A. C. Heidebrecht

NUMBER OF PAGES: 465, xxxii

ABSTRACT

Although panel buildings have been constructed since before World War II, there is very little known about their ultimate capacity when subjected to lateral loads. The existing methods of analysis and design are based on tests conducted on isolated vertical and horizontal joints, and empirical relationships derived from these experiments.

Very little attention has been paid to the influence of joint behaviour on the response of an assembly of panels. The studies of the overall behaviour of panel buildings which have been done by constructing mathematical models for panel assemblies, have not in general devised realistic models for the joints.

Since the joints are weaker than the panels they connect, and because failure in almost every case occurs in the joints, a realistic joint representation is very important if a true prediction of lateral load response of panel buildings is to be provided.

In this work an attempt has been made to develop a realistic model for both the horizontal and the vertical joints of the assemblies of panels forming the shear walls in panel buildings. In determining the joint model, joint details as well as existing experimental information

and on-site construction techniques (and possible imperfections) were taken into account. The mathematical model was based on the finite element method of analysis. Due to practical limitations of computer storage and computation time, modifications had to be made to reduce the total number of elements used to simulate the panel assemblies.

The results confirmed the immense importance of the realistic modelling of joints, and also illustrated the susceptibility of horizontal joints to failure due to the redistribution of gravity loads during lateral loading. It was shown that the method is capable of predicting the ultimate lateral load capacity of panel buildings.

Recommendations were made regarding an acceptable limit for drift to height ratio (Δ/H) for panel construction. Factors of safety against collapse were also established based on the maximum allowable lateral loads to which an assembly of panels could be subjected without compromising the overall integrity of the structure, or incurring minor local failures.

ACKNOWLEDGEMENTS

The author wishes to express his gratitude to his supervisors, Dr. R. G. Drysdale and Dr. A. C. Heidebrecht, for their help and guidance throughout the preparation of this thesis.

Appreciation is extended to the members of the Supervisory Committee, and especially to Dr. W. K. Tso for his continuous encouragement and assistance.

The author also wishes to thank his friend and colleague Dr. A. V. Rutenberg for his encouragement and many stimulating discussions throughout his residency at McMaster University.

Special thanks to Miss Deborah Pitkin, Mrs. Amy Stott and Mrs. Sue Saracini for their careful typing of this manuscript.

The financial support provided by McMaster University is gratefully acknowledged.

The author also wishes to express his deepest gratitude to his wife Christine and his parents Dr. and Mrs. Y. M. Navabi, without whose help and sacrifices this work would not have been possible.

TABLE OF CONTENTS

LIST OF FIGURES

LIST OF TABLES

NOMENCLATURE

Each symbol listed below is also explained in the text when it first appears. In some cases, more than one symbol has been used to describe a parameter. This is done in order to create as little confusion as possible where the works of other authors are discussed.

A	~~a cons~~tant used in modification process
A_g	gross area
A_s	reinforcement area
A_v	cross-sectional area of vertical joint
a	thickness of wall (or joint)
a_e	average effective width of joint
B	a constant used in modification process
b	thickness of sub-zone A
c	calibration coefficient
[D]	composite material stiffness matrix
$[D^c]$	material stiffness matrix associated with concrete component
$[D^s]$	material stiffness matrix associated with steel component
$[D_m]$	elasticity matrix
$[D^x]$	material stiffness matrix associated with steel component in x-direction
$[D^y]$	material stiffness matrix associated with steel component in y-direction
d	width of the joint
$\{d_i\}$	displacement vector after i^{th} increment (or i^{th} cycle)

$\{d_o\}$	initial displacement vector
E	modulus of elasticity
E_c	modulus of elasticity of concrete
E_s	modulus of elasticity of steel
E_x	modulus of elasticity for composite material in x-direction
E_y	modulus of elasticity for composite material in y-direction
$\bar{E}$	modulus of elasticity for composite material with identical reinforcing steel in x and y directions
F_{BL}	yield force in the vertical spring of a joint reinforcing element when the force acting in the horizontal spring is zero
F_{BR}	the force capable of causing yield in the vertical spring in the presence of a force acting on the horizontal spring
F_{DL}	yield force in the horizontal spring of the joint reinforcing element when the force acting in the vertical spring is zero
F_{DR}	the force capable of causing yield in the horizontal in the presence of a force acting on the vertical spring
$\{F_c^t\}$	force vector of vertical joint concrete element in transition stage
$\{F_c^I\}$	force vector of vertical joint concrete element in phase I
$\{F_c^{II}\}$	force vector of vertical joint concrete element in phase II

$\{F_c^{II}\}_f$ cumulative force vector of vertical joint concrete element in phase II

F_n normal force component of force vector $\{F_c^I\}$

F_n^{II} normal force component of vector $\{F_c^{II}\}_f$

F_s shear force component of force vector $\{F_c^I\}$

$\{F_s^t\}$ force vector of vertical joint steel element in transition stage

F_s^{II} shear force component of vector $\{F_c^{II}\}_f$

$\{F_s^{II}\}$ force vector of vertical joint steel element in phase II

$\{F_s^{II}\}_f$ cumulative force vector of vertical joint steel element in phase II

f_{cmax} maximum allowable concrete compressive stress in horizontal joints

f_c^* permissible concrete strength

f_n normal stress in horizontal or vertical joint elements

f_n' normal stress acting over the bonded part of slip surface 2

f_n^{II} normal stress corresponding to F_n^{II}

f_s shear stress in horizontal or vertical joint elements

f_{sm} maximum shear steresses in horizontal joints

f_{st} stress in steel bar

f_s^{II} shear stress corresponding to F_s^{II}

f_t tensile strength of concrete

f_t^* maximum principal stress

G	shear modulus
H	height of building (complex cantilever)
$[K]$	assembly stiffness matrix
$[\bar{K}]$	matrix containing the stiffness matrices of component elements
$[K^e]$	element stiffness matrix
K_B	stiffness of reinforcing element's vertical spring representing bond-slip action
K_D	stiffness of reinforcing element's horizontal spring representing dowel action
$[\bar{K}_J^I]$	stiffness matrix of vertical joint element in phase I
$[K_c^t]$	vertical joint concrete element property matrix in transition stage
$[K_c^I]$	concrete element property matrix in phase I
$[\bar{K}_c^I]$	stiffness matrix of vertical joint concrete element in phase I
$[K_c^{II}]$	vertical joint concrete element property matrix in phase II
$[\bar{K}_c^{II}]$	stiffness matrix of vertical joint concrete element in phase II
K_h	tie beam link horizontal spring stiffness
$[K_i]$	stiffness matrix belonging to the i^{th} increment (or i^{th} cycle)
K_n	normal spring element stiffness
K_{nc}^t	normal stiffness of vertical joint concrete element in transition stage

K_{nc}^{I}	normal stiffness of vertical joint element in phase I
K_{ns}^{II}	normal stiffness of vertical joint steel element in phase II
K_{nt}	normal stiffness of tie beam element
K'_{nt}	normal stiffness of tie-beam element after cracking
K_s	shear spring element stiffness
K_s^m	modified shear spring stiffness
$[K_s^t]$	vertical joint steel element property matrix in transition stage
$[\overline{K}_s^I]$	stiffness matrix of vertical joint steel element in phase I
$[K_s^{II}]$	vertical joint steel element property matrix in phase II
$[\overline{K}_s^{II}]$	stiffness matrix of vertical joint steel element in phase II
K_{sc}^t	shear stiffness of vertical joint concrete element in transition stage
K_{sc}^I	shear stiffness of vertical joint element in phase I
K_{ss}^{II}	shear stiffness of vertical joint steel element in phase II
K_{st}	shear stiffness of tie-beam element
K'_{st}	shear stiffness of tie-beam element after cracking
K_v	tie-beam link vertical spring stiffness
$[K_o]$	initial stiffness matrix

$[\bar{K}]_B$	stiffness matrix of bar element
$[K]_E$	diagonal material property matrix for slip surface element (or horizontal joint element)
$[\bar{K}]_E$	stiffness matrix for slip surface element (or horizontal joint element)
$[K]_F$	property matrix for friction element
$[\bar{K}]_F$	stiffness matrix for friction element
$[\bar{K}]_R$	stiffness matrix for horizontal joint reinforcing element
$[K]_{TB}$	property matrix for tie-beam element
$[K']_{TB}$	material property matrix of tie-beam element after cracking
$[\bar{K}]_{TB}$	stiffness matrix for tie-beam element
k_n	normal stiffness per unit area of slip surface element (or horizontal joint element)
k_{nc}^{I}	unit normal stiffness coefficient in phase I
k_{ns}^{II}	unit normal stiffness coefficient of steel in phase II
k_s	shear stiffness per unit area of slip surface element (or horizontal joint element)
k_{sc}^{I}	unit shear stiffness coefficient in phase I
k_{sc}^{II}	unit shear stiffness coefficient of concrete in phase II
k_{ss}^{II}	unit shear stiffness coefficient of steel in phase II
L	length of slip surface represented by a single element

L_A	embedment length
L_b	length of bar element
l_c	length of that portion horizontal joint contributing to the stiffness of one element
m	number of shear-keys
N	clamping force
n	$\frac{ES}{E_c}$
P	normal force
{P}	slip surface element (or horizontal joint element) force vector
P_d	compressive force acting on inclined side of a shear-key
P_n	an element of vector {P} representing normal force
P_r	shear (or slipping) force acting on inclined side of a shear-key
P_s	an element of vector {P} representing shear force
p	steel ratio
{p}	vector of internal nodal forces
p_x	steel ratio in x-direction
p_y	steel ratio in y-direction
Q_t	resisting shear force
{q}	vector containing the nodal displacements of component elements
R	interface reduction factor (vertical joints)
{R}	external load vector
$\{R\}^o$	sub vector of {R} corresponding to zero external loads

$\{R\}^*$	sub vector of {R} corresponding to none zero external loads
$\{s\}$	composite material stress vector
$\{s^c\}$	concrete stress vector
$\{s^s\}$	steel stress vector
S_R	reduction coefficient for simplified vertical joint for single concentrated shear force
s_x^c	composite material stress in x-direction
s_{xy}^c	composite material shear stress
s_y^c	composite material stress in y-direction
s_1^c	stress in an arbitrary direction 1
s_2^c	stress in direction 2(perpendicular to 1)
s_{12}^c	shear stress associated with 1 and 2 reference directions
s_x^s	reinforcement stress in x-direction
s_{xy}^s	reinforcement shear stress associated with x and y reference directions
s_y^s	reinforcement stress in y-direction
T	total shear force carried by vertical joint
T_1	shear force carried by one shear-key
t	depth of floor slab (or horizontal joint)
t_t	thickness of a finite element
u_A	average bond stress
$\{u\}$	assemble nodal displacement vector
$\{u\}^o$	nodal displacement vector corresponding to zero nodal loads
$\{u\}^*$	nodal displacement vector corresponding to none zero nodal loads

v	shear force associated with clamping force N
w	potential energy of load system
$\{W_{eq}, i-1\}$	equilibrated load vector after i-1 cycles
$\{w_r\}$	vector of relative nodal displacements
w_x	an element of vector $\{w_r\}$ representing the x component of relative nodal displacements
w_y	an element of vector $\{w_r\}$ representing the y component of relative nodal displacements
$\{w_o\}$	initial load vector
y_1	relative normal deformation between the left corner of the panel and the bar element
y_2	relative normal deformation between the right corner of the panel and the bar element
Δ	drift or horizontal displacement at the top of building
Δv	increment of shear displacement
Δz	horizontal component of slipping force
$\{\Delta d_j\}$	displacement vector associated with j^{th} increment or (j^{th} cycle)
Δ_t	area of a finite element
$\{\Delta w_j\}$	incremental load vector
$\Delta\tau$	increment of shear stress
θ	plasticity index ($o \leq \theta \leq 1.0$)
ϕ	total potential energy
ϕ^e	potential energy of an element
υ	strain energy
υ^e	strain energy of an element
α	angle of shear-keys

β	normal separation associated with slip
$[\beta]$	matrix relating $\{\delta\}$ and $\{u\}$
$[\beta]^o$	submatrix of $[\beta]$ corresponding to zero nodal loads
$[\beta]^*$	submatrix of $[\beta]$ corresponding to none zero nodal loads
γ	shear strain
γ_m	behavioural coefficient associated with the strength of concrete
γ_{xy}	shear strain associated with x and y reference direction
γ_{12}	shear strain associated with 1 and 2 reference directions
δ	shear deformation in phase II measured w.r.t. x-y co-ordinate system shown in Fig. 4-8
$\{\delta\}$	structure nodal displacement vector
$\{\delta_i\}$	displacement vector of node i
δ_{x1}	displacement of end 1 of element in x direction
δ_{x2}	displacement of end 2 of element in x direction
δ_{y1}	displacement of end 1 of element in y direction
δ_{y2}	displacement of end 2 of element in y direction
ϵ	normal deformation
$\{\epsilon\}$	strain vector
ϵ_x	strain in x-direction
ϵ_y	strain in y-direction
ϵ_1	strain in arbitrary direction 1
ϵ_2	strain in direction 2 (perpendicular to 1)
λ_s	load factor of safety
μ	coefficient of friction

$\bar{\mu}$	apparent coefficient of friction for a shear-key joint
ν	Poisson's ratio
$\bar{\nu}$	Poisson's ratio for composite material with identical reinforcing steel in x and y directions
ν_c	Poisson's ratio of concrete
ν_{py}	plastic shear strength at level y
$\nu_{\hat{y}}$	elastic shear stress
ν_x	$\varepsilon_x/-\varepsilon_y$
ν_y	$\varepsilon_y/-\varepsilon_x$
	reduction coefficient associated with the type of horizontal joint
τ	shear stress
ψ	angle between compression struts and vertical direction

CHAPTER 1

INTRODUCTION

1.1 Historical Development and Background Information

In recent years there has been a tendency towards a more frequent use of factory produced components in building structures. The transition from the Primitive building methods to more 'industrialized' techniques has been a painfully slow process. The term industrialized or factory produced encompasses all off-site produced components including large panels that are used as primary load bearing structural members. Generally, the construction of buildings has progressed from Primitive to Traditional to Improved Traditional to Monolithic and finally to highly industrialized Large-panel type of construction.

Even today depending on the location and the type of building being constructed, the Traditional and/or Improved Traditional methods still prevail. The term Traditional in this context means a system of construction whereby all the building components are made out of locally available raw materials and are fashioned on the site by local craftsmen. There is practically no standardization and each building is tailored according to the user's needs.

The Improved Traditional system represents the first step in the direction of industrialization. Masonry, for example, is still laid by hand, but many elements of the building such as lintels, floor and roof slabs, stair flights and landings are made away from the site and are erected as the construction progresses. The degree of industrialization as defined by the ratio of work done in the factory to the total construction work, improves as the transition is made towards Large-panel type structures.

The following are some of the advantages of moving towards a more industrialized building construction:

1. smaller labour requirements,
2. more efficient use of materials,
3. shortening of overall construction time,
4. decreased dependence on seasonal changes, and
5. improved economy.

In the years immediately following the Second World War, many war-ridden countries especially in Eastern Europe were faced with the problem of acute housing shortages due to large scale destruction, mass migration and displacements. The industrialization techniques, leading to quicker construction times and more economical buildings, seemed to provide the logical solution. Although some prefabricated buildings were constructed on an experimental basis during the pre-war years, the real interest in industrialization was

born out of necessity in the late Nineteen-forties. The continual experimental research work conducted in Poland, Czechoslovakia, Germany, Russia, France, Denmark, Hungary and Sweden, in addition to the experience gained from the construction of scores of prefabricated buildings, has established these countries as undisputed leaders in the field of industrialized construction.

In the mid nineteen-sixties patented building systems were imported to this country from Europe, but to date most have not been successful. The most important reason for this seems to be the lack of a large guaranteed market for successful and efficient mass production. Unlike the case in Europe and more recently in the Middle East, North American governments have not supplied this guaranteed market. However, in spite of the set backs in North America, industrialized building markets in North Africa and especially in the oil-rich nations of the Middle East seem to be flourishing.

It has long been felt that existing methods of analysis for large-panel buildings in which lateral loads are resisted by a series of 'complex cantilevers', leave a lot to be desired. The term complex cantilever will be defined in the following section. Here, it will suffice to say that a complex cantilever is the basic structural component resisting the vertical and the horizontal loads of all large-panel (industrialized) buildings. As will be discussed in detail later, the analytical methods needed to fully understand the

behaviour of these complex cantilevers has lagged significantly behind their actual construction. Thus, the purpose of the study presented in this thesis is to develop a realistic analytical model for a complex cantilever (including its various components), and to develop a computer-aided analysis technique capable of predicting its ultimate strength and the corresponding inelastic deformation. To this end, the materials presented in this and the follwoing chapters are compiled in a way that the author trusts will assist the reader to readily follow the logical sequence of development.

1.2 Complex Cantilever

A complex cantilever is a shear wall composed of a number of large prefabricated reinforced concrete panels. These panels are arranged side by side and atop one another to form a cantilever the basic function of which is to resist vertical (gravity) loads, and horizontal (lateral) wind and earthquake forces. They are connected along their edges by means of in situ concrete joints. These joints are of two basic types. Those connecting the vertical edges of the neighbouring panels are called vertical joints. The basic function of these is to resist the longitudinal shear stresses which are created in the assembly when the complex cantilever is subjected to lateral loads.

The connections between the panels' horizontal boundaries are referred to as horizontal joints. The

primary function of these is to transfer the vertical (gravity) loads and to resist the transverse shears caused by the lateral loads.

For horizontal joints it is the gravity force which is usually relied upon to preserve the joint integrity. However, both the reinforced and the unreinforced joints will be investigated. To reinforce a horizontal joint a pair of steel dowels is usually incorporated transversely through the joint and is anchored in the panels immediately above and below the joint. Thus, some degree of vertical continuity is provided against the possibility of separation.

Vertical joints are usually reinforced. The reinforcement is very often in the form of steel loops protruding from the panels' vertical edges.

The physical characteristics of both vertical and horizontal joints are discussed in more detail in chapters 3 and 4. A schematic representation of a complex cantilever defining its various components is shown in Fig. 1.1.

1.3 Scope of the Investigation

It is very important to be able to predict the ultimate strength of a complex cantilever, since without it any estimate of the factor of safety can be greatly in error. To be able to predict the capacity, the most important aspect requiring attention is the behaviour of the joints. The joint behaviour is entirely depend-

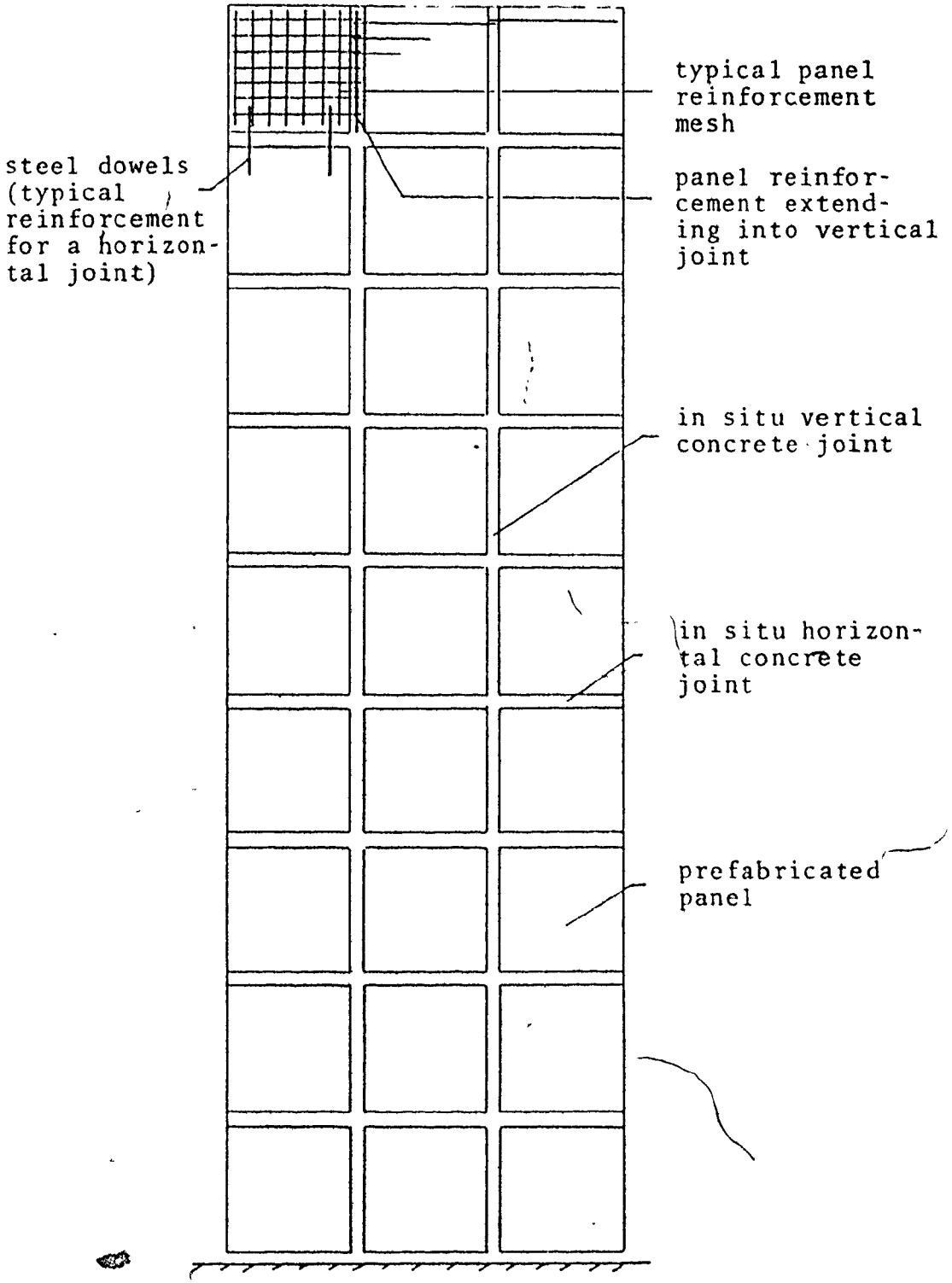

Fig. 1.1 Schematic Representation of a Typical Complex Cantilever

ent on its configuration and construction.. Thus, any realistic estimate of ultimate strength of a complex cantilever should incorporate a joint model which would allow partial or complete failure of horizontal and vertical joints as these connectors between the panels slip, separate, split, crack or crush.

It is therefore, the aim of this investigation to construct a realistic model for the joints of complex cantilevers taking into account such factors as the joints' geometric parameters, the strengths of various components and the actual in situ construction. Once this model has been constructed, the non-linear behaviour of complex cantilevers under a combined action of gravity and lateral loads will be investigated with the aim of predicting their ultimate strength and corresponding deformation.

To achieve this, the finite element method will be used. The finite element method provides a good way to model panel behaviour, and may be adopted to simulate the non-linear behaviour of the joints. Finite elements have been used by several researchers in their studies of various aspects of the behaviour of panel buildings and other reinforced concrete structures[9, 41, 43, 61, 70, 19, 33]. Details of finite element models of panels, joints and complex cantilevers will be discussed in greater length in the following chapters (also see section 1.5) and will not be elaborated upon further at this time.

1.4 Previous Studies

The available research information in the area of panel buildings may be broadly divided into two main categories: (a) experimental reserach work on joints, and (b) theoretical work on assemblies of panels. There are also a number of other studies that, although not specifically developed to further the study of panel buildings, are none the less quite important. The study of bond-slip characteristics of reinforced concrete and the investigation of dowel action are examples of this type of contribution. These related contributions will be discussed where they are referenced in this study.

The literature on topics specifically related to the study of panel buildings are discussed here under subsections (a) and (b), in Chapter 4 and in Appendix A. In general, the type of information which is either utilized in this study or is directly related to it, is presented in this section and in Chapter 4. Materials not specifically used in this study which nevertheless are considered important are discussed in Appendix A.

(a) Experimental Research on Joints

With the exception of a recent and as yet unpublished progressive collapse test carried out at Building Research Station, Watford, U.K., and the tests by Armer and Kumar (2) which were conducted on 1/2 scale cantilever panels, the experimental research work has been mainly concerned with the behaviour of vertical joints as determined by push-off tests. These studies were

mostly concerned with joint behaviour and strength and the influence of various physical characteristics and parameters. The most important of these were the joint type, its geometry, and the effect of in-fill concrete strength and steel ratio.

Chapter 4, which contains a study of vertical joints, has a review of the most relevent of these studies. Additional selected information is summarized in Appendix A.

(b) Theoretical Research on Assemblies of Panels

The available research information on assemblies of panels fall under three different categories as follows:

1. lateral load studies,
2. progressive collapse investigations, and
3. stability studies.

Items 2 and 3 are not directly related to the study reported in this thesis, and will not be elaborated upon in the main text. However, the interested reader will find a summary of these studies in Appendix A.

Most investigators who have studied the behaviour of panel buildings (lateral loads, progressive collapse or stability studies) have in general paid very little attention to proper modelling of the joints. With the possible exception of the work done by Mehlhorn and Schwing[41, 42, 43] the author is aware of no studies in which attention was given to a realistic representation of the joints. Furthermore, an in-depth study of non-linear behaviour of Large-panel structures encompasses

a wide range of distinct structural topics, some of which have not yet been sufficiently investigated. These include such independent topics as the dowel action, the bond-slip characteristics of joint reinforcement, the composite action of reinforced concrete panels and the nonlinear behaviour of the connections.

Most of the theoretical investigations on panel assemblies have been limited to the structural behaviour in the linear elastic range. In addition the joint response was usually determined using simplifying assumptions, the validity of which may in some cases be open to question.

To illustrate the general degree of development in this area of research (behaviour of panel buildings subjected to lateral loads), the published works of several authors are reviewed here.

The behaviour of coupled panelized shear walls was investigated by Burnett and Rajendra[9]. The coupling effect was produced by the floor slabs (or floor panels) connecting the two complex cantilevers. The lateral load response was significantly influenced by the nature of the connection between the floor slab and the wall panels. The factors influencing the coupling were:

1. the effective width of the floor slab, ranging from a full bay to considerably smaller widths,
2. the effective depth of the equivalent floor slab, accounting for the effect of tensile cracks and

reduction in flexural rigidity, and

3. the influence of the degree of rigidity (fixity).

For monolithic structures the degree of rigidity between the connecting beams and the walls was assumed to be unity (completely fixed). For fully panelized buildings the degree of rigidity was taken to be zero. Therefore, depending upon the connection detail, the service load response of the connection had to lie between these two extremes rendering the joint partially rigid. The authors, however, made no recommendation as to the actual rigidity values for partially rigid structures. In addition, to ensure joint integrity, tensile stresses were not allowed in the horizontal joints. The vertical joint stresses were also monitored to make certain that the maximum principal stresses did not exceed the tensile strength of concrete.

Burnett and Rajendra also developed a method of analysis involving elastic-plastic behaviour of vertical joints which was used to determine the lateral load response for various plasticity indices.

Assumptions inherent in this approach were pinned wall-floor connections, proportioned loading, elastic-plastic response and instantaneous plastification of the entire joint for some statically admissible stress field corresponding to an elastic configuration of stresses. The plasticity index was defined in the following relationship

$$v_{py} = \theta \lambda_s v_{wy}$$

where v_{py} = the plastic shear strength at some level y in the vertical joint,

v_{wy} = the elastic shear stress at working load in the vertical joint at level y

λ_s = the load factor of safety, and

θ = the plasticity index ($o \leq \theta \leq 1.0$)

Burnett and Rajendra investigated the deformational aspect of this approach by assigning an arbitrary value of 1.5 to λ_s and evaluating the deflection versus height ratio, Δ/H, for various plasticity indices. Horizontal joints were assumed to remain completely intact. No indication was given as to what actual plasticity index should be used to determine the reserve strength of panel buildings.

Unlike most experimental researchers who have made strength studies on the basis of variations in the physical parameters of joints, Mehlhorn and Schwing[41, 42, 43] investigated the effect of joint characteristics on the overall behaviour of complex cantilevers.

The finite element method was used to simulate the wall behaviour taking into account several sources of non-linearity. It was assumed that cracks and slips occur only in the joints, and that panels themselves remain unbroken. The behaviour of reinforced concrete was idealized as shown in Fig. 1.2. Concrete was represented in the form of rectangular finite elements with a total of 8 degrees of freedom, connected to orthogonal bar elements (representing steel reinforcing

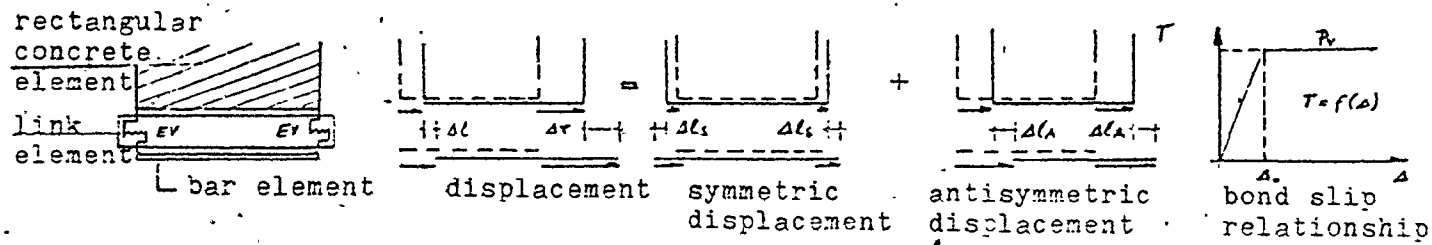

link element spring stiffness

case a: $|\Delta l_A + \Delta l_S| \leq \Delta_0$ $\qquad EV = \frac{P_v \cdot a}{2 \cdot \Delta_0}$

case b: $|\Delta l_A - \Delta l_S| < \Delta_0 < |\Delta l_A - \Delta l_S|$ $\qquad EV = \frac{P_v \cdot a}{2 \cdot \Delta_0} \cdot \left(1 - \frac{(|\Delta l_A + \Delta l_S| - \Delta_0)^2}{4 \cdot \Delta l_S \cdot \Delta l_A}\right)$

case c: $|\Delta l_A - \Delta l_S| \geq \Delta_0$ $\qquad EV = \frac{P_v \cdot a}{2 \cdot \Delta l_A} \cdot \frac{|\Delta l + \Delta r|}{|\Delta l| + |\Delta r|}$

Fig. 1.2 Mehlhorn and Schwing's Finite Element Representation of Reinforced Concrete (41)

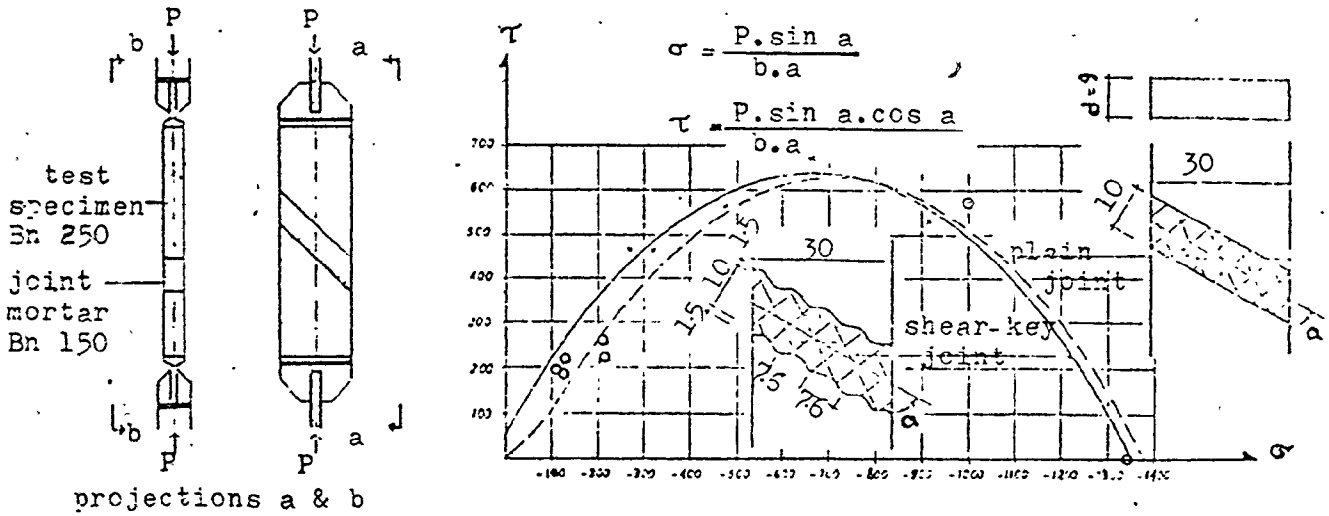

Fig. 1.3 Mehlhorn and Schwing's Test Set Up and Graph of τ-σ Relationship (41)

bars) by means of dimensionless linkage elements simulating a bilinear bond-slip relationship between steel and concrete. This type of finite element representation of reinforced concrete was first introduced by Ngo and Scordelis [48] and was later utilized by Nilson[47]. Its usefulness, however, is in dealing with cracked concrete, as the contribution of steel bars to the strength or the stiffness of uncracked sections is marginal. The panels in the Mehlhorn-Schwing approach were assumed to remain uncracked. In addition, to be meaningful a rather large number of elements and links must be used.

The stress-strain relationship for both the steel and the concrete was approximated by bilinear elastic-plastic curves, and the yielding of concrete was determined on the basis of the Von Mises yield criteria.

The joint behaviour was based on experimentally determined 'joint characteristics'. These were estimated from tests carried out on small panel segments with plane and shear-key joints as shown in Fig. 1.3. Iterative techniques were used to simulate the behaviour of the assembly. The joints were simulated by springs, the stiffness of which was determined from stress-strain and/or shear-slip relationships.

It must be noted that the joints used in the above investigation were generally unreinforced. Although until recently it was a common practice not to use reinforcement in horizontal joints, vertical joints were almost always reinforced. Vertical joints in

panelized construction are the equivalent of lintels or beams in coupled shear walls. They add tremendously to the strength and the stiffness of the building. Since in practice it is so easy to reinforce a vertical joint, neglecting to do so, especially in tall buildings, amounts to bad design.

Numerical investigations of panel shear walls were restricted to those consisting of vertical unreinforced joints of waved profile. Horizontal reinforcement was provided within the tie beams at the level of the floor slab. There was no continuity of steel across horizontal joints. The relationship between τ and σ which was determined experimentally, was simulated using a computer by means of a number of different curves fitted to the experimental points shown in Fig. 1.3. Because of an insufficient number of points, the fitted curves were very likely unreliable. Furthermore, as the author himself points out in his final conclusions, the normal stresses acting on a vertical joint are almost always very close to zero. Thus, it would have been much more logical to utilize one of the existing test results for vertical joints subjected to pure shearing action. For the horizontal joints, again the experimental model did not constitute a realistic situation. The influence of floor panels, partial bonding of various components of horizontal joints, shrinkage and other problems associated with joint grout and the prevailing on-site construction techniques were not taken into account at all.

In studying the behaviour of panel assemblies, three different combinations of lateral and vertical loads were considered. As lateral loads were increased, vertical loads were also increased. This was done, presumably, to help preserve the integrity of the horizontal joints. However, this again represents an unrealistic situation, since vertical gravity loads invariably remain nearly constant.

To the best of the author's knowledge, the work of Mehlhorn and Schwing, although in many respects unrealistic, represents the only attempt by any researcher to take into account the joint behaviour in determining the overall behaviour of panel shear walls.

The linear elastic behaviour of three dimensional structures consisting of two dimensional panels arranged in orthogonal or oblique panels was investigated by Stamato and Stafford-Smith[61]. The structural scheme could include frames, trusses or shear walls. The method assumes vertical concentrated forces to be induced along the vertical intersections of panels at each storey to ensure compatibility of displacements. The solution was based on the displacement method. By incorporating various simplifications and refinements, the method was made suitable for analysis for large structures. Where vertical displacements could be neglected, as in buildings of moderate height and slenderness with columns or walls at the intersections of the panels, the method becomes especially efficient. The floors in this analysis were

assumed to be rigid diaphragms of infinite in-plane stiffness and zero transverse stiffness, and were thus able to transmit only horizontal forces to the panels. The analysis deals entirely with uncracked, unseparated joints between panels, or between panels and other structural components.

The validity of the usual assumption that in slab-wall panel buildings the primary load bearing action is through in-plane or membrane forces was investigated by Zienkiewicz, Parekh and Teply[70]. They demonstrated this on the basis of comparison of solutions for idealized cases involving full bending-membrane action, and membrane action alone. Although only the results for simple buildings were presented, the membrane solution may be applied to all sizes and shapes of structures. The advantage of this approach over the full bending-membrane solution is the reduction of the volume of computations required in the full analysis. It appears that little is to be gained in terms of accuracy of the analysis by including bending action in the floor diaphragm. It must be born in mind that in this analysis the structure was treated as linear and elastic, and that no cracking or separation of the joints was considered.

A method of analysis for lateral loads acting on three dimensional buildings with elastic linear properties was presented by Dickson and Nilson[19]. Each concrete floor and wall panel was idealized as a sub-

structure of two dimensional finite elements joined to the adjacent panels at discrete points along their common boundaries. The analysis took into account the deformation of floor panels in their own plane as well as that of vertical wall panels. Holes of any shape or size located in floors or walls could also be accounted for. The stiffness method of analysis was used and the solution of the equilibrium equations was by successive elimination of displacements from top to bottom of the structure. This provided the values for the base reactions, the substructure displacements and the internal forces. The joints were assumed to remain intact.

The architectural considerations, layouts and inherent limitations of large panel multistorey buildings were studied by Levy and Varga[33]. To investigate the drift a method given by Coull and Chowdhury (see ref. 33) for the analysis of coupled shear walls was modified to include wall openings. The analysis dealt with the linear range only and the joints between panels were assumed to remain completely intact.

Figure 1.4 summarizes the panel building related literature referenced in this thesis in a schematic fashion. The numbers given within each box identify the relevant literature. Under the box marked 'general' are included such references as texts on design and construction, building materials, information on design, evaluation and economy, and building codes and regulations. So far very little work has been reported on lateral

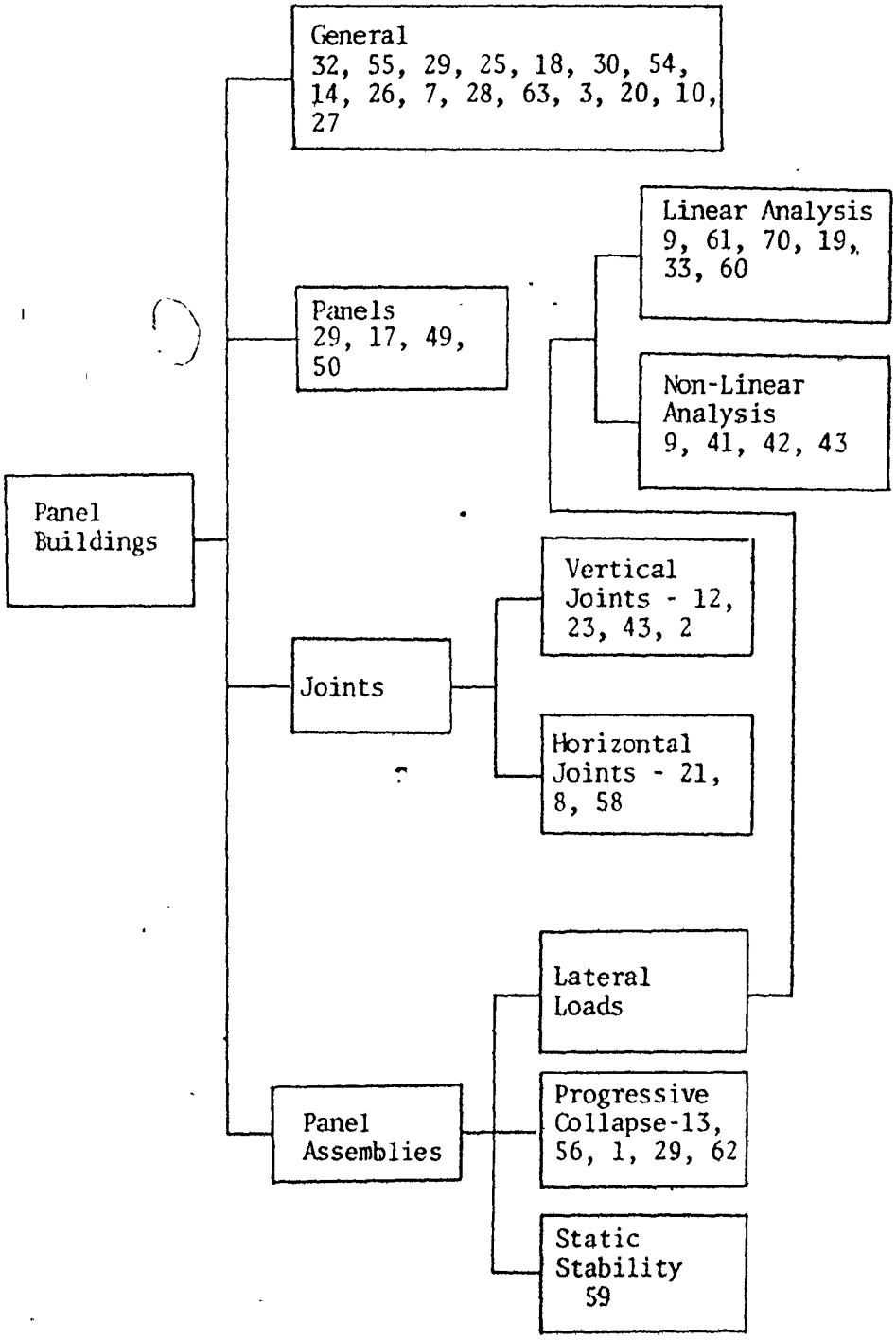

Fig. 1.4 A Schematic Survey of Literature Relevent to Panel Buildings

load analysis of panel buildings. The relevant studies were briefly outlined in this section. Further information on joints will be given in Chapters 3 and 4 where horizontal and vertical joints are discussed. A summary of related test data, empirical design formulae, and other related studies which are felt to be of general interest but not directly related to this thesis will be outlined in Appendix A.

1.5 Organization of the Thesis

The organization of this thesis parallels the actual research approach which was to initially investigate the separate characteristics of the major components. This approach provides an efficient mechanism for defining the accuracies and determining the sensitivities of the analysis to various assumptions prior to investigating the complex cantilever behaviour. Generally, with finite elements, the larger the number of elements, the more accurate is the solution. This approach however, in addition to being laborious, becomes unfeasible due to insufficient computer storage space when a large complex cantilever is studied. Thus it is necessary to find a method to reduce the number of elements without drastically reducing the accuracy of the solution.

The investigation of panels is reported in Chapter 2. The purpose of Chapter 2 is to arrive at a form of panel representation which produces reasonably accurate results using the least possible number of

elements, and minimizing the computational time and effort.

Details of the behaviour of horizontal and vertical joints are described in Chapters 3 and 4 respectively. At this stage, one joint between a pair of panels is considered. The joints are investigated under a variety of loading conditions using a relatively large number of joint elements to ensure reasonably accurate results. Once the detailed behaviour is established, the joints are simplified (calibrated) using fewer elements and the results are compared. In Chapter 5 modifications to the stiffness of the joint elements to improve the accuracy of using fewer elements are reported and evaluated.

In Chapter 6 the results of the studies described in the previous chapters are incorporated into a single program, thus making it possible for the behaviour of complex cantilevers to be studied.

Chapter 7, simply deals with conclusions and recommendations.

CHAPTER 2

MODELLING OF PANELS

2.1 Introduction

Precast concrete wall panels are among the major load resisting components of panel buildings. Although these panels are much stronger and stiffer than their interconnecting joints, their deformation may have a significant effect on the response of the panel assembly to gravity and lateral loads. The response of a panel assembly is more complex than would be indicated by a planar elastic analysis. This is partly because of the shape of the panels. Their relatively low height to length ratio can make shear distortion a major factor. Perhaps an even more important factor is the effect of joints which create regions of non-uniformity in the panel assembly. Therefore, considering the problem of non-uniform, non-linear behaviour, and taking into account the work done by other investigators[19, 48, 59, 60, 61, 70], it was concluded that the finite element method of analysis offered by far the best possibility for proper modelling of this complex behaviour.

The use of finite elements for analysing complex cantilevers requires that all the building components including the joints be represented by a finite number

of elements. Initial studies showed that the joint behaviour could be simulated by a series of elements, each in the form of a pair of dimensionless springs. This type of element will be discussed in detail in Chapters 3 and 4. The panel behaviour can be simulated by a large variety of different types of finite elements. The number of these will be governed by accuracy requirements and the need to accommodate connections to the joint elements. It is mainly the former aspect which will be dealt with in the remainder of this chapter.

The joints in a complex cantilever are weaker than those of factory produced panels because of a reduction in the amount of reinforcement, weaker concrete and the existance of discontinuities created by casting in situ joints. Shrinkage of the cast-in-place joint concrete is another factor contributing to the weakening of the joints. The assumption of inherent weakness of the joints has been confirmed by tests conducted by Sementsov, Shapiro and Sokolov. An outline of their investigations is given in reference 58. Armer and Kumar's[2] tests also support this assumption. The observations of actual failures of panelized buildings[13], and in some cases even monolithic structures[50] confirms the greater susceptibility of joints (construction joints in the case of monolithic structures) to failure. The "International Recommendations for the Design and Construction of Large-Panel Structures"[29] recognizes this by imposing rather severe strength reduction factors on the allowable stresses

in the joints.

Joints will be discussed in more detail in Chapters 3 and 4. They were introduced here to provide background for the following important assumptions concerning the panel behaviour. These are:

1. the behaviour is linear-elastic, and
2. the panels remain uncracked.

These assumptions greatly simplify the analysis of complex cantilevers but do not in any way prohibit or impede the possible occurrence and detection of either cracking or stressing of the panel into the inelastic range. Therefore, although it is not anticipated that these assumptions will be violated, except possibly at imminent collapse, it is important to emphasize that inelastic behaviour or cracking can be identified.

Aside from the practical reason that inelastic behaviour and cracking are not expected, an additional consideration is the capacity of computational facilities. Among the authors who have investigated the non-linear behaviour of reinforced concrete structures, the names Ngo and Scordlis[48], Nilson[47], Valliappan[65] and Cervenka[11] may be mentioned. Their proposed analyses are not only extremely involved and time consuming (in terms of computer time), but also require a fine finite element mesh to achieve reasonable accuracy. Providing a fine mesh for an assembly of perhaps 30 panels and solving the resulting equilibrium equations repeatedly on an iterative or incremental basis would be completely

beyond the capacity of available computers. If inelastic behaviour or cracking in the panels were found to occur, then it is anticipated that an alternative form of modelling would have to be developed.

The use of the finite element method requires that the elastic properties of the continuum under study be established. In the case of reinforced concrete panels this would require the development of composite material properties. This topic will be discussed in the next section, followed by a brief discussion of the basic principles of the finite element method, and a short study of various types of elements which could be used to simulate panel behaviour. The behaviour of a single panel will then be studied with the aim of developing a simple model which would provide sufficient accuracy while minimizing the computational effort.

2.2 Determination of Equivalent Modulus of Elasticity, Modulus of Rigidity and Poisson's Ratio for Reinforced Concrete Panels

The determination of the equivalent values for the elastic constants of the composite panel material is fundamental to the proposed analysis. These constants will be determined using a method proposed by Cervenka[11]. In Cervenka's analysis the composite material stiffness matrix is defined as the sum of the component (steel and concrete) material stiffnesses. This approach is only applicable to cases where steel is uniformly distributed

within concrete. Thus

$$[D] = [D^C] + [D^S] \tag{2.1}$$

where $[D]$ = composite material stiffness matrix

$[D^C]$ = material stiffness matrix associated with the concrete component, and

$[D^S]$ = material stiffness matrix associated with the steel components.

The steel reinforcing bars are assumed to be arranged in two orthogonal directions (coinciding with x and y directions of the element coordinate system), and uniformly distributed throughout the concrete element. Implicit in the relationship, is also the assumption of consistant deformation between the component materials. This simply means that the bond versus slip relationship is ignored for uncracked elements (i.e. for uncracked sections the rate of change of steel stress is very low). The stress-strain relationship for an element of unit thickness can therefore be written as

$$\{s\} = [D] \{\varepsilon\} \tag{2.2}$$

where $\{s\}$ = total stress vector, and

$\{\varepsilon\}$ = strain vector

The total stress vector is equal to the sum of the component stress vectors and is given by

$$\{s\} = \{s^C\} + \{s^S\} \tag{2.3}$$

Furthermore, $\{s^C\} = [D^C] \{\varepsilon\}$ (2.4)

and $\{s^S\} = [D^S] \{\varepsilon\}$ (2.5)

It should be noted that $[D^S]$ is the sum of steel material stiffness matrices in the two orthogonal directions,

$$[D^S] = [D^X] + [D^Y] \tag{2.6}$$

The material stiffness matrix for concrete, $[D^C]$, according to Hooke's Law for a plane stress isotropic material is

$$[D^C] = \frac{E_c}{1-v_c^2} \begin{bmatrix} 1 & v_c & 0 \\ v_c & 1 & 0 \\ 0 & 0 & \frac{1-v_c}{2} \end{bmatrix} \tag{2.7}$$

where E_c = modulus of elasticity of concrete, and

v_c = Poison ratio of concrete.

The reinforcement stress-strain relationship in the x and y directions is given by

$$\begin{Bmatrix} s_x^s \\ s_y^s \\ s_{xy}^s \end{Bmatrix} = \begin{bmatrix} P_x E_s & 0 & 0 \\ 0 & P_y E_s & 0 \\ 0 & 0 & 0 \end{bmatrix} \begin{Bmatrix} \varepsilon_x \\ \varepsilon_y \\ \gamma_{xy} \end{Bmatrix} \tag{2.8}$$

where P_x = steel ratio in x direction,

P_y = steel ratio in y direction, and

E_s = modulus of elasticity of steel.

The composite material stiffness matrix can now be given by

$$[D^C] + [D^S] = E_c \begin{bmatrix} (\frac{1}{1-v_c^2} + nP_x) & \frac{v_c}{1-v_c^2} & 0 \\ \frac{v_c}{1-v_c^2} & (\frac{1}{1-v_c^2} + nP_y) & 0 \\ 0 & 0 & \frac{1}{2(1+v_c)} \end{bmatrix} \tag{2.9}$$

where $n = \frac{E_s}{E_c}$

The orthotropic properties of the composite element can be described by means of the orthotropic elastic constants in the relationship

$$\begin{Bmatrix} \epsilon_x \\ \epsilon_y \\ \gamma_{xy} \end{Bmatrix} = \begin{bmatrix} \frac{1}{E_x} & \frac{-v_y}{E_x} & 0 \\ \frac{-v_x}{E_y} & \frac{1}{E_y} & 0 \\ 0 & 0 & \frac{1}{G} \end{bmatrix} \begin{Bmatrix} s_x^c \\ s_y^c \\ s_{xy}^c \end{Bmatrix} \tag{2.10}$$

where $v_x = \frac{\epsilon_x}{-\epsilon_y}$ and $v_y = \frac{\epsilon_y}{-\epsilon_x}$. E_x and E_y are the orthotropic elastic moduli in the x and y directions respectively, and G is the shear modulus. The inverse relationship is

$$\begin{Bmatrix} s_x^c \\ s_y^c \\ s_{xy}^c \end{Bmatrix} = \begin{bmatrix} \frac{E_x}{1-v_x v_y} & \frac{v_y E_x}{1-v_x v_y} & 0 \\ \frac{v_x E_y}{1-v_x v_y} & \frac{E_y}{1-v_x v_y} & 0 \\ 0 & 0 & G \end{bmatrix} \begin{Bmatrix} \epsilon_x \\ \epsilon_y \\ \gamma_{xy} \end{Bmatrix} \tag{2.11}$$

The new elastic constants can be related to the original parameters by comparing the coefficients in equations (2.9) and (2.11). Thus

$$E_x = E_c \left[\frac{1}{1-v_c^2} + nP_x - \frac{\left(\frac{v_c}{1-v_c^2}\right)^2}{\frac{1}{1-v_c^2} + nP_y}\right]$$

$$E_y = E_c \left[\frac{1}{1-v_c^2} + nP_y - \frac{\left(\frac{v_c}{1-v_c^2}\right)^2}{\frac{1}{1-v_c^2} + nP_x}\right]$$

$$v_x = \frac{\frac{v_c}{1-v_c^2}}{\frac{1}{1-v_c^2} + nP_y} \qquad (2.12)$$

$$v_y = \frac{\frac{v_c}{1-v_c^2}}{\frac{1}{1-v_c^2} + nP_x} = \frac{E_y}{E_x} v_x$$

$$G = \frac{E_c}{2(1+v_c)}$$

If the same percentage of steel is used in both directions as is usually the case with panels, then

$$E_x = E_y = \bar{E} \quad \text{and} \quad v_x = v_y = \bar{v}$$

Substituting the new symbols in equation (2.11) gives

$$\begin{Bmatrix} s_x^c \\ s_y^c \\ s_{xy}^c \end{Bmatrix} = \begin{bmatrix} \frac{\bar{E}}{1-\bar{v}^2} & \frac{\bar{v}\bar{E}}{1-\bar{v}^2} & 0 \\ \frac{\bar{v}\bar{E}}{1-\bar{v}^2} & \frac{\bar{E}}{1-\bar{v}^2} & 0 \\ 0 & 0 & G_c \end{bmatrix} \begin{Bmatrix} \varepsilon_x \\ \varepsilon_y \\ \gamma_{xy} \end{Bmatrix} \qquad (2.13)$$

Comparing this with the stress-strain relationship for unreinforced uncracked concrete (assumed isotropic) which is

$$\begin{Bmatrix} s_1^c \\ s_2^c \\ s_{12}^c \end{Bmatrix} = \begin{bmatrix} \frac{E_c}{1-v_c^2} & \frac{v_c E_c}{1-v_c^2} & 0 \\ \frac{v_c E_c}{1-v_c^2} & \frac{E_c}{1-v_c^2} & 0 \\ 0 & 0 & G_c \end{bmatrix} \begin{Bmatrix} \varepsilon_1 \\ \varepsilon_2 \\ \gamma_{12} \end{Bmatrix} \qquad (2.14)$$

it is observed that the equations are of exactly the same form. However, it must be noted that in contrast with equation (2.13), which is applicable to stresses and strains in the directions of the reinforcement, equation (2.14) can be used to relate stresses and strains in any two arbitrary orthogonal directions 1 and 2.

In practice panel reinforcement is determined on the basis of design considerations, handling needs and transportation requirements. However, it should not be less than a minimum specified for temperature and shrinkage requirements[17]. As with reinforced concrete cast-in-place walls, the temperature and shrinkage requirements are usually the governing consideration. The numerical values for panel steel ratios needed to simulate this behaviour were arbitrarily chosen as $P_x = P_y = 0.003$, which is slightly in excess of the minimum requirement. The concrete strength used for the purpose of simulating the behaviour was chosen as 5,000 psi, which is consistant with the common design practice of favouring a slightly stronger concrete for wall panels.

No reliable information on the variation of Poisson's ratio with age, strength, duration of loading or other properties of concrete is available. According to Neville[44] Poisson's ratio of concrete varies in the range 0.11 to 0.21 when determined from strain measurements, both for ordinary and lightweight concrete. A dynamic determination yields values averaging about 0.24.

For the purpose of this study Poisson's ratio for concrete (v_c) was taken as 0.15 which is well within the acceptable range.

Information on the variation of the modulus of elasticity of concrete with compressive strength is outlined in reference 44 . For the purpose of this study, a value of 4.5×10^6 was obtained for the modulus of elasticity of concrete (E_c) for 5,000 psi concrete. The value of the modulus of elasticity for steel is fairly independent of the grade, and the widely accepted value of 3.0×10^7 psi was chosen.

Incorporating the numerical values discussed above in equations (2.12), the following values for the properties of the composite materials are obtained:

$$E_x = E_y = 4.6 \times 10^6 \text{ psi and } v_x = v_y = 0.1455$$

Theoretically, these new values for E and v must be used when determining the panel element stiffness matrix. From a practical point of view, however, it should be pointed out that the values obtained for E_c and v_c depend to a large degree on the method of

evaluation. The observed variations as indicated in reference (44) are greater than those produced by the introduction of reinforcing bars. Thus, for all practical purposes, when the steel ratio is small, the changes in the values of modulus of elasticity and Poisson's ratio can be neglected.

2.3 Finite Element Analysis

A detailed discussion of the finite element method of analysis is presented in references 16 and 69. The method is based on minimizing the total potential energy of an element. Only a very brief outline of the method is given in this section for the sake of continuity and in order to introduce the terminology.

The procedure consists of separating the continuum by imaginary lines into a number of finite elements. The elements are assumed to be interconnected at a discrete number of nodal points situated on their boundaries. A function is chosen to define uniquely the state of displacement within each element in terms of its nodal displacements. The strains and hence the stresses are then uniquely determined throughout the element. The element stiffness matrix is determined by minimizing the total potential energy of a typical element.

The total potential energy is defined as

$$\phi = U + W \qquad (2.15)$$

where ϕ is the total potential energy,

U is the strain energy, and

W is the potential energy of load system

To minimize the total potential energy, a system of equations of the type

$$\frac{\partial \phi}{\partial \{\delta_i\}} = 0 \qquad (2.16)$$

where $\{\delta_i\}$ is the nodal displacement vector for node i, must be established. The total potential energy may be considered as the sum of the potential energies, ϕ^e, contained within individual elements, and the potential energy of the nodal loads. Thus,

$$\phi = \Sigma \phi^e - \{R\}^T \{\delta\} \qquad (2.17)$$

where $\{R\}$ is the nodal load vector, and

$\{\delta\}$ is the nodal displacement vector.

Equations (2.16) can then be written as

$$\frac{\partial(\phi)}{\partial\{\delta_i\}} = \Sigma \frac{\partial(\phi^e)}{\partial\{\delta_i\}} - \{R_i\} \qquad (2.18)$$

It is therefore necessary to consider only the changes of potential energy within a typical element. Equation (2.18) may be recognized as the condition of equilibrium at node i.

The detailed derivation of the stiffness matrix for a typical finite element is well established and will not be repeated. Suffice it to say that, by considering the variation of the total potential energy of an element it may be shown that

$$[k^e] = \int [B]^T [D_m] [B] \, d(\text{vol.}) \qquad (2.19)$$

where $[k^e]$ is the element stiffness matrix, $[B]$ is a matrix relating the strains at any point within an element to its nodal displacements and $[D_m]$ is the elasticity

matrix.

For the plane stress case of an isotropic material $[D_m]$ is given by

$$[D_m] = \frac{E}{1-\nu^2}\begin{bmatrix} 1 & \nu & 0 \\ \nu & 1 & 0 \\ 0 & 0 & \frac{1-\nu}{2} \end{bmatrix} \qquad (2.20)$$

where E and ν are the elastic constants of the material.

For an orthotropic material such as reinforced concrete with different ratios of steel in the two orthogonal directions (which in this particular case are coincident with the x and y directions of the coordinate system), matrix $[D_m]$ is deduced from equations (2.11) and (2.12).

2.4 Selection of Finite Elements Suitable for Modelling a Panel as a Constituent Part of a Complex Cantilever

There are various types of elements which can be used in the analysis of panels in buildings. Lau[31] has provided a comprehensive summary of most of these. The simple triangular element with 2 degrees of freedom per node is one of the most widely used elements and was employed extensively throughout this work. The stiffness matrix of this element may be determined by assuming a set of displacement functions of the form given in Fig. 2.1. The step by step details of the derivation of the stiffness matrix of this element may be found in any standard text on finite elements[16, 69] and will not be repeated. The final product however, is given by the following equation,

$$[k^e] = [B]^T [D_m] [B] t_t \Delta_t \qquad (2.21)$$

where matrices [B] and $[D_m]$ were defined in the previous section, and t_t and Δ_t are the element thickness and its area respectively.

Other types of elements which are useful in the analysis of panel buildings are:

1. the triangular element with mid-side nodes and 2 degrees of freedom per node (u, v),
2. the simple rectangular element with 2 degrees of freedom per node (u, v), and
3. the rectangular element with mid-side nodes and 2 degrees of freedom per node (u, v)

The displacement functions and other pertinent information for these elements are given in tabular form in Fig. 2.1.

There are a number of more elaborate elements such as rectangular elements with 3, 4 or 6 degrees of freedom per node including such nodal parameters as θ (average rotation) and γ (shear strains) as well as $\frac{\partial u}{\partial x}$, $\frac{\partial u}{\partial y}$, $\frac{\partial v}{\partial x}$ and $\frac{\partial v}{\partial y}$. In general the use of elements with more degrees of freedom improves the accuracy of the analysis. However, because of their complexity, they also require greater computer core capacity which in the case of larger structures constitutes an important limiting factor. Moreover, in a non-linear analysis such as the present work, it is extremely difficult to realistically allow for partial relaxation of rotations or to

Type	Shape	No. of Nodes	Degrees of freedom per node	Total number of degrees of freedom	Displacement Functions
Triangular element with 2 degrees of freedom per node	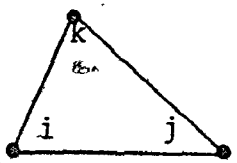	3	2	6	$u = \alpha_1 + \alpha_2 x + \alpha_3 y$ $v = \alpha_4 + \alpha_5 x + \alpha_6 y$
Triangular element with mid-side nodes and 2 degrees of freedom per node	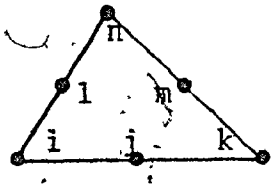	6	2	12	$u = \alpha_1+\alpha_2 x+\alpha_3 y+\alpha_4 x^2+\alpha_5 xy+\alpha_6 y^2$ $v = \alpha_7+\alpha_8 x+\alpha_9 y+\alpha_{10} x^2+\alpha_{11} xy+\alpha_{12} y^2$
Rectangular element with 2 degrees of freedom per node	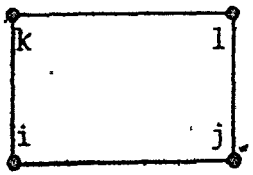	4	2	8	$u = \alpha_1 + \alpha_2 x + \alpha_3 y + \alpha_4 xy$ $v = \alpha_5 + \alpha_6 x + \alpha_7 y + \alpha_8 xy$
Rectangular element with mid-side nodes and 2 degrees of freedom per node	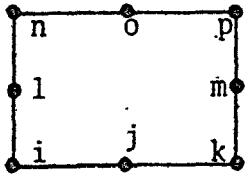	8	2	16	$u = \alpha_1+\alpha_2 x+\alpha_3 y+\alpha_4 xy+\alpha_5 x^2+$ $\alpha_6 x^2 y+\alpha_7 xy^2+\alpha_8 y^2$ $v = \alpha_9+\alpha_{10} x+\alpha_{11} y+\alpha_{12} xy+\alpha_{13} x^2+$ $\alpha_{14} x^2 y+\alpha_{15} xy^2+\alpha_{16} y^2$

Fig. 2.1 Most Commonly Used Elements in Panel Building Analysis

meaningfully account for parameters such as $\frac{\partial u}{\partial x}$, $\frac{\partial u}{\partial x}$, etc., as the joints between panels crack, slip or separate. Thus further elaboration on elements with more than 2 degrees of freedom per node will not be included. Furthermore, rather than experimenting with the other elements shown in Fig. 2.1, simple triangular elements were used in conjunction with the method of condensation of internal nodes to construct rectangular elements with 4 (corner) and 8 (corner and mid-side) nodes. It was thought that by eliminating the internal nodes of an appropriately assembled cluster of simple triangular elements, sufficient accuracy could be obtained without either sacrificing the simplicity or increasing the computational effort.

The method of condensation of internal nodes which is used extensively throughout this work is presented in detail in Appendix B. The method may be used to eliminate the internal node of an arrangement of 4 simple triangular elements to obtain a rectangular element with the same total number of degrees of freedom as the simple rectangular element shown in Fig. 2.1. Since the condensed element utilizes a total of 10 degrees of freedom (including 2 degrees of freedom for the centre node) and satisfies the compatibility of displacements along the diagonals as well as the boundary lines, it provides for a more accurate solution.

Similarly, 16 simple triangular elements may be used to construct a rectangular element with 4 corner and

4 mid-side nodes. Rather than eliminating the 5 resulting internal nodes in one operation which requires more computer storage, the process of condensation may be carried out in 2 successive stages. This aspect is explained in more detail in Appendix B.

A rather general description of the method of condensation of internal nodes is presented in reference 53 . The method is discussed in detail in Appendix B with reference to the particular arrangement of the elements used in this study. Since the 2 types of elements considered form the basis of the analytical treatment of complex cantilevers, it was felt that a precise description of the method would be essential to the understanding of the computational procedures should modifications to present work be contemplated by other researchers. Thus, Appendix B is entirely devoted to the development of the method of condensation of internal nodes with specific reference to the type of elements utilized in this study.

It should be pointed out that the elements constructed by the method of condensation are meant to represent the individual panels in the context of an assembly of panels. For the study of the behaviour of an individual panel, the number of elements can usually be increased without much restriction to achieve the desired accuracy. More accurate results may be obtained either by using more elaborate elements, or by increasing the number of simple elements. The choice between using

either a large number of simple elements, or a smaller number of more elaborate elements is made on the basis of economy or more often the availability of sufficient storage space. The accuracy of the proposed condensed elements will be tested by comparing the stress and deformation results with those for a small panel with identical physical parameters and loading, but utilizing a large number of elements. The result of this comparison will be presented in the following section. For further information regarding the method of condensation of nodes, reference should be made to Appendix B.

2.5 Investigation of the Effect of Reducing the Number of Nodes in a Panel

A detailed investigation of the effect of reducing the number of nodes in a panel was performed using deformations and stresses as the basis for comparison. The comparison was carried out considering a basic finite element mesh composed of 72 triangular elements. This is labeled scheme 1, where the results are illustrated on Figures 2.2 and 2.3. The vertical load corresponded to the dead weight of a 20 ft. bay of a five story panel building. An arbitrary horizontal load of 20 kips was applied to the top of the panel alternately as either a distributed load along the top or as a concentrated load at the edge.

In scheme 2 (see Fig. 2.2) the panel was represented by a single rectangular element containing 8 boundary nodes (4 corner and 4 mid-side). The stiffness matrix

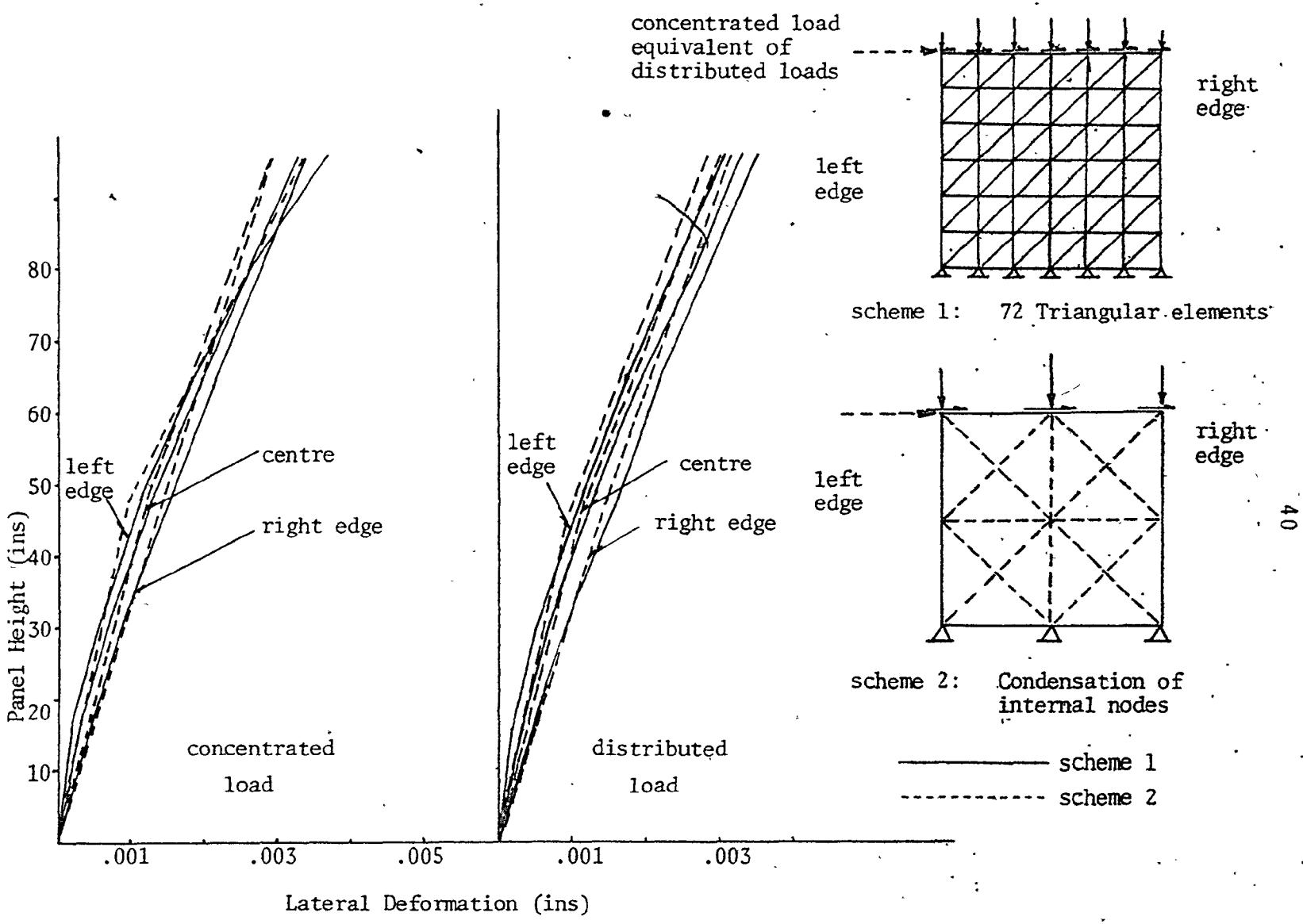

Fig. 2.2 Lateral Deformations for a Panel Using the Condensation Method Compared to Using a Dense Triangular Mesh of 72 Elements

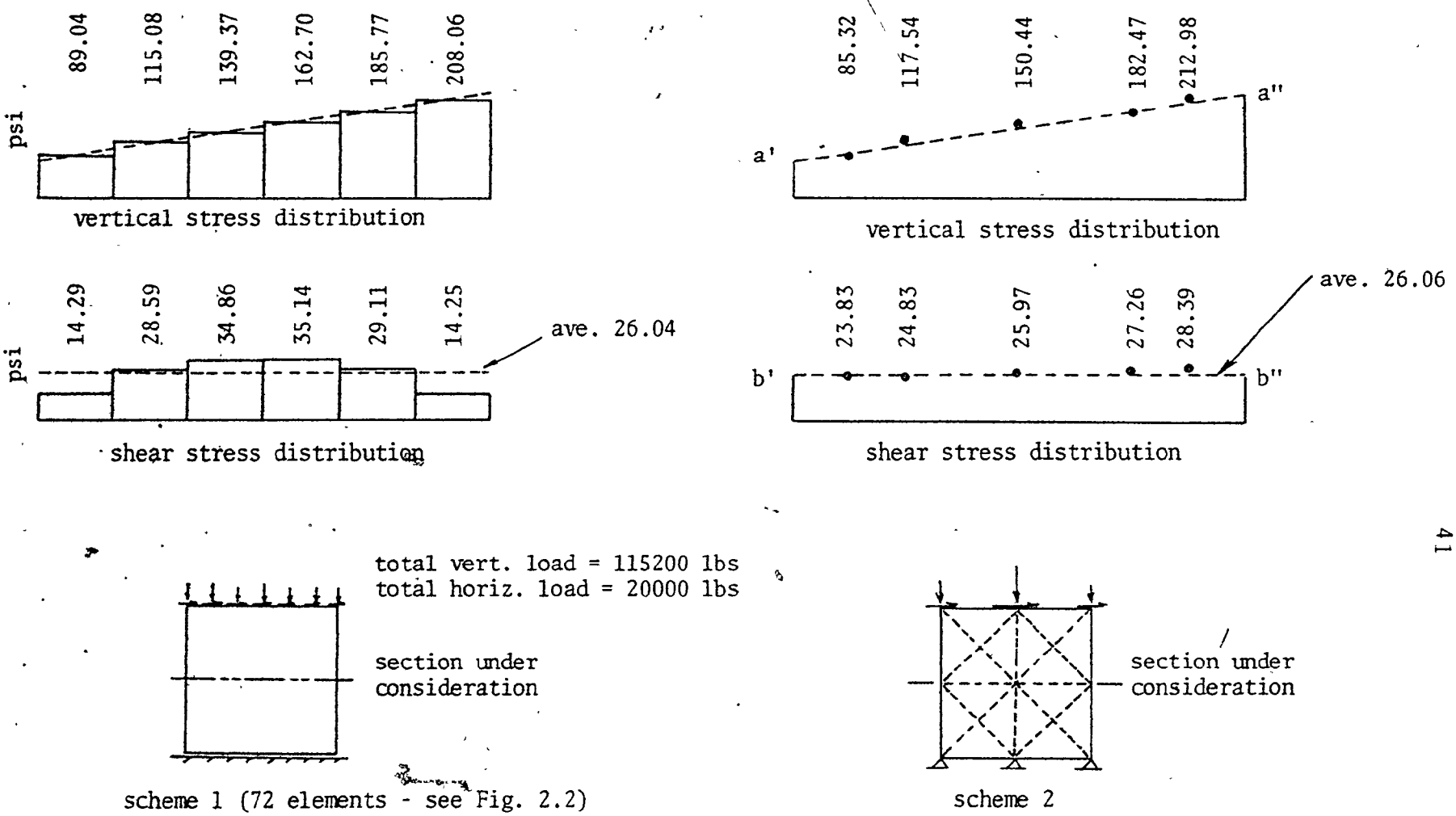

Fig. 2.3 Stresses at Mid-Section Through a Panel Using the Condensation Method Compared to Using a Dense Triangular Mesh of 72 Elements

of this element was obtained by condensing 5 internal nodes of the arrangement of elements shown in Fig. 2.2. The process of condensation was carried out in 2 stages. To start with, the nodes marked 'a' were condensed, thereby, reducing the total number of elements from 16 (triangular) to 4 (rectangular) elements. The node designated with letter 'b' was then condensed to obtain the final stiffness matrix. All the internal nodes could have been condensed in one step. However, since both 4-noded and 8-noded rectangular elements will be used in investigating the complex cantilevers, the 2-stage condensation was preferred. The process also saves computer storage space which is often a practical consideration.

The panels considered were 8 ft. square with a uniform thickness of 8 inches. A steel ratio of 0.003 and a uniform distribution of reinforcement were assumed in each direction.

Fig. 2.2 shows the comparison between the lateral deformations of panels for schemes 1 and 2. The deformations are considered along the left edge, the right edge and the centre of the panels. The maximum discrepancy in lateral deformations between the two schemes for uniformly distributed load is 9.9% and it is encountered at the right top corner of the panel. In the case of the concentrated load, the maximum discrepancy is 6.4% and it is measured at the point where the load is applied. The stress comparison for the two schemes for a section taken at mid-height of the panel is illustrated

in Fig. 2.3. The indicated stresses are found by averaging the element stresses on either side of the section. For scheme 1, equilibrium between the externally applied loads and the internal forces is satisfied to within 0.01% for normal forces and 0.002% for shear forces. The corresponding figures for scheme 2, using the approximate stress distribution illustrated by the dashed lines a'a" and b'b" are respectively 0.17% and 0.07%. The shear stress distribution for scheme 1 shows a gradual increase towards the centre of the section. However, the average shear stress is in close agreement (26.04 psi versus 26.06) with the average shear stress resulting from the analysis of scheme 2.

Three other arrangements of elements were also investigated under the same load conditions as in schemes 1 and 2. These are labelled 3, 4 and 5. The graph of lateral deformations together with the arrangement of the elements are shown in Fig. 2.4. Scheme 3 is the simplest possible way of representing a panel, and hence was the first arrangement to be studied. The comparison of lateral deformations with scheme 1 indicates the need for a more complex arrangement of elements if panels are compared on a 1 to 1 basis. In general, when a panel forms part of a complex cantilever composed of a large number of panels, the need to introduce more elaborate elements becomes less important. This is certainly true of the linear range. To illustrate this point, the lateral deformation of a complex cantilever

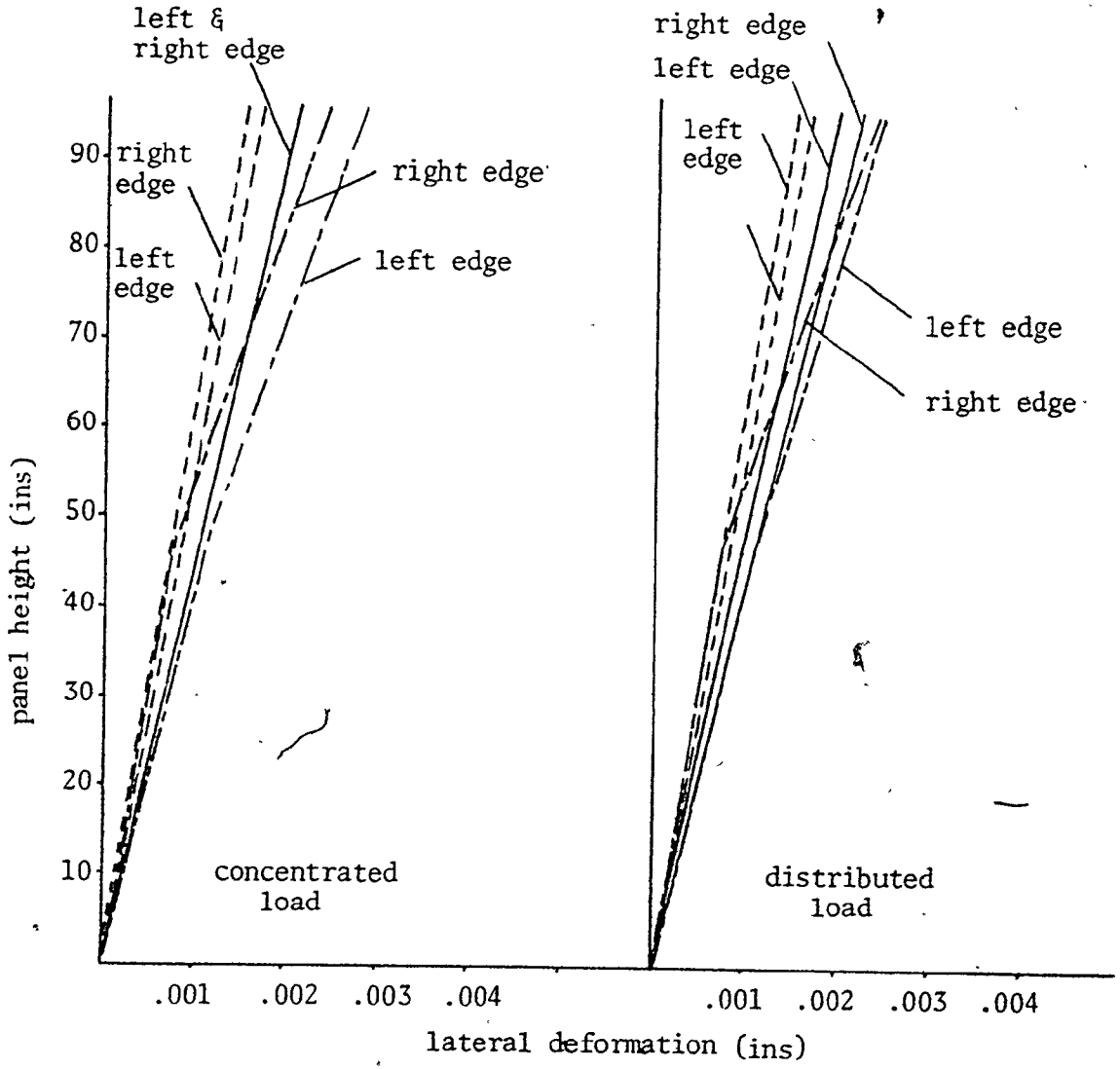

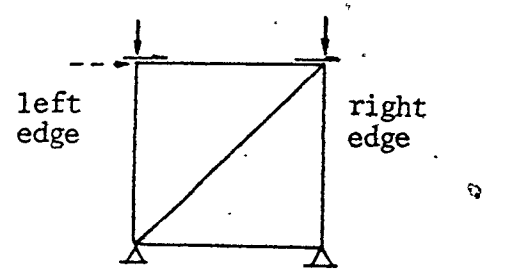

scheme 3 - 2 triangular elements

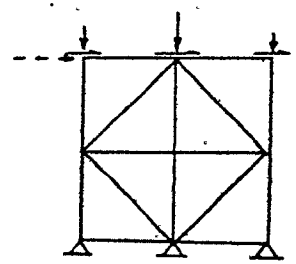

scheme 4 - 8 triangular elements

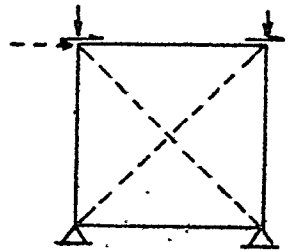

scheme 5 - condensation of one internal node

scheme 3

scheme 4

scheme 5

Fig. 2.4 Comparison of Lateral Deformations for Schemes 3, 4 & 5

composed of 30 panels was investigated using the panel elements of schemes 2 and 5.

The results were compared with those of the simple theory of bending. For all practical purposes the three methods yielded identical results as shown in Fig. 2.5. This illustrates the effect of the size of the element relative to the size of the structure being analysed. Although the panel element of scheme 2 (composed of 16 elements) is more accurate than the panel element of scheme 5 (composed of 4 elements) for a single panel analysis as shown in Fig. 2.6, as the size of the structure increases both schemes yield results which converge and become identical. It must be pointed out that in the example of the 30 panel complex cantilever, the joints were rigidly connected.

In the non-linear range it is very difficult to estimate the influence of the number of panel elements, on the behaviour of complex cantilevers. In order to achieve a realistic estimate of this influence, a fine finite element mesh of the entire assembly of panels must be considered. This would impose serious practical limitations, even on computers of very large capacity. Since the aim of the analysis is to estimate the ultimate (lateral load) strength of complex cantilevers, in a range where the joints slip, separate, crack and disintegrate, it is argued that slight discrepancies in simulating the linear behaviour of panels, will not effect the final results more than a few percentage points.

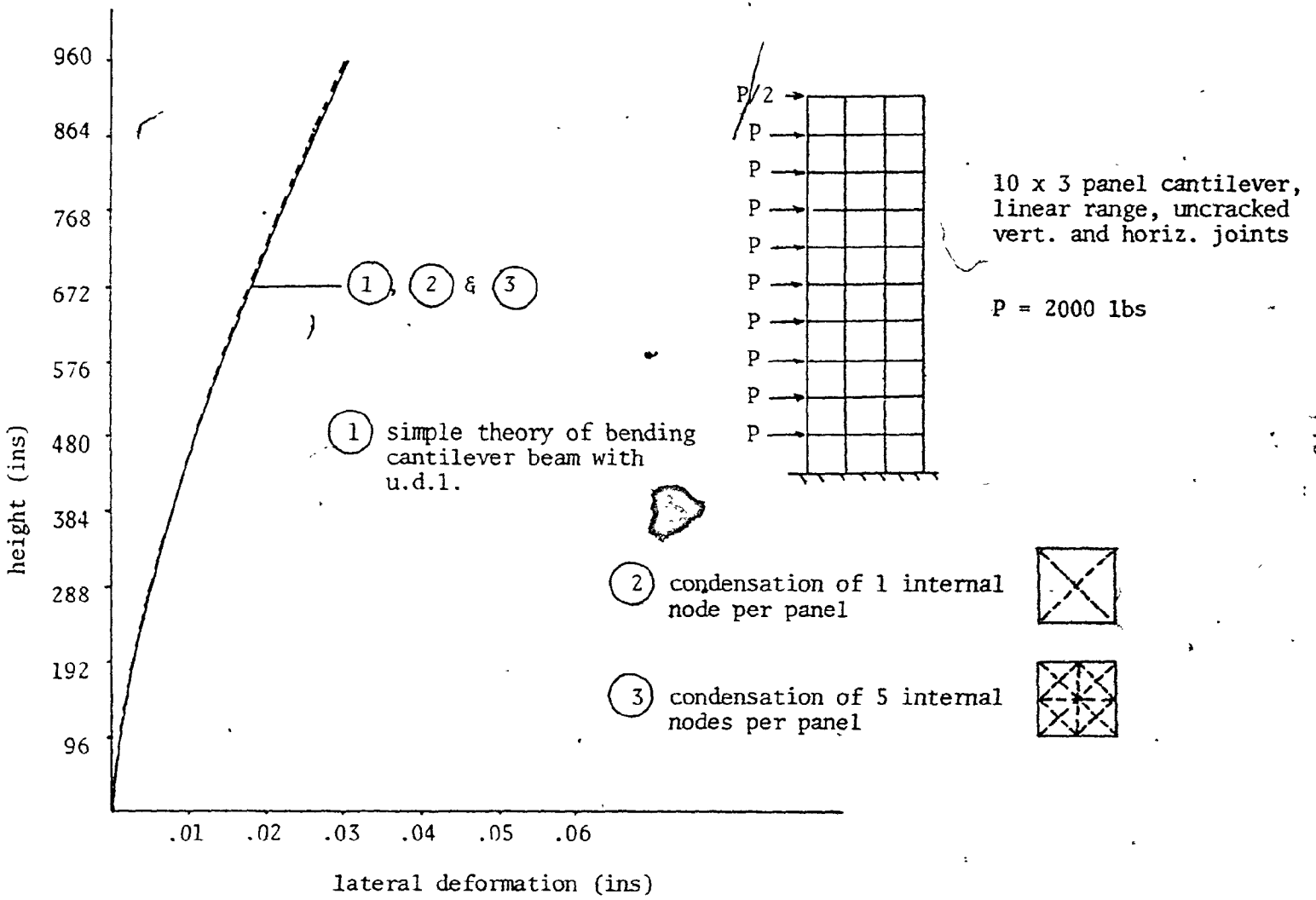

Fig. 2.5 Comparison of Lateral Deformations for a 30 Panel Complex Cantilever in Linear Range Using 2 Different Types of Finite Elements and Simple Theory of Bending

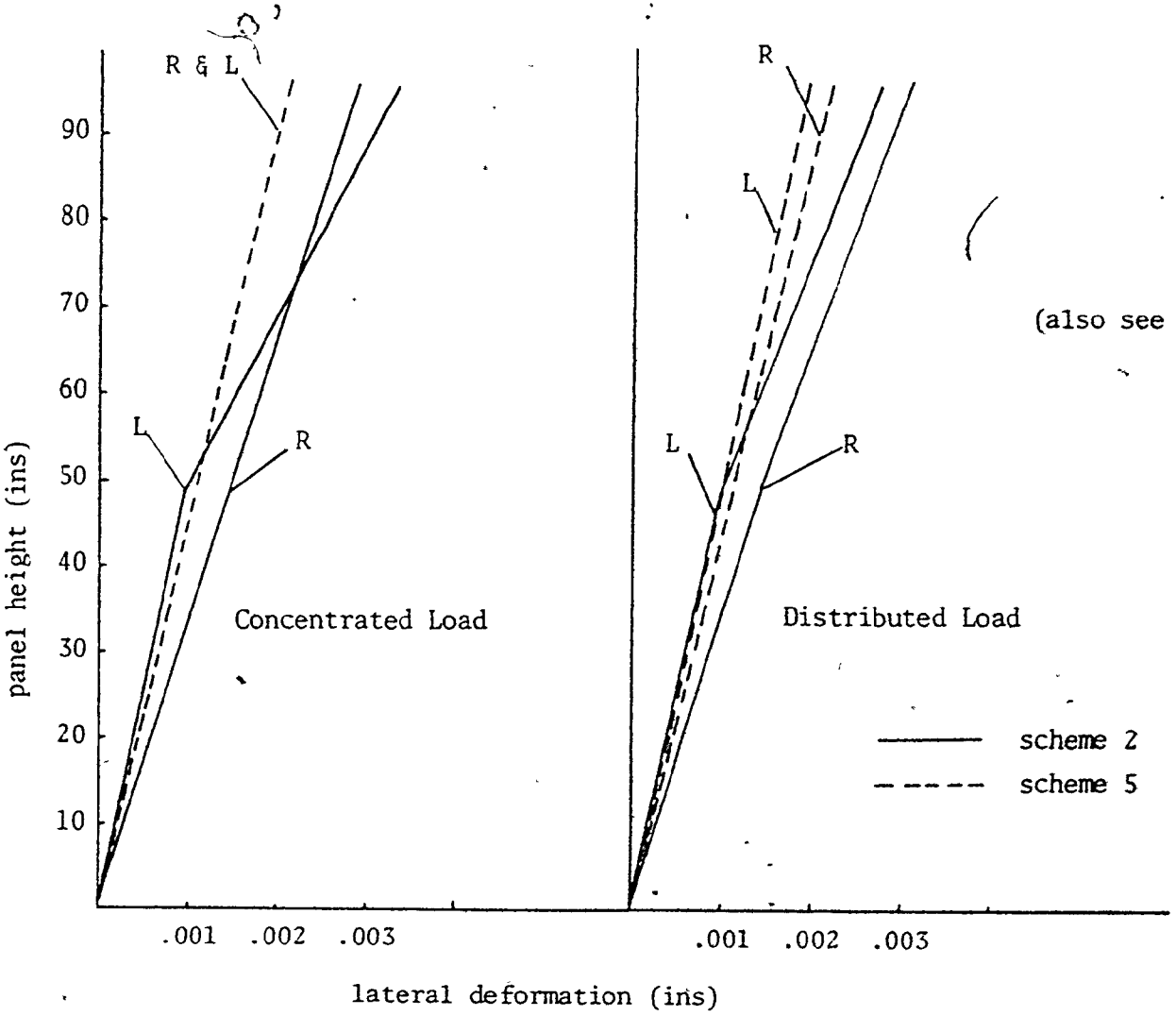

Fig. 2.6 Comparison of Lateral Deformations for Schemes 2 & 5

The non-linear behaviour of complex cantilevers will be examined in Chapter 6 after the joint behaviour has been studied.

2.6 Summary

Chapter 2 deals with panels as a constituent component of complex cantilevers and discusses the assumptions governing their behaviour.

The assumptions relating to panel behaviour, the basic principles of the finite element method, and various types of elements commonly used to simulate panel behaviour were briefly discussed. The method of condensation of internal nodes was mentioned with reference to its detailed development in Appendix B. Finally, the suitability of various schemes of representing panels, when they form a constituent part of a complex cantilever, were investigated. Special emphasis was placed upon the method of condensation of internal nodes as a means of obtaining good accuracy, without sacrificing either the simplicity or increasing the total number of degrees of freedom beyond what might be accommodated by most computers.

The condensation method was shown to produce acceptable results when a single panel so analysed was compared with a similar panel using a fairly dense mesh. The effect of the relative size of the element to the structure, in the linear range, was illustrated by comparing the lateral deformation of a complex cantilever composed of 30 panels with rigid joints using 4 and 16

condensed elements per panel respectively, with that obtained using simple bending theory. Almost identical results were obtained. In the non-linear range, it was assumed that minor discrepancies resulting from linear panel behaviour would not have a significant effect on the behaviour of complex cantilevers, as long as drastic changes occurring within the joints were accounted for.

The non-linear behaviour of complex cantilevers will be discussed in Chapter 6, after joint behaviour is studied in Chapters 3, 4 and 5.

CHAPTER 3

ANALYSIS OF HORIZONTAL JOINTS

3.1 Introduction

The overall behaviour of a complex cantilever depends to a very large degree on the performance of its horizontal joints. Very little is known about the behaviour of horizontal joints under the combined action of vertical and horizontal loads. The few investigators who have reported studies of the behaviour of panel assemblies, have usually used simplifying assumptions to model the behaviour of the joints. A summary of most of these investigations was given in Section 1.4.

The purpose of this chapter is to develop a more realistic analytical model for the behaviour of horizontal joints. This model should be able to account for their partial or complete separation, cracking and slip as well as to allow for shear and normal deformations of the joint material.

A detailed analysis of the behaviour of an individual joint involves the use of a large number of elements. Representation of the many joints contained in a complex cantilever in this fashion would be unrealistic, if for no other reason than practical limitations on computer storage capacity. In addition, even if sufficient storage

space could be provided, the computer time required to solve the equations repeatedly as lateral loads gradually increase would prove quite uneconomical. Thus, in order to perform a detailed joint analysis, a single isolated horizontal joint cast between a pair of prefabricated panels is considered. This arrangement is shown in Fig. 3.1(a). It is intended that once the behaviour of an isolated joint has been documented using the detailed model, a simplified model can be developed employing fewer elements to approximate the detailed behaviour. This procedure has been followed and a simplified model is presented in Chapter 5 and is subsequently used in the study of complex cantilevers to determine the behaviour of the whole assembly.

The material presented in this chapter is divided into two parts. Initially, the behaviour associated with unreinforced joints is studied, taking into account separation, cracking and slip along two possible surfaces. These will be discussed further in Sections 3.2 and 3.4. Other topics discussed are establishment of the various criteria and modes of joint failure, derivation of stiffness matrices for elements representing the slip surfaces (defined in the next section), and investigation of various methods of nonlinear analysis with emphasis on the method selected for this study. The joint behaviour under various loading conditions is illustrated by means of a series of graphs.

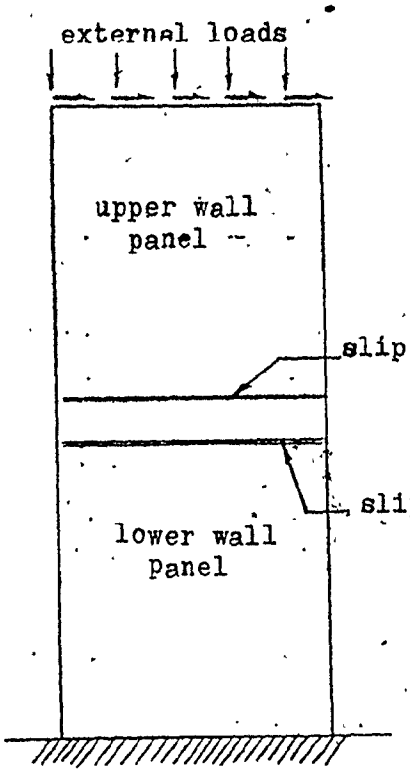

(a) Schematic Representation of an Isolated Horizontal Joint

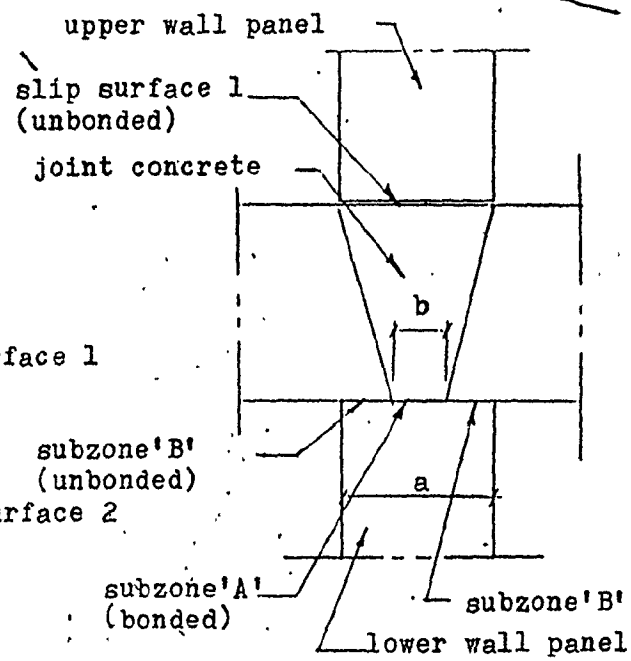

(b) Idealized Horizontal Joint

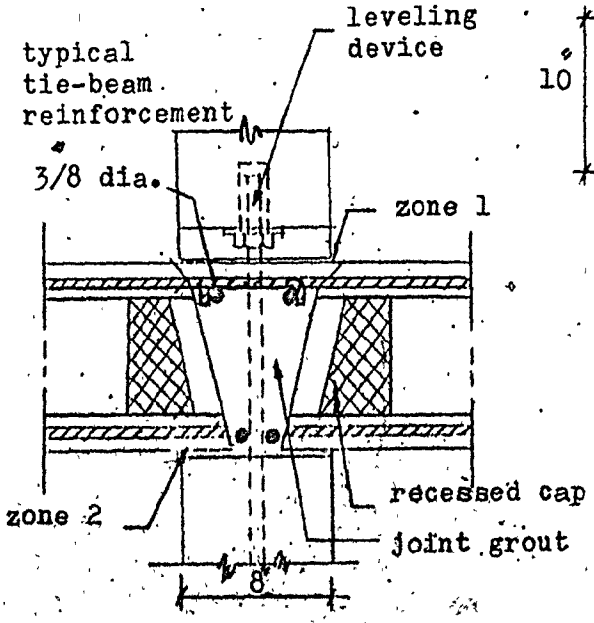

(c) Actual Horizontal Joint

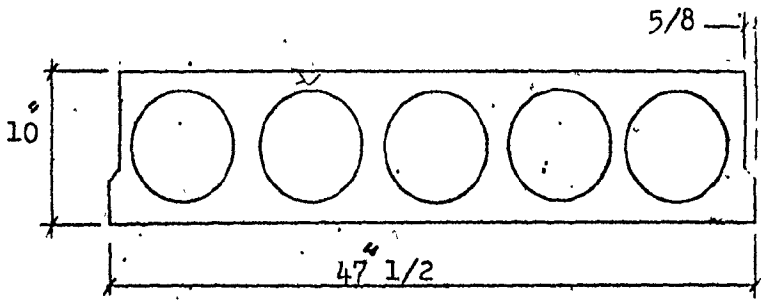

(d) Cross Section of Floor Slab

Fig.3.1 Horizontal Joint Components and Details

The behaviour of reinforced joints is investigated in the latter part of this chapter. The representative reinforcement consists of two vertical dowel bars extending from the upper surface of the wall panel below the joint, passing through the joint-filler region, and grouted or otherwise anchored in the preformed cavities in the wall panel immediately above. These dowels may also be used as a leveling aid. In addition, they serve to support the upper wall panel while the joint concrete is hardening. (Although the same method of support may also be used in unreinforced joints, it is assumed that the dowels' function in this case is purely non-structural. Here, inadequate development length or the lack of proper anchorage will not allow significant forces to be developed in them. Alternatively, unreinforced joints could be supported or shims or wedges which are removed after in-situ concrete has hardened.)

The stiffness of a reinforced joint element is determined using experimental results for bond-slip and for dowel bar force-displacement relationships to establish the material property matrix. Once the reinforced joints have been modelled and analyzed, their behaviour is compared to those of unreinforced joints to determine the effect of joint reinforcement on strength and ductility.

However, before proceeding with the actual analysis, it is important to describe the horizontal joints and the manner in which they are actually constructed in the field.

Although for the purpose of actually simulating the behaviour, specific typical joint dimensions and other characteristics have to be selected, the method will be developed so that it is capable of accommodating different joint parameters and characteristics. Thus, the remainder of this introductory section will be used to describe the most common types of horizontal joints and the rationale behind choosing the particular joint for this study.

(a) Horizontal Joints

The basic functions of a horizontal joint are to accommodate the floor panels, to transmit the interpanel gravity and shear forces, and to provide some resistance against separation if the joint is subjected to vertical tensile forces.

In almost all systems, it is the friction force which is relied upon to resist the shear. Furthermore, the strength and integrity of a joint is greatly influenced by the type of joint and the degree of care (proper placing, compaction and curing of in situ concrete) used during its construction.

The various ways in which horizontal joints are constructed depend to a large extent on the manner in which the floor slabs are supported on the wall panels. There are three basic methods of supporting floor slabs on load bearing panels [32, 55]:

1. continuously along the ends,
2. on lugs of steel or concrete, and

3. on reinforced concrete dowels used in conjunction with hollow reinforced concrete floor slabs.

There are four basic types of floor panel commonly in use in fully panelized and semi-panelized construction. These are:

1. cast in-situ floor slabs on load carrying precast wall panels,
2. solid precast floor panels,
3. hollow precast floor panels, and
4. ribbed and corrugated precast floor panels.

Type 1 is sometimes designed as a continuous slab over the wall panels. It may also be designed as a simply supported slab. This type of floor slab is usually supported continuously along both ends. Type 2 may be similarly supported or supported on lugs of steel or reinforced concrete. Type 3 may be supported continuously along its ends or on reinforced concrete dowels. Type 4 which is the least frequently used type, may also be supported continuously along its ends, or on lugs.

It is usually considered good practice to provide reinforcing steel both to tie the floor panels together end to end, and to control the development of tension cracks. Three basic ways to achieve this are:

1. over-lapping the steel bars protruding through the edges of the floor panels and welding them,
2. welding the protruding bars to a steel connecting plate or angle, and

3. anchoring the bars in grout in the joint space between the floor panels.

When floor panels are supported on lugs, the bottom edge of the upper wall panel is usually provided with a key[32]. Sometimes what appears to be a key is in fact a cavity provided for the purpose of accommodating a leveling mechanism. This is one of the most commonly used methods of leveling and supporting the upper wall panels prior to placing and curing the joint concrete.

In a system which was modified for use in North America (Jesperson-Kay), the bolts used for leveling were welded to a steel bracket type of arrangement and the bracket bars were carried through the height of the panel to give the joint some resistance to separation.

Different joint details have been devised by various manufacturers. Although the details may seem to be different, most may be classified under one of the types described above with only superficial differences in behaviour. More information on joint details may be found in references 14, 18, 32, 45 and 55.

Since there have been a large number of joints which differ from one another in their details, the choice of a representative model for the purpose of studying the behaviour of panel buildings, is very important. Furthermore, the choice must reflect current good practice. However, the analytical model developed for this study is such that other types of joints may be substituted without requiring major changes in the

analytical scheme.

The joints to be modelled for this study were selected to conform to the following basic requirements:

1. the strength requirement provided for by the inclusion of tying steel, and
2. the requirements for conformance with the current construction practices taking into account economy and other practical considerations.

In general, the CEB Recommendations[29] were used as a guide along with information on typical joints. (The above comments also refer to vertical joints). It must be mentioned that the choice of typical components was made on the basis of an extensive preliminary investigation of a number of wall-floor combinations, and after it was ascertained that the chosen combination contained all the necessary features to allow a comprehensive study of the problem.

The joint selected for the purpose of this study is shown in Fig. 3.1(c). Wall panels were 8 ft. square with a thickness of 8". Floor slabs were the hollow precast type and were 10 inches thick as shown in Fig. 3.1(d). They are assumed to span a distance of approximately 20 feet[32, 55]. The width of the floor panel was taken to be 48 inches including clearances. (The size of panels used in panelized construction is usually limited by practical considerations of lifting and erecting.) The slabs' top reinforcement was extended into the joint and welded to that of the adjacent floor panel to ensure

continuity. The concrete strength selected for wall and floor panels were 5,000 psi and 4,000 psi respectively. Tie beam reinforcement was provided in the form of 4 #3 bars. The purpose of these bars is to provide the panel assembly with transverse continuity. Floor slabs were assumed to be continuously supported along their ends with a bearing width of 2 inches[32, 21, 8, 58].

3.2 Characteristics of Slip Surfaces

Before discussing the structural behaviour of a horizontal joint, it is convenient to initially define the following joint components which are also shown in Fig. 3.1.

(1) Slip surface 1, slip zone 1, or simply zone 1, are used synonymously to define the contact surface between the bottom face of a wall panel and the concrete joint and/or the floor slab.

(2) In-fill concrete, joint concrete or joint filler identify the in-situ concrete used to fill the cavity between the floor slabs and wall panels.

(3) Slip surface 2, slip zone 2, or simply zone 2 define the interface between the top surface of a wall panel and the concrete joint and/or the floor slab.

Under the combined action of gravity loads and horizontal shear forces, slip is likely to occur in the locations identified as slip surfaces 1 and 2. Slip surface 1 is assumed to be unbonded. To support this assumption the sequence of the construction operations for the erection of a wall panel must be examined.

A common method of construction is to initially support the wall panel on a leveling device, fill the joint cavity with concrete (grout), and allow the concrete (grout) to harden. When it is strong enough to support the weight of the panel, the supporting device is removed, by turning down the nuts on leveling screws or by removing the wedges, and the entire weight of the panel is transferred to the joint.

As a result of shrinkage, or the settlement associated with the possible leakage of water and cement due to improper sealing, there will in all likelihood be a prevention or breakage of bond along slip surface 1. Furthermore, due to the phenomenon commonly known as bleeding[40], the top surface of concrete is often of inferior quality compared with the rest of the concrete. (Bleeding is the tendency of water to rise to the surface of freshly placed concrete.) This bleeding and the accompanying phenomenon of laitance formation also provides reason for assuming no bond at slip surface 1.

For these reasons and because it is a conservative assumption, slip surface 1 is assumed to be unbonded for the analysis of joints. The external shear forces are thus resisted only through friction along this surface.

Slip zone 2 is assumed to be comprised of 2 sub-zones. Sub-zone 'A' (Fig. 3.1(b)) is assumed to be bonded in all cases. Sub-zone 'B' may in reality be partially bonded or unbonded depending on the method used to support the floor panels. It is difficult to estimate the degree

of bonding that might be provided by a thin layer of mortar (approximately 3/8")[32,55]. The primary purpose of this layer is to provide an even support for the floor panels. For this reason and because it is a more conservative approach, this latter sub-zone is assumed to be unbonded in the analysis which follows. The idealized horizontal joint is shown in Fig. 3.1(b).

The concept of shear-friction will be introduced before continuing with the analysis since frequent reference will be made to it is the subsequent sections.

3.3 Shear-Friction Theory[6]

Referring to the block of concrete shown in Fig. 3.2(a), a crack is assumed to exist along surface S-S. The external shear force V which is sufficient to produce slip along S-S is resisted by friction force μp.

Because the crack surface is rough, a sliding motion along it will cause a separation between the two halves of the block. This is produced by riding up of one of the halves over the asperities of the other. If well anchored steel bars are placed across the interface, the separation will develop a tensile force in the reinforcement. This force will create a clamping force of equal magnitude on the concrete. The roughness may be visualized as a frictionless series of fine saw-tooth ramps having a slope of ϕ. Comparing Fig. 3.2(a) and Fig. 3.2(b), $N \tan\phi$ is seen to be similar to the friction

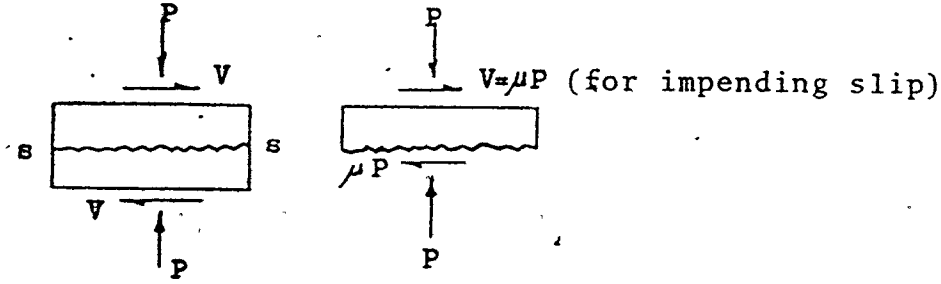

(a) Compressive Force Supplied by Gravity

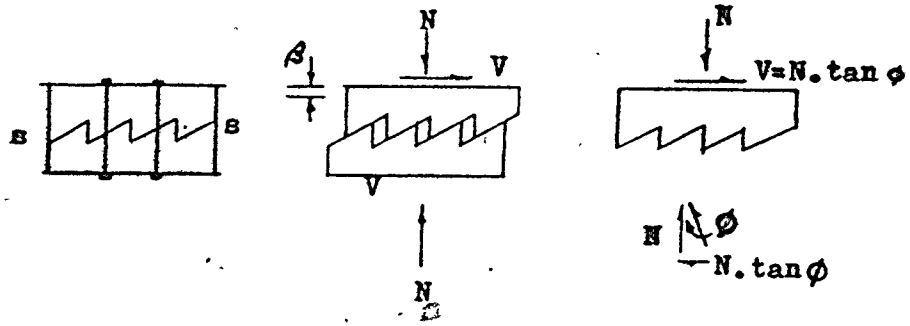

(b) Compressive Force Supplied by Clamping
Action of Dowel Bars

Fig.3.2 Shear-Friction Theory

force μp. Consequently,

$$V = N \tan\phi = A_s f_s \tan\phi \qquad (3.1)$$

$$\tau = V/A_g = P f_s \tan\phi \qquad (3.2)$$

where

V = shear force

N = clamping force

A_g = gross area

A_s = area of reinforcement

$p = A_s/A_g$

τ = shear stress

$\tan\phi = \mu$ = coefficient of friction

This representation of shear friction theory will be referred to again when discussing the various modes of failure for slip surfaces 1 and 2.

3.4 Modes of Failure Under the Combined Action of Gravity Loads and Lateral Loads

Under different loading conditions failure may occur in slip surfaces 1 and/or 2. The failure in each slip surface will be discussed separately in the following sub-sections.

(a) Slip Surface 1

As was previously mentioned, slip surface 1 is assumed to consist of an unbonded surface capable of resisting shear forces through frictional resistance only. The values of the coefficients of friction for various types of surfaces recommended by Birkeland[6],

Mast[38] and the ACI Standard 318-71 are summarized in Table 3.1.

The structural behaviour of slip surface 1, and the accompanying modes of failure may be classified as follows:

	Birkeland	Mast	ACI Standard 318-71
Monolithic concrete	1.7	1.4-1.7	1.4
Rough surface between precast and cast-in-place concrete	1.4	1.4	
Concrete cast against smooth concrete or steel	0.8-1.0	0.7-1.0	
Concrete cast against hardened concrete			1.0
Concrete cast against steel			0.7

Table 3.1 Values of Coefficients of Friction for Various Surfaces

(i) Separation

If tensile forces are acting on a portion of slip surface 1 due to, say a bending moment, then separation will immediately occur over that part of the surface. Since this zone is assumed to be unbonded, the surface cannot provide resistance against separation. Furthermore, as soon as separation has occurred, slip zone 1 loses all its ability to resist shear forces over the separated segment.

(ii) Slip Resulting from Exceeding Maximum Shear Resistance

If f_n and f_s represent respectively the compressive and shear stresses acting over a given segment of slip surface 1, then with μ as the coefficient of friction, the maximum shear stress, f_{sm}, that may be sustained over the segment is

$$f_{sm} = \mu f_n$$

as long as $f_{sm} \geq f_s$ no slip will occur. Thus the slip condition for zone 1 may be stated as

$$f_s > \mu f_n \qquad (3.3)$$

(iii) Slip Resulting from Exceeding Concrete Strength

If the compressive stress, f_n, is large, a correspondingly large shear stress, f_s, is required to cause slip. In such cases, the strength of the concrete forming the slip surface may be overcome before f_s exceeds μf_n. The transfer of shear to the joint is through asperity interlock along the slip zone which forms localities of high stress concentration. Thus the combined effect of compressive and shear forces tend to create diagonal cracks commencing in the vicinity of the slip surface. There is experimental evidence[40] suggesting that immediately after the formation of these small inclined cracks there will be a relative movement between the components on either side of the slip surface. Failure will then follow almost immediately as additional cracks are formed interconnecting the original tension cracks.

The process will also be accompanied by spalling of concrete in the region of the slip surface leading to a reduction in the value of the coefficient of friction.

The tests conducted by Mattock[40] on initially cracked (unbonded) and uncracked push-off specimens indicate clearly the mode of failure in the presence of large compressive forces. Although, there are basic differences in the load-slip behaviour of push-off specimens compared to horizontal panel joints, the behaviour at failure directly supports the failure pattern described for slip zone 1.

For unbonded specimens, Mattock observed that for high percentages of steel, it was the strength of concrete which governed the failure. For these specimens, diagonal tension cracks crossed the pre-existing crack in the shear plane. Failure finally occurred as a result of the formation of additional cracks (linking the diagonal tension cracks) and by disintegration of concrete in the region of the tension cracks adjacent to the shear plane.

It is important to be aware of certain differences which exist between the structural behaviour of the slip surfaces and that of a push-off specimen. To start with, it must be noted that the compressive (clamping) force in a push-off specimen is supplied by the reinforcing bars crossing the shear plane. For a compressive force to exist, first a slip and hence a separation (denoted by β in Fig. 3.2(b)) between the two halves of the specimen must take place. Thus, slip becomes a prerequisite for

the creation of the clamping force necessary to resist shears. Fig. 3.3 gives a schematic representation of the shear-friction cycle. It is seen that it forms a closed loop.

For slip surfaces 1 and 2, however, the compressive force is supplied by gravity. It remains constant, and slip occurs only when the shear force exceeds the gravity force times the coefficient of friction. The typical load-slip curves for the two cases are shown in Fig. 3.4.

In addition, it must be remembered that in push-off specimens the applied shear force is resisted by friction as well as the dowel action of the reinforcements. For unreinforced horizontal joints, the entire shear force is resisted by friction alone.

Another possible mode of failure which has been suggested by Phillips[52] for bonded push-off specimens under shear and bending condition is that of a diagonal crack extending right through the depth of the member. It is extremely unlikely that this situation could be duplicated for a horizontal joint. That is, for a push-off specimen the section properties remain relatively unchanged at various perpendicular distances from the shear plane. This, however, is not the case for the horizontal joints. The slip surfaces constitute the weakest link in the chain of components resisting the loads. Because of the contribution of the floor slabs to the strength of the joint, the shear failure is assumed to be confined to

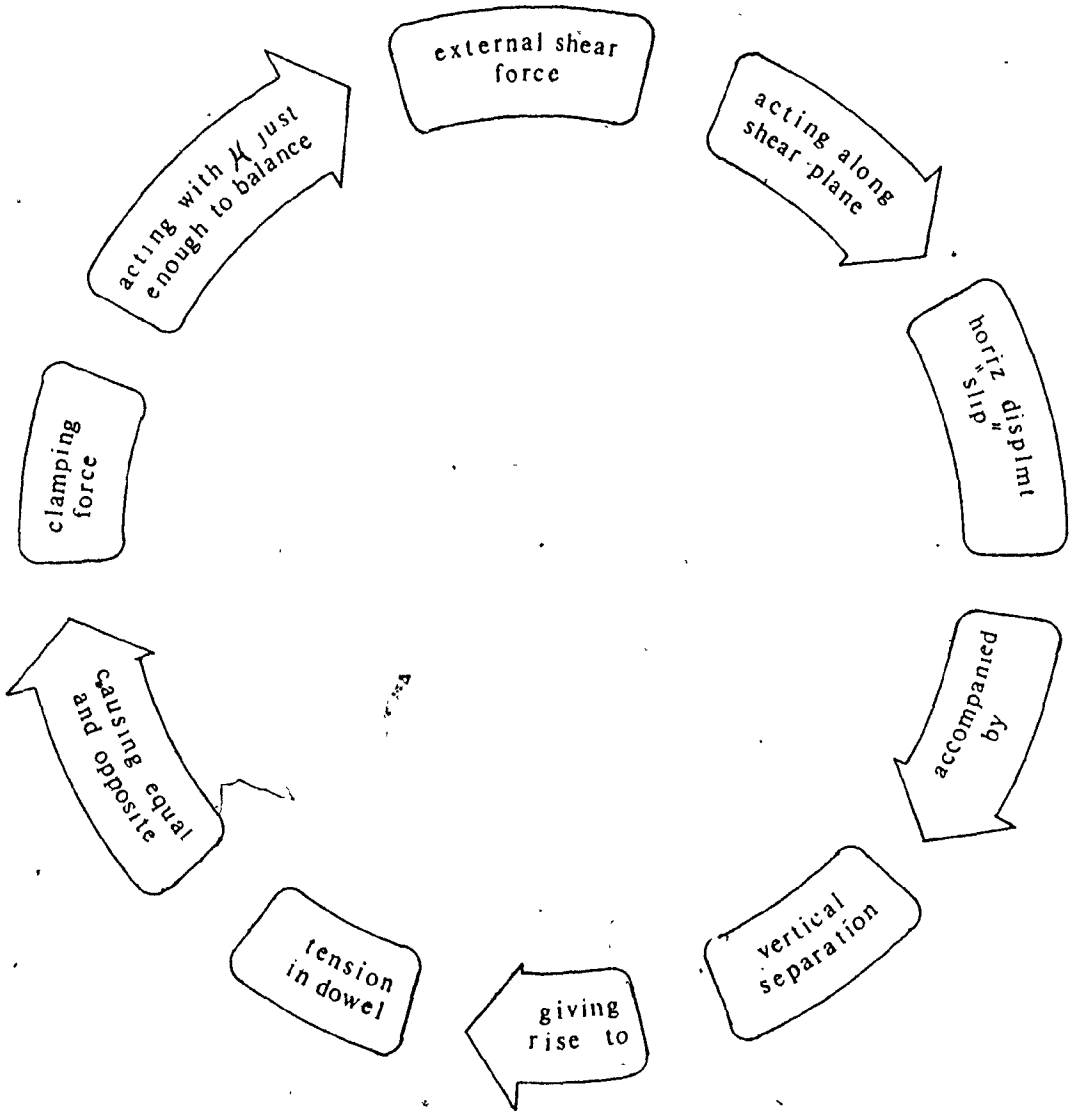

Fig.3.3 Schematic Representation of Shear-Friction Cycle

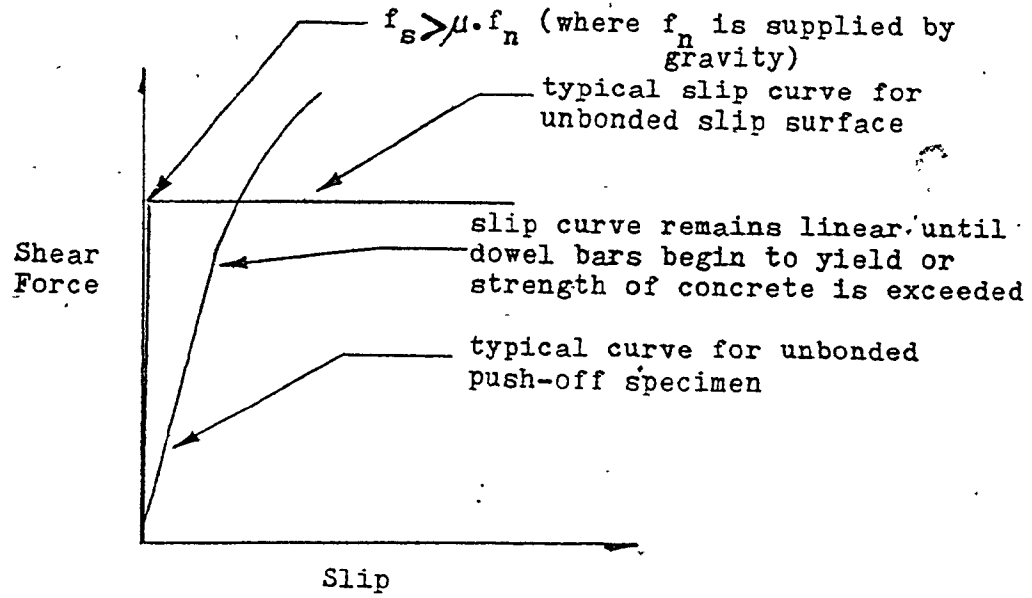

Fig.3.4 Typical Shear Force Versus Slip Curves for Push-Off Specimens and Slip Surfaces

the immediate vicinity of the slip surfaces rather than penetrating deep into the joint section.

Considering an element in the joint filler region and immediately below slip surface 1, the maximum principal stress created by a combination of vertical compressive stress, f_n, and shear stress, f_s, can easily be determined (Fig. 3.5). This stress is denoted by f_t^*. If f_t^* is greater than the tensile strength of concrete, f_t, short diagonal cracks will develop. For the reasons stated in the previous paragraph, these cracks tend to remain confined to the immediate vicinity of the slip surface. With a slight increase in shear forces, additional cracks are formed joining the diagonal cracks together and resulting in the so called shear failure of the joint. Because the behaviour of the joint at failure is quite brittle, the failure load is taken as that causing the formation of the diagonal cracks.

In the above analysis, the cracking criterion is based on maximum stress or Rankin's theory. The assumption here is that the cracking of the stressed element is governed by the maximum principal stress only, and is not influenced by the presence of the other principal stress.

(iv) Compression Failure

From experimental work[58] it has been found that the failure load for horizontal joints subjected to compression is less than the product of the contact area and the ultimate strength of concrete f_c'. The amount by which

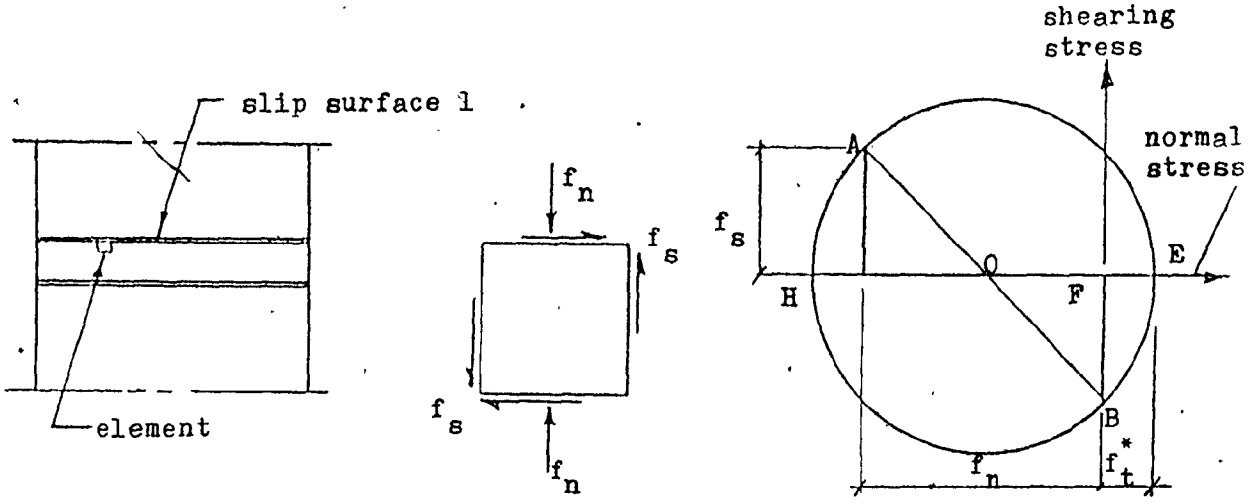

$OA = OE$

$$f_t^* = FE = OE - OF = \sqrt{(f_n/2)^2 + f_s^2} - f_n/2$$

$f_t^* \geqslant f_t$ for crack development

Fig.3.5 Maximum Stress or 'Rankin's' Theory(37)

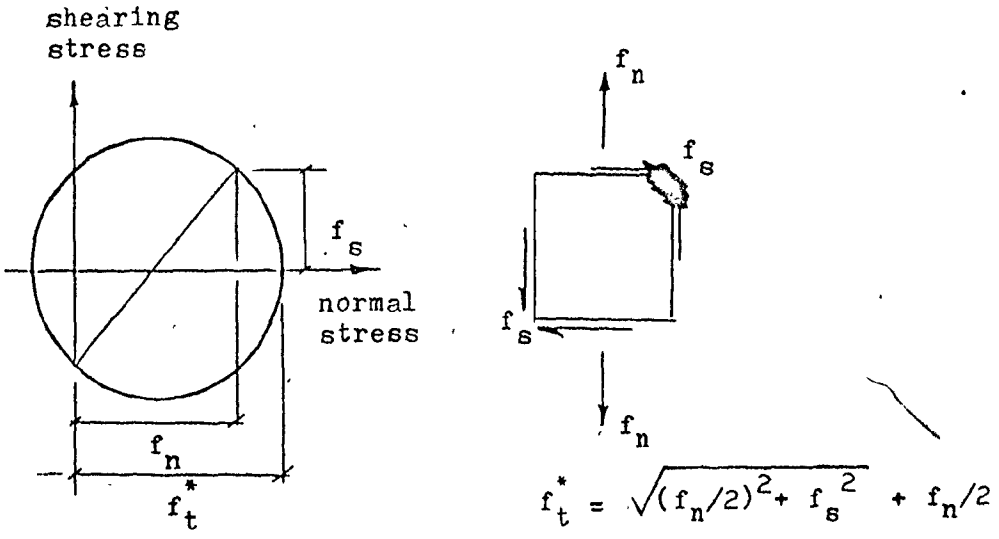

$$f_t^* = \sqrt{(f_n/2)^2 + f_s^2} + f_n/2$$

Fig.3.6 Mohr's Circle for an Element Subjected to Shear and Tension

the joint strength is reduced, however, depends on the type of the joint, provisions for mechanical continuity across the joint, attention to detailing, and good workmanship to ensure uniform distribution of stresses.

This reduction is recognized by the CEB[29] in their recommendation for the introduction of two factors of safety ξ and γ_m. It is recommended that these be applied to all horizontal joints in the absence of specific experimental information. For this reason, they are quite conservative. The CEB relationship for maximum allowable compressive stress, assuming that all materials at the joint have similar properties, is of the form

$$f_{cmax} = \xi \frac{f_c^*}{\gamma_m} \qquad (3.4)$$

where f_c^* = permissible concrete strength,

ξ = reduction coefficient depending upon the type of horizontal joint, and

γ_m = behavioral coefficient associated with the strength of concrete.

Although, equation (3.4) deals with allowable rather than ultimate stresses, the roles of ξ and γ_m remain unchanged. According to the CEB[29] recommendations, ξ must be taken as 1.0 for monolithic construction, 0.8 for precast wall panels and cast-in-place floor, and 0.7 for precast wall and precast floor panels. If no mechanical continuity is provided at the horizontal junctions, ξ is further reduced to 0.5. As was mentioned earlier these values

are conservative. Thus for the type of joint used in the present investigation a ξ value of 0.75 to 0.8 is probably more appropriate to represent the actual conditions. A value of $\xi = 0.8$ will be used in this investigation.

The CEB recommendations on the use of γ_m are rather ambiguous. They state that due to certain 'heat treatments' a loss of strength of up to about 25% might result depending on concrete composition and the duration and the method of treatment. The recommended values vary between 1.0 and 1.60 depending on the type of construction, the component (wall panel, floor panel or cast-insitu joint concrete) and whether the limit states of resistance, cracking or deformation are considered.

In the present analysis it is assumed that there is no reduction in strength of joint concrete. This is one of the variables over which the designer has a great deal of control. The strength can be specified in such a way as to provide high probability that the minimum required strength will be achieved. As far as the strength of the prefabricates is concerned, it is an observed fact that the actual strengths achieved are usually in excess of the minimum specified values. This is due to the fact that factory produced panels are not only very well compacted, but are also cured in a very highly controlled environment.

It must also be noted that compression failure effects the entire joint. Thus, it is no longer possible

to talk about failure in the vicinity of the slip surfaces.

(b) Slip Surface 2

The physical characteristics of zone 2 are slightly different from those of zone 1. Sub-zone 'A' Fig. 3.1(b) is assumed to be bonded. Sub-zone 'B' on the other hand is taken to be unbonded. The structural behaviour under load and the possible modes of failure are classified as follows.

(i) Splitting

The tendency to separate along slip surface 2 is counteracted by the bonding resistance existing between the top of the wall panel and the joint filler. If f_n is the mean normal (tensile) stress across slip zone 2, then the actual stress, f_n', acting over the bonded portion (assuming no resistance to separation is offered by sub-zone 'B') is given by

$$f_n' = a.f_n/b \qquad (3.5)$$

where a and b are the width of the wall and the width of sub-zone 'A' respectively. Splitting or separation will then occur when the maximum principal stress, f_t^*, exceeds the tensile strength of the concrete. With reference to Fig. 3.6

$$f_t^* = \sqrt{(\frac{f_n'}{2})^2 + f_s'^2} + \frac{f_n'}{2} \qquad (3.6)$$

In this equation $f_s' = a.f_s/b$, where f_s is the mean shear stress. The condition for splitting is therefore given by

$$f_t^* > f_t \tag{3.7}$$

where

f_t = tensile strength of concrete

Waters[66], Bates[5], and the United States Army Engineer Waterways Experimental Station (reported by Phillips[52]) have investigated the tensile strength between cast-in-place and preformed concrete for a variety of surface treatments. It is generally concluded that tensile strength across a joint formed by placing concrete against a pre-existing concrete member is less than that existing in an unjointed concrete of similar composition. According to Troxell[64], the bond strength between the cement paste and the aggregates in concrete depends on physical, chemical mineralogical and electrostatic properties of the aggregate surface. Similarly, the bond strength between the cement paste in cast-in-place concrete and a precast surface is governed by the properties of the surface. If this bond strength is less than that existing between the cement paste and the aggregate, failure will occur at the interface as reported in the above references.

Although there is general agreement among investigators that there is a reduction in strength across a construction joint, the quantitative values are not readily available. The amount by which the strength is reduced seems to depend not only on the surface texture and dryness, but also on the type of loading. The experimental values for the ratio of jointed to unjointed

strengths vary from about 0.50 to 0.95 depending on the surface treatment and the type of loading. For the type of joint studies here this value is chosen as 0.8 which is thought to reflect the existing joint conditions. The criteria for splitting is then modified to:

$$(\sqrt{(\frac{f'_n}{2})^2 + f'^2_s} + \frac{f'_n}{2}) > 0.8\ f_t \qquad (3.8)$$

(ii) Cracking Resulting from Exceeding Concrete Strength

The failure mechanism is similar to that discussed for slip surface 1 (3.4(a)(iii)). It is assumed that the initial cracks are very short diagonal cracks commencing at the slip surface. In the case of zone 1 it was possible under the right conditions for the slip to occur without shearing off of the asperities. In the case of zone 2, cracking must precede slip as this zone is considered to be unbonded.

To formulate the cracking criterion for slip surface 2, f_n and f_s are designated to represent the mean normal (compressive) and shear stresses acting on zone 2. If $f_s < \mu f_n$ where μ is the coefficient of friction associated with the unbonded region of the slip surface (sub-zone B), then the principal tensile stress is given by

$$f^*_t = \sqrt{(\frac{f_n}{2})^2 + f_s^2} - \frac{f_n}{2} \qquad (3.9)$$

If $f^*_t > 0.8$ ft. then cracking will commence.

Conversely, $f_s > \mu f_n$ would indicate an impending slip on the unbonded portion of the slip surface. When it is known that the maximum shear stress which can be carried by the unbonded region is $\mu . f_n$, the excess shear must be resisted by the bonded portion. The magnitude of the shear force to be carried by the bonded portion may be determined by considering the forces acting on a unit length of the slip surface. Referring to Fig. 3.1 (b) the shear force on the unbonded region is given by

$$F_{s\,(unbonded)} = (a-b).\mu f_n$$

where the total shear force is

$$F_{s\,(total)} = af_s$$

The strength criterion for unbonded region may be written as

$$f_{s\,(bonded)} = a.f_s/b - \mu(\frac{a}{b} - 1)f_n \qquad (3.10)$$

Thus, the principal tensile stress,

$$f_t^* = \sqrt{(\frac{f_n}{2})^2 + f_{s\,(bonded)}^2} - \frac{f_n}{2} \qquad (3.11)$$

Cracking commences when f_t^* becomes the greater than $0.8\ f_t$.

3.5 Finite Element Representation of the Slip Surfaces

A dimensionless element consisting of a pair of springs at right angles to one another is used to represent the slip surfaces. This type of element which was introduced by Ngo and Scordelis[48] in a paper on the application of the finite element technique to the analysis

of reinforced concrete beams, is shown in Fig. 3.7(a). In the following presentation, the stiffness matrix for this element is developed using a slightly different approach. The stiffness matrix is then modified to apply to a friction type joint.

Utilizing the principle of minimum potential energy, the equilibrium condition for a typical node i can be written as

$$\frac{\partial(\phi)}{\partial\{\delta_i\}} = \Sigma \frac{\partial(v^e)}{\partial\{\delta_i\}} - R_i = 0 \qquad (3.12)$$

Equation (3.12) is a modified form of equation (2.18) where the external load system is assumed to consist entirely of concentrated loads acting at the nodes.

The strain energy stored in the element shown in Fig. 3.7(a) due to the applied forces is (in matrix form) given by

$$(v^e) = \{w_r\}^T \{P\} \qquad (3.13)$$

where

$$\{w_r\} = \begin{Bmatrix} w_x \\ w_y \end{Bmatrix} = \begin{bmatrix} -1 & 0 & 1 & 0 \\ 0 & -1 & 0 & 1 \end{bmatrix} \begin{Bmatrix} \delta_{x1} \\ \delta_{y1} \\ \delta_{x2} \\ \delta_{y2} \end{Bmatrix} = [B]\{\delta^e\} \qquad (3.14)$$

and

$$\{P\} = \begin{Bmatrix} P_s \\ P_n \end{Bmatrix} = \begin{bmatrix} K_s & 0 \\ 0 & K_n \end{bmatrix} \{w_r\} = [K]_E\{w_r\} \qquad (3.15)$$

If k_s and k_n are shear and normal stiffnesses per unit length of the slip surface respectively, then

$$K_s = k_s \cdot L$$

and $$K_n = k_n \cdot L$$

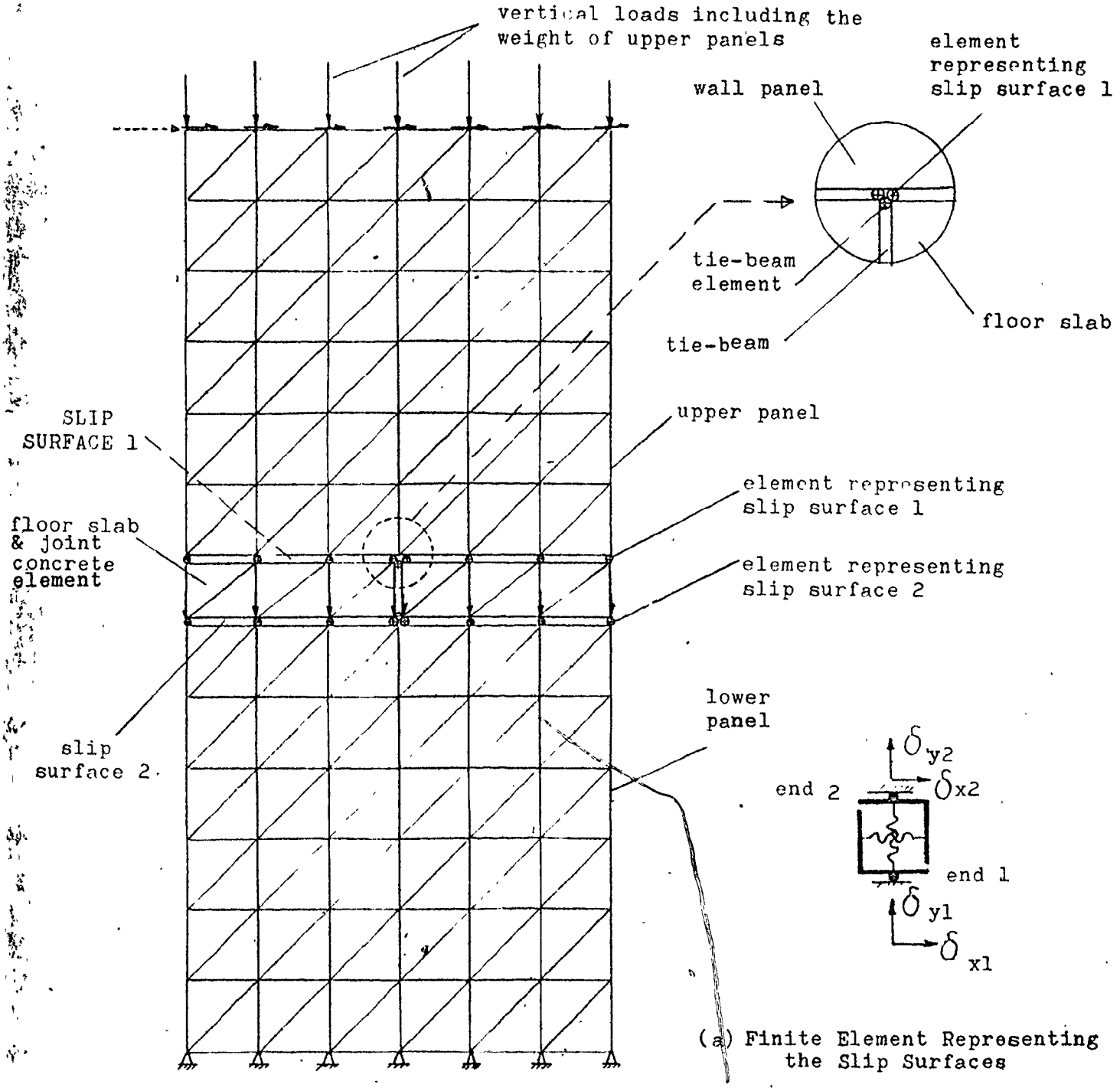

(a) Finite Element Representing the Slip Surfaces

(b) Finite Element Representation of a Horizontal Joint and the Adjoining Panels

Fig.3.7 Finite Element Model Used to Study Horizontal Joints

where L is the length of the slip surface represented by a single element. Substituting for $\{P\}$ and $\{w_r\}$ in equation (3.13)

$$(v^e) = \{\delta^e\}^T [B]^T [K]_E [B] \{\delta^e\} \tag{3.16}$$

It must be noted that in general where the element coordinate system is inclined at an angle θ with respect to the global coordinate system, matrix [B] is of the form

$$\begin{matrix} -\cos\theta & -\sin\theta & \cos\theta & \sin\theta \\ \sin\theta & -\cos\theta & -\sin\theta & \cos\theta \end{matrix}$$

According to equation (2.18), the partial derivative of the element strain energy (v^e) with respect to any component of $\{\delta\}$ gives the corresponding component of $\{R\}$. Using the expression for strain energy from equation (3.16) and determining the partial derivatives with respect to each element of $\{\delta\}$, a set of equations of the form

$$[B]^T [K]_E [B] \{\delta\} = \{R\} \tag{3.17}$$

is obtained. Comparing equation (3.17) with the definition of stiffness matrix, namely

$$[\bar{K}]_E \{\delta\} = \{R\} \tag{3.18}$$

it is immediately apparent that the element stiffness matrix is given by

$$[\bar{K}]_E = [B]^T [K]_E [B] = \begin{bmatrix} K_s & 0 & -K_s & 0 \\ 0 & K_n & 0 & -K_n \\ -K_s & 0 & K_s & 0 \\ 0 & -K_n & 0 & K_n \end{bmatrix} \tag{3.19}$$

3.6 Modification of a Slip Surface Element to Represent Friction Behaviour

With reference to equation (3.15), as long as $P_s \leq \mu.P_n$ for slip surface 1 or if cracking has not occurred along slip surface 2, the stiffness matrix of the elements representing the slip zones is given by equation (3.19). In actual calculations a very large value is assinged to the unit shear stiffness k_s, since under the conditions stated above, no slip can occur along the interfaces. In addition, because the slip surfaces are assumed to have no thickness, they are essentially incompressible and thus k_n is also chosen to be very large.

The largest shear force which can be sustained along slip surface 1 is $\mu.P_n$. Thus $P_s > \mu.P_n$ serves as a signal to indicate that the element stiffness matrix must be modified. In modified form equation (3.15) may be written as

$$\begin{Bmatrix} P_s \\ P_n \end{Bmatrix} = \begin{bmatrix} 0 & -\mu K_n \\ 0 & K_n \end{bmatrix} \begin{Bmatrix} w_x \\ w_y \end{Bmatrix} \tag{3.20}$$

or $$P_n = K_n w_y$$

$$P_s = -\mu K_n w_y = -\mu P_n$$

By convention the shear force is chosen as being positive when end 2 of the element shown in Fig. 3.7(a) moves to the right relative to end 1. For a monotonic gradually increasing external shear force, this is always the case. Since compressive forces are assumed

to be negative, it is necessary to introduce a minus sign in the property matrix as shown in equation (3.20).

The element stiffness matrix for the friction model can thus be written as

$$[\bar{K}]_F = [B]^T[K]_F[B] = \begin{bmatrix} 0 & -\mu K_n & 0 & \mu K_n \\ 0 & K_n & 0 & -K_n \\ 0 & \mu K_n & 0 & -\mu K_n \\ 0 & -K_n & 0 & K_n \end{bmatrix} \qquad (3.21)$$

This is the condition of an impending slip. The shear force carried by the element is exactly proportional to the compressive force acting on the element. The actual occurence of slip depends on whether or not this condition is satisfied for all the elements comprising the slip surface.

As the compressive force acting on an element decreases, so does the shear force which can be carried by that element prior to separation. The stiffness matrix of the element, after separation, becomes a null matrix, i.e.

$$[\bar{K}]_s = \begin{bmatrix} 0 & 0 & 0 & 0 \\ 0 & 0 & 0 & 0 \\ 0 & 0 & 0 & 0 \\ 0 & 0 & 0 & 0 \end{bmatrix} \qquad (3.22)$$

3.7 Modelling of the Region Between the Two Slip Surfaces

A horizontal joint is comprised of slip surfaces 1 and 2, the joint in-fill concrete and the floor slab. The interaction is complicated by the existance of a weaker

section where the longitudinal joint between the floor panels (if they are not of the same width as the wall panels) joins the horizontal joint. The contribution of the floor panels to the strength of that part of the joint which is sandwiched between the two slip surfaces, the physical characteristics of the local zone of weakness, and the manner in which these factors are accounted for are discussed below.

It must be noted that if longitudinal steel bars are used in the region of the joint filler, the region also serves as a tie-beam. Thus the word tie-beam is sometimes used in the following sections to describe this region.

(a) Modelling of the Joint In-Fill Concrete and the Floor Slab

Simple triangular finite elements of the type used for panels (Fig. 3.7) are also employed to represent the floor slab and the joint filler region. The joint filler is assumed to form an integral part of the floor slab. In support of this assumption it can be argued that:

1. A prefabricated floor slab is self-supporting during the construction stage. Thus deflections due to its own weight (plus possibly added construction loads) and the resulting rotations of the ends occur prior to placing the joint concrete. This eliminates the possibility of cracks forming over the support due to dead load.

2. Negative reinforcement is provided to resist live-load bending moments over the support. Thus any tensile cracks forming will in all probability be no more severe than those existing in cast-in-place floor slabs under service conditions.

The effective width of the region between the two slip surfaces is estimated on the basis of the 45° line assumption for the distribution of compressive loads. If a and t denote the thicknesses of the wall and the floor panels respectively, then the average effective width of the joint is given by

$$a_e = a + \frac{1}{2}t \qquad (3.23)$$

(b) Modelling of the Local Zone of Weakness in the Tie Beam

Tie beams exist as a result of incorporating steel in the cavity existing at the junction of wall and floor panels. Tie beams are not bending members. They are essentially tensile components provided to guarantee the building's transverse continuity.

Where floor slabs are continuous over the supports, they contribute to the strength of tie beams. The exception, however, is where the longitudinal joints between the floor panels meet the supporting walls. These regions which reoccur at regular intervals (depending on the width of the floor panels), are the intermittent weak regions along the length of the tie beam, and any cracking that might occur is assumed to be concentrated at these locations.

The formation of a crack at any other location is not anticipated because such a crack would have to propagate through a reinforced floor slab which is much stronger than the tie beam is at a longitudinal floor joint.

The structural behaviour of tie beams at these locations which are most susceptible to cracking is modelled with the aid of a pair of dimensionless finite elements of the type shown in Fig. 3.7(a). Figure 3.8 gives an exaggerated view of the whole assembly including the slip surface elements. Because the connecting elements are dimensionless, points a, b, c and d originally occupy the same location. The stiffness matrix of the tie beam element is of the form

$$[K]_{TB} = [B]^T [K]_{TB} [B] \qquad (3.24)$$

where $$[K]_{TB} = \begin{bmatrix} K_{nt} & 0 \\ 0 & K_{st} \end{bmatrix}$$

Considering a two inch length of tie beam between two successive floor panels, and utilizing the elastic properties of the joint concrete, the unit normal and shear stiffnesses of the tie beam (k_{nt} and k_{st} respectively) can easily be determined prior to cracking. After cracking, however, the normal and shear stiffnesses of the elements will become a function of the bond-slip and the dowel bar characteristics of the reinforcing elements crossing the cracked section. The stiffness matrix of the elements at this stage will be of the same general form as was given by equation (3.24), except that the property matrix will

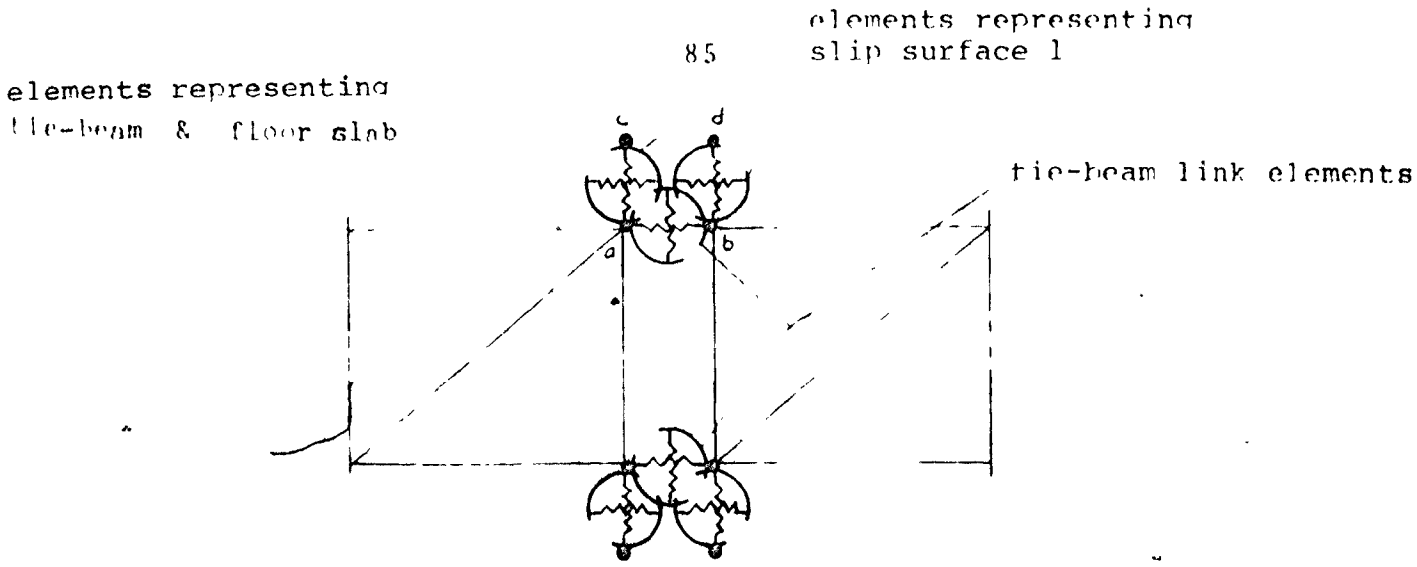

Fig.3.8 Tie-Beam Finite Element Representation

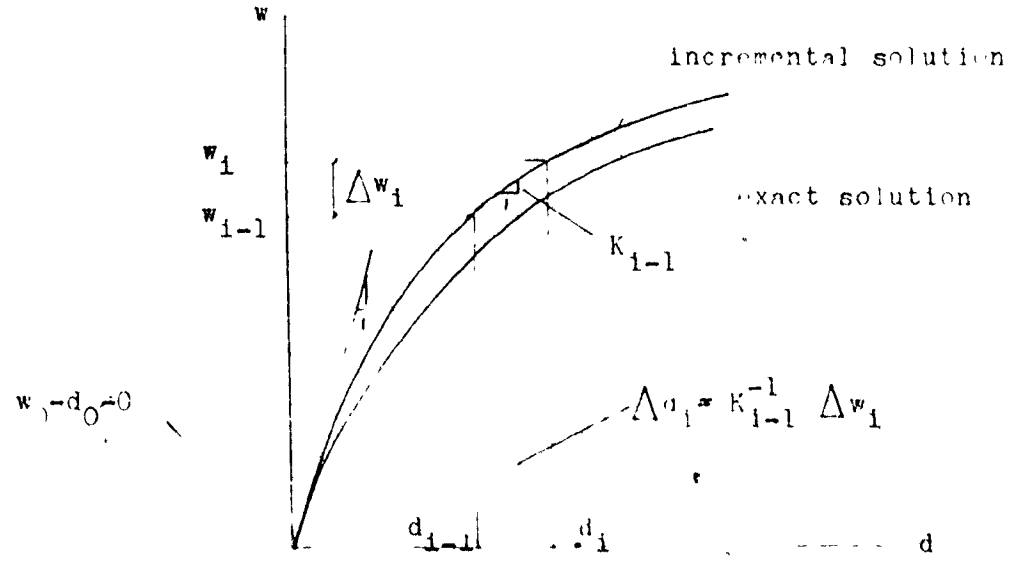

Fig.3.9 Incremental Method

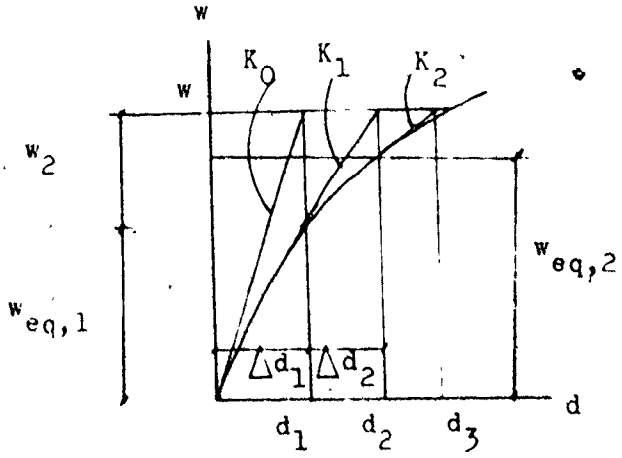

Fig.3.10 Iterative Method

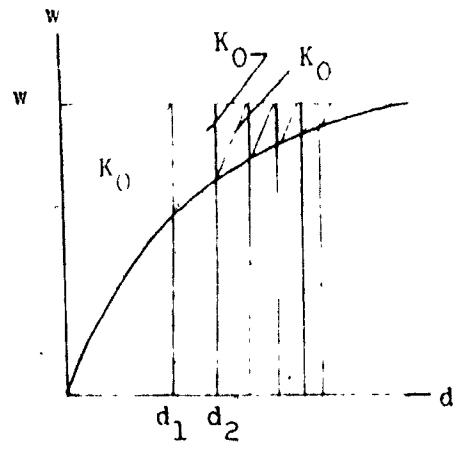

Fig.3.11 Modified Iterative Method

now be given by

$$[K']_{TB} = \begin{bmatrix} K'_{nt} & 0 \\ 0 & K'_{st} \end{bmatrix} \qquad (3.25)$$

The actual numerical values for K'_{nt} and K'_{st} are determined on the basis of tests conducted by Mathey [39], Phillips [52], and Paulay [51]. They will be discussed in detail in Sections 3.12 to 3.14.

3.8 Discussion of Possible Methods of Nonlinear Analysis [16]

(a) Types of Nonlinear Problems

On the basis of the source of nonlinearity, three categories of nonlinear problems may be identified. These are: 1. problems involving material nonlinearity alone, 2. problems involving geometric nonlinearity alone, and 3. problems involving both material and geometric nonlinearities.

The first category is comprised of problems in which stresses are not proportional to strains, but in which only small strains and displacements are considered. Displacements in this case refer to changes in the overall geometry of the body whereas strains refer to internal deformations. The displacements are said to be small when the geometry of the loaded structure can be assumed to be uneffected by the deformations. The elastoplastic analysis of various structures is an example of this category of problems.

The second category is comprised of problems in which significant changes in geometry may take place. Problems involving the elastic post buckling behaviour of structures are examples of this type.

The final category of nonlinear problems involves both material and geometric nonlinearity. The deformation of a rubber-like material is an example of this group of problems.

(b) Methods of Solution

The approaches to solving all three groups of problems are fundamentally the same. Thus for the sake of brevity the various techniques are illustrated with reference to the first category of nonlinear problems only.

For the aspects of nonlinearity encountered in this study, the complicating feature of a highly redundant structure and interdependent properties effectively reduces the possible methods of solution to:

(i) incremental or stepwise method,

(ii) iterative method, and

(iii) step-iterative or mixed method

(i) Incremental Method

In this approach the load is applied in small increments. During the application of each incremental load, stiffnesses are assumed to remain constant. For succeeding increments, however, stiffnesses may assume different values as determined by the behaviour during the previous increments.

With reference to Fig. 3.9, if $\{w_o\}$ and $\{d_o\}$ denote the initial load and nodal displacement vectors respectively, then the load after the application of i^{th} increment is given by

$$\{w_i\} = \{w_o\} + \sum_{j=1}^{i} \{\Delta w_j\} \qquad (3.26)$$

where $\{\Delta w_j\}$ is the incremental load vector. Similarly, the displacement, d_i, after applying the i^{th} load increment is

$$\{d_i\} = \{d_o\} + \sum_{j=1}^{i} \{\Delta d_j\} \qquad (3.27)$$

where Δd_j = displacement associated with the j^{th} increment as j goes from 1 to i.

To compute incremental displacements d_1, a fixed value of stiffness computed at the end of the previous increment is used. Thus, during the first application of the incremental load, the equilibrium equation is of the form

$$[K_o]\{\Delta d_1\} = \{\Delta w_1\} \qquad (3.28)$$

where $[K_o]$ is computed using material constants derived from stress-strain curve at the start of the loading. For the i^{th} increment equation (3.28) assumes the general form given by

$$[K_{i-1}]\{\Delta d_i\} = \{\Delta w_i\} \quad \text{where } i = 1, 2, \ldots, n \qquad (3.29)$$

To evaluate $[K_i]$ either the functional or the tabular representation of the stress-strain curve may be used.

The accuracy of the incremental method may be improved by taking smaller increments. The midpoint Runge-Kutta procedure is another method of increasing accuracy[16]. In this approach two cycles of analysis are performed for each load increment. Thus greater accuracy is obtained at the expense of more computational effort.

(ii) Interative Method

In this approach, unlike the incremental method, the structure is fully loaded for each iterative cycle. Since the initial estimates of material constants are usually approximate, equilibrium is not necessarily satisfied when the stresses are evaluated. Thus after each cycle of analysis that portion of the load which is not balanced is calculated and is applied in the next cycle to determine an additional increment of displacement. This process is repeated until equilibrium is satisfied within the prescribed limits.

If vectors $\{w_o\}$ and $\{d_o\}$ are the same as defined in the previous article, then for the i^{th} cycle the out of balance force is given by

$$\{w_i\} = \{w\} - \{w_{eq,\ i-1}\} \tag{3.30}$$

where $\{w\}$ is the total load vector, and $\{w_{eq,\ i-1}\}$ is the equilibrated load vector after $i-1$ cycles. The increment of displacement during the i^{th} cycle is determined using the following equation

$$[K_{i-1}]\ \{\Delta d_i\} = \{w_i\} \tag{3.31}$$

the total displacement after i cycle is calculated from

$$\{d_i\} = \{d_o\} + \sum_{j=1}^{i} \{\Delta d_j\} \tag{3.32}$$

The equilibrated load after the i^{th} cycle $\{w_{eq,\ i}\}$ is determined using the actual stress-strain relationship in either the tabular or the functional form. The process is repeated until the increments of displacements and the out of balance forces become sufficiently small.

A modified iterative technique uses the initial stiffness $[K_o]$ for all iterations rather than modifying it at each step. As a result the computational effort is greatly reduced at the expense of an increased number of cycles to reach convergence (Fig. 3.10 and Fig. 3.11).

(iii) Step-Iterative Method

This method combines both the iterative and incremental techniques to gain more accuracy at the expense of more computational effort. A graphical example of this type of approach is shown in Fig. 3.12 where for each increment of load as in (i), the equilibrium is reached by iteration as in (ii).

3.9 The Method of Nonlinear Analysis Used in the Present Investigation

The analysis outlined here belongs to the first category of nonlinear problems namely those concerning material nonlinearity alone. Moreover, nonlinear behaviour is restricted only to the joints. For reasons stated in Chapter 2 the panels' behaviour is assumed to be linear.

Implicit in the assumptions relating to the first category of nonlinear problems is the limitation to small deflections (or in our case distortion of elements). The validity of this assumption is confirmed on the basis of the results obtained in this chapter and in Chapters 5 and 6.

An iterative technique very similar to that employed for elastic-plastic behaviour[16] may be used

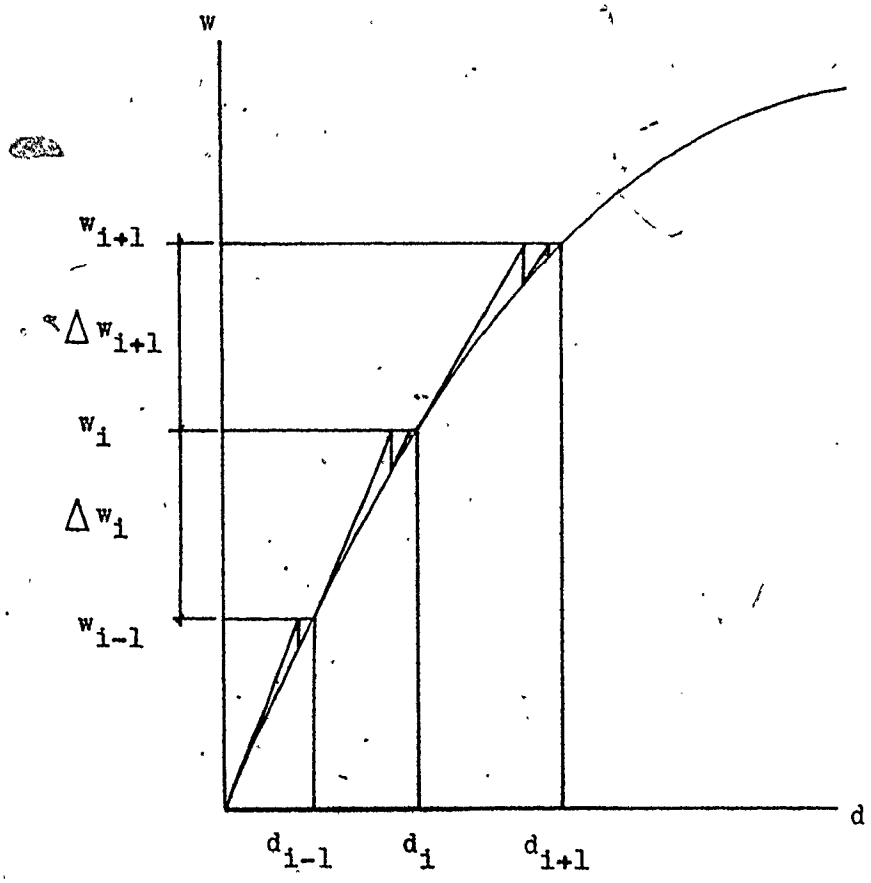

Fig.3.12 Step-Iterative or Mixed Method

in this study. Here the stiffness matrix is modified after each iteration step on the basis of the behaviour outlined in sections 3.4 to 3.6, and the total load is applied for each iteration. For each and every step, the equilibrium equation remains in the form

$$[K_i] \{d_i\} = \{w\} \tag{3.33}$$

where $\{w\}$ is the total external load vector. $[K_i]$ and $\{d_i\}$ denote respectively the stiffness matrix and the nodal displacement vector belonging to the i^{th} cycle.

It is important to note that each stiffness $[K_i]$ is utilized as if it described a linear elastic body. Thus, in a sense each step is equivalent to an elastic analysis for the body under full loading.

The basic aim of the analysis is to predict the behaviour over the full range of loading in addition to determining the ultimate load at which a structure fails. Failure is indicated when a structure or part of it becomes unstable.

To arrive at the failure load, incrementally increasing lateral forces must be applied to the structure. A complete nonlinear analysis of the above iterative type must be performed every time there is an increase in lateral forces. Thus, a set of computations of the type indicated by equation (3.33) is necessary after each and every load increase. The process continues until the structure fails. It must be noted that the external load vector $\{w\}$ for each set of nonlinear analyses represents the total load applied to the structure at that instant.

A schematic representation of the process can be seen in Fig. 3.13.

In the event of an element yielding, the stiffness matrix of that element is changed to a null matrix. The forces acting at the element's nodal points just before yielding are reversed and applied to the same points in the form of external loads.

3.10 Discussion of the Results of the Investigation for Unreinforced Joints

This section is devoted to the study of the behaviour of an isolated horizontal joint subjected to the combined action of horizontal and vertical loads. The arrangement of elements used is shown in Fig. 3.7(a). The panels are 8 feet square with a thickness of 8 inches. The material properties are as indicated in Chapter Two. Each panel is modelled using 72 triangular elements. The slip surfaces are represented utilizing a total of 16 dimensionless elements of the type introduced in section 3.5.

The detailed behaviour of the finite element model used to represent the slip surfaces is presented in Subsection (a), where a zone of weakness between floor slabs of smaller width is considered. The accompanying diagram (Fig. 3.14) shows how the individual elements modelling the slip surfaces progressively slip, separate, crack and shear as the lateral load increases. In addition, the effect of changes in the physical characteristics of the panels, namely the rigidity, size and

⊙ — Conditions of Section 3.4 are satisfied. Corresponding displacements are true equilibrium displacements.

• — Conditions of Section 3.4 are violated. Stiffnesses must be modified and the anallsis repeated for the same total load.

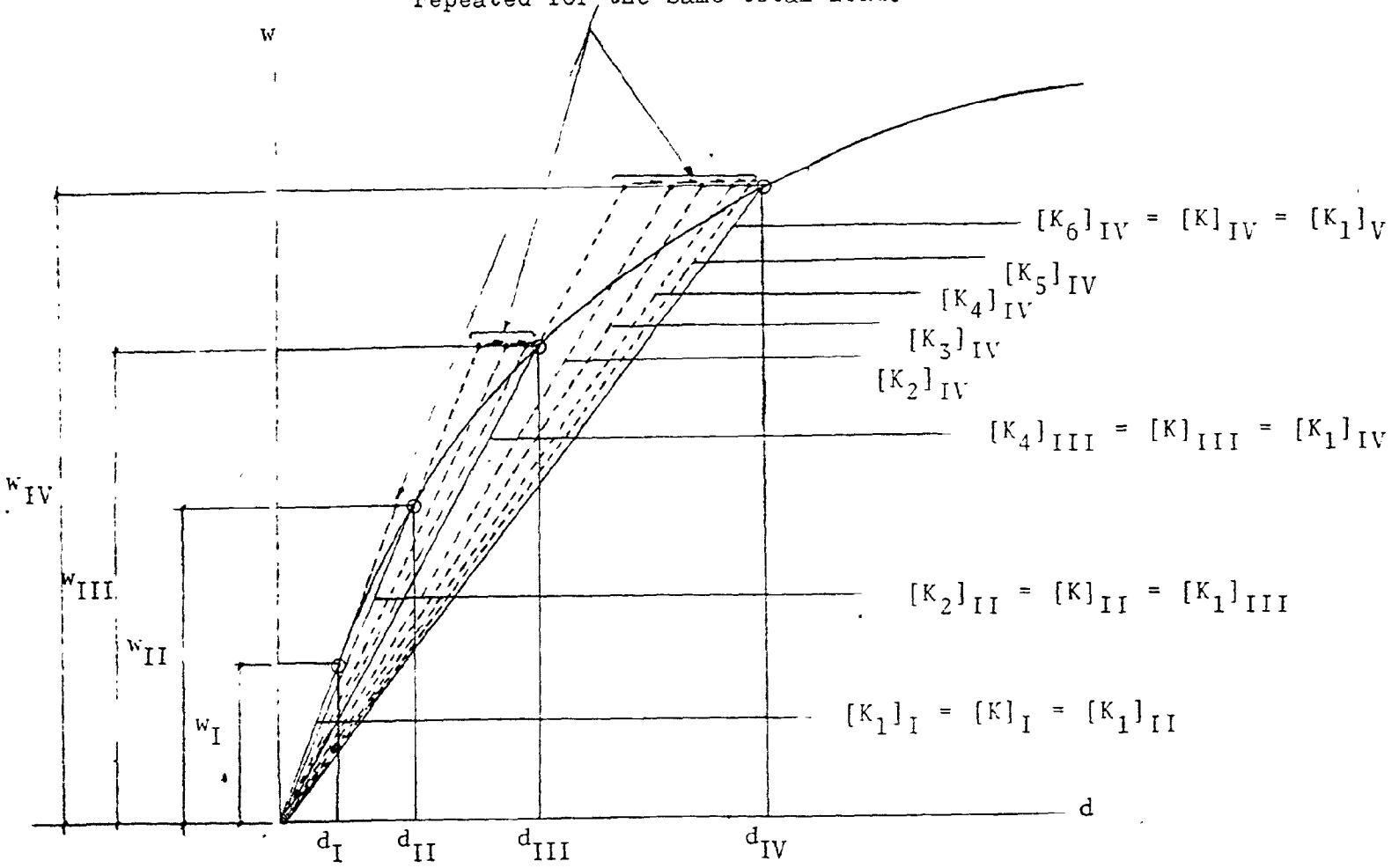

Fig. 3.13 Iterative Method for Gradually Increasing Load Using Secant-Type Stiffness Modification

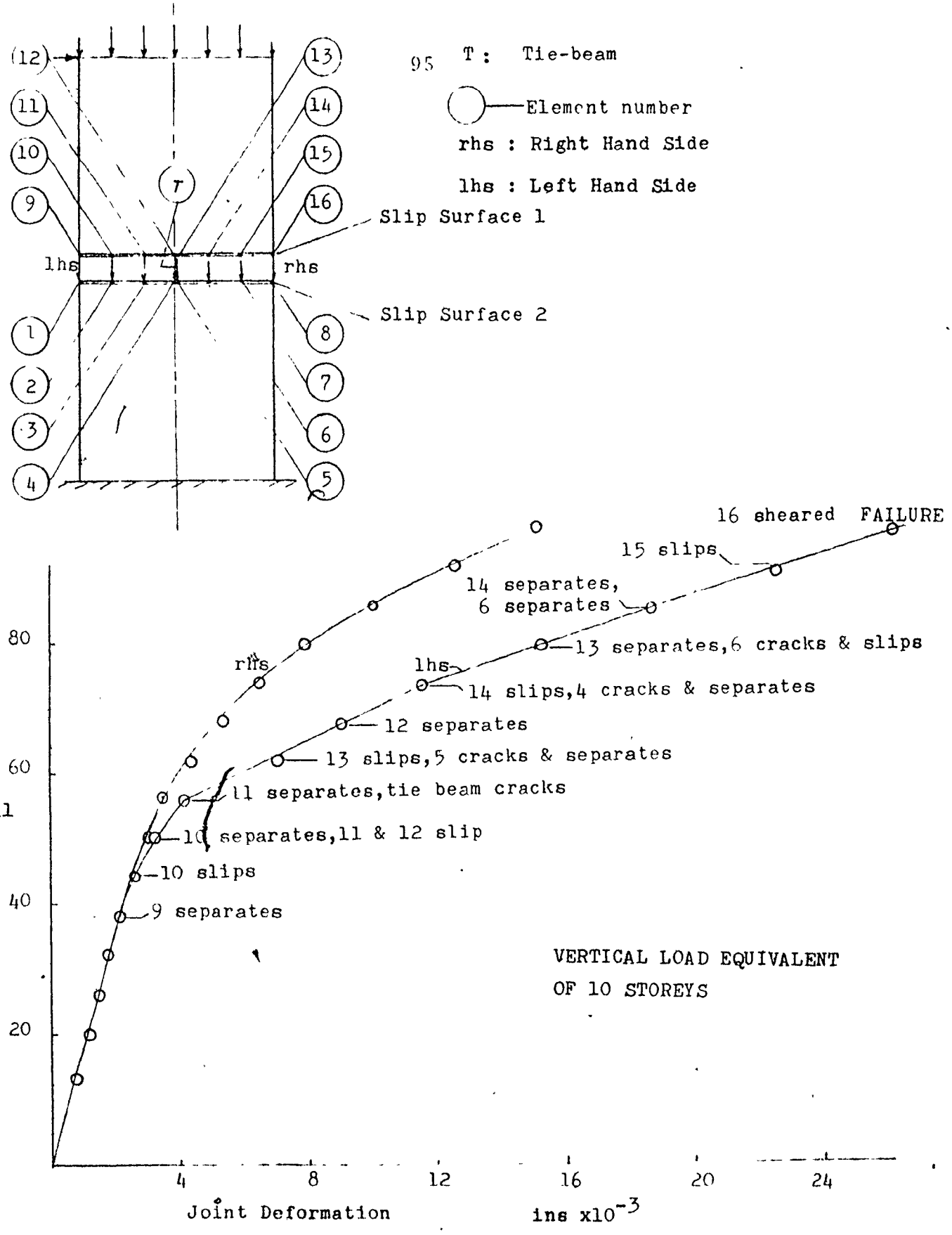

Fig.3.14 Lateral Load Versus Joint Deformation: Detailed Joint Behaviour

shape, and the effect of variation in the position and magnitude of the applied loads on the deformation response of the joint, are also presented. These effects will be discussed in Subsections (c), (d), (e), (f) and (g). Subsection (b) is devoted to the case where the floor panel is of the same width as the wall panels. The zone of weakness between the floor panels discussed previously in Subsection 3.7(b) no longer exists, and thus the tie beam is assumed to remain uncracked(due to the contribution of floor slabs to the strength of the tie-beam). The resulting joint deformation graph is compared with that of a case where cracking of the tie beam is considered.

(a) Behaviour of Slip Surface Elements

(Tie-Beam Cracking Considered)

A graph of the horizontal deformation over the height of a joint resulting from a gradually increasing concentrated lateral shear force applied to the top of the panel is shown in Fig. 3.14. Since the floor panels are assumed to be 4 feet wide, each wall panel is equivalent to two floor panels in width. In practice the small opening in the longitudinal joint existing between the floor panels is usually filled with grout. For the purpose of this investigation, the strength of this grouted joint is assumed to be negligible. Continuity in the region where this longitudinal joint meets the vertical plane of the supporting wall is provided by the cross section of the tie beam alone. It is assumed that the floor slabs do not contribute to the strength

at this location thus making it most susceptible to cracking. After cracking, some degree of continuity is provided by the longitudinal reinforcing bars in the tie beam crossing the cracked section.

Figure 3.14 contains a detailed description of the changes in behaviour of each element along the slip surfaces during the application of shear force which gradually increases to failure. The deformation graph represents the horizontal displacements of the lower corners (left and right) of the upper panel relative to the corresponding upper corners of the lower panel. Therefore it represents the total horizontal joint deformation. (The deformation of the material between the wall panels as well as any displacements occurring along the slip surfaces are included.)

The behaviour of the individual elements forming the slip surfaces during the application of the increasing shear force is as follows. For the elements representing slip surface 1, no slip will take place as long as the shear force acting on that portion of the slip surface represented by the element is less than the corresponding normal compressive force times the coefficient of friction. Alternatively slip may take place as a result of exceeding the concrete strength as was explained in Subsection 3.4(a) part (iii). For slip surface 2 (partly bonded) the behaviour is further complicated by the fact that slip or separation can not occur until the surface is cracked. The criteria for this type of behaviour was

outlined in Subsection 3.4(b).

Before the start of nonlinear behaviour the shear stress distribution along the slip surfaces is similar to that existing at any other section through the assembly with the possible exception of the sections considered near the point of application of the concentrated external shear force. For the type of loading shown in Fig. 3.14, as the shear force increases the normal compressive forces on the joint elements located to the left of the centre line decrease and the compressive forces on the elements located to the right of the centre line increase. The process continues until shear stress exceeds the shear resistance for the element located at the extreme left of slip surface 1. At this stage the stiffness of the element is modified in accordance with equation (3.21) so that the shear stress carried by the element is now a function of the compressive force acting on that element. When a tensile normal force acts on the element, the stiffness matrix of the element is reduced to a null matrix.

Figure 3.14 shows the above process for the elements comprising slip surfaces 1 and 2, and the resulting nonlinear behaviour for the joint as a whole. As can be observed from the graph there exists a marked increase in the rate of deformation for the left hand side of the joint after the tie-beam has cracked. The cracking of the tie-beam occurs after separation is spread to approximately 50% of the surface area of zone 1. To elaborate, cracking takes place when elements 9, 10 and 11 are

separated and a state of impending slip exists for element number 12.

The elements designated as having slipped are in fact assigned a stiffness matrix given by equation (3.21), and the shear force resisted by each slipped element is a function of the compressive force acting on that element. The actual slip at this stage is quite small and is the result of deformation of the elements surrounding the slip zones. The overall joint slip would in fact occur only when the condition of impending slip exists for all the elements constituting a slip surface.

The diagram shows that the joint failure occurs when element number 16 is sheared off. That is failure occurs as a result of exceeding the concrete strength as indicated in Subsection 3.4(a), part (ii). At the instant of failure, all the remaining elements of slip surface 1 are separated with the exception of element number 15 which is subject to the condition of impending slip. Slip surface 2 is only partly cracked and separated.

(b) Joint Behaviour Associated with Uncracked Tie-Beams

In order to determine the effect of tie-beam cracking on horizontal joint deformation, a situation may be envisaged where cracking is presented by removing the joint between floor panels (i.e. selecting the floor panels as wide as the wall panels). The resulting deformation curve is illustrated in Fig. 3.15. The figure also shows the deformation comparison with a similar case where

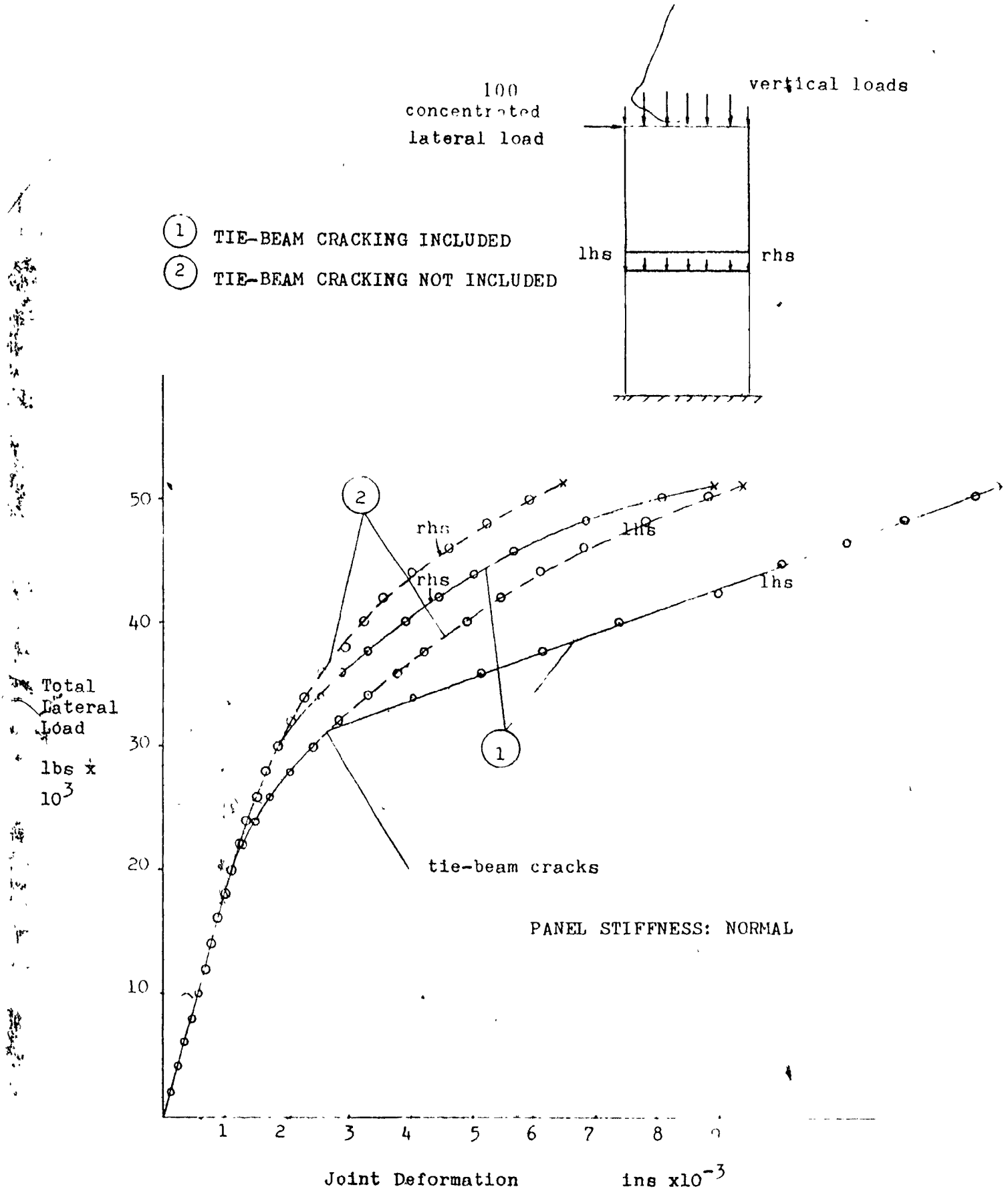

Fig.3.15 Lateral Load Versus Joint Deformation: Effect of the Cracking of Tie-Beam

cracking of the tie-beam was considered. Although, the ultimate loads in both cases are the same, the joint deformation just before failure for the case where cracking is considered, is approximately 38 and 44 percent greater for the right and left hand sides of the joint respectively. The two curves follow identical paths until cracking occurs.

The above comparison shows that where floor panels are narrower than the wall panels, thereby creating a local zone of weakness, the possibility of a crack forming in this region must be accounted for. This is evident from the marked difference which exists between the deformation curves of the two cases considered.

(c) Effect of the Mode of Application of Shear Forces (Distributed Versus Concentrated Shears)

It was originally thought that the mode of transferring shear forces to panels might influence the joint behaviour. Therefore, joint deformation is investigated using a set of gradually increasing distributed shear forces and the results are compared with those determined using a gradually increasing equivalent concentrated shear force. The results for the case where tie-beam cracking is allowed are illustrated in Fig. 3.16. It is observed that the mode of application of shear forces when these loads are applied to the top of the upper panel produces only very small changes in the graph of joint deformation. Hence, it is concluded that the effect produced in the vicinity of the joint is independent of the mode of shear transfer, for loads must be transmitted through the upper

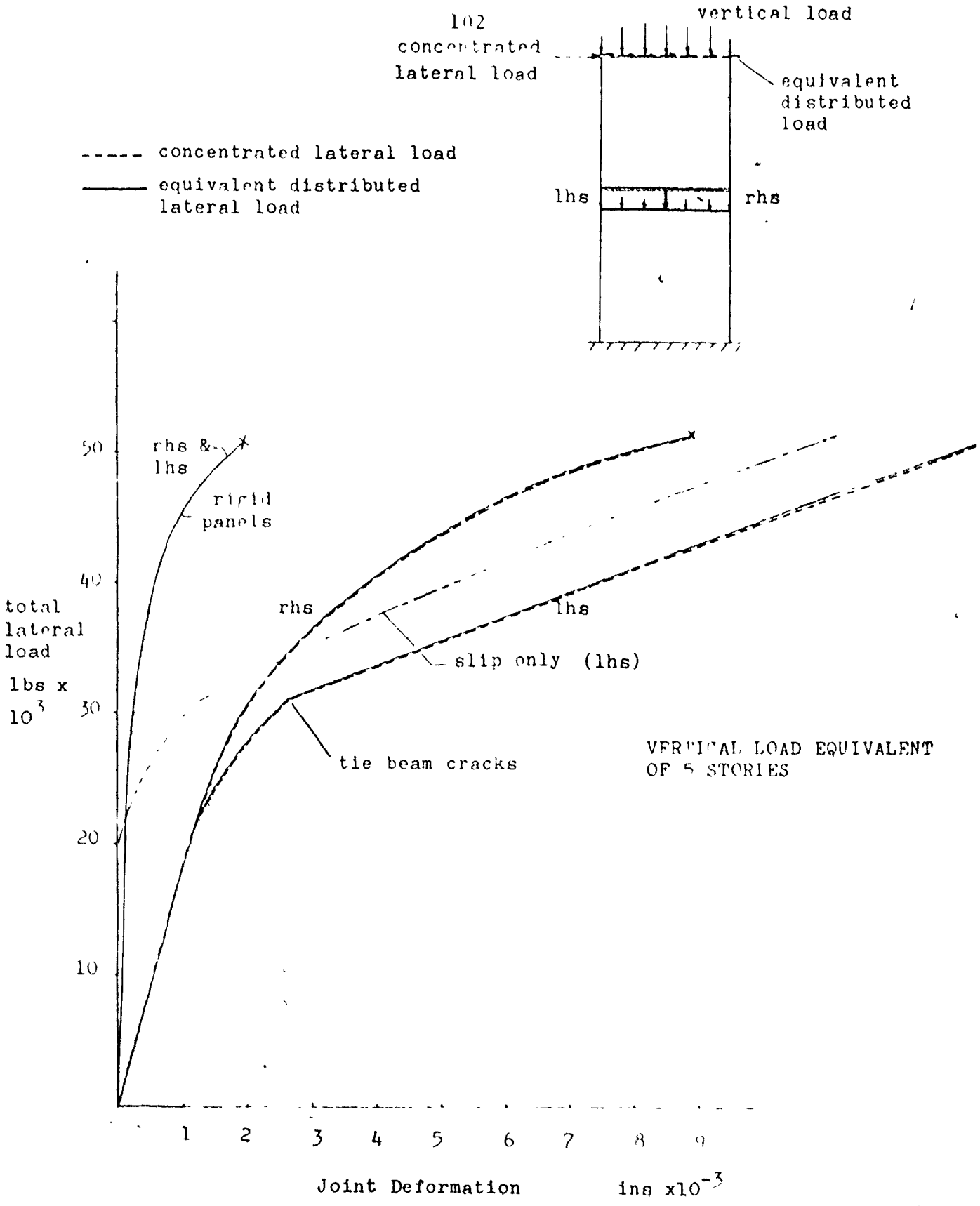

Fig.3.16 Lateral Load Versus Joint Deformation: Effect of Panel Rigidity and the Mode of Application of Shear Forces on Joint Deformation

panel to reach the joint.

There was also uncertainty as to whether the results of the investigation of the mode of shear transfer were effected by the behaviour of the tie-beams. For this reason the effect of the mode of shear transfer was investigated for a case where tie-beam cracking was prevented. The results are shown in Fig. 3.17. It is seen that joint deformation is again independent of the mode of transfer of shear forces.

For the rest of this study in keeping with the normal practice of constructing the floor panels narrower than the wall panels, the possibility of tie-beam cracking is taken into account. The case of wider floor panels will not be investigated further.

The effect of the mode of shear transfer becomes important when shear forces are applied at the level of slip surface 1. In this case no moments are acting on slip surface 1, and those applied to slip surface 2 are greatly reduced. The joint deformation curves for the two cases of concentrated and distributed shear forces are illustrated in Fig. 3.18. For distributed shear forces the deformation curves for the left and right hand sides of the joint coincide. In contrast, when a concentrated shear force is considered, there is a marked increase in the deformation curve of the left hand side of the joint due to local deformations occurring at the point of application of the load. Although allowance is made for cracking of the tie-beam, the analysis indicates

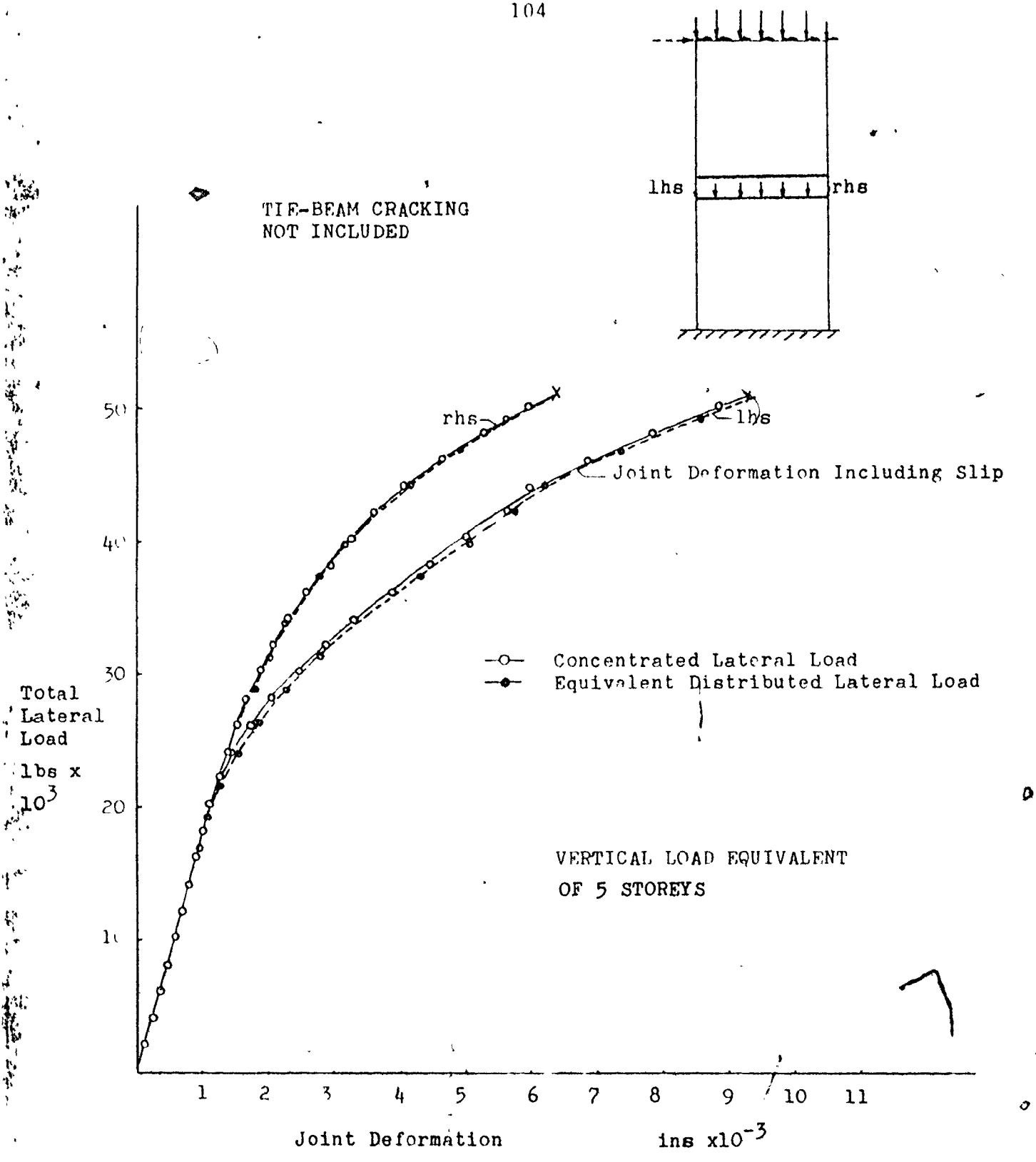

Fig.3.17 Lateral Load Versus Joint Deformation: Effect of the Mode of Application of Shear Forces on Joint Deformation

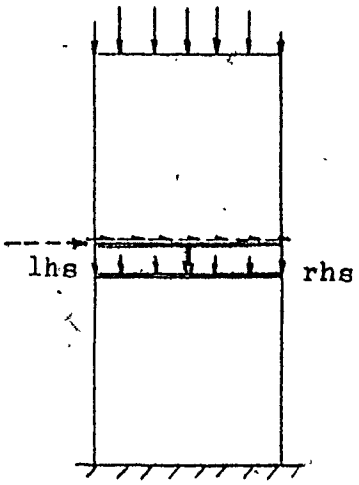

TIE-BEAM CRACKING INCLUDED

——— concentrated shear force

----- equivalent distributed shear force

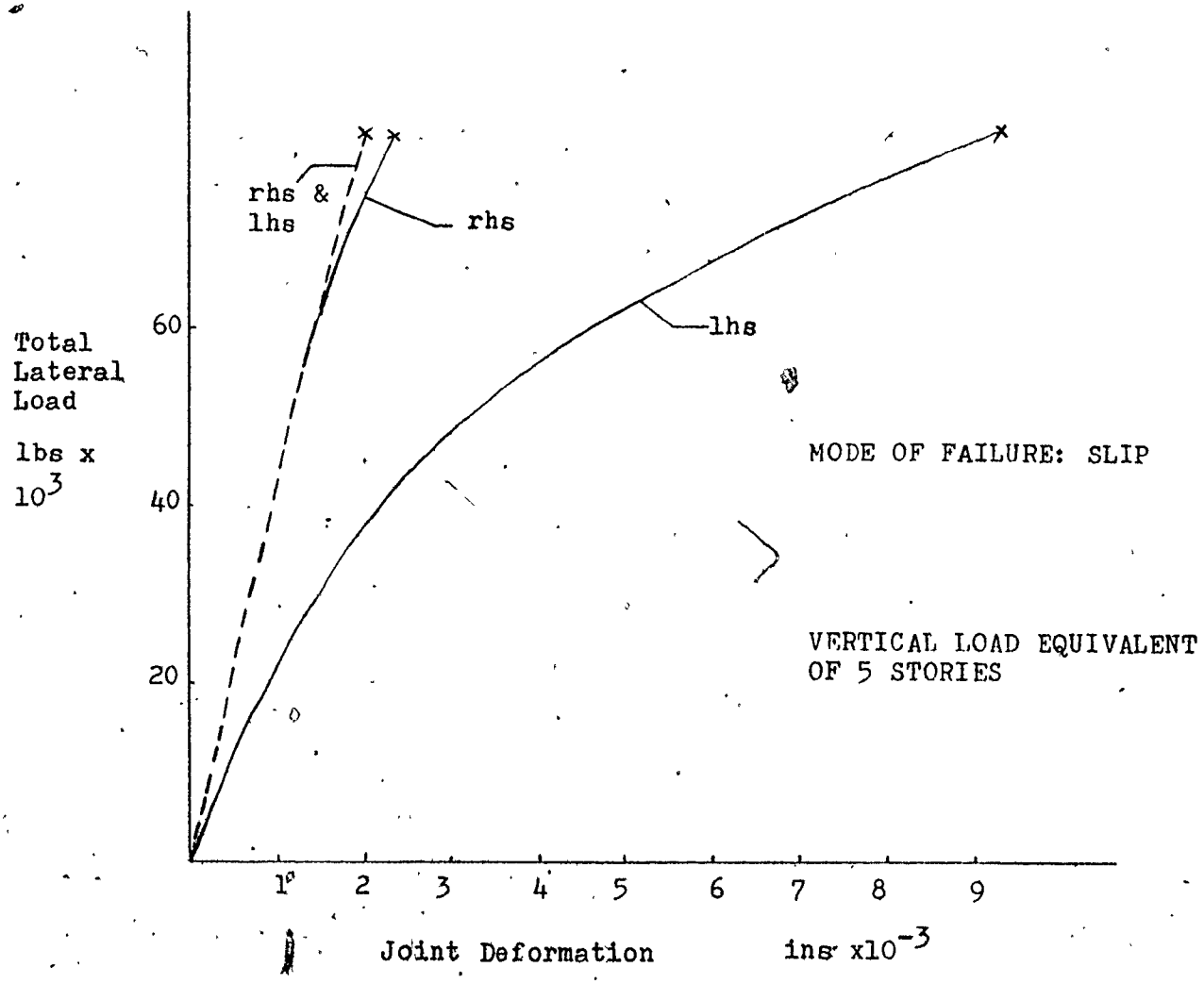

Fig. 3.18 Lateral Load Versus Joint Deformation: Distributed and Concentrated Shear Forces Applied at the Level of Slip Surface 1

that the tie-beam remains uncracked. It may thus be concluded that in this particular case the joint deformation is independent of the relationship between the widths of wall and floor panels. Failure occurs as a result of exceeding the maximum shear resistance along slip surface 1 in accordance with the principles outlined in Subsection 3.4(a), part (ii).

(d) Effect of Rigidity of Panels on Joint Deformation

The possibility of simplifying the process of analysing complex cantilevers by treating the panels as rigid components is investigated by determining the effect of panel rigidity on the behaviour of the joint. The results are then compared with those using elastic panels of normal rigidity. The panel dimensions in both cases are identical and the panels are subjected to the same loading conditions.

To simulate a rigid panel, the modulus of elasticity of the elements representing the wall panels is assigned a very large value ($E = 10^{15}$) and Poisson's ratio is assumed to be zero. To be able to easily compare the effect of panel rigidity on joint behaviour, the deformation curve is superimposed on Fig. 3.16. As illustrated the deformation curves for the two sides of the joint are identical. Furthermore, the joint deformation at failure for the case where panel rigidity is normal is at least 4-1/2 times greater than that obtained using panels of very high rigidity. It is thus concluded that for the

purpose of analysing panel buildings, the panels cannot be treated as rigid components.

(e) Components of Joint Deformation

So far the joint deformations referred to have been the total displacements between the lower edge of the upper panel and the upper edge of the lower panel at the two corners. These points are important because in the simplified model which will be discussed later, panels will be connected at these locations. The deformation is the sum of two components. These are the slip along the interfaces and the deformation of the joint materials between the two panels.

As will be discussed in Chapter 5, the thickness of the material between the two panels will be eliminated. Therefore, it is the overall joint deformation which is of most interest. However, in order to understand the joint behaviour it is necessary to study the various components which constitute the total deformation. Referring to Fig. 3.16 the graph labeled 'slip only' indicates the slip occurring along slip surface 1 at the left corner. There is no slip at the other corner. The bond along slip surface 2 at the corners is not broken and thus no slip is indicated on the diagram. The material deformation at the left corner is the difference between the graph marked 'slip only' and either of the solid or dashed lines representing the overall deformation for the left side of the joint. The overall deformation of the right side of the joint is entirely due to the material deformation.

In the following pages of this chapter and in the subsequent chapters the term joint deformation refers to the overall joint deformation including slip. Again it should be noted that in the simplified model it is the overall deformation which will be simulated.

(f) Effect of Variation in Magnitude of Gravity Loads on Joint Deformation

A horizontal joint may be situated at any level in a multi-story building and thus be subjected to vertical loads of various intensities. It is possible that variation in the magnitude of vertical loads might produce different types of failures. Furthermore, the simplified model of the joint which will be introduced in Chapter 5 must be able to simulate the joint behaviour regardless of the magnitudes of horizontal and vertical loads acting on the joints. To be able to confirm that the simplified model is adequate, its behaviour should be compared with that of a joint which is simulated with more accuracy, and is subjected to an identical range of loading conditions. For these reasons the joint behaviour was investigated using three sets of gravity loads which were approximately equivalent to the weight of one bay of a 10 storey, 5 storey and 2½ storey panel building of the size selected for this study. In Subsection (g) the joint behaviour under very high gravity loads will be investigated.

Figure 3.19 shows the results for the above-mentioned three cases. It is observed that as gravity load acting on the joint increases, so does the shear force

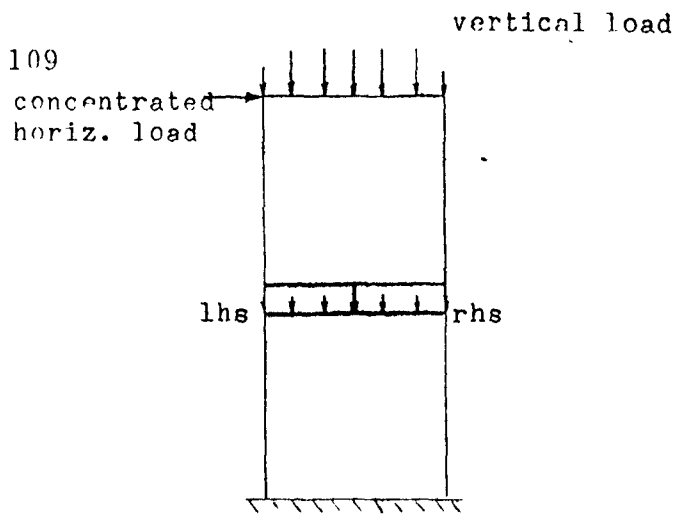

(1) - vert. load equivalent of 10 stories (204 kips)
(2) - vert. load equivalent of 5 stories (102 kips)
(3) - vert. load equivalent of 2½ stories (51 kips)

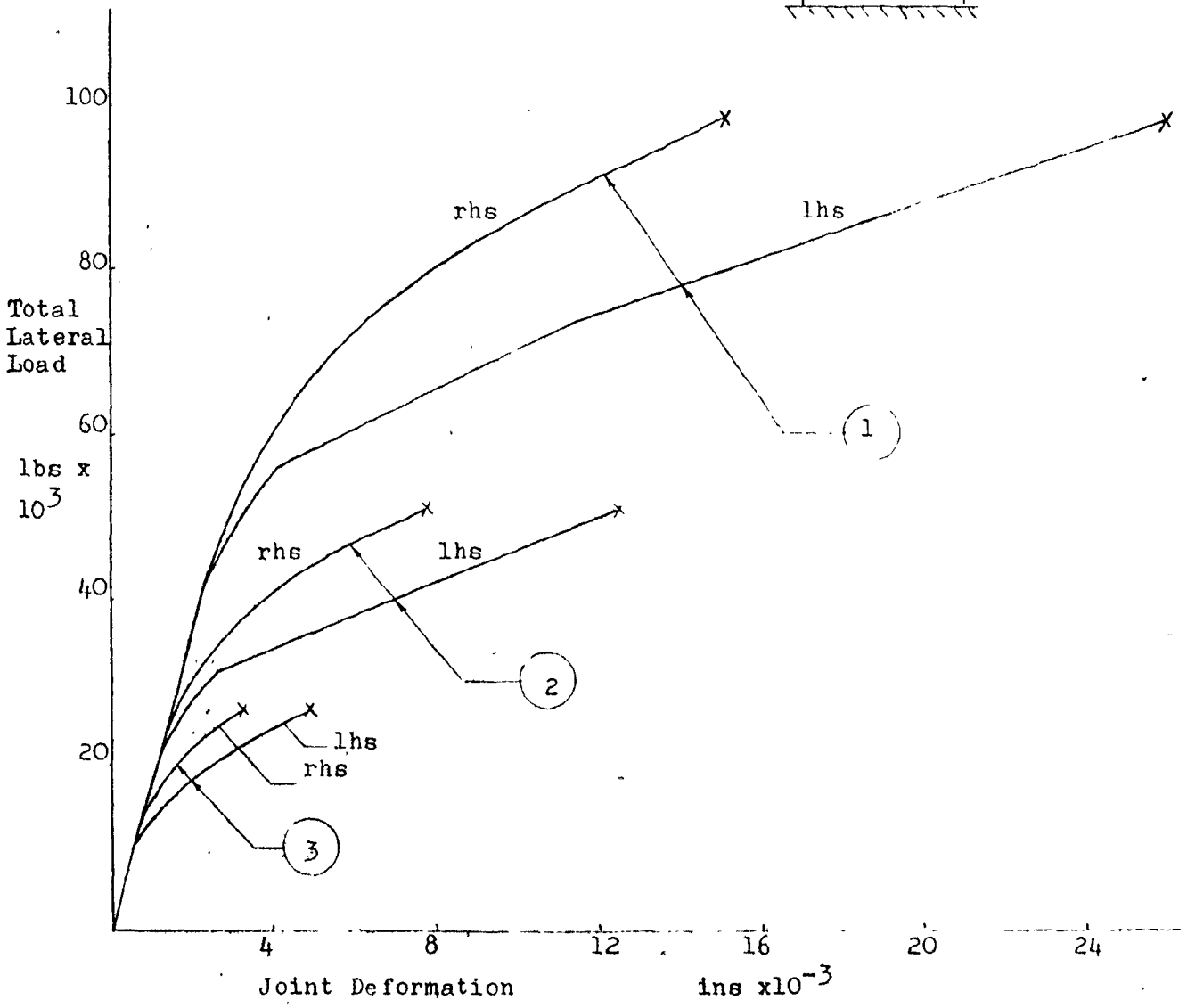

Fig.3.19 Lateral Load Versus Joint Deformation: Effect of Increasing Vertical Load

necessary to cause failure. For case 1 (indicated on the diagram) failure occurred as a result of separation along slip surface 1 which ultimately led to a shear type failure at the extreme right of the same surface. The detailed behaviour was illustrated in Fig. 3.14. In this case the combined effects of gravity, and bending resulting from the application of lateral loads to the top of the panel, produced such high compressive forces on the right side of the joint that the shear friction capacity along zone 1 could not be overcome. Instead, failure occurred as a result of exceeding the strength of concrete as was explained in Subsection 3.4(a), part (iii). For cases 2 and 3, where smaller gravity loads were applied to the joint, this type of failure was not indicated and the ultimate capacity was reached as a result of separation along zone 1 and the eventual overturning of the upper panel.

The results found in this Subsection will be used in Chapter 5 as a standard for comparison of the joint behaviour using a simplified joint model.

(g) Effect of Very Large Gravity Loads in the Range Producing Compression Failure

The joint behaviour when capacity is governed by a compression type failure involves criteria different from those investigated so far. These were indicated in Subsection 3.4(a), part (iv). In addition, it must be determined whether the simplified model of Chapter 5 would be capable of reproducing this behaviour.

Therefore, to provide an extreme condition, the joint behaviour was investigated under the combined action of a very large gravity load (equivalent of 40 storeys) and a gradually increasing horizontal load applied to the top of the upper panel. As illustrated in Fig. 3.20, when the horizontal force reaches a value of approximately 150 kips,nonlinear behaviour begins to occur. Slip and separation start at the left side of slip surface 1 and propagate towards the centre. When the shear force reaches a value of about 205 kips, the stresses which were building up along slip surface 2 cause it to suddenly crack. The analysis indicates that this crack extends over three elements. As a result of cracking a sudden release of stresses takes place which in turn leads to an instantaneous increase in the joint deformation. As the shear force is further increased compression failure begins to occur. The compression failure occurs because the vertical loads now acting over a much smaller area due to partial separation caused by the bending moment. The failure begins at the extreme right of the joint, propagates towards the centre, and eventually leads to the total failure of the joint. It must be recognized that this type of failure is quite brittle in nature. (It happens without warning and the propagation is very rapid). A more detailed presentation of this behaviour is shown in Fig. 3.20.

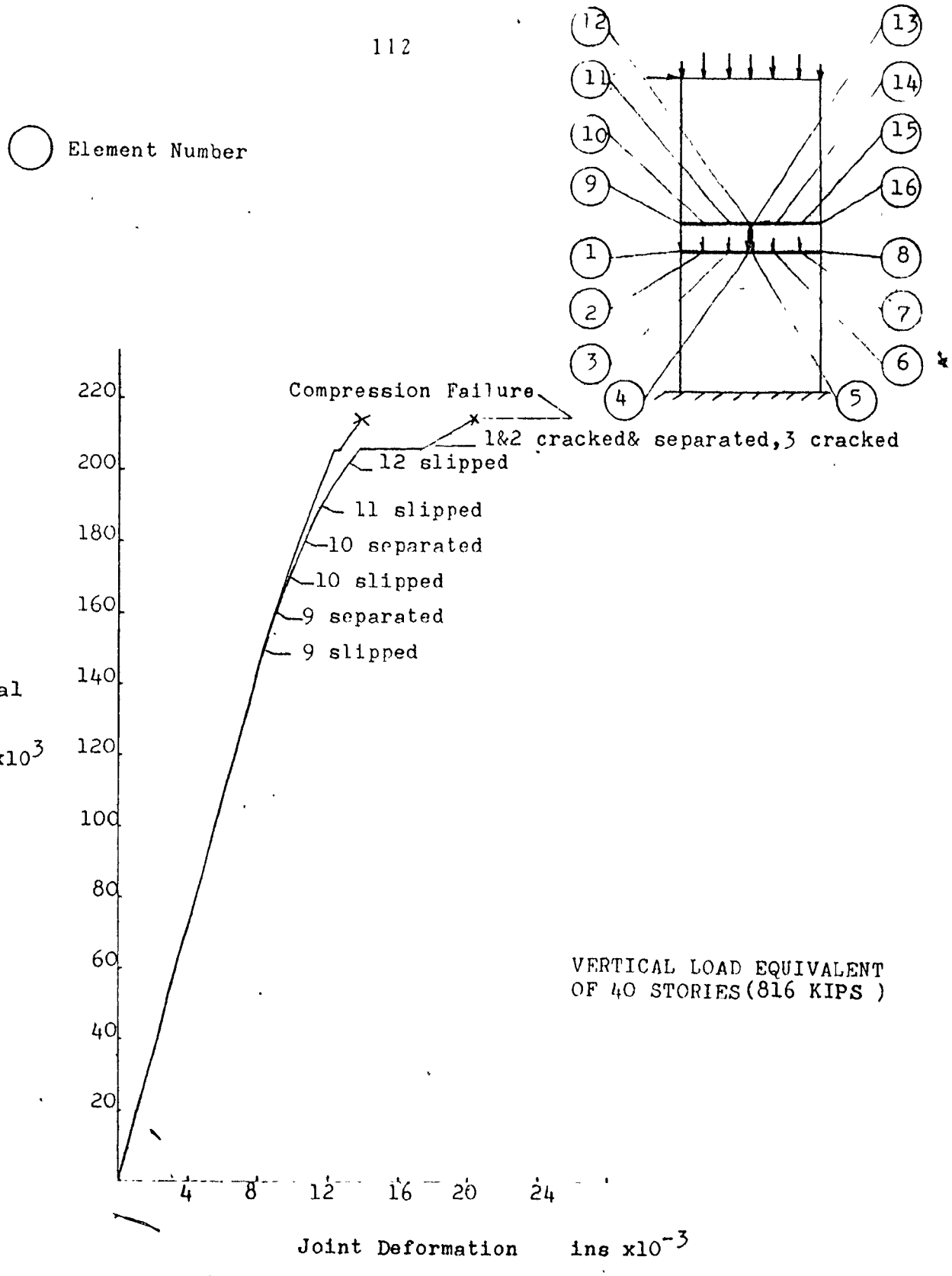

Fig.3.20 Lateral Load Versus Joint Deformation: Compression Failure

(h) Effect of Varying the Number of Joint Elements on Predicted Behaviour

It was anticipated that the number of elements used to represent a horizontal joint would have a significant effect on the shape of the resulting deformation graphs. Therefore when the number of elements per slip surface is reduced to 2 or 3 as will be the case with the simplified analysis proposed in Chapter 5, other modifications may have to be introduced to ensure that the joint deformation curves are similar to those found using more elements. Thus the results of this chapter will be used to judge the adequacy of modifications introduced in Chapter 5. It is therefore important to make sure that the results obtained here are sufficiently accurate.

In order to determine whether or not the joint behaviour is accurately represented using eight element per slip surface, two further analyses are carried out using six and ten elements per slip surface. The results are illustrated in Fig. 3.21. It is observed that using six elements per slip surface leads to a considerable difference in the deformations. However, using ten elements per slip surface results in marginal improvement over the 8-element case in terms of the definition of gradual change, and the overall behaviour remains virtually the same. Thus it is concluded that sufficient accuracy is attained using eight elements per slip surface. Furthermore, the use of 8 elements per slip surface is a reasonable compromise between accuracy and computer time and space economy.

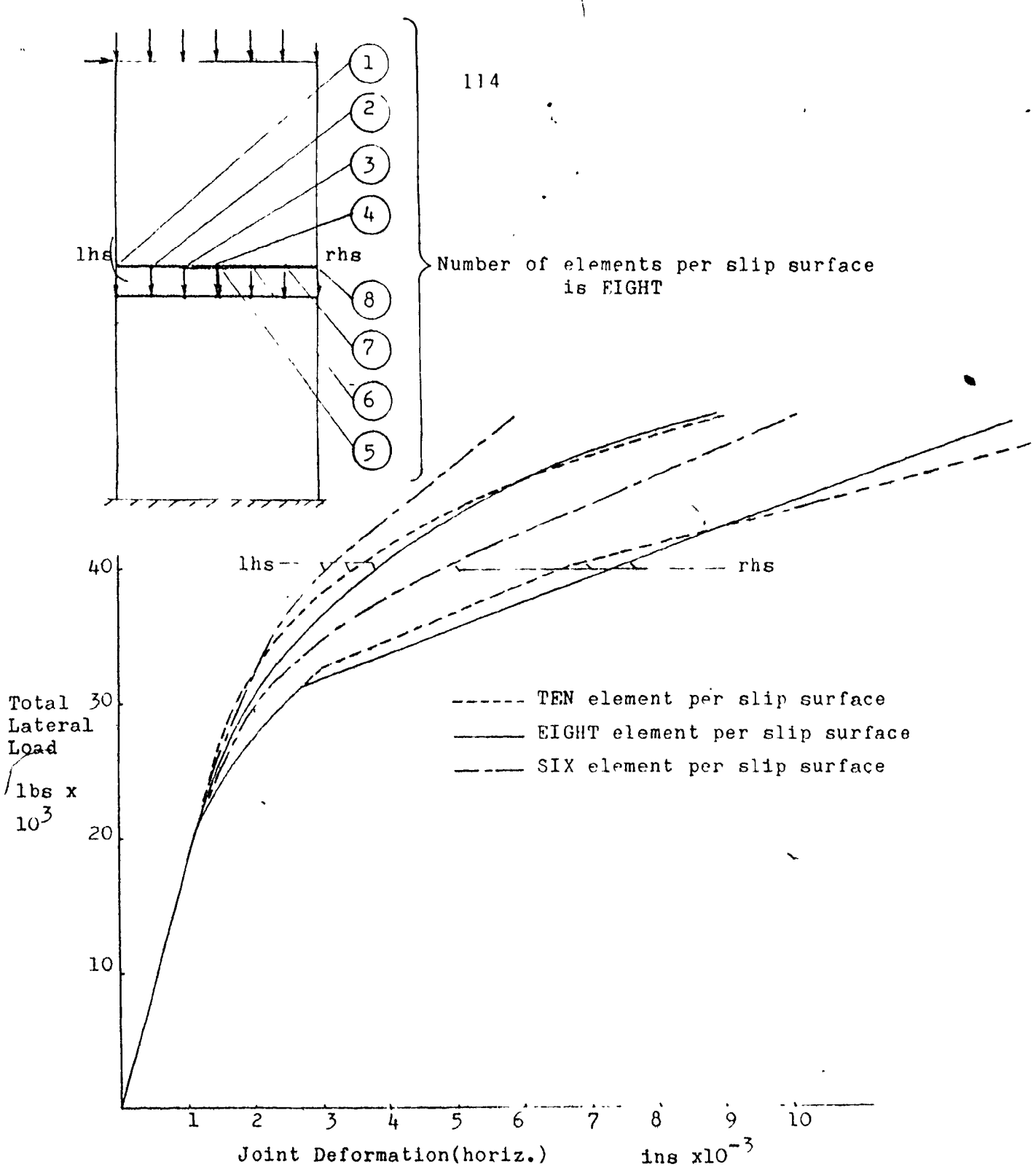

Fig.3.21 Lateral Load Versus Joint Deformation: Effect of Number of Elements per Slip Surface on Behaviour

(1) Effect of Size and Shape of Wall Panels

As was mentioned in the previous subsection, the information obtained in this chapter will be used in Chapter 5 to assess the accuracy of the simplified analysis. Another factor to consider is whether the coefficients for successive modification of the slip surface element stiffnesses used in the simplified analysis would remain unchanged for panels of various sizes and shapes. The purpose of this subsection is to provide the necessary information which will be referred to in Chapter 5 where the effects of panel size and shape are investigated again using the simplified model.

Figure 3.22 illustrates the effect on joint deformation of changing the size and shape of the wall panels. The three different sizes of square wall panels used in this study are 8 ft., 10 ft. and 12 ft. In all three cases the vertical load acting on the joint is assumed to represent the gravity load equivalent of a 5 storey building. The vertical load per linear foot of the horizontal joint of a 12 ft. square panel assuming the floor contribution to remain unchanges, is approximately 16% more than that of an 8 ft. square panel as the weight is assumed to be directly proportional to the size. Thus a greater shear force was necessary to cause failure in the larger panel. This is illustrated in Fig. 3.22.

The deformation curve for the case of a rectangular 8 x 10 panel was also investigated to determine the effect of an increase in the height of the panel on the joint

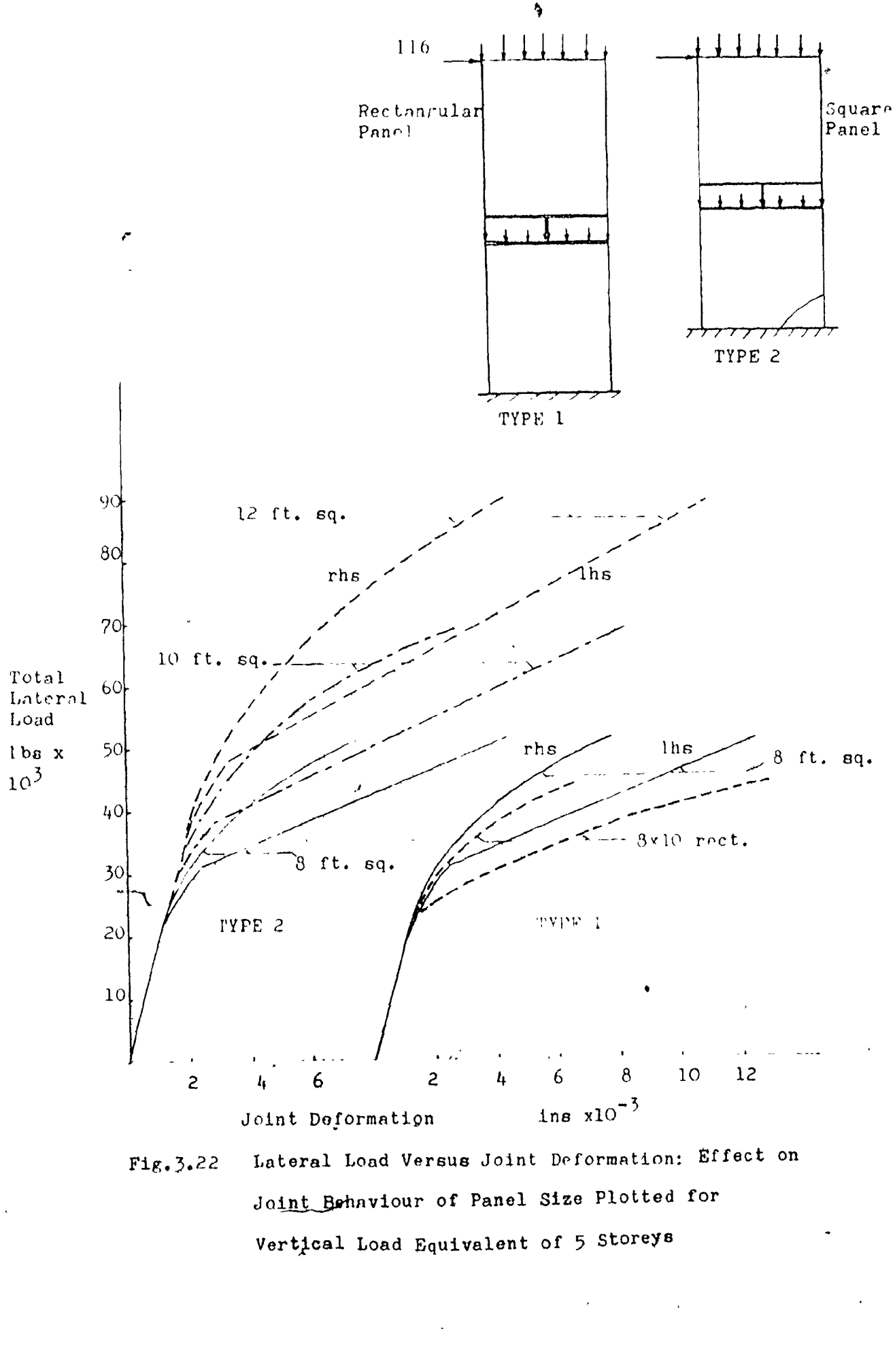

Fig.3.22 Lateral Load Versus Joint Deformation: Effect on Joint Behaviour of Panel Size Plotted for Vertical Load Equivalent of 5 Storeys

behaviour. This result is also shown in Fig. 3.22. To make comparison easier, the deformation graph for the 8 ft. square panel is represented again. The shear force in both cases is assumed to be concentrated at the top left hand corner of the upper panel. For equal shear forces acting on the joints, the joint moment for the 8 x 10 ft. panel is greater since the point of application of the lateral load is at a greater height. Hence the joint fails at a lower ultimate load by overturning the upper panel.

This concludes the detailed investigation of unreinforced horizontal joints. In the following sections reinforced horizontal joints will be studied.

3.11 Introduction to Reinforced Horizontal Joints

As was mentioned in Subsection 3.1(a) a representative type of joint reinforcement consists of a pair of steel bars protruding from the upper surface of a wall panel below a given floor level, passing through the joint-filler region and being anchored in the pre-formed cavities in the wall panel above the joint. The continuity provided by the bar causes the joint to develop some resistance against separation along the slip surfaces.

The greater shear resistance exhibited by the reinforced joints is the result of two distinct actions. Part of the additional shear resistance is provided by the dowel action of the reinforcing bars crossing the slip surface. However, the greater part of the shear resistance occurs as a result of the reinforcing bar being subjected

to tension (as in a reinforced concrete beam), and hence creating an additional balancing compressive force on the other end of the joint.

In the following sections of this chapter, various behaviour mechanisms of dowel bars and the tendency of the reinforcing bars to pull out of the concrete (hand-slip) will be investigated. Later the stiffness matrix of the element representing the reinforcing bars will be investigated taking into account both dowel and hand-slip behaviours. Finally the results of the investigation in graphical form will be presented to illustrate the difference in behaviour when joints are reinforced.

3.12 Dowel Bar Behaviour

Dowel action has been investigated by Mattock[40] and Hanson[24] and more recently by Phillips[52] and by Paulay and Hitchings[51]. To isolate the dowel action, Mattock wrapped the reinforcing bars near the joints in push off specimens in rubber sleeves. This method of studying the dowel action does not realistically model the actual situation as it provides for an unbonded and unsupported length of the bar in the vicinity of the interface and hence reduces the stiffness.

Phillips[52] and Paulay-Hitchings[51] measured the dowel bar effect for various sizes of reinforcing bars by coating the first half of the push-off specimens with candle wax before casting the second half and were thus able to eliminate both bond and friction. Their test

results are shown in Fig. 3.23 and Fig. 3.24.

Phillips investigated the dowel action for 3 different bar sizes. The surface area of push off specimen was 96 square inches and 6 dowel bars were used in all cases. His load-slip curves are illustrated in Fig. 3.23. The shear force applied to the push off specimen is plotted (at) the shear stress on the joint surface area.

Paulay and Hitchings[51] extended Phillips' tests to larger diameter dowel bars namely #5, #7 and #9 as shown in Fig. 3.24. However, for bar #7 and #9 crushing and splitting of the specimens occurred at early stages of loading due to poor detailing of the reinforcements within the specimen. Thus for these bars the results are reliable only at the very early stages of loading.

As can be observed in Fig. 3.24, although the stiffness and the maximum average shear stress for specimens with different steel ratios (bar sizes) are different, all curves have an almost identical shape. Furthermore, Phillips[52] indicates that the shear resisted by a joint is proportional to the area of the bars. Thus it seems justifiable to use interpolation (within a reasonable range of bar sizes and steel ratios) to derive load-slip curves for other size bars and steel ratios. Such a graph for 2 #8 bars, with a steel ratio of 0.0165 used to reinforce the horizontal joints, is also illustrated in Fig. 3.24.

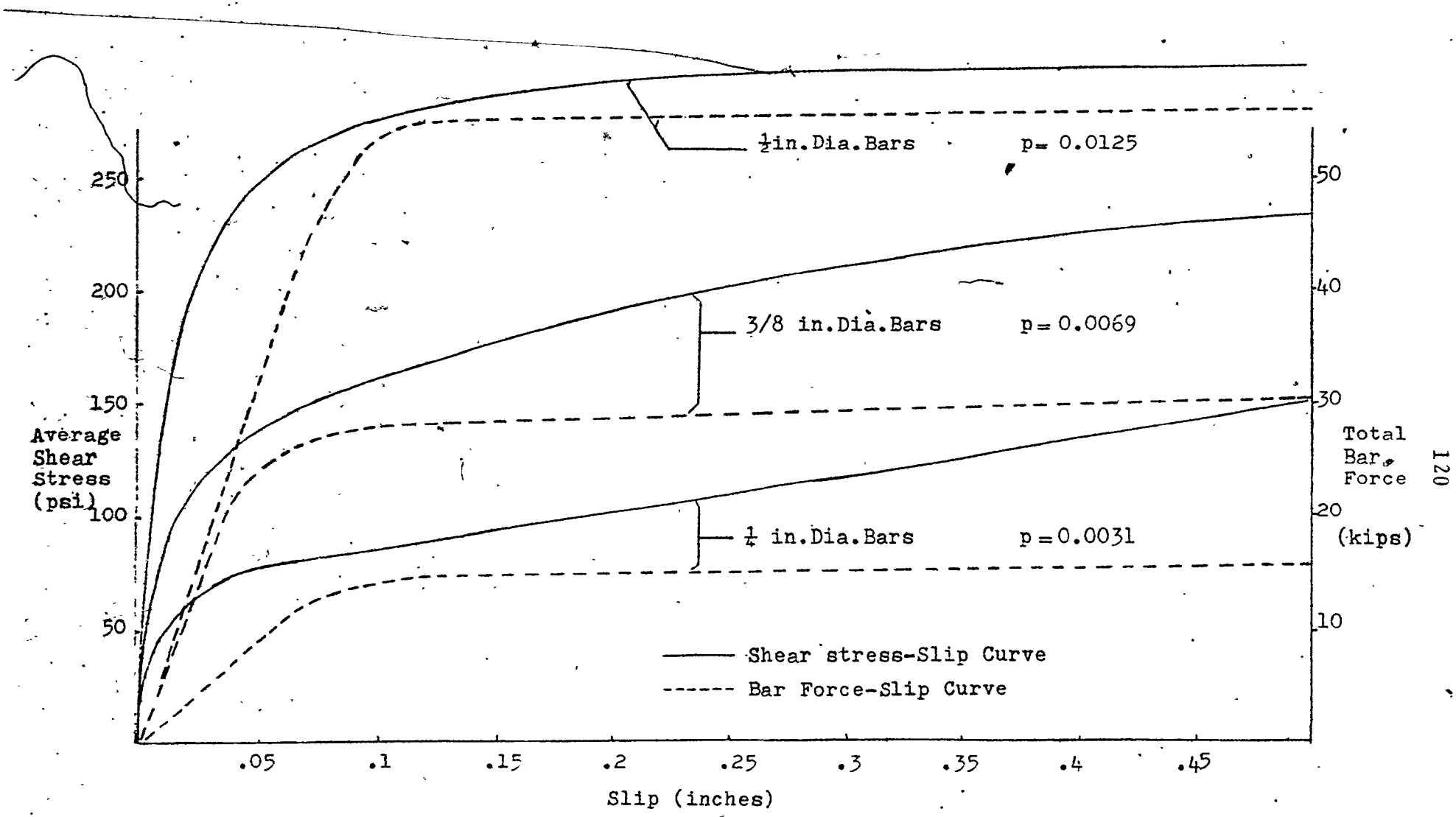

Fig.3.23 Load-Slip Curves for Dowel Action for Phillips' Push-Off Specimens(52)

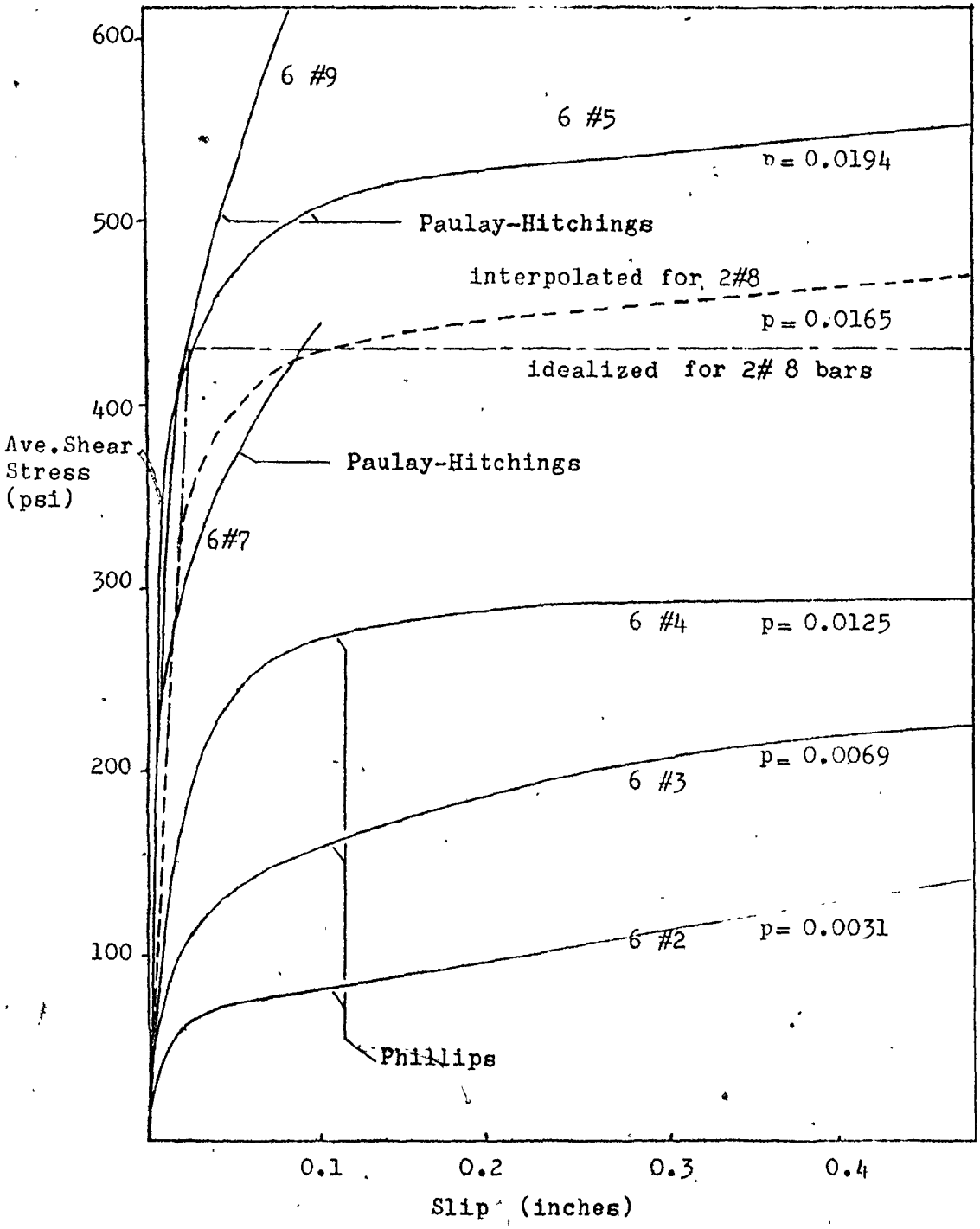

Fig.3.24 Load-Slip Curves for Dowel Action

There are 3 possible dowel bar mechanisms which could contribute to shear resistance through dowel bar action. These are:

1. bending,
2. shear, and
3. kinking[52].

It is important to note that all the above mechanisms occur simultaneously, and that the contribution of each action depends to a great degree on the size of the bar, the strength of concrete surrounding the dowels and the amount of slip which has already occurred. The crushing of concrete in bearing around the dowels as slip becomes greater is also a definite possibility and a cause for further complication as it allows continual change in the orientation of the dowels as they cross the interface.

Referring once again to Fig. 3.23, it is very interesting to note that:

1. bar force (dashed line) after yielding remains approximately constant, whereas dowel bar action continues to increase at a constant rate, and
2. this phenomenon is more pronounced for bars with smaller diameters.

A possible reason for this behaviour is the effect of the continual change in the slope of the kinked portion of the dowel bars (dowel action being the horizontal component of the bar force). Also the fact that for 1/2 inch diameter bars the load-slip curve assumes an almost horizontal slope strongly suggests that the dowel bar

action for smaller diameter bars is mostly due to the kinking type mechanism.

3.13 Bond-Slip Behaviour

The bond-slip relationship for reinforced concrete has been studied by numerous researchers[34, 35, 36, 39, 45, 46, 67, 68].

Tests to determine bond-slip behaviour have been carried out utilizing either beams in bending or pull-out specimens. Because of the differences in the physical make-up of the specimens, and the method in which the loads are applied, the resulting bond-slip graphs might be expected to exhibit considerable differences.

The type of finite element model proposed by Ngo[48], Nilson[47] and other researchers for simulating the behaviour of reinforced concrete members, utilizes many elements to represent the bond-slip relationship at regular intervals along the length of the steel bars. It is very important to use realistic values for the stiffnesses of these elements, and therefore Nilson's[45, 46] work is quite valuable when this type of bond-slip simulation is used.

However, in the present work an attempt has been made to use a single element to represent the effect of reinforcing a horizontal joint. An element is located at the point where a reinforcing bar crosses the slip surface. The element is composed of two independent springs located at right angles to one another. The bond-slip characteristics of the reinforcing bars is simulated by the stiffness of the vertical spring.

The test conducted by Mathey and Watstein[39] on pull-out specimens are used to determine the stiffness of the vertical spring. The test results give the relationship between the force applied to the steel bar and the resulting end slip relative to the surrounding concrete. This provides the required information so that the effects of reinforcing bars on joint strength (additional shear resistance resulting from the added compression force exerted on the joint) and on separation can be adequately simulated.

The graph of average bond stress versus loaded end slip constructed by the author on the basis of the relationship

$$u_A = \frac{f_s A_s}{\Sigma_o L_A}$$

for the results obtained by Mathey and Watstein is shown in Fig. 3.25. As observed there is some scatter in the results of similar specimens especially for bars with smaller embedment lengths. Rather than deal with bond stress, Mathey and Watstein[39] suggest a process of averaging for bars of various embedment lengths. Their results for #4 and #8 bars drawn as a graph of reinforcing bar stress (force) versus loaded end slip are shown in Fig. 3.26 and Fig. 3.27 respectively. The points very nearly fall on a straight line. The stiffness of the vertical spring mentioned above can be determined on the basis of the slope of these lines. The computed stiffnesses are 9.25×10^5 lb/in and 1.38×10^6 lb/in for #4 and #8 bars respectively.

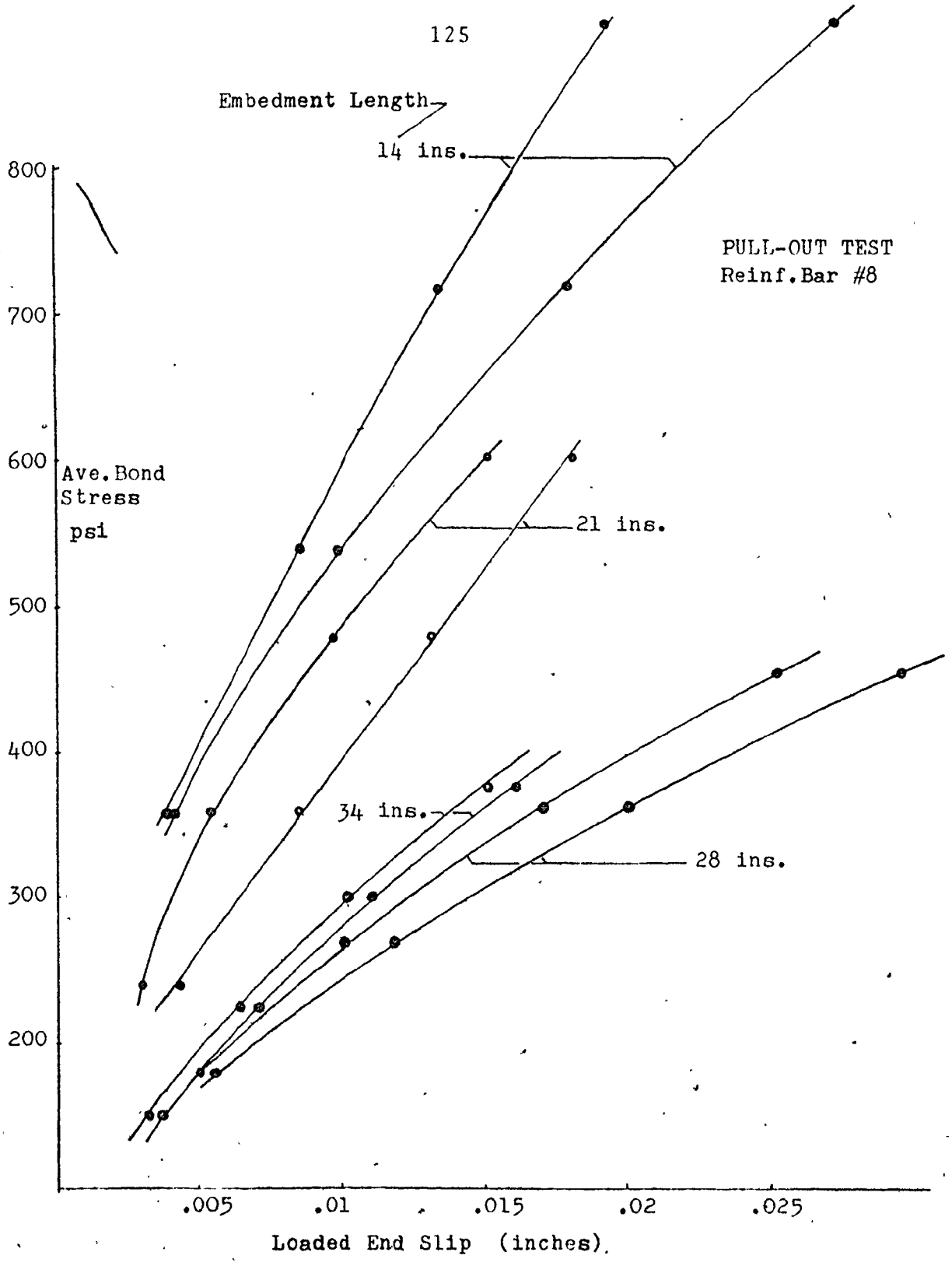

Fig.3.25 Computed Average Bond Stress Versus Loaded End Slip (Constructed by the Auther from Mathey-Watstein's Test Results [39])

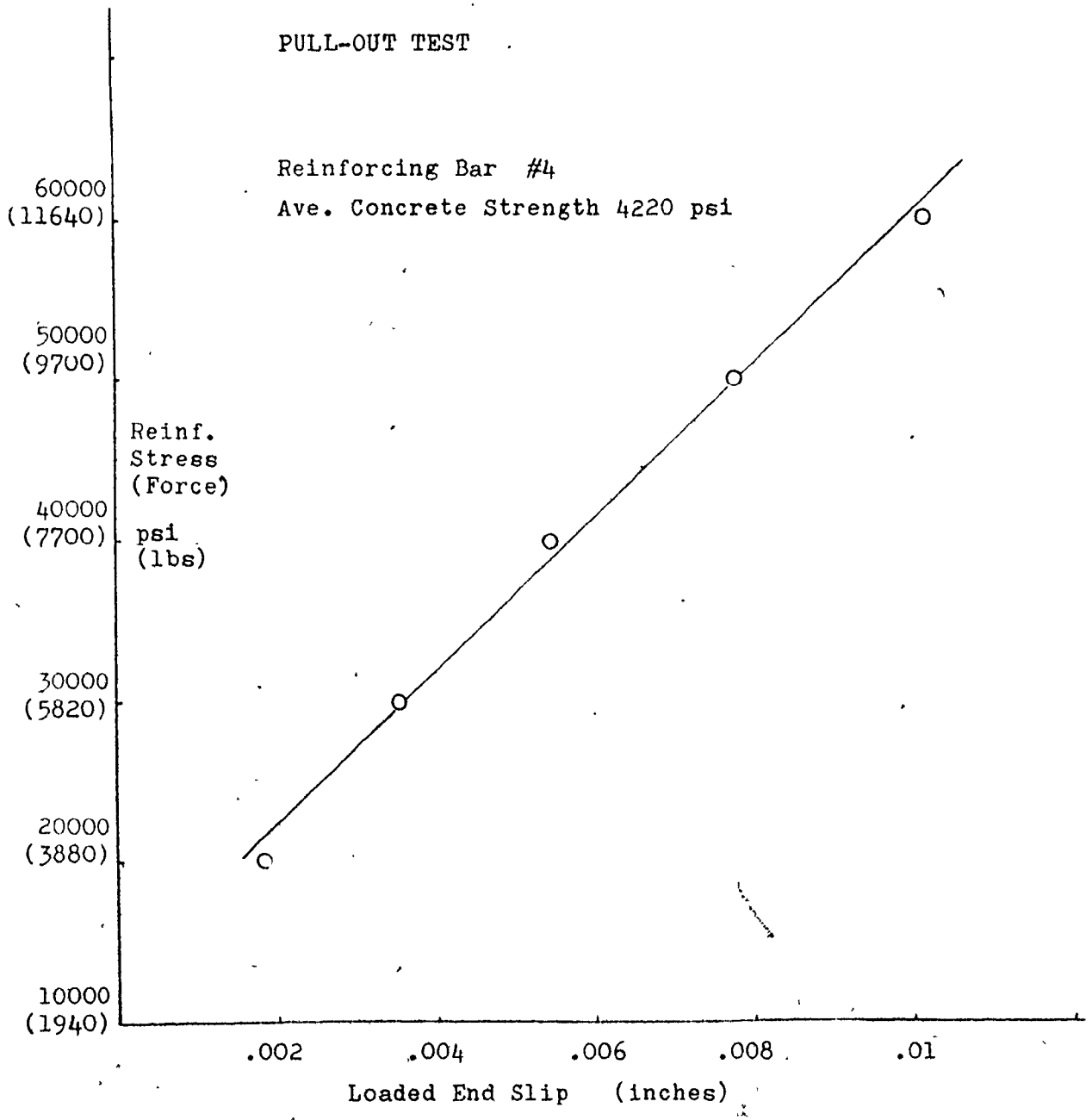

Fig.3.26 Computed Stress(Force) in Reinforcing Bar Versus Loaded End Slip (Mathey-Watstein[39])

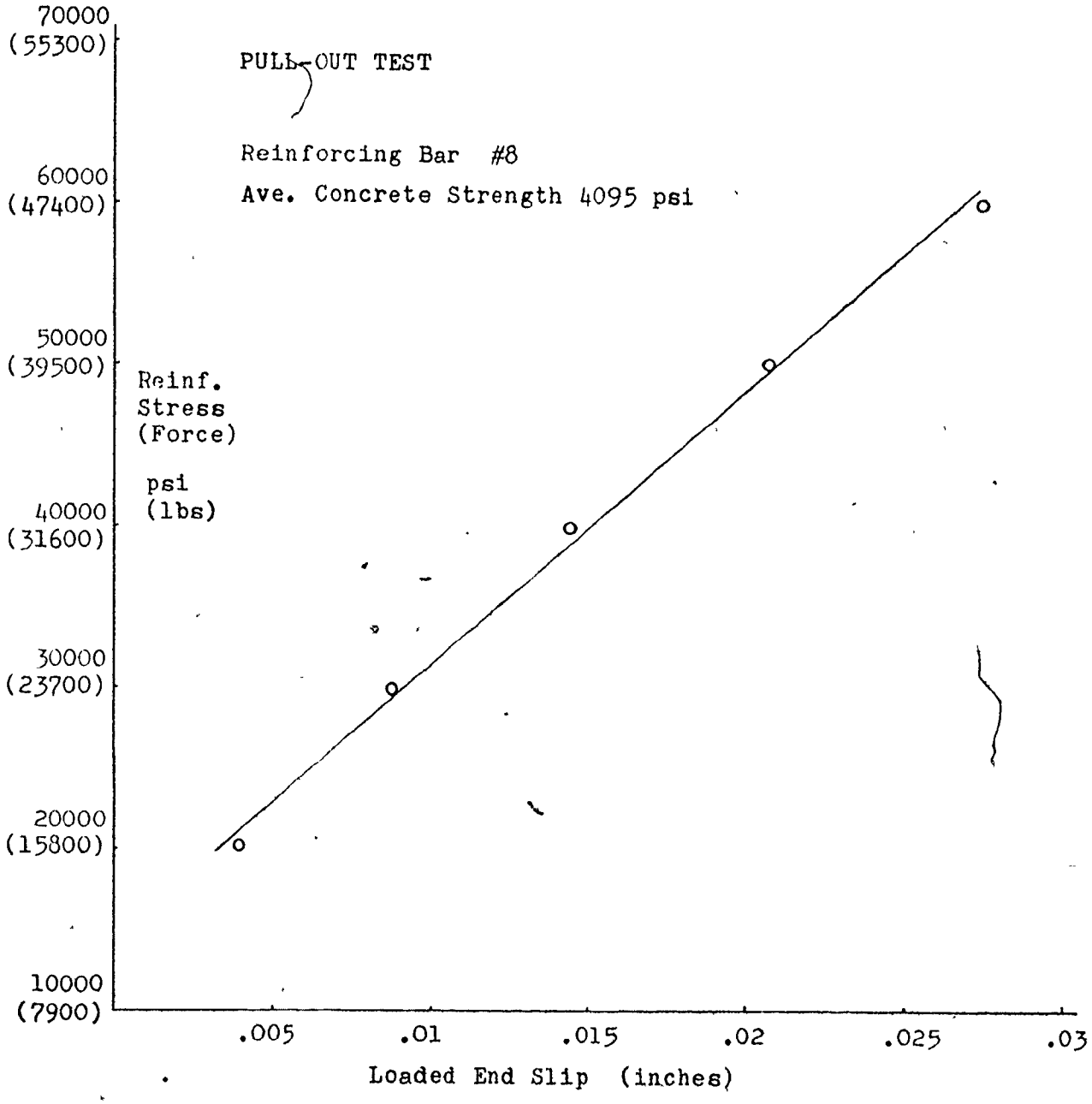

Fig.3.27 Computed Stress(Force) in Reinforcing Bar Versus Loaded End Slip (Mathey-Watstein[39])

It must, however, be noted that the stiffnesses at very early stages of loading are quite different from those obtained from Fig. 3.26 and Fig. 3.27. In all likelihood the stiffnesses at very small values of slip are quite high. For the purpose of this analysis a linear bond-slip relationship is assumed throughout. This assumption is justified because the emphasis here is on the strength and stiffness near the ultimate load. Furthermore, the linear bond-slip relationship yields results which are on the safe side. It must also be noted that embedment length is assumed to be sufficient to develop the bars' yield strength.

3.14 Finite Element Representation of Joint Reinforcement

As mentioned in the previous section, a joint reinforcement bar is represented by an element composed of a pair of dimensionless independent springs situated at right angles to one another. Dowel bar behaviour is simulated by the action of the horizontal spring, whereas vertical continuity (taking bond-slip characteristics of the bar into account) is represented by the action of the vertical spring. The element is physically similar to that shown in Fig. 3.7(a) for modelling the slip surfaces. The stiffness for the vertical spring is based on the information presented in the previous section. The horizontal spring stiffness is determined in accordance with the slope of the interpolated dowel bar graph for 2 #8 bars as illustrated in Fig. 3.24. The interpolated curve is further idealized to represent the yielding of

the dowel bar by a horizontal line at an average shear stress of approximatley 428 psi. The horizontal line is drawn to intersect the interpolated curve at a slip of 0.1 inch. This is consistent with Paulay and Hitchings[51] suggestion for determination of a theoretical dowel failure force. The equivalent stiffness for 2 #8 bars is estimated to be 1.73×10^6 lb/in.

In this analysis it is assumed that the springs representing the dowel action and the vertical continuity are independent. How realistic is this assumption? Hitchings[51] observed that for push-off specimens with tensile forces acting normal to the surface of the joint, slip at ultimate capacity was uneffected by the magnitude of tensile stresses up to 80% of yield. Even though this has not been conclusively proved, it seems logical that this should be realistic as long as the joint separation is small in comparison with the diameter of the reinforcing bar. Furthermore, the increased joint capacity resulting from the dowel bar action constitutes only a small part of the total shear resisted by the joint. Thus even large variations in the dowel spring stiffnesses resulting from the action of the vertical spring will produce only relatively small differences in the overall capacity.

The stiffness matrix of the reinforcing element is given by equation (3.34) and is derived using a procedure similar to that outlined in Section 3.5.

$$[\bar{K}]_R = \begin{bmatrix} K_D & 0 & -K_D & 0 \\ 0 & K_B & 0 & -K_B \\ -K_D & 0 & K_D & 0 \\ 0 & -K_B & 0 & K_B \end{bmatrix} \qquad (3.34)$$

where K_D and K_B represent the horizontal (dowel) and vertical (bond-slip) spring stiffnesses respectively.

It is assumed that the forces existing in one spring can effect the yield in the other spring in accordance with the following relationship:

$$F_{BR} = F_{BL} \cdot R_D$$

$$\text{and} \qquad F_{DR} = F_{DL} \cdot R_B \qquad (3.35)$$

F_{BL} and F_{DL} are the yield forces in the vertical and horizontal springs respectively when there is no force activating the other spring.

F_{BR} and F_{DR} are the forces capable of causing yielding in the presence of a force activating the other spring.

$$R_D = 1 - \frac{F_D}{F_{DL}} \quad \text{and} \quad R_B = 1 - \frac{F_B}{F_{BL}}$$

F_D/F_{DL} is the ratio of the actual force existing in the dowel spring to that force which (in the absence of other forces) would cause yielding of the element. R_B can be similarly defined. At yielding where $F_D = F_{DR}$ and $F_B = F_{BR}$ equations (3.35) may be written as

$$\frac{F_{BR}}{F_{BL}} + \frac{F_{DR}}{F_{DL}} = 1 \qquad (3.36)$$

Although equations (3.35) seem to be subjective and rather conservative, the author feels that they are justifiable in the absence of rigorous experimental evidence regarding the yield behaviour.

3.15 Discussion of the Results of the Investigation for Reinforced Joints

(a) Detailed Account of Slip Surface Element Behaviour

The joint behaviour under the combined actions of a concentrated lateral force applied to the top left hand corner of the upper panel and a gravity load equivalent of a 5 story building is illustrated in Fig. (3.28). Separation starts at the left hand side of slip surface 1 and propagates to the right. The shear force carried by an element labelled 'slipped' is a function of the compressive force acting on that element. The actual slippage occurring for a particular element is quite small and depends on the relative deformations of the concrete elements surrounding the slip surface. Slip for the zone as a whole does not occur because the shear resistances of the elements to the right of the slipped element are not as yet exceeded.

Since slip surface 1 is assumed to be unbonded, the process of separation is gradual as reflected by the load-deformation graph which does not show the sudden increases in deformation normally associated with cracking of the bonded components. When cracking is not excessive, the instantaneous increase in deformation is small and depending on the size of the increment by which the total

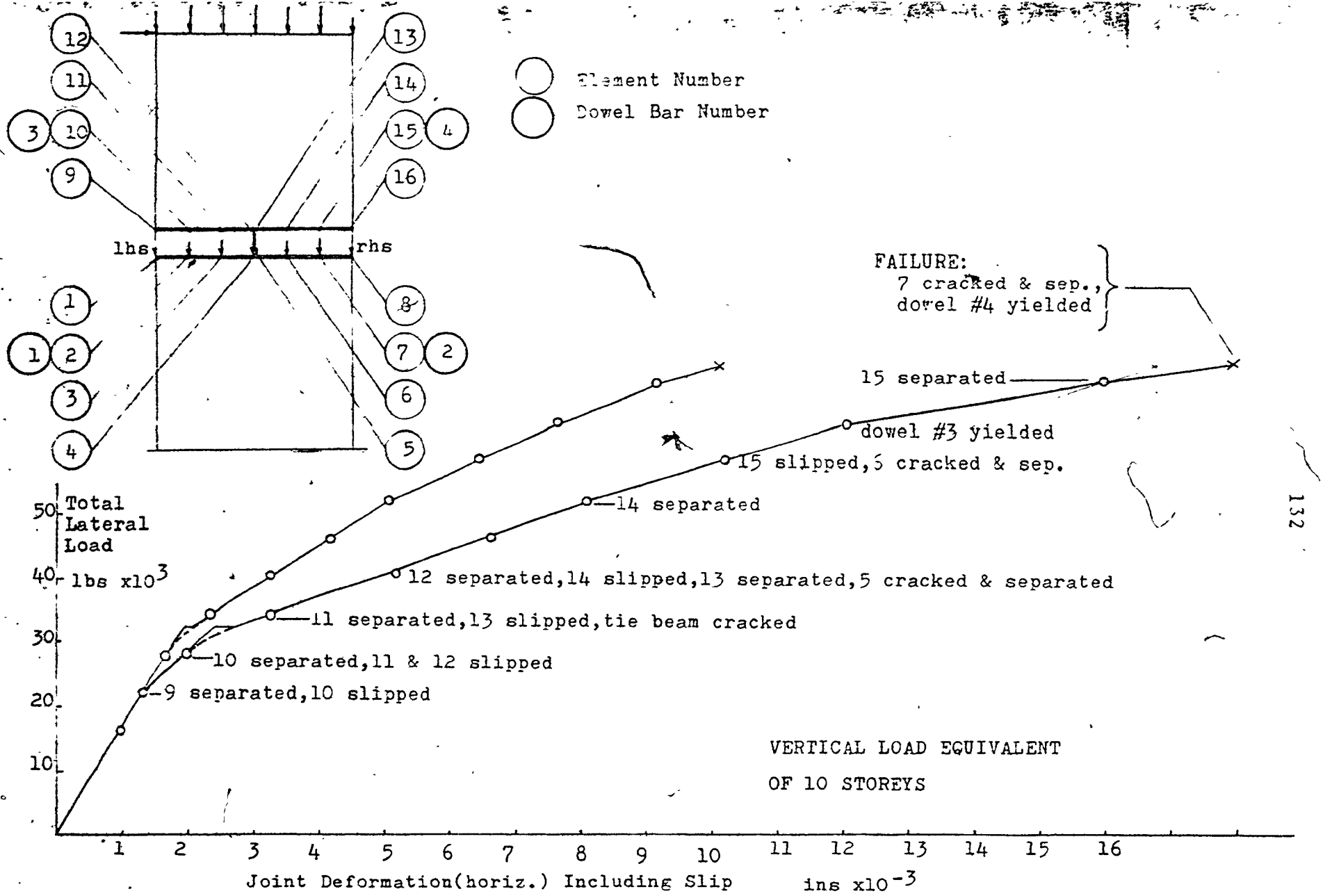

Fig.3.28 Lateral Load Versus Joint Deformation: Detailed Behaviour of Reinforced Joint with Narrow Floor Panels

load is increased, it might sometimes be possible to remove the discontinuity by a smoothing process. Such a situation is observed for the graph shown in Fig. 3.28 at a total lateral load of approximately 30 kips.

The behaviour of the joints with wide floor panels (sections 3.7 and 3.10) is shown in Fig. 3.29. By comparison with Fig. 3.28, it is observed that with narrower floor panels where cracking of the tie-beam occurs, the deformation curve shows a smoother transition as it inhibits the sudden release of energy resulting from cracking along slip surface 2 at a lateral load of about 63 kips (Fig. 3.29).

The effect of a change in the magnitude of the gravity load can be illustrated by comparing Fig. 3.28, and Fig. 3.30 and Fig. 3.33. The graphs of deformations for unreinforced joints are also compared with their reinforced counter-parts and are shown in Fig. 3.31, Fig. 3.32 and Fig. 3.33. As can be observed the effect of reinforcing a joint is much more dramatic for joints with smaller gravity loads, as in Fig. 3.31. For a gravity load equivalent of 2-1/2 stories, the lateral force resisted by the unreinforced joint is about 50% of the force carried by its reinforced counter-part. When gravity loads are increased to the equivalent of 10 stories, the unreinforced joint capacity increases to about 85% of the reinforced joint capacity. Under the action of very high gravity loads, i.e. the weight of 40 stories, the introduction of reinforcing bars will have no effect at

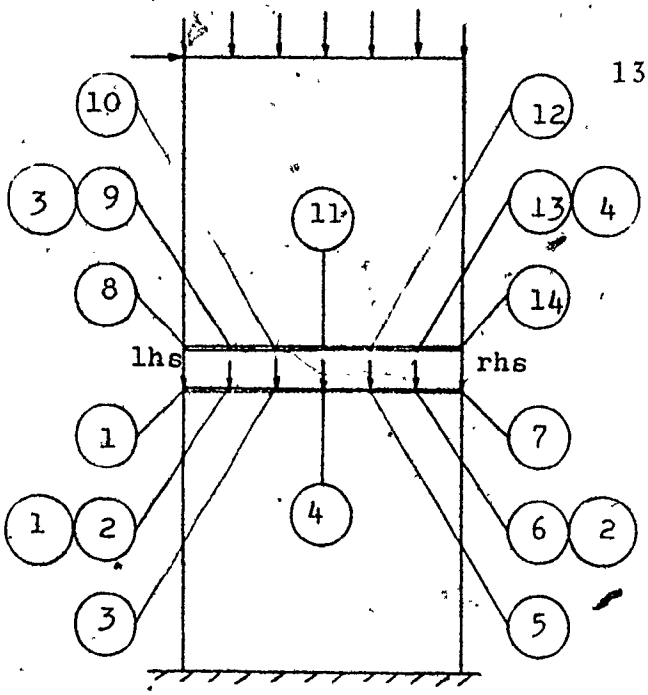

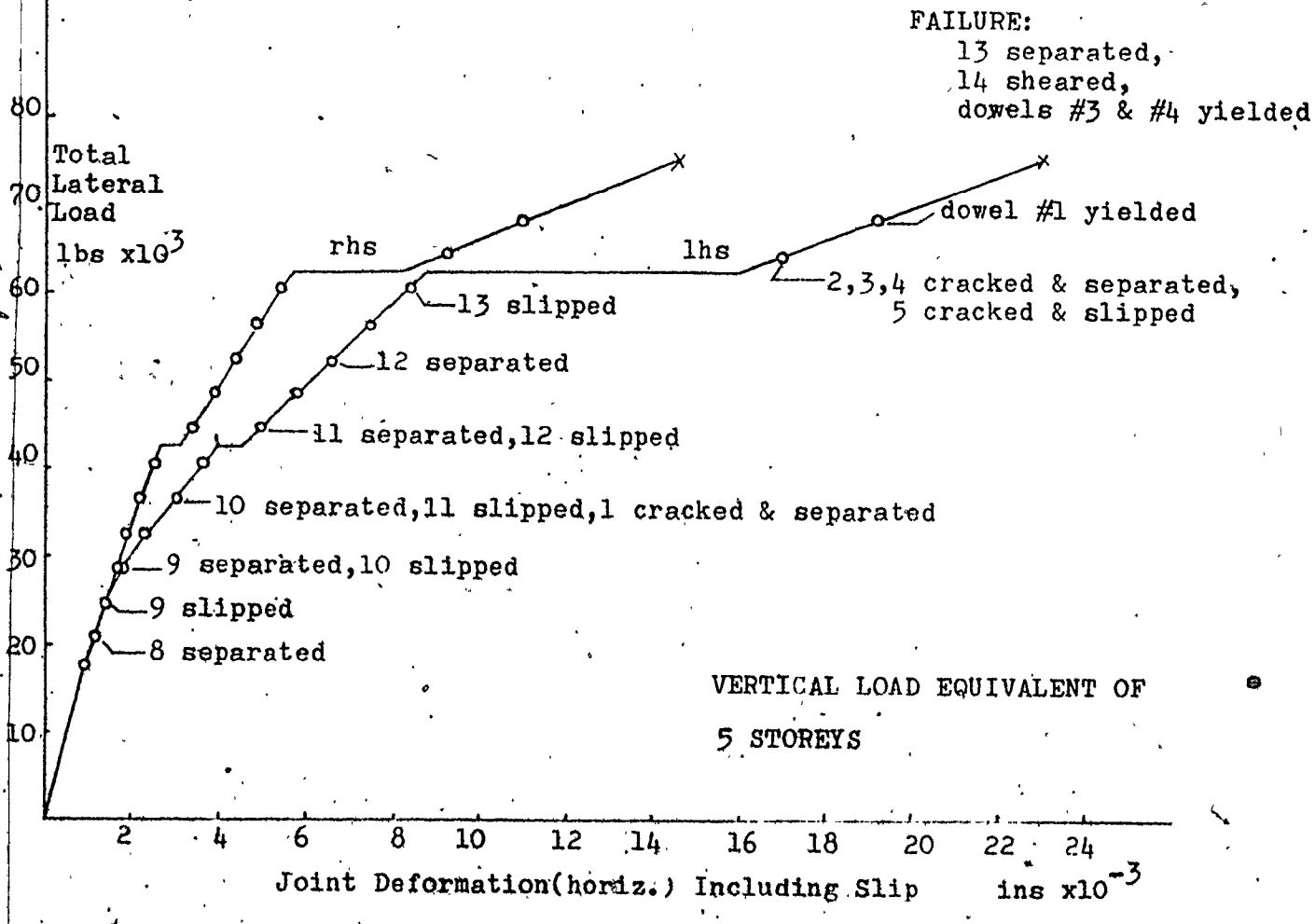

Fig.3.29 Lateral Load Versus Joint Deformation: Detailed Behavfour of Reinforced Joint with Wide Floor Panel

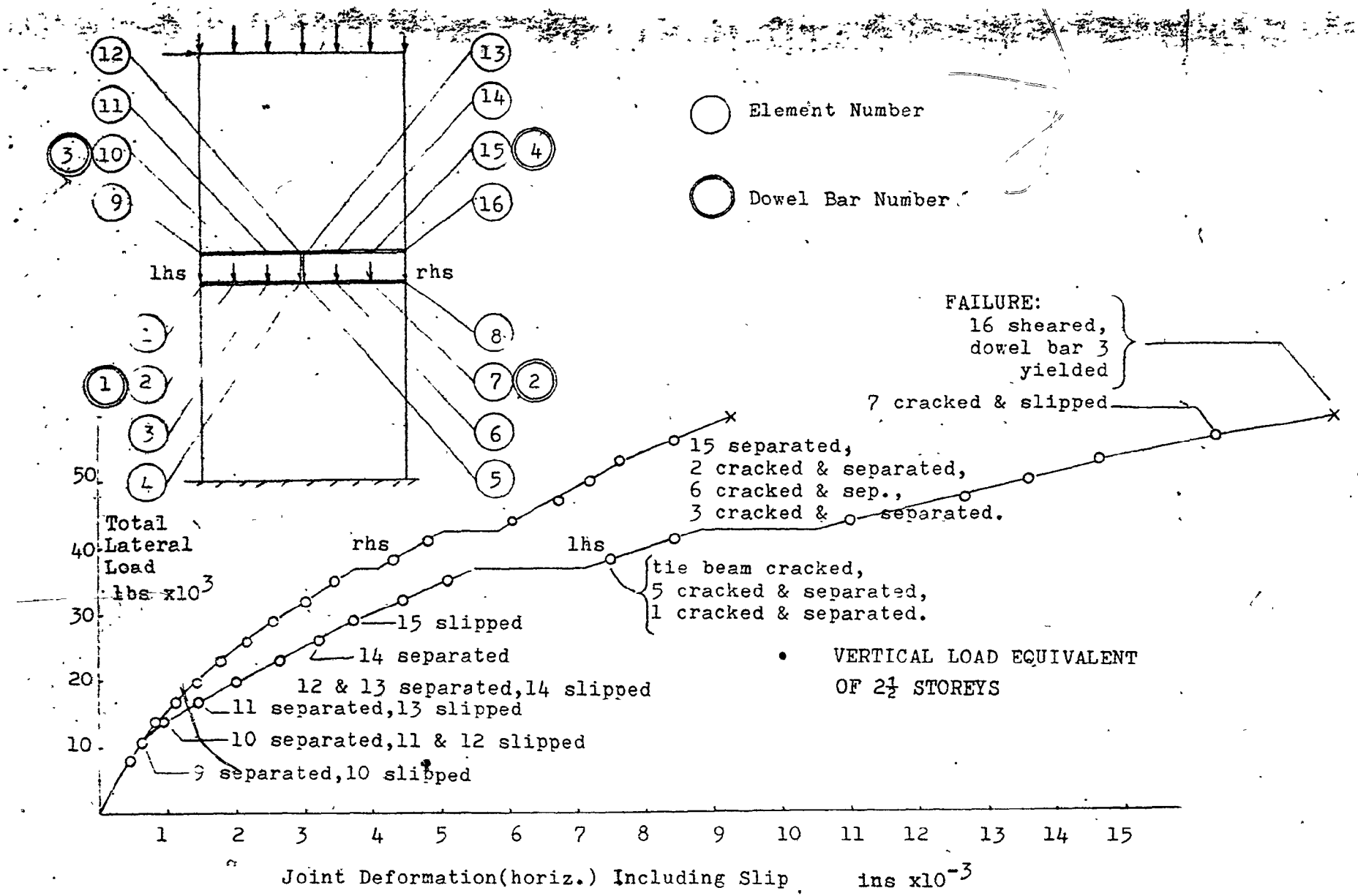

Fig.3.30 Lateral Load Versus Joint Deformation: Detailed Behaviour of Reinforced Joint For Vertical Load Equivalent of 2½ Storeys

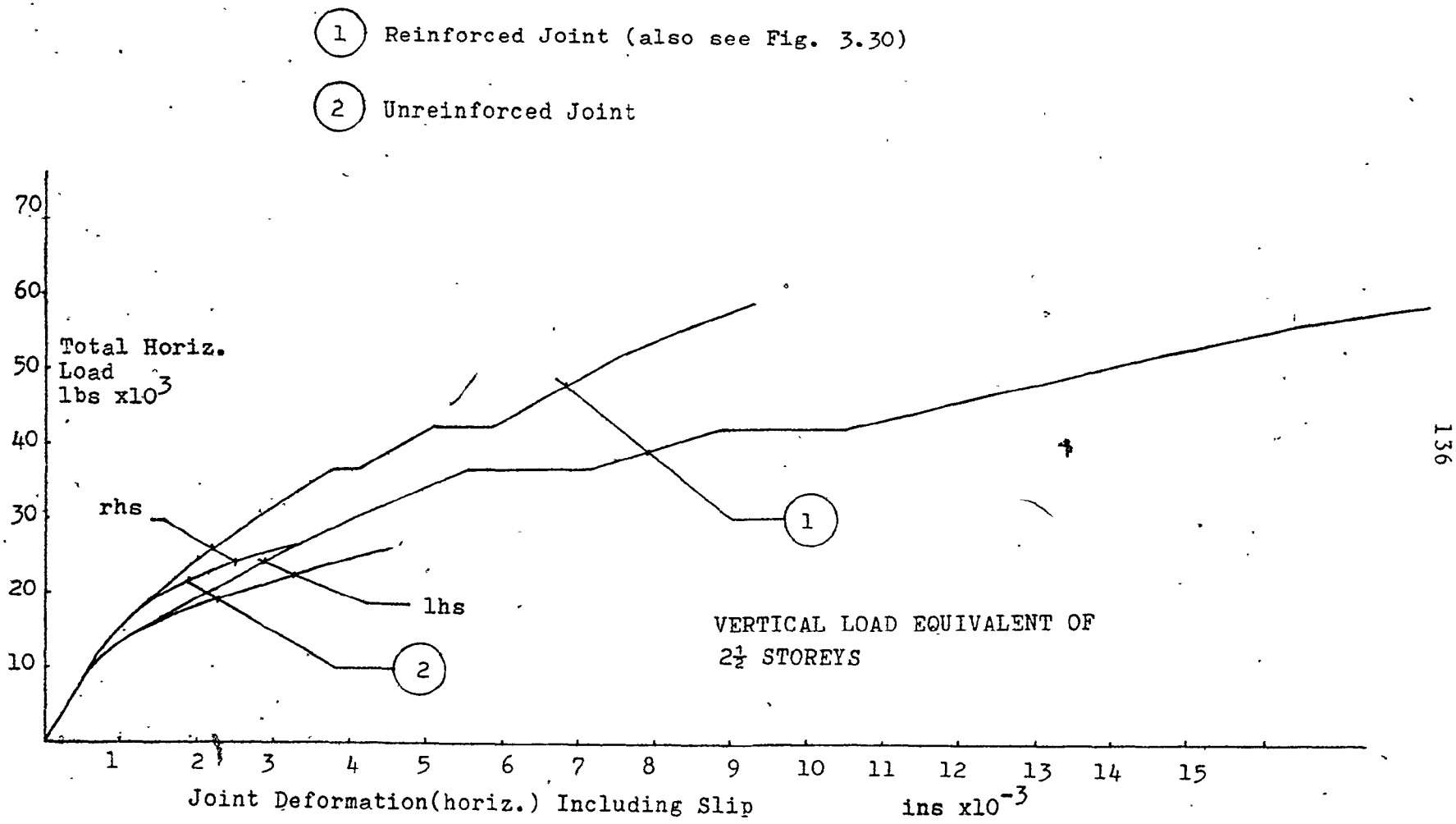

Fig.3.31 Comparison of Horiz. Deformations of Reinforced and Unreinforced Joints For Vertical Load Equivalent of 2½ Storeys

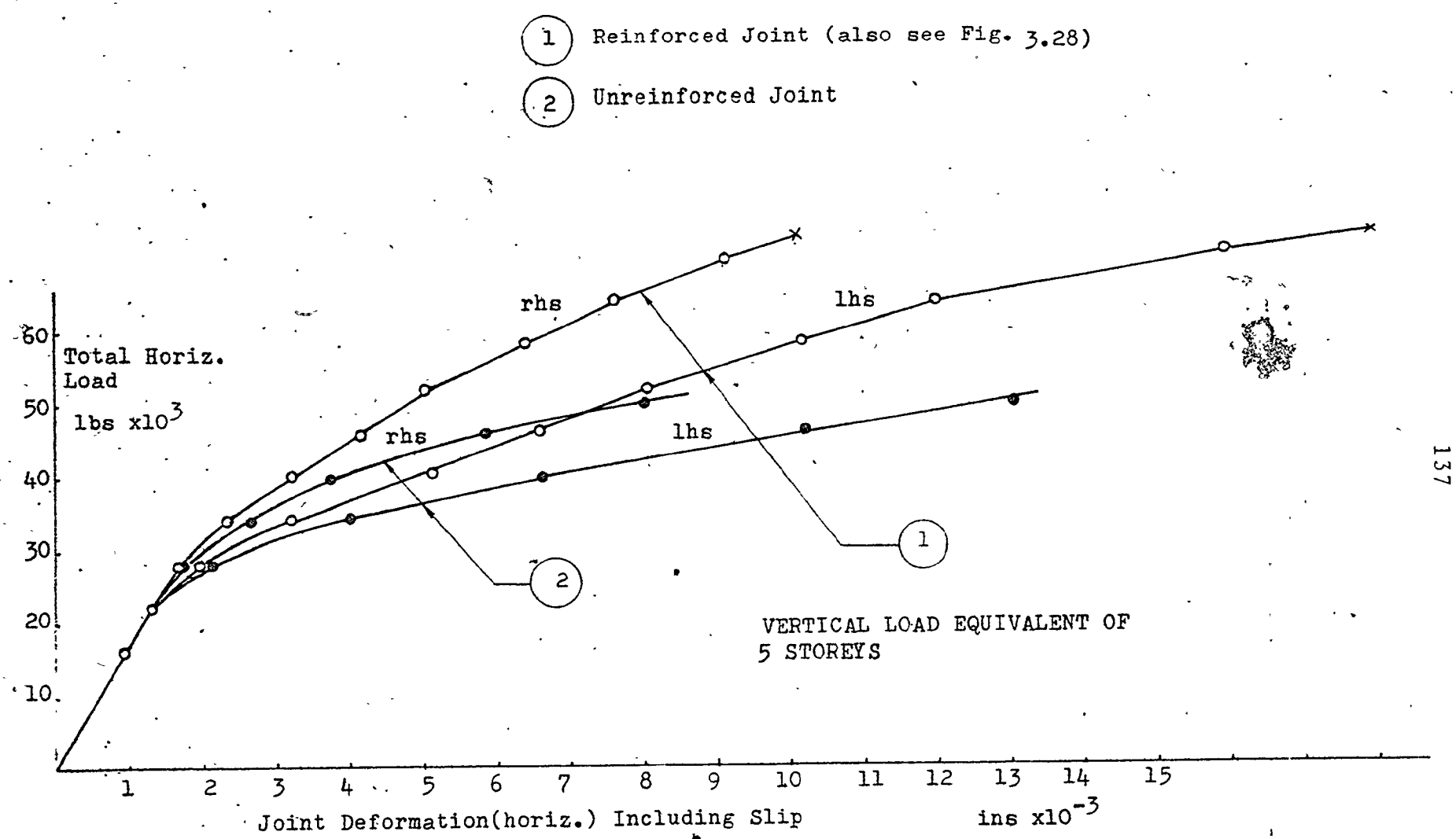

Fig.3.32 Comparison of Horiz. Deformations Of Reinforced and Unreinforced Joints For Vertical Load Equivalent of 5 Storeys

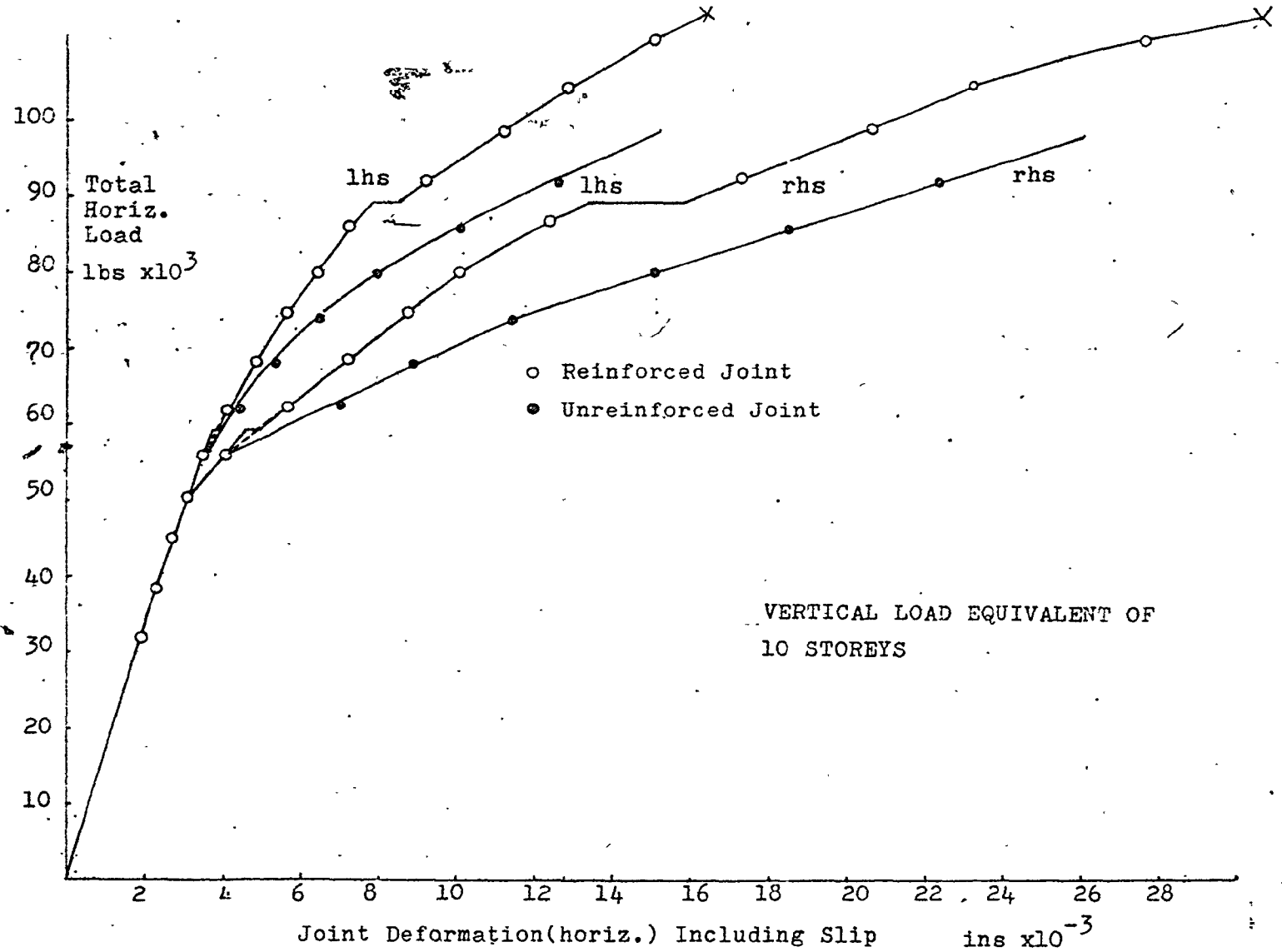

Fig.3.33 Comparison of Horiz. Deformations of Reinforced & Unreinforced Joints For Vertical Load Equivalent of 10 Storeys

all since the failure mode would be compressive (see Fig. 3.20).

The behaviour of joints subjected to a shear force applied at the joint (to eliminate bending on slip surface 1) was also investigated. The graphs showing the comparison between the reinforced and the unreinforced joints are shown in Fig. 3.34. The contribution of the dowel bars to the strength of the joint is quite small until the friction capacity of the joint is overcome. The dowel contribution will then become significant. A comparison of the capacities of reinforced and unreinforced joints subjected to nearly pure shear, as shown in the joint sketch in Fig. 3.34, shows that the capacity of an unreinforced joint is about 73% of that of its reinforced counter-part when the vertical gravity load is the equivalent of 5 stories.

(b) Effect of Dowel Bar Location

The reinforcing bars are normally located some distance away from the vertical edges of the wall panels. This distance varies according to the manufacturer's specifications and it is determined mainly on the basis of practical considerations. Generally, the dowels are located from 12 to 20 inches away from the vertical panel edge.

In the present investigation, the exact edge distance used is dependent on the number of elements used to represent the slip surfaces (and hence the distance between them). For the analysis shown in

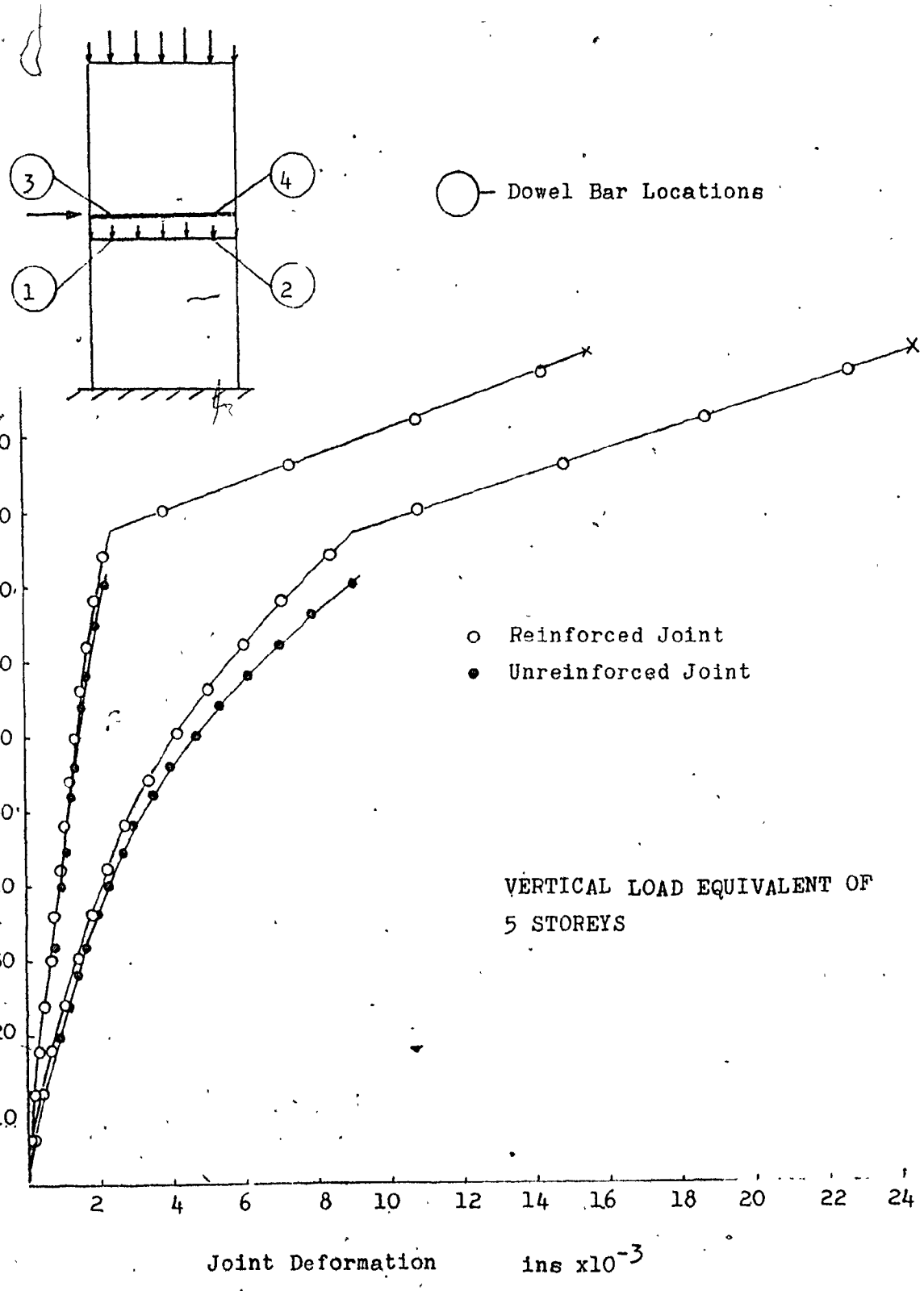

Fig.3.34 Comparison of Horiz. Deformation of Reinforced and Unreinforced Joints For Nearly Pure Shear

Fig. 3.35, the edge distance is 16 inches for locations 'A' of the dowel bars.

In order to be able to investigate, the behaviour must be simplified. As will be seen in Chapters 5 and 6, this simplification results in using far fewer elements to simulate the joint behaviour (usually 2 or 3 elements per slip surface). In this case there is no choice but to connect the reinforcing elements at the very edges of the panels.

The effect of changing the reinforcing bar locations from 'A' (16 inches away from the edge) to 'B' (at the edges) is shown in Fig. 3.35. As can be observed, changing the dowel bar location by 16 inches produces only marginal changes on the overall behaviour of the joint. Thus it would be feasible to install the dowel bars at the edge of the panel in the simplified analysis without effecting the outcome appreciably.

Figure 3.36 illustrates the case where an edge distance of 12 inches (obtained by using more elements per slip surface) is compared with the edge locations of the dowels. The analysis again indicates that a change in the location of the dowel bars does not produce significant changes in the overall behaviour of the joint.

(c) Reinforcing Bar Forces

Horizontal and vertical spring forces for the reinforcing elements are shown in Figs. 3.37, 3.38 and 3.39 for cases where the gravity loads are the equivalent of 2-1/2, 5 and 10 stories respectively. The forces in

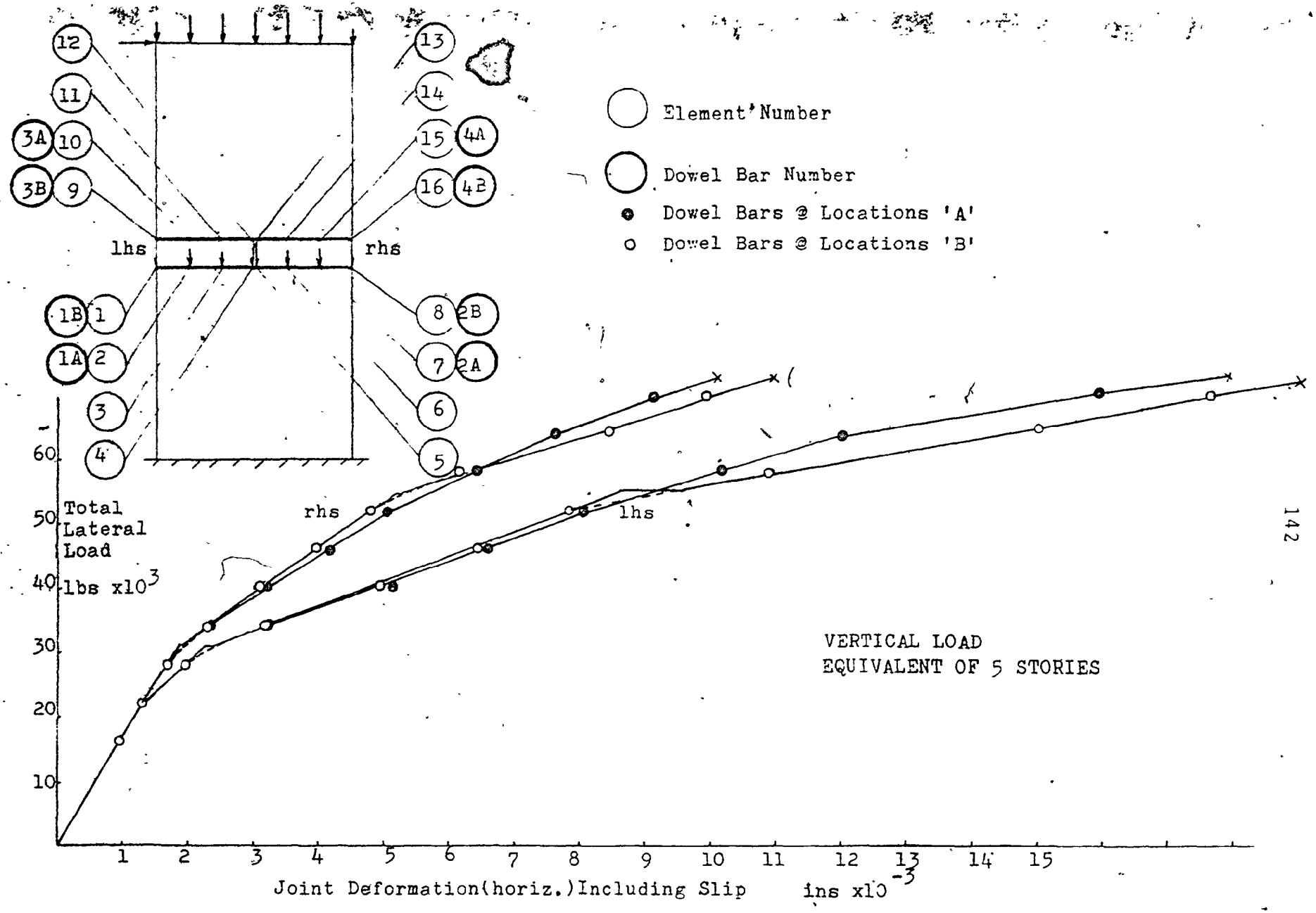

Fig.3.35 Lateral Load Versus Joint Deformation: Effect of Changing Bar Position Utilizing 8 Elements per Slip Surface

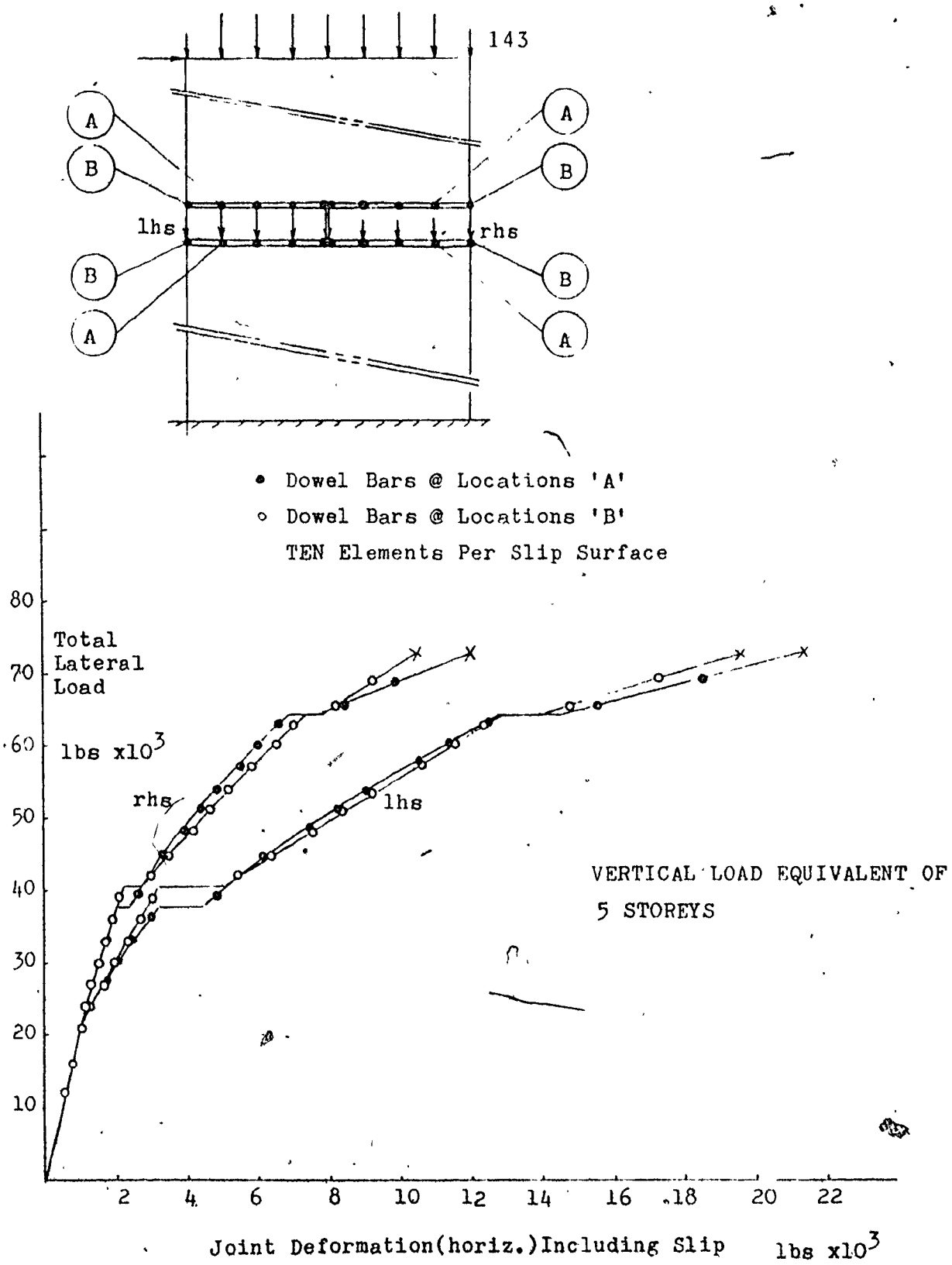

Fig.3.36 Lateral Load Versus Joint Deformation: Effect Of Changing Dowel Bar Position Utilizing 10 Elements per Slip Surface

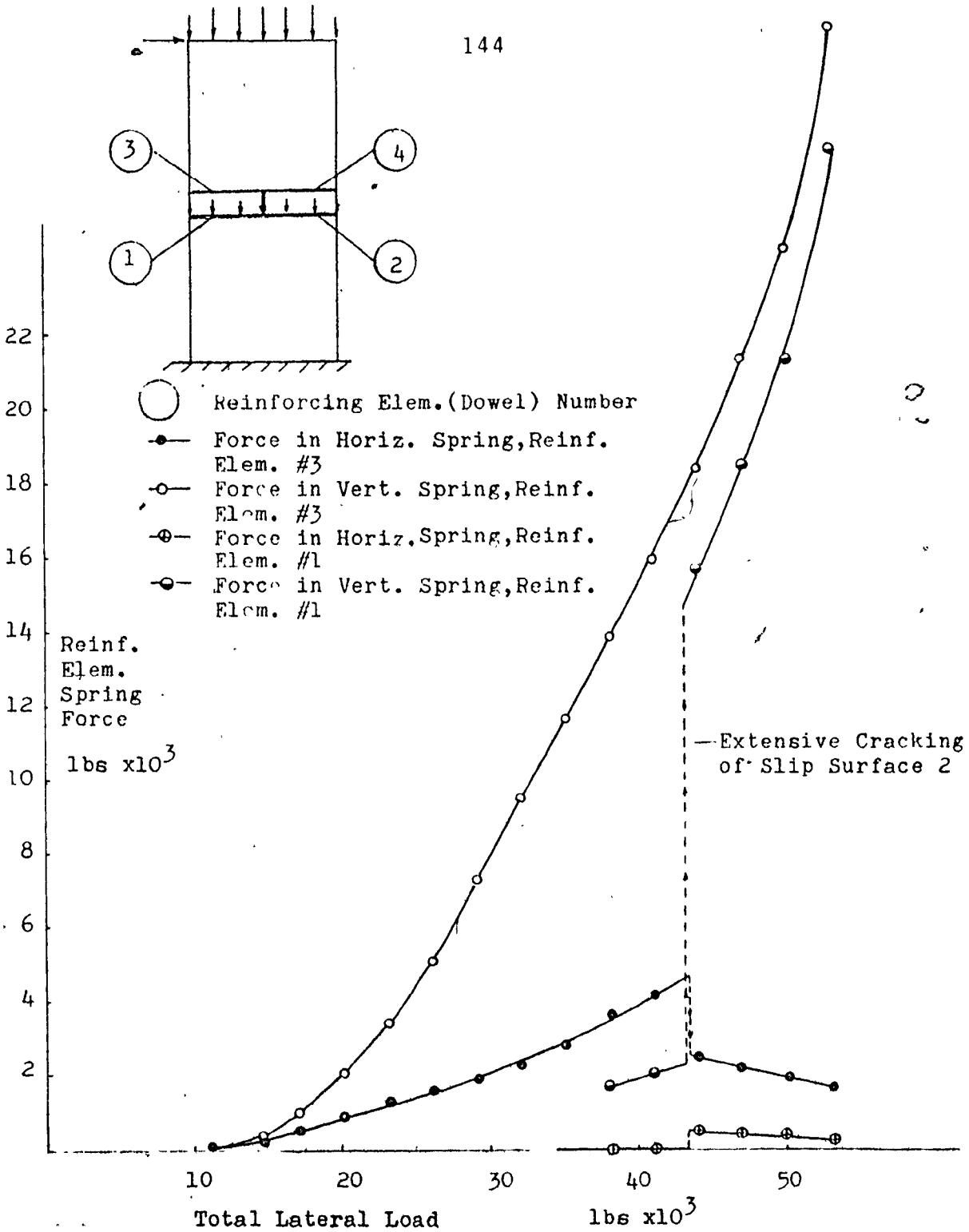

Fig.3.37 Forces in Reinforcing Elements Versus Total Lateral Load For Vertical Load Equivalent of $2\frac{1}{2}$ Storeys

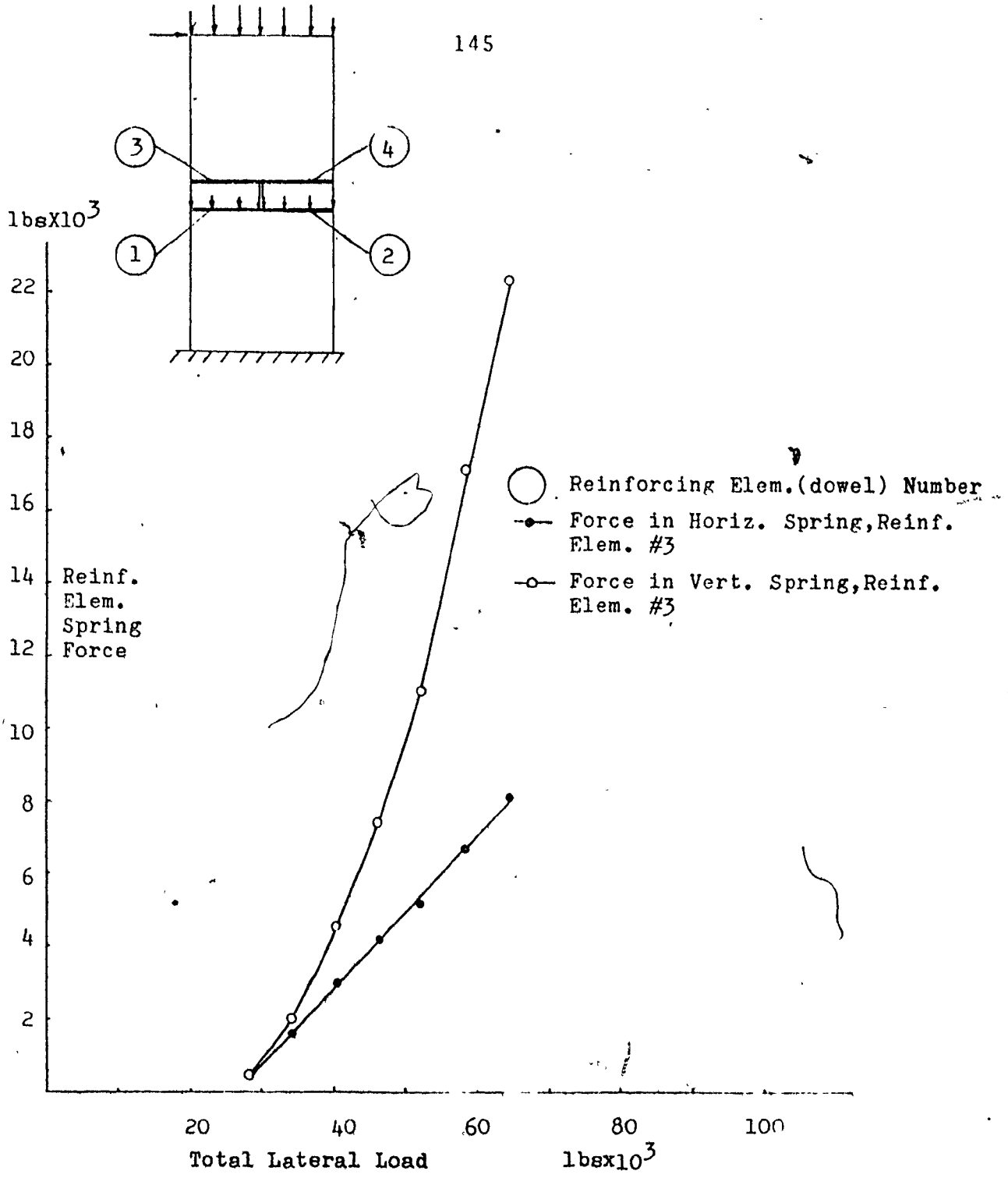

Fig.3.38 Force in Reinforcing Elements Versus Total Lateral Load For Vertical Load Equivalent of 5 Storeys

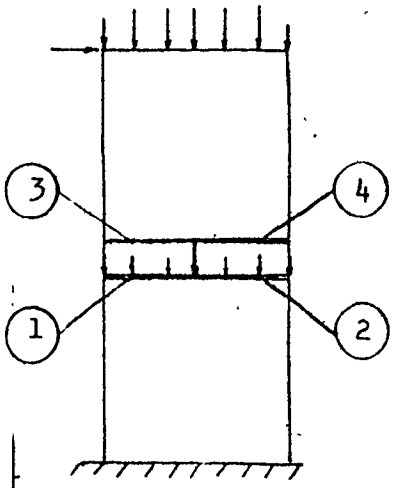

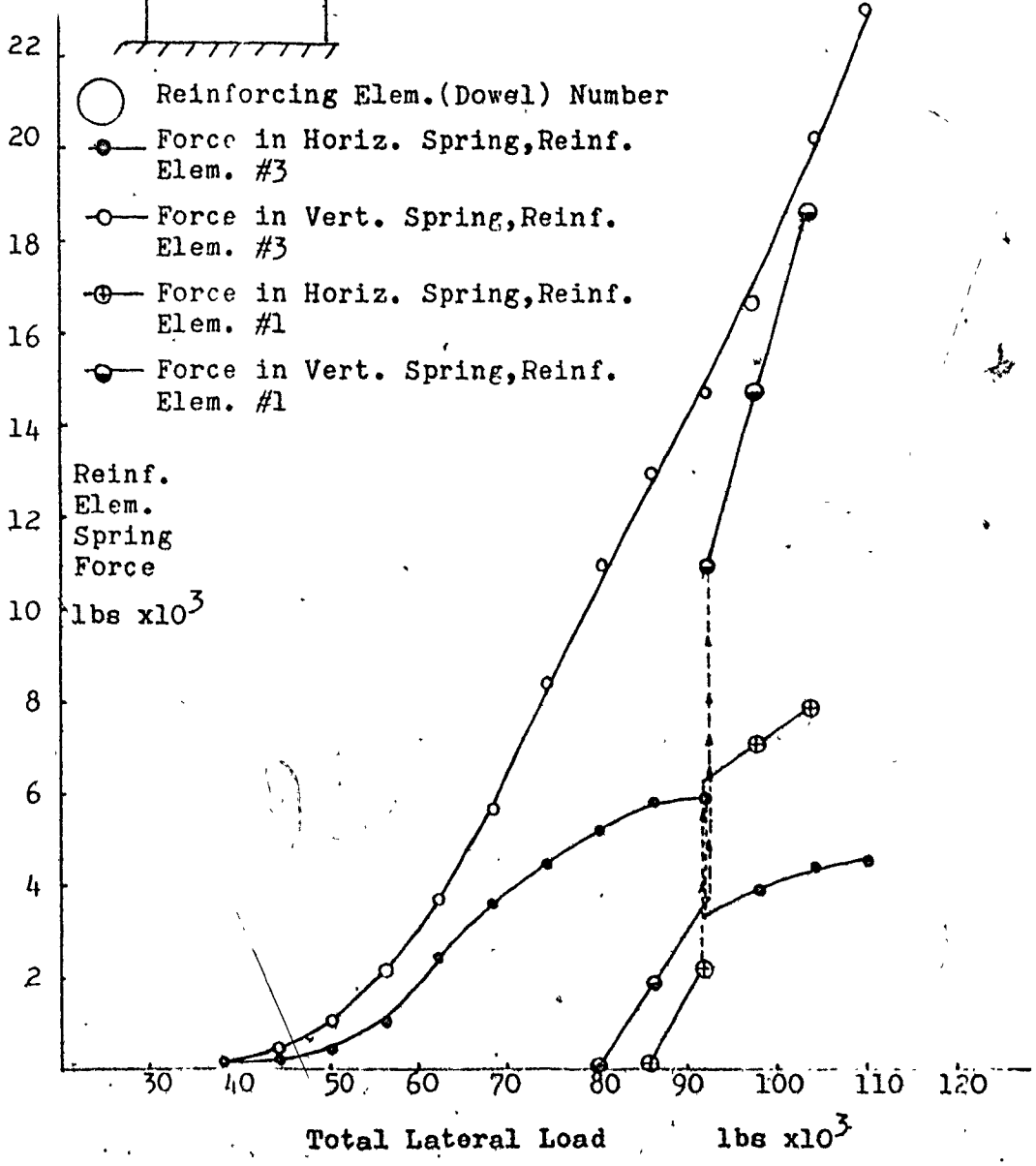

Fig.3.39 Force in Reinforcing Elements Versus Total Lateral Load For Vertical Load Equivalent of 10 Storeys

the dowels situated on the right hand side of the joint are so small that they are not shown. For reinforcing element #3 the force in the vertical spring begins to increase rapidly after separation occurs in the vicinity of the element on slip surface 1. The forces in the horizontal spring (representing the dowel action) also increase,but at a much slower rate since no significant slip takes place at this stage. In Fig. 3.37 this trend continues until, at a total lateral load of approximately 43 kips, extensive cracking and separation occur on the left side of slip surface 2. This leads to a dramatic increase in the vertical spring force representing the reinforcing element #1. At the same time, the left hand portion of the concrete component of the joint including the floor slab separates from the rest of the structure (the connection is only through reinforcing elements #1, #3, the floor panels and the tie-beam's longitudinal reinforcement). As a result there is an appreciable and sudden reduction in the force carried by the horizontal spring of reinforcing element #3.

The above agrument can be applied to explain the behaviour of the reinforcing elements in Fig. 3.38 and Fig. 3.39. Any discrepancy that may be observed is simply due to the combined effects of normal and shear stresses acting on the joint arising from differences in the magnitude of the gravity loads. For example in Fig. 3.38, the load combination, the extent of cracking on slip surface 1, and the force in the horizontal spring of element #3 are

such that element #3 yields prior to cracking of the left hand portion of slip surface 2. Thus unlike the other two cases (Fig. 3.37 and Fig. 3.39), forces acting on element #1 are quite small and are not shown in Fig. 3.38.

3.16 Summary

Chapter 3 dealt with the behaviour of an isolated horizontal joint. The purpose of this study was to develop a realistic model for the joint and to use this model to investigate the behaviour of both reinforced and unreinforced joints. The joint behaviour was simulated using the finite element method for a variety of loading conditions. This was felt to be necessary, since the results obtained in this chapter will be used as the criteria for developing a simplified model which will be discussed in Chapter 5.

As expected, the joint response was found to be influenced by the magnitude of the gravity loads. With larger gravity loads, the capacity of the joint to resist shear forces increased. However, the joint response was found to be unaffected by the mode of shear transfer (for concentrated or distributed shear forces applied to the top of the upper panel). The ability of the joint to resist shear forces was also increased with the introduction of joint reinforcement. The effect of reinforcement was found to be more pronounced for joints with smaller gravity loads. For very large gravity loads, reinforcing a horizontal joint did not effect the joint capacity since

the

or shear. Another result of reinforcing a joint was to increase its ductility. This effect was again more pronounced for joints with smaller gravity loads.

The cracking of the tie-beams in cases where the floor panels were selected to be half as wide as the wall panels, caused a considerable increase in the deformation of the joint. In reinforced joints, however, the cracking of the tie-beam had a smoothing effect on the deformation curve of the joint. For joints with the floor panels as wide as the wall panels, a sudden increase in the joint deformation was observed. This was due to the formation of cracks along slip surface 2, and the accompanying sudden release of energy.

The accuracy of the analysis was tested by increasing the number of finite elements representing the joint. The differences in the results were marginal. It was thus concluded that the accuracy of the analytical prediction of the joint behaviour was not improved significantly by using more than a total of 16 joint elements.

It was originally thought that perhaps this analysis could be simplified by treating the panels as rigid components. The validity of this assumption was tested by assigning a very high value to Young's modulus for panels and reducing Poission's ratio to zero. The joint response was found to be significantly effected by the assumption of rigid panels and thus it was decided that the deformations in panels would have to be incorporated in the analysis.

The effect of the shape and size of panels on the joint response was also briefly investigated. The study was aimed at establishing the joint response for panels of various sizes and shapes, so that it could serve as a basis for establishing the accuracy of the simplified model of Chapter 5. Except for minor variations, the joint response was found to be similar to the other cases reported previously.

The effect of a change in the location of the reinforcing bars was investigated by moving them from their usual location 16 inches in from the edge to the edge of the panel. The reason for this was that in the simplified 2 or 3-3-element joint model which will be investigated later, there is no choice but to connect the reinforcing bars to the panel nodes located at the very edge of the panel. The analysis showed that a change in the location of the reinforcing bars, produced only marginal effects on the joint response.

The analysis also provided an indication of the magnitude of dowel and tensile forces developed in the reinforcing bars, and the criterion for yielding allowed for the prediction of the ultimate loads for the reinforced horizontal joints.

CHAPTER 4

ANALYSIS OF VERTICAL JOINTS

4.1 Introduction

The lateral deflection of a complex cantilever is influenced to a great extent by the behaviour of its vertical connections. For complete interactions (assuming a no-tension situation for the horizontal joints) the complex cantilever is equivalent to a simple cantilever of equal second moment of area. If there is no interaction along the vertical joints, the complex cantilever behaves like a number of independent simple cantilevers. In reality the degree of interaction is between the above two extremes and is dependent on the deformation of the joint as will be explained in the following sections.

In this chapter the element stiffness matrices at various stages of deformation referred to as phases are developed. These matrices are used to simulate the behaviour of the joint. The available experimental data is employed to determine the unit shear stiffness coefficients. These coefficients are necessary in constructing the joints material stiffness matrix after a splitting crack has appeared along the joint. To simulate the behaviour of the elements representing a split joint, an additional term referred to as the apparent coefficient of friction for shear-key joints is also developed. After constructing the element stiffness matrices

for various phases of joint behaviour, the behaviour of a push-off specimen for which test results are available is simulated. Once it is determined that the finite element model produces reasonable results compared with a simple test specimen, the behaviour of vertical joints is investigated using the same criteria.

As will be indicated in Section 4.3, in order to be able to proceed with the analysis of vertical joints, some important background material must first be introduced. The author has chosen to do this by referencing the experimental and/or theoretical studies of a number of recent investigators. For the sake of brevity only the most relevent topics will be mentioned. Appendix A should be consulted for other details.

However, before proceeding with the background material and the actual analysis, it is important to introduce the vertical joints and the various techniques used to achieve interaction. Although for the purpose of actually simulating the behaviour, certain specific dimensions and characteristics have to be considered (based on good current construction practices), it is important to emphasize that the method of analysis developed will be applicable to various types of vertical joints with only minor adjustments.

The remainder of this introductory section will be devoted to a brief discussion of various types of vertical joints.

(a) Vertical Joints

In complex cantilevers, the rigidity of the assembly as well as the distribution of internal stresses are greatly

influenced by the degree of interaction provided by their vertical connections. The degree of interaction in turn, is very much dependent on the type and the strength of the vertical joints used in construction. Thus, the study of complex cantilevers especially in the nonlinear range is meaningless, without a thorough understanding of the behaviour of their vertical joints.

One of the most important factors affecting the vertical joint behaviour is the type or the shape of joint as determined by its dimensions and profile. Fig. 4.1(a) illustrates, schematically, some types of vertical joints used in panel buildings. These can be divided into 3 basic groups as follows:

1. plane joints,
2. grooved joints and
3. shear-key joints

The shear-keys may be distributed along the entire length of the joint or they may be localized. The joints may also be divided into two categories on the basis of being reinforced or unreinforced. However, good practice dictates that only reinforced joints be used in complex cantilevers. This is because normal compressive forces (if any) acting on vertical joints are quite small, and thus once the joint is split (with the possible exception of shear-key joints), the shear resisting capacity is completely destroyed. Even with shear-key joints the performance is improved by reinforcing the joint. Reinforcing a vertical joint is in general much simpler than reinforcing a horizontal joint. The most common methods of

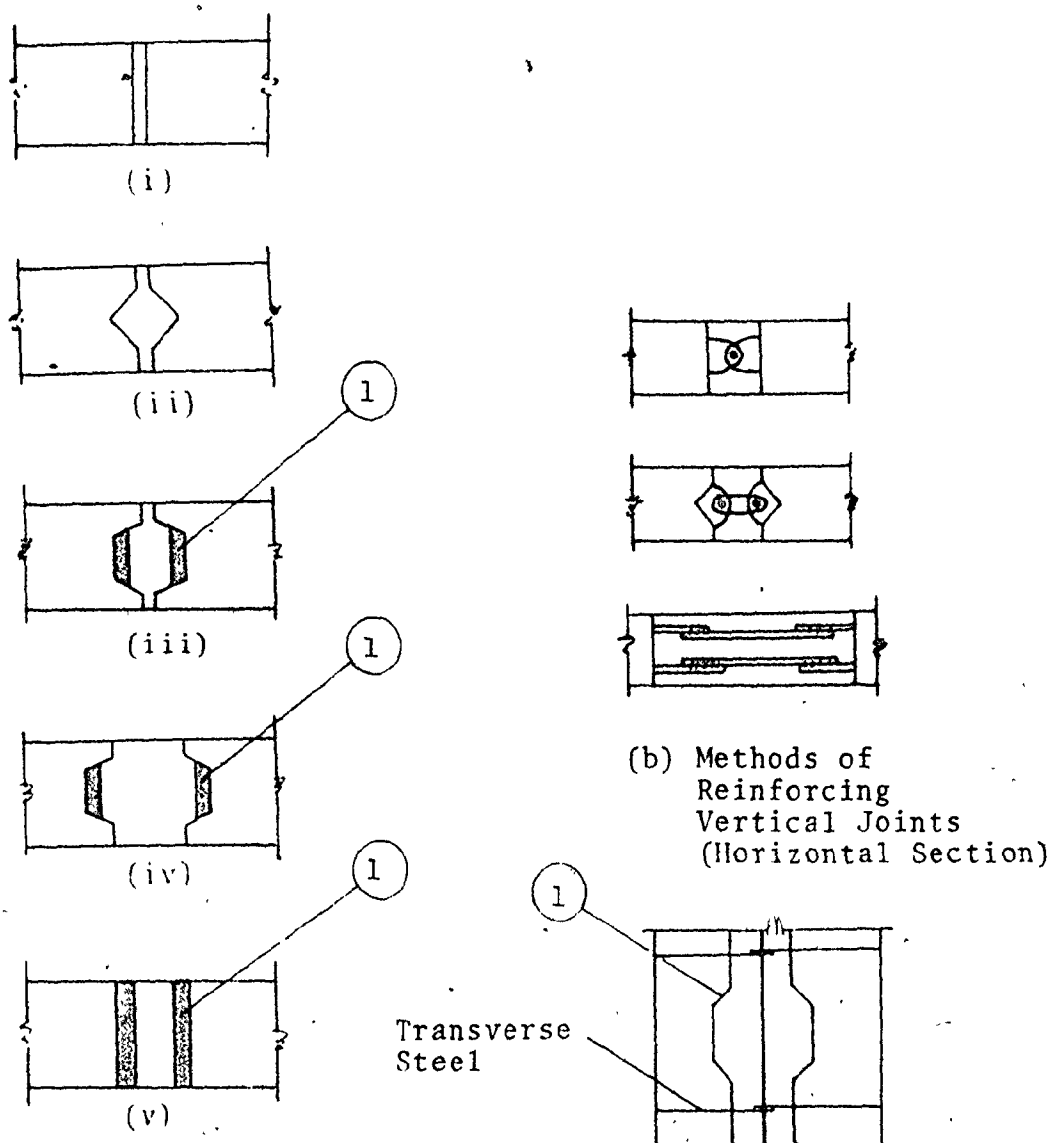

Fig. 4.1 Schematic Representation of Some Typical Vertical Joints

achieving this are illustrated in Fig. 4.1(b). Typical joint dimensions are given in Fig. 4.1(c) for a reinforced vertical joint with distributed shear keys. More will be said about vertical joints in the following sections in which a typical model will be developed for inclusion in the analysis of complex cantilevers.

4.2 Previous Contributions

(a) Cholewicki's Work[12]

One of the most interesting recent studies dealing with the behaviour of vertical joints is that of Cholewicki[12]. His work is particularly valuable because he supplemented his experimental investigations with theorectical considerations and arrived at a number of semi-emperical relationships for the assessment of the shear capacity of vertical joints.

Under the action of shear forces, vertical joints are likely to behave in one of two characteristic ways (Fig. 4.2). As long as bond is not broken, the joint is said to be in phase I. The range of loading associated with the phase extends up to the point where splitting takes place along at least one face of the panel. When bond is broken the joint is said to be (where applicable) in phase II. The loading range for phase II extends to failure.

Both of these phases are not necessarily observed in all types of joints. For example, in some grooved joints tested by Cholewicki, splitting did not occur at all, and the joint ultimately failed by cracking within the body of the in-fill concrete.

The pattern of behaviour is influenced by the following

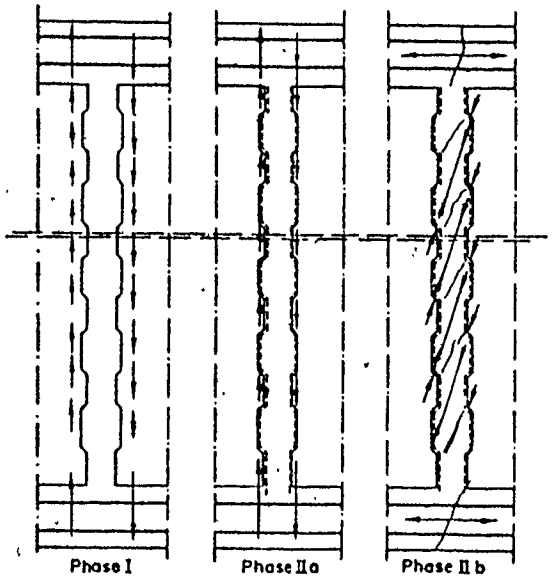

(a) Schematic Representation of Various Working Phases

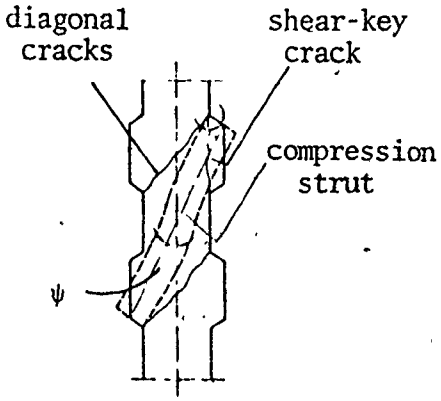

(b) Schematic Representation of a Joint in phase IIb and Formation of an Inclined Compression Strut

Fig. 4.2 Various Phases of a Shear-Key Joint (Cholewicki[12])

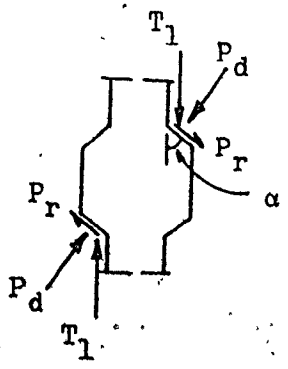

Fig. 4.3 Shear Force Components in Shear-Key Joints After Splitting (Cholewicki[12])

physical characteristics of the joint:

1. the type of joint (plane, grooved or keyed),
2. the strength of the in-fill concrete or grout, and
3. the amount, distribution and strength of transverse reinforcing steel

By studying the test results reported by several researchers (a summary of their work is given in reference 12), it may be concluded that in almost all cases for reinforced joints, ultimate failure is preceded by cracking and disintigration of the in-fill concrete. This, however, may occur in phase I or the joint could split (phase II) before cracking and disintegration occurs. The term 'cracking' as used here refers to both the diagonal cracks and the possible shearing off of the keys.

For an unreinforced joint, splitting or cracking, whichever occurs first, marks the end of the joint's shear capacity. For an isolated joint, there is no possibility of the joint transmitting forces in phase II.

A reinforced joint may continue to function in phase II. In this situation Cholewicki made the following distinction (Fig. 4-2):

1. phase IIa - working phase after splitting but before the appearance of diagonal cracks, and
2. phase IIb - after the formation of diagonal cracks.

In phase IIb the joint still functions because of the formation of a system of small concrete columns which act like inclined compression struts between the adjacent faces of the

panel. This is shown in Fig. 4.2(b). Although shear key cracks may have appeared at this stage, it is assumed that transverse steel prevents the dislocation of the keys and hence enables them to continue functioning.

Joint reinforcement produces different effects for different phases. In phase I, regardless of the type of joint, the stresses in the reinforcement are very small and their effect on the overall behaviour of the joint is negligible. According to Cholewicki, the effect of the steel in this phase is to limit microcrack propagation along the contact faces, and hence to increase the splitting loads. Halasz [23], however, found that increasing the steel ratio did not increase the splitting loads.

In phase II, the role of the steel is influenced by the shape (type) of the joint. Cholewicki suggested that for plane and grooved joints the transverse steel carries the full shear force. This assumption completely neglects the clamping effects and the resulting shear resisting capacity produced by transverse steel (see Shear-Friction Theory, Section 3.3).

Cholewicki proposed the following scheme for the determination of stress in a shear-key type of joint after splitting assuming that no cracks appear in the body of the in-fill concreate. Referring to Fig. 4.3, if T_1 represents the shear force carried by one key, then

$$T_1 = T/m \qquad (4.1)$$

where T is the total shear force carried by the vertical joint and m is the number of keys.

The compressive and slipping forces are expressed by

the following relationship respectively.

$$P_d = T_1 \sin \alpha \tag{4.2}$$

and

$$P_r = T_1 \cos \alpha \tag{4.3}$$

The resistance to slipping provided by the force Q_t, is expressed as

$$Q_t = \mu \cdot P_d \tag{4.4}$$

where μ is the coefficient of friction between the edge of the panel and the in-fill concrete. To avoid slip, P_r should not exceed Q_t

$$P_r < Q_t \tag{4.5a}$$

or

$$T_1 \cos \alpha < T_1 \sin \alpha \cdot \mu \tag{4.5b}$$

or

$$\therefore \quad \text{Tan } \alpha > \frac{1}{\mu} \tag{4.5c}$$

If μ is taken to be 0.7, then

$$\alpha > 55 \tag{4.6}$$

This means that slip does not occur if angle α is greater than 55° provided that the coefficient of friction has a value of 0.7.

When $\alpha < 55°$ the transverse steel provides resistance against slipping by taking the horizontal component, ΔZ, of the slipping force.

$$\Delta Z = \frac{m\ (P_r - Q_t)}{\sin \alpha} = \frac{m\ (T_1 \cos \alpha - T_1 \sin \alpha \cdot \mu)}{\sin \alpha}$$

$$= mT_1\ (\cot \alpha - \mu) \tag{4.7a}$$

Equation (4.7a) overestimates the force produced in the transverse steel because it does not take into account the extra compression produced on the inclined surfaces of the shear-keys due to the clamping action of the transverse reinforcement. Taking clamping into account, equation (4.7a) may be modified as follows:

$$\Delta Z = m \frac{T_1 \cos \alpha - T_1 \sin \alpha \cdot \mu}{\sin \alpha + \cos \alpha \cdot \mu} \qquad (4.7b)$$

After the appearance of the diagonal cracks (phase IIb), the tensile forces in the reinforcing bars increase up to a maximum value given by

$$Z = mT_1 \tan \psi \qquad (4.8)$$

where ψ is the angle between the compression strut and the vertical.

Based on test results, Cholewicki found that it was more effective to disperse the transverse steel through the length of the joint rather than to concentrate it at the level of the tie-beams.

The effect of longitudinal steel was to strengthen the transverse steel anchorage when it was made in a loop form and dispersed through the length of the joint. It also helped to protect the joint against horizontal shrinkage cracks and acted to inhibit further cracking when the system of small concrete columns appeared in phase IIb.

Based on tests conducted on a number of joints of varied physical characteristics (see Appendix A), Cholewicki produced an empirical formula to represent the joints' load bearing capacity. These relationships together with an out-

line of the experimental work are pressented in Appendix A.

The deformation of the joints in phase I may be approximated by the following relationship (using Cholewicki's notation)

$$\Delta = \frac{\tau}{G} a = \frac{T}{A_v G} a \qquad (4.9)$$

where τ = shear stress,

a = width of the joint,

G = shear modulus,

T = shearing force

A_v = cross sectional area, and

Δ = shear deformation of the joint.

For joints which are split (phase IIb), the shear stiffness may be given by the following relationship:

$$K_{II} = \frac{\Delta\tau}{\Delta v} \qquad (4.10)$$

where $\Delta\tau$ = increment of shear stress, and

Δv = increment of shear displacement

The reason that this is based on an incremental analysis is evident from Fig. 4.4, where in phase II the behaviour is not linear and the magnitude of deformation is predominant. Thus, in phase II the values of K_{II} must be found experimentally.

(b) Halasz's Tests

Halasz's[23] test results are particularly interesting because they exhibit the type of behaviour and phases discussed above. He found that the shear capacity of shear-key type joints was much higher than that of plane joints even though

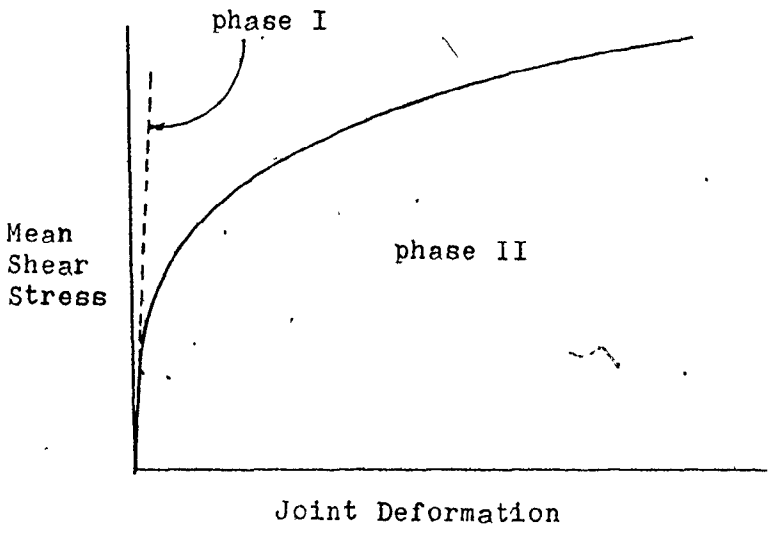

Fig. 4.4 Typical Shear Deformation Curve for a Vertical Joint

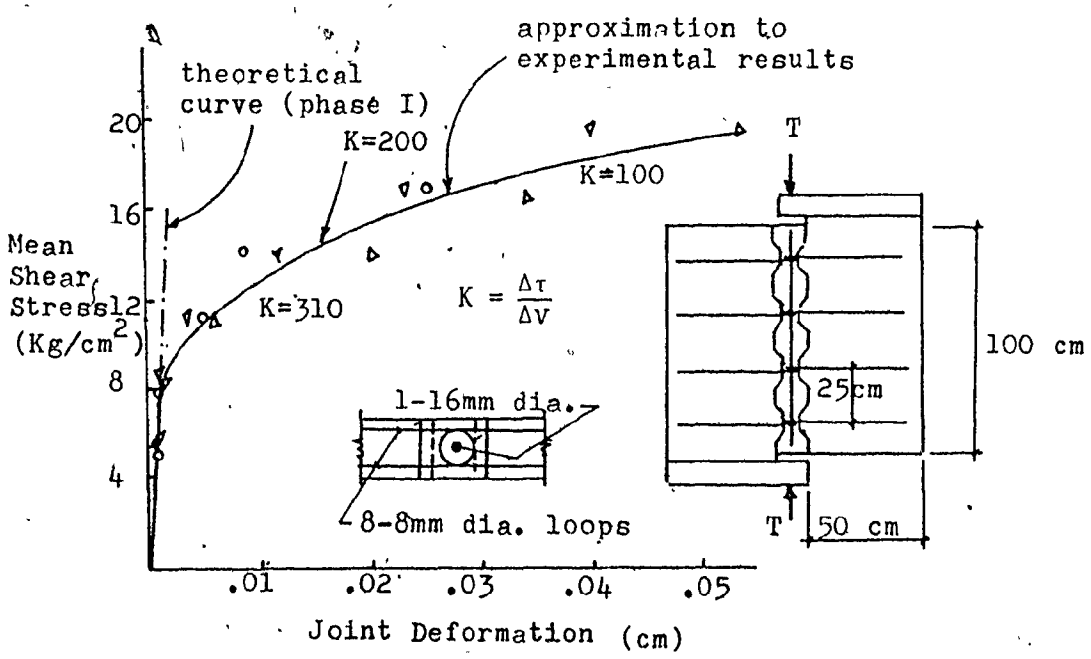

Fig. 4.5 Halasz's Mean Shear Stress Versus Deformation Curve for Reinforced Shear Key Joints

both types were filled with concrete of the same strength and were identically reinforced. He also found that splitting along the contact surfaces was independent of the transverse steel ratio, and occurred at an average shear stress of about 8 kg/cm^2 (112 psi). Joints exhibited high stiffness prior to splitting. After splitting, however, the joint stiffness was reduced considerably and deformations at failure were many times greater than those measured at the end of phase I. For reinforced shear-key type joints failure occurred at shear stresses two to five times greater than those which caused splitting. Failure immediately followed the formation of diagonal cracks and the local crushing of concrete around the steel loops. One type of joint which was not transversely reinforced failed due to slippage along the contact surfaces in all cases.

Halasz's test results for reinforced shear-key type joints exhibited good strength and ductility properties, represented simplicity of construction and produced the various phases of deformation. Therefore, they have been utilized for determining the unit stiffness coefficients for a typical vertical joint. These coefficients are in turn used in subsequent sections to develop the material stiffness matrices for joint elements after splitting.

A sketch of Halasz's test specimen and his experimental results for stress versus slip are shown in Fig. 4.5.

(c) Other Works

The behaviour of vertical joints has been investigated experimentally by a number of other researchers. Some of these

works are summarized in Appendix A. Among these the contributions made by Pommeret[12] and Armour[2] are particularly interesting.

Pommeret tested a large number of joints having varied physical characteristics. His experiments are very useful in studying the influence of various joint parameters such as tranverse steel ratio, concrete strength and shear-key dimensions on ultimate load capacity.

Armer and Kumar[2] investigated the behaviour of large panel assemblies under the combined action of shear and bending moments. These tests are quite interesting because the vertical joint is studied in the context of an assembled structure. Details of Armer's tests are summarized in Appendix A, part (e). The physical characteristics of these joints were not the same as those studied here; nevertheless, they provide worthwhile evidence of the general behaviour.

There are a number of other studies which could be mentioned in relation to vertical joint behaviour. Although these studies promote a general understanding of the problem, they are not used in the present study, and hence will not be discussed further.

4.3 Finite Element Representation of a Push-Off Test Specimen

The next few sections of this chapter are devoted to the development of a finite element model capable of simulating the behaviour of vertical joints. Before actually analyzing the joint used in this study, it is interesting to

compare the finite element prediction with Halasz's test results in order to evaluate the accuracy of the model. Therefore, the initial discussion of development of the analytical model will be with reference to Halasz's test specimen.

Figures 4.6(a) to (d) diagrammatically represent Halasz's test specimen and its finite element model. The two halves of the test specimen are modelled using a number of rectangular elements, each consisting of 4 triangular elements with the centre node eliminated. The procedures dealing with this type of element and the formation of its stiffness matrix were discussed in Chapter 2, and will not be repeated here. The joint itself is represented by means of a number of joint elements evenly spaced along the vertical edge. These elements connect the two halves of the test specimen. A joint element consists of a pair of dimensionless springs which simulate the normal and the shear stiffnesses of the corresponding area of the joint, and are denoted by K_{nc} and K_{sc} respectively (Fig. 4.6(e)).

4.4 Determination of Unit Stiffness Coefficients

(a) Phase I

In phase I the specimen acts essentially as a monolithic material. Therefore, the unit shear and normal stiffness coefficients are determined on the basis of the elastic properties of concrete. Concrete is assumed to behave in an elastic-plastic fashion. As was pointed out by Cholewicki[12] and Halasz[23], the contribution of transverse steel can be considered to be negligible in this phase.

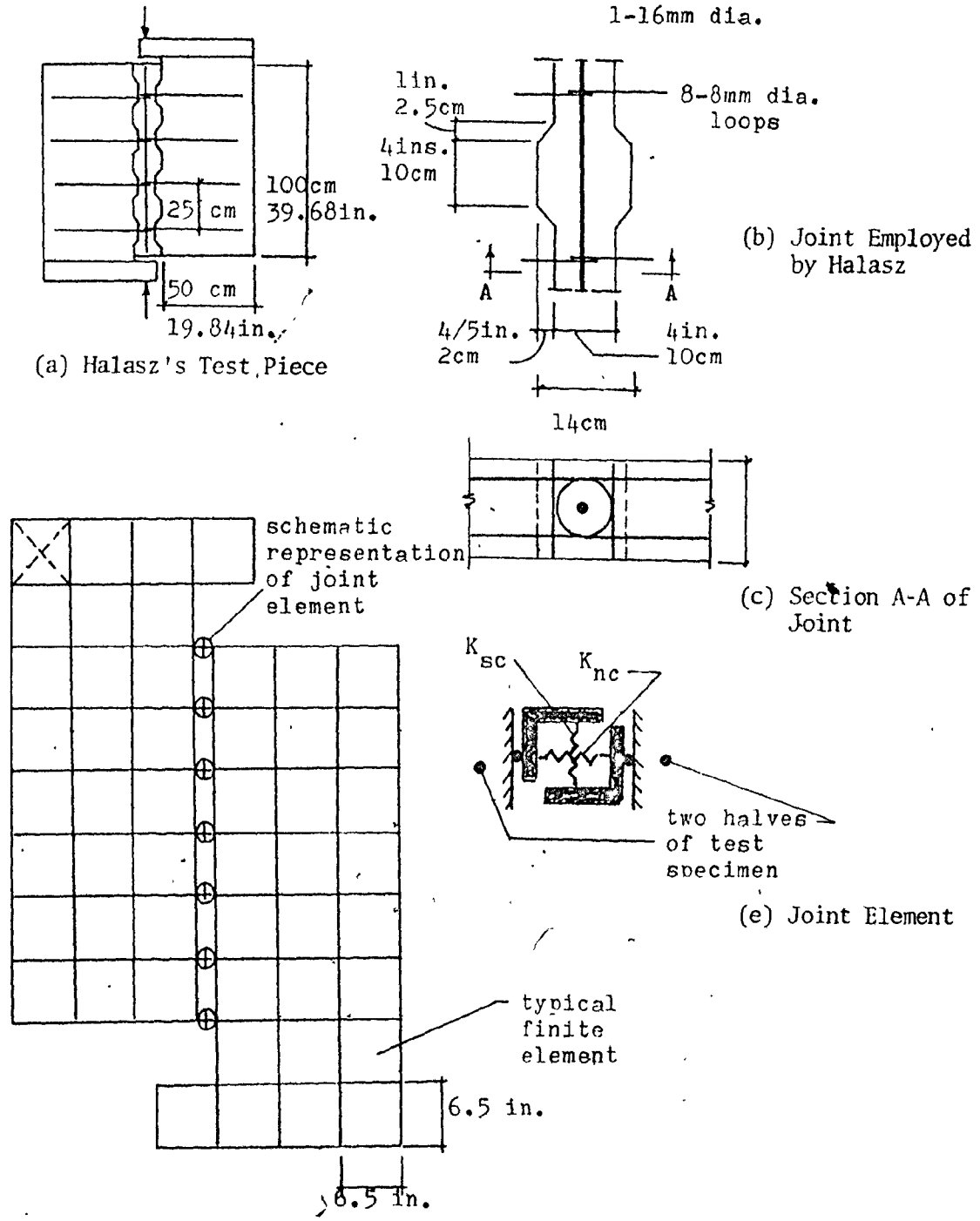

(a) Halasz's Test Piece

(b) Joint Employed by Halasz

(c) Section A-A of Joint

(e) Joint Element

(d) Finite Element Model of Halasz's Test Specimen

Fig. 4.6 Finite Element Representation of Halasz's Test Specimen

With reference to Fig. 4.7(a), the unit shear stiffness coefficients can be determined as follows:

$$G = \frac{\tau}{\gamma} = \frac{\tau}{\Delta/a} \text{ and } G = \frac{E}{2(1+\nu)}$$

where G = shear modulus,

γ = shear strain,

τ = shear stress,

a = width of the joint,

Δ = shear deformation, and

ν = Poisson's ratio.

For the purpose of the analysis, the block shown in Fig. 4.7(b) must be replaced by a fictitious dimensionless spring which would deform a distance of Δ when subjected to a shear force of equal magnitude. The unit shear stiffness coefficient, k^I_{sc}, is therefore defined as being numerically equal to the force which is required to cause a shear deformation, Δ, of unity. Hence

$$k^I_{sc} = \frac{\tau}{\Delta} = \frac{G}{a} \qquad (4.11)$$

In equation (4.11), with unit shear deformation, Δ, τ is numerically equal to the shear force when the side of the block in Fig. 4.7 has a unit area. The contribution of a concrete element to the shear stiffness of the joint is then given by

$$K^I_{sc} = k^I_{sc} \cdot A \qquad (4.12)$$

where A = area of the concrete joint element.

A similar procedure can be adopted to determine the unit normal stiffness coefficient, k^I_{nc}. This can be defined as being numerically equal to the normal force required to

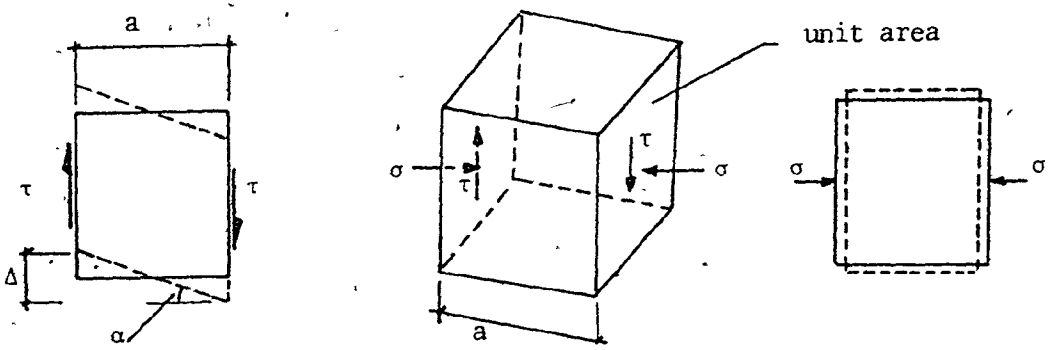

(a) Shear Deformation (b) Free Body Diagram of an Element in the Joint Region (c) Normal Deformation

Fig. 4.7 Determination of Unit Shear and Normal Stiffness Coefficients

cause a normal deformation of unity. Thus if

$$P = \frac{AE\varepsilon}{a} \qquad (4.13a)$$

where E = elastic modulus, P = normal force, and ε = normal deformation

then $$k^{I}_{nc} = \frac{E}{a} \qquad (4.13b)$$

and $$K^{I}_{nc} = k^{a}_{nc} \cdot A \qquad (4.14)$$

where K^{I}_{nc} = Normal stiffness associated with a joint element of area A.

(b) Phase II

Unit shear stiffness coefficients in phases II must be determined on the basis of experimental results. Halasz's test results in Fig. 4.5 have been converted to imperial units and are shown in Fig. 4.8. As can be seen, the behaviour in phase II can be approximated by a straight line. The unit shear stiffness coefficient, k^{II}_{sc}, is then obtained directly from the slope of this line.

or $$k^{II}_{sc} = \frac{\tau}{\Delta} \qquad (4.15)$$

and $$K^{II}_{sc} = k^{II}_{sc} \cdot A \qquad (4.16)$$

where K^{II}_{sc} = shear stiffness associated with a joint element of area A.

It is important to note that the contribution of the transverse steel to the shear strength has already been taken into account in equation (4.16) and should not be included again when the stiffness matrix of steel element is constructed. Thus

$$K^{II}_{ss} = k^{II}_{ss} = 0 \qquad (4.17)$$

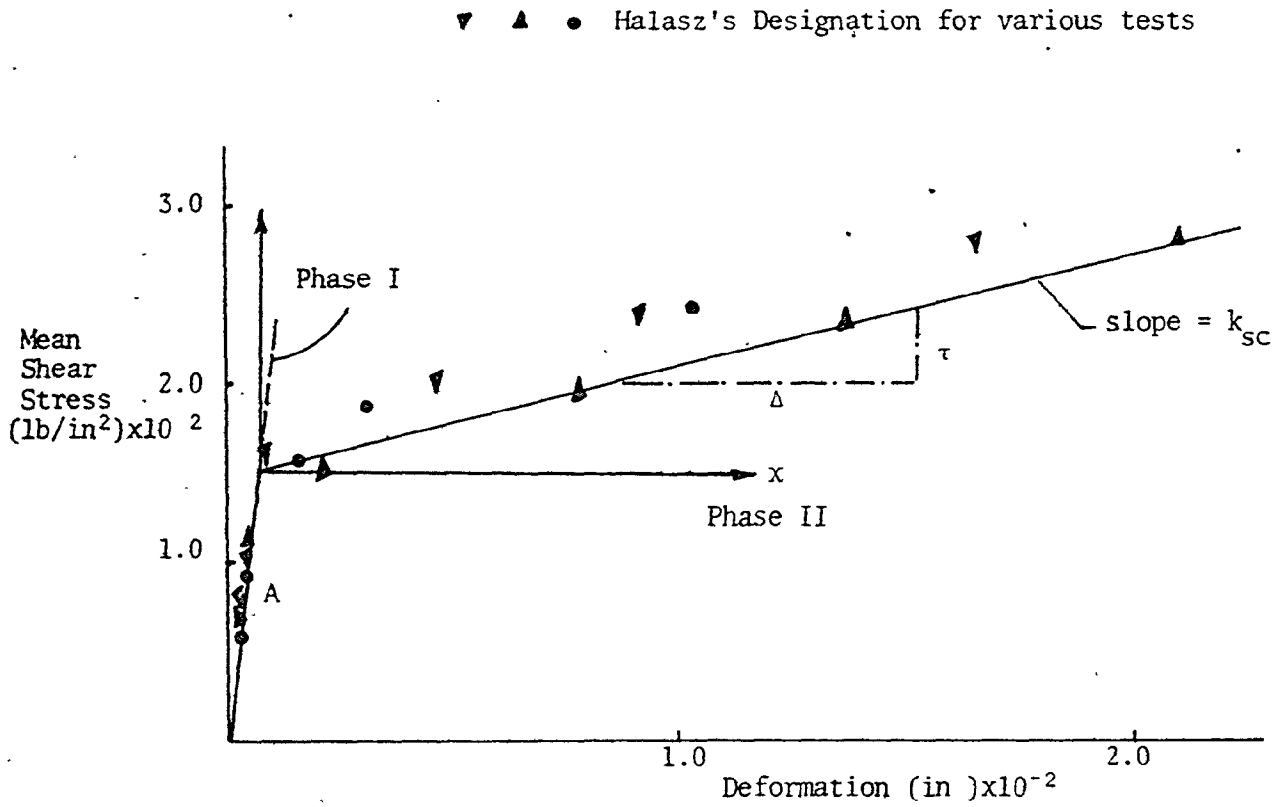

Fig. 4.8 Halasz's Test Results Drawn in Imperical Units

The normal stiffness of the joint in phase II depends on the stiffness provided by the transverse steel. After splitting, steel provides for continued functioning of the joint by producing the necessary clamping force. The normal stiffness in phase II may be estimated quite easily if its shear stiffness in phase II, its geometry and its coefficient of friction at the interface are known. However, before proceeding to determine the normal stiffness of a joint, an additional term henceforth referred to as the apparent coefficient of friction for a shear-key joint must be introduced.

4.5 Development of the Apparent Coefficient of Friction For Shear-Key Joints and the Vertical Joint's Normal Stiffness Coefficient

Recalling the shear friction theory discussed in Chapter 3, and referring to Fig. 4.9(a) it is observed that slip along surface s-s will not occur unless the shear force, V, is greater than P times the coefficient of friction, μ. When reinforcement is provided (Fig. 4.9(b)) a clamping force is created by the steel as one surface slips up the asperities of the other surface. If N is the tensile force created in the steel reinforcement, then the shear force, V, corresponding to the clamping force, N, is given by

$$V = N \cdot \mu \tag{4.18}$$

Replacing mT_1 by T_m in equation (4.7b) and isolating T_m yields

$$T_m = \Delta Z \left(\frac{\sin \alpha + \cos \alpha \cdot \mu}{\cos \alpha - \sin \alpha \cdot \mu}\right) \tag{4.19}$$

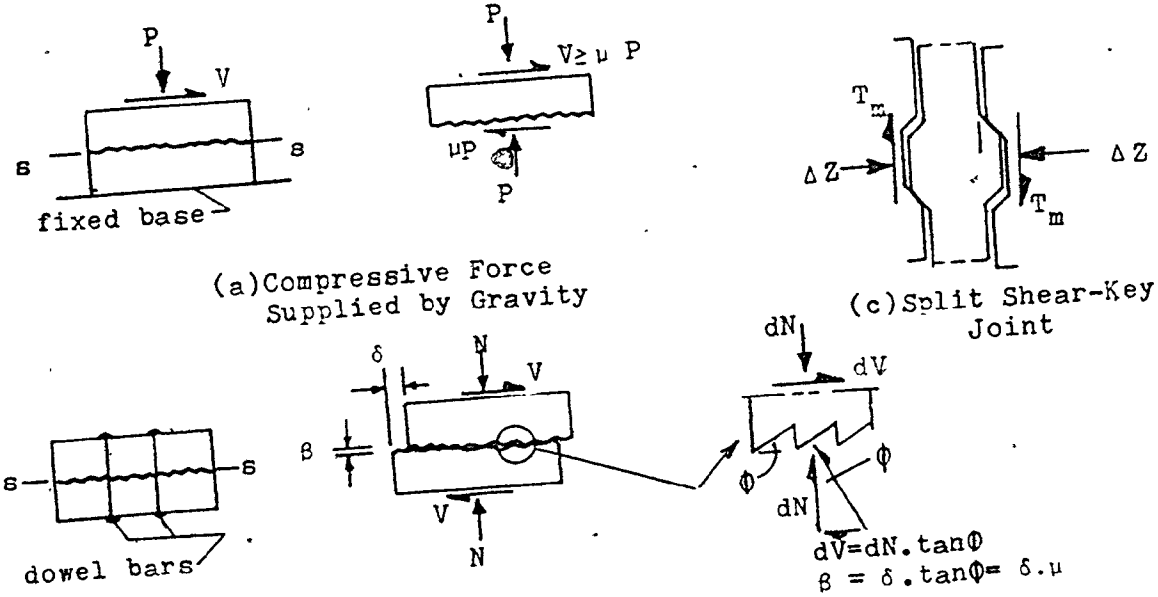

(a)Compressive Force Supplied by Gravity

(c)Split Shear-Key Joint

(b)Compressive Force Supplied by Clamping Action of Dowel Bars

Fig. 4.9 The Apparent Coefficient of Friction by Comparison with Shear Friction Theory

where ΔZ = the clamping force provided by the transverse steel, and

T_m = the shear force

Comparing equations (4.18) and (4.19) term by term yields a value for the apparent coefficient of friction of a shear-key joint as given by

$$\bar{\mu} = \frac{\sin \alpha + \cos \alpha \cdot \mu}{\cos \alpha - \sin \alpha \cdot \mu} \qquad (4.20)$$

where $\bar{\mu}$ = apparent coeff. of friction for a shear-key joint

μ = coeff. of friction for a joint surface after splitting, and

α = angle of inclination of the shear-key (see Fig. 4.9(c)).

Returning to the problem of determining the normal stiffness of a joint in phase II, equation (4.19) may be written as

$$\frac{Tm}{Av} = \frac{\Delta Z}{Av} \bar{\mu} \qquad (4.21)$$

where Av = total area of the joint

With reference to Fig. 4.8 $\frac{Tm}{Av}$ can be written as

$$\frac{Tm}{Av} = k_{sc}^{II} \cdot \delta \qquad (4.22)$$

where δ = shear deformation in phase II corresponding to $\frac{Tm}{Av}$ measured with respect to the x-y coordinates.

For $\delta = 1$, equation (4.21) reduces to $\frac{\Delta Z}{Av} = k_{sc}^{II} \cdot \frac{1}{\bar{\mu}}$ (4.23)

In equation (4.23) ΔZ is the clamping force corresponding to a unit shear deformation. As may be seen from Fig. 4.9b, a normal separation β is always associated with δ as one surface slides up the asperities of the other surface. Referring to the enlarged portion of the slip surface shown in Fig. 4.9b, β may be written as $\delta \cdot \tan \phi$ or $\delta \cdot \mu$. Thus, utilizing the apparent coefficient of friction for a shear-key joint, the normal separation associated with a unit shear deformation is given by

$$\beta = \bar{\mu} \text{ for } (\delta=1)$$

By definition the normal stiffness coefficient is numerically equal to that force (per unit area) which causes a normal deformation of unity. Hence,

$$k_{ns}^{II} = k_{sc}^{II} \frac{1}{\bar{\mu}^2} \tag{4.24}$$

The numerical values for the unit stiffness coefficients and the apparent coefficient of friction used in this analysis are summarized in the following table.

Notation	Numerical Values	
k_{sc}^{I}	3.25×10^5	lb/in^3
k_{nc}^{I}	7.50×10^5	"
k_{sc}^{II}	6.30×10^3	"
k_{ss}^{II}	0	
k_{ns}^{II}	5.4×10^2	"
$\bar{\mu}$	3.41	

Table 4.1 Numerical Values for Unit Stiffness Coefficients and the Apparent Coefficient of Friction for a Shear-Key Joint

In table 4.1, Roman numerals I and II refer to phase I and II respectively. The first subscript of k indicates direction (s and n for shear and normal) and the second subscript denotes the material (concrete or steel).

4.6 Meaning of Apparent Coefficient of Friction

Referring to Fig. 4.3 it is noted that a portion of the externally applied shear force T_1 is used to provide resistance against slip by creating compression over the inclined side of the key. As long as P_r is less than Q_t (see equations (4.3) and (4.4)), slip does not occur. After the occurrence of slip, additional clamping forces are provided by the transverse steel. In the finite element representation of the joint (Fig. 4.6(d)), no allowance is

made for that portion of the shear force which provides resistance against slip. After the splitting of the joint all resistance to shear must be provided through the clamping action of the transverse steel. By the use of the apparent coefficient of friction which includes the contribution of the shear-key, it is possible to get a more realistic estimate of the clamping forces.

The following example in which a plane and a shear-key joint are compared for their respective clamping forces, may help to clarify the discussion.

If F_{sp}, K_{sp}, W_{sp} and F_{sk}, K_{sk}, W_{sk} are the shear forces, the stiffnesses and the deformations for plane and shear-key joints respectively, than

$$F_{sp} = K_{sp} \cdot W_{sp} = F_{np} \cdot \mu$$

and

$$F_{sk} = K_{sk} \cdot W_{sk} = F_{nk} \cdot \bar{\mu}$$

where F_{np} and F_{nk} are the normal clamping forces for plane and shear-key joints and $\bar{\mu}$ is the apparent coefficient of friction.

$$F_{nk} = \left[K_{sk} / \bar{\mu}\right] W_{sk} \qquad)$$

or $$\frac{F_{nk}}{F_{np}} = \frac{0.7}{3.41} \cdot \frac{K_{sk} \cdot W_{sk}}{K_{sp} \cdot W_{sp}} = \frac{0.7}{3.41} \cdot \frac{F_{sk}}{F_{sp}}$$

where $\mu = 0.7$ and $\bar{\mu} = 3.41$

if $\frac{F_{sk}}{F_{sp}} = 1$, i.e. requiring both joints to resist the same shear force, then $$\frac{F_{nk}}{F_{np}} = \frac{.7}{3.41} = 0.21$$

Thus a plane joint must develop approximately five times the clamping force required of a shear-key joint to resist the same shear force.

4.7 Development of the Joint Element Stiffness Matrices

(a) Phase I

The stiffness matrix of a concrete element in phase I (no slip) is very similar to that of a horizontal joint element when the shear force carried by the element had not yet become a function of the normal force. In this phase vertical and horizontal springs act completely independantly. With reference to Fig. 4.10 if vectors $\{W_1\}$ and $\{W_2\}$ denote the nodal displacements vectors of ends 1 and 2 respectively, then

$$\begin{Bmatrix} W_1 \end{Bmatrix} = \begin{Bmatrix} \delta_{x1} \\ \delta_{y1} \end{Bmatrix}$$

$$\begin{Bmatrix} W_2 \end{Bmatrix} = \begin{Bmatrix} \delta_{x2} \\ \delta_{y2} \end{Bmatrix}$$

If $\{W_r\}$ denotes the relative displacement vector between ends 1 and 2, then

$$\begin{Bmatrix} W_r \end{Bmatrix} = \begin{Bmatrix} W_x \\ W_y \end{Bmatrix} = \begin{Bmatrix} W_2 \end{Bmatrix} - \begin{Bmatrix} W_1 \end{Bmatrix} = \begin{bmatrix} -1 & 0 & 1 & 0 \\ 0 & -1 & 0 & 1 \end{bmatrix} \begin{Bmatrix} \delta_{x1} \\ \delta_{y1} \\ \delta_{x2} \\ \delta_{y2} \end{Bmatrix} \qquad (4.25)$$

$$= [B] \begin{Bmatrix} \delta_{x1} \\ \delta_{y1} \\ \delta_{x2} \\ \delta_{y2} \end{Bmatrix}$$

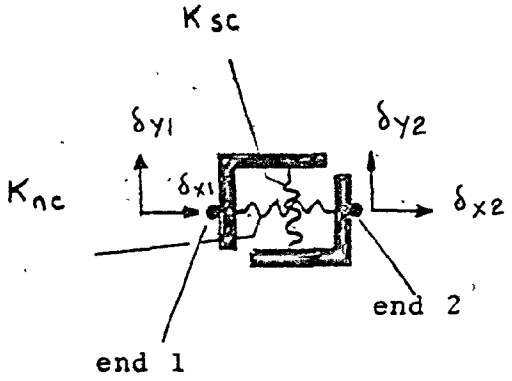

Fig. 4.10 Fictitious Dimensionless Finite Element for Vertical Joints

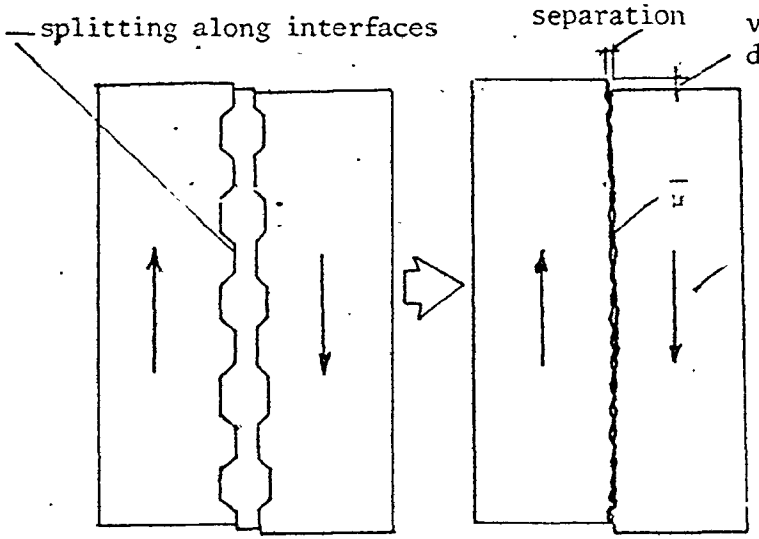

(a) A Shear-Key Joint in phase II (b) Model of a Shear-Key Joint using $\bar{u}$

Fig. 4.11 Modelling of a Shear-Key Joint Using the Apparent Coefficient of Friction

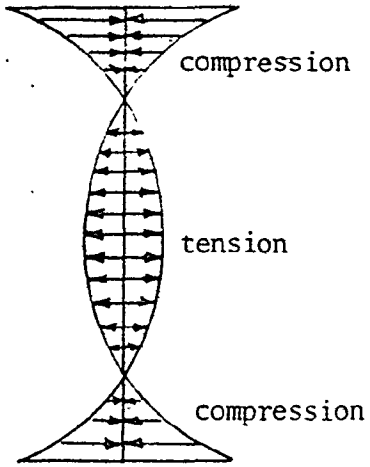

Fig. 4.12 Normal Stress Distribution Resulting from the Deformation of the Material Surrounding the Joint

If $[K_c^I] = \begin{bmatrix} K_{nc}^I & 0 \\ 0 & K_{sc}^I \end{bmatrix}$ is the diagonal concrete element property matrix for phase I conditions, then the stiffness matrix of concrete element in phase I (see Section 3.5) is given by

$$\bar{K}_c^I = [B]^T [K_c^I][B] = \begin{bmatrix} K_{nc}^I & 0 & -K_{nc}^I & 0 \\ 0 & K_{sc}^I & 0 & -K_{sc}^I \\ -K_{nc}^I & 0 & K_{nc}^I & 0 \\ 0 & -K_{sc}^I & 0 & K_{sc}^I \end{bmatrix} \qquad (4.26)$$

As was mentioned previously, the contribution of transverse steel before splitting (phase I) is negligible. Thus the stiffness matrix of steel element in this phase is in the form of a null matrix.

$$\bar{K}_s^I = \begin{bmatrix} 0 & 0 & 0 & 0 \\ 0 & 0 & 0 & 0 \\ 0 & 0 & 0 & 0 \\ 0 & 0 & 0 & 0 \end{bmatrix} \qquad (4.27)$$

The stiffness matrix of a joint element before splitting, is then given by the following equation

$$\bar{K}_j^I = \bar{K}_c^I + \bar{K}_s^I = \bar{K}_c^I \qquad (4.28)$$

The forces in the normal and shear springs are given by

$$\{F_c^I\} = \left[\bar{K}_c^I\right] \{W_r\} \qquad (4.29a)$$

In expanded form equation (4.29a) may be written as

$$\begin{Bmatrix} F_n \\ F_s \end{Bmatrix} = \begin{bmatrix} K_{nc}^I & 0 \\ 0 & K_{sc}^I \end{bmatrix} \begin{Bmatrix} W_x \\ W_y \end{Bmatrix} \qquad (4.29b)$$

(b) Phase II

In order to simulate the behaviour of a shear-key joint after splitting without constructing an intricate mesh of elements representing the various joint components, the shear-key joint is replaced by a plane joint using the apparent coefficient of friction. This is shown schematically in Fig. 4.11.

The development of joint element of stiffness matrices for phase II behaviour is slightly more complicated than for phase I because the property matrices for both steel and concrete involve off-diagonal elements. These represent the interaction which exists between the shear and normal joint springs after splitting.

Preliminary investigations showed that the deformation of the prefabricated components surrounding the joint has considerable influence on the stress distribution within the joints. The resulting normal stress distribution is shown in Fig. 4.12. When the joint is subjected to a shearing action, compressive stresses are over the top and bottom regions of the joint, while tensile stresses are created in the middle region. Furthermore, the normal stress distribution associated with the deformation of the prefabricated components is such that the sum of all the resulting normal forces is equal to zero. This kind of stress distribution is the result of an arching action which is created between the two prefabricated halves of a test (push-off) specimen.

Consequently, the material property matrix of a joint for the concrete element after splitting may be written as

$$\left[K_c^{II}\right] = \begin{bmatrix} K_{ns}^{II} & -K_{sc/\bar{\mu}}^{II} \\ -\bar{\mu}K_{ns}^{II} & K_{sc}^{II} \end{bmatrix} \qquad (4.30a)$$

Element (2,2) in this matrix represents the shear stiffness of the concrete element and by definition is numerically equal to the shear force created in the element when the joint undergoes a unit shear deformation. As the joint deforms, the clamping action of the joint's transverse reinforcement causes compressive forces to be generated along the joint surface. The magnitude of this force for a unit shear deformation is $-K_{sc/\bar{\mu}}^{II}$. This constitutes element (1,2) in the above matrix with minor sign signifying a compressive action. The effect of the deformation of the material surrounding the joint is taken into account by including elements (1,1) and (2,1) in the material property matrix. Element (1,1) represents the normal stiffness of the joint element after splitting (phase II). Element (2,1) reflects the influence of the deformation of the materials surrounding the joint on shear stress distribution along the joint.

The material property matrix for the steel element may be written as

$$\left[K_s^{II}\right] = \begin{bmatrix} K_{ns}^{II} & K_{sc/\bar{\mu}}^{II} \\ 0 & 0 \end{bmatrix} . \qquad (4.31a)$$

Elements (2,1) and (2,2) of this matrix are zero because it is assumed that no shear forces are directly resisted by the transverse steel. Whatever the contribution of steel, it is already incorporated in the shear stiffness of

the concrete element as indicated by element (2,2) in the property matrix of the joint element for concrete. As the joint undergoes a shear deformation of unity, tensile forces are created in the steel elements. The magnitude of these forces is the same as those exerted on the concrete element but are of opposite sign. Thus element (1,2) is given by $K^{II}_{sc/\bar{\mu}}$. Element (1,1) represents the influence of the deformation of the materials surrounding the joint on the distribution of the stresses in the transverse steel along the joint.

The stiffness matrices of the joint's concrete and steel elements are then given by

$$\bar{K}^{II}_c = [B]^T [K^{II}_c] [B] \tag{4.32}$$

for the concrete element, and

$$\bar{K}^{II}_s = [B]^T [K^{II}_s] [B] \tag{4.33}$$

for the steel element.

The stiffness matrix for the joint element after splitting (phase II), can then be expressed by the following equation:

$$\bar{K}^{II}_J = \bar{K}^{II}_c + \bar{K}^{II}_s \tag{4.34}$$

The normal and shear forces in the concrete and steel elements are given by equations 4.35 and 4.36 respectively.

$$\{F^{II}_c\} = \left[K^{II}_c\right] \{W_r\} \tag{4.35}$$

$$\{F^{II}_s\} = \left[K^{II}_s\right] \{W_r\} \tag{4.36}$$

where $\{W_r\}$ is the vector of relative nodal displacements.

4.8 Splitting Criterion

The maximum principal stress as determined from the normal and shear stresses existing for phase I conditions is used to determine the stress at which splitting commences in a vertical joint. If f_t is the tensile strength of the in-fill concrete, and f_t^* is the maximum principal tensile stress, then splitting is initiated when

$$f_t^* > R.f_t \qquad (4.37a)$$

where R is referred to as the interface strength reduction factor. The numerical value of R can vary from 0.5 to 0.95 as was discussed in subsection 3.4 (b), Part (i). Shrinkage stresses existing between the precast halves of the test specimen and the in situ joint concrete is another factor contributing to the weakness of the interface. For monolithically cast concrete R may be assumed to be unity.

The reduction in tensile strength across joints has been observed even for ordinary construction joints (15,16). In the case of construction joints, however, the cause is not likely to be shrinkage. (Bleeding and honeycombing are the more probable causes.) Regardless of the actual process, there is general agreement that the interface constitutes a definite zone of weakness.

As the maximum principal stress f_t^* approaches $R.f_t$, micro-cracks begin to form in the vicinity of the zone of weakness. As loads increase, micro-cracks also increase both in number and in size, and eventually join other micro-cracks and propagate along the interface to cause splitting.

With reference to equation (4.31a), if $\{F_c^I\} = \begin{Bmatrix} F_n \\ F_s \end{Bmatrix}$ is the vector of element forces for phase I, and if f_n and f_s are the normal and shear stresses corresponding to F_n and F_s, then

$$f_t^* = \sqrt{(\frac{f_n}{2})^2 + f_s^2} + \frac{f_n}{2} \qquad (4.38)$$

and the criterion for splitting (equation (4.37)) could be written as

$$\frac{\sqrt{(\frac{f_n}{2})^2 + f_s^2} + \frac{f_n}{2}}{R} > f_t \qquad (4.37b)$$

4.9 Transition from Phase I to Phase II

Considering a joint for which the τ-Δ graph is similar to that shown in Fig. 4.5 (i.e. both phases I and II exist), microcracks begin to form along the interface as joint approaches the end of phase I. Splitting, as mentioned earlier, is the result of these microcracks eventually propagating along the weaker interface surface as applied shear forces increase in magnitude. This tends to create a situation whereby one surface could slide over the asperities of the other surface causing a gap or a horizontal separation which at the same time is accompanied by a vertical deformation (slip). However, the distance that one surface can separate from the other (or slip vertically relative to the other) is governed by the stiffness of the transverse steel located across the interface. The stiffness of the transverse steel is in turn a function of the distance over which bond is broken

around the reinforcement. As more and more microcracks are formed and joined together to form a splitting crack, the mode of shear transfer between the two halves of the test specimen changes from one of transmitting forces through bond, to transmitting forces by means of shear-friction. The breakdown of bond around the steel bars will not, however, be significant until the splitting crack has been formed over a fairly large part of the interface area. This constitutes the beginning of the transition stage. Since the bond breakdown at the early stages of this transition is very small, the reinforcement stiffness is very high, and large amounts of shear can be transmitted without significant deformation (Fig. 4.13). This explains why in Fig. 4.8, there is no sudden increase in deformation as splitting starts at a value of shear stress of about 112 psi. In other words, the shear forces of phase I are sustained after splitting without a sudden increase in deformation because of the very high stiffnesses exhibited by the transverse steel bars.

It must be noted that during the transition stage the shear stiffness of the spring representing the joint changes from a value given by K_{sc} for phase I to K_{sc} for phase II. In the simulation of the joint behaviour only one transitional step is used. The shear stiffness of the element in the transitional stage lies between K_{sc} of phase I and K_{sc} of phase II. The stiffness matrices of the concrete and steel elements in the transition stage have the same general form as those given by equations (4.32) and (4.33) respectively. However, instead of employing K_{ns}^{II} and K_{sc}^{II}, K_{ns}^{t} and K_{sc}^{t} are

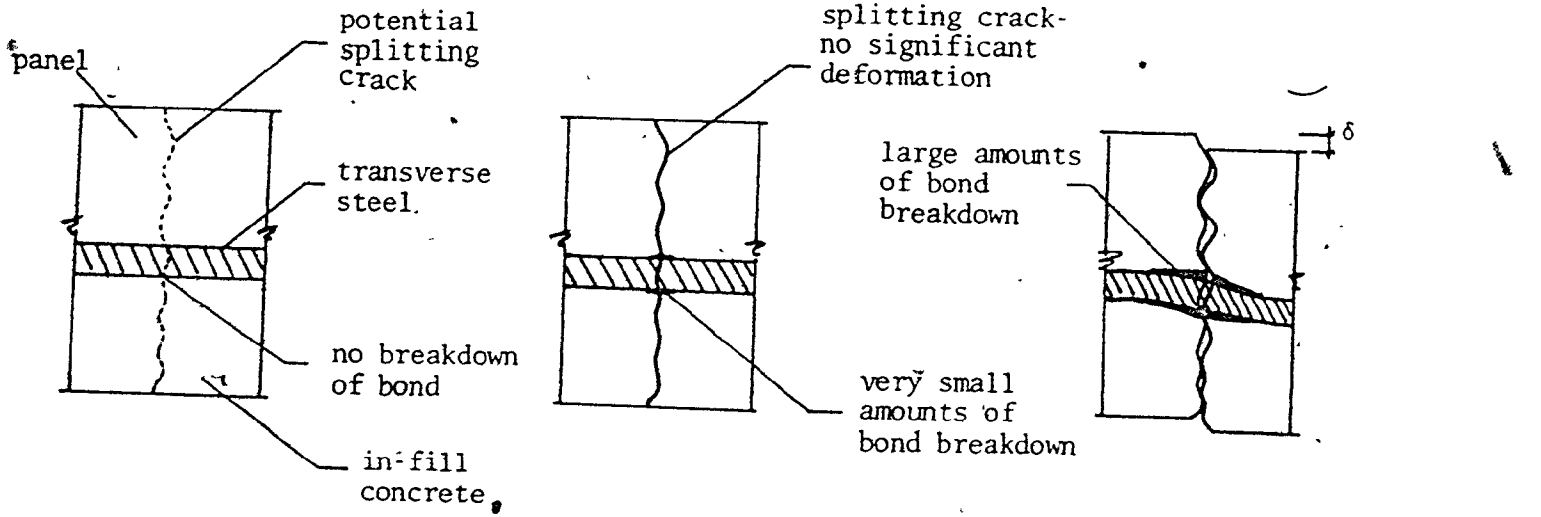

(a) Phase I. No Splitting Cracks

(b) Transition Stage

(c) Phase II. Splitting and Separation

Fig. 4.13 Transition from Phase I to Phase II for Vertical Joints

used. The latter two symbols represent the normal and shear spring stiffnesses respectively during this transition.

In determining the numerical values of K_{ns}^{t} and K_{sc}^{t}, the following conditions are imposed:

1. K_{sc}^{t} is determined such that the shear deformation of the joint immediately after splitting (when the stiffness of the transverse steel is very large) is consistent with the joint deformation immediately prior to splitting (end of phase I), and

2. The ratio of K_{ns}^{t} to K_{sc}^{t} is the same as the ratio of K_{ns}^{II} to K_{sc}^{II} (see equation 4.24).

(A more realistic way of simulating the transition stage, would be to change the joint stiffness gradually in accordance with a fitted mathematical function, or by selecting an arbitrary number of joint stiffnesses based on experimental considerations. However, since this analysis is basically concerned with the ultimate rather than the transitory capacities, and because a multi-step transition approach would be both numerically complex and uneconomical (in terms of computer time), a one step transition was considered to be sufficiently accurate for the purpose of this study.)

By applying the two conditions stated above, the numerical values of the transitory spring stiffnesses are found to be:

$$K_{sc}^{t} = 1.92 \times 10^{5} \cdot A(\text{lbs/in}), \qquad (4.38)$$

and

$$K_{ns}^{t} = 1.65 \times 10^{4} \cdot A(\text{lbs/in}) \qquad (4.39)$$

where A = area represented by the joint element.

The transitional property matrices are given by

$$[K_c^t] = \begin{bmatrix} K_{ns}^t & -K_{sc}^t/\bar{\mu} \\ -\bar{\mu}K_{ns}^t & K_{sc}^t \end{bmatrix} \tag{4.30b}$$

for the concrete element, and

$$[K_s^t] = \begin{bmatrix} K_{ns}^t & K_{sc}^t/\bar{\mu} \\ 0 & 0 \end{bmatrix} \tag{4.31b}$$

for the steel element.

The transition force vectors for the concrete and steel elements are then given by equations (4.40) and (4.41) respectively.

$$\{F_c^t\} = \left[K_c^T\right] \{W_r\} \tag{4.40}$$

$$\{F_s^t\} = \left[K_s^T\right] \{W_r\} \tag{4.41}$$

In computing the elemental forces for the transition to phase II behaviour, the transition forces are applied to the nodal points of the joint elements in such a way as to resist the externally applied shear forces. It must be remembered that these forces result from the application of the same external shear force which exists at the end of phase I. However, they represent a change in load resisting mechanism from bond to shear-friction. As the external loads increase, the joint undergoes deformations which are characteristic of phase II, and the total loads carried by the joint elements in phase II are given by

$$\{F_c^{II}\}_f = \{F_c^t\} + \{F_c^{II}\} \qquad (4.42)$$

for the concrete elements, and

$$\{F_s^{II}\}_f = \{F_s^t\} + \{F_s^{II}\} \qquad (4.43)$$

for the steel elements.

4.10 Joint Failure

The failure of a moderately reinforced vertical joint begins with the formation of diagonal cracks within the body of the joint's in-fill concrete (phase IIb). It was observed by Halasz[23] and Hansen[see(12)], (and reaffirmed by the analysis in this study) that diagonal cracks started near the end regions of the joint and progressed toward the middle as the loads were increased. If the transverse steel does not yield, the joint continues to resist loads until the entire body of the joint is cracked. In all probability, redistribution of stresses takes place for densely cracked regions of the joint where local compression struts can not sustain the load levels which initiated their formation (i.e. between successive compression struts there will be regions for which the joint material is not effective in transmitting shear forces). The redistribution of stresses from densely cracked regions of the joint to uncracked or lightly cracked regions, contributes to further cracking and eventually to ultimate failure.

If F_n^{II} and F_s^{II} are the force components of vector $\left\{F_c^{II}\right\}_f$ (equation 4.4 2) representing the total normal and

shear forces acting on a concrete element for phase II, and if f_n^{II} and f_s^{II} are the normal and shear stresses corresponding to F_n^{II} and F_s^{II}, then diagonal cracks are initiated when

$$\sqrt{(\frac{f_n^{II}}{2})^2 + (f_s^{II})^2} + (\frac{f_n^{II}}{2}) \geq f_t \qquad (4.44)$$

where f_t is the tensile strength of the in-fill concrete.

When the condition imposed by equation (4.44) is satisfied, the stiffness matrices for the steel and concrete elements are reduced to null matrices. Even though the joint is cracked, it is still capable of resisting shear forces in a purely plastic fashion (system of small compression struts). The load at which this occurs depends entirely on the configuration, dimensions and properties of the joint, and must be determined experimentally. Thus, after the stiffness matrices are reduced to zero, shear forces corresponding to the joint's plastic limit must be applied to the nodal points of the joint in such a way as to resist the external shear forces. This joint at this stage may undergo plastic deformation while sustaining this constant load. Experimental results indicate[23] that for the type of joint used in this study, the plastic limit was reached at an average shear stress of approximately 275 psi.

The same procedure may also be used, when failure is the result of yielding of the transverse steel.

4.11 Experimental Versus Analytical Results

The analytical results obtained by utilizing the ideas outlined in sections (4.3) to (4.10) are super-imposed

on Halasz's experimental results and are shown on Fig. 4.14. The reduction factor R takes into account all the factors (shrinkage, partial loss of bond, existance of debris on the face of the panels, etc) which contribute to the loss of strength at the interface. A zero value of R indicates a complete loss of bond. When R is 0.5, the analytical and experimental results seem to be in fairly good agreement. The value of R depends on so many different factors[5],[52],[66] that a true estimate of its value could only be found from experimental considerations. Thus, in the absence of a better estimate of its value, a R of 0.5 is used to indicate the interface strength reduction factor for this type of joint (considering all its physical characteristics). This value will also be utilized in the analysis of the vertical joints.

After splitting has taken place, as can be observed in Fig. 4.14, the τ mean versus slip curve for phase II is for all practical purposes, linear until failure. Diagonal cracks begin to appear at the top and the bottom of the specimen at a value of mean shear stress of approximately 188 psi. However, the appearance of these cracks does not apparently affect the linearity of τ mean versus slip diagram. The ultimate load is reached at a value of τ mean of approximately 275 psi. At this stage diagonal cracks suddenly propagate towards the middle of the joint and cause failure.

For a rigid specimen, which is simulated by assigning a very high stiffness value to its two halves, the slip curve phase II remains completely linear until failure. In Fig. 4.14

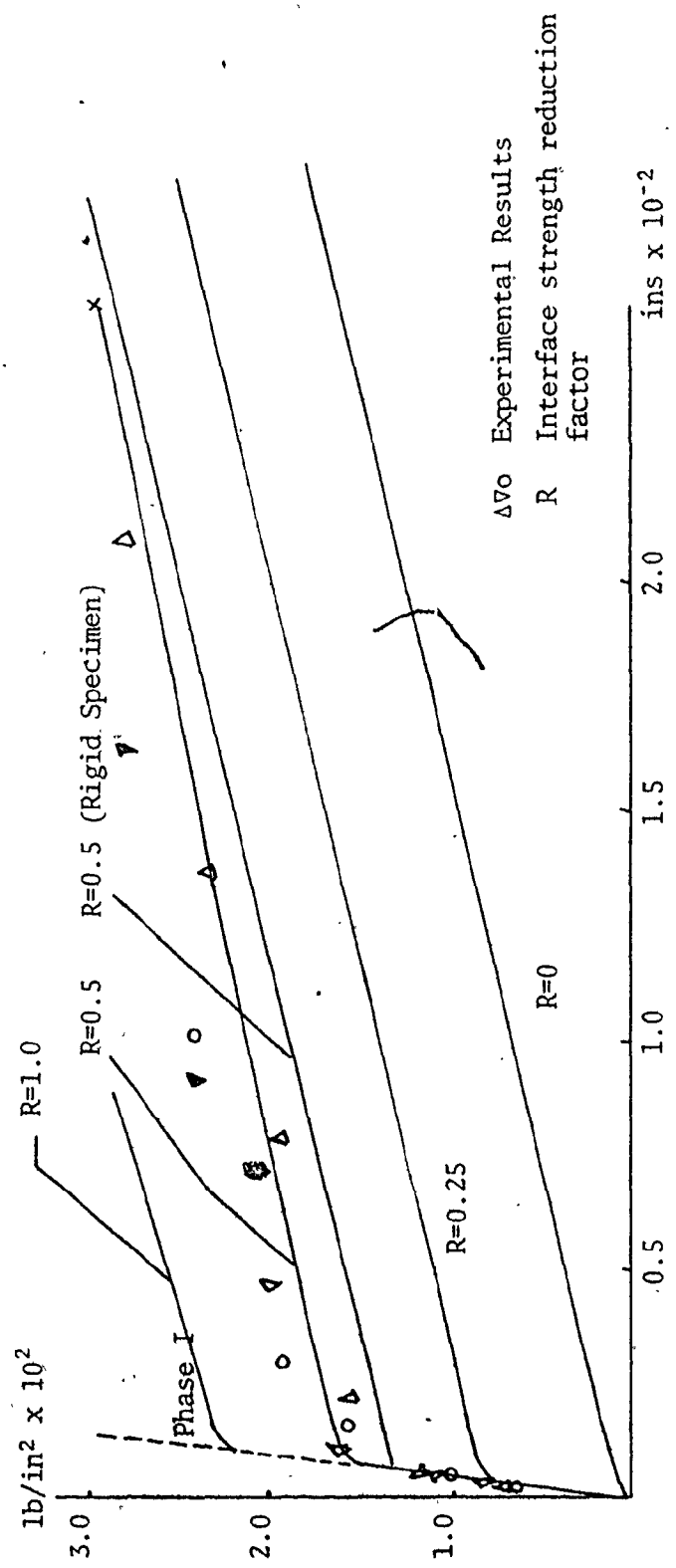

Fig. 4.14 Experimental versus Analytical Results for Halasz's Test Specimen

this curve is identified by the words 'rigid specimen'. An R value of 0.50 is used in this case to provide comparable results to evaluate the effect of using a rigid rather than a deformable specimen. For the rigid specimen the stresses are uniformly distributed along the length of the joint and the condition imposed by equation (4.44) is satisfied simultaneously by all the joint elements causing failure to follow immediately. For a deformable specimen, the shear stresses are not uniformly distributed. Because of the presence of compressive stress in the regions of high shear stress, a splitting occurs at slightly higher values of τ mean.

The joint behaviour is also investigated using an R value of 0.25. With the exception of the splitting crack which occurs at a lower τ mean value, the behaviour was the same as that with an R value of 0.5. However, the ductility of the joint is greatly improved. For a zero value of R (i.e. and unbonded joint surface), ductility is still greater, and the distribution of stresses is more uniform.

When R is chosen as unity (i.e. no reduction of strength is assumed for the interface surface), the splitting and diagonal cracks appear simultaneous (in practice one or the other can occur first due to localized effects of non-homogeneity of concrete). The joint shows improved splitting properties in phase I, at the expense of greatly reducing the ductility in phase II.

4.12 Influence of Normal Forces on the Splitting Strength of a Joint

Figure 4.15 illustrates the effect of an external

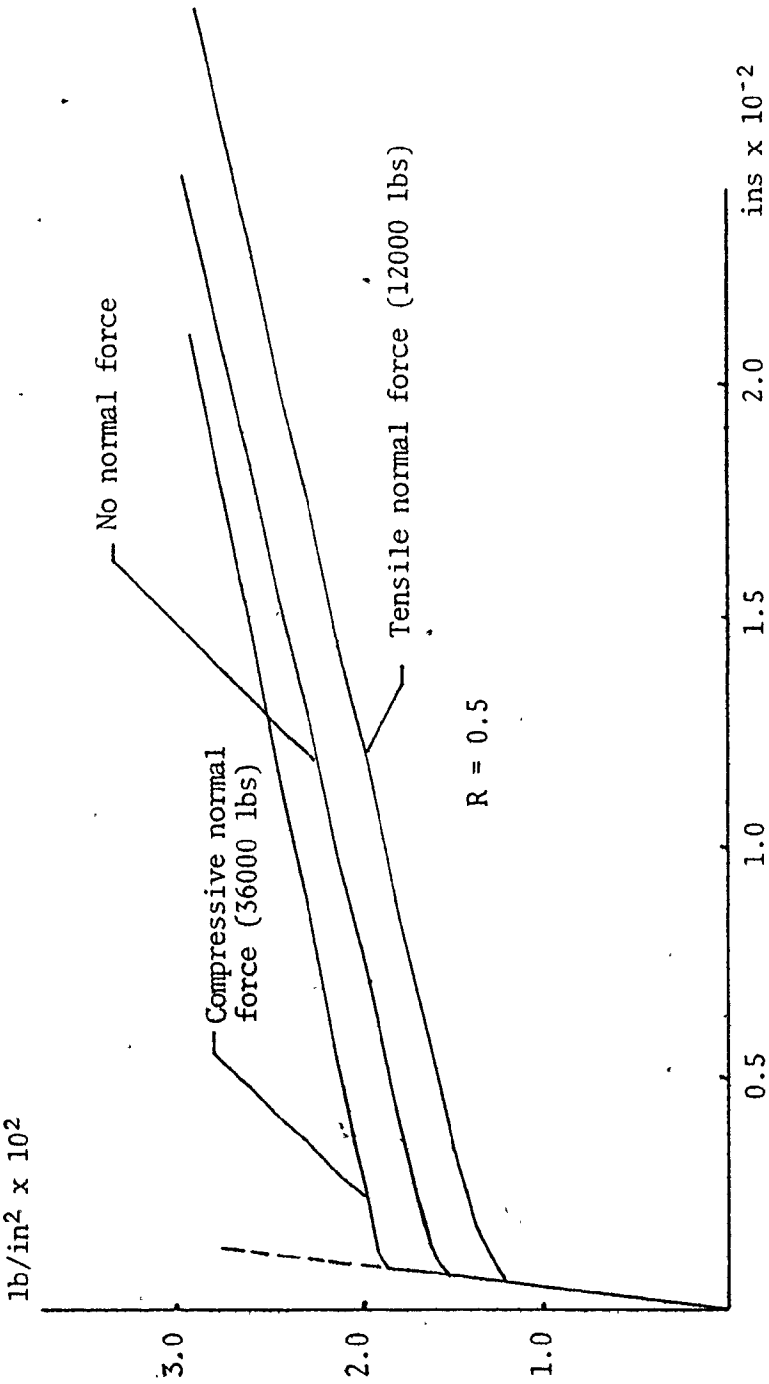

Fig. 4.15 Effect on Joint Slip of Forces Normal to the Joint Surface

normal tensile or compressive force on shear stresses at which splitting occurs. A normal compressive force increases the mean shear stress at which splitting occurs. The opposite is true for a tensile force. The failure loads are affected only slightly, while the amounts of slip at failure are affected to a larger extent.

Fig. 4.16 shows the effect of normal forces on an unbonded joint. The general behaviour of an unbonded joint acted upon by compressive normal forces would be the same as that of bonded joints, except that in this case the slip criterion is different. The property matrix for concrete element changes from $[K_c^I]$ to $[K_c^t]$ to $[K_c^{II}]$ when for each element $F_s > \bar{\mu} F_n$. The joint behaviour for a normal tensile force of 12000 lbs is also shown on Fig. 4.16.

An initial tensile force has the effect of separating the joint without any vertical displacement. When the joint is unbonded all resistance to separation must be provided by the transverse steel alone. By applying the slightest shear force, a vertical displacement proportional to the already imposed horizontal separation would occur. The amount of this vertical displacement is given by $W_y^i = W_{x/\bar{\mu}}^i$, where W_y^i and W_x^i are the initial shear and normal relative displacements respectively. After the gap is closed the joint can resist shear forces in the same fashion as when the joint was initially unstressed.

4.13 Joint Stresses in Various Phases

Figures 4.17 and 4.18 illustrate schematically the distribution of stresses at various stages of loading.

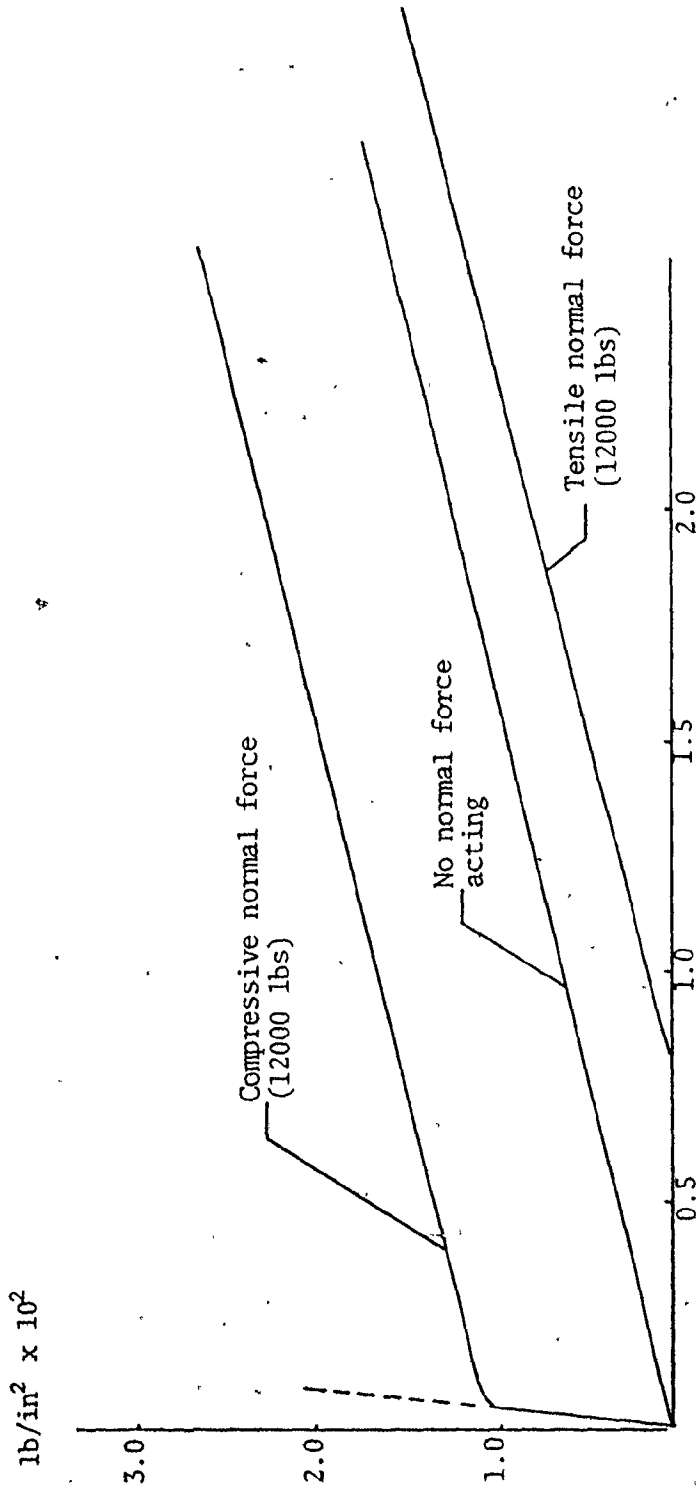

Fig. 4.16 Effect on Joint Slip of Forces Normal to the Joint Surface for R=o (Unbonded Surface)

Loads* (lbs.)	12000 lbs.	24000 lbs.	34000 lbs.	42000 lbs.	60000 lbs.
Shear stresses (PSI)	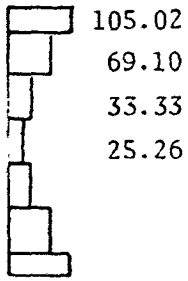	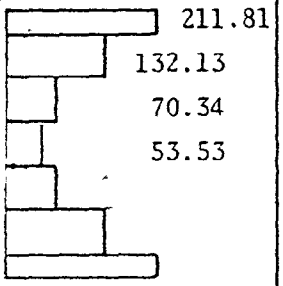	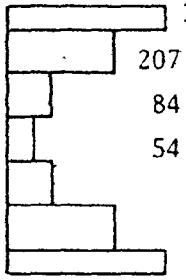	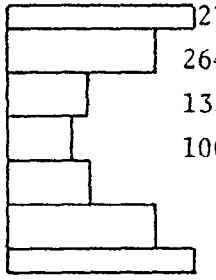	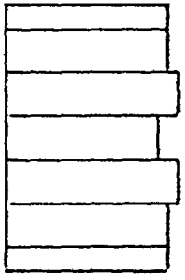
Comments	Phase I . Mode of shear transfer: bond	Top and bottom elements split . Mode of shear trans: shear friction and bond	Transition stage ended. Mode of shear transfer: shear friction	Phase II . Mode of shear transfer: shear friction. End elements yielded	Phase IIb . Diagonal cracks on shaded elements
Normal stresses (PSI)	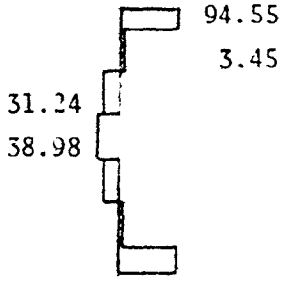	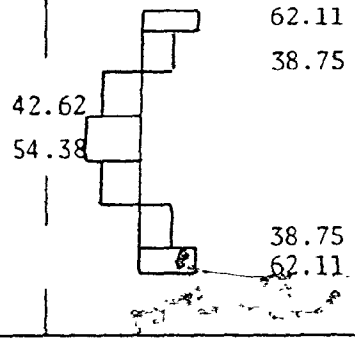	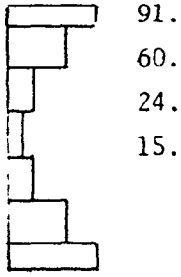	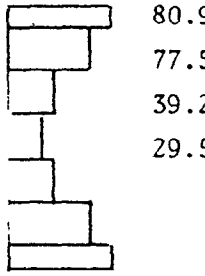	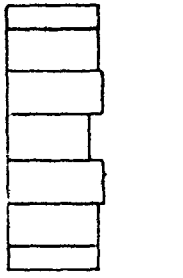

*Total External Shear Force

Fig. 4.17 · Normal and Shear Stresses at Various Stages of Loading. R = 0.50

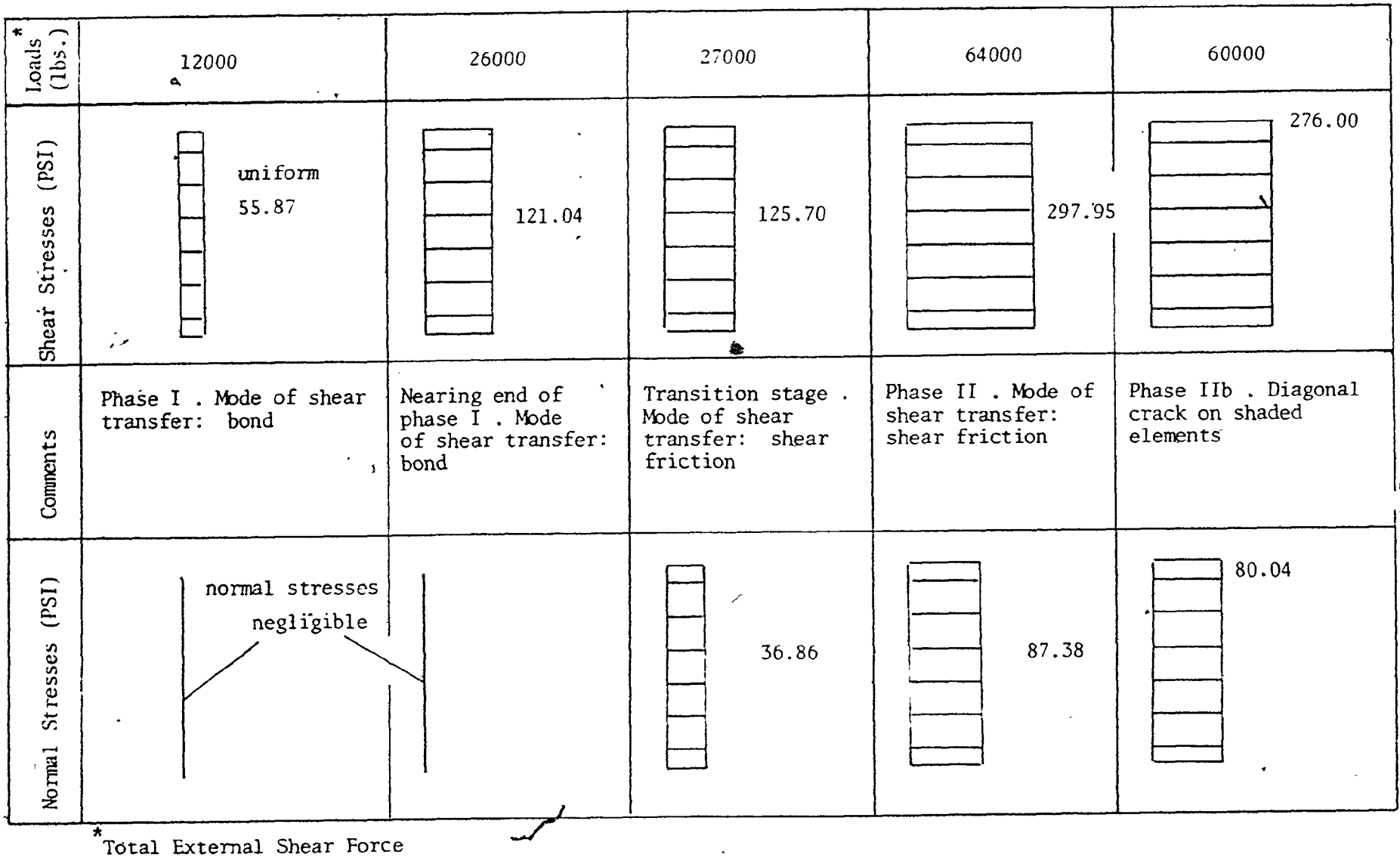

Fig. 4.18 Normal and Shear Stresses at Various Stages of Loading.
Rigid Specimen R = 0.50

Referring to Fig. 4.17, it is observed that bond is the mode of shear transfer in phase I. The stress distribution diagrams exhibit the usual characteristics associated with this type of shear transfer mechanism. As a result of panel deformation, normal compressive stress is one created in the regions close to the top and bottom of the joint, while the middle region is dominated by normal tensile stresses. As the transition stage is reached, a splitting crack is formed along the top and bottom 2 elements of the joint, and the mode of shear transfer for these elements changes from bond to shear-friction. The middle elements, however, are still bonded. At this stage the joint undergoes only slight shear deformations characteristic of the transition stage. As the shear loads increase, the splitting crack propagates through the entire length of the joint, and the normal stresses acquire the characteristics associated with the shear-friction mechanism. Diagonal cracks start to appear when the condition imposed by equation (4.44) is satisfied. This condition is initially satisfied for the most highly stressed elements near the ends of the specimen. After the formation of diagonal cracks, the affected elements lose some of their load resisting capacity. The released stresses are redistributed to the other elements causing their stresses to increase accordingly. If this increase is large enough to produce further cracking, the stresses are again released and redistributed to unaffected elements. The process continues in this fashion until either a stable condition is reached, or the entire joint is cracked.

Figure 4.18 shows the stress distribution diagrams for a hypothetical rigid specimen. Because of the rigidity of materials surrounding the joint, the stress distribution is found to be uniform at every stage. This is in marked contrast to the previous case where the two halves of the specimen were deformable. In phase I, the normal stresses acting along the joint are so small that they could be neglected. The fact that they do exist at all is because absolute rigidity, which implies an infinitely large modulus of elasticity for the material surrounding the joint, cannot be simulated.

The uniformity of stress distribution shown in Fig. 4.18 clearly indicates the important influence of the deformation of the material surrounding the joint on stress distribution along the joint. As the transition stage is reached and a splitting crack is formed, the mode of shear transfer changes from bond to shear-friction, and normal uniform clamping forces are created along the split surface. As shear loads increase, so do the corresponding shear and normal stresses, until the condition imposed by equation (4.44) is satisfied. As a result of the uniform stress distribution, this happens simultaneously for all the elements. After the formation of diagonal cracks, the joint is still capable of sustaining loads due to the formation of the aforementioned system of compression struts in a purely plastic fashion. However, failure follows immediately if loads are slightly increased.

During the course of the development of the techniques

used to simulate the behaviour of a push-off specimen, numerous other cases were investigated to ensure that the method was workable under a large variety of loading conditions. The basic features relating to deformation and stress distribution were similar to those reported in this section and since no new information may be obtained by including them, their presentation is omitted. However, there is one very important point which must be clarified before proceeding to simulate the behaviour of an isolated vertical joint.

Referring to Fig. 4.19, line No.1 is obtained by fitting a curve to the experimental results obtained by Halasz[23], and closely approximates the actual behaviour of the specimen. This curve is seen to be composed of 3 distinct segments which represent the joint behaviour in phases I and II and in the transition stage. During the transition stage the stiffness of the joint gradually changes from that of the joint for phase I to that given by the almost linear portion of line No.1 for phase II. As was experienced in section 4.9 a multi-step transition stage could be used to present this segment of the line. But this would be both involved and uneconomical in terms of computor time. Instead it was chosen to use a one step transition stage. The graph of this for R=0.5 is illustrated by line No.2. Because of the nature of the transitional stiffnesses (see section 4.9), the joint as a whole exhibits high stiffness characteristics, which in turn tend to retard the simulated crack (splitting) propagation. Thus, the one-step approach tends to underestimate the rapidity of crack (splitting) development. This small discrepancy

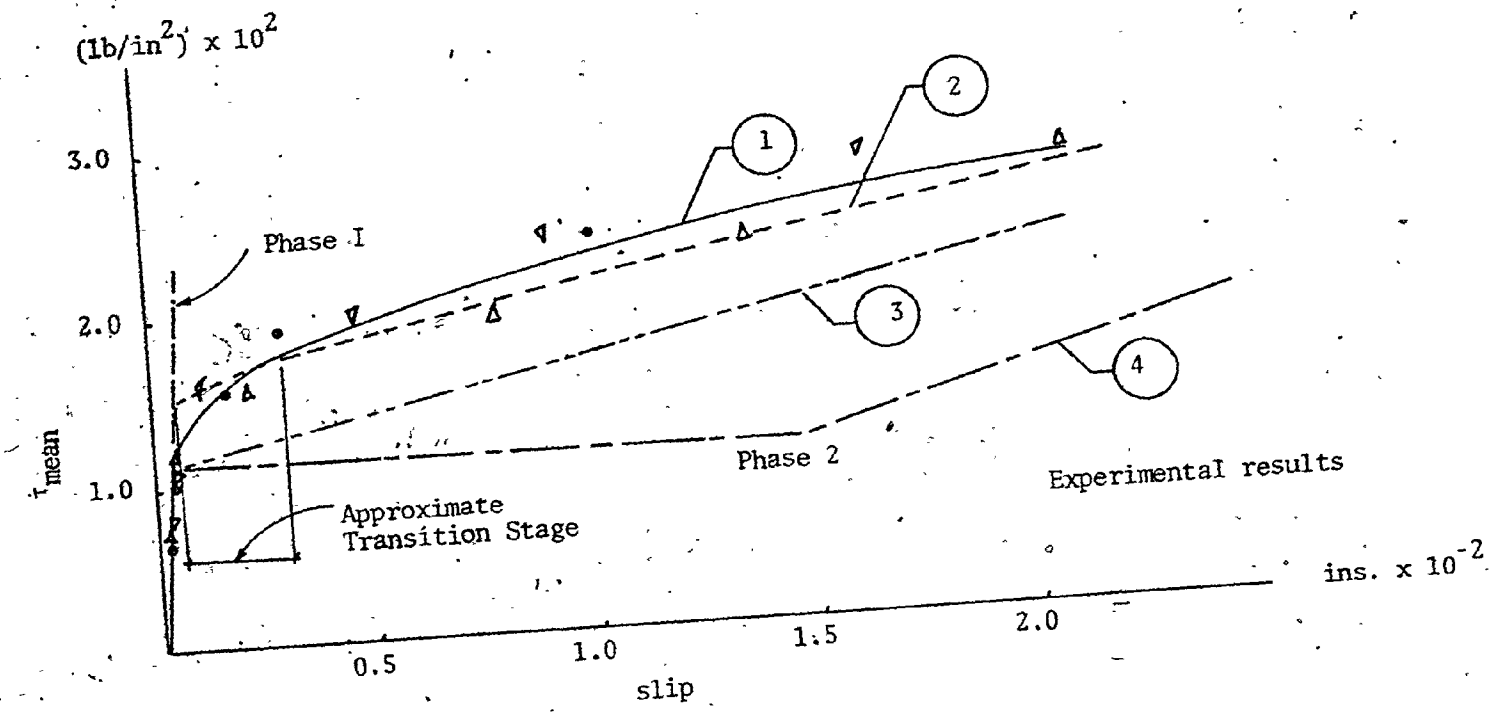

Fig. 4.19 A Comparison of Various Methods of Simulating Joint Behaviour

is not an important drawback since in actual practice the crack propagation could vary even for otherwise identical test specimens.

Line No.4 represents a situation where the transition stage was completely bypassed. As soon as a splitting crack is observed in an element, the stiffness of that element is replaced by that representing the joint in phase II. Since the stiffness of the element is reduced appreciably, the sudden release of stresses leads to an almost explosive crack (splitting) propagation resulting in loss of stiffness throughout the entire joint and the creation of large overall deformations. Obviously, this is not an acceptable simulation of the behaviour.

Line No.3 represents a case which bridges the gap between the solutions represented by lines 2 and 4, and in some cases may provide a valuable analytical tool. It represents a method of solution where one transition step is used under the same conditions as in the solution represented by line 2 except for one difference. Instead of satisfying the condition imposed by equation (4.37b) for each and every element of the joint, the splitting crack is permitted to propagate, when the condition imposed by equation (4.37b) is satisfied for any one of the elements in the joint. This method of crack prediction may in some cases over estimate the rapidity of crack propagation, but the error is on the conservative side. For a given τ mean it also over estimates the joint ductility, which depending on the level of τ mean, may be considerable. However, by adjusting the stiffness

values for phase II, it is possible (if experimental results for a given type of joint exist) to construct a useful tool for predicting the joint behaviour with the added built-in feature of perhaps slightly over estimating the rapidity of crack propagation.

The τ mean versus slip curves using this approach for Halasz's test specimen, are superimposed on his experimental results, and are shown in Fig. 4.20 for two values of R. The main features of these curves are identical to those of Fig. 4.14, and will not be elaborated upon further.

This concludes the study of the behaviour of a vertical joint as predicted by a push-off specimen. The method of analysis developed in the preceeding sections will now be utilized to study the behaviour of a vertical joint as it might appear between a pair of panels under a variety of loading conditions.

4.14 Behaviour of Vertical Joints

It must be mentioned at the outset that simulating the joint behaviour on the basis of tests on push-off specimens, is probably one of the best ways of predicting the vertical joint behaviour in a panel assembly under most loading conditions. However, in order to test the applicability of the analysis to some unusual loading conditions which may occur near collapse, (where for example, some panels may be cantilevering from the adjacent panels due to a separation along their horizontal joints) a number of other loading conditions are studied in this section.

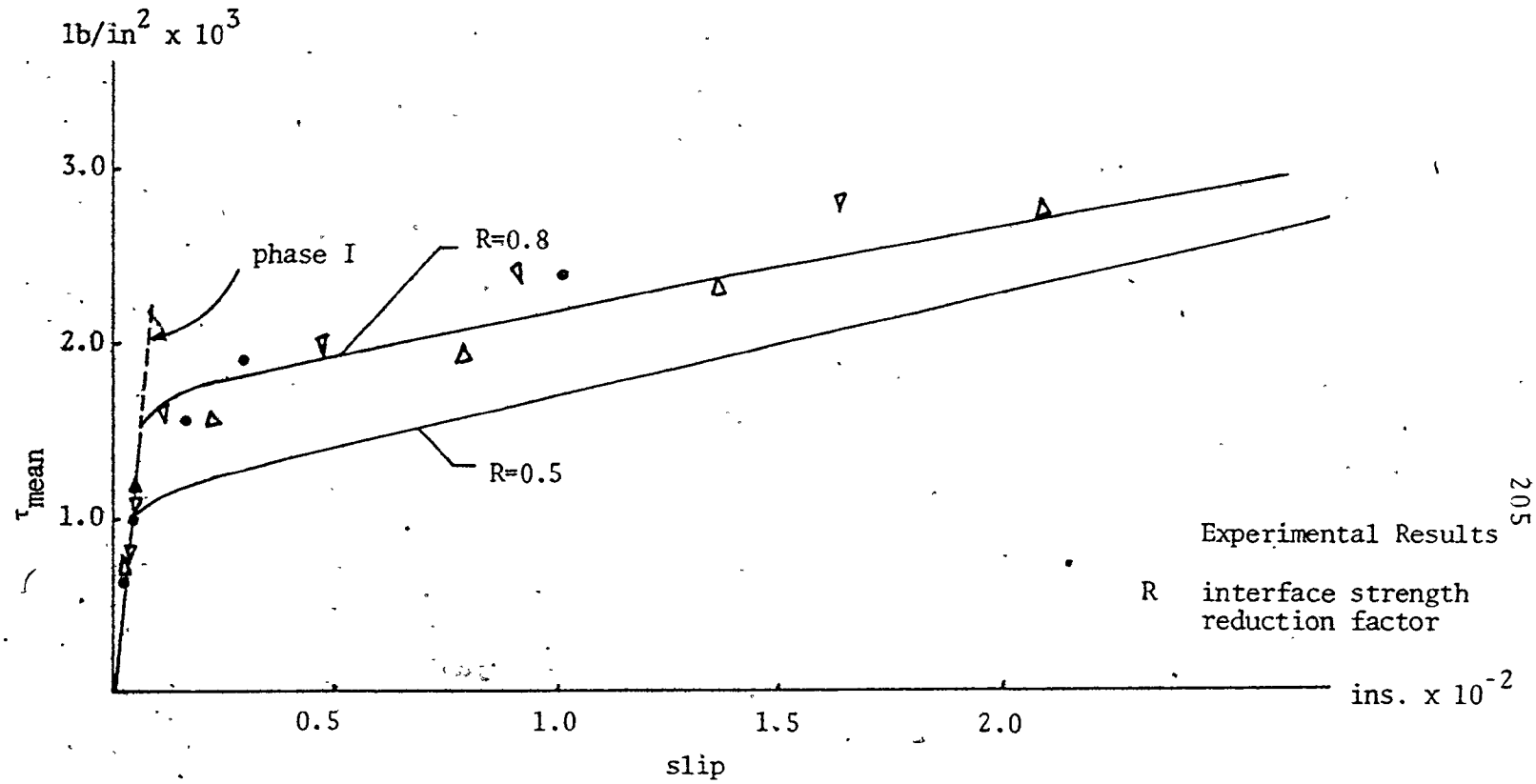

Fig. 4.20 Analytical Results for Rapid Split of the Joint Compared to Halasz's[23] Test Results

The finite element representation of a vertical joint situated between a pair of panels is shown in Fig. 4.21. Each rectangular panel element is composed of 4 triangular elements with the centre node eliminated (Fig. 4.21(b)). The joint elements are shown in Fig. 4.21(c) and are of the same configuration as used for the horizontal joints in Chapter 3, and in the analysis of the push-off specimens. A sketch of the vertical joint as it is actually constructed is shown on Fig. 4.22. The shear-key dimensions are the same as those used by Halasz in his experimental investigation. The thickness of the joint, however, is increased to 8. Since the stress distribution across the thickness of the joint is assumed to be uniform, the unit stiffness coefficients in phase II remain unchanged. The transverse steel ratio is kept constant at a value of 0.00286.

In order to study the joint behaviour under the action of both shear forces and bending moments, three basic loading schemes are devised. These are as follows:

1. a single force applied in such a way as to impose no bending moment on the joint,

2. a distributed shear force applied as in scheme 1, and

3. a pair of forces applied in such a way as to create bending and shear simultaneously.

(a) Scheme I - Action of a Single Concentrated Shear Force

Fig. 4.23 shows the load slip curves for two values

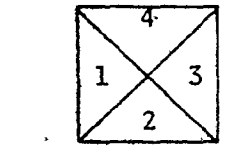

(b) Makeup of Each Rectangular Element

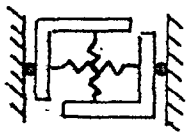

(c) The Joint Element

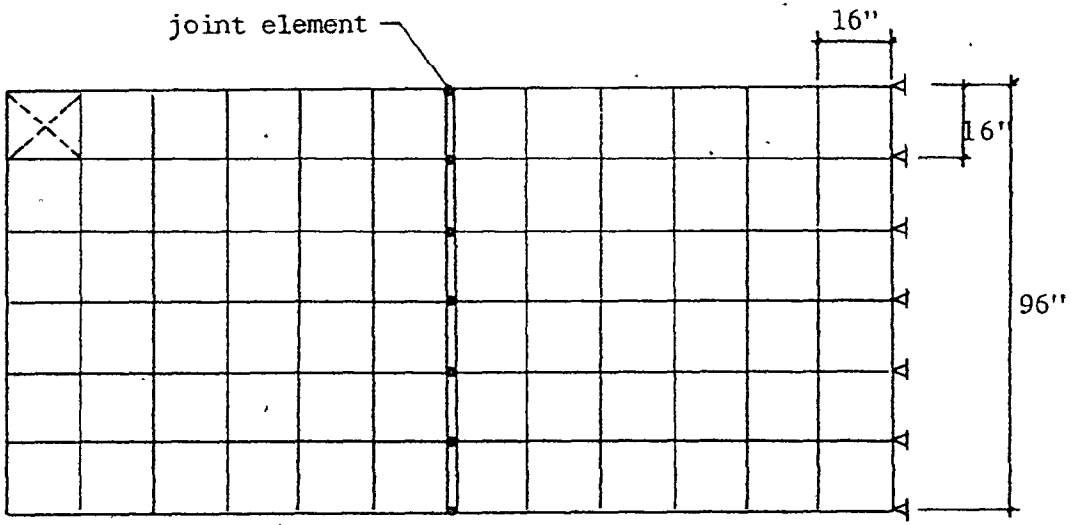

(a) Panel Elements and Support System

Fig. 4.21 Finite Element Representation of Vertical Joints and the Adjoining Panels

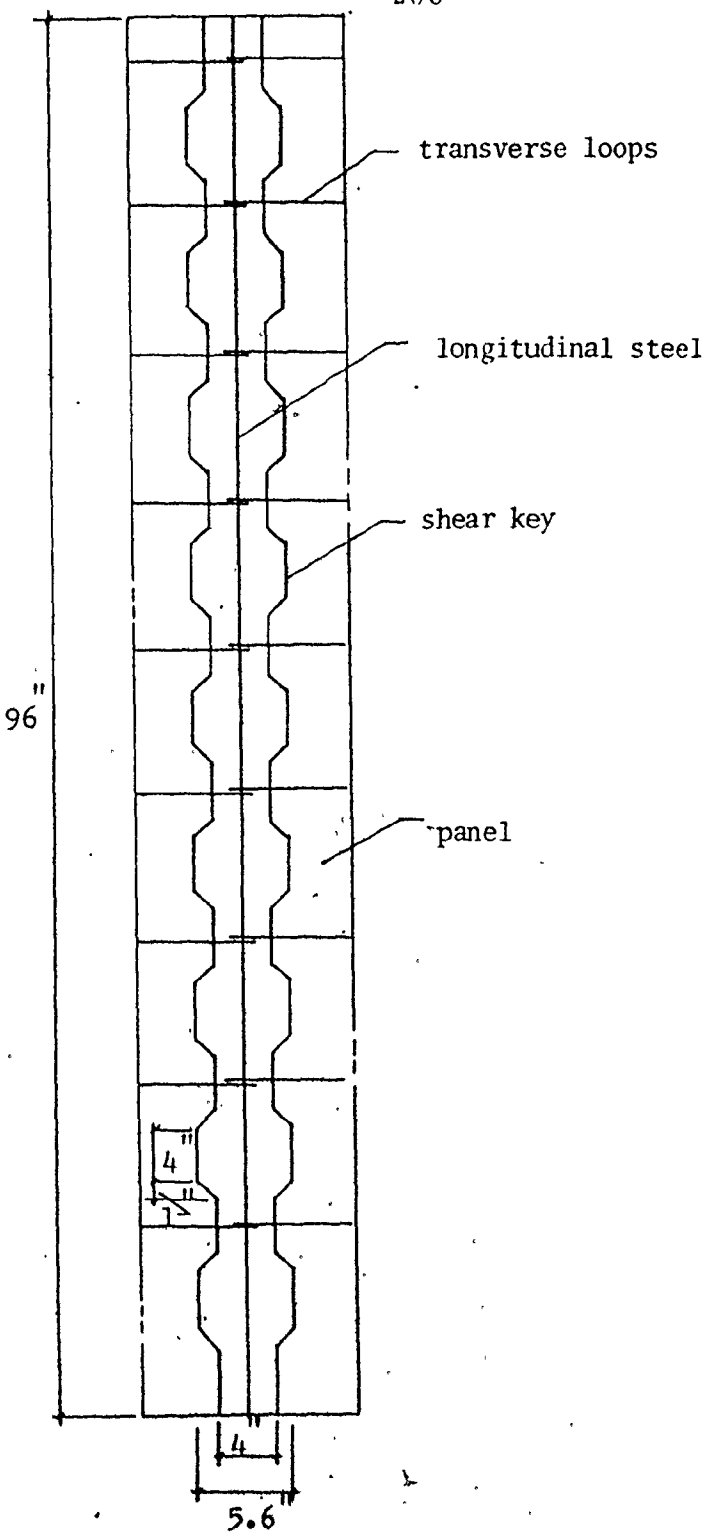

Fig. 4.22 Actual Vertical Joint

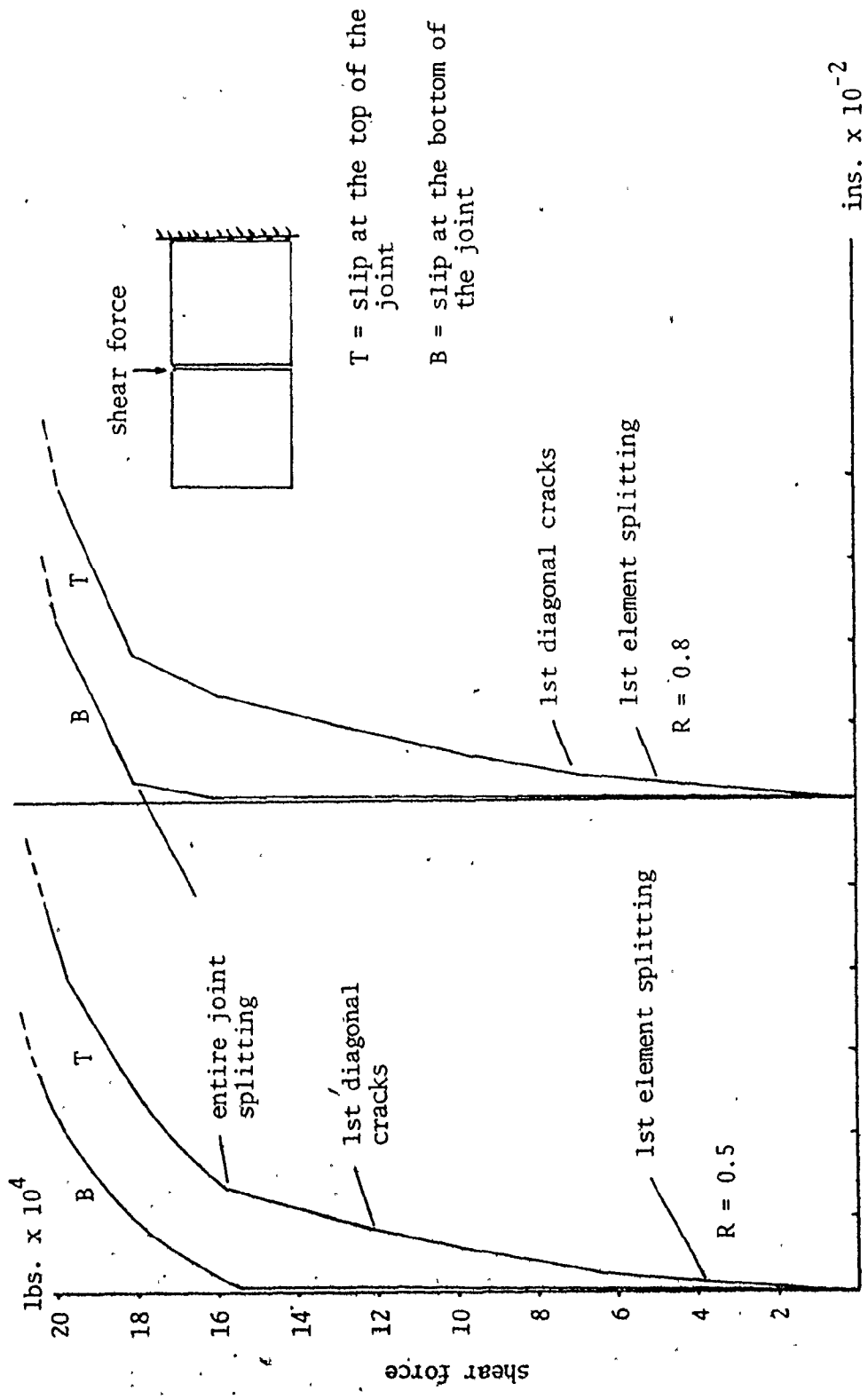

Fig. 4.23 Effect on Joint Slip of a Shear Force Applied to the Top of the Joint

at R. The curve marked T denotes the slip at the top of the joint and between the two corners of the adjoining panels. The curve marked B signifies the bottom slip (deformation) between the corresponding panel corners. Curve B in both cases exhibits very large stiffness until the applied load reaches a value of approximately 15 x 10^4 lbs. This occurs because the concentrated load produces localized effects and as a result the splitting crack propagation is very slow.

The top deformation over most of the loading range is many times greater than the bottom deformation due to the higher stresses resulting from the local effects produced just below the point of application of the load. As expected the load at which splitting commences is directly related to the assumed value of R. The loads at which diagonal cracks first appear on the other hand, are reversely related to the R value. This occurs because at higher R values, the stresses at which splitting originally commences are already very close to those which cause diagonal cracking (i.e. for R=1, splitting and diagonal cracking theoretically occur simultaneously). After splitting more load is transferred to the stiffer elements, because the split elements still sustain the load already imposed on them (through shear-friction mechanism resulting from the existance of compressive forces). However, the available range of loading to reach the diagonal cracking stresses is smaller with higher R values.

In the case of a single concentrated shear force, the diagonal cracking of the first element which is the direct result of the proximity of the point of application of the

load, does not immediately extend to the adjacent elements. The joint as a whole continues to function until diagonal cracks are extended to other elements at higher load levels. For joint elements near the bottom of the joint, splitting and diagonal cracking follow in short order for both R values. The joint as a whole fails at a predicted ultimate load of 21×10^4 lbs.

It would be interesting to see what differences would result if the method represented by line 3 in Fig. 4.19 (and henceforth referred to as method 3) were used instead of the method represented by line 2 (method 2), which has predominated in this study. The result of investigation for the same 2 cases is shown in Fig. 4.24. In this analysis (as was explained in section 4.13), the splitting crack is assumed to propagate through the entire length of the joint when the condition imposed by equation (4.37b) is satisfied for any one element in the joint. The method is obviously unreliable for predicting the joint deformations when the effects of a concentrated shear force are studied. Splitting, however, commences at the same load level as found from method 2 and its dependence on the R value is of the same nature. The method also illustrates how the stiffness of the joint is reduced when a splitting crack propagates through the entire joint. This of course, is not the case for a concentrated shear force as its effects on the joint for a major portion of the loading range are localized.

The joint stresses for the case shown in Fig. 4.24 are shown in Fig. 4.25. The top element as expected for a

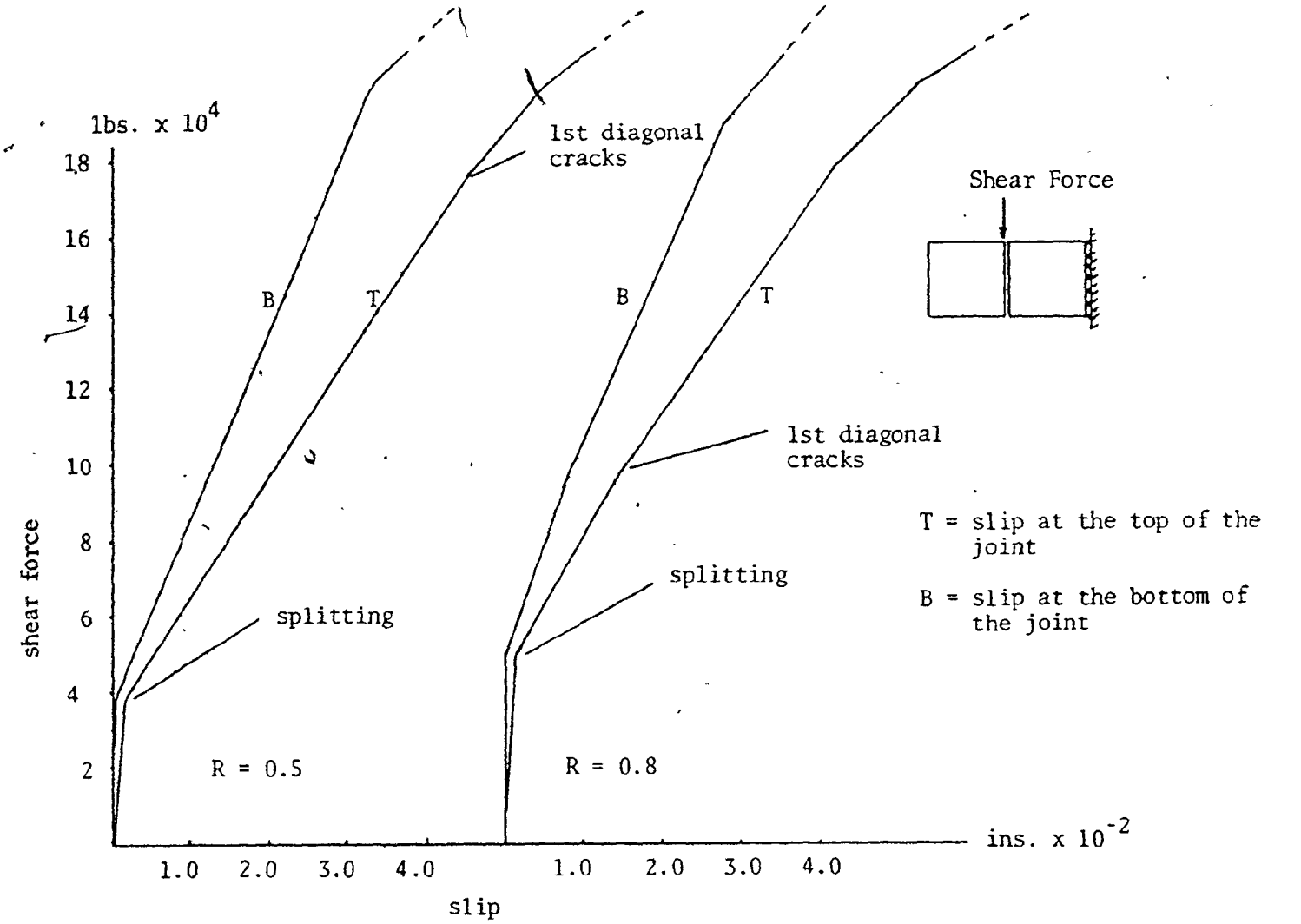

Fig. 4.24 Effect on Joint Slip of a Shear Force Applied to the Top of the Joint - Rapid Splitting of the Joint Elements

*Load (lbs.)	30000	54000	54000	98000	194000
Shear Stresses (PSI)	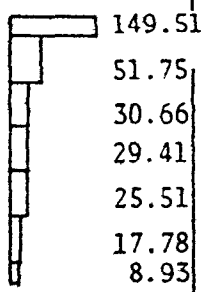	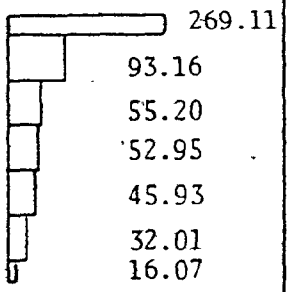	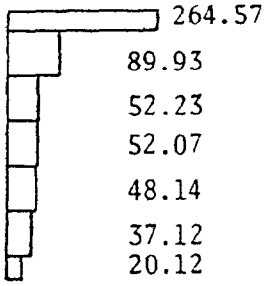	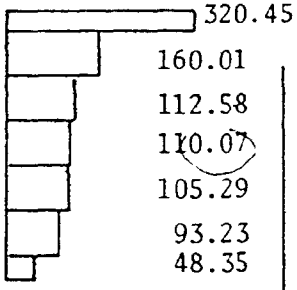	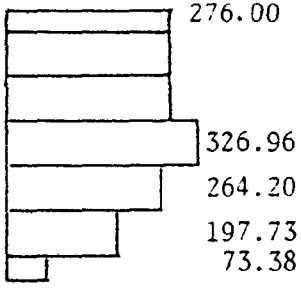
Comments	Phase I . Mode of shear transfer: bond	End of phase I . Mode of shear transfer: bond	Transition stage . Mode of shear transfer: shear friction	Phase II . Mode of shear transfer: shear friction	Phase IIb . Diagonal cracks on shaded elements
Normal Stresses (PSI)	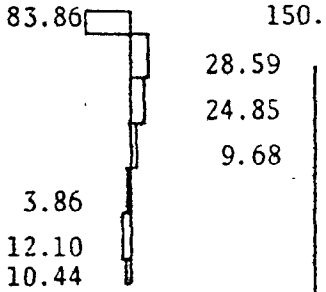	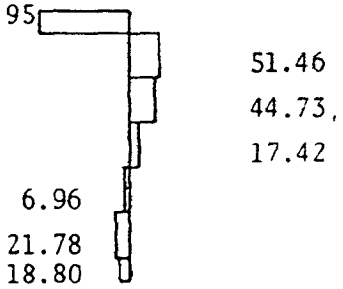	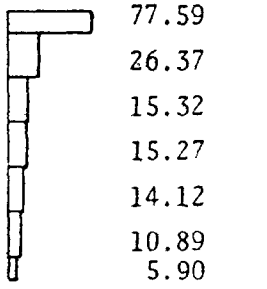	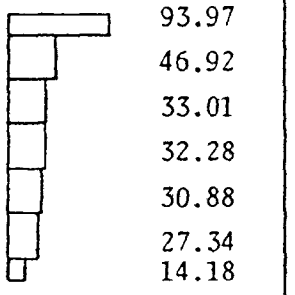	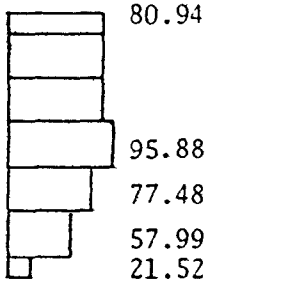

*Total External Shear Force

Fig. 4.25 Vertical Joint Normal and Shear Stresses along the Vertical Joint at Various Stages of Loading. R = 0.8

concentrated shear load, exhibits very large stresses when compared to other elements. It is also interesting to note the normal compressive stress distribution before and after complete splitting. The top element cracks diagonally at a load of approximately 10^5 lbs. However, diagonal cracks remain confined to the top element and the joint as a whole continues to function until diagonal cracks spread to the other elements at a much higher load level.

By assigning a very high modulus of elasticity to the panel elements, they could effectively be made rigid. Fig. 4.26 shows the joint deformation curves for rigid panels for two values of R. As expected, the deformations at the top and at the bottom of the joint are equal. The load at which splitting occurs is directly related to the value of R. It is interesting to note that both analytical methods 2 and 3 yield identical results for rigid panels due to equal distribution of stresses (see Fig. 4.27). This is not surprising since splitting occurs simultaneously for all the joint elements regardless of the method used. The deformation curve after splitting remains linear until failure occurs as a result of diagonal cracks appearing simultaneously throughout the entire joint.

Fig. 4.27 shows the stress conditions at various stages of loading. The interesting feature here, is the absence of normal stresses prior to splitting which illustrates the effect of panel deformation on joint stresses. It is also interesting to note that the load at which splitting commences is approximately 3 times greater than that indicated for a

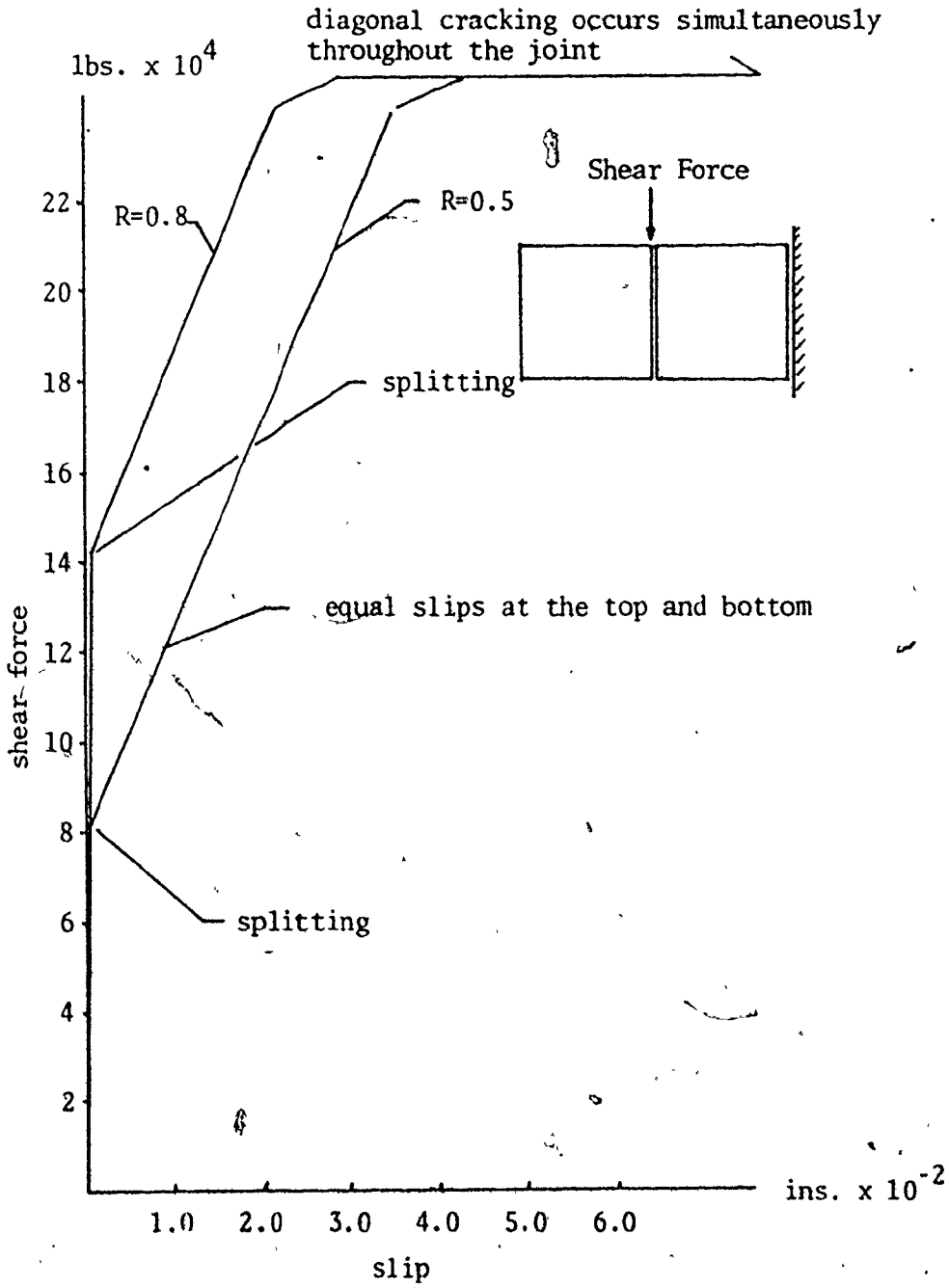

Fig. 4.26 Vertical Joint Load-Slip Curves for Rigid Panels

Load (lbs.)	90000	142000	142000	182000	211968
Shear Stresses (PSI)	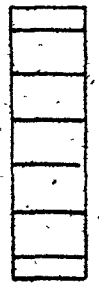	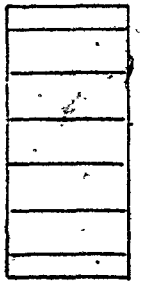 184.90	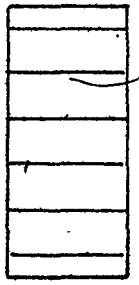 184.90	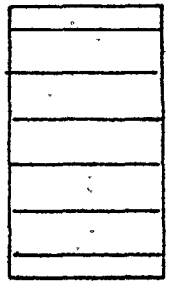 236.98	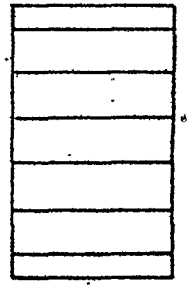 276.00
Comments	Phase I . Mode of shear transfer: bond	End of phase I . Mode of shear transfer: bond	Transition stage . Mode of shear transfer: shear friction	Phase II . Mode of shear transfer: shear friction	Phase IIb . Diagonal cracks on shaded elements
Normal Stresses (PSI)	normal stresses very small		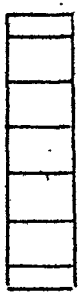 54.22	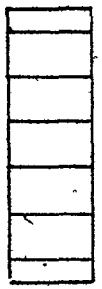 69.50	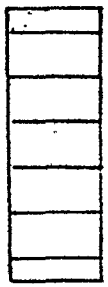 80.94

*Total External Shear Force

Fig. 4.27 Vertical Joint Normal and Shear Stresses along Vertical Joint at Various Stages of Loading . Rigid Panels. R = 0.8

deformable panel. This is again due to uniform stress distribution.

(b) Scheme II - Action of a Distributed Shear Force

The slip curves for uniformly distributed shear forces are shown in Fig. 4.28. It is interesting to note that as was the case of the rigid panels, slip values at the top and at the bottom of the joint are equal for both values of R, and again methods 2 and 3 yield identical solutions. The reason again is the more or less uniform stress distribution within the joint. As illustrated in Fig. 4.29, the shear stresses in phase I are symmetrical with respect to the centre of the joint. The normal stresses on the other hand, are anti-symmetric with stresses at the centre of the joint being zero.

The load at which splitting occurs is a little lower than that observed for the case of a rigid panel. The reason for this is the presence of tensile stresses in certain joint elements.

In phase II, due to the effects of panel deformation, the shear stress symmetry is slightly distorted. Although the shear stresses in phase II are not entirely uniform, they are close enough in value from one element to the next, so as to set up a diagonal crack propagation effect with the cracking of the first element. This leads to the joint cracking simultaneously throughout its entire length.

(c) Scheme III - Action of a Pair of Shear Forces

In order to produce bending moments as well as shear forces on a vertical joint, a pair of equal forces are

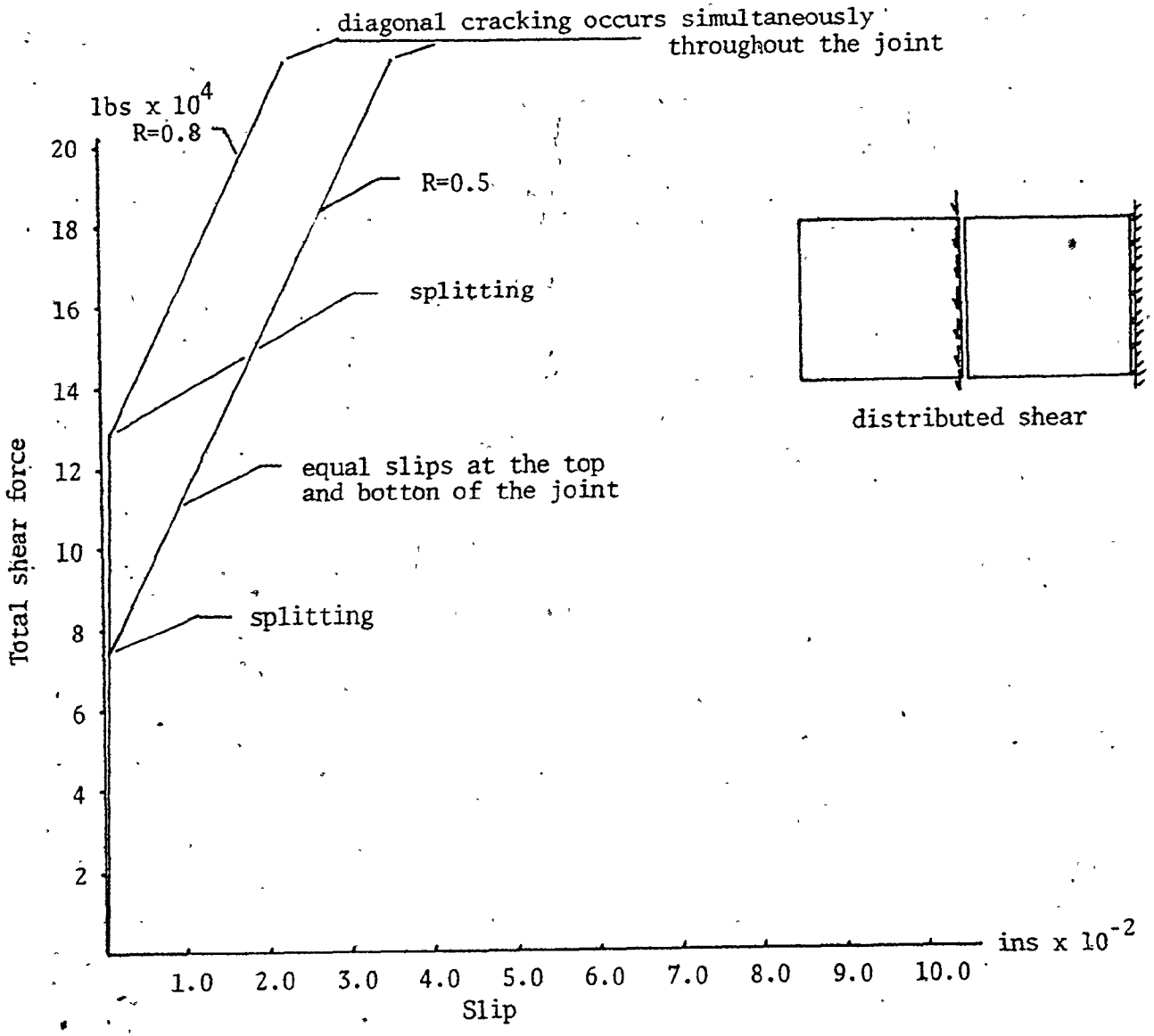

Fig. 4.28 Vertical Joint Load Slip Curves for Panels of Normal Rigidity

*Loads (lb.)	90000	126000	126000	186000	211968
Shear Stresses (PSI)	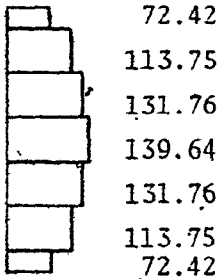	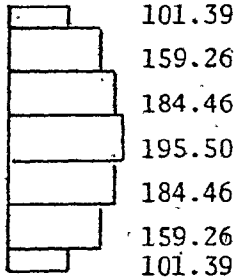	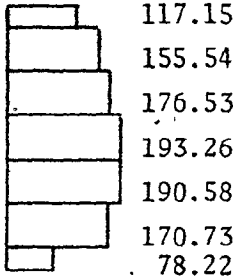	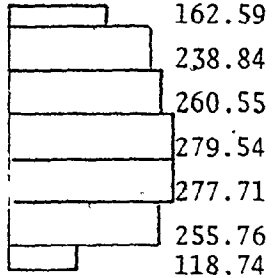	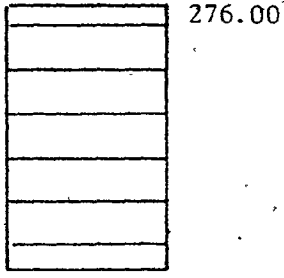
Comments	Phase I . Mode of shear transfer: bond	End of phase I . Mode of shear transfer: bond	Transition stage . Mode of shear Transfer: shear friction	Phase II . Mode Mode of shear Transfer: shear friction	Phase IIb . diagonal cracks on shaded elements
Normal Stresses (PSI)	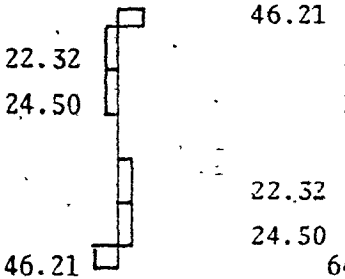	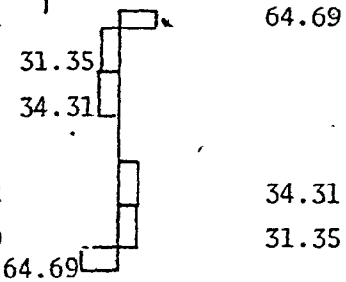	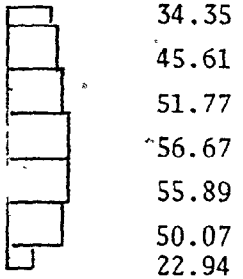	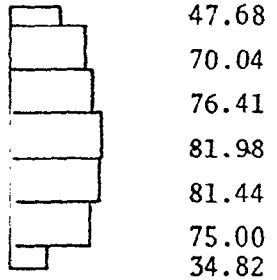	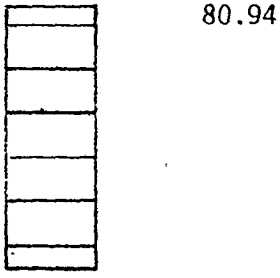

*Total External Shear Force

Fig. 4.29 Vertical Joint Normal and Shear Stresses along Vertical Joint at Various Stages of Loading. Uniformly Distributed Applied Shear Forces. R = 0.8

applied to the top corners of the outer panel as shown on Fig. 4.30. This situation may be encountered in a complex cantilever subjected to lateral loads, when there is a separation in the horizontal joints above and below a given panel. The analysis was carried out for three different values of R, and in each case the joint failed in tension resulting from the bending action. The effect of shear stresses on failure is considered to be of secondary importance. The tension failure (splitting) starts at the top of the joint and propagates almost instantaneously towards the bottom. The last element, however, fails in shear.

The joint deformation at the top is very much longer than that at the bottom because of the local effects produced by one of the concentrated shear forces. The two methods of analysis (2 and 3) yield identical results because splitting is again instantaneous.

These results are noteworthy since they are in agreement with the tests carried out by Armer and Kumar[2] on large scale panel assemblies (Appendix A). In their case, however, the transverse steel ratio was much higher than that used here. This enabled the joint to carry moments after the formation of the vertical crack in much the same way as does a reinforced concrete beam. In the case studied here, yielding of the transverse steel immediately folows the formation of the tensile crack which results in total failure.

4.15 - Summary

In order to study the behaviour of a complex cantilever subjected to lateral loads, it is essential to thoroughly

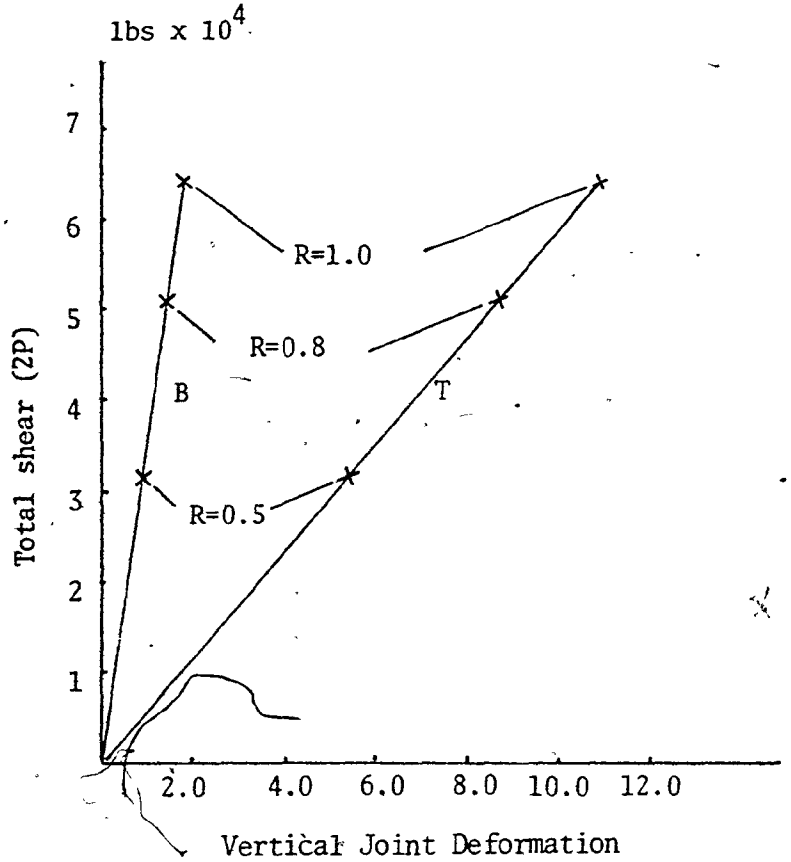

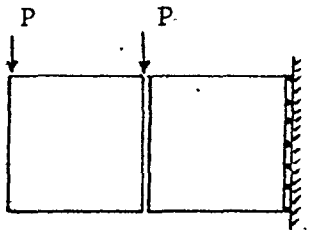

T = vertical deformation at the top of the joint

B = vertical deformation at the bottom of the joint

x indicates failure

Tensile splitting due to bending is the primary cause of failure. Splitting starts at the top and propagate to the bottom. Bottom element fails by shear.

Fig. 4.30 Shear Force Versus Joint Deformation Curves for the Effects of Shear plus Bending. Normal Panel Rigidity

understand the structural behaviour and the limitations of the joints used to connect these precast panels. In this chapter the behaviour of a typical vertical joint was investigated.

With the aid of the experimental work, the observations and the recommendations of several authors, an analytical technique was developed which allowed the stresses and the deformations in a joint to be predicted. As the physical state of a joint changes, so does the distribution of stresses acting upon it. By developing a finite element capable of representing a split joint, and by introducing a transition stage between phases I and II (representing the joint behaviour before and after the development of a splitting crack along the panel interface) the joint stresses and deformations may be accounted for throughout the entire loading range.

The joint model was tested by simulating the test results for a push-off specimen. The model also served to determine, by comparison with actual experimental results, an interface reduction factor R for the particular joint considered. The model was also used to investigate the joint behaviour as it might appear between a pair of precast panels under a variety of loading conditions which might arise in complex cantilevers near collapse.

The ideas put forth in this chapter should lead to a better understanding of the behaviour of vertical joints. To the best of the author's knowledge, no previous information was available to explain the joint

behaviour as a change from the bond transfer mechanism to the shear-friction transfer mechanism occurs. Also the ability to simulate the joint stresses during and after splitting is an important feature of this part of the study.

CHAPTER 5

SIMPLIFIED HORIZONTAL AND VERTICAL JOINTS

5.1 Introduction

In Chapters 3 and 4 a detailed investigation of the behaviour of horizontal and vertical joints was carried out utilizing a relatively large number of joint elements to simulate their load response. As previously mentioned, from a practical point of view, it is impossible (given the limitations of computer core space and the time involved to carry out this type of nonlinear analysis) to determine the response of a complex cantilever using the same number of elements per joint. Thus, in order to extend the analysis to complex cantilevers, the number of elements must be reduced.

This chapter is devoted to the development of a simple technique whereby the number of joint elements may be reduced to a manageable size without altering the joint response appreciably. It was originally anticipated that the number of finite elements representing each joint could be reduced to two. However, after a number of preliminary studies, it became apparent that the 2-element joint representation could not model the separation of the horizontal joints. Thus, the introduction of a third element became necessary to

make modelling separations possible.

In the analysis that will follow, the 2-element and the 3-element horizontal and vertical joints will be investigated. The joint response to various loading conditions investigated in Chapters 3 and 4 will be used as a guide to determine the accuracy of the simplified analysis. In the simplified analysis, in order to achieve reasonable accuracy, the stiffnesses of the elements representing the joints must be modified in accordance with a set of procedures which will be developed in the following sections. However, before describing the modification procedures, the physical representation of the mathematical model will be explained in the following section.

5.2 Simplified Horizontal Joints with 2 or 3 Elements per Slip Surface Representation of the Mathematical Model

Figure 5.1 shows the physical model for the 2 and 3-element representation of horizontal joints. In the 2-element representation (Fig. 5.1(a)) panel behaviour is simulated using a square element composed of 4 triangular elements with the centre node condensed. In the 3-element representation (Fig. 5.1(b)) 16 triangular elements are used to create a square element having mid-side as well as corner nodes. For details of the condensation technique and the accompanying case studies please refer to Chapter 2.

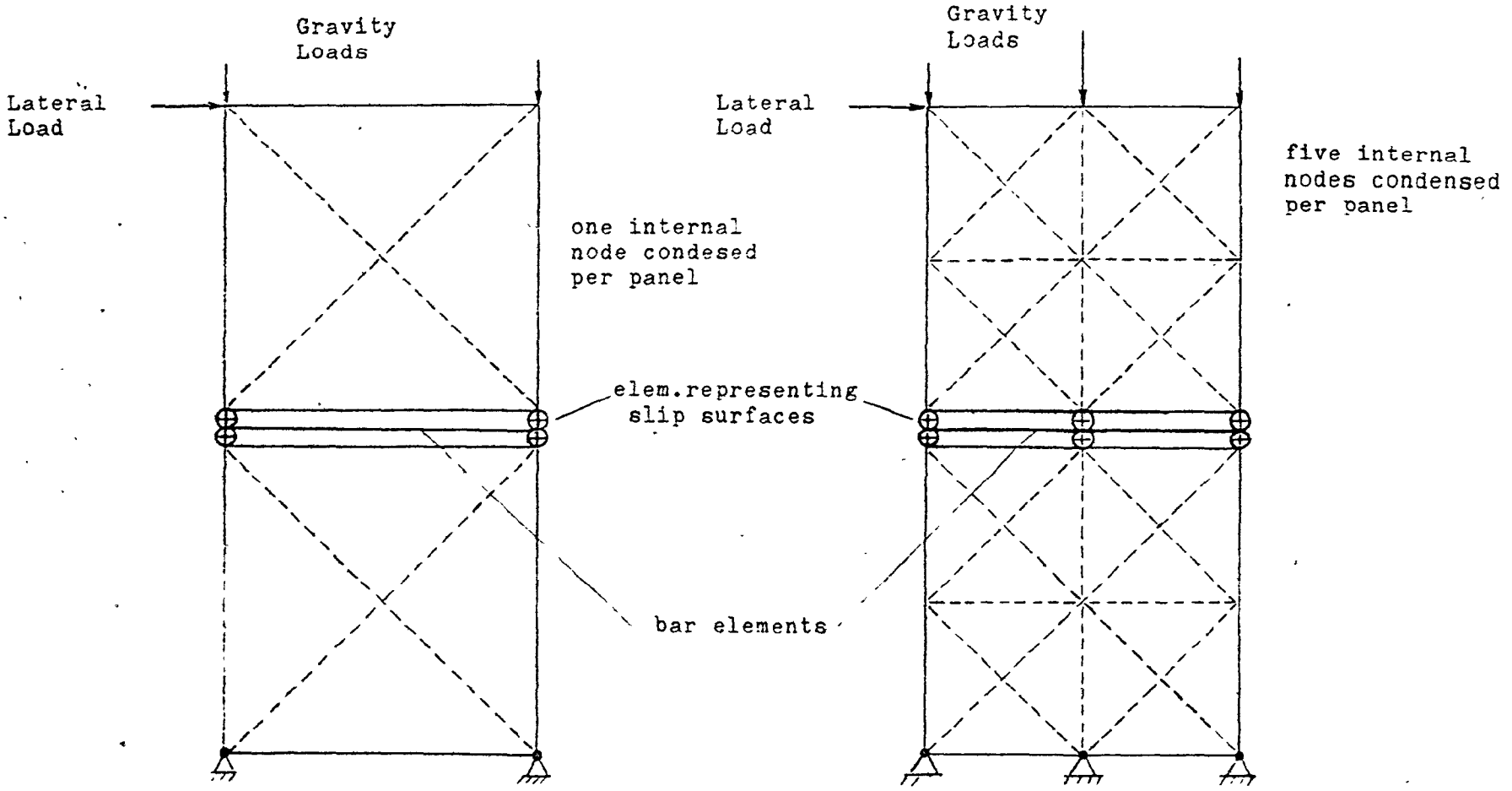

(a) 2-Element Representation of Slip Surface

(b) 3-Element Representation of Slip Surface

Fig.5.1 Physical Model of Simplified Horizontal Joints and the Adjoining Panels

The joint elements used in the simplified analysis have the same characteristics and stiffness matrices as those used for the detailed analysis except that the numerical values of the stiffnesses are now different. As will be explained in sections 5.3 and 5.5 these values are continually modified as lateral loads increase.

In the 2-element representation, a total of 4 dimensionless elements in 2 layers are used to simulate the behaviour of the joint filler and the slip surface components. Each layer is assumed to possess the deformation characteristics associated with one half of the thickness of the joint filler component. The same approach is used for the 3-element representation, except that each half layer is now composed of 3 elements.

The bar elements shown in Fig. 5.1 represent the horizontal continuity provided by the joint filler (including the floor panel contribution). This element is capable of taking axial loads only. Treating the joints in this fashion makes it possible to investigate the tie-beam effect when the behaviour of complex cantilevers is studied.

The procedures used in section 4.4 are employed once again to determine the unit shear and normal stiffness coefficients. Thus

$$k_s = \frac{G}{\frac{1}{2}t} \quad , \text{ and } \quad k_n = \frac{E}{\frac{1}{2}t} \qquad (5.1)$$

where G = shear modulus,

E = modulus of elasticity, and

t = joint thickness (10 ins.).

The stiffness matrix of the elements is similar to that indicated by equation (3.19). However, the spring element stiffnesses, K_s and K_n, now acquire values given by:

$$K_s = k_s \cdot l_c \cdot d \text{ , and } K_n = k_n \cdot l_c \cdot d \qquad (5.2)$$

where d is the width of the joint, and l_c is the length contributing to the stiffness of one element. For the 2-element representation l_c is equal to one half of the total length of the joint.

The stiffness matrix for a bar element is of the form

$$[\overline{K}]_B = \frac{EA_b}{L_b} \begin{bmatrix} 1 & 0 & -1 & 0 \\ 0 & 0 & 0 & 0 \\ -1 & 0 & 1 & 0 \\ 0 & 0 & 0 & 0 \end{bmatrix} \qquad (5.3)$$

where $A_b = t \cdot d$, and L_b is equal to the total length of the joint for the 2-element representation or one half that amount for its 3-element counterpart.

5.3 2-Element Simplification by Successive Modification of the Stiffnesses

As will be explained later in this section the process of successive modification of stiffnesses is based on relative normal deformations occurring at the corners where the two panels are connected. Since elements simulating the joints have zero dimensions in the simplified analysis, the upper edge of the lower panel, the bar

element and the lower edge of the upper panel occupy the same physical location in space as long as the structure remains unstressed. When loaded, however, relative displacements (horizontal and/or vertical) will take place. For a uniform vertical compressive force, for example, it appears that the lower edge of the top panel is protruding into the lower panel. This in no way complicates the analysis, and the resulting relative displacements are indeed a measure of the deformability of the joint filler component.

In reality, panels are in contact along their entire lengths by means of the joint filler component. For the analysis discussed in Chapter 3, a relatively large number of elements were used to simulate the behaviour along these contact surfaces. For the simplified analysis, where the stiffness of the entire joint is accumulated at the two corners, the physical model can not correctly represent the joint resistance. This is because instead of having a large number of weaker spring elements distributed along the surface of the joint, the joint now is simulated by only two elements of much greater stiffness at its two extremeties. In the detailed case investigated in Chapter 3, separation occurred gradually as lateral loads increased. This in turn gradually reduced the area over which the shear forces were resisted and resulted in greater deformations. However, in the simplified case studied in this section, separation does not occur until the joint reaches its ultimate capacity.

A preliminary analysis showed that if joint springs in the simplified analysis were not modified, the joint deformation near failure was approximately 1/20 of that of the detailed analysis under similar loading conditions. It was thus concluded that the joint spring stiffnesses had to be modified if the simplified analysis was to produce acceptable results.

Before proceeding further, the word modification must be defined. Modifications as used in this chapter, means changing the stiffnesses of the elements representing the simplified model during the application of the shear forces. By successively modifying the element stiffnesses, the behaviour of a simplified model may be altered in such a way that its deformation curves can lie close to those obtained by using the more elaborate models of Chapter 3.

Thus, the next step in developing a simplified model was to develop a workable modification technique which could later be incorporated into the analysis of complex cantilevers. After a number of preliminary trials it was decided to use a modification technique based on joint deformation. The procedure was implemented utilizing a variable referred to as the modification coefficient which was to be constantly re-evaluated as the joint deformations increased under the action of gradually increasing lateral loads.

Referring to Fig. 5.2, y_1 and y_2 are the relative normal displacements occurring at the two ends of the joint between the lower edge of the upper panel

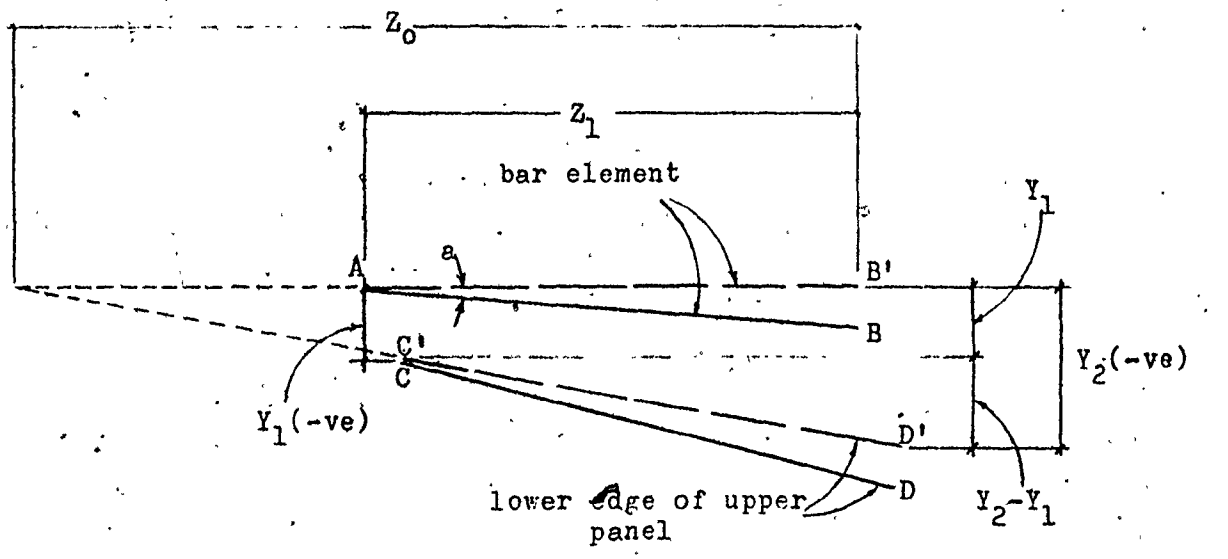

(a) First Case

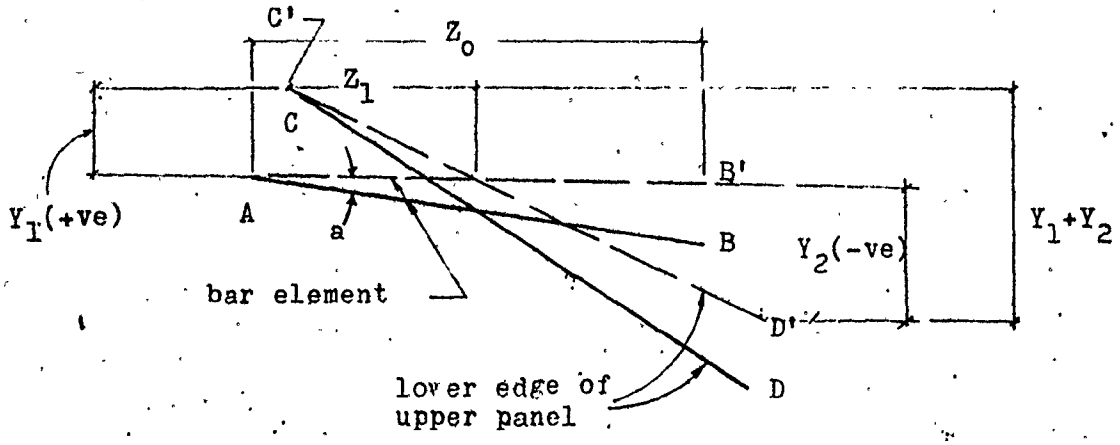

(b) Second Case

Fig.5.2 Determination of Coefficient C Based on Relative Normal Corner Deflections

and the bar element (representing the joint filler component) under a combined action of vertical compressive forces and lateral forces.

A similar diagram could have been drawn to show the relative normal corner displacements between the upper edge of the lower panel and the bar element.

Lines AB and CD in Fig. 5.2 illustrate schematically the positions taken by the bar element and the lower edge of the upper panel respectively. Two possible situations are considered. Figure 5.2(a) shows a situation where the entire surface of the joint is in compression. In Fig. 5.2(b) the joint is partially separated. To make the diagram simpler to work with, the system is rotated about point A, so that lines AB and CD assume the new positions indicated by the dashed lines AB' and C'D' respectively. Neglecting the relative horizontal deformations resulting from the application of the horizontal and vertical loads, and assuming that the relative vertical deformations y_1 and y_2 are uneffected by rotation through angle a (which is very small), relationships expressing the tilting of the panels in terms of z_1/z_o (Fig. 5.2) can be established. For the two cases shown in Fig. 5.2(a) and Fig. 5.2(b), the ratio z_1/z_o in terms of y_1 and y_2 is given by $\frac{|y_2| - |y_1|}{|y_2|}$ and $\frac{|y_1|}{|y_1| + |y_2|}$ respectively.

It must be emphasized, that the above ratios must be continually re-evaluated during the application of the

loads so that the element stiffnesses can also be continually re-evaluated.

Using these ratios as a measure of the tilt and/or the separation of the panels, two empirical relationships can be developed. These relationships define a modification coefficient used for the successive modification of the element stiffnesses in the simplified model. With the aid of this coefficient which will be called C and another constant B (equation 5.6), the stiffness of the elements in the simplified model can be modified so that its deformation curve is similar to that determined for the detailed model. The expressions for C (equations (5.4) and (5.5)) involve another constant A. The significance of the coefficient C and the related constants A and B will be discussed later. It must, however, be mentioned that constants A and B are determined using a combinatorial approach incorporated in a simple computer program. The joint deformation curves determined in this manner are then compared to that of the detailed analysis to determine constants A and B for the best fitting curve.

Referring to Fig. 5.2(a), coefficient C may be expressed in terms of the relative normal corner deformations y_1 and y_2 by the following relationship:

$$C = 1 - \frac{|y_2| - |y_1|}{|y_2|} \cdot A \qquad (5.4)$$

for $|y_1| \leq |y_2|$. The numerical value of a will lie between zero and one. When $y_1 = y_2$, then C = 1. The other limit

is when $y_1 = 0$ or just before separation for which C = 1-A. For $|y_2| \leq |y_1|$, the subscripts 1 and 2 in equation (5.4) must be reversed.

The second situation arises when forces are acting over only a portion of the surface of the joint (ie. partial separation). It is very important to realize that this situation can exist only if the panels form part of a complex cantilever. For an isolated horizontal joint between a pair of panels as shown in Fig. 5.1(a), $y_1 = 0$ indicates the end of the analysis as separation (or disconnection of the element) will cause the upper panel to become unstable and the stiffness matrix to become singular.

Referring to Fig. 5.2(b), coefficient C for the second situation was found to give satisfactory results when expressed in the form:

$$C = (1-A) - \frac{|y_1|}{|y_1| + |y_2|} \cdot (1-A) \qquad (5.5)$$

for $y_2 \leq 0$. It must be noted that in equation (5.4), both y_1 and y_2 had negative values. In equation (5.5) only y_2 is negative.

Examining the boundary values for equation (5.5), it is observed that for $y_1 = 0$, C = 1-A. This is the same value of C that was obtained from equation (5.4) at $y_1 = 0$. At the other extreme, when $y_2 = 0$ (which represents the case just before the entire joint is separated), C = 0. It should be remembered that equation (5.5) is only used

where the joints are in the redundant system of a complex cantilever.

The same argument could be repeated for the interface between the upper edge of the lower panel and the bar element representing the joint filler components. The coefficient C in this case is used to modify the element stiffnesses along slip surface 2.

The joint element spring stiffness, K_s, is modified before each loading cycle in accordance with the following equation:

$$K_s^m = K_s \cdot C \cdot B \qquad (5.6)$$

where K_s^m is the new modified shear spring stiffness, K_s is the original unmodified shear spring stiffness, and B is the aforementioned constant determined in conjunction with A. The constants A and B and the coefficient C interact to adjust the shape of the joint deformation curve. Although the influence of each cannot be totally isolated, their significance may be illustrated by keeping one constant and varying the other. The sensitivity of the deformation curve to changes in each constant was studied using the simplified model shown in Fig. 5.1(a). The deformation curve for the detailed model shown in Fig. 3.15 (line 1) was used as the criterion for the determination of the most suitable values of these constants. Using a simple computer program, the optimum values for A and B were computed to be 0.76 and 0.12 respectively. This was achieved by a systematic examination of various combinations of A and B. A graphical representation of the effects of

A and B on joint deformation is given in Figs. 5.3 and 5.4. In Fig. 5.3 constant B remains unchanged at its optimum value of 0.12. It is observed that changes in constant A, alter the slope of the deformation curve especially at the higher load levels where the effect of relative corner deformations (equations (5.4) and (5.5)) become more pronounced. In Fig. 5.4 constant A remains unchanged at its optimum value of 0.76. The changes in constant B affect the slope of the deformation curve more drastically at the lower load levels. It must be noted that although both sets of curves seem rather sensitive to changes in A and B, the controlling mechanism in both cases is the changes in relative normal corner deformations. This is illustrated in Fig. 5.5 where the changes in the value of C are plotted against the total horizontal loads applied to the top of the upper panel for the model shown in Fig. 5.1(a). The value of constant B has no direct influence on changes in C. However, its value when these curves were computed was 0.12. As shown in Fig. 5.5, the sensitivity of C to changes in A was studied by plotting C for 3 values of A including the optimum value of 0.76. The dashed lines indicate the changes in C for slip surface 2. Because of the load contributed to slip surface 2 by the floor slabs, the graphs of changes in C for the 2 surfaces are not identical. The figure shows how the changes in relative normal corner deformations (tilting of the upper panel relative to the lower panel) influence the value of the coefficient C.

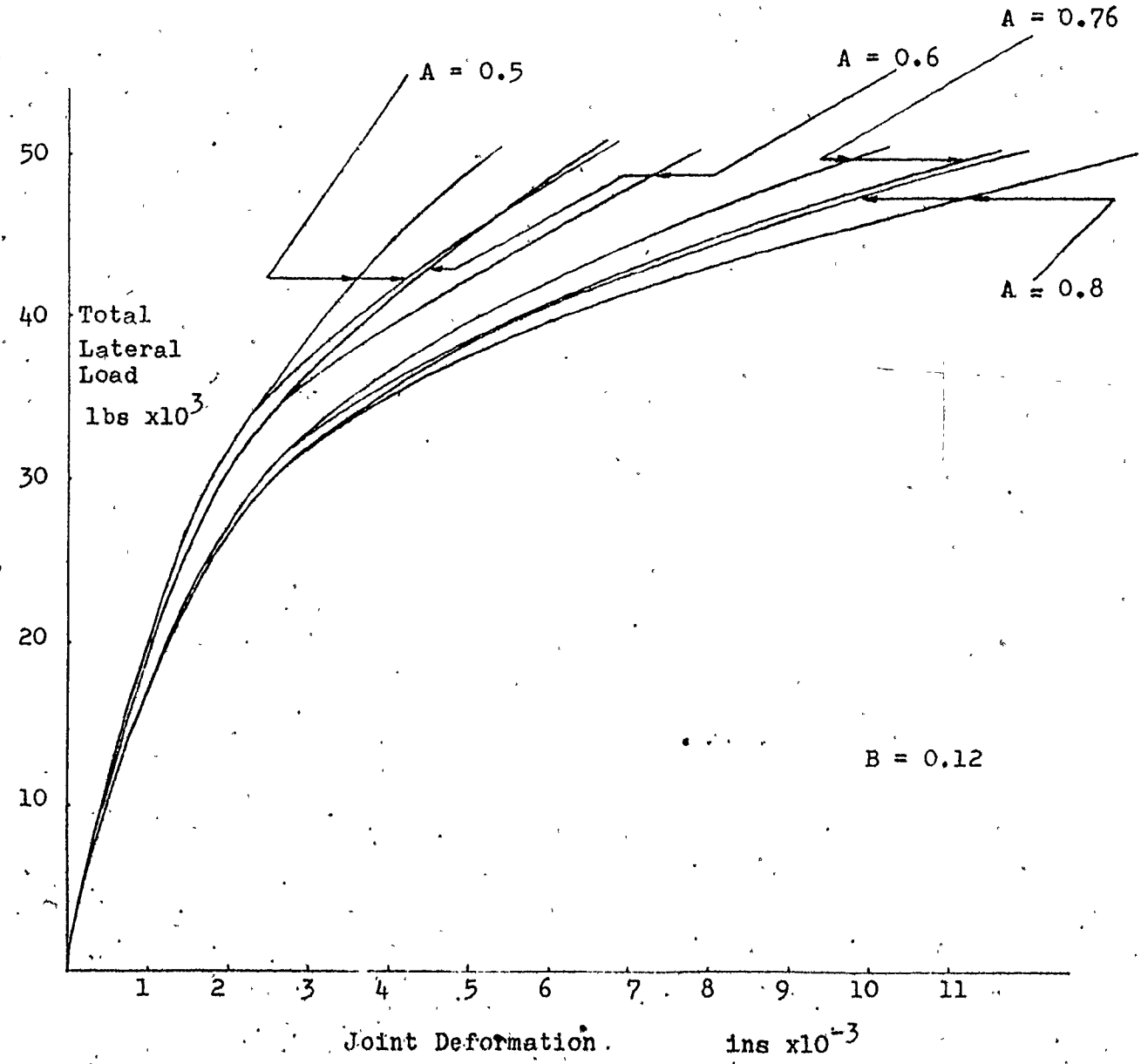

Fig. 5.3 The Effect of Varying Coefficient A for the 2-Element Joint Simplification

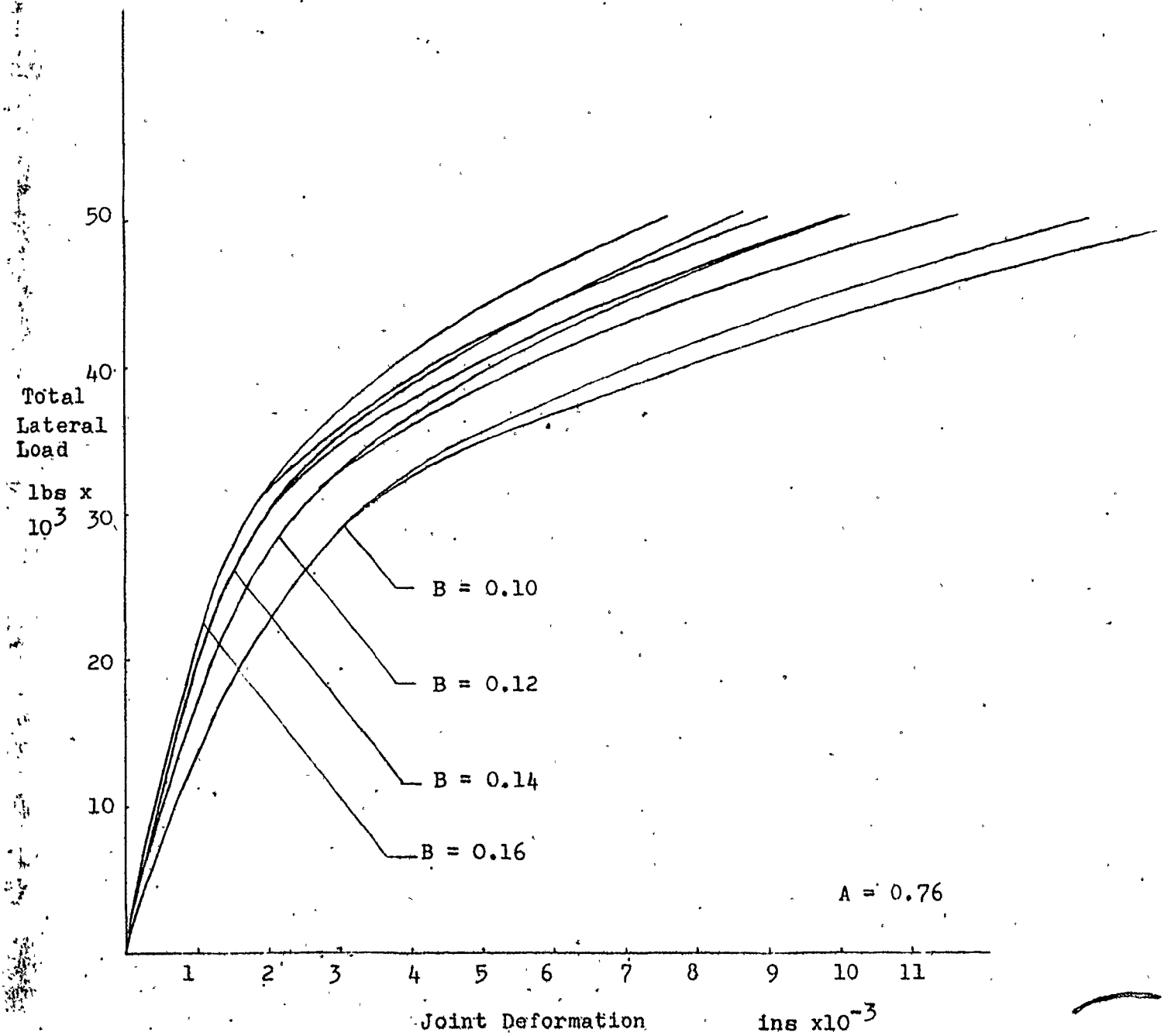

Fig.5.4 The Effect of Varying Coefficient B for the 2-Element Joint Simplification

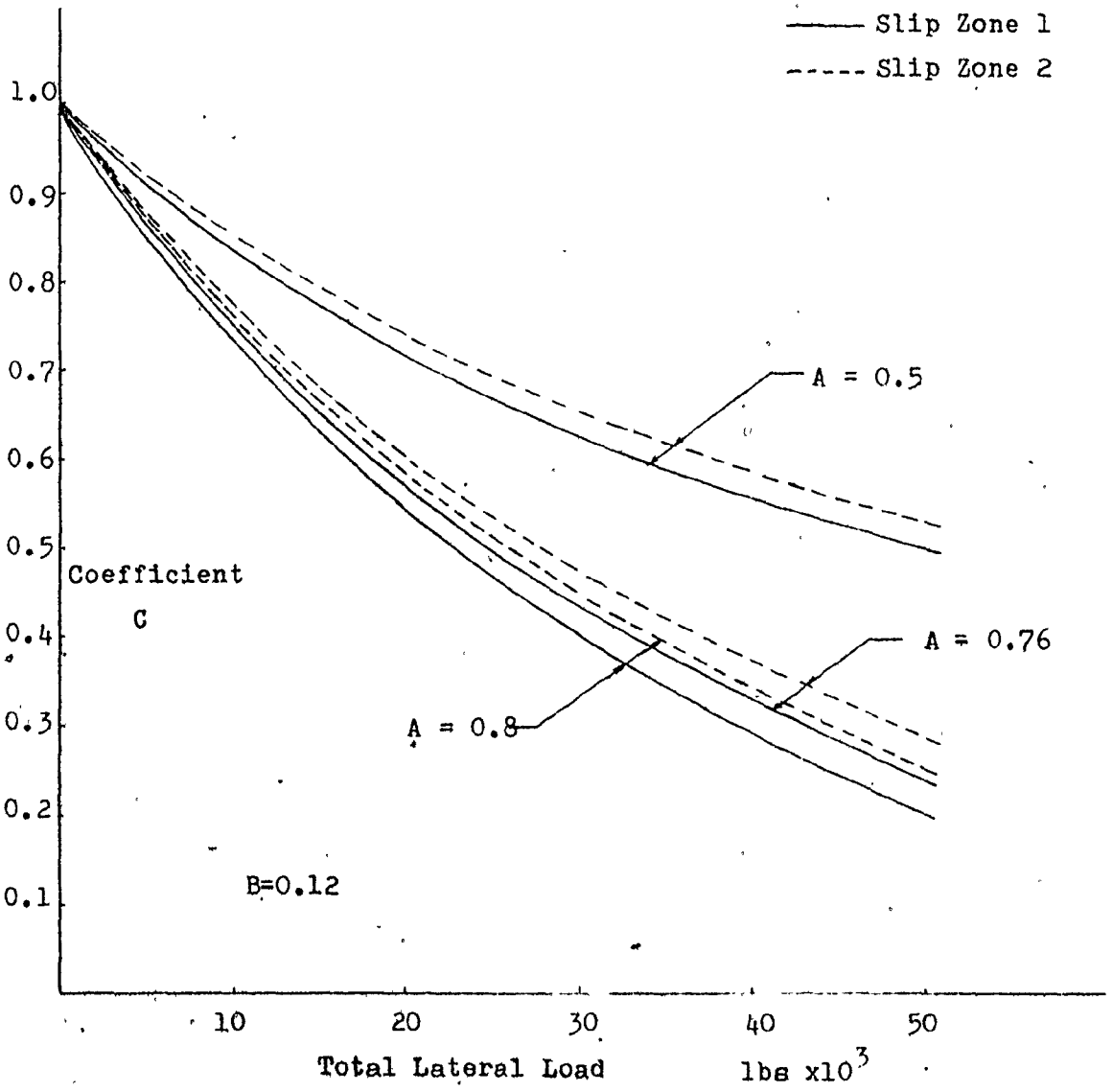

Fig.5.5 Graph of Coefficient C Versus Total Lateral Load

In a complex cantilever, the horizontal joints located at various floor levels are subjected to various combinations of horizontal and vertical loads. Moreover, the load combination for a particular joint changes as the loads applied to the complex cantilever gradually increase. A simplified joint model should be able to accurately simulate the behaviour of all the joints under all loading conditions. For this reason the modification technique was based on the relative normal corner deformations which directly reflect the unique conditions prevailing at a certain joint.

The validity of the modification technique developed here will be tested in the following section, where a number of different cases will be examined using the optimum values of A and B.

It is very important to note that dowel bar action cannot be accurately simulated using a simplified 2-element joint model. As was indicated in section 5.1 and again in section 5.3, for the one panel to one panel connection studied here, separation between the panels cannot be simulated, because disconnection of either of the 2 elements creates instability and indicates the end of the analysis. The effect of joint reinforcement is relatively unimportant prior to separation. However, to be able to model the joint behaviour after separation, the 3-element simplification is also investigated as will be explained in section 5.5.

5.4 Results of the Analysis for the 2-Element Simplification

The deformation curves using the simplified analysis for the effect of increasing vertical loads are shown in Fig. 5.6. The constants A and B selected for this analysis are 0.76 and 0.12 respectively. As the analysis of the previous section indicated, these were found to be the most suitable values for simulating the behaviour of the 2-element joints. To make comparison with the detailed analysis (using 8 elements) easier, the corresponding curves shown in Chapter 3 are also presented on the same diagram. The curves are equally applicable to concentrated as well as distributed shear forces applied to the top of the panel.

With reference to the simplified case, the differences in displacements between the two sides of the joint are quite small when compared with the corresponding differences obtained from the detailed analysis. This discrepancy is primarily a function of the number of elements used to represent the system. A more accurate representation of the system, as will be seen in the following sections, will produce results which are much closer to those of the detailed analysis.

When the vertical load is the equivalent of 2-1/2 stories, it is seen that the simplified analysis slightly overestimates the deformations. This is because constants A and B were chosen to be equally applicable to all joints. Most of the joints investigated

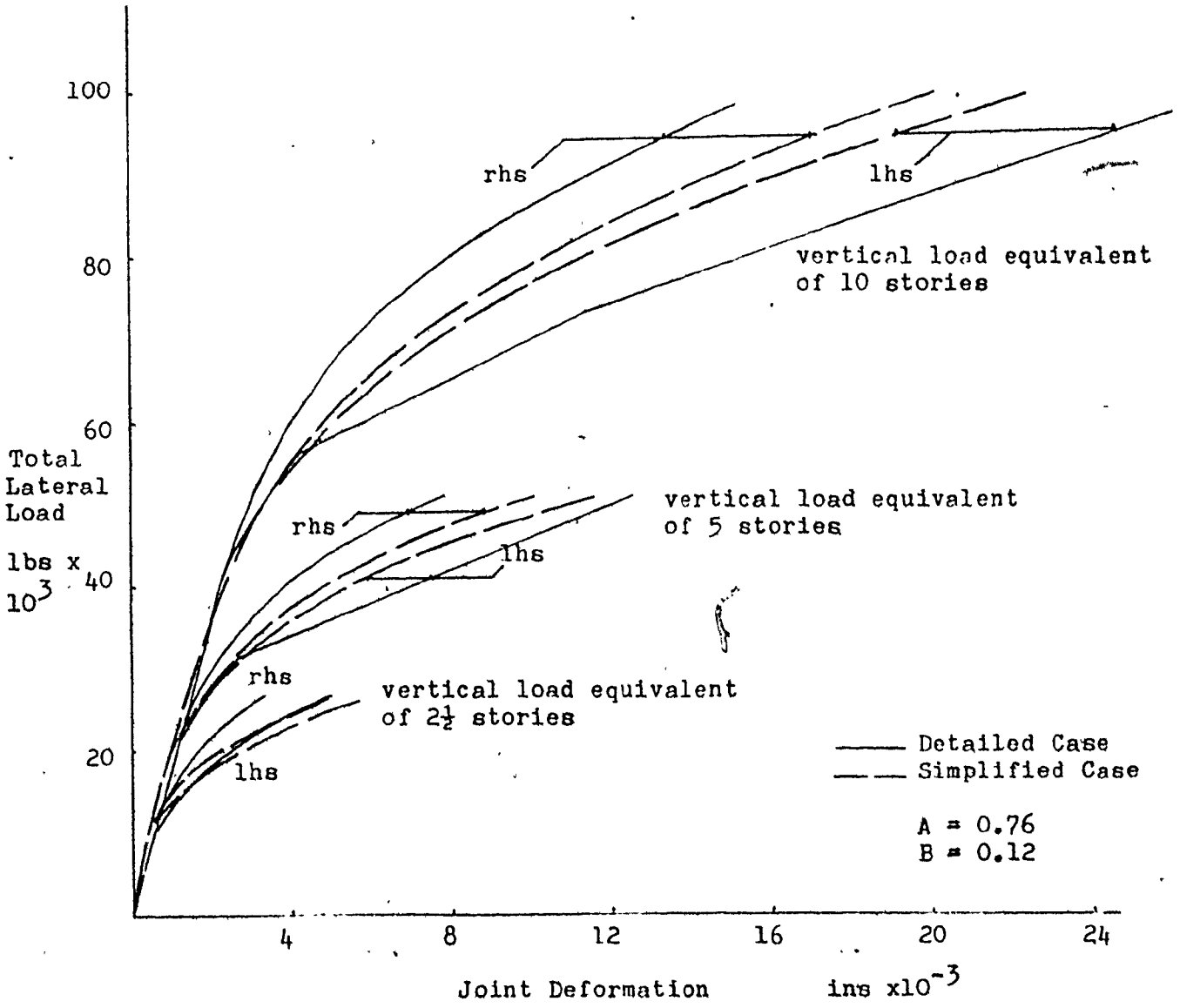

Fig.5.6 Comparison of the Lateral Deformation for the 2-Element Simplified Horizontal Joint and the Detailed Analyses

using the detailed analysis show cracking along slip surface 2 in addition to the cracking of the tie-beam. However, when the vertical load is the equivalent of 2-1/2 stories, tie-beam cracking does not occur, and as a result, the deformation curve does not exhibit the sudden increase in deformation which characterizes the other cases.

The effect of very high gravity loads (equivalent of 40 stories) is shown in Fig. 5.7. The simplified analysis overestimates the deformation by approximately 10%.

It must be noted that when considering compression-type failure, the effect of accumulating the stiffnesses at the two extremities of the joint requires that a further reduction factor be imposed on the ultimate compressive strength of the concrete. Using the rotation of panels as a measure of this reduction factor, the calibration coefficient C can again be utilized as a means of modifying the ultimate compressive strength of the concrete.

The effect of panel size is illustrated in Fig. 5.8. It is found that changing the size of the panels does not effect the modification coefficient, C, or the constants A and B required to approximate their deformation curves. Thus, the correlation is consistent for all sizes.

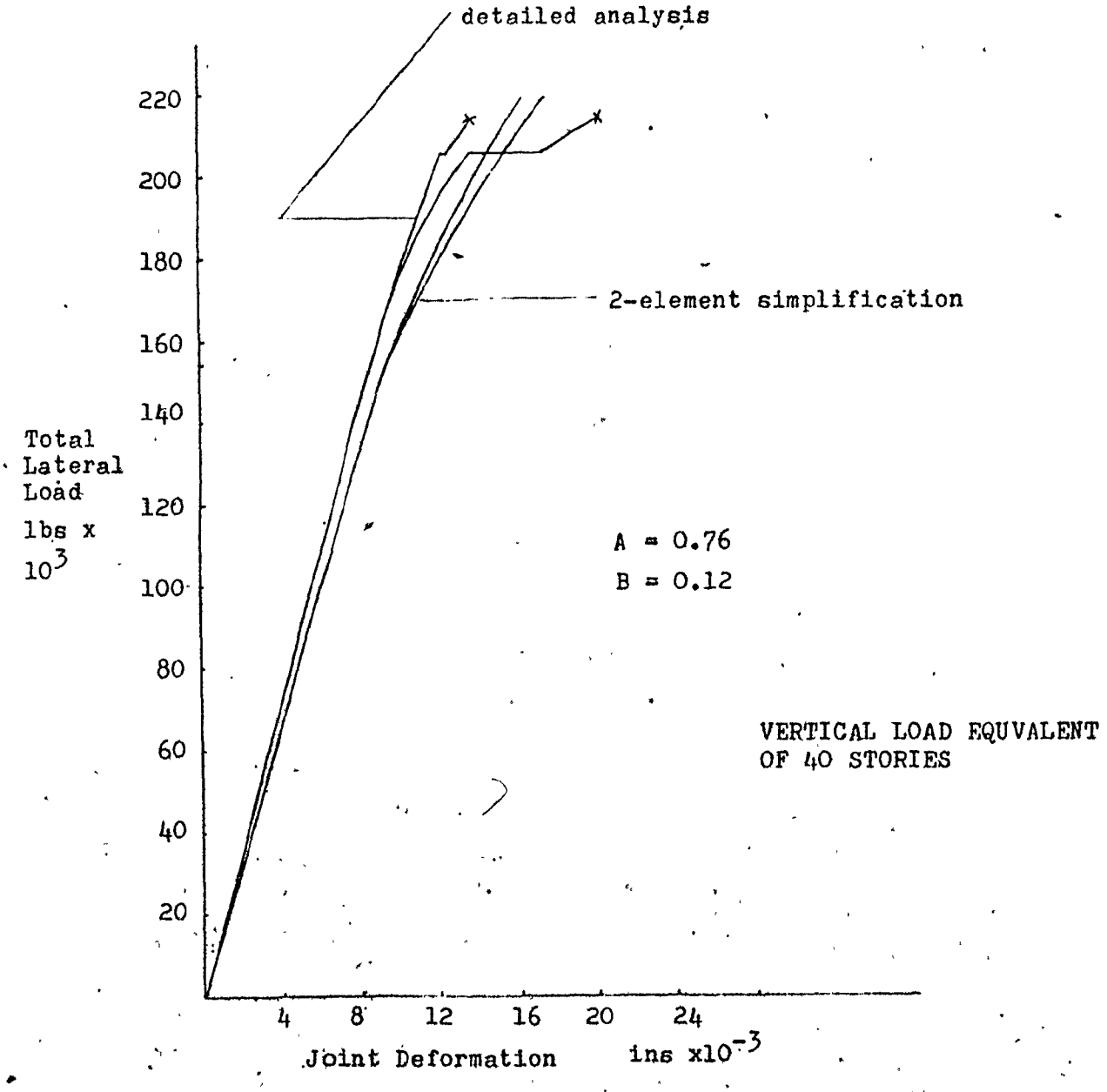

Fig. 5.7 Compression Failure: Comparison of the Lateral Deformation for the 2-Element Simplified Horizontal Joint and the Detailed Analyses

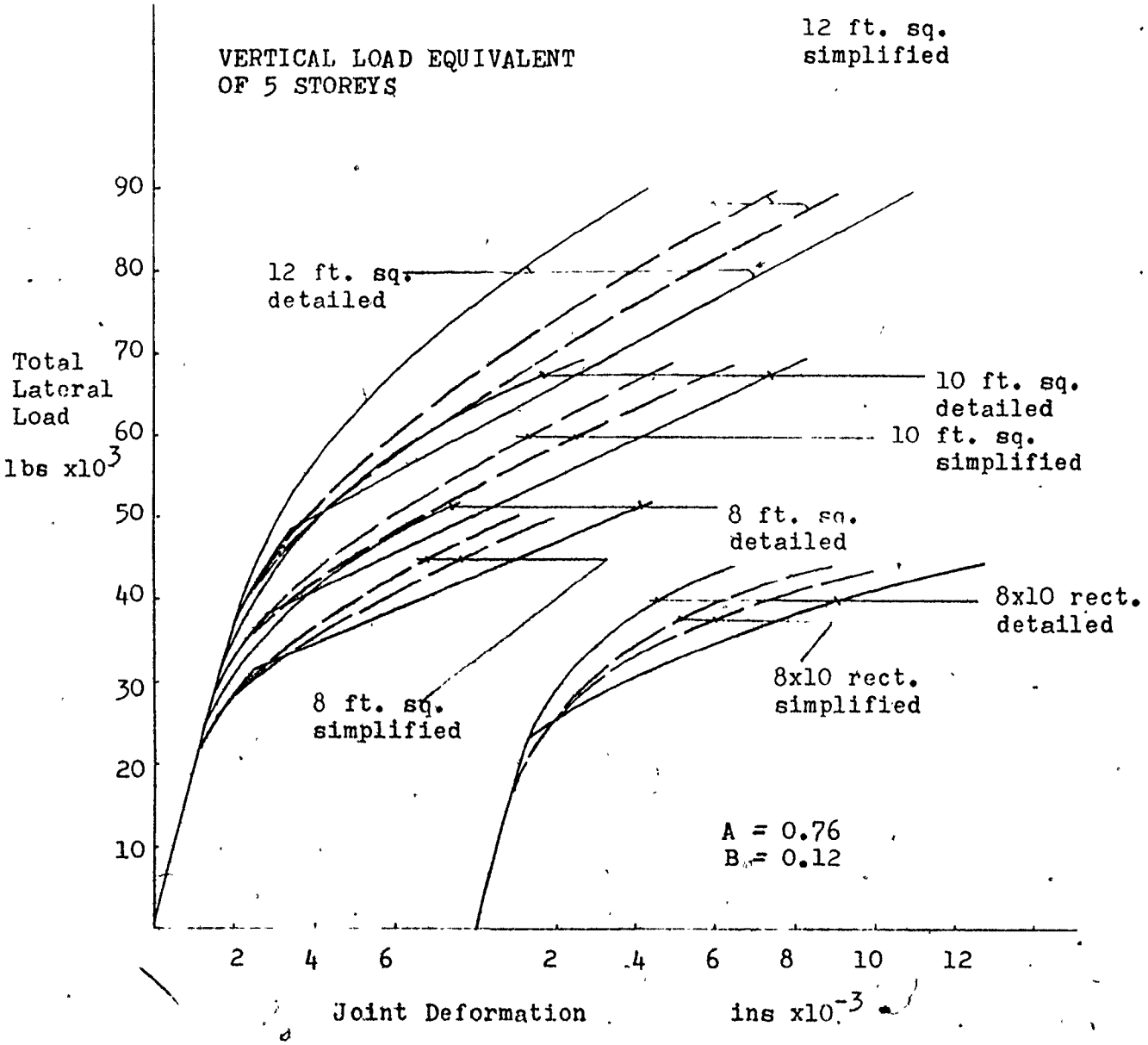

Fig.5.8 Effect of Panel Size: Comparison of Lateral Deformation for the 2-Element Simplified Horizontal Joint and the Detailed Analyses

5.5 3-Element Simplification by Successive Modification of the Stiffnesses

Relative normal deformations are again used as a means of successively modifying the spring stiffnesses. Starting from the left side (Fig. 5.1(b)) and identifying the three joint elements by numbers 1, 2 and 3, coefficient 'C' before separation of the second element is given by the following relationship:

$$C = 1 - \frac{|y_i| - |y_2|}{|y_i|} \cdot A \qquad (5.7)$$

Subscript i is either 3 or 1 depending on whether there is a tendency for separation at the left or the right side of the joint. A has the same meaning as in section 5.3.

If a joint forms part of a complex cantilever, there is a possibility of separation extending to 2 elements. The coefficient C in this case is given by:

$$C = (1-A) - \frac{|y_2|}{|y_2| + |y_i|} (1-A) \qquad (5.8)$$

Subscript i has the same meaning as in equation (5.7).

Figure 5.9 shows the graph of C versus total lateral load for a value of A = 0.55 which is found to be suitable for the 3-element simplification. As observed there is a sharp drop in the value of C for slip zone 1 after the first element is separated. The elements on slip surface 2 do not separate. The sharp drop in the value of C is the result of an accelerated change in the values of the relative normal deformations of elements 2 and 3. However, before the separation of the first element,

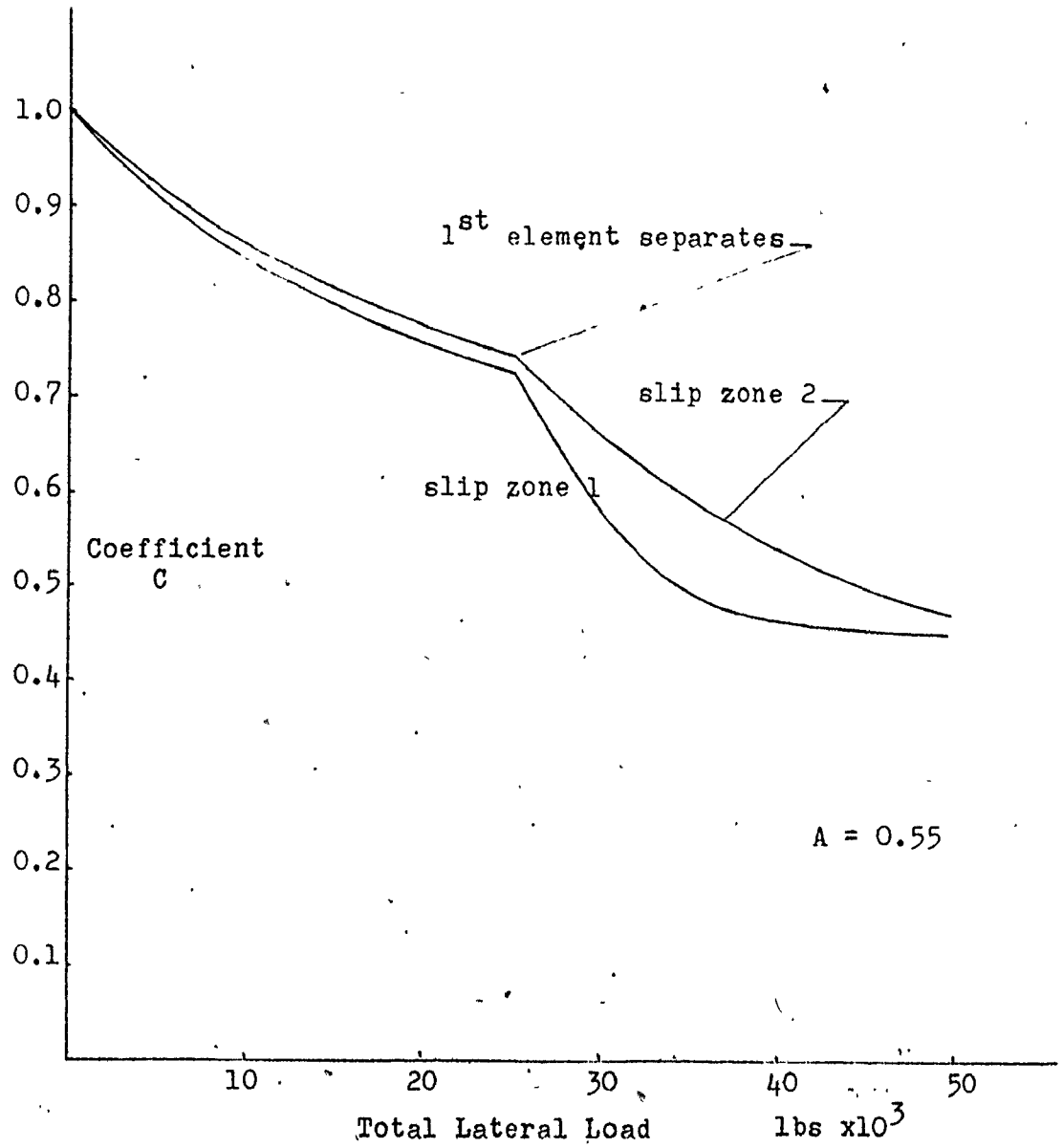

Fig.5.9 Graph of Coefficient C Versus Total Lateral Load for the 3-Element Simplified Analysis

the curves for the two slip surfaces lie very close to one another. They do not coincide because relative normal corner deformations between the edges of the upper and the lower panels and the bar element are not the same. The difference in deformation is due to the floor loads being applied directly to the bar element.

As was stated previously, the 3-element simplification to some degree allows for joint separations to be simulated. In Fig. 5.10, the solid lines represent the normal corner deformations as determined by the detailed analysis. The dashed lines represent the same for the 3-element simplified case when the normal spring stiffnesses of the joint elements are left unmodified. The third set of lines illustrates the corner deformations when a vertical spring modification coefficient D is introduced in the analysis. D is taken as a 2nd degree polynomial in terms of C and for the 3-element modified case shown in Fig. 5.10 it was found to give satisfactory results when expressed in the form:

$$D = 1.5C^2 - 0.5C \qquad (5.9)$$

Equation (5.9) was derived on the basis of the following basic premise. It was argued that by a proper reduction in the stiffnesses of the vertical springs of the joint elements in the simplified model, it had to be possible to obtain a closer approximation to the curve of the detailed analysis shown by solid lines in Fig. 5.10. After a number of unsuccessful preliminary attempts, in which relationships of the type indicated by equation (5.6)

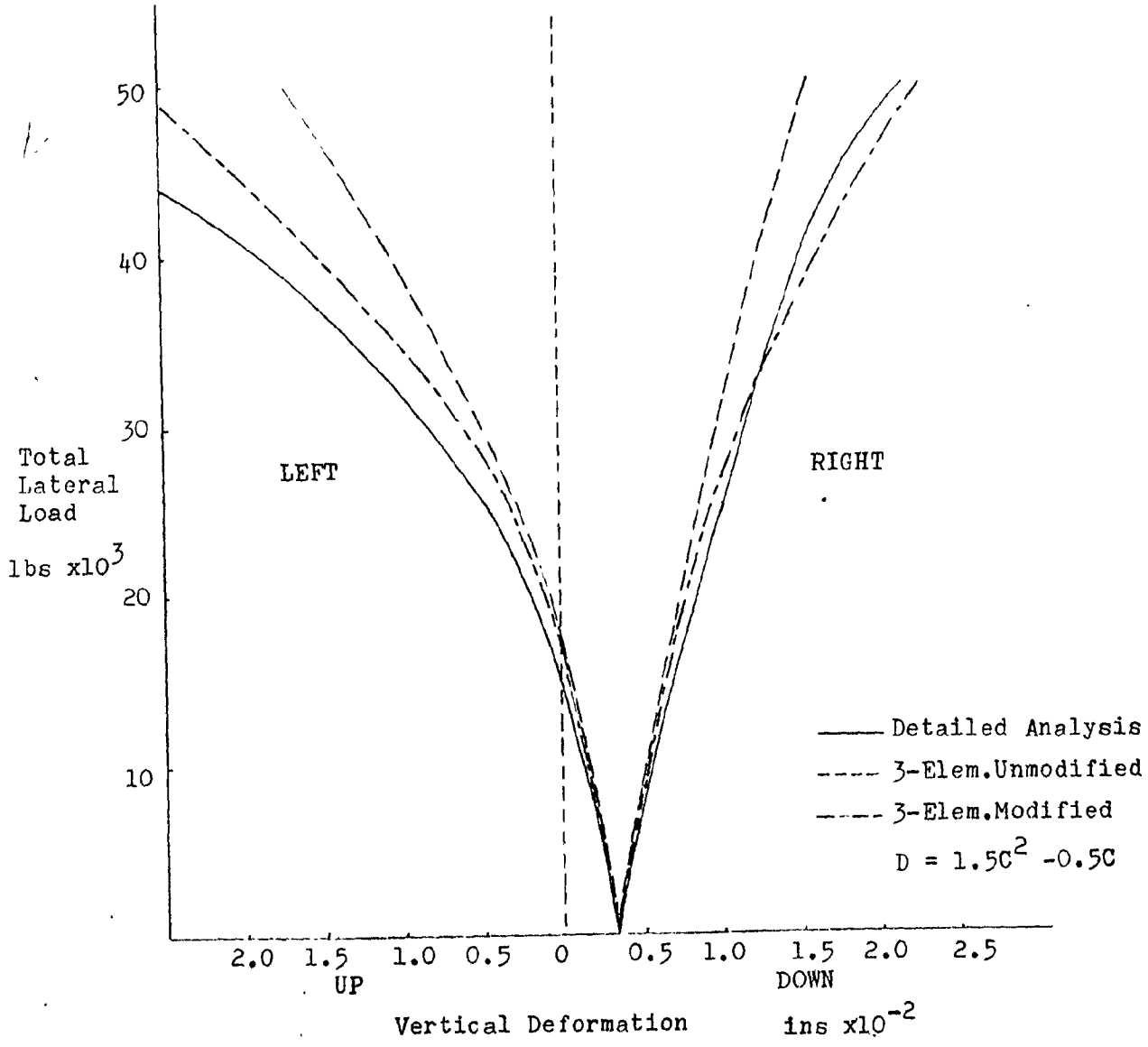

Fig.5.10 Lateral Load Versus Vertical Corner Deflections of the Upper Panel for the Simplification Shown in Fig. 5.1 (b)

were used for the modification of the vertical spring stiffnesses, it was concluded that a more complicated form of modification was necessary.

This was accomplished by the appropriate choice of the coefficients in a general polynomial equation of the form $D = a_1 + a_2 C + a_3 C^2 + \ldots$ The coefficients in equation (5.9) were determined using a simple computer program which systematically examined a range of coefficients starting with the simplest possible form of the equation given by $D = a_1 + a_2 C$. The optimum values for the coefficients were those which produced a deflection curve best fitting both branches of the solid line shown in Fig. 5.10. This was accomplished by modifying the vertical springs of the elements in accordance with the following equations:

$$(K_n^m)_i = (K_n)_i \cdot D, \quad i = 1, 2, 3 \qquad (5.10a)$$

where K_n^m is the new modified normal spring stiffness, K_n is the original unmodified normal spring stiffness and subscript i denotes the element number. Equation (5.10a) is applicable as long as there is no separation.

After separation, however, equation (5.10a) may be written as follows:

$$(K_n^m)_i = (K_n)_i \cdot D, \quad i = 1 \text{ or } 3 \qquad (5.10b)$$

In this case subscript i is either 3 or 1 depending on whether there is a tendency for separation at the left or the right side of the joint.

The process of successive modification of the horizontal springs is more complicated in the case of the

3-element simplification since a single modifying function cannot be found to be applicable throughout the entire loading range. Depending on the behaviour of the 3 joint elements, 4 loading stages may be distinguished. A different modification coefficient must be found for each stage.

First stage: There is no separation in this stage. In addition, the vertical and horizontal element springs act independently of one another. Under these conditions the shear spring stiffnesses may be modified as follows:

$$(K_s^m)_i = (K_s)_i \cdot C \cdot B_1, \quad i = 1, 2, 3 \qquad (5.11)$$

where K_s^m and K_s are the modified and original shear spring stiffnesses, respectively, C is given by equation (5.7) and B_1 is yet another coefficient. Its numerical value of 0.106 was obtained using the same technique as was adopted for determination of B in equation (5.6). Subscript i denotes the element number. Equation (5.11) has the same form as equation (5.6) for 2-element simplification.

Second stage: Stage 2 is the same as stage 1 except that element 1 is in a slipped condition. The shear and normal spring stiffnesses are no longer independent and the modified shear spring stiffnesses are given by:

$$(K_s^m)_i = (K_s)_i \cdot B_2, \quad i = 2, 3 \qquad (5.12)$$

It is very difficult to evaluate B_2 in such a way that the boundary deformations at the transition from one stage to the next remain perfectly compatible under all loading conditions. It is, however, possible to approximate

B_2 so that reasonable accuracy is obtained in all cases. The same condition is true for stages 3 and 4. Thus in stage 2, B_2 may be expressed as a function of C by the following approximate relationship:

$$B_2 = 0.695C - C^3 \qquad (5.13)$$

Equation (5.13) was obtained following procedures similar to those adopted for the determination of D (equation 5.9), namely, systematic examination of a range of coefficients starting with the simplest form of a general polynomial equation. The appropriate coefficients were those which produced optimum joint deformation curves in terms of both the orientation and the compatibility of the deformations at the boundary between the first and the second stages. The same type of procedure was adopted for the determination of the expressions for the modification of the shear spring stiffnesses in the third and fourth stages.

Third stage: Stage 3 is the same as stage 2 except that element 1 is separated. The modified shear spring stiffnesses may be written as:

$$(K_s^m)_i = (K_s)_i \cdot B_{3i}, \quad i = 2, 3 \qquad (5.14)$$

Coefficients B_{3i} may again be expressed in terms of C as given by the following relationships (adopting the same approach used for the determination of B (Section 5.3) and B_2)

$$B_{32} = -0.055C + 0.307C^2$$

$$B_{33} = 0.199C - 0.0473C^2 \qquad (5.15)$$

Fourth stage: For stage 4 element 1 is separated and a state of slip exists for element 2. This is the last phase of the analysis as separation of element 2 indicates instability and causes the stiffness matrix to become singular. The stage 4 modification relationship may be written as:

$$(K_s^m)_3 = (K_s)_3 \cdot B_4 \qquad (5.16)$$

where B is given by the following approximate equation:

$$B_4 = 0.603C - 0.889C^2 \qquad (5.17)$$

5.6 Results of the Analysis for the 3-Element Simplification

The graph of lateral load versus joint deformation for the 3-element simplification and under the vertical load equivalent of 10 storeys is shown in Fig. 5.11. The corresponding curve utilizing the detailed analysis of Chapter 3 is also drawn for the purpose of comparison. The results are on the whole more representative than those obtained using the 2-element simplification.

It must be emphasized that the procedures developed for the modification of the simplified analysis remained unchanged for the various cases studied in this section.

The difference in deformations between the two ends of the joint in all cases reported in this section are less than the corresponding cases reported in Chapter 3. As was discussed in relation to the 2-element simplification, the discrepancy is the function of the number of elements used to represent the system. The 3-element representation

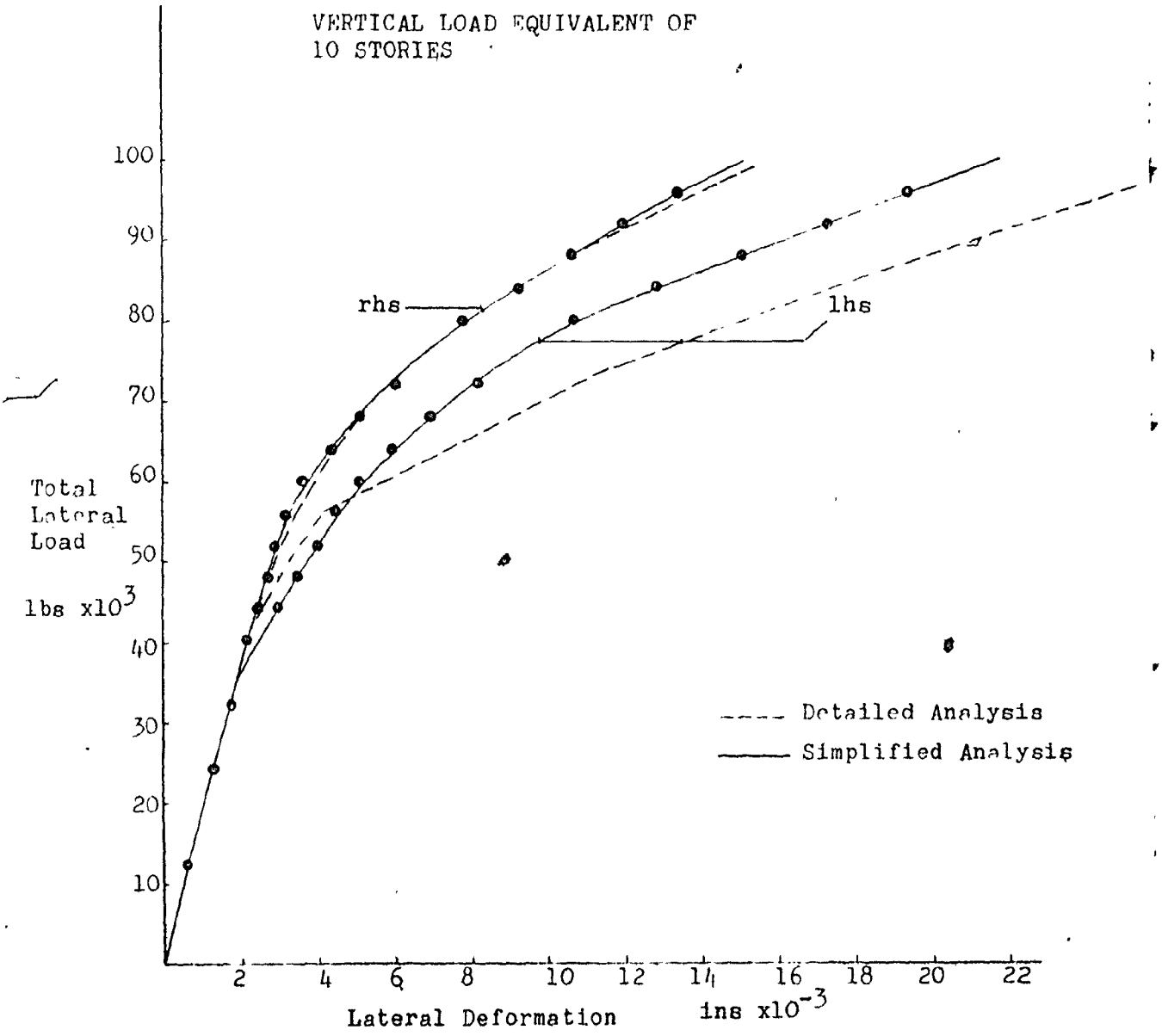

Fig.5.11 Comparison of the Lateral Deformation for the 3-Element Simplified Horizontal Joint and the Detailed Analyses (Vertical Load Equivalent of 10 Storeys)

simulates this aspect of the behaviour with a lot more accuracy than its 2-element counterpart.

Similar curves for cases where the vertical load is the equivalent of 5 and of 2-1/2 storeys are shown in Fig. 5.12. As expected, the simplified analysis in the case of the lower gravity load slightly overestimates the deformations. As was discussed in Section 5.4 this is because the simplified analysis is geared to take into account the effect of tie-beam cracking which becomes prominent with higher gravity loads.

The effect of very high gravity loads is shown in Fig. 5.13. Except where separation occurs, the curve seems to be in very good agreement with the detailed analysis.

The effect of panel size was studied using 12 ft. square and 8 x 10 rectangular panels. The resulting curves are shown in Fig. 5.14. As can be observed fairly good agreement is obtained between the deformation curves of the detailed and the simplified models.

The effect of lateral loads on the behaviour of reinforced horizontal joints for the vertical load equivalents of 2-1/2, 5 and 10 stories is shown on Figs. 5.15, 5.16, and 5.17 respectively. As was explained in Chapter 3, the effect of joint reinforcement as measured by increased ability to resist shear forces, is a lot more pronounced for joints with lower gravity loads. With reference to Figs. 5.15, 5.16 and 5.17, it is observed that, as the effect of joint reinforcement becomes less significant,

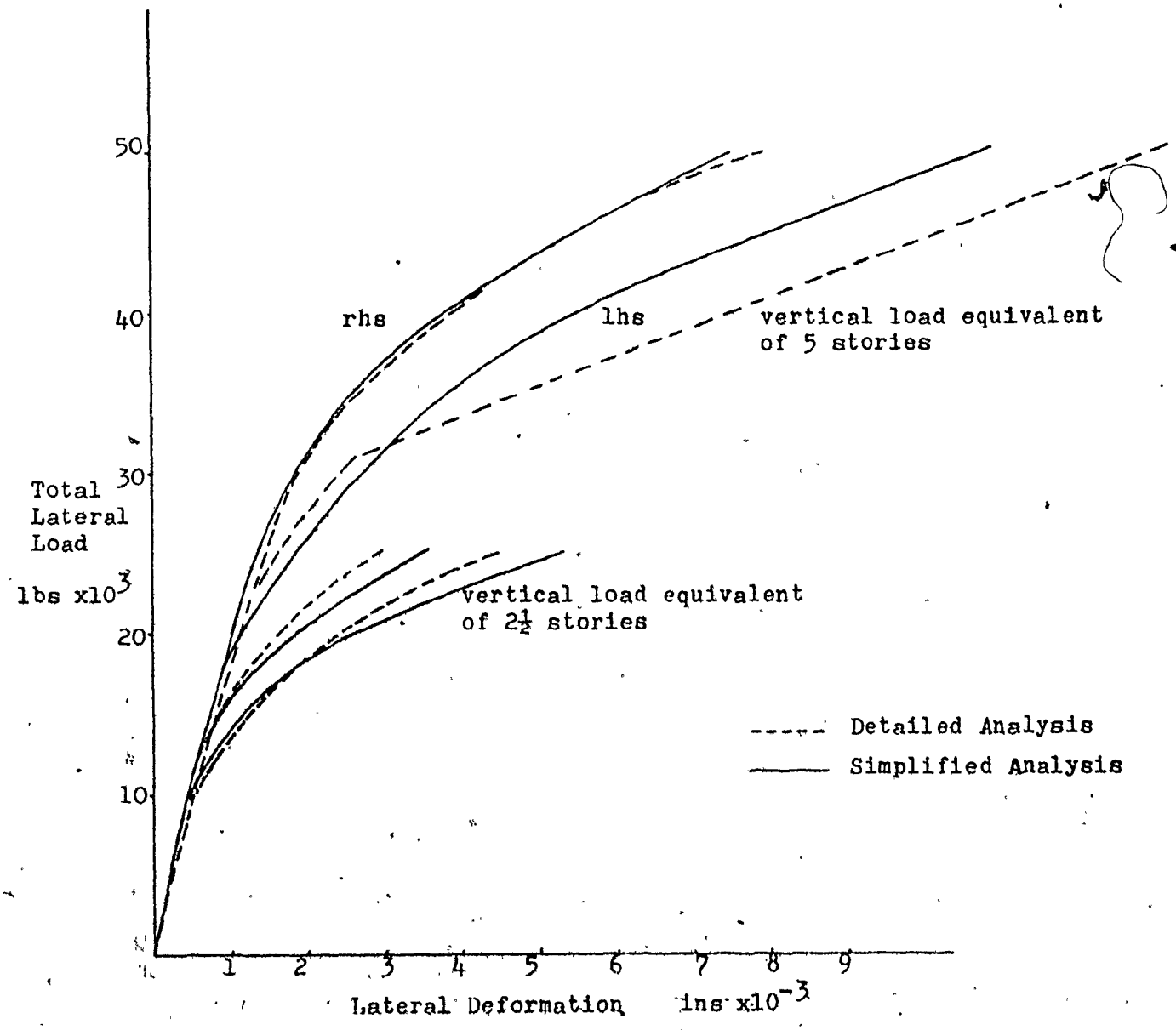

Fig.5.12 Comparison of the Lateral Deformation for the 3-Element Simplified Horizontal Joint and the Detailed Analyses (Vertical Load Equivalent of 5 and 2½ Storeys)

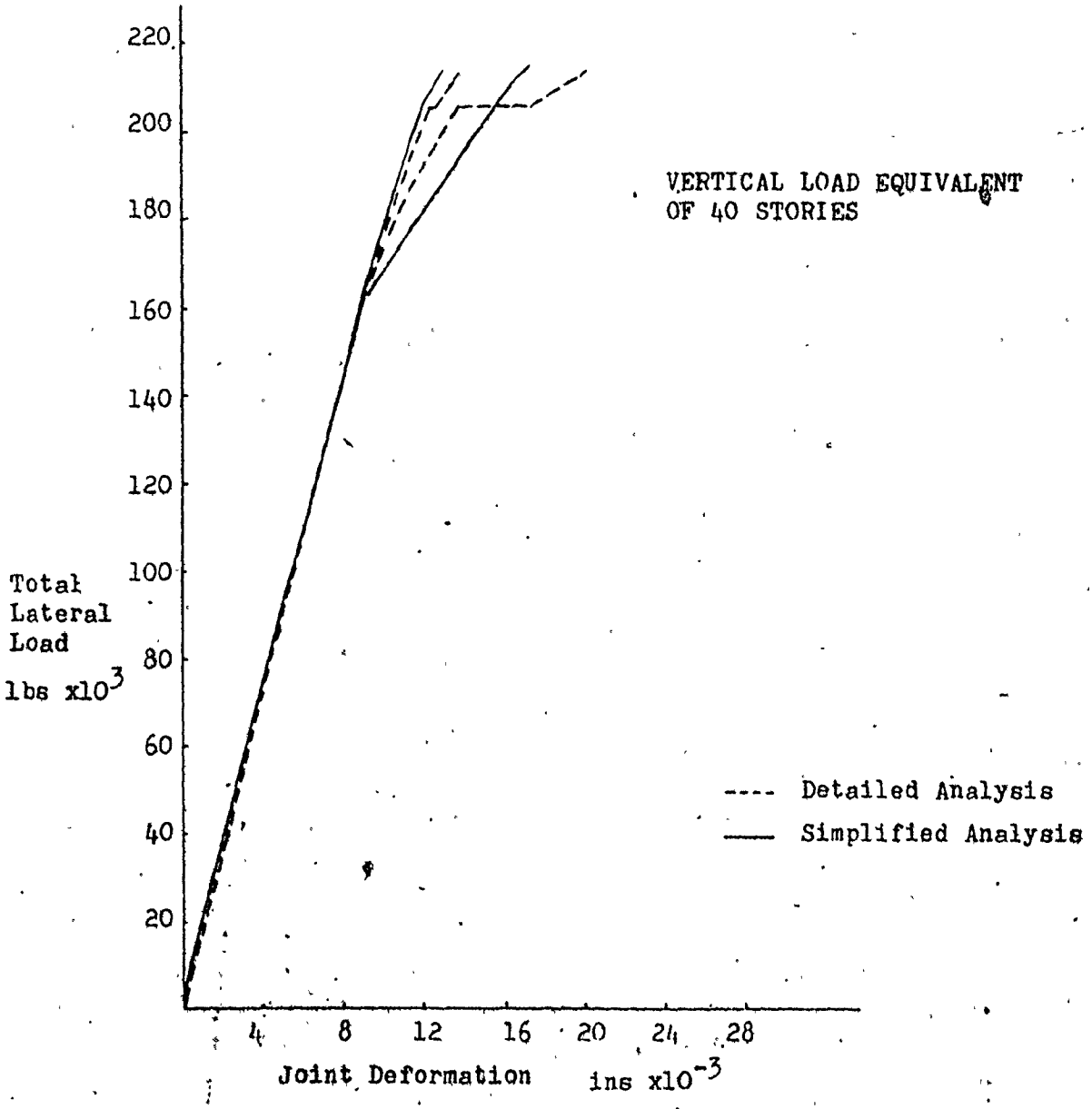

Fig.5.13 Compression Failure: Comparison of the Lateral Deformation for the 3-Element Simplified Horizontal Joint and the Detailed Analyses

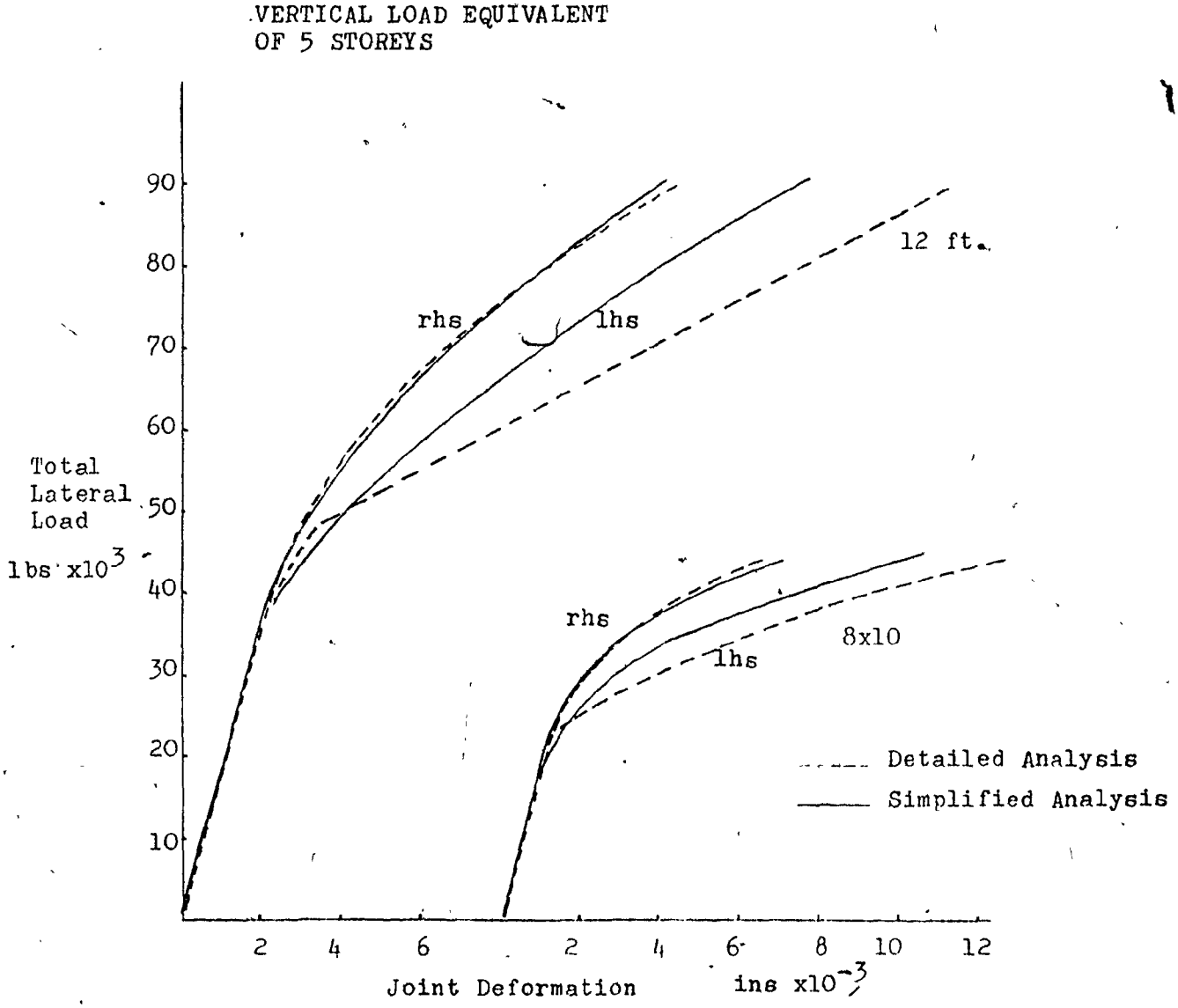

Fig.5.14 Effect of Panel Size: Comparison of Lateral Deformation for the 3-Element Simplified Horizontal Joint and the Detailed Analyses

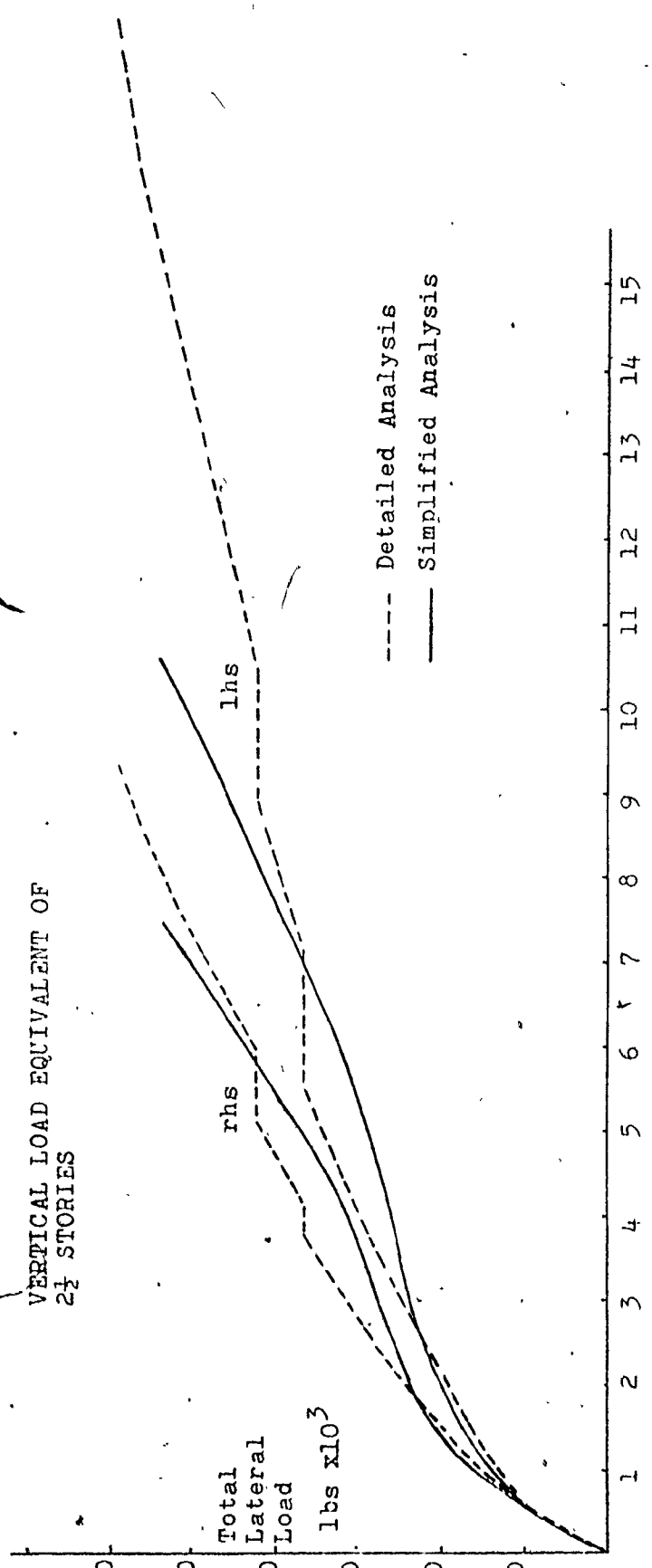

Fig.5.15 Lateral Load Versus Reinforced Joint Deformation: Comparison of the Results for the 3-Element Simplification and the Detailed Model Developed in Chapter 3 (Vertical Load Equivalent of 2½ Storeys)

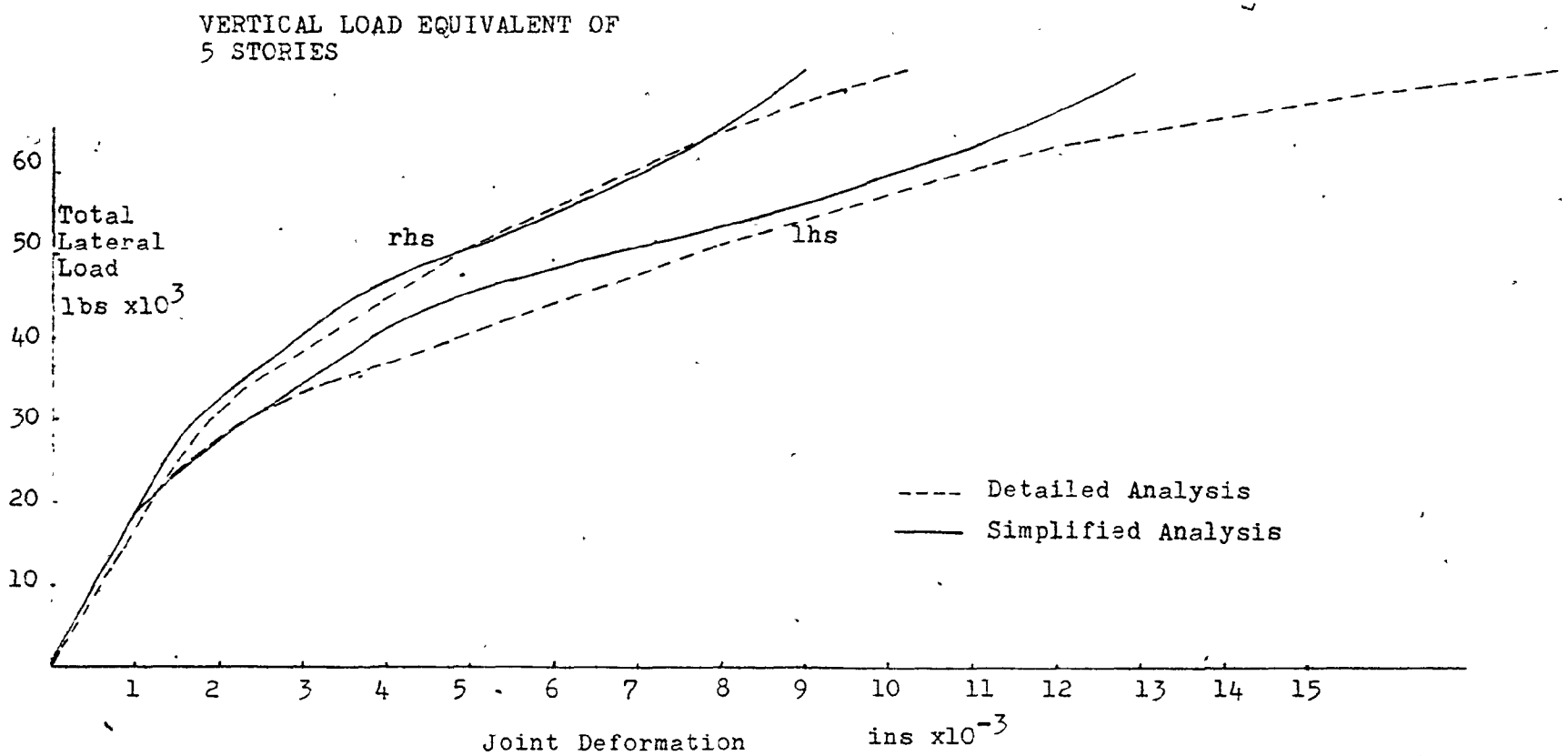

Fig.5.16 Lateral Load Versus Reinforced Joint Deformation : Comparison of the Results for the 3-Element Simplification and the Detailed Model Developed in Chapter 3 (Vertical Load Equivalent of 5 Storeys)

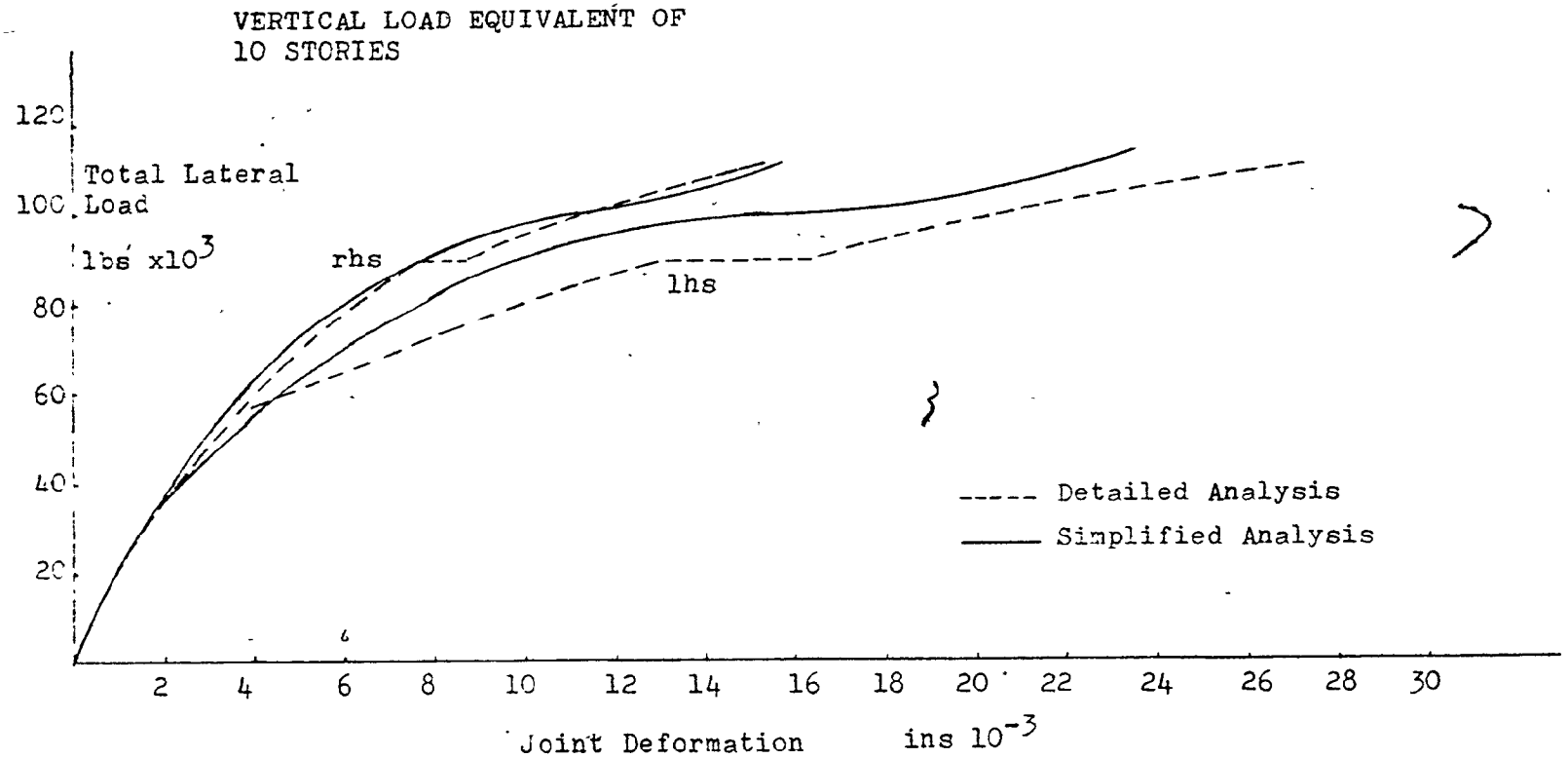

Fig.5.17 Lateral Load Versus Reinforced Joint Deformation :Comparison of the Results for the 3-Element Simplification and the Detailed Model Developed in Chapter 3(Vertical Load Equivalent of 16 Storeys)

the deformation curves obtained using the simplified analysis become more representative of those determined using the detailed method.

The forces in the reinforcing elements' horizontal and vertical springs which represent respectively the dowel action and the vertical continuity (provided by the bars) are shown in Figs. 5.18, 5.19 and 5.20. The dashed lines represent the curves obtained from the detailed analysis of Chapter 3. The solid lines are the corresponding forces determined using the simplified analysis. Considering the amount of approximation used in the simplified analysis, the results shown in Figs. 5.18, 5.19 and 5.20 are a surprisingly good representation of the detailed behaviour.

This concludes the development and discussion of the simplified analysis for the horizontal joints. The remainder of this chapter will be devoted to the analysis of simplified vertical joints and to comparing the results with those presented in Chapter 4.

5.7 3-Element Analysis of Simplified Vertical Joints

It was the author's original intention to simplify the vertical joint analysis so that each vertical joint could be represented by two joint elements. However, as the process of simplification of the horizontal joints progressed, it became obvious that in order to be able to adequately represent the horizontal joint behaviour and to allow for joint separation, at least 3 elements were necessary. This meant the introduction of a mid-side

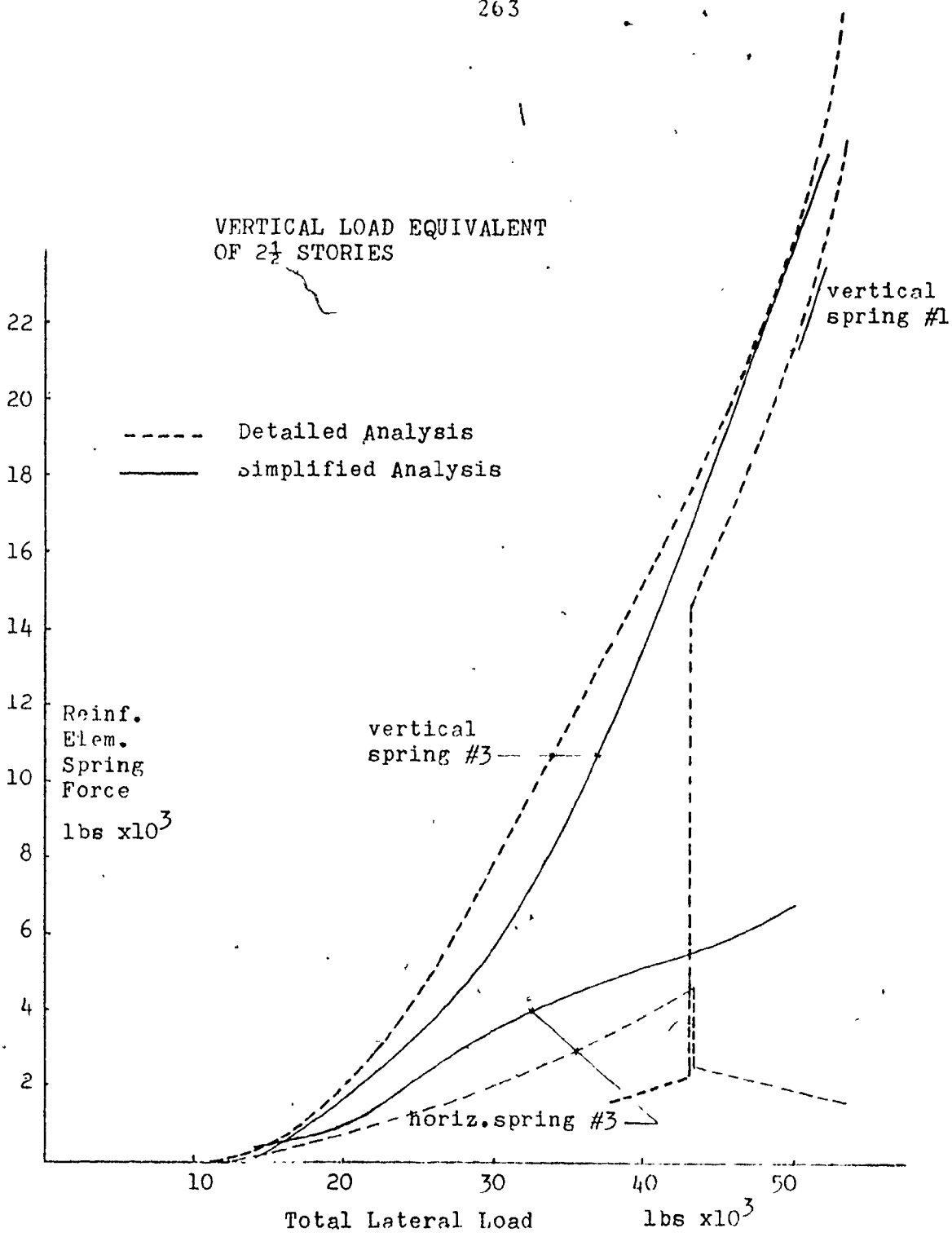

Fig.5.18 Forces in Reinforcement Elements: Comparion of the Results for the 3-Element Simplification and the Detailed Model Developed in Chapter 3(Vertical Load Equivalent of 2½ Storeys)

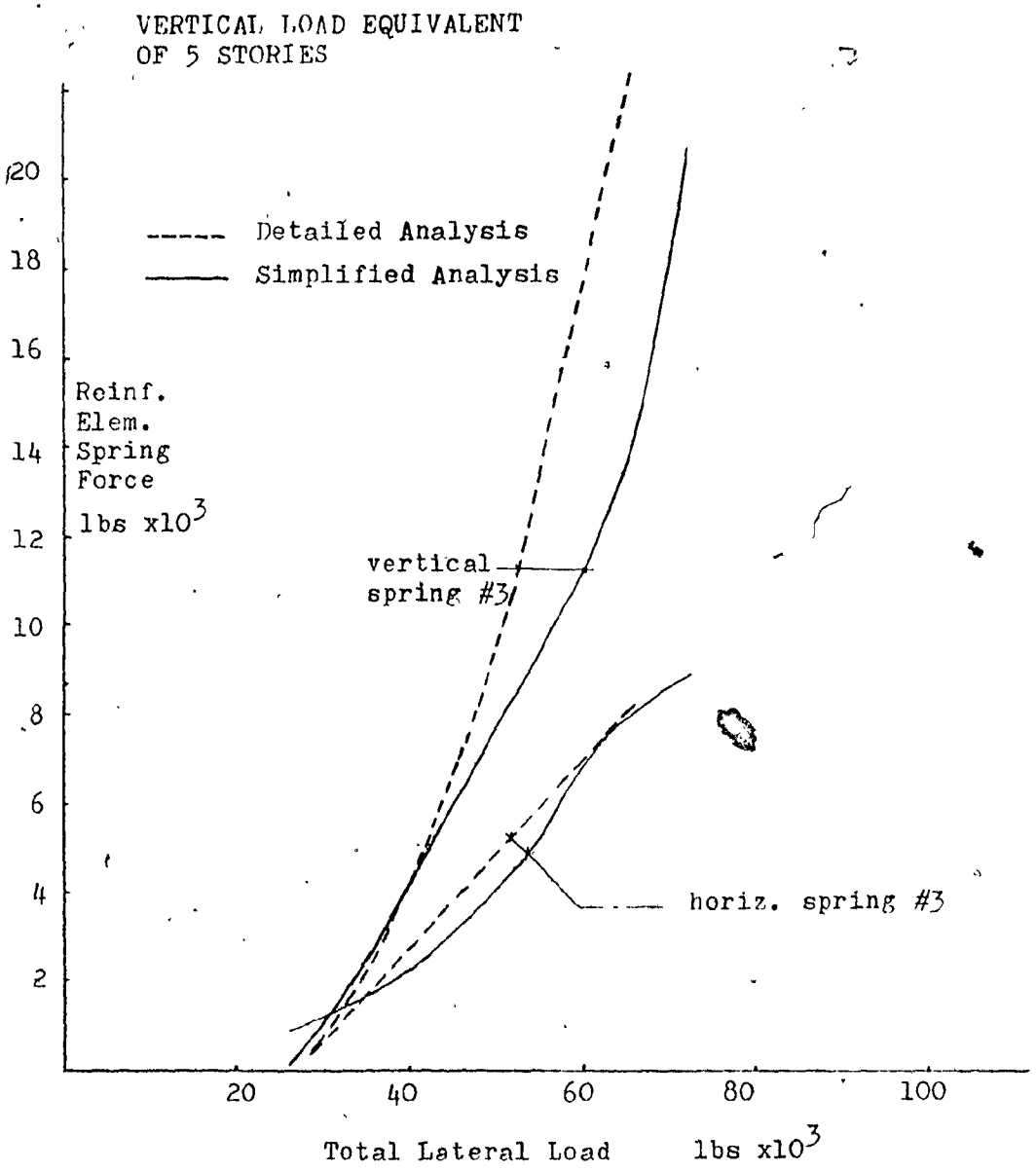

Fig.5.19 Forces in Reinforcement Elements: Comparison of the Results for the 3-Element Simplification and the Detailed Model Developed in Chapter 3 (Vertical Load Equivalent of 5 Storeys)

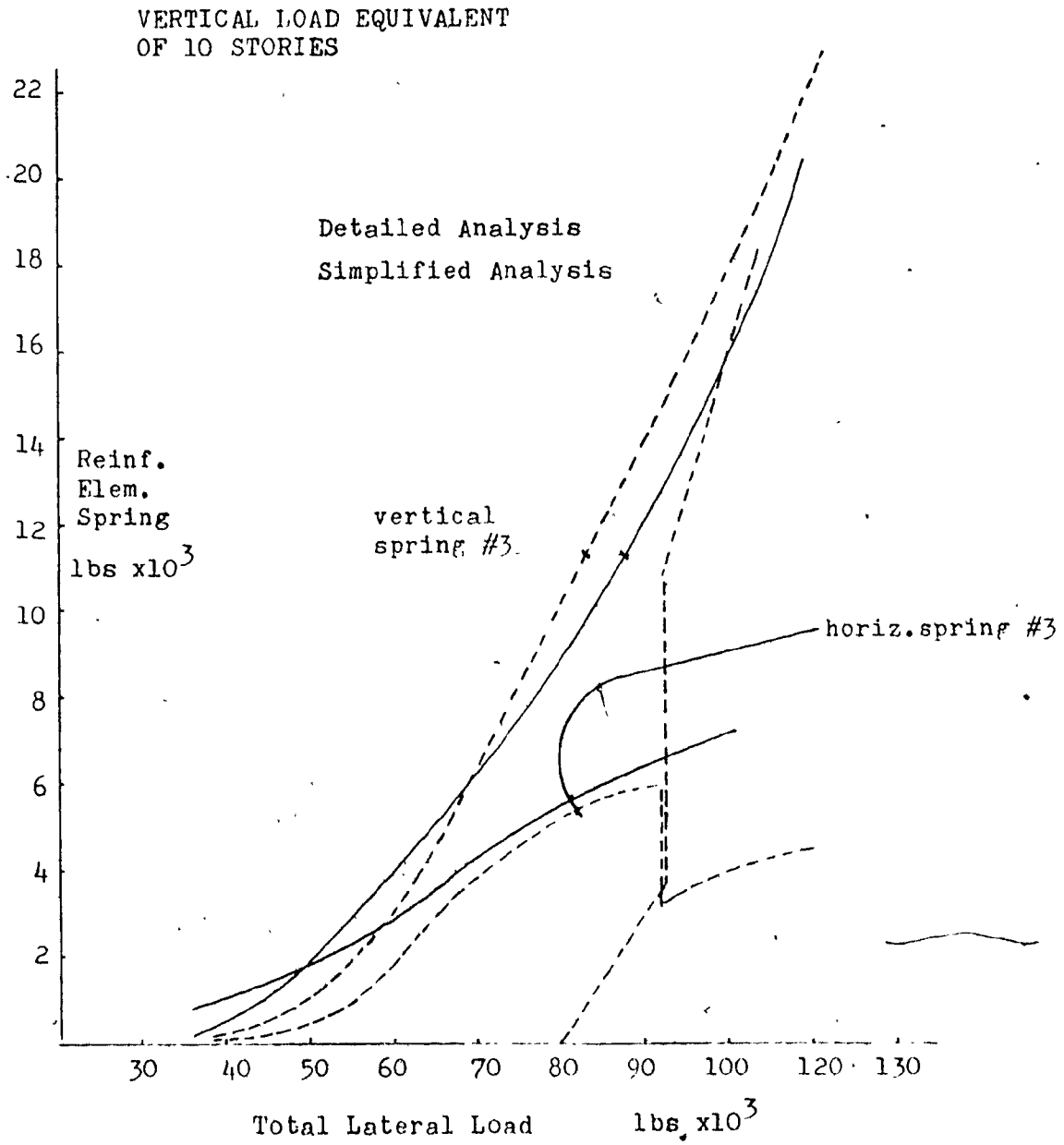

Fig.5.20 Forces in Reinforcement Elements: Comparison of the Results for the 3-Element Simplification and the Detailed Model Developed in Chapter 3 (Vertical Load Equivalent of 10 Storeys)

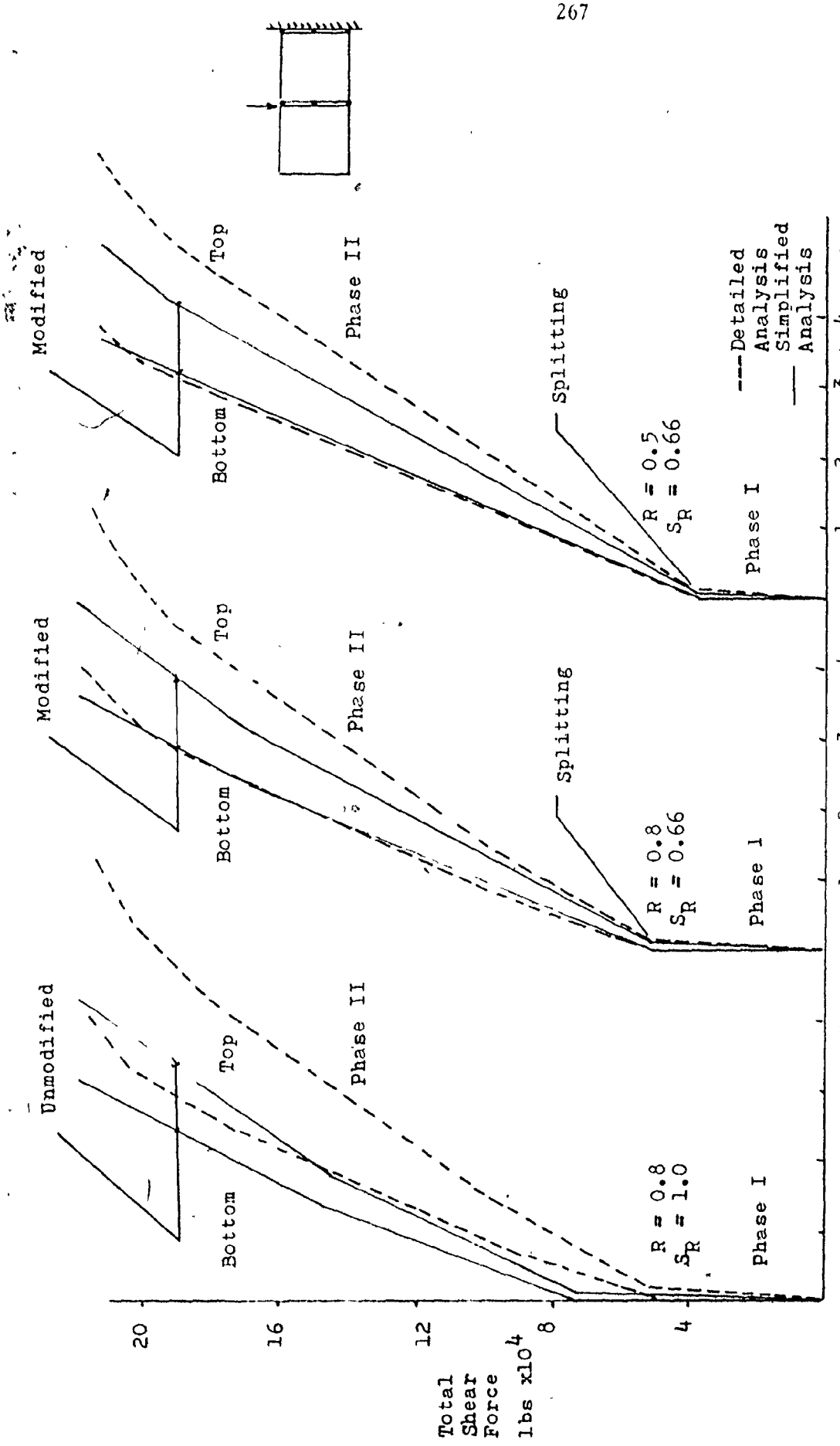

Fig.5.21 Vertical Joint Load-Slip Curve for the 3-Element Simplified Analysis Using Rapid Splitting Criterion (Single Concentrated Shear Force)

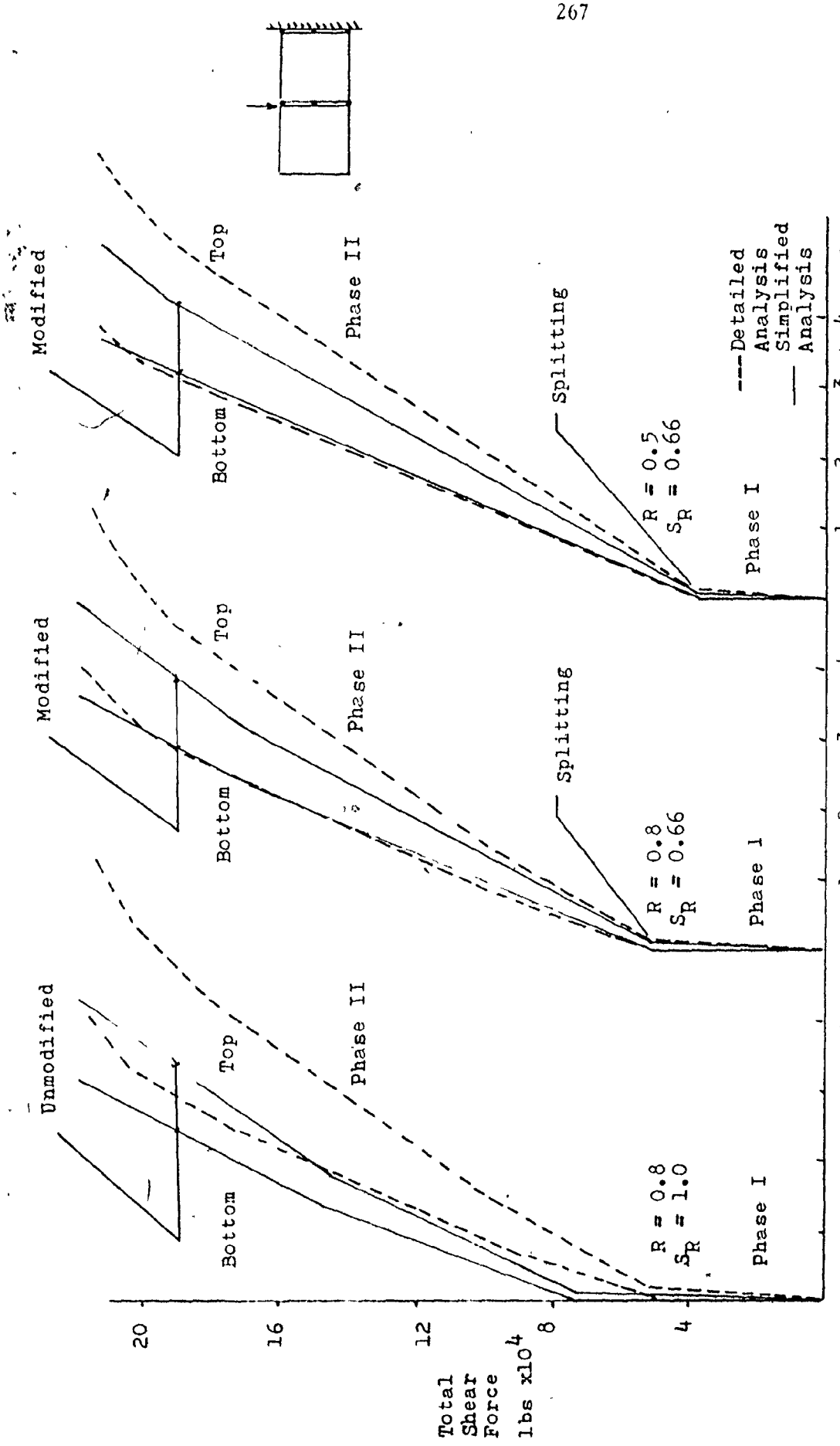

Fig.5.21 Vertical Joint Load-Slip Curve for the 3-Element Simplified Analysis Using Rapid Splitting Criterion (Single Concentrated Shear Force)

bond which might exist at the interface between the panel edges and the joint concrete or grout.

As illustrated in these graphs the prediction of slip at the bottom of the joint (indicated by the left branch of the curve) for the simplified model is in good agreement with that of the detailed model obtained in Chapter 4. The slip at the top, however, shows a discrepancy of approximatley 15% at a load level of 10×10^4 lbs. This is due to the local effects of the concentrated load which are not fully represented when larger elements are used in the simplified case.

Figure 5.22 shows the shear and the normal stress distribution for the 3-element simplified analysis of the vertical joint subjected to a single concentrated shear force. The top element, being closest to the point of application of the load, is stressed most heavily. As was indicated in Chapter 4, bond is the mode of shear transfer before the transition. After the transition, however, shear friction becomes the mode of shear transfer from one panel to the next. By comparing Figs. 5.22 and 4.25 it is observed that stresses using the 3-element simplification are much more uniformly distributed. This fact, as mentioned earlier, contributes to a rise in the level of the splitting load. Another interesting feature is the distribution of normal stresses prior to splitting. When the area of a joint is represented by 3 elements, and the area of the middle element is twice the area of the others, the symmetrical distribution of normal stresses prior

bond which might exist at the interface between the panel edges and the joint concrete or grout.

As illustrated in these graphs the prediction of slip at the bottom of the joint (indicated by the left branch of the curve) for the simplified model is in good agreement with that of the detailed model obtained in Chapter 4. The slip at the top, however, shows a discrepancy of approximatley 15% at a load level of 10×10^4 lbs. This is due to the local effects of the concentrated load which are not fully represented when larger elements are used in the simplified case.

Figure 5.22 shows the shear and the normal stress distribution for the 3-element simplified analysis of the vertical joint subjected to a single concentrated shear force. The top element, being closest to the point of application of the load, is stressed most heavily. As was indicated in Chapter 4, bond is the mode of shear transfer before the transition. After the transition, however, shear friction becomes the mode of shear transfer from one panel to the next. By comparing Figs. 5.22 and 4.25 it is observed that stresses using the 3-element simplification are much more uniformly distributed. This fact, as mentioned earlier, contributes to a rise in the level of the splitting load. Another interesting feature is the distribution of normal stresses prior to splitting. When the area of a joint is represented by 3 elements, and the area of the middle element is twice the area of the others, the symmetrical distribution of normal stresses prior

Load* (lbs)	34000	54000	54000	160000	170000
Shear Stresses(psi)	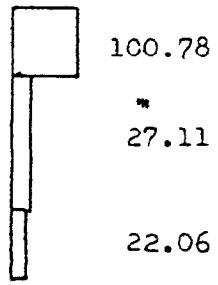	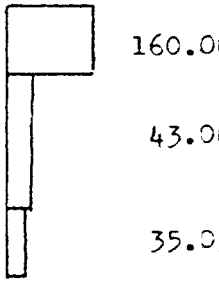	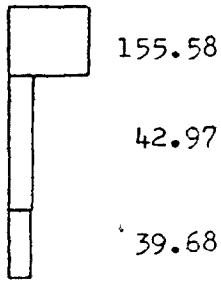	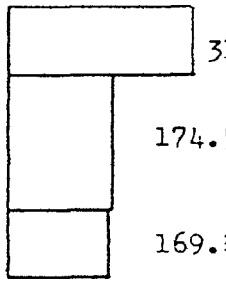	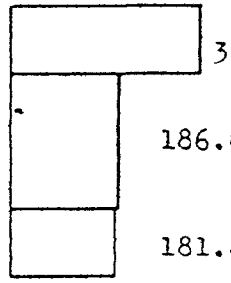
Comments	Phase I. Mode of shear transfer: bond	End of phase I. Mode of shear transfer: bond	Transition stage. Mode of shear transfer: shear-friction	Phaes II. Mode of shear transfer: shear-friction	End of phase II & start of phase IIb. 1st element starting to crack diagonally
Normal Stresses(psi)	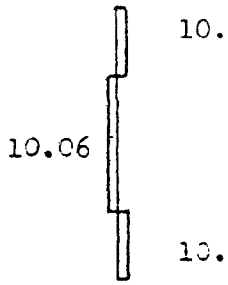	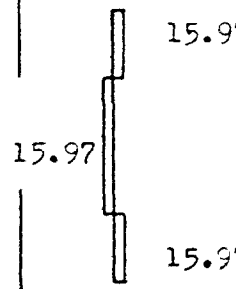	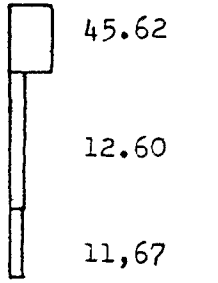	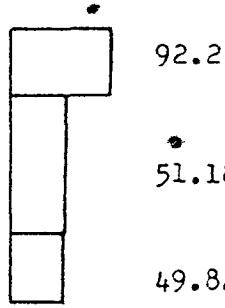	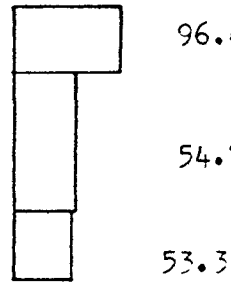

* Total External Shear Force

Fig.5.22 Shear and Normal Stresses for Vertical Joints at Various Stages of Loading for the 3-Element Simplified Analysis Shown in Fig. 5.21($R=0.8, S_R=0.8$)

to splitting is inevitable. After splitting, however, the joint stress distribution is dictated by the shear-friction requirements.

A more likely loading situation for a joint is when the joint is subjected to distributed shear forces. This situation occurs in the vertical joints of a complex cantilever when the whole assembly is subjected to lateral loads. Furthermore, under the action of excessive lateral loads, there is the possibility of the horizontal joints above and below a given panel opening up, and hence leaving the panel to cantilever from its neighbour. In this situation the joint is subjected to the combined actions of shear plus bending. These two cases are discussed in the following two sections.

5.9 Effect of a Distributed Shear Force on the Behaviour of 3-Element Vertical Joints

The load-slip curves using the 3-element simplification for the case where a distributed shear force is applied to the joint is shown in Fig. 5.23 along with its detailed analysis from Chapter 4. The top curve labeled unmodified with $S_R = 1.0$ represents the case where the analysis of Chapter 4 is in no way altered, except that the number of elements is reduced to 3. For reasons stated in section 5.8, a rise is apparent in the level of the splitting load. The reduction factor for splitting, S_R, in this case, is found to be 0.8. This differs from the previous case, because of the more uniform distribution of stresses through the joint.

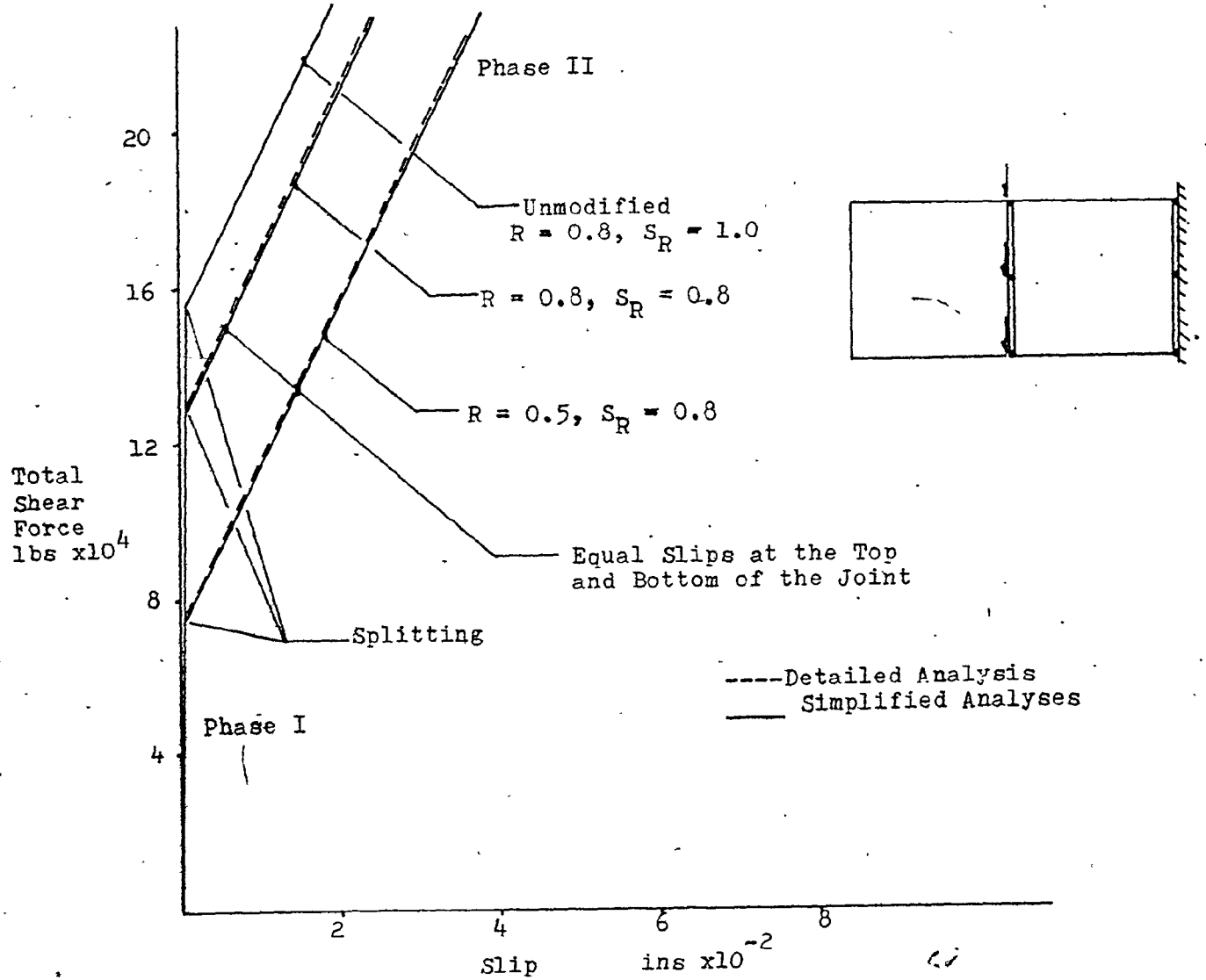

Fig.5.23 Vertical Joint Load-Slip Curves for the 3-Element Simplified Analysis Using the Gradual Splitting Criterion (Distributed Shear Forces)

The middle curve shows the load-slip relationship after the introduction of S_R. The curve is in very good agreement with the detailed case except for the ultimate load which is higher by approximately 10 percent. The last curve shows the relationship for the case where R is 0.5. The agreement with the detailed case is again very good if $S_R = 0.8$.

The stress distribution at various stages of loading for a distributed shear force is illustrated in Fig. 5.24. Since the main features of this diagram are the same as those for Fig. 5.22 except for the more uniform stress distribution, they will not be discussed again.

5.10 Effect of Shear Plus Bending on the Behaviour of a 3-Element Vertical Joint

The sketch in Fig. 5.25 illustrates a condition where both shear and bending are acting on a simplified vertical joint. This situation can exist when there is a separation in the horizontal joints above and below a given panel forming part of a complex cantilever under large lateral loads. However, it must be emphasized that although the computational necessities of the finite element method, may require the loads to be applied in a concentrated form to the few nodal points available, the corresponding loads in the real structure are distributed more or less uniformly along the top edge of the cantilevered panel. Thus the application of concentrated shear forces to a few nodal points and the resulting large local deformations represent an unrealistic test for the

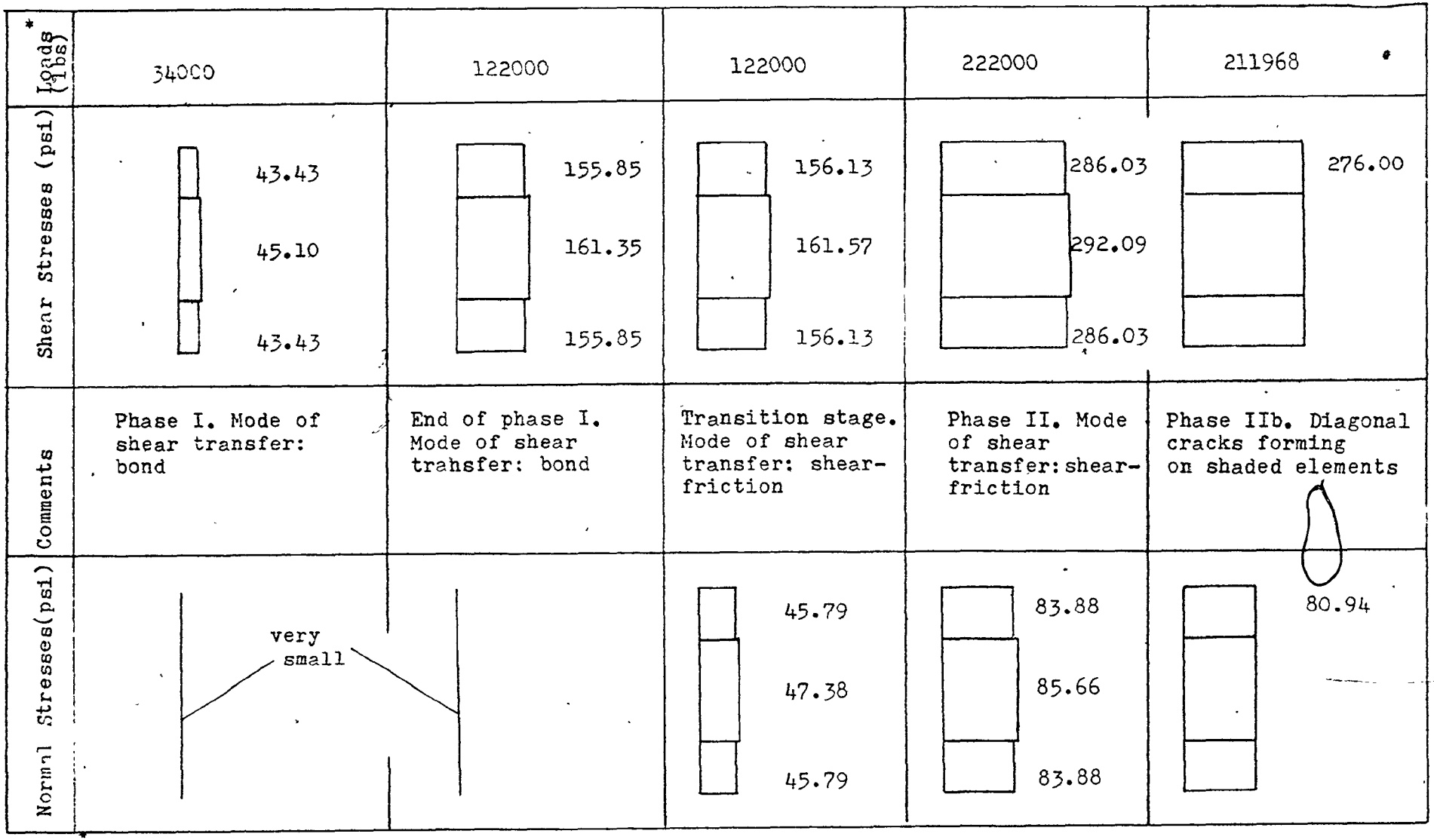

*Total External Shear Force

Fig.5.24 Shear and Normal Stresses for Vertical Joints at Various Stages of Loading for the 3-Element Simplified Analysis Shown in Fig. 5.23 (R- 0.8)

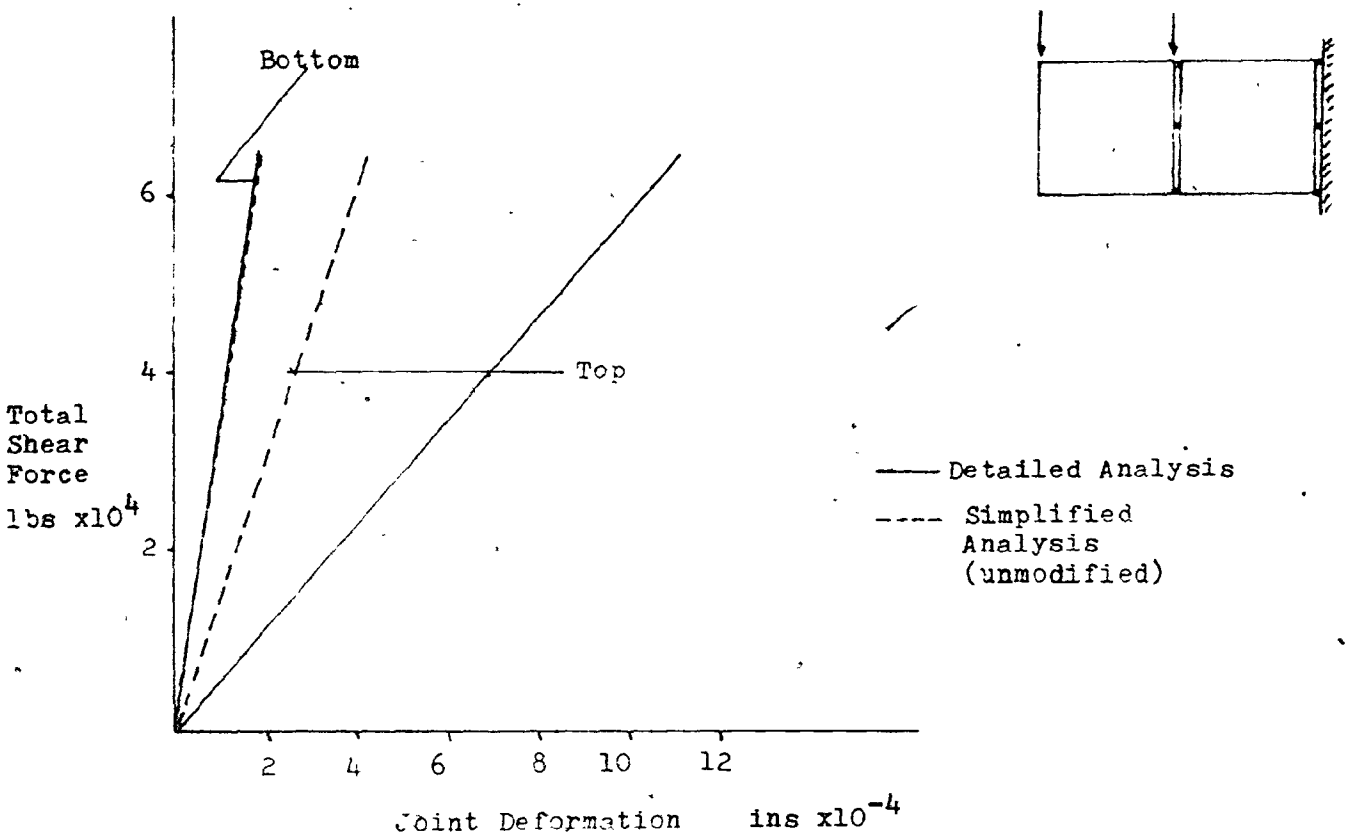

Fig.5.25 Vertical Joint Load-Deformation Curves for the 3-Element Simplified Analysis Showing the Effects of Shear plus Bending(Two Concentrated Shear forces)

joint deformations. The reason for investigating this case for both the detailed and the simplified analyses is to insure that the proposed method of analysis has the capability of predicting tension cracks (resulting from bending) in the vertical joints.

Lines (1) in Fig. 5.25 indicate the deformations at the top and the bottom of the joint for the detailed analysis reported in Chapter 4. The corresponding deformations for the unmodified simplified case are identified by lines (2). Deformations at the bottom of the joint for both cases are the same. The top deformations, however, are considerably different. Although it is possible to bring the top deformations in line with those for the detailed analysis by devising a sophisticated stiffness modification technique (which alleviates the effect of concentrating the entire joint stiffness in 3 localities), the author feels that this is neither necessary nor justified. In addition to the reasons given previously, it must be noted that the entire range of deformation shown in Fig. 5.25, constitutes only the equivalent of the very bottom portions of the curves shown on Fig. 5.21. These are pre-splitting deformations and their magnitude when compared with the nonlinear post splitting/cracking deformations are very small. Furthermore, the bending action is usually quite small unless a panel is forming a cantilever (due to separation along its horizontal joints) and the vertical joint is its only link to the rest of the structure. Thus, the fact that the

deformations along this linking vertical joint might differ from those reported in Chapter 4, is not anticipated to have a major effect on the behaviour of the rest of the complex cantilever.

For the reasons given above, it is concluded that no further modification, other than that required for the uniformly distributed forces of section 5.9, will be necessary when the 3-element simplification for the vertical joints is incorporated in the analysis of a complex cantilever.

This concludes the investigation of the 3-element simplification of vertical joints. In the next section, the analysis of the 2-element simplification for vertical joints will be considered.

5.11 2-Element Analysis of the Simplified Vertical Joints

To illustrate the effects of a further reduction in the number of elements the use of 2-element vertical joints is now considered. Figure 5.26 shows the response of the joint when it is subjected to a concentrated shear force applied at the top of the joint. The behaviour is first studied using the same values of R and S_R which were found suitable for the 3-element joint simplification shown in Fig. 5.21. To make comparison easier, the joint response for the detailed analysis is also presented. As expected the splitting load using the 2-element simplification is slightly higher because of concentrating the stiffnesses. It may be recalled that when 3 elements were used to

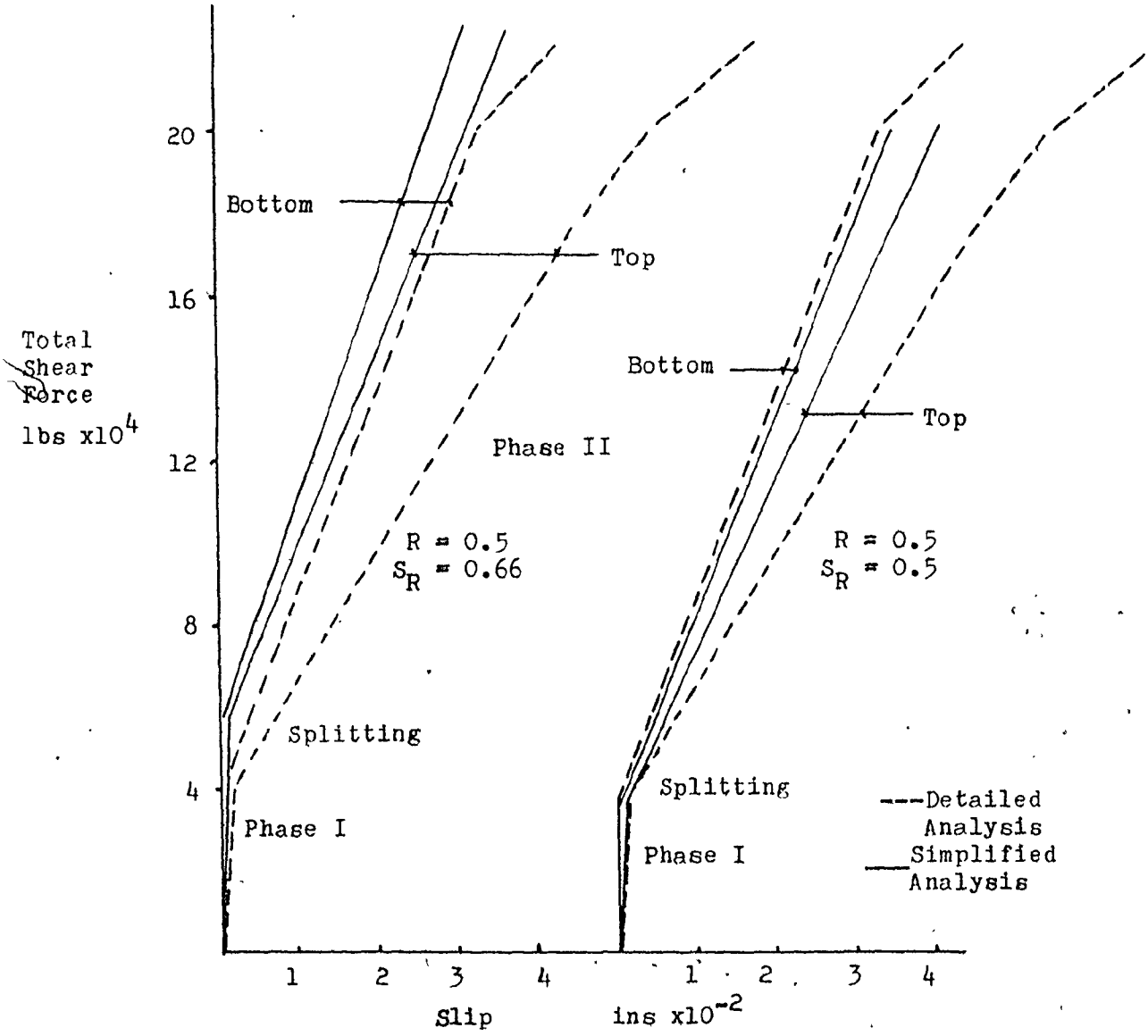

Fig.5.26 Vertical Joint Load-Slip Curves for the 2-Element Simplified Analysis Using the Rapid Splitting Criterion (Single Concentrated Shear Force)

represent the joint, a value for S_R of 0.66 caused the splitting load to coincide with that of the detailed analysis. Reducing S_R to 0.5 produces the same trend for the 2-element joints.

Referring to the set of curves on the right side of Fig. 5.26, it is seen that the slip at the bottom of the joint is fairly accurately represented by the simplified analysis. The top slip, however, is not very representative because the larger panel elements used in the simplified case do not adequately simulate the local effects produced by the concentrated shear force. This should not cause undue concern because shear forces are distributed along the length of the joint in a complex cantilever, and concentrated forces, as has been mentioned several times before, do not represent a very real situation.

Figure 5.27 shows the same joint subjected to distributed shear forces. It is observed that reducing the number of joint elements to 2 does not affect the joint response. Thus the same coefficients as used for a 3-element joint are also utilized in the analysis of its 2-element counterpart.

For the reasons stated in section 5.10, other loading conditions are not considered important, and will not be investigated further.

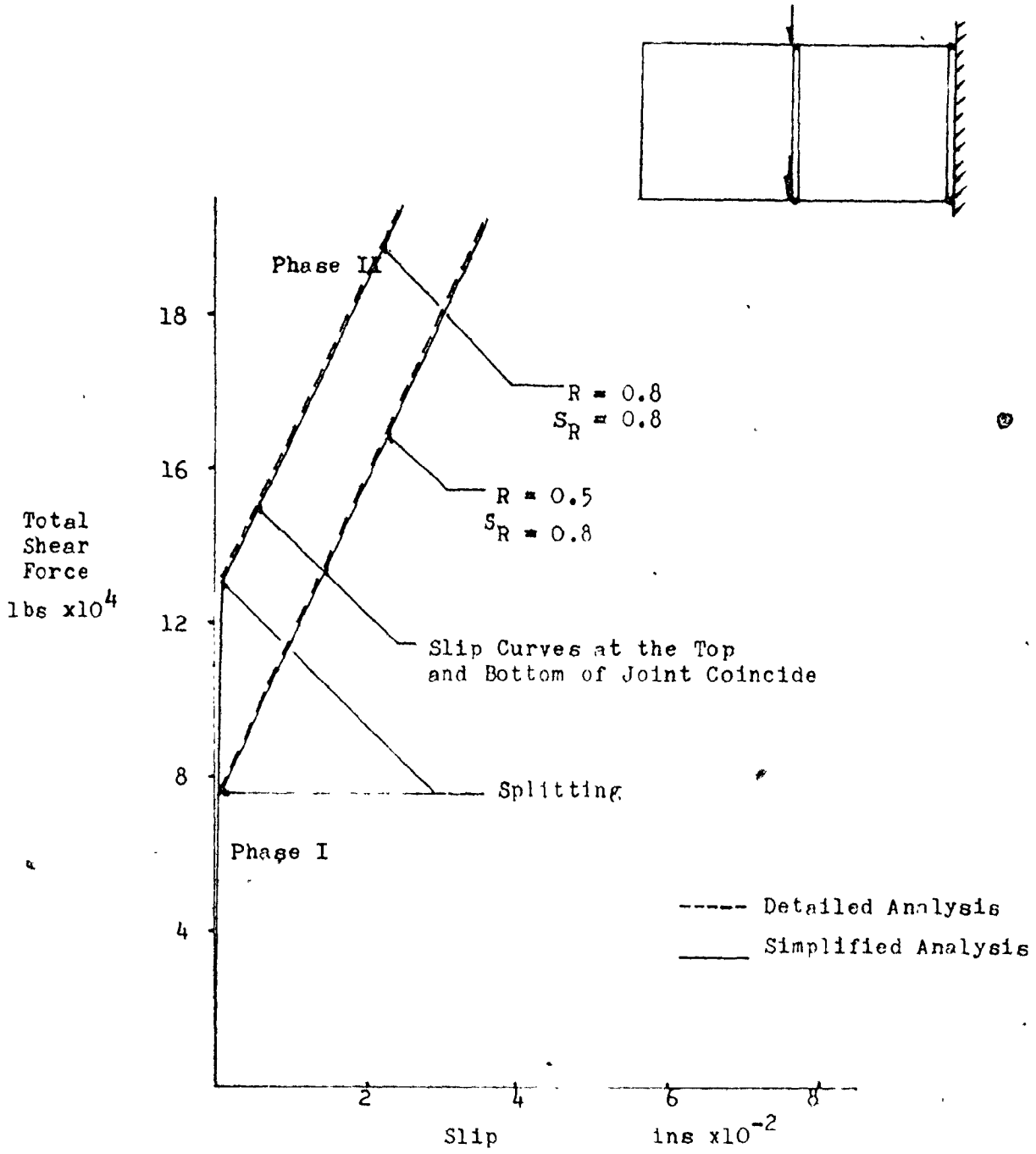

Fig.5.27 Vertical Joint Load-Slip Curves for the 2-Element Simplified Analysis using the Gradual Splitting Criterion(Distributed Shear Forces)

5.12 Summary

In this chapter a simplified analytical model for the horizontal and vertical joints was investigated. Initially, the behaviour of horizontal joints were studied using 2-element and 3-element joint simplifications. The detailed analyses of Chapter 3 were used as a guide to measuring the degree of accuracy achieved. It was found that in order to represent the joint deformations with reasonable accuracy, stiffnesses of the joint elements had to be continually modified. Furthermore, it was observed that when 2-element simplification was used, joint separation could not be simulated. However, the 3-element simplification, yielded acceptable results for both the deformation of the reinforced joint and for the actual forces existing in the reinforcing elements.

Next, simplified vertical joints were studied. It was shown that the behaviour predicted by the detailed joint analysis could be duplicated quite accurately by taking 3 or 2 elements per vertical joint, and by introducing a number of coefficients aimed at modifying certain patterns of behaviour which were distorted as a result of reducing the number of elements. Among the different loading cases considered, the distributed shear force was considered to be the most representative of those existing in a cantilevered assembly of panels.

Either of the 2 or 3-element joint representations together with their appropriate modifying coefficients will

thus be used in the next chapter to investigate the overall behaviour of complex cantilevers.

CHAPTER 6

ANALYSIS OF COMPLEX CANTILEVERS

6.1 Introduction

In recent years more effort has been devoted to the study of different aspects of the behaviour of panel buildings. Most of these were briefly oulined in Chapter 1 and in Appendix A. These studies, although valuable in establishing certain characteristic patterns of behaviour associated with panel buildings, were not, in general, deeply concerned with the behaviourr of the joints.

During the early stages of this investigation, and after a number of preliminary attempts at formulating an approach for finding the ultimate load response of complex cantilevers, it became apparent that no realistic estimate of lateral deformations and the ultimate strength of these structures could be found without a detailed study of the behaviour of their connections. For this reason, the major part of this thesis was devoted to the study of the behaviour of horizontal and vertical joints. For practical reasons and in order to apply the analysis to large assemblies of panels, the joints were then simplified as was reported in Chapter 5.

In this chapter, the ideas and the methods developed in the previous chapters are brought together and assembled

in a form suitable for analyzing complex cantilevers. To begin with, a description of the complete physical models are presented. This is basically a summation of the ideas developed in the previous chapters. A 2 bay by 5 storey complex cantilever is then analysed using the 3-element joint representation of both the horizontal and the vertical joints. The same cantilever is also analyzed using the 2-element joint representation. The results of the two analyses are then compared. Finally, using the 2-element representation of the joints a 3 bay by 10 storey complex cantilever is studied. (It should be noted that with the available computer (CDC 6400) the above structures were the largest which could be analysed using the model developed in this study. In fact for the 10 storey structure part of the analysis had to be carried out separately, stored on permanent files and called upon when needed in the main program.)

6.2 Physical Model

The principle structural components of a complex cantilever assembled for the purpose of this investigation are as follows:

1. PANELS Cracking is assumed to be confined to the joint regions. Panels, therefore remain uncracked and are assumed to behave in a linear fashion. For the 2-element joint representation each panel is made up of 4 triangular elements with the centre node eliminated by condensation, yielding a 4 noded rectangular element. Each node is assumed to have 2 degrees of freedom constituting a total of 8 degrees of

freedom per panel. For the 3-element joint representation each panel is composed of 16 triangular elements. When all of the internal nodes are eliminated, the resulting rectangular element has 4 mid-side nodes in addition to the corner nodes and has a total of 16 degrees of freedom. For further details reference should be made to Chapter 2.

The panel material is treated as being homogeneous. The effect of panel reinforcement is taken into account by utilizing equations (2.12). The material properties for the panels are given as follows (Section 2.2):

Modulus of Elasticity (E) = 4.6×10^6 psi

Poisson Ratio (V) = 0.1455

2. HORIZONTAL JOINTS The joint elements are of the type shown in Fig. 3.7(a) with horizontal and vertical springs representing the shear and normal joint stiffnesses respectively. The numerical values for the stiffnesses of the springs are determined as a product of the joints contributory area and the unit shear and/or normal joint stiffness coefficients. These constitute the initial joint stiffnesses. During the application of loads the initial stiffnesses are successively modified using equation (5.6) for the 2-element representation and equations (5.9) to (5.17) for the 3-element representation. The numerical values of the initial unit stiffness coefficients in accordance with the procedures established in Section 5.2 are given as follows:

Unit shear stiffness coefficient = 5.65×10^5 lbs/in^3,

and Unit normal stiffness coefficient = 1.3×10^6 lbs/in^3

The reinforcing elements are also of the same config-

uration shown in Fig. 3.7(a). The normal stiffness representing the vertical continuity provided by the bar is determined from the bond-slip considerations outlined in Section (3.13). The horizontal stiffness representing the dowel action is estimated on the basis of the experimental results. The values used for the purpose of this analysis are:

vertical spring stiffness (K_B) = 6.9×10^5 lbs/in, and

horizontal spring stiffness (K_D) = 8.65×10^5 lbs/in

For the yield behaviour of the reinforcing element reference should be made to Section (3.14).

3. VERTICAL JOINTS The physical configuration of the elements representing the joints is shown in Fig. 4.6(c). For the type of joint selected two distinct phases are encountered when considering the behaviour of vertical joints. Phase I is associated with the behaviour of unsplit joints. Phase II is related to the behaviour after splitting but before the formation of diagonal cracks. A transition phase is also introduced to account for the gradual loss of stiffness as the transition is made from phase I to phase II.

The actual numerical values representing the joints unit stiffness coefficients are indicated in Table 4.1.

4. BAR ELEMENTS As outlined in the simplified analysis of Section 5.2, the joint filler - floor slab component of the joint is represented by a simple axial member.

The normal and shear stiffnesses of the joint filler-slab components are incorporated in the stiffnesses of the elements representing the horizontal joints. For further details reference should be made to Section 5.2.

5. TIE-BEAM LINK ELEMENTS To allow for possible cracking of the tie beams a link element is introduced where a tie beam crosses a vertical joint. The physical configuration of this link element is very similar to that introduced in Section 3.8 to account for the effect of the longitudinal joint existing between 4 ft. wide floor panels. The stiffnesses of the springs representing the link element are, however, very different from those of Section 3.8. The cracking of the link element is very much dependent on the behaviour of both the vertical and the horizontal joints. The stiffnesses prior to cracking are determined using basically the same procedures as those used to obtain the stiffnesses of vertical joints before splitting. The numerical values of the stiffnesses used in this study are:

vertical spring stiffness (K_v) = 1.95×10^7 lbs/in, and

horizontal spring stiffness (K_h) = 4.50×10^7 lbs/in.

After cracking, however, the behaviour of the reinforcing bars crossing the cracked section determines the stiffness values. By adopting procedures similar to those outlined in Sections 3.7 and 3.8, the following spring stiffness values may be determined:

vertical spring stiffness (K_v) = 6.48×10^5 lbs/in, and

horizontal spring stiffness (K_h) = 1.85×10^6 lbs/in.

Having introduced the physical model which is used in studying the behaviour of complex cantilevers, the results of the investigation can now be presented.

The following presentation is sub-divided into three

separate parts and will be outlined in the next three sections of this chapter. As was also indicated in the introduction to this chapter, three representative assemblies of panels (complex cantilevers) will be looked at in this study.

6.3 Analysis of 10-panel Complex Cantilevers Utilizing 3-Element Joint Simplification

The finite element arrangement used for this example is shown in Fig. 6.1. The cantilever is attached to a fixed base through elements representing slip surface 1. Each panel element is composed of 16 elements with the central nodes condensed as was explained in Chapter 2.

The joint filler-floor slab portions of the cantilever are represented by means of one dimensional bar element. This type of arrangement was discussed in chapters 3 and 5. Also as was indicated at the beginning of Chapter 5, the elements representing slip surface 1, the joint filler-floor slab elements, and the elements representing slip surface 2 initially occupy the same physical location (co-ordinates) in space, although for the sake of being able to identify the elements, they are shown in expanded from in Fig. 6.1.

The loads acting on the structure are applied in the following manner. Gravity loads representing the self weight of each wall panel are applied to the bottom row of nodes of that panel. For example the self weight of panel element 5 is applied vertically to nodes 50, 51 and 52 with the load of node 51 being twice that of the other two nodes. The self weight of floor panels is applied to the nodal joints

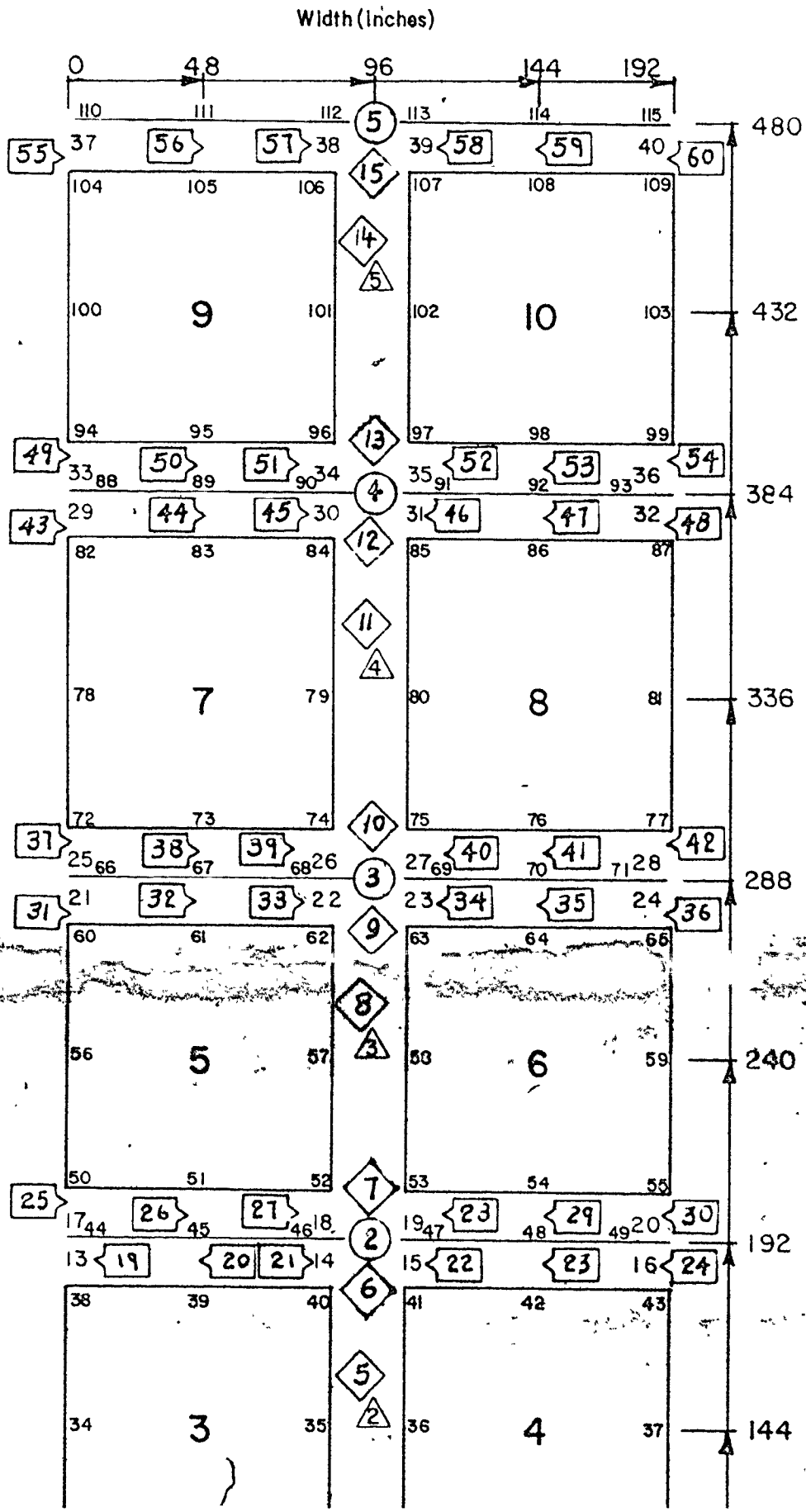
Width (Inches)
0
48
96
144
192
480
432
384
336
288
240
192
144
Height (Inches)
9
10
7
8
5
6
3
4

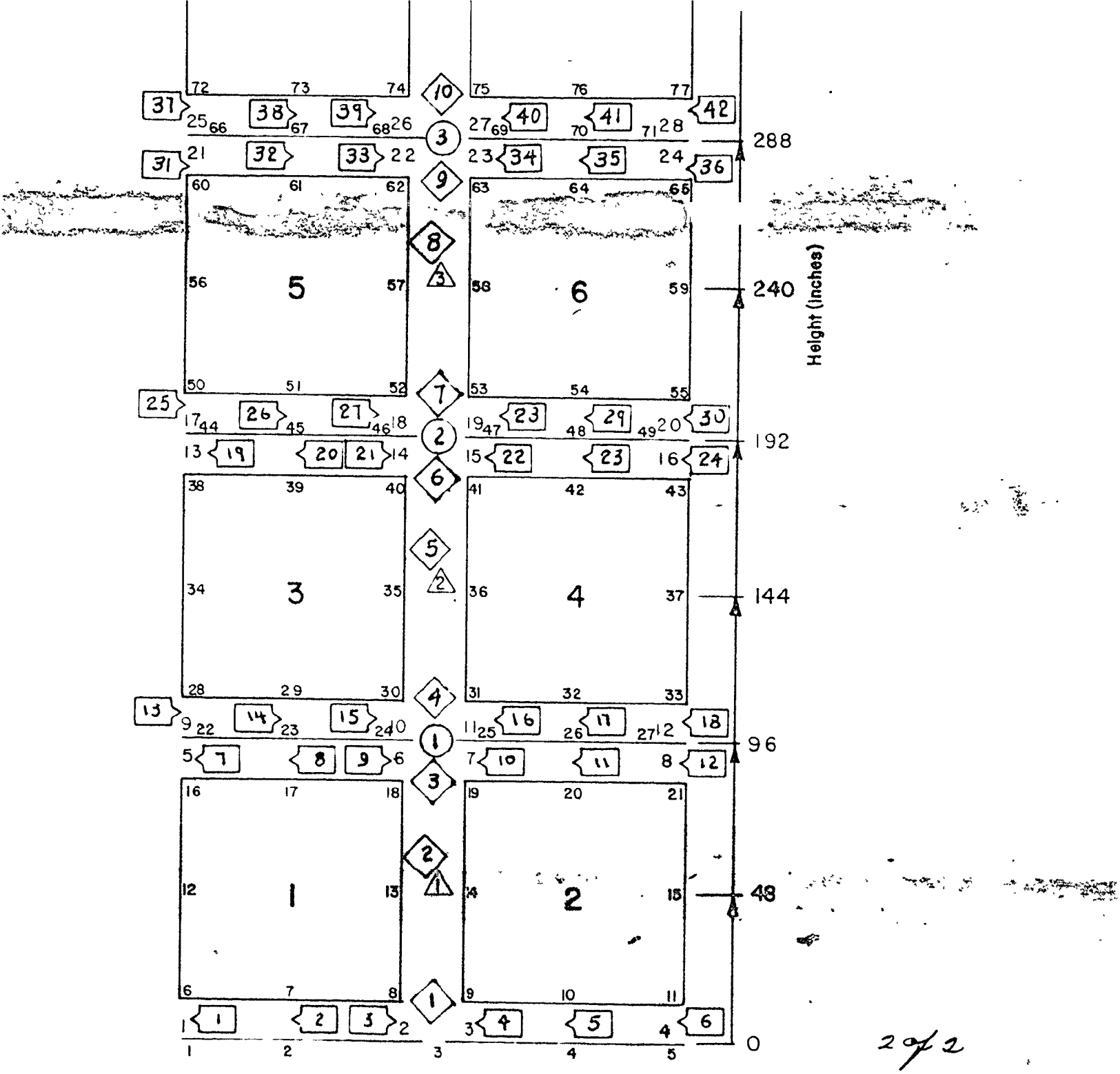

Legend

- Horizontal Joint Element No.
- △ Vertical Joint No.
- ◇ Vertical Joint Element No.
- ○ Tie-Beam Element No.
- 4 Typical Panel No. (Digit-Size 3/8")
- 4 Typical Horizontal Joint Reinforcement No. (Digit Size 1/4")
- 4 Typical Nodal No. (Digit Size 3/16")

Fig. 6.1 Finite Element Representation of a Complex Cantilever Composed of 10 panels Arranged in 2 Bays and 5 Storeys Using 3 Elements per Joint

of the bar elements representing the joint filler-floor slab components. Thus the weight of the floor slabs resting on the upper edge of panel 5 is applied to nodes 66, 67 and 68 with the middle node taking twice as much load as the other two. The gravity loads remain unchanged throughout the analysis.

Uniform lateral loads are applied to the nodes located along the left profile of the complex cantilever with the middle nodes again taking twice as much load as the corner nodes. The lateral loads are increased in equal increments until structural failure occurs.

The procedures for the type of non-linear analysis used in the previous chapters are extended to include the entire complex cantilever. The details are identical to those discussed in relation to isolated vertical and horizontal joints and will not be repeated here.

In this section which deals with the behaviour of 10-panel complex cantilevers using the 3-element simplified analysis, three different problems are investigated. These problems are discussed in the following subsections.

(a) Unreinforced Horizontal Joints (Distributed Lateral Loads)

In this portion of the study, the horizontal joints are assumed to contain no reinforcing bars. As was explained in Chapter 3 in connection with the detailed analysis of horizontal joints, and again in Chapter 5 in connection with the simplified analysis of the same joints, bond is assumed to exist along slip surface 2. Slip surface 1 is assumed to

be unbonded and the gravity forces resulting from the weight of the structure are the only shear transfer mechanism existing along this interface. The lateral loads are increased in increments of 300 lbs per corner node (600 lbs per mide-side nodes). The slip and separation along the joints of the complex cantilever under the action of gradually increasing lateral loading is shown in Table 6.1. This table when examined together with Fig. 6.1 illustrates the sequence in which slip and separation occur along the horizontal joints under the action of ever increasing lateral loads. A schematic presentation of the failure sequence as complied in Table 6.1, is illustrated in Fig. 6.2 for 4 different stages during loading. The vertical joints in this case remained intact. The failure of the structure occurred by separation along the base when the lateral loads applied to the nodes are equivalent to approximately 2025 pounds per linear foot along the height of the structure. The word approximately is used here in describing the failure load since the exact load at which the structure actually fails is not determined.

The failure load was taken as the sum of the highest stable total load and one half of the final increment of load which produced failure. The maximum possible error which might occur as a result of adopting this procedure is less than one half of the load increment or in this case 3.7%. Preliminary attempts at pin pointing the failure load which involves a complicated process of successively halving the load increment, proved too costly in terms of computer time.

Lateral Load per Corner Node (lbs)	Lateral Load per Panel (lbs)	Lateral Load per Linear foot (lbs/ft)	Failure Sequence
1500	6000	750	elem. 1 slip.
1800	7200	900	elem.1, sep. , elem. 13 slip.
2100	8400	1050	elem.2, slip. , elem.13 sep. elem.25 slip.
2400	9600	1200	elem.2 sep. , elem.14 slip.
2700	10800	1350	elem.4 slip. , elem.25 sep. elem.26 slip. , elem.37 slip.
3000	12000	1500	elem.14 sep. , elem.15 slip.
3300	13200	1650	elem.3 sep. , elem.4 sep. elem.16, slip. , elem.28 slip.
3600	14400	1800	elem.5 slip., elem.37 sep. elem.38 slip.
3700	15600	1950	elem.15 sep. , elem.16 sep. elem.26 sep. , elem.40 slip. elem.49 slip.
4200	1680	2100	elem.5 sep. , elem.17 slip.
4200	16800	2100	failure

Table 6.1 Failure Sequence for the 10-Panel Complex Cantilever with Unreinforced Horizontal Joints Using the 3-Element Joint Simplification (Distributed Lateral Loads)

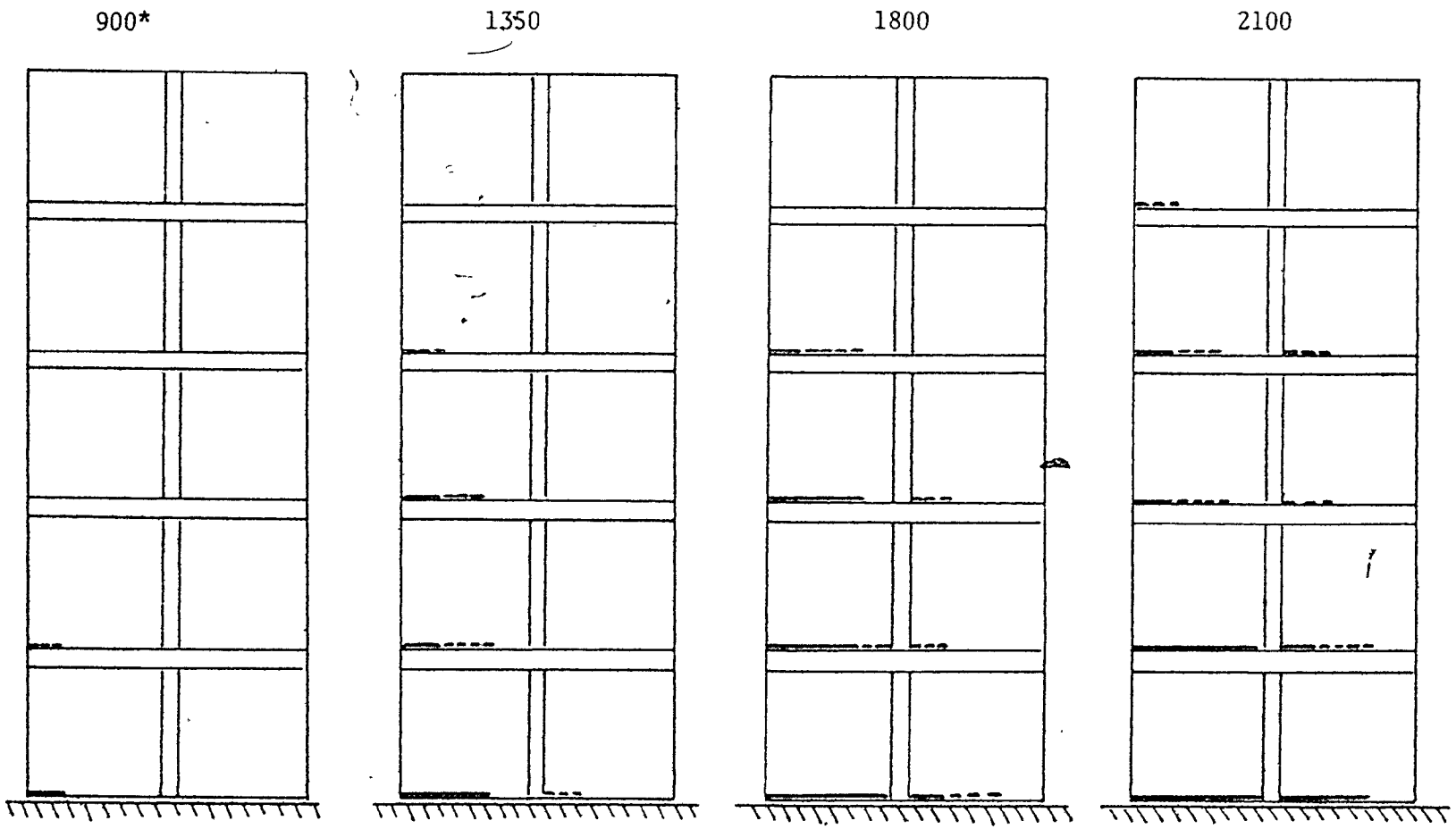

*Horizontal load per linear ft. of height (lbs.)

--- slip

—— separation

Fig. 6.2 Schematic Presentation of Failure Sequence for the 10-Panel Complex Cantilever as Documented in Table 6.1

Therefore, no further attempts were made to reduce the error.

As was indicated in the previous paragraph, the vertical joints in this example remain completely intact. The normal and shear stresses acting perpendicular to and parallel to the surface of the vertical joints respectively, are shown in Table 6.2. The combined effects of these forces are such that splitting cannot occur along the vertical joints. This is because of the separation which occurs along the horizontal joints. If the complex cantilever were heavily reinforced in the vertical direction, as is the case with the piers of coupled shear walls for example, or if very high gravity loads were applied to horizontal joints as is the case with complex cantilevers of very high structures, then sufficient longitudinal shear stresses would develop along the vertical joints to cause splitting. In the case studied here, it is observed (Table 6.2) that as lateral loads increase, and as separations occur along the horizontal joints, the left panels at each level starting from the bottom, tend to cantilever from their neighbouring panels and to give rise to tensile stresses at the top of their respective vertical joints. These stresses, however, are not sufficiently large to cause cracking.

The graph of lateral forces versus drift (lateral deflection) at the top of the assembly is shown in Fig. 6.3. For small values of lateral loads, and while separation and slip are confined to only a few elements near the bottom of the cantilever, drift (lateral deflection) at the top remains

Element	Joint	600 *		900		1050		1350		1650		1950		2100
No.	No.	N**	S+	N	S	N	S	N	S	N	S	N	S	
1	1	-9.28	6.26	-6.31	16.71	-10.00	31.27	-30.31	35.63	-38.49	12.70	-46.22	.96	
2	1	-7.03	16.70	-9.65	28.02	-15.06	34.41	-28.25	38.15	-48.58	35.13	-47.11	21.03	
3	1	-4.49	13.86	-8.12	20.02	-11.96	23.66	4.79	19.54	33.71	32.25	48.99	43.85	
4	2	-3.09	13.66	-7.29	23.03	-6.04	28.19	-37.33	52.71	-52.74	44.88	-51.25	22.21	
5	2	-3.15	15.37	-6.17	23.21	-7.79	27.62	-19.32	38.06	-28.87	42.26	-42.07	41.52	
6	2	-3.61	11.37	-5.16	16.27	-6.30	18.59	-7.97	23.82	18.01	26.44	31.05	26.88	
7	3	-2.23	9.93	-4.58	15.87	-6.20	19.18	-9.26	27.44	-17.73	33.92	-87.08	36.89	
8	3	-3.16	10.99	-4.75	16.53	-5.79	19.31	-9.01	25.30	-21.58	32.50	-28.06	37.87	
9	3	-4.09	7.75	-5.33	11.43	-5.97	13.18	-6.83	16.25	-6.79	19.78	12.98	20.38	
10	4	-2.10	6.41	-3.89	9.94	-4.89	11.79	-7.32	15.80	-13.20	21.51	-62.07	28.59	
11	4	-3.20	6.00	-4.74	9.91	-5.51	11.57	-6.88	14.88	-8.93	18.42	-17.08	22.49	
12	4	-4.15	4.07	-5.59	6.06	-6.29	7.05	-7.34	8.98	-7.20	10.40	-69.37	12.39	
13	5	-1.98	3.06	-3.59	4.67	-4.42	5.49	-6.11	7.18	-8.24	9.19	-12.03	11.60	
14	5	-2.81	2.04	-4.34	3.60	-5.11	4.21	-6.59	5.42	-7.74	6.62	-8.68	7.91	
15	5	-3.44	1.02	-4.91	1.54	-5.63	1.80	-7.03	2.32	-7.82	2.85	-7.17	3.34	

FAILURE

*Lateral Load per Linear ft. of height of complex cantilever(lb)**Normal(psi) +Shear(psi)

Tabel 6.2 Normal and Shear Stresses for Vertical Joint Elements for Various Lateral Load Levels

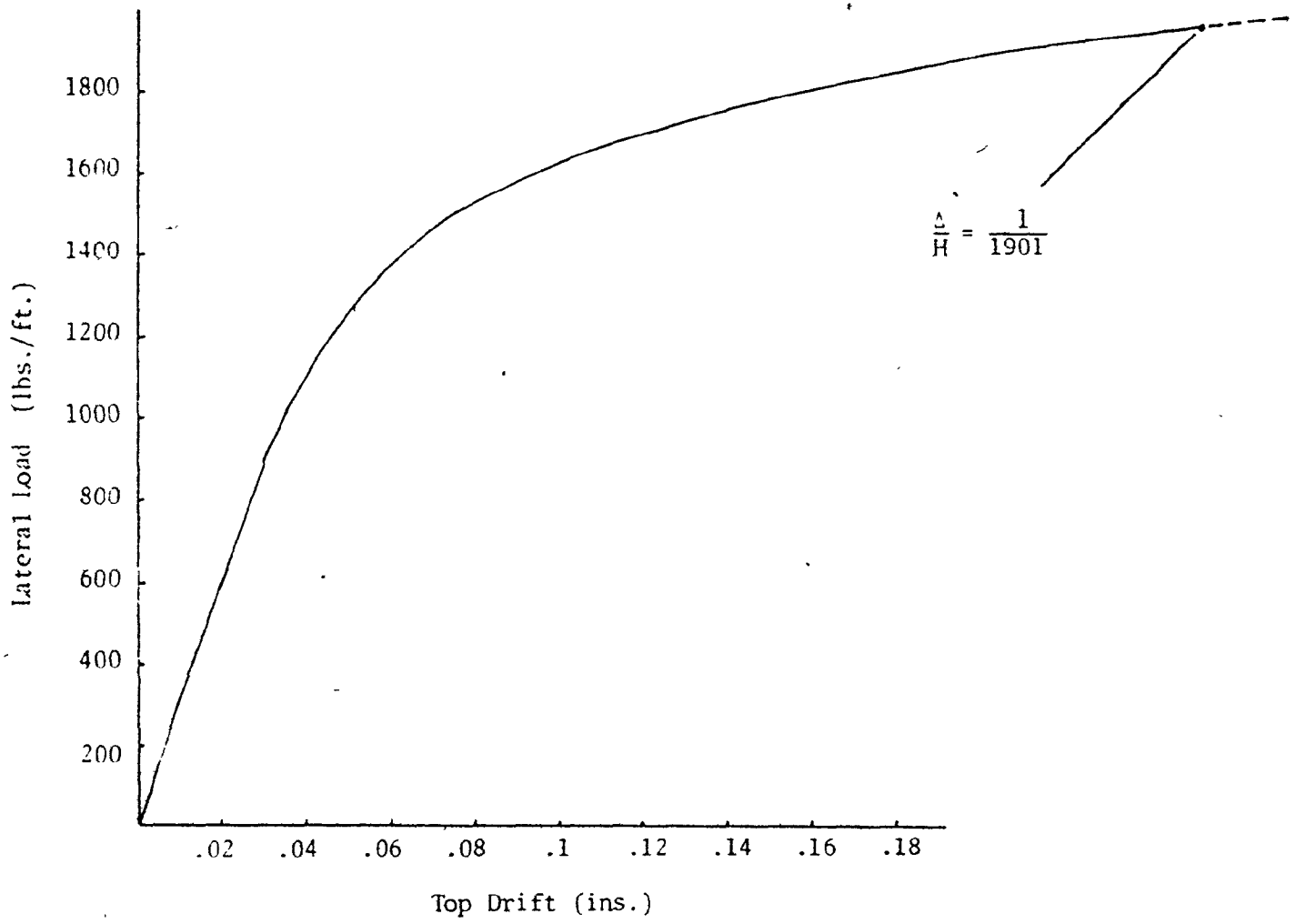

Fig. 6.3 Graph of Lateral Load Versus Drift for 10-Panel Complex Cantilever with Unreinforced Horizontal Joints Using 3-Element Joint Simplification (Distributed Lateral Loads)

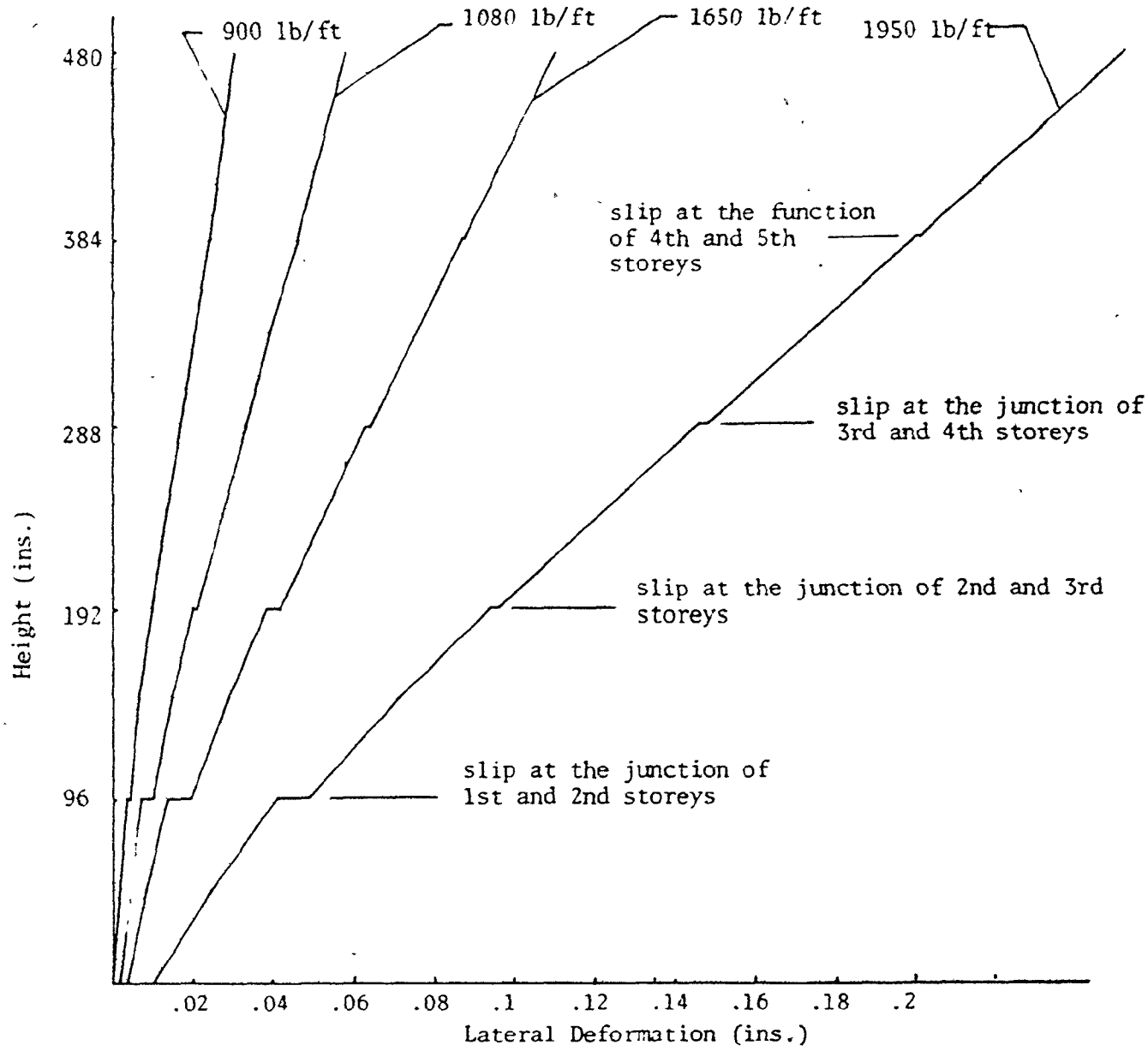

Fig. 6.4 Deflected Profile of 10-Panel Complex Cantilever with Unreinforced Horizontal Joints Using 3-Element Joint Simplification (Distributed Lateral Loads)

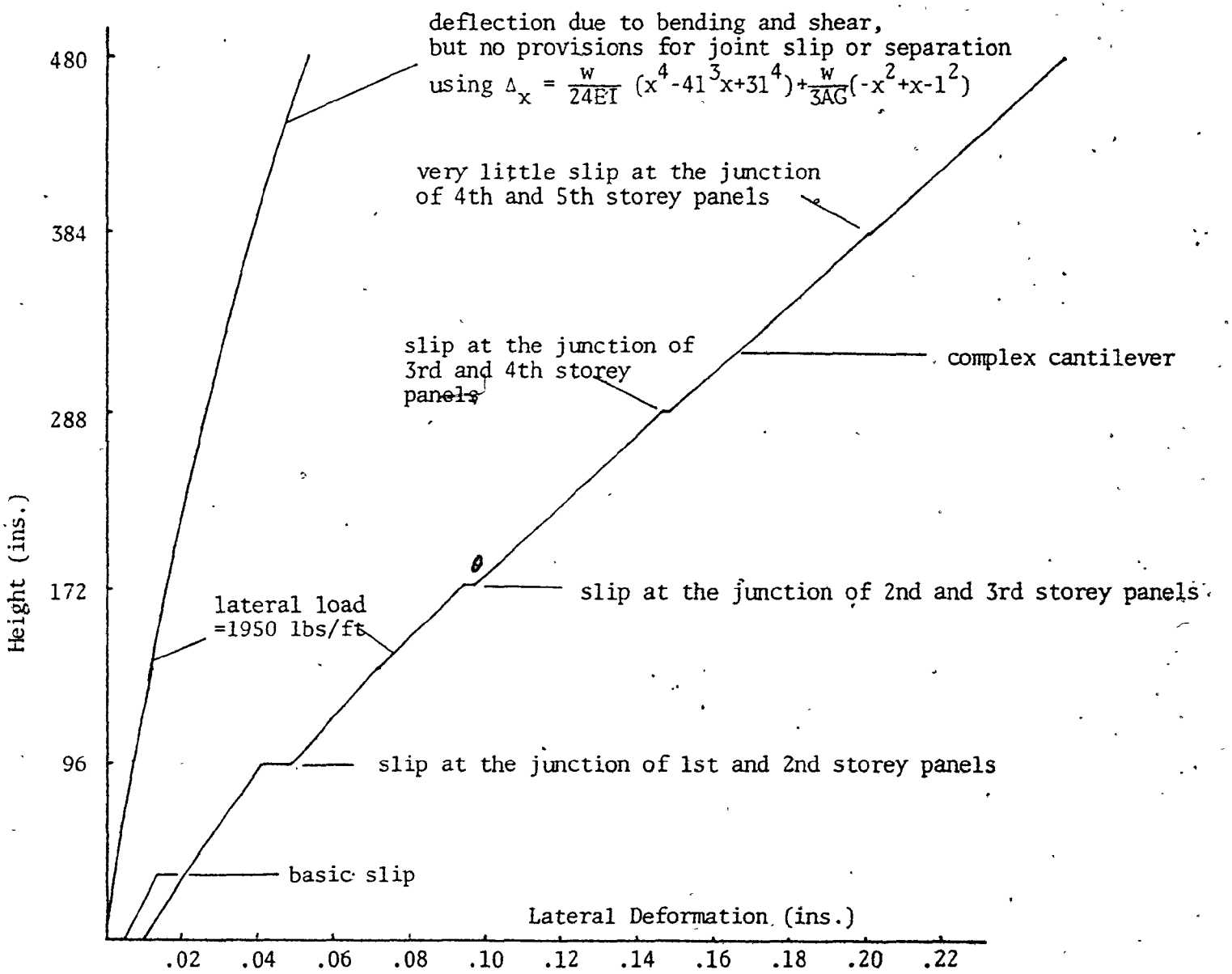

Fig. 6.5 Comparison of the Deflected Profiles of a 10-Panel Complex Cantilever with Unreinforced 3-Element Horizontal Joints and a Monolithic Cantilever of the Same Physical Dimensions and Properties (Distributed Lateral Loads)

relatively small and is approximately linear. At high lateral load values, as the process of slip and separation along horizontal joints is accelerated, drift at the top becomes proportionately much larger with 50% of the ultimate lateral delfection occurring for the final 11% of the ultimate load.

The deflected profile of the complex cantilever at various stages of loading is shown in Fig. 6.4. The total delfection at the top of the cantilever is dependent upon panel deformation, a change in the overall orientation of the panels, and joint slip and separation. The horizontal lines at the panel junctions represent slip which become larger towards the bottom of the cantilever. At any given level however, slip increases as the lateral loads acting on the assembly are increased. The change in the orientation of the panels is best observed by comparing the deflected profile of the complex cantilever with that of a cantilever beam with comparable dimensions and stiffness, and acted upon by similar lateral loads. This comparison is illustrated in Fib. 6.5 for a lateral load of 1950 lbs/linear ft of height. With no provisions for slip and separation along the joints, the deflection of the cantilever beam at any point may be computed from the relationship $\Delta_x = \frac{W}{24EI}(x^4-4l^3+3l^4)+\frac{W}{3AG}(l^2+x-x^2)$ for the combined effects of shear plus bending. The effect of the joints on the behaviour of the complex cantilever may thus be illustrated by observing that the deflection at the top of a complex cantilever in this case is approximately 5 times greater than that of a comparable structure constructed without joints. As indicated in Fig. 6.3, the $\frac{\Delta}{H}$ ratio for a complex cantilever at the given load level is equal to $\frac{1}{1901}$ as

compared to $\frac{1}{9230}$ for a jointless cantilever of similar stiffness and material properties.

(b) Unreinforced Horizontal Joints (Concentrated Lateral Load)

The case of a complex cantilever with a concentrated lateral load acting at the top was investigated because it was thought that the failure pattern would provide an interesting contrast with the case outlined in (a). The sequence of joint slip and separation is shown in Table 6.3. A schematic presentation of the failure sequence as indicated in Table 6.3 for 4 different values of lateral loads is shown in Fig. 6.6. The complex cantilever arrangement is the same as that of the previous example shown in Fig. 6.1. A concentrated load increasing gradually in 4000 pound increments is applied to the top left corner of the complex cantilever. Unlike the previous case where the first indications of slip and separation appeared at the base of the cantilever, in this case slip and separation are first indicated at the junction of the 4th and 5th storey panels. With further increase in the concentrated load the slip and separation of the joint elements spreads to the other parts of the structure, and failure finally occurs at the junction between the 4th and the 5th storey panels. In contrast with the previous case where separation at the base was the failure mode, the present case is distinguished by a slip type failure.

The reason for this is that the concentrated load applied to the top of the complex cantilever causes the

Total Lateral Load (lb)	Failure Sequence
12000	elem. 49 slip.
16000	elems. 1,13,25,37,49 sep. elem. 50 slip.
20000	elems. 14,26,38,52 slip.
20000	elem. 50 sep.
24000	elems. 2,14,26,38 sep. elems. 39,51 slip.
24000	elems 27,40,53 slip.
28000	elems. 16,28 slip.
32500	elems. 3,4,15,16,27,28,39, 40,51,52 sep.
36000	elems. 29,41,54 slip.
36000	failure

Table 6.3 Failure Sequence for the 10-Panel Complex Cantilever with Unreinforced Horizontal Joints using the 3-Element Joint Simplification (Concentrated Lateral Load Applied to the Top of the Complex Cantilever)

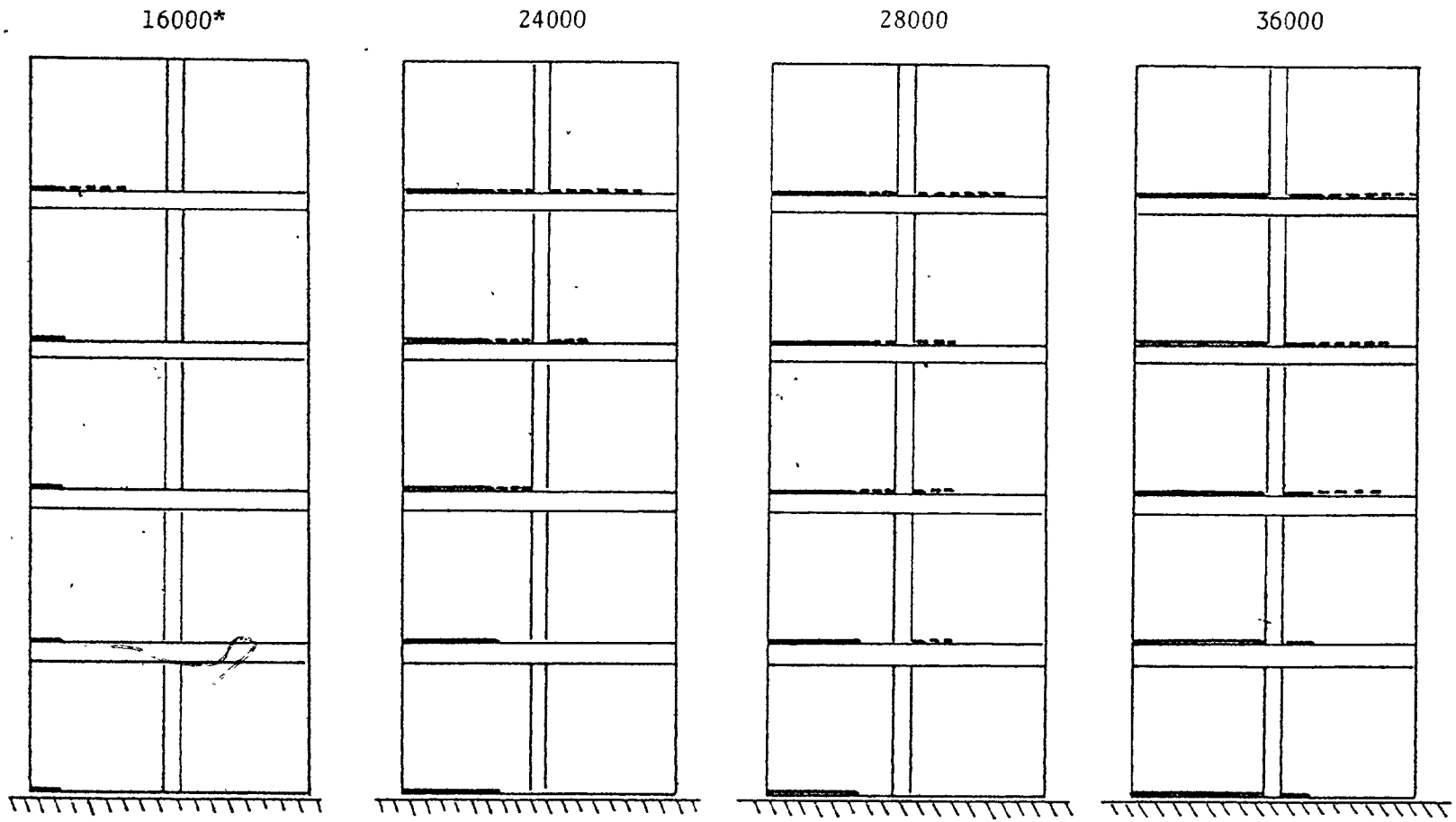

Fig. 6.6 Schematic Presentation of Failure Sequence for the 10-Panel Complex Cantilever as Documented in Table 6.3

friction force resulting from the weight of only one storey (at the junction of the 4th and the 5th storeys) to be exceeded before total separation at the base (i.e. overturning) occurs. As before, no splitting is observed in the vertical joints.

The graphs of lateral load versus drift is illustrated in Fig. 6.7. The curve appears to be approximately linear for loads up to about 50% of the ultimate load. Beyond this level there is a sharp increase in the rate of drift with about 50% of the total drift before failure occuring for the final 11% to 14% of the ultimate load. The ratio $\frac{\Delta}{H}$ just before failure is found to be equal to $\frac{1}{.2304}$.

Another interesting contrast with the previous case is shown in Fig. 6.8. The curve shows the deflected profile of the cantilever just before failure. Unlike the previous case where joint slip was most significant at the base, and gradually decreased towards the top, in this case the most significant joint slip occurs at the junction of the 4th and the 5th storey panels. This is explained simply by remembering that slip is a function of gravity loads acting at right angles to the surface of the joint as well as the bending and the shearing effects produced by the lateral loads. Although the bending effect of the concentrated load increases as the distance from its point of application increases, its shearing effect remains constant throughout the height of the cantilever. It is the combination of this shearing effect acting in conjunction with lower gravity loads towards the top of the structure, that gives rise to higher slips and

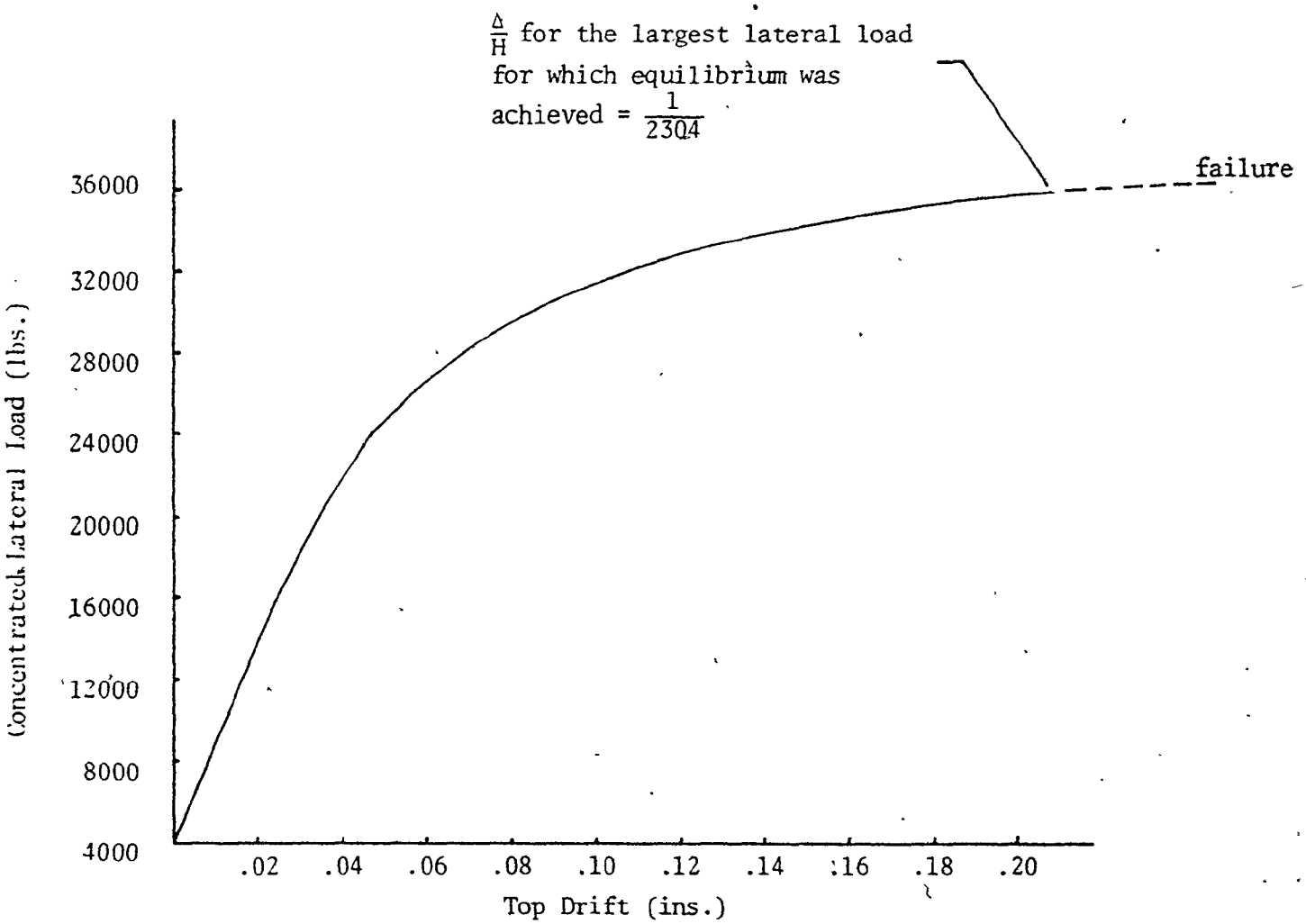

Fig. 6.7 Graph of Lateral Load Versus Drift for 10-Panel Complex Cantilever With Unreinforced Horizontal Joints Using 3-Element Joint Simplification (Concentrated Lateral Load)

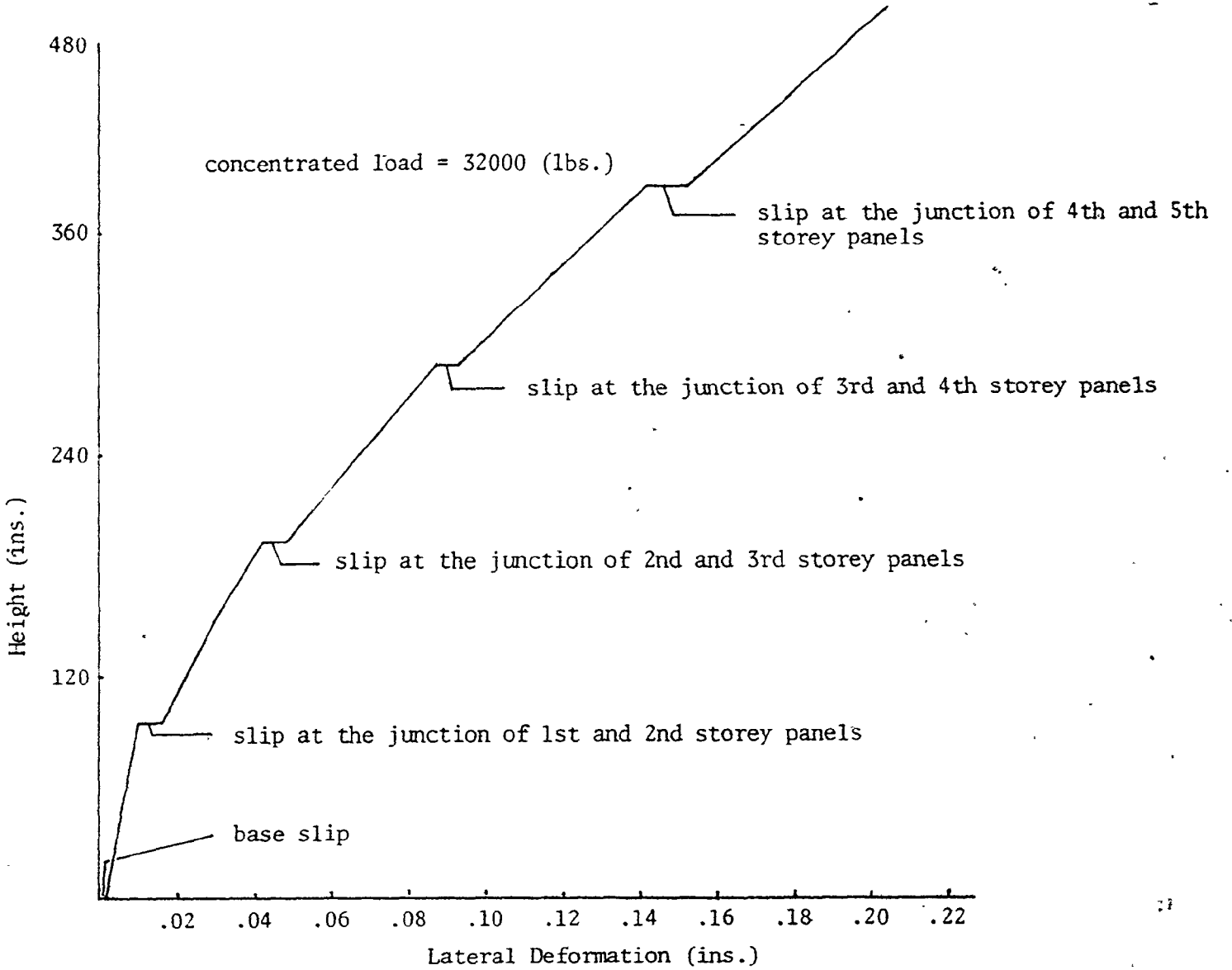

Fig. 6.8 Deflected Profile of 10-Panel Complex Cantilever with Unreinforced Horizontal Joints Using 3-Elements Joint Simplification (Concentrated Load Applied to the Top of the Complex Cantilever)

eventually failure near the top of the cantilever. The bending effect of the concentrated force in this case, does not seem to be insignificant enough to produce a separation failure.

(c) Reinforced Horizontal Joints (Distributed Lateral Loads)

The arrangement and the number of panels forming the complex cantilever in this investigation are the same as those used in (a) and (b). The exception, however, is the introduction of two reinforcing bars across each of the horizontal joints. Because the procedures for modelling these bars were introduced in Chapter 3, and dealt with again in Chapter 5, they will not be discussed further.

The sequence of joint slips and separations leading to the complete failure of the complex cantilever is shown in Table 6.4. A schematic presentation of the failure sequence as indicated in Table 6.4, is illustrated in Fig. 6.9. There is again no indication of splitting along the vertical joints, and the failure of the complex cantilever occurs by overturning along the base at an ultimate load of approximately 2475 pounds per linear foot of height. The effect of reinforcing the horizontal joints is to increase the failure load by 20% over case (a) where the joints were unreinforced.

Table 6.5 shows the forces developed in the joint reinforcements. As was mentioned in Chapter 3, reinforcing bars crossing the joints contribute to shear resistance along the joints acting as dowels while at the same time offering

Lateral Load per Corner Node (lbs)	Lateral Load per Panel (lbs)	Lateral Load per Linear ft. (lbs/ft)	Failure Sequence
1500	6000	750	elem.1 slip
1800	7200	900	elem.1 sep., elem.13 slip
2100	8400	1050	elem.2 slip., elem.13 sep. elem.25 slip.
2400	9600	1200	313m.14 slip.
2700	10800	1350	elem.2 sep., elem.3 slip., elem.25 wep., elem.26 slip.
3000	12000	1500	elem.4 slip., elem.14 sep., elem.15 slip., elem.37 slip.
3300	13200	1650	elem.4 sep., elem.16 slip., elem.28 slip. elem.3 sep.
3600	14400	1800	elem.37 sep., 38 slip.
3900	15600	1950	elem.26 sep., elem.40 slip., elem.49 slip.
4200	16800	2100	elem.15 sep.,
4500	18000	2250	elem.16 sep.,
4800	19200	2400	elem.29 slip., elem.50 slip. elem.27 sep.
5100		2550	dowels 1,2,3, yield. leading to failure.

Table 6.4 Failure Sequence for the 10-Panel Complex Cantilever with Reinforced Horizontal joints Using the 3-Element Joint Simplification (Distributed Lateral Loads)

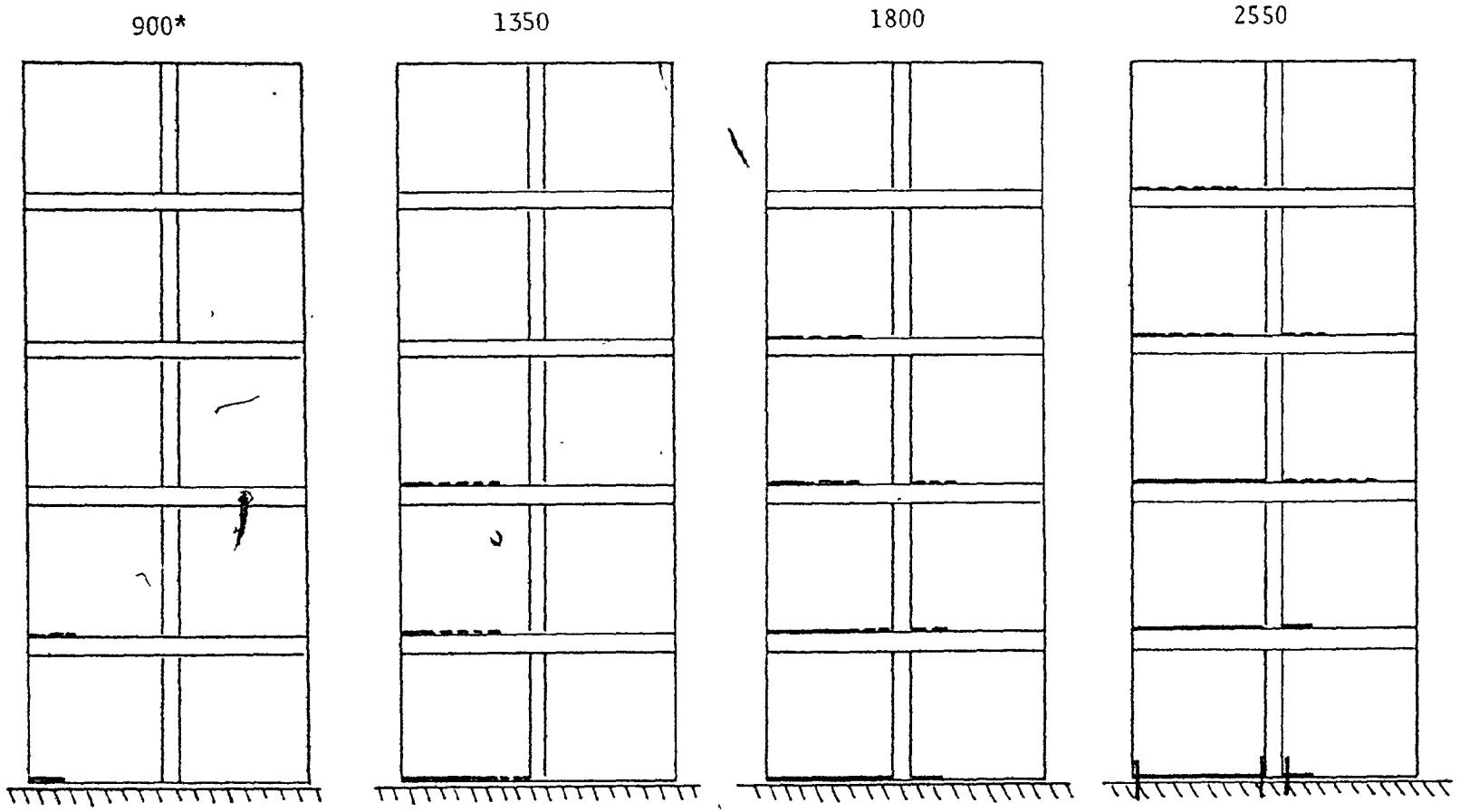

* horizontal load per linear ft. of height

--- slip

—— separation

| yielding of dowel bars (horizontal joint reinf.)

Fig. 6.9 Schematic Presentation of Failure Sequence for the 10-Panel Complex Cantilever as documented in Table 6.4

Dowel Bar Number \ Load lb/L.ft	700		1050		1200		1350		1500	
	H*	V**	H	V	H	V	H	V	H	V
1	478	394	702	799	1319	1038	1637	2135	2383	3254
2										
3										
9			875	138	1385	673	2132	1084	2767	1720
10										
11										
17						907		74	1791	371
25										

Table 6.5 Forces in the Joint Reinforcements for Various Levels of Lateral Loads Expressed in Pounds per Linear Foot of Height (Table Contains the Forces in only Those Joint Reinforcements which were Activated by Separation)

* Force in the Horizontal Springs of Joint Reinforcement Element representing the Dowel Action.

** Force in the Vertical Spring of Joint Reinforcement Element representing the Vertical Continuity

	1650		1800		1750		2100		2250		2400		2550
	H	V	H	V	H	V	H	V	H	V	H	V	
1	2420	4444	2892	7438	3595	10723	4598	11365	5396	14599	6057	17627	yield
2	2060	34	2368	1208	2875	2491	3618	3896	4256	5321	4748	6707	yield
3	2028	72	2326	1246	2822	2528	3554	3933	4187	5360	4672	6747	yield
9	3323	3043	6223	4226	6254	5666	6661	7094	6599	9526	7243	10478	Failure of complex Cantilever
10							6305	5	6198	884	6460	1806	
11									5884	868	6108	1784	
17	2450	619	1842	868	1723	1339	1805	2068	1984	2797	1420	3634	
25			1107	20	1839	150	1565	244	1932	373	2262	455	

Table 6.5 (cont'd)

resistance to separation. The forces developed in the joint reinforcement are indicated under the appropriate columns in Table 6.5. As the increasing lateral forces result in joint slip and separation, reinforcing bars become activated one by one. A total of 8 reinforcing bars become activated in this case, before yielding of bars number 1, 2 and 3 and failure of the complex cantilever by separation along the base occur.

The graph of lateral load versus drift (lateral deflection at the top) is illustrated in Fig. 6.10. The drift remains linear up to approximately 50% of the ultimated load. For loads greater than 50% of the ultimate, an accelerated drift rate is observed with 50% of the ultimate drift caused by the final 14% of the ultimate load. The $\frac{\Delta}{H}$ ratio just before failure is $\frac{1}{1476}$. The $\frac{\Delta}{H}$ ratio at the highest stable load level for the case where joints were not reinforced was $\frac{1}{1901}$. This was determined at a load of 1950 pounds per linear foot of height. For the reinforced case at the same load, the $\frac{\Delta}{H}$ ratio was $\frac{1}{3535}$ or a decrease in drift of approximately 46%. Thus introduction of even a small quantity of reinforcement (in this case 2 one inch diameter bars per joint), improves the resistance to lateral deformation appreciably.

6.4 Analysis of 10-panel Complex Cantilevers Utilizing the 2-Element Joint Simplification

The second example which will be studied in this chapter consists of 10 panels arranged in 2 bays and 5 storeys.

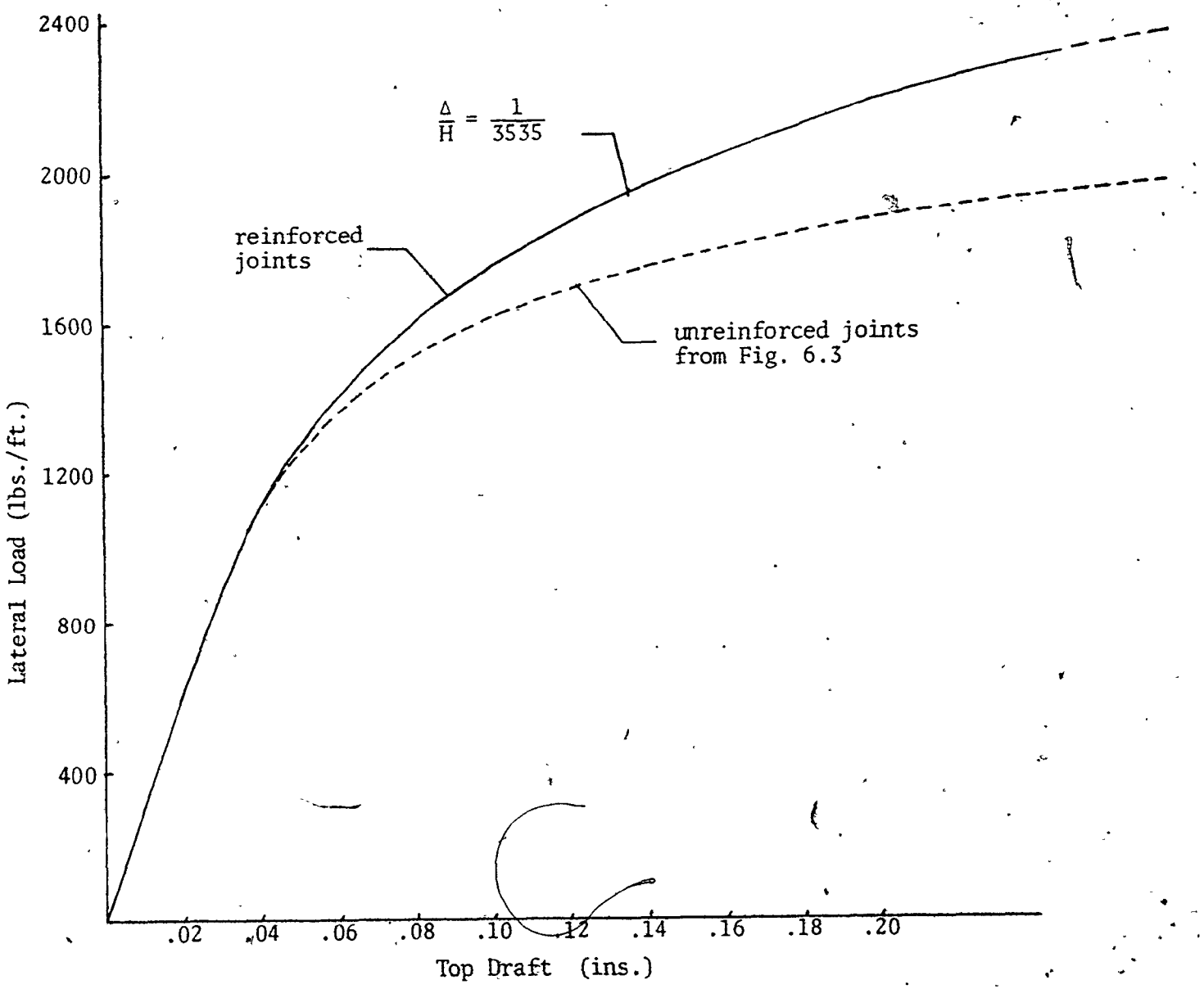

Fig. 6.10 Graph of Lateral Load Versus Drift for 10-Panel Complex Cantilever with Reinforced Horizontal Joints Using 3-Element Joint Simplification (Distributed Lateral Loads)

The 2-element representation is used for each of the joints. These elements, which incorporate all the joint properties, are located at the corners of the panels. The successive joint element stiffness modification outlined in Chapter 5 is utilized in simulating the joint behaviour. Although the 3-element per joint model of a complex cantilever is probably a more reasonable method of modelling these structures, the procedure still requires a computer with very large storage capacity if large complex cantilevers are to be investigated. As mentioned previously, the largest complex cantilever which could be investigated using the CDC 6400 computer at McMaster University was that studied in the previous section. If larger structures are to be studied, further joint simplifications have to be made. That is basically why the possibility of representing the joints using 2 elements only was also investigated in Chapter 5. However, before studying the behaviour of larger complex cantilevers using 2-element joints, it was deemed necessary to reinvestigate the behaviour of the 10-panel complex cantilever of the previous section using 2-element joints and to compare the results. Thus, in the remaining parts of this section, the behaviour of reinforced and unreinforced 10-panel complex cantilevers under the action of distributed lateral loads will be studied.

(a) Unreinforced Horizontal Joints (Distributed Lateral Loads)

The finite element representation of a 10-panel complex cantilever using the 2-element joint simplification is shown in Fig. 6.11. Each panel is composed of 4 triangular

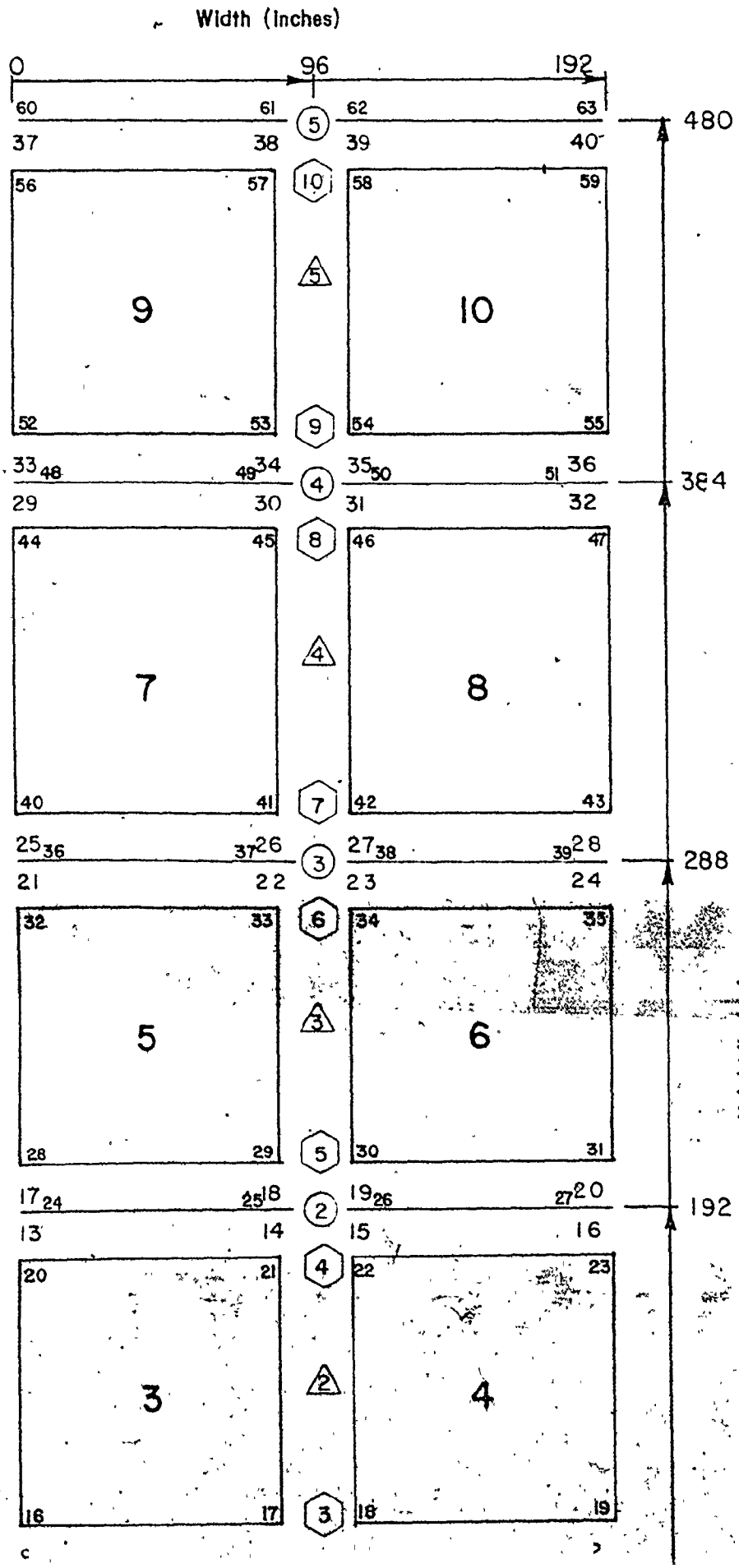
Width (Inches)
0
96
192
480
384
288
192
Height (Inches)
60 61 62 63
37 38 39 40
56 57 58 59
9
10
52 53 54 55
33 48 49 34 35 50 51 36
29 30 31 32
44 45 46 47
7
8
40 41 42 43
25 36 37 26 27 38 39 28
21 22 23 24
32 33 34 35
5
6
28 29 30 31
17 24 25 18 19 26 27 20
13 14 15 16
20 21 22 23
3
4
16 17 18 19
1
2
3
4
5
6
7
8
9
10

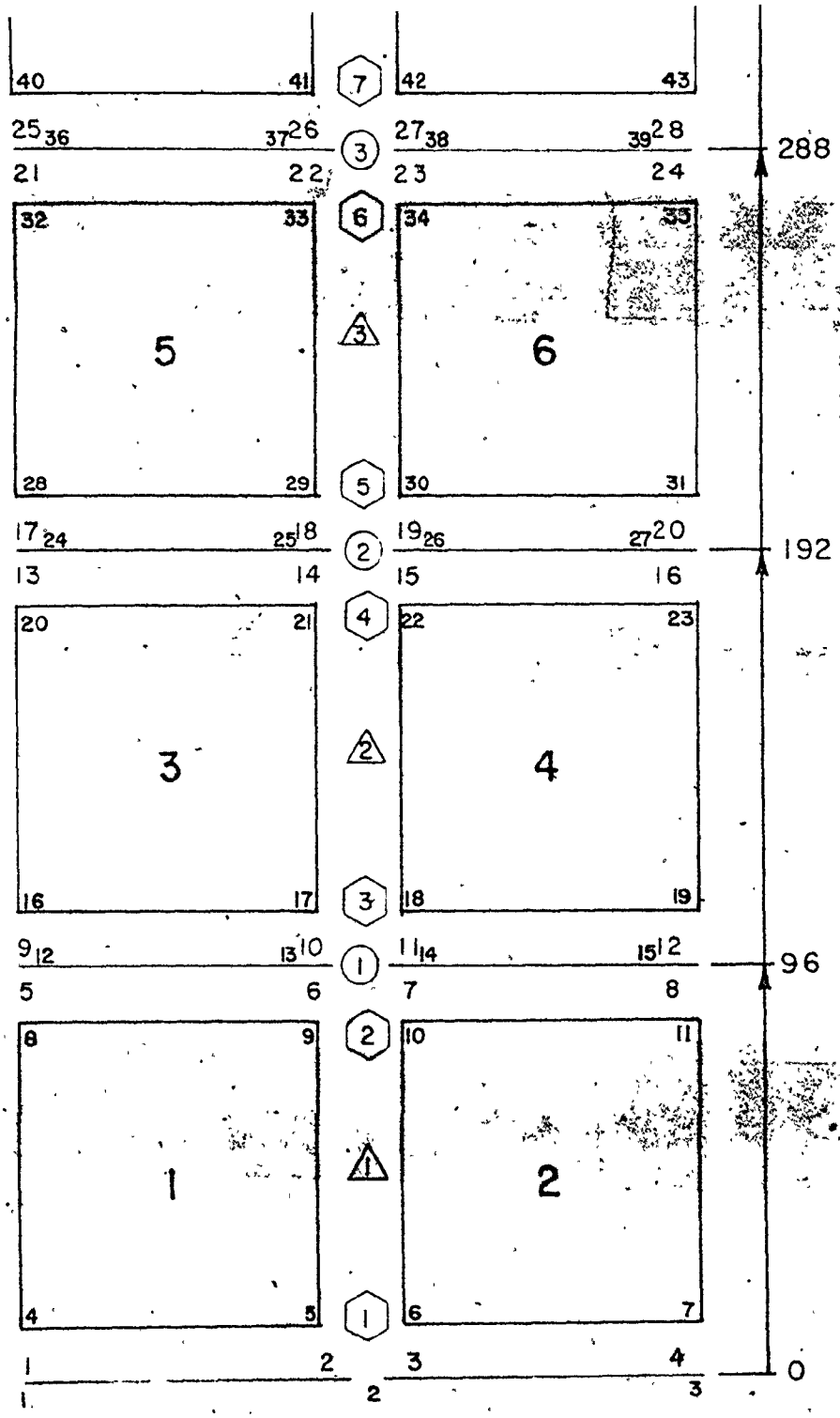

Legend

△ Vertical Joint No.

⬡ Vertical Joint Element No.

◯ Tie-Beam Element No.

4 Typical Panel No. (Digit Size 3/8")

4 Typical Horizontal Joint Element and horizontal Joint Reinforcement No. (Digid Size 1/4")

4 Typical Nodal No. (Digit Size 3/16")

Fig. 6.11. Finite Element Representation of a Complex Cantilever Composed of 10 panels Arranged in 2 Bays and 5 Storeys Using 2 Elements per Joint

elements with the centre node condensed. The sequence of slips and separations is illustrated in Table 6.6 and Fig. 6.12. When examined together with Fig. 6.11, Table 6.6 illustrates the manner in which the slip and separation of joint propagate through the complex cantilever leading to failure by separation along the base of the cantilever.

The failure occurs at the same lateral load level as when the 3-element joint model was used. However, an examination of Fig. 6.13 which shows the graph of lateral loads versus drift, indicates that the model exhibits more stiffness for the 2-element joint simplification. This is not entirely unexpected since a comparison of simplified horizontal joints in Chapter 5 also showed the 2-element joint to be stiffer than its 3-element counterpart. The difference in drift, however, is greater near the ultimate load. At 75% of the ultimate load, the discrepancy in drift is approximately 21%. At 50% of the ultimate load the discrepancy reduces to 17%. Therefore although the 2-element joint will be utilized for the purpose of analysing larger structures, it must be remembered that lateral deformations are generally under estimated.

(b) Reinforced Horizontal Joints (Distributed Lateral Loads)

The bahaviour of the 10-panel complex cantilever with reinforced horizontal joints utilizing the 2-element simplification are also compared with their 3-element counterparts. The sequence of joint slip and separation is indicated in Table 6.7 and schematically presented in Fig. 6.14. The

Lateral Load per Corner Node (lbs)	Lateral Load per Panel (lbs)	Lateral Load per Linear ft. (lbs/ft)	Failure Sequence
3600	7200	900	elm.1 slip.
4200	8400	1050	elem.9 slip.
4800	9600	1200	elem.1 sep., elem.17 slip.
5400	10800	1350	elem.9 sep.
6000	12000	1500	elem.3 slip., elem.25 slip.
6600	13200	1650	elem.11 slip.
7200	14400	1800	elem.17 sep.
7800	15600	1950	elem.19 slip.
"	"	"	elem.33 slip.
8400	16800	2100	elem.2 sep., elem.3 sep. leading to failure

Table 6.6 Failure Sequence for the 10-Panel Complex Cantilever with Unreinforced Horizontal Joints Using the 2-Element Joint Simplification (Distributed Lateral Loads)

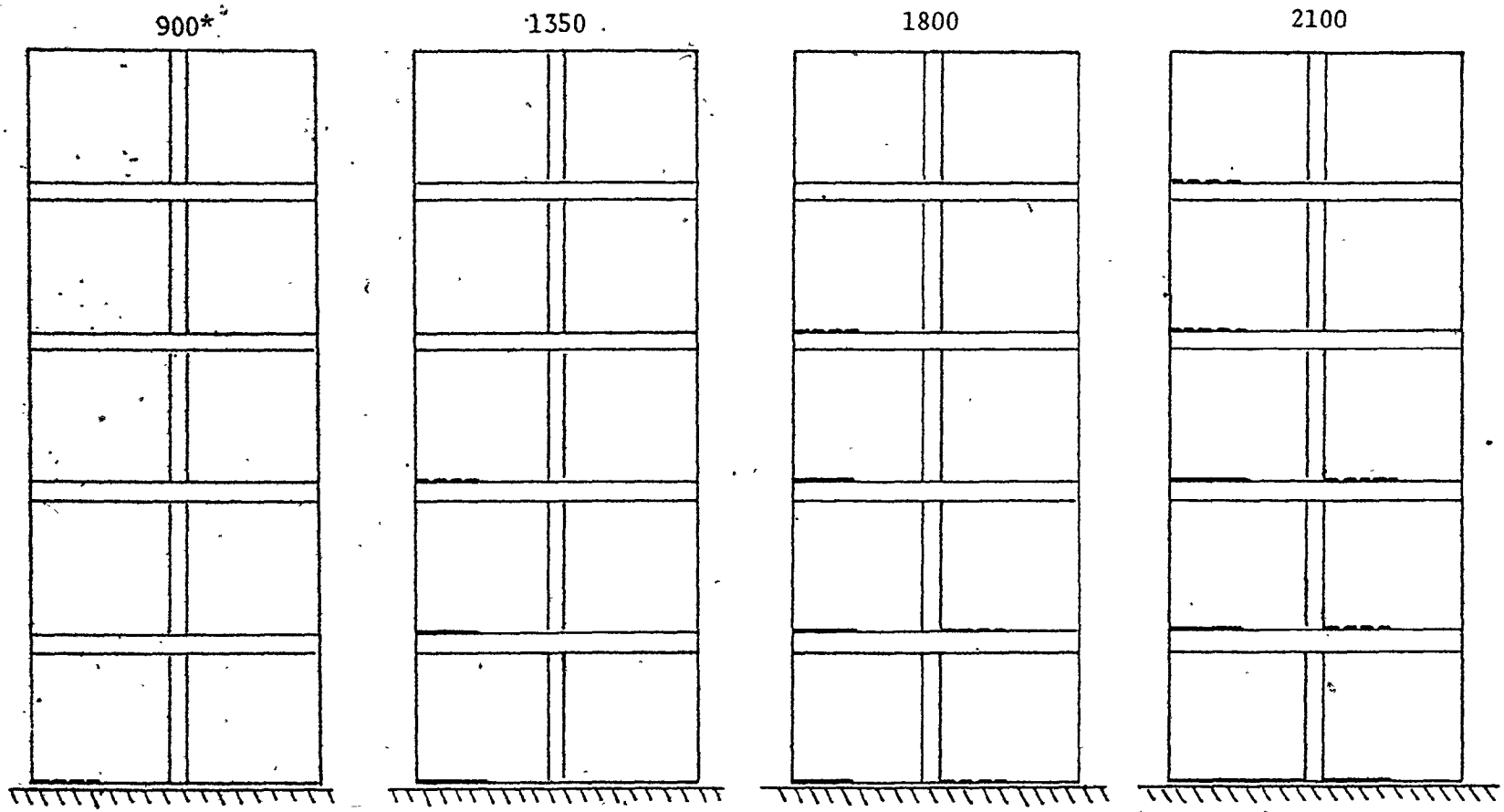

* horizontal load per linear ft. of height (lbs.)

--- slip

—— separation

Fig. 6.12 Schematic presentation of Failure Sequence for 10-Panel Complex Cantilever as Documented in Table 6.6

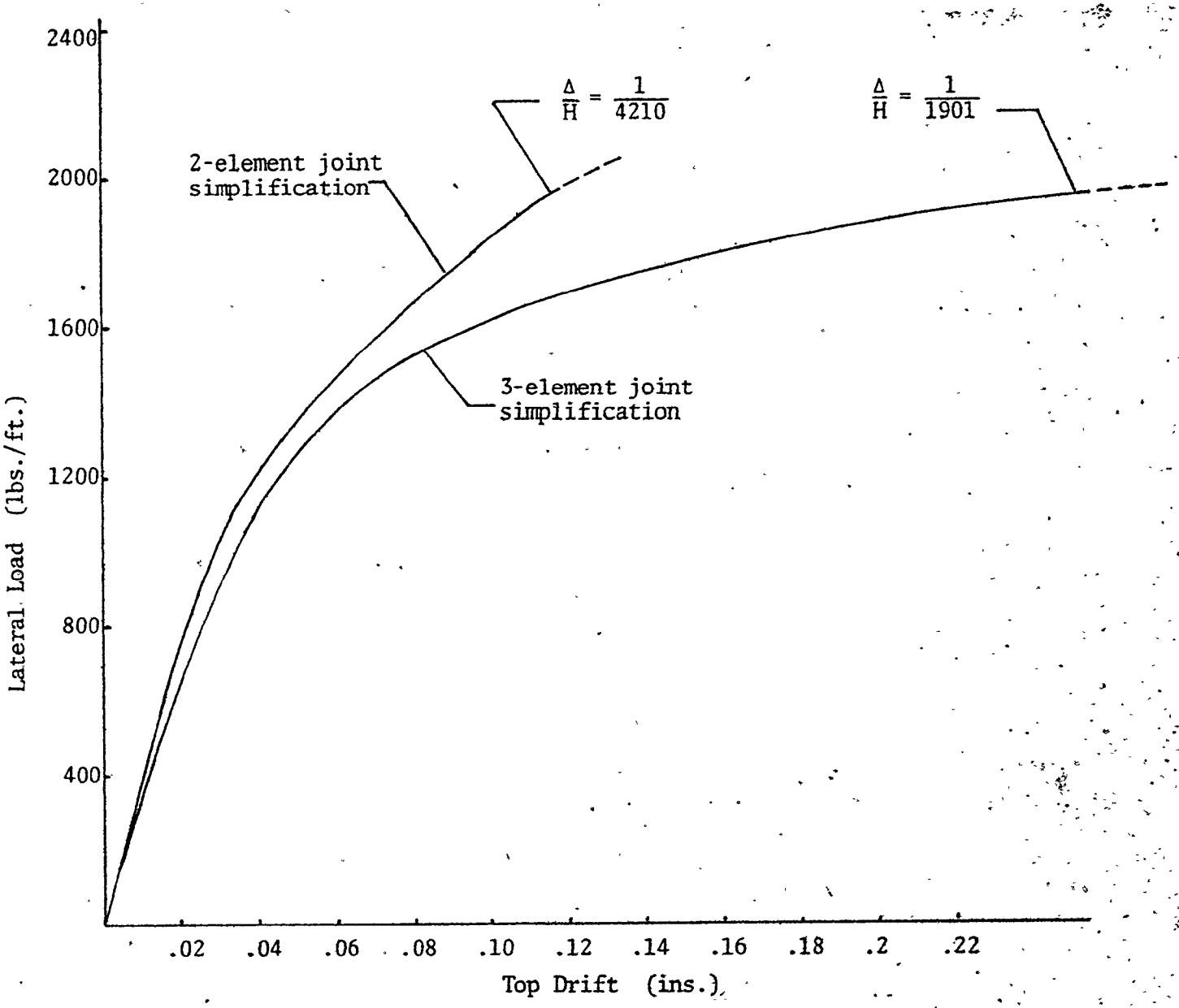

Fig. 6.13 Graph of Lateral Load Versus Drift for 10-Panel Complex Cantilever with Unreinforced Horizontal Joints Using 2-Element Joint Simplification (Distributed Lateral Load)

Lateral Load per Corner Node (lbs)	Lateral Load per Panel (lbs)	Lateral Load per Linear foot (lbs/ft)	Failure Sequence
3600	7200	900	elem.1 slip.
4200	8400	1050	elem.9 slip
4800	9600	1200	elem.1 sep., elem.17 slip.
5400	10800	1350	elem.9 sep.
6000	12000	1500	elem.3 slip., elem.25 slip.
6600	13200	1650	-
7200	14400	1800	elem.11 slip.,elem.17 sep.
7800	15600	1950	elem.19 slip.
8400	16800	2100	elem.23 slip.
7000	18000	2250	elem.2 sep., elem.3 sep.
9600	19200	2400	dowels 1,2,3 yield. leading to failure

Table 6.7 Failure Sequence for the 10-Panel Complex Cantilever with Reinforced Horizontal Joints Using the 2-Element Joint Simplification (Distributed Lateral Loads)

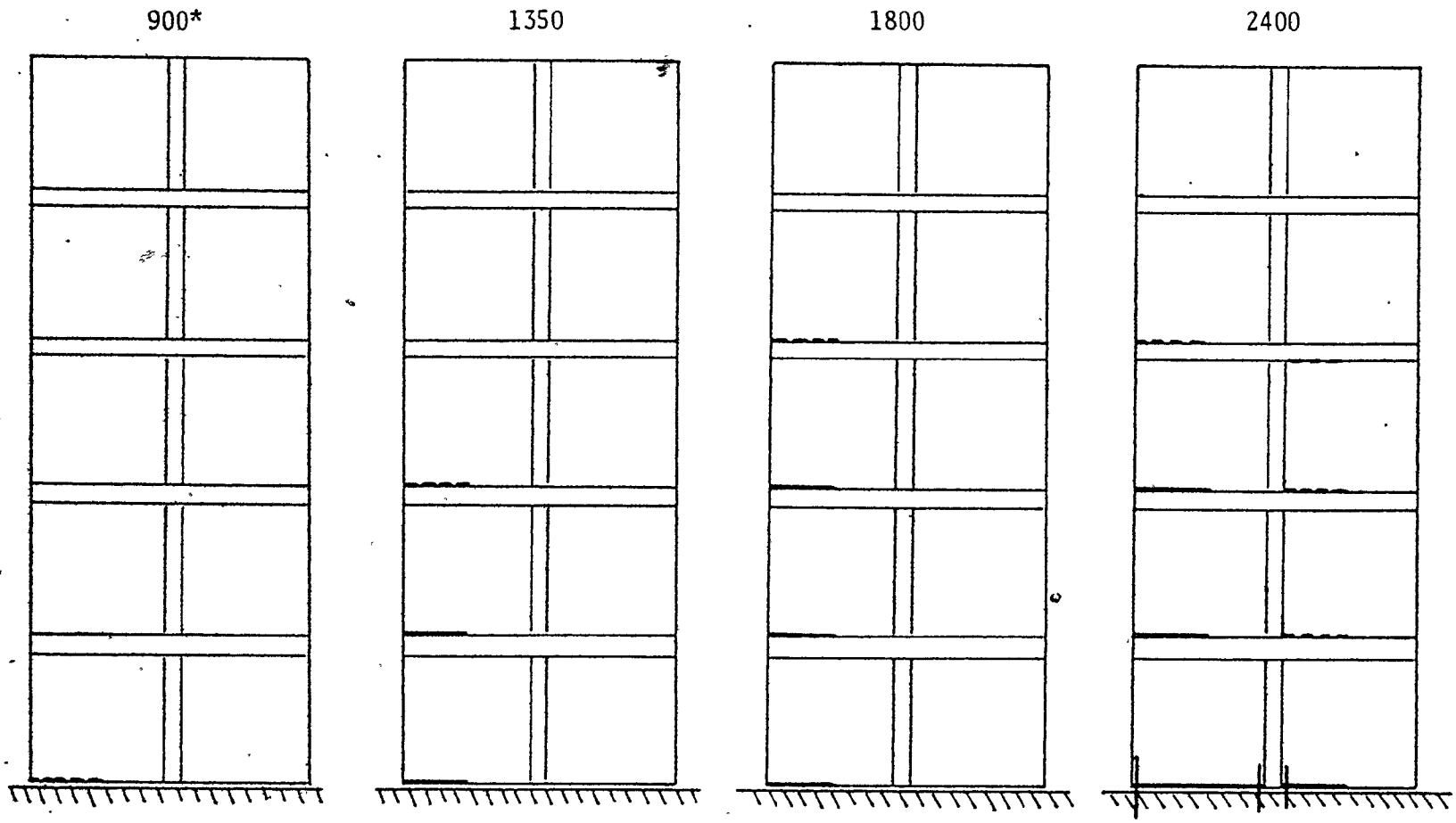

* horizontal load per linear ft. of height (lbs.)

--- slip

—— separation

yielding of dowel bars (horizontal joint reinf.)

Fig. 6.14 Schematic Presentation of Failure Sequence for 10-Panel Complex Cantilever as documented in Table 6.7

physical model is the same as that shown in Fig. 6.11 except that elements representing the joint reinforcement are added to the horizontal joints and accounted for in the overall stiffness matrix of the structure. The failure of the structure is once again by separation along the base of the structure when yielding occurs in the base reinforcement elements 1, 2 and 3. When this case is compared with its 3-element counterpart (outlined in Subsection 6.3(c)), it is observed that its failure load is slightly lower. Therefore although the maximum possible discrepancy between this case and the 3-element one could be as high as 12%, the actual discrepancy in all likelihood is much less. For all practical purposes it can be said that changing the number of joint elements does not effect the ultimate load capacity of the cantilever. An examination of ultimate failure loads for 2 and 3 element joints outlined in Chapter 5 further reinforces this conclusion.

A comparison of drifts at the top of the structure for the 2 and 3-element joint simplification is illustrated in Fig. 6.15. The same slight increase in stiffness observed in the previous case is also apparent here with a discrepancy of about 19% at 75% of the ultimate load. This discrepancy is very similar to the 21% found for the similar but unreinforced joint model.

6.5 Analysis of 30-panel Complex Cantilevers Utilizing the 2-Element Joint Simplification

The final model that will be investigated in this chapter is that of a 30-panel complex cantilever arranged in

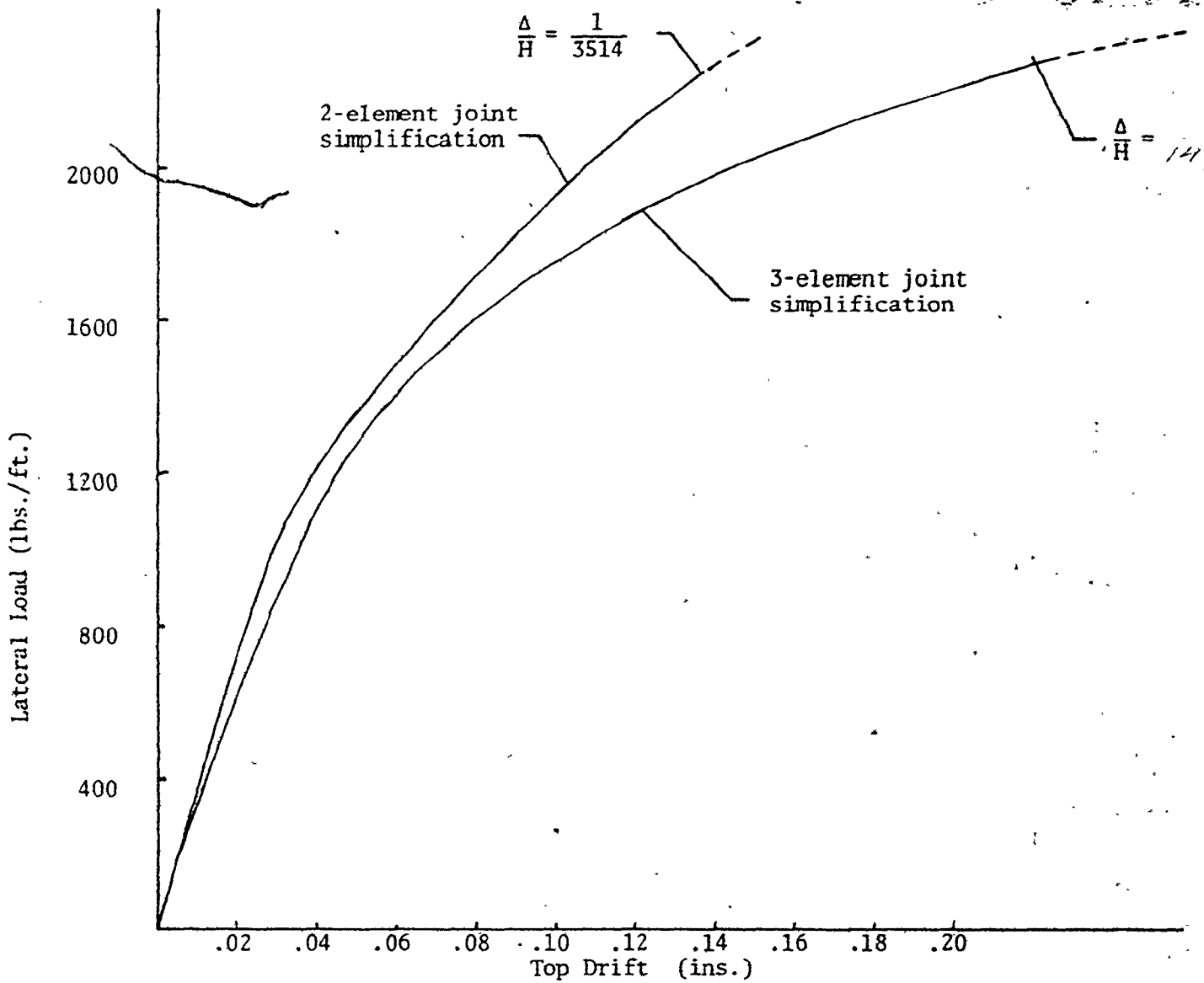

Fig. 6.15 Graph of Lateral Load Versus Drift for 10-Panel Complex Cantilever with Reinforced Horizontal Joints Using 2-Element Joint Simplification (Distributed Lateral Load)

3 bays and 10 storeys. The physical properties and dimensions of the individual panels are identical to those already studied in connection with the 10-panel complex cantilevers of Sections 6.3 and 6.4. The finite element model of the assembly is shown in Fig. 6.16. Each interface is composed of 2 elements located at the corners of the panels. The behaviour for a gradually increasing lateral load applied to the nodes located on the vertical edge of the complex cantilever for the 2 cases of unreinforced and reinforced horizontal joints is studied in the following Subsections.

(a) Unreinforced Horizontal Joints (Distributed Lateral Loads)

The sequence of the slipping and separation of the joints is indicated in Table 6.8, and is schematically presented in Fig. 6.17. When reviewed together with Fig. 6.16, Table 6.8 illustrates the manner in which horizontal joints gradually separate with final failure of the complex cantilever occurring by separation along the base of the structure. As expected, the joint separation is initiated at the bottom left corner of the complex cantilever. (Lateral loads are applied from left to right.) As lateral loading increases, separation extends to the upper floor joint elements situated on the left vertical edge of the structure. By the time that the entire base of the first panel has separated, the corner element separation has extended to the bottom of the 4th storey panel.

As was the case with the 10-panel complex cantilever, no splitting of the vertical joints is observed. The reason

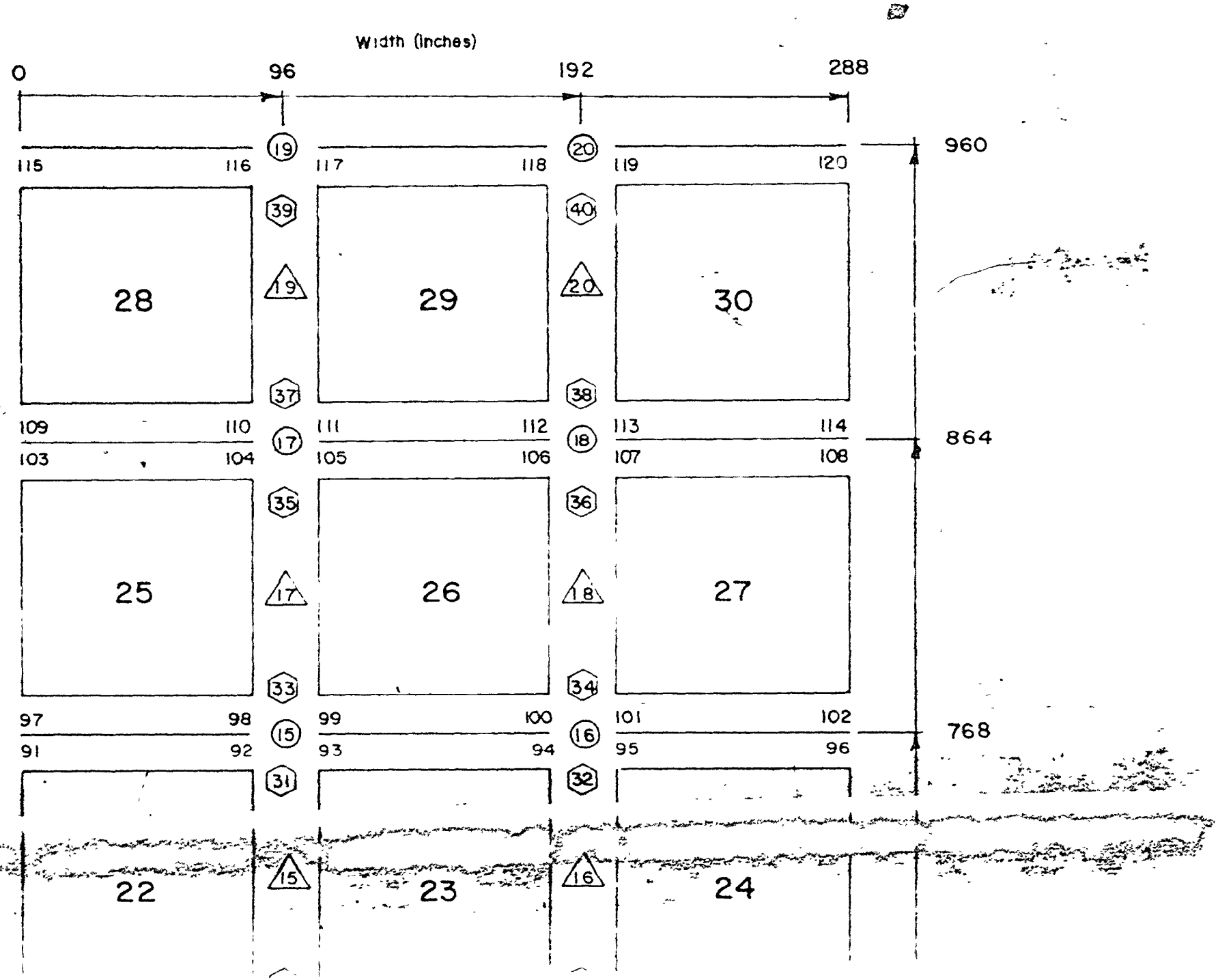
Width (inches)
0
96
192
288
960
864
768
19
20
115
116
117
118
119
120
39
40
28
29
30
19
20
37
38
109
110
111
112
113
114
17
18
103
104
105
106
107
108
35
36
25
26
27
17
18
33
34
97
98
99
100
101
102
15
16
91
92
93
94
95
96
31
32
22
23
24
15
16

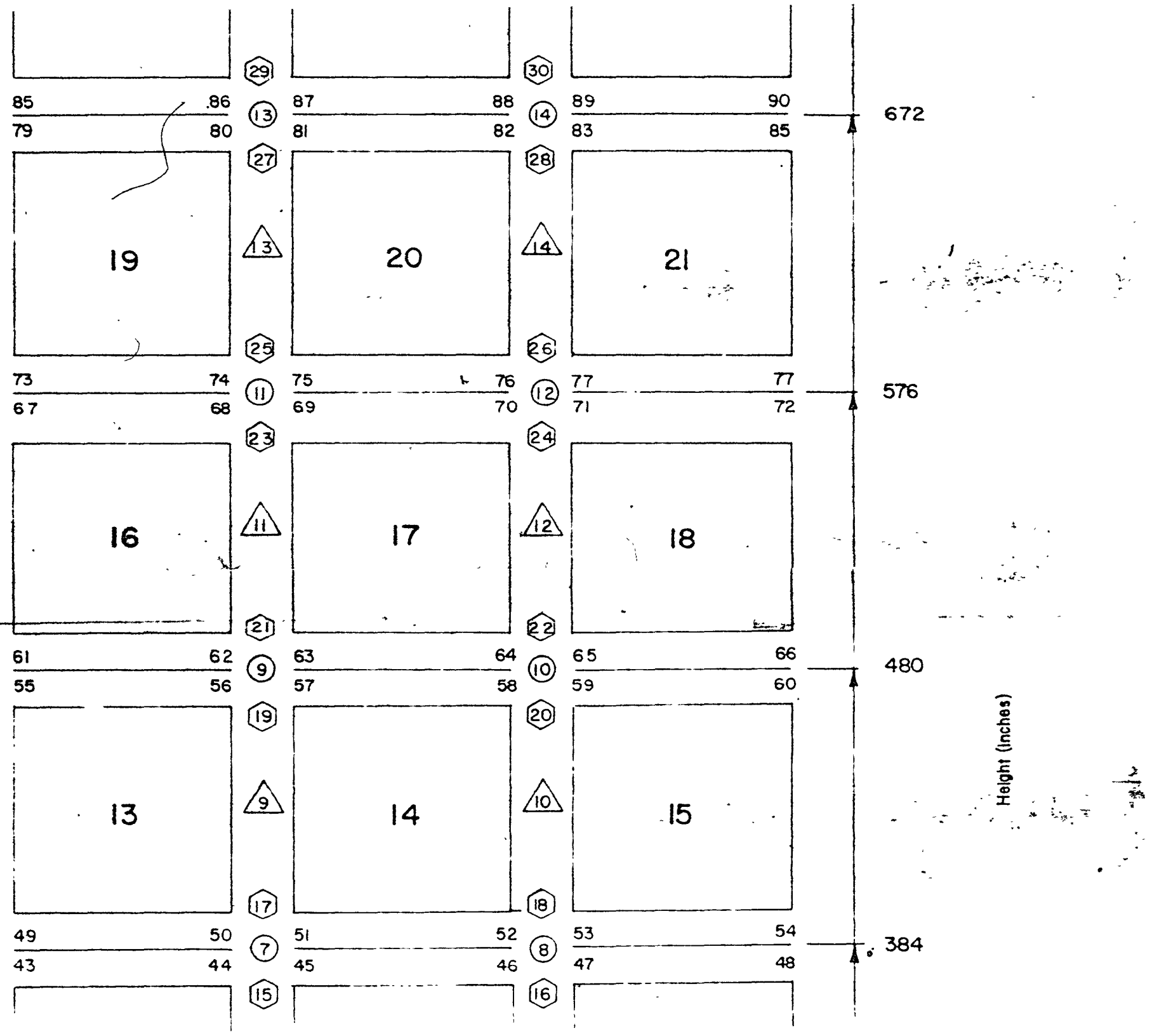
29
30
85
86
87
88
89
90
13
14
79
80
81
82
83
85
672
27
28
19
13
20
14
21
25
26
73
74
75
76
77
77
11
12
576
67
68
69
70
71
72
23
24
16
11
17
12
18
21
22
61
62
63
64
65
66
9
10
480
55
56
57
58
59
60
19
20
13
9
14
10
15
17
18
49
50
51
52
53
54
7
8
384
43
44
45
46
47
48
15
16
Height (inches)

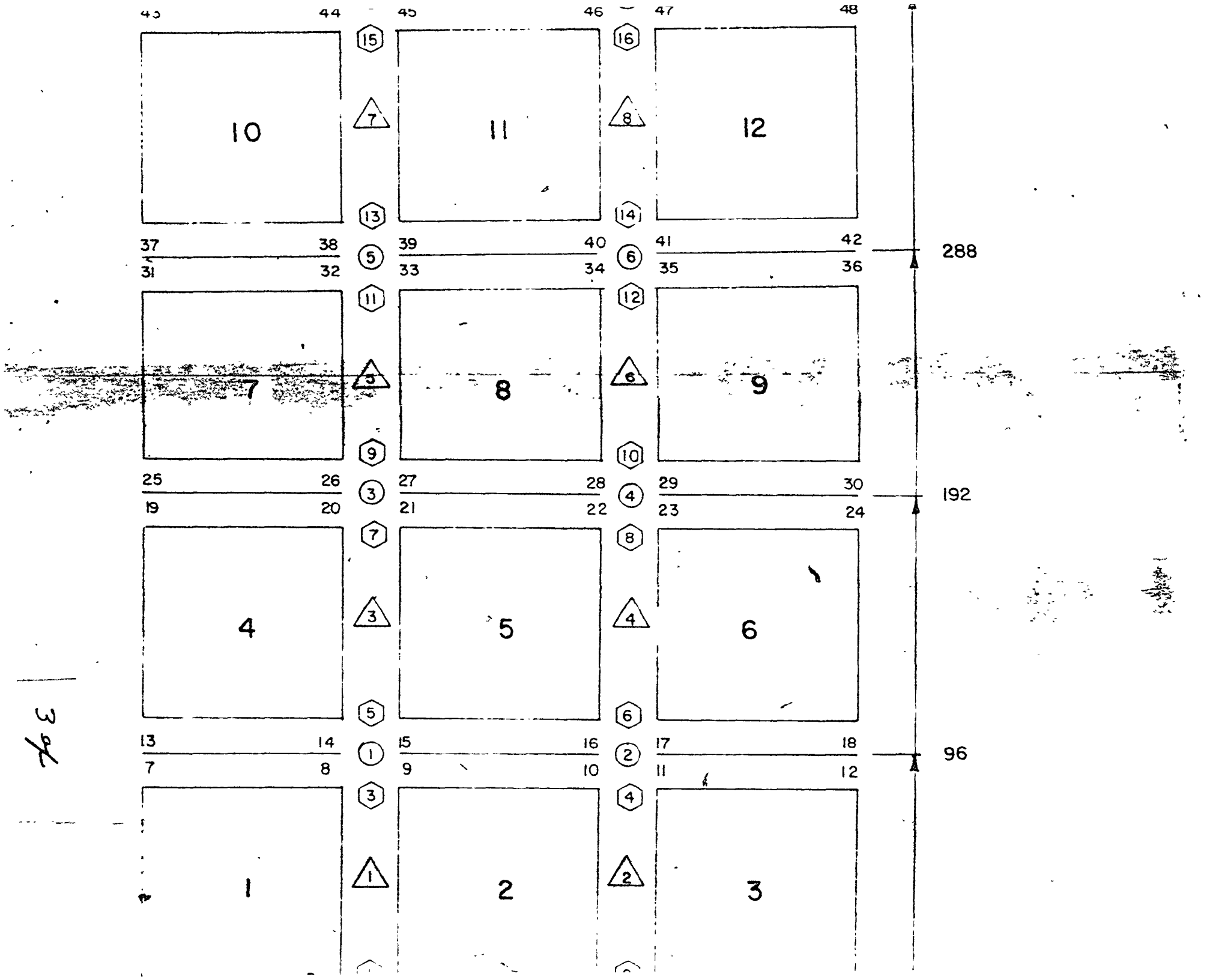
43
44
45
46
47
48
15
16
10
7
11
8
12
13
14
37
38
39
40
41
42
288
31
32
33
34
35
36
11
12
7
3
8
6
9
9
10
25
26
27
28
29
30
192
19
20
21
22
23
24
7
8
4
3
5
4
6
5
6
13
14
15
16
17
18
96
7
8
9
10
11
12
3
4
1
1
2
2
3

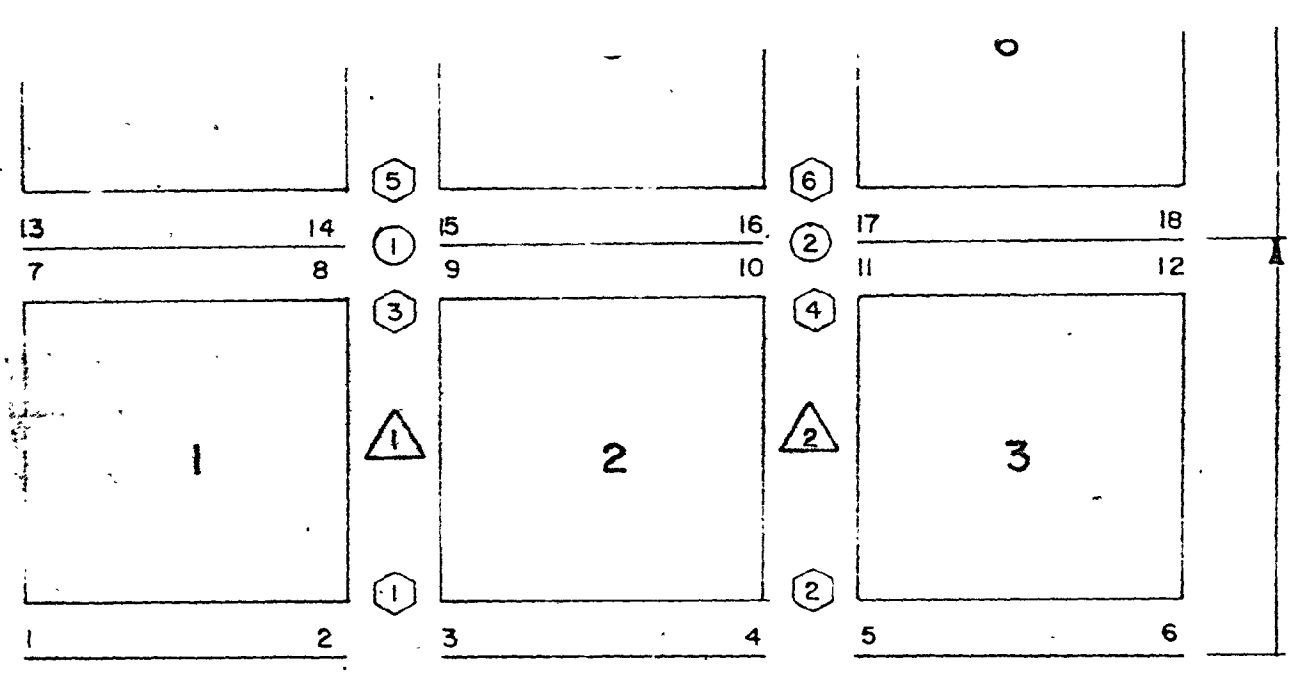

△ Vertical Joint No.

⬡ Vertical Joint Element No.

◯ Tie-Beam Element No.

4 Typical Panel No. (Digit Size 3/8")

4 Typical Horizontal Joint Element and Horizontal Joint Reinforcement No. (Digit Size 1/4")

Fig. 6.16 Finite Element Representation of a Complex Cantilever Composed of 30 Panels Arranged in 3 Bays and 10 Storeys Using 2 Elements per Joint

Lateral Load per Corner Node (lbs)	Lateral Load per Panel (lbs)	Lateral Load per Linear ft. Height (lbs/ft)	Failure Sequence
3600	7200	900	elem.1 slip.
4000	8000	1000	elem.1 sep., elem.13 slip., elem.25 slip.
4400	8800	1100	elem.13 sep.
4800	9600	1200	elem.37 slip.
5200	10400	1300	elem.3 slip., 25 sep., elem.49 slip.
5600	11200	1400	elem.15 slip.
6000	12000	1500	elem.27 slip., elem.37 sep., elem.61 slip.
6400	12000	1600	elem.3 sep., elem.39 slip., elem.2 sep.
6800	13600	1700	elem.14 sep., elem.49 sep., elem. 73 sep.
7200	14400	1800	elem.15 sep., elem.26 sep., elem. 51 slip.
7600	15200	1900	elem.5 slip., elem.61 sep.
8000	16000	2000	elem.27 sep.
8400	16800	2100	elems.17,63,85 slip.
8800	17600	2200	elems. 4,38 sep.
7200	18400	2300	elems 5,16 sep., elem 29 slip. elems 39,73 sep. leading to failure.

Table 6.8 Failure Sequence for the 20-Panel Complex Cantilever with Unreinforced Horizontal Joints Using the 2-Element Joint Simplification (Distributed Lateral Loads)

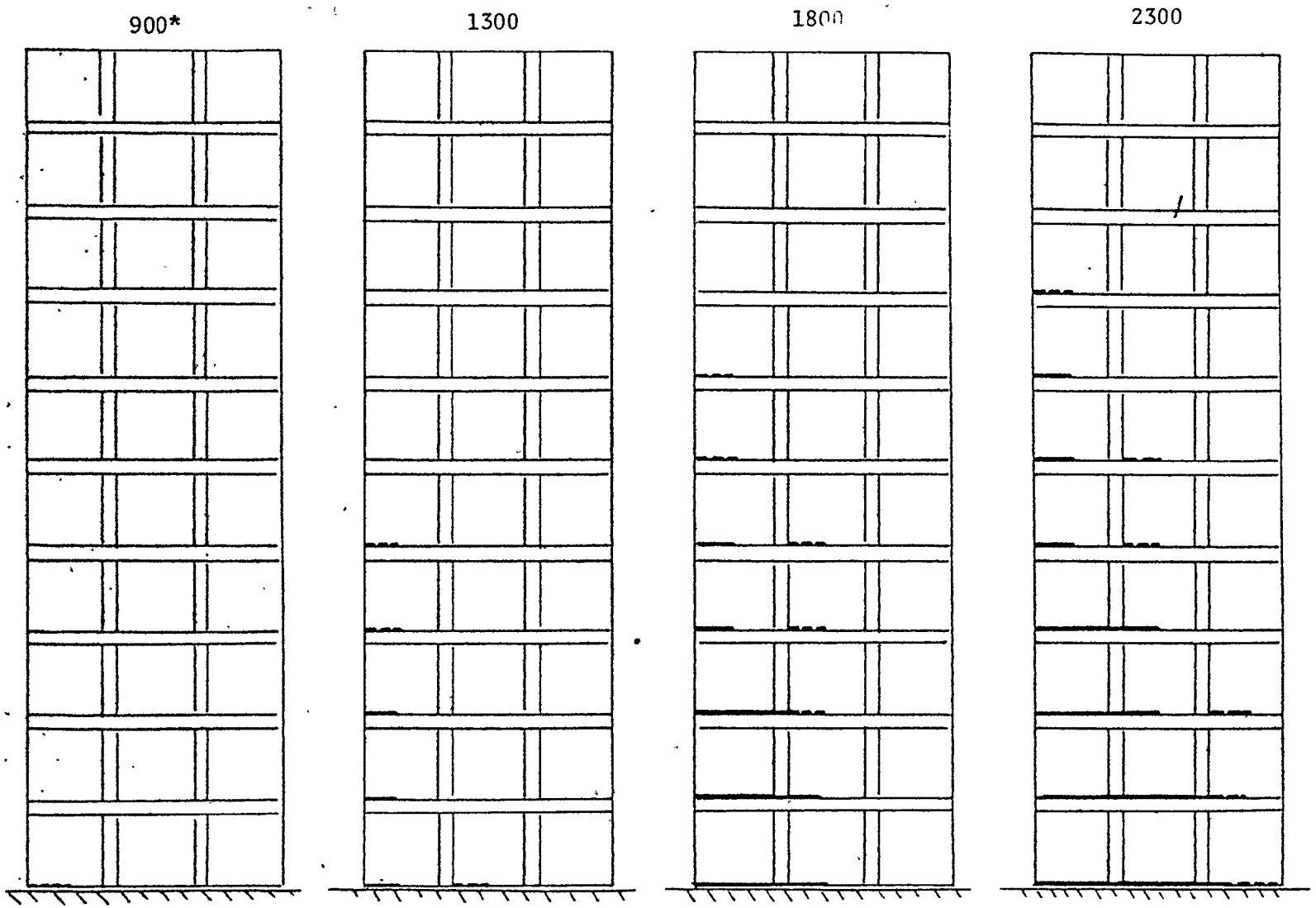

Fig. 6.17 Schematic Representation of Failure Sequence for 30-Panel Complex Cantilever as Documented in Table 6.8

for this was explained in Section 6.3 and will not be repeated here. The fact that neither shear nor tension cracks appear along a vertical joint, even though the panel immediately to the left of it may have lost all contact with its neighbouring panels above and below while carrying the imposed dead loads, may appear to be somewhat puzzling. It must, however, be remembered that the lateral loads acting on the structure (including the panel under consideration) tend to reduce the cantilever action by producing bending moments in the opposite direction, thus reducing the stresses sufficiently to prevent cracking of the vertical joints. Even so, the contribution of lateral loads is not enough to prevent cracking of the vertical joints when more shear loads are transmitted to them due to the introduction of horizontal joint reinforcement. This will be dealt with in the next subsection.

The graph of lateral loads versus drift is shown in Fig. 6.18. If it is assumed that the results of Section 6.4 regarding the comparative stiffnesses of the 2 and 3-element joint models are also applicable in this case, it may be concluded that Fig. 6.18 underestimates the lateral deflection of the complex cantilever. The failure load, however, is considered to be reliable. The amount by which the deflections are underestimated varies with the load level. Again with reference to the results of Section 6.4, the discrepancy at 75% of the ultimate load could be as high as 20%.

If the allowable $\frac{\Delta}{H}$ ratio for panelized structures is

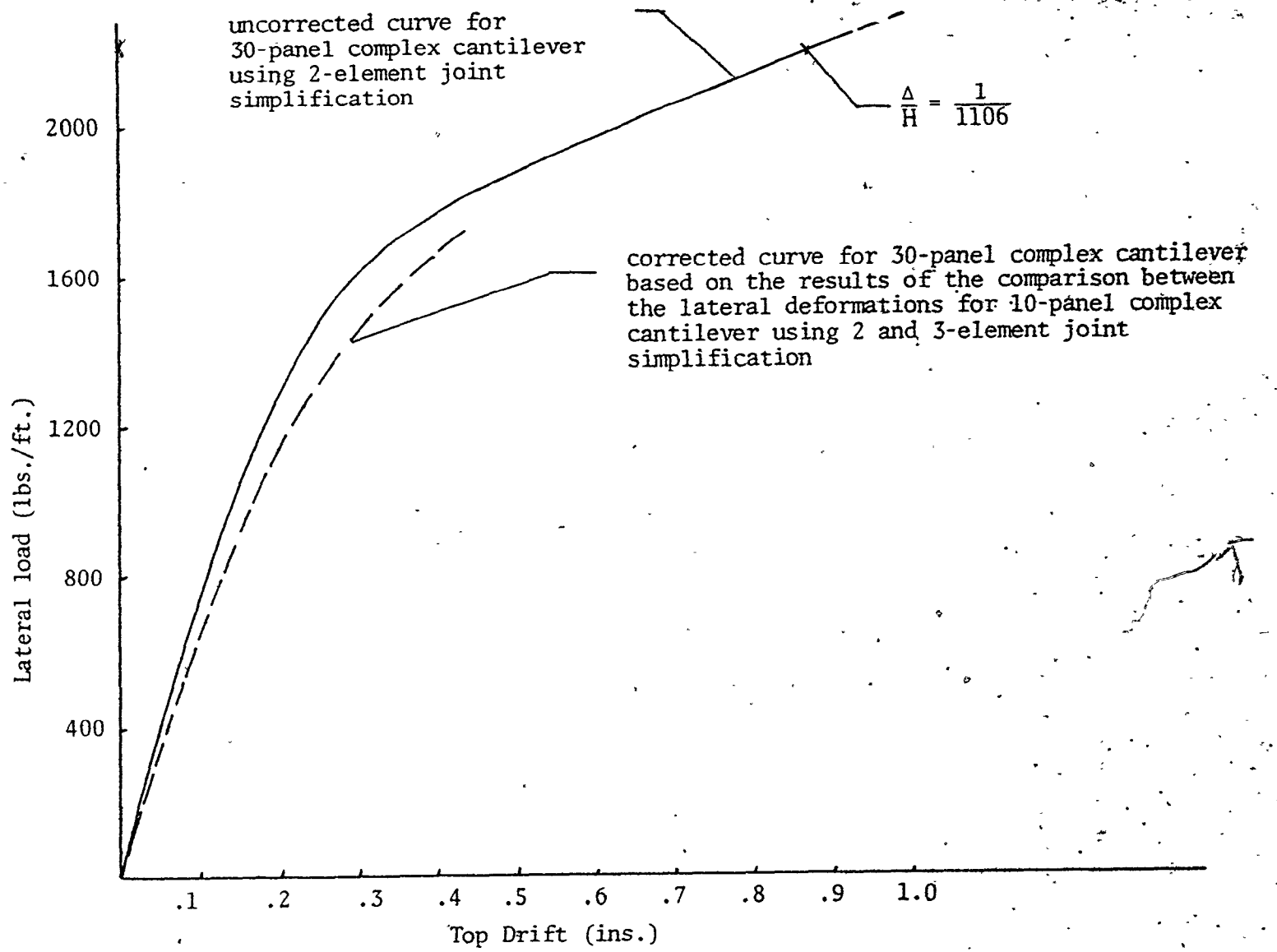

Fig. 6.18 Graph of Lateral Load Versus Drift for 30-Panel Complex Cantilever with Unreinforced Horizontal Joints Using 2-Element Joint Simplification (Distributed Lateral Load)

taken to be equal to $\frac{1}{2000}$ [26], the ratio of the ultimate load to the load corresponding to a $\frac{\Delta}{H}$ ratio of $\frac{1}{2000}$ is found to be 1.21. With a limiting $\frac{\Delta}{H}$ of $\frac{1}{4000}$, the corresponding load ratio is increased to 1.56. This would coincide with lateral load of 1440 pounds per linear ft. of height of the complex cantilever with horizontal joints exhibiting a moderate amount of slipping and separation. Therefore, it must be concluded that in order for the joints to maintain their integrity allowable values of $\frac{\Delta}{H}$ must be reduced. More about this will be said in Chapter 7.

(b) Reinforced Horizontal Joints (Distributed Lateral Load)

In this model the joint reinforcement is identical to those described in Subsections 6.3(c) and 6.4(b). The sequence of joint slip and separation is illustrated in Table 6.9 and in Fig. 6.19. The sequence follows a pattern similar to that indicated for the previous case until the lateral load reaches the 2000 pound per linear foot level Fig. 6.16. At this load level, complete separation of panels 1 and 4, and partial separation of panels 2 and 5 from their neighbouring panels above and below has already taken place. At this stage, the primary means of connection of these panels to the rest of the structure is through their respective vertical joints and the steel reinforcement incorporated in their horizontal joints. With further increase in lateral loads panels 1 & 2, and panels 4 & 5 start to cantilever from panels 3 and 6 respectively, thereby causing tension cracks to appear

Lateral Load per Corner Node (lbs)	Lateral Load per Panel (lbs)	Load per Linear ft. height (lbs/ft)	Failure Sequence
3600	7200	900	elem.1 slip.
4000	8000	1000	elem.1 sep., elem.13 slip., elem.25 slip.
4400	8800	1100	elem.13 sep.
4800	9600	1200	elem.37 slip.
5200	10400	1300	elem.25 sep., elem.49 slip.
5600	11200	1400	elem.3 slip., elem.15 slip. elem.37 sep.
6000	1200	1500	elems.27,61 slip.
6400	12800	1600	-
6800	13600	1700	elems.2,3,14 sep. elem.39 slip. elem.49 sep., elem.73 slip.
7200	14400	1800	elem.15 sep. elem.51 slip.
7600	14200	1900	elem.26 sep.
8000	16000	2000	elem.27 sep. elem.61 sep., elem. 85 slips.
8400	16800	2100	elem.63 slip., vert.joint elem.4 crack in tension elem.5 slip., vert.joint elem.8 crack in tension, elem.38 sep. vert.joint elem.6 split
8800	17600	2200	dowel bar 25 yield.
9200	18400	2300	elem.39 sep., vert.joint elem.10 split.

Table 6.9 Failure Sequence for the 30-Panel Complex Cantilever with reinforced Horizontal Joints Using the 2-Element Joint Simplification (Distributed Lateral Loads)

Lateral Load per Corner Node (lbs)	Lateral Load per Panel (lbs)	Load per Linear ft. height (lbs/ft)	Failure Sequence
9200	18400	2300	dowel bars 26 & 27 yield,, elem.16 sep., dowel bar 1 yields.
9600	19200	2400	elem.73 sep. elem.75 slips, DB 2 & 3 yield. elem.5 sep., elem.4 sep.
10000	20000	2500	elem. 17,97 slip. dowel bar 4,5 yield, elem.6 crack diagonally leading to failure.

Table 6.9 (cont.)

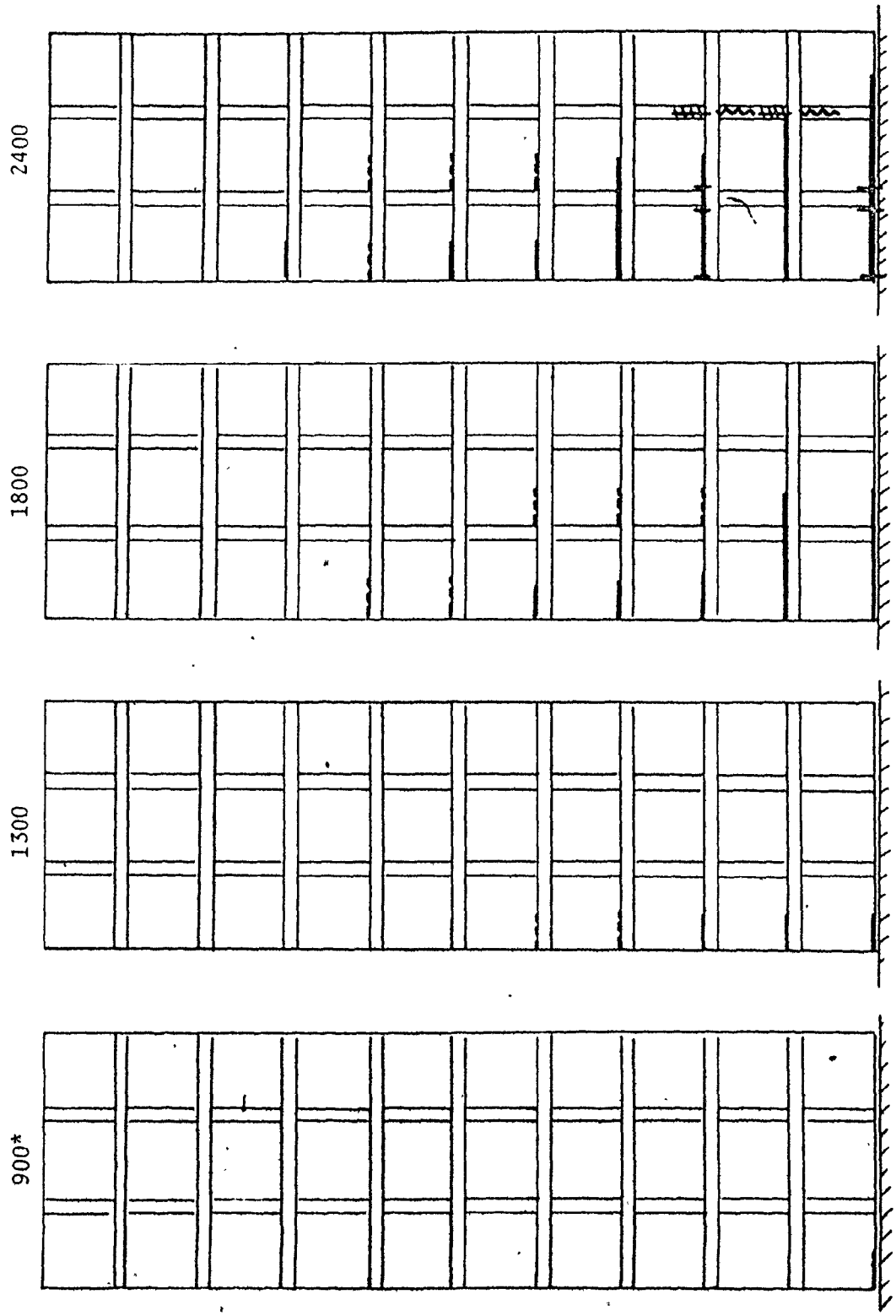

Fig. 6.19 Schematic Representation of Failure Sequence for 30-Panel Complex Cantilever as Documented in Table 6.9

in vertical joint elements 4 and 8. The expression tension cracks as used here signifies cracks resulting primarily from a bending type action. The word splitting is used in connection with a shear type crack running along the interface between the vertical edge of a panel and the joint concrete. The expression diagonal cracks is used to indicate the formation of cracks within the body of the joint concrete.

The cracking of vertical joint element 8 leads to a sudden increase of shear stresses in the vertical joint element 6 causing it to split. The same type of behaviour would be expected to occur in relation to the vertical joint element 2. However, no splitting of this joint is indicated. The author can attribute this only to the effects of the fixed boundary, that is, the rigid base of the structure.

The splitting of the vertical joint element 6 and the formation of tensile cracks in the vertical joint element 8 cause panels 4 and 5 to practically hang from the neighbouring panels above resulting in yielding of horizontal joint reinforcing elements 25, 26 and 27. Final failure occurs by separation along the base and by yielding of horizontal joint reinforcing elements 1, 2, 3, 4 and 5. The improvement in load capacity over the previous case with unreinforced horizontal joints is about 9%.

Figure 6.20 shows the graph of lateral load versus drift, for the cantilever with reinforced horizontal joints. Assuming that the comparison between the 2 and 3-element joint representation of the reinforced joints for the complex

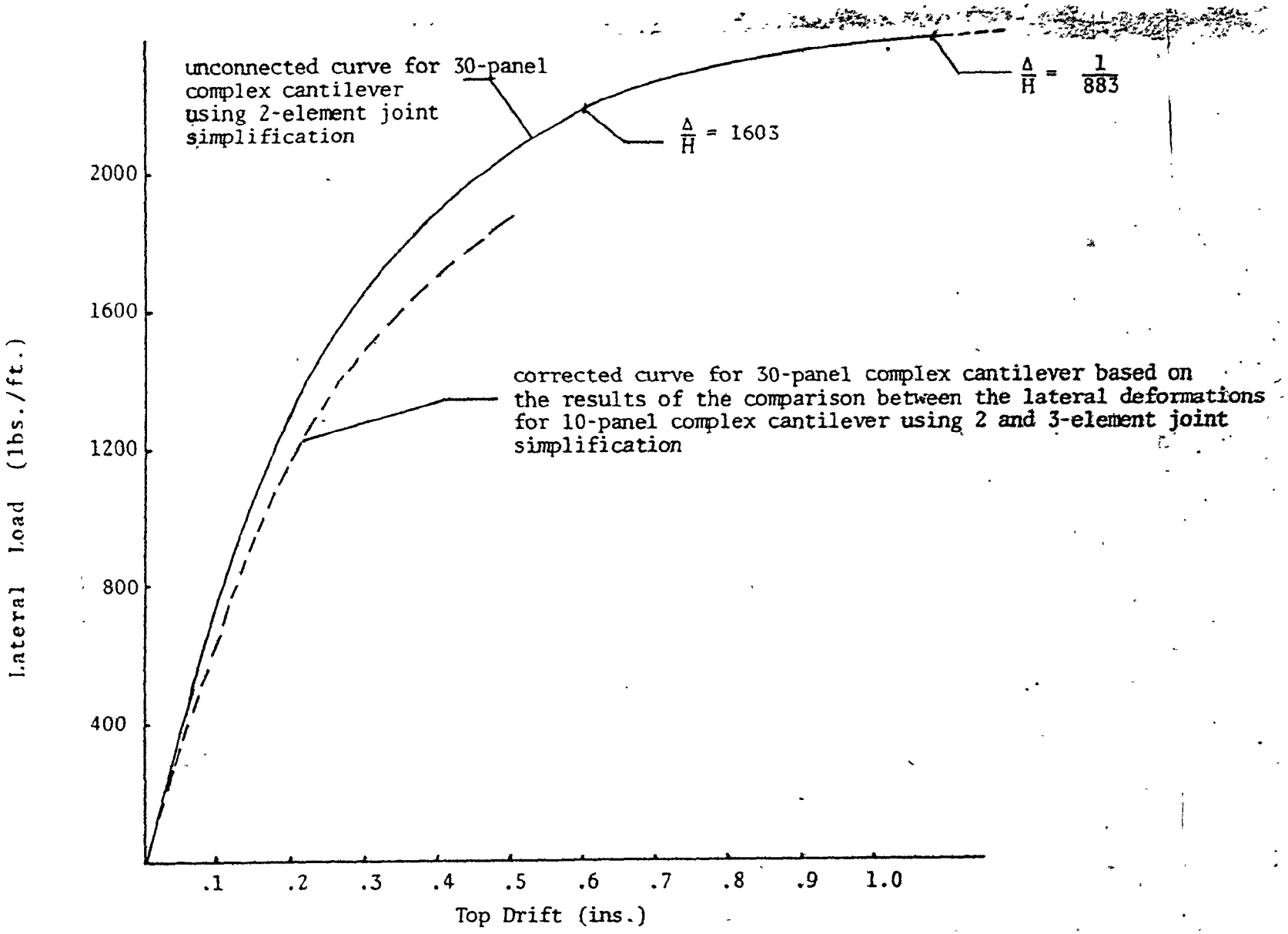

Fig. 6.20 Graph of Lateral Load Versus Drift for 30-Panel Complex Cantilever with Reinforced Horizontal Joints Using 2-Element Joint Simplification (Distributed Lateral Load)

cantilevers of Subsection 5.4(b) is also valid in this case the deformation graph shown (solid line) probably underestimates the actual deformation of the complex cantilever. Thus, if the deformation curve shown in Fig. 6.20 is increased by the same proportions, a more realistic estimate of the actual deformations (dashed line) might be obtained. The $\frac{\Delta}{H}$ ratio for the unreinforced case (Subsection 6.5(a)) at a lateral load level of 2200 pounds per linear foot of height was found to be equal to $\frac{1}{1106}$ (Fig. 6.12). For the reinforced case at the same level of loading the ratio is $\frac{1}{1603}$. The actual drifts for the two cases are 0.868" and 0.598" respectively. The effect of reinforcing the joints is to reduce the drift by 21%.

The ratio of the ultimate load to the load corresponding to a $\frac{\Delta}{H}$ ratio of $\frac{1}{2000}$ utilizing the uncorrected curve in Fig. 6.20, is 1.23. The load ratio corresponding to a $\frac{\Delta}{H}$ ratio of $\frac{1}{4000}$ is 1.66. The load corresponding to the $\frac{\Delta}{H}$ ratio of $\frac{1}{4000}$ is 1480 lbs per linear foot of height of the complex cantilever

At this load level the horizontal joints exhibit a moderate amount of slipping and separation.

This would indicate that excessive deflection is not a likely source of trouble with panel buildings. Although the loads causing slipping and separation for a $\frac{\Delta}{H}$ of $\frac{1}{4000}$ are far in excess of normal service loads, the fact that separation and slip do occur indicates that the horizontal joints of complex cantilevers are perhaps far more susceptible

than is nly

6.6 Summary

The 2 and 3-element simplified joint models developed in Chapter 5, were used in this chapter to simulate the behaviour of several complex cantilever models. The largest of these which could be investigated using McMaster University's CDC 6400 computer were 10-panel complex cantilevers with 3-element joints, and 30-panel complex cantilevers with 2-element joints. The investigation for each model included the reinforced as well as the unreinforced horizontal joints. With the aid of these models it was possible to estimate the ultimate lateral load capacity for complex cantilevers. It was also possible to compute the lateral deformation curves resulting from the increasing lateral loads. Lateral deformations at the top of the cantilever were found to be small and remained linear for up to 50% of the ultimate load capacity. Thereafter the deformations increased rapidly in a nonlinear fashion so that most of the total ultimate deformation resulted from the application of the final 10 or 15 percent of the ultimate (total) load.

The effect of joint reinforcement on the behaviour was to increase the load capacity by 9 to 20 percent and to inhibit lateral deformations. It was difficult to compare the changes in the deformations near the ultimate load. For various models tested, the effect of reinforcing the horizontal joints was to inhibit lateral deformations by approximately 16 to 20 percent at 75 percent of the ultimate load capacity.

A comparison of lateral deformations for 10-panel complex cantilevers which were identical in every respect, except for the number of elements used to simulate the joint behaviour, indicated that the complex cantilevers with 2-element joints appeared stiffer than their 3-element counterparts. At 75 percent of the ultimate load, deformations for the cantilever utilizing the 2-element joint model were approximately 17 percent less than those computed for the complex cantilever utilizing the 3-element joint model. In the cantilevers using the 2-element simplification, the joint slip and separation was also delayed.

These observations are quite important, because they indicate that by reducing the number of joint elements and concentrating the stiffnesses at the two corners (of the joint), the overall behaviour of a complex cantilever is changed even when the modification approach is adopted. Although it has not been conclusively proved, because joint separation was included in the 3-element joint model, it is anticipated that the results of the analyses (using the 3-element model) will be much more representative of the actual situation.

Based on the comparison of the results for the 10-panel complex cantilever using the 2 and 3-element joint simplifications, the deformation curve for the 30-panel complex cantilever with the 2-element joint model could be adjusted to represent the actual situation more realistically.

If the allowable $(\frac{\Delta}{H})$ ratio for panel buildings is

taken to be $\frac{1}{2000}$ [26], then the ratio of the ultimate load to the load corresponding to $(\frac{\Delta}{H})$ of $\frac{1}{2000}$ may be used as an indication of the factor of safety against collapse. It is important to realize that this definition of the factor of safety should be based on an allowable lateral deformation for which the permissible limits on stresses and deformations for the constituent components are not violated.

Based on a $\frac{\Delta}{H}$ ratio of $\frac{1}{2000}$ the factor of safety against collapse was found to be approximately 1.20. However, the lateral loads corresponding to $\frac{\Delta}{H}$ ratio of $\frac{1}{2000}$ produced extensive slipping and separation along the horizontal joints. Even when the ratio was reduced to $\frac{1}{4000}$, the corresponding loads produced moderate amounts of slipping and separation. It is therefore concluded that the allowable lateral deformations for panel buildings should be reduced so that joint integrity is not compromised under the service loads. More about this will be said in the concluding chapter where recommendations for allowable $\frac{\Delta}{H}$ ratios for panel buildings under service loads will be made.

CHAPTER 7

CONCLUSIONS AND RECOMMENDATIONS FOR FUTURE RESEARCH

7.1 Conclusions

The purpose of the investigation presented in the preceding chapters was to study the behaviour of complex cantilevers under the action of gradually increasing lateral loads, and to be able to predict their ultimate strengths. After a number of preliminary studies it was concluded that in order to be able to realistically simulate the overall behaviour of complex cantilevers, the detailed behaviour of the joints had to be modelled adequately. Therefore, a large part of the effort in this study was devoted to the development of realistic models for the joints of complex cantilevers. The joint models were then simplified and modified so that larger complex cantilevers could be analyzed using the average capacity (approximately 120 K) computers. The study culminated in Chapter 6 where simplified joints were used to simulate the behaviour of a number of complex cantilevers.

The simplified joints fell into 2 basic categories. In the first category, the joint behaviour was simulated using 3 elements per each of the horizontal and the vertical joints. The largest cantilever that could be analysed

using a 3-element scheme (due to limitations in computer storage capacity) was a 2 bay by 5 storey complex cantilever. In the second category, the joint behaviour was simulated using 2 elements per joint. The largest cantilever which could be analyzed using this scheme was a 3 bay by 10 storey complex cantilever. In each case the influence of reinforced and unreinforced horizontal joints on the behaviour was investigated, under the action of gradually increasing lateral loads until failure of the assembly occurred.

By analyzing the results obtained in Chapter 6 and making a comparative study of various cases, keeping in mind the implications of the results of other chapters, the following conclusions may be drawn:

1. The behaviour of a complex cantilever cannot be simulated realistically by concentrating the entire joint stiffness in 2 or 3 nodal points without incorporating some form of stiffness modification. This is particularly true for the horizontal joints. By concentrating large stiffnesses at the 2 ends of a joint, resistance to deformation for both shearing and bending actions is greatly exaggerated. In the case of a vertical joint subjected to distributed longitudinal shear stresses, the difference is due mostly to the imposed uniformity of stresses on the joint.

For an isolated horizontal joint where stiffnesses were concentrated at the 2 extreme ends of the joint

without further stiffness modification, it was found that joint deformation at failure was less than 1/20 of that computed for a more detailed joint representation.

By modifying joint stiffnesses when they are concentrated at 2 or 3 points, it is possible to obtain results which are in good agreement with those obtained using a more detailed joint representation.

2. It is very difficult to realistically represent separations along horizontal joints when the number of joint elements representing a horizontal joint is reduced. In joints represented by 2 elements, the effect of partial separation can not be simulated. In fact, as the comparison of 2 element and multi-element joints of Chapter 5 indicated, 2-element joints remain unseparated for loads causing almost complete separation in their multi-element counterpart. If horizontal joints are reinforced, forces in the reinforcing bars are greatly influenced by the discrepancies in joint separations.

   In joints represented by 3 elements, some separation is indicated even if the joint stiffnesses are unmodified. By modifying the joint stiffnesses, the joint separations can be simulated with even greater accuracy. This leads to a better estimation of the forces developed in the joint reinforcement.

3. The analysis of complex cantilevers also indicates that horizontal joints are much more susceptible to slip and separation than would be expected from a review of previous investigators. Again, this inconsistency may be attributed to the effects of concentrating the joint stiffnesses without stiffness modification. As a result, the horizontal joints appear to be much stronger than indicated by a more detailed analysis.

Slip and separation of the horizontal joints also influence the development of stresses in vertical joints. It is for this reason that the complex cantilevers analyzed in Chapter 6 show so few splitting cracks even though the structural behaviour is well within the non-linear range.

In order to make full use of the strength of vertical joints, horizontal joints must remain intact. In high buildings, this is guaranteed because of high gravity loads. Alternatively, large amounts of longitudinal steel could be provided to guard against separation. If the joint stiffnesses are modified (to counteract the effects of stiffness concentrations), and if the joints are not heavily reinforced or, vertical loads are not very large, then there would be very little cracking (diagonally) or splitting of the vertical joints even when a complex cantilever is subjected to large lateral loads. Such is the case with the examples of complex cantilevers

analyzed in Chapter 6.

Thus in very high buildings although there might be extensive cracking of vertical joints near the base, slip and separation will in all likelihood be more predominant towards the middle or near the top.

4. Reinforcing the horizontal joints produces beneficial results both by increasing the ultimate load and by reducing the lateral deflection for a given load level. The ultimate load for the 5 storey complex cantilever when reinforced by 2 #8 bars increases by approximately 20%. For the 10-storey complex cantilever, the increase is approximately 9%. Not enough cases were investigated to permit predictions for complex cantilevers of other heights or widths. As expected, reinforcing the horizontal joints also reduces the drift for both the 5-storey and the 10-storey complex cantilevers. At a load level measured just before the collapse of the unreinforced complex cantilevers, the drift is reduced by approximately 46% and 21% for 5-storey and 10-storey cantilevers respectively. Again no general prediction can be made as to the amount of improvement for cantilevers of other sizes.

When 3-element joints are used, horizontal joint reinforcement also delays the occurrence of the 1st slip. However, as indicated in Section 6.4 this effect is not noticeable with 2-element joints.

5. The acceptable values of $\frac{\Delta}{H}$ ratio for panel buildings should be based on a limiting lateral deformation which would allow both the horizontal and the vertical joints to remain completely intact. Based on this criteria, the recommended permissible $\frac{\Delta}{H}$ ratio for complex cantilevers documented in Chapter 6 is found to be approximately $\frac{1}{10000}$. However, it must be remembered that this ratio is suggested on the basis of assuming an unbounded surface for slip zone 1. The reasons for this were fully discussed in Chapter 3. Under this condition slip occurs on portions of the joint before any tensile stresses are created. If slip is not taken into account or if horizontal joints are heavily reinforced and complex cantilevers are treated like coupled or independent shear walls, then much larger lateral deformations could be tolerated.

   If the slipping of the first horizontal joint is considered to be the criterion for determining an acceptable $\frac{\Delta}{H}$, then the load factor of safety against failure will be approximately 2.5 for examples documented in Chapter 6.

6. The static design wind pressure which is expected to produce the same peak load effects as the actual turbulent wind, may be estimated on the basis of the information provided in supplement No. 4 of the 1977 edition of the National Building Code of Canada.

Considering the most stringent design criterion (i.e. the reference velocity pressure for the design of structural members for strength for buildings essential for post disaster services based on a probability of being exceeded in any one year of 1 in 100), the design wind pressure on a building in an area exposed to high wind velocities, may be found to be approximately 40 psf. The factor of safety against the occurrence of slip in the 1st joint based on a wind pressure of 40 psf. for 30 panel complex cantilever documented in Chapter 6, would be approximately 1.1. The factors of safety against failure would be between 2.8 and 3.0 depending upon whether the horizontal joints are reinforced or not.

For buildings not essential for post-disaster services the reference velocity pressure is based on a probability of being exceeded in any one year of 1 in 30. The corresponding design pressure may be found to be about 35 psf. The factor of safety against the occurrence of slip in the 1st joint for the above mentioned complex cantilever would be approximately 1.3. The corresponding factors of safety against failure would be 3.2 and 3.5 depending on whether the joints are reinforced or not.

7. It is commonly believed that shear stresses on vertical joints become uniformly distributed after splitting in phase II. The analysis in Chapter 4 indicates that there is certain a tendency towards the

equalization of shear stresses along the vertical joint surface. However, for reasons which were fully explored in Chapter 4, full equalization of shear stresses cannot materialize. The analysis in Chapter 4 indicated that the slips along the joints in phase II do indeed become nearly equal. But this does not necessarily mean that there is an equalization of stresses. Such equalization would have been possible, only if the panels on either side of the joint had been perfectly rigid. The deformationof the panels results in a non-uniform normal stress distribution which in turn leads to a non-uniform shear stress distribution sustained by the shear-friction mechanism.

8. The behaviour of complex cantilevers after a splitting crack is formed along the length of their vertical joints is very much dependent on the type of vertical joint utilized in design. Joint reinforcement is absolutely essential if the joints are to exhibit some degree of ductility. For vertical joints without either shear keys or joint reinforcement, the occurrence of splitting terminates any real interaction between the panels adjacent to the joint. Those portions of a complex cantilever, for which interaction along vertical joints has ceased to exist, would then become independent. By incorporating reinforcement, the interaction along vertical

is sm:

For joints with shear-keys, there would be some degree of interaction along the joints even without reinforcing bars. The angle of the shear-key may theoretically be designed such that slip is prevented. The failure may then occur as a result of shearing off of the shear-keys with very little or no ductility. In order to provide some degree of ductility, the angle of the shear-keys should be designed such that slip can occur. At the same time the joint should be reinforced so that shear forces can be resisted through the shear friction mechanism.

It is strongly recommended that only reinforced vertical joints be used in practice. Reinforcing a vertical joint by looping the panel reinforcement and anchoring it within the body of the joint, or welding it, is usually a simple matter from a practical point of view and is relatively inexpensive. This should not be overlooked especially where high buildings are concerned.

9. Where modelling a shear-key joint for the purpose of analyzing a complex cantilever, a very large number of finite elements will be required if the jagged profile of the interface created by the shear-keys is to be accounted for. The number of elements necessary to achieve this for a sizeable complex cantilever, makes this approach totally impractical. However, the effect of shear-keys which is to impart a much greater shear resistance to the joint, may be

taken into account by defining a term called the apparent coefficient of friction for shear-key joints. Using this coefficient, the derivation of which was explained in Chapter 4, the behaviour of a shear-key joints may be simulated using significantly fewer elements.

10. Experimental evidence[12, 23] indicates that as a joint passes from phase I to phase II, there is a definite and pronounced but not sudden (catastrophic) loss of stiffness for reinforced vertical joints. However, the mechanics of the behaviour had not been fully explained.

The shear-friction theory together with the idea of gradual loss of bond and hence loss of stiffness for reinforcing bars is used in Chapter 4 to explain this phenomenon. The idea that the total shear forces imposed on a vertical joint in phase I, could be sustained in phase II (after the formation of a splitting crack) without a sudden increase in deformations, is attributed to the fact that reinforcing bars during and immediately after splitting exhibit very large stiffnesses. The shear-friction theory is used to explain how pre-splitting loads could be sustained through a transition stage while the shear carrying mechanism undergoes an actual transformation from bond to friction. A one step transition stage is found to be sufficient to represent the behaviour adequately, although several steps will provide a

better representation at the cost of greater computational effort and the use of more computer storage space.

11. In the detailed horizontal joint model developed in Chapter 3, the joint consists of 2 slip surfaces identified as 1 and 2 and a joint filler or joint concrete region. For reasons which were fully explained in Chapter 3, slip surface 1 is assumed to be unbonded whereas slip surface 2 is assumed to be bonded. For this reason, and because of the additional compression forces due to the weight of the floor panels which act on slip surface 2 only, joint slip and separation occurs mostly along slip surface 1. The occurrence of slip and separation along the slip surfaces is also influenced by the width of the floor panels. Where the width of the floor panels is chosen as 1/2 of that of the wall panel, the joint slip and separation is confined mostly to slip surface 1. The tie-beam, however, shows extensive cracking where the longitudinal joint between the successive floor panels intersects the horizontal joint. The detailed analysis of Chapter 3, for an isolated horizontal joint indicates that where floor panels are chosen as wide as the wall panels, there could be extensive cracking and separation along slip surface 2.

In the light of the information provided by this

and their influence on the overall behaviour of complex cantilevers, it is felt that the considerable effort devoted to the development of a comprehensive horizontal joint model is justified. The study further points to some large errors which could result if simplifying assumptions are used without proper joint stiffness modifications.

12. In order to account for the shear forces resisted along slip surface 1, a friction type finite element was developed in Chapter 3, which allows the shear forces to be resisted along the slip surface in proportion to the available normal compressive forces, without impeding the slip. This type of element is not only extremely useful in the analysis of panel buildings, but may be applied in other situations where previously, the cracking of a finite element usually indicated the end of the useful life of that element. The main difficulty here, would be the determination of the orientation of the new element which is decided on the basis of one of the usual failure theorys. However, for practical reasons it must be located between the existing nodal points of the finite element mesh. Another problem would be the necessity of allowing for cracks to open or to slip which would require the superposition of a second set of nodal points on the original mesh, so that the nodes occupying the same physical location in space before cracking can move relative

to one another after cracking. Such superposition of nodes, would immediately increase the total number of computer storage spaces needed to carry out the analysis, and could produce serious practical limitations.

13. The imposed gravity loads maintain the integrity of the horizontal joints. Due to the bending action of the lateral loads, vertical compressive forces acting on the horizontal joints can be greatly reduced or eliminated. Therefore it is recommended that vertical joints be reinforced.

In general, the joint ductility and strength is considerably improved even for very small steel ratios. However, the improvement is much greater for joints with low gravity loads such as those existing near the top of a complex cantilever. The improvement becomes less noticeable as gravity loads are increased towards the base of the building. For very high gravity loads, there is no improved performance for the reinforced joints, since the mode of failure is no longer slip or separation but rather a compression type failure due to the combined effects of bending and superimposed vertical (gravity) loading.

7.2 Recommendations for Future Research

The complex cantilever used for the purpose of the present study has practical limitations arising basically from architectural needs for openings in the internal complex cantilevers. It is thus logical that

the present study should be extended to include complex cantilevers with openings and those consisting of panels of various sizes. However, joint behaviour and the associated characteristics from this study may be used directly in the new system.

As in the case of coupled shear walls, the contribution of floor slabs to the degree of interaction between various complex cantilever piers is another important consideration. The problem is complicated even further by the fact that the ability of the floor panels to provide the needed interaction between successive complex cantilevers is not only a function of the effective width of the floor panels. It is also a function of the arrangement of the floor panels and the slip, separation and cracking of the joints. A suggested method of approaching this problem would be to conduct a parametric study of a small structure (2 or 3 piers by 2 storeys) similar to that used in Chapters 3 and 4 for the study of isolated joints.

In the study presented in the preceding chapters the effects of gradually increasing lateral loads acting on complex cantilevers were considered. An important question which arises immediately is what would happen if, due to severe wind gusts or seismic forces, the structure was pushed far into the non-linear range causing the joints to slip, separate and crack, and how would these changes effect the subsequent joint performance? Very little experimental work has been done on the effects of

cyclic loading on joint performance. Cyclic loading, no doubt, would effect the value of the coefficient of friction which is a very important factor in determining the joint resistance to shear forces. The breakdown of bond around the joint reinforcing bars is another factor which influences the subsequent joint behaviour. Thus it is important that the effect of cyclic loading on joint behaviour, specifically its influence on the coefficient of friction and bond breakdown around the bars, be fully investigated and understood.

Even with monotonic type loading, there is the possibility of the breakdown of the joint surface asperity. The separated particles trapped between the two surfaces might tend to act somewhat like ballbearings contributing to reductions in the coefficient of friction between the two surfaces. This is another aspect of the problem which has not been fully investigated.

Another problem which is worthy of research, is the effect of diaphragm action of the floor panels. Unequal lateral deformations of parallel complex cantilevers, which may be the result of either lack of physical symmetry or unequal loading of various cantilevers, can cause an in-plane rotation of the floor slab leading to cracking and disintegration of the horizontal joints. The existence of mechanical continuity from floor panel to floor panel and the construction of peripheral tie-beams may reduce or eliminate this problem. However, no estimate of the actual forces and hence the

required amount of reinforcement may be obtained without a 3-dimensional analysis.

The influence of stiffening components such as corridor walls or cladding on the longitudinal stiffness of the building is again a problem which can be investigated only if a 3-dimensional analysis of panel buildings is undertaken.

In closing, it must be emphasized that there are also a number of related problems such as bond-slip behaviour of bars of various sizes, dowel bar action, bonding between preformed concrete and fresh concrete, etc. which need a great deal more research. The construction of panel buildings is still in a state of infancy and the investigation of the problems associated with it is far from being complete. The study presented in the preceding pages is only a starting point towards a more comprehensive and in-depth study of panel buildings.

APPENDIX A

RELATED STUDIES

A.1 A Summary of Related Experimental Results and Empirical Formulae

a) Cholewicki[12]

i) Empirical Formulae

The load bearing capacity of the joint in Phase IIa may be given by the following empirical relationship (Cholewicki's notation):

$$T_n = R_t n F_1 + \mu F_z \sigma_z \qquad (A.1a)$$

or alternatively by

$$T_n = nF_1(R_t + \delta\mu\sigma_z) \qquad (A.1b)$$

where T_n = load bearing capacity,

R_t = shear strength of concrete,

F_1 = area of one key,

F_z = area of steel reinforcement,

σ_z = tensile stress in transverse steel $<$ yield stress, and

$\delta = F_z/nF_1$

Polish Standards PN-B/03260 defines R_t as follows:

$$R_t = 2R_r \text{ and } R_r = 0.5\sqrt[3]{R_b^2}$$

where R_r = tensile strength of concrete, and

R_b = compressive strength of concrete

The effect of tensile stresses in transverse steel is to create compressive stresses at right angles to the direction of the shear plane. These stresses according to Mohr's hypothesis cause an increase in shear capacity of concrete. In addition since shear stresses are not uniformly distributed along the shear plane, two correction coefficients are introduced in equation (A.1b). The values of these coefficients are determined empirically. Equation (A.1b) can now be written in the following form:

$$T_n = nF_1(m_b R_t + m_z \delta \mu \sigma) \qquad (A.1c)$$

The load bearing capacity for Phase IIb, where failure is caused by shearing off of the keys is approximated by the following relationship:

$$T_n = nF_1(cC + \mu \delta Q_r) \qquad (A.2)$$

where Q_r = yield stress of transverse steel, and

c = concrete cohesion.

The produce cC is introduced to account for the increase in shear capacity of concrete when compressive forces are acting on the shear plane.

The values of correction coefficients m_b and m_z are determined by Hansen[12] and Pommeret[12] and are indicated in the following table:

	m_b	m_z
Hansen	0.96	1.24
Pommeret	0.93	1.74

Table A.1 Correction Coefficients for Calculation of Shear Capacity of Shear-Key Joints

The relationship (A.1a) may now be written as:

$$T_n = 0.95\ R_t n F_1 + \xi\ \sigma_z F_z \qquad \text{(A.1d)}$$

where ξ is a coefficient accounting for the influence of the joint's reinforcement on its strength.

ii) Experimental Results

Two basic test schemes were adopted by Cholewicki in his attempt to investigate the behaviour of vertical joints. These are shown in Fig. A.1.

Tests utilizing scheme I were carried out to investigate 6 different types of joint geometry. Except for type 6, the joints were all unreinforced. These are shown in Fig. A.2. Figure A,3 shows the graphs of mean shear stress versus slip for each type.

Cholewicki's second scheme of testing was conducted for two basic types of joints. Although, both types were of the shear-key kind, one employed four shear-keys per joint, while the other contained only one key. The load bearing capacity for all cases with 4 keys was considerably higher than those containing only one key although the same in-fill concrete was used for both types.

In the sake of simplicity and since no reference to these tests is made in this thesis, their full presentation is omitted.

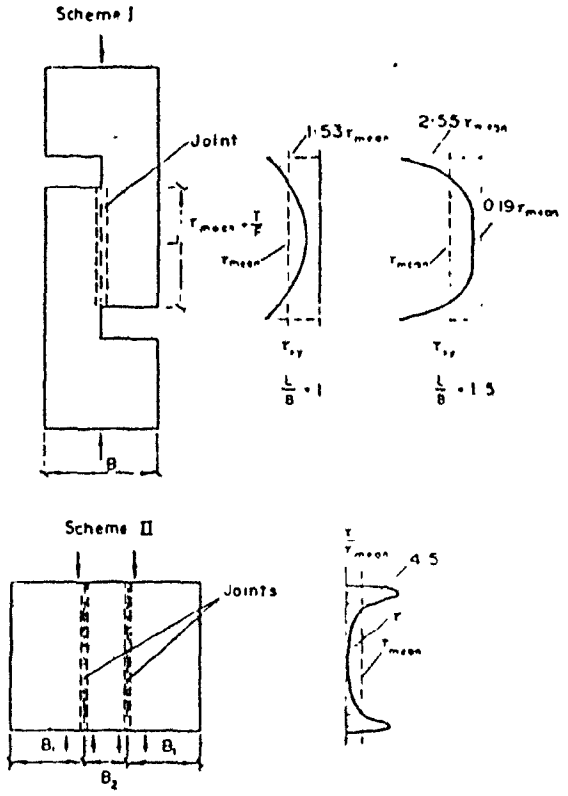

$$\tau_{mean} = \frac{T}{F} = \text{(ave. shear stress)}$$

Fig. A.1 Test Schemes Employed by Cholewicki[12]

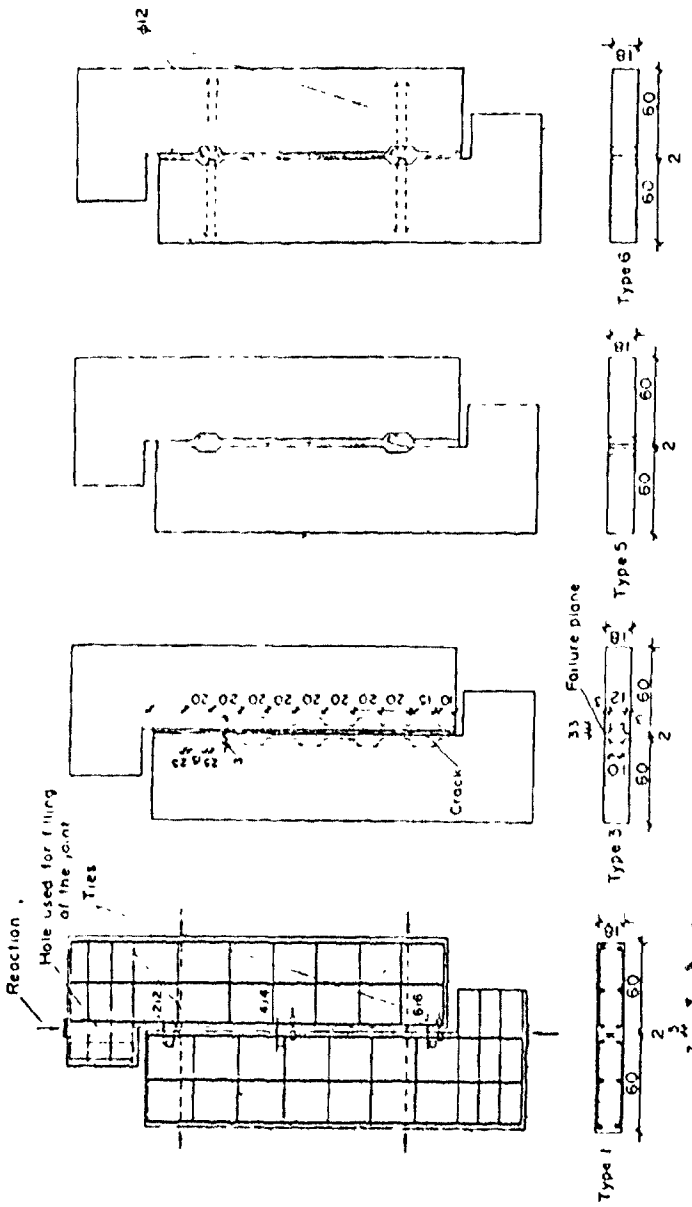

Fig. A.2 Types of Joints Tested in Conjunction with Cholewicki's Scheme I[12]

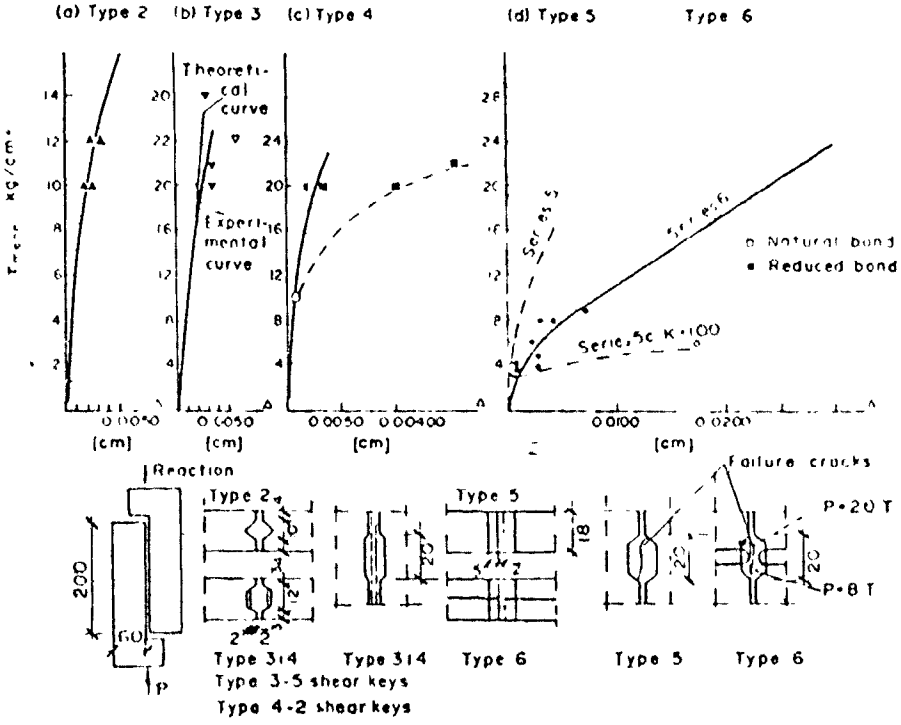

Fig. A.3 Cholewicki's Mean Shear Stress (τ_{mean}) Versus Joint Deformation (Δ) Curves for Vertical Joints, Scheme I[12]

b) Hansen[12]

Joints of the type shown in Fig. A.1, scheme II, were used by Hansen in his experimental investigations. The joint configuration itself was of the same type as those commonly used by the Larsen & Nielsen Large Panel Building System. Three series of tests were carried out. In the first series bond existed between the panel edges and the in-fill concrete in the joints. In the remaining 2 series the bond was reduced or destroyed before the panels were loaded. The joints of the 1st series failed with the appearance of cracks along the contact surfaces (beginning of Phase II) and exhibited relatively small deformations. The joints of the other 2 series failed in Phase II and their deformations were many times greater than those of the first series. The failure in these joints followed immediately after the keys were sheared off or disintegrated.

The load bearing capacity of the joints with artifically destroyed bond was higher than those with bond intact, due to a more uniform distribution of shear stresses along the length of the joints. Figure A.4 shows the graphs of mean shear stress versus deformation as reported by Hansen.

c) Pume[12]

Test scheme II of Fig. A.1 was also used by Pume in his experimental investigations. All the joints used with the exception of one were of the shear-key type,

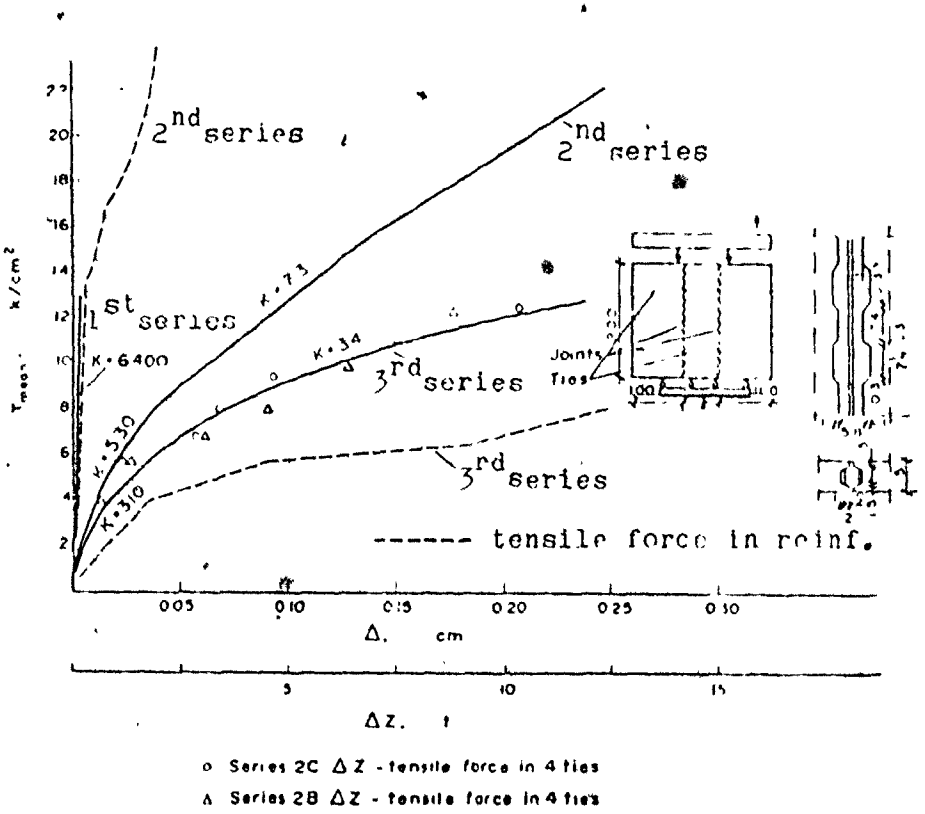

Fig. A.4 Hansen's Mean Shear Stress (τ_{mean}) Versus Joint Deformation (Δ) Curves for Vertical Joints[12]

and all were unreinforced. As expected, failure in all cases followed shortly after the occurance of the splitting crack between the edge of the panel and the in-fill concrete. The range over which the loads were resisted in Phase II, even for dey type joints was very small.

Pume proposed the following empirical relationship for calculation of the ultimate shear stresses:

$$\tau_{alt} = \kappa_3(0.4R_r + 0.8\kappa_4\sigma) \qquad (A.3)$$

where R_r = tensile strength of concrete,

σ = stresses acting at right angles to the surface of the joint,

κ_3 = a coefficient expressing the effect of joint type; with a value of 1.1 for key type joint and 1.0 for joints without keys, and

κ_4 = a coefficient expressing the influence of the supporting system for the whole set up; its value varying between 1.0 and 1.27.

Figure A.5 shows Pume's experimental results, his test set up, and a theoretical check made by Cholewicki on the basis of the following empirical relation:

$$R_t = 0.75\sqrt{R_{20}R_r} \qquad (A.4)$$

where R_{20} = compressive strength of concrete as determined by tests on cubes $20_{cm}x20_{cm}x20_{cm}$, and

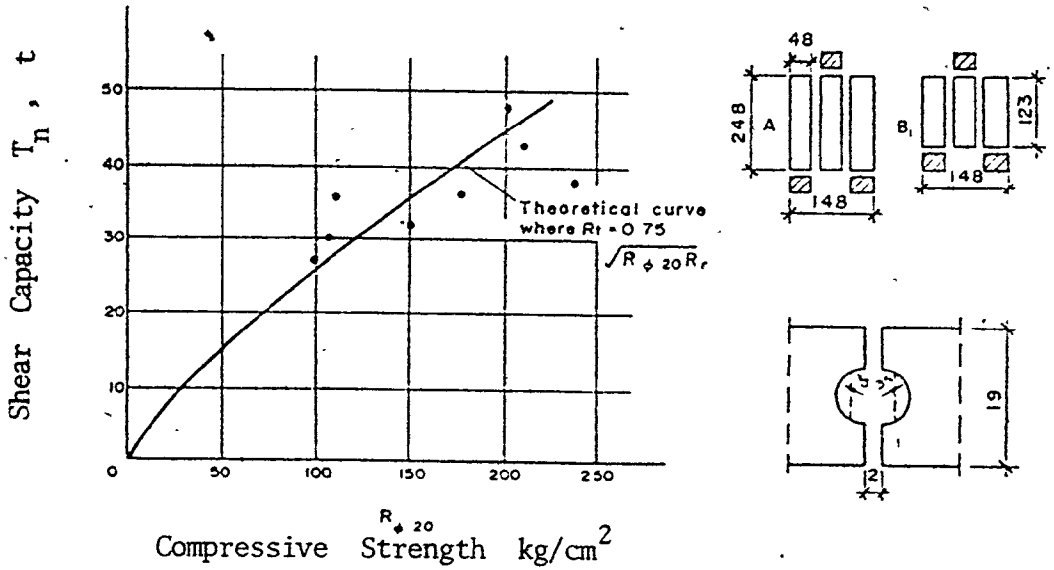

Fig. A.5 Pume's Results and Test Set Up[12]

R_t = shear strength under direct shear.

d) Pommeret[12]

Pommeret tested a large number of different types of vertical joints all of which were reinforced. Transverse reinforcement was distributed along the joint and was well anchored. Through these tests, Pommeret hoped to produce experimental confirmation of a theory proposed by Robinson[9, 12] for calculation of multicantilevered shear walls with vertical joints capable of elastic-plastic behaviour.

Pommeret's experimental results, test set up, and joint details are shown in Fig. A-6. These tests are very valuable in that they cover a wide range of variations in the basic structural parameters. These tests also confirmed the interrelation between these basic parameters and the load bearing capacity of the joint. Pommeret expressed this by the following empirical relationships for the strength of the joint in the elastic and the plastic ranges:

$$T_{nel} = \sqrt{R_b}(2nF_1 + 0.08F_zQ_r) \qquad (A.5a)$$

or

$$T_{nel} = \sqrt{R_b}[8.2\sqrt{(F_zQ_r)} + 0.42(1+F_z)/nF_1] \qquad (A.5b)$$

and

$$T_{npl} = 0.1F_zQ_r\sqrt{R_b} \qquad (A.6)$$

where R_b = compressive strength of concrete,

n = number of keys,

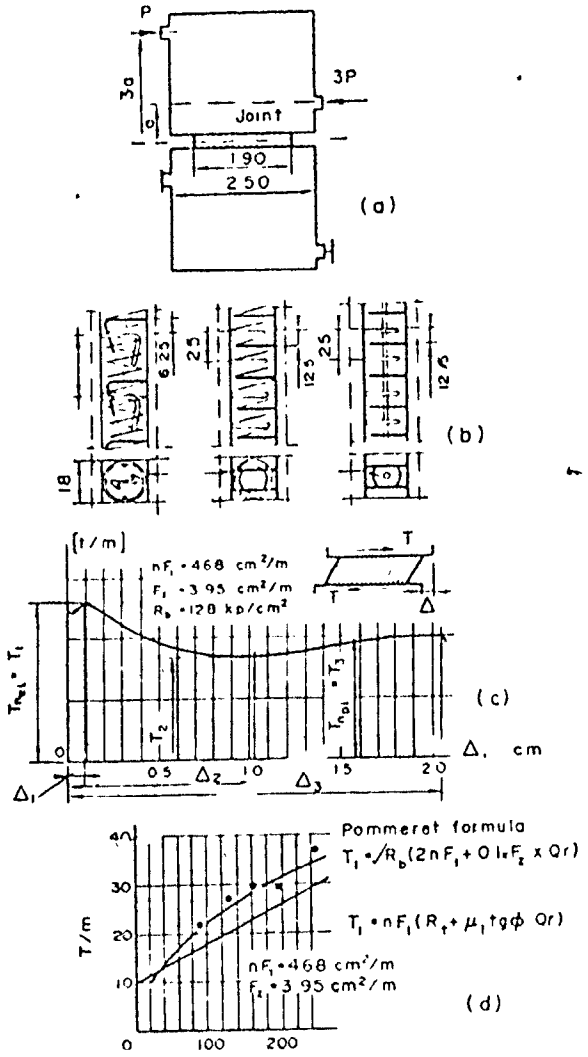

(a) testing scheme (b) joint details

(c) typical joint deformation diagram where T_{nel} is the shear capacity in elastic range, T_{npl} is the shear capacity in plastic range and Δ is the joint deformation

(d) joint shear capacity versus joint's concrete strength relationship

Fig. A.6 Pommeret's Test Set Up Joint Details and Deformation Curves[12]

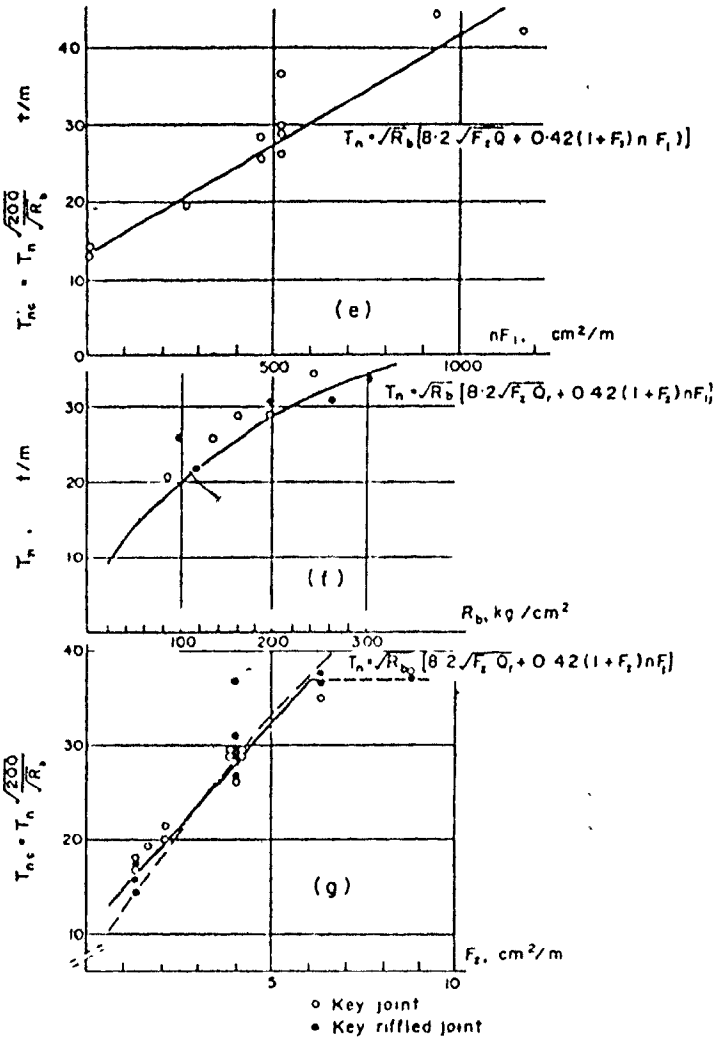

(e), (f) and (g) shear capacity of shear key joints versus joint parameters where T_n is the shear capacity of the joint, R_b is the concrete compressive strength, F_z is the reinforcement area, Q_r is the reinforcement yield stress, F_1 is area of one shear-dey and n is the number of shear-keys.

Fig. A.6(cont.) Pommeret's Test Set Up Joint Details and Deformation Curves (12)

F_1 = area of one key,

F_z = transverse steel area, and

Q_r = steel yield stress.

e) Hansen-Olesen[12]

The cracking pattern observed by Halasz[23] was confirmed by the tests carried out by Hansen and Olesen. Diagonal cracks, however, appeared gradually, beginning at 0.5 T_n, where T_n was the shear capacity of the joint. The cracked portions of the joint became more extensive and cracks propagated towards the middle of the joint as the shear forces were increased. Failure followed immediately after the shear-keys were sheared off.

The Hansen-Olesen test set up, and their joint deformation curves are shown in Fig. A.7.

f) Armer and Kumar[2]

The behaviour of large panel assemblies under the action of bending and shear forces was investigated by Armer and Kumar. The test assemblies were of 3 different types. These are shown schematically in Fig. A.8. Figures A.8(a), (b) and (c) represent panels and assemblies of panels cantilevering from their neighbours after the removal of their primary support, in this case the panels above and/or beneath them. This situation can exist when in a panelized shear wall the horizontal joints above and/or below a given panel open up due to the action of lateral loads on the assembly. The cantilevered

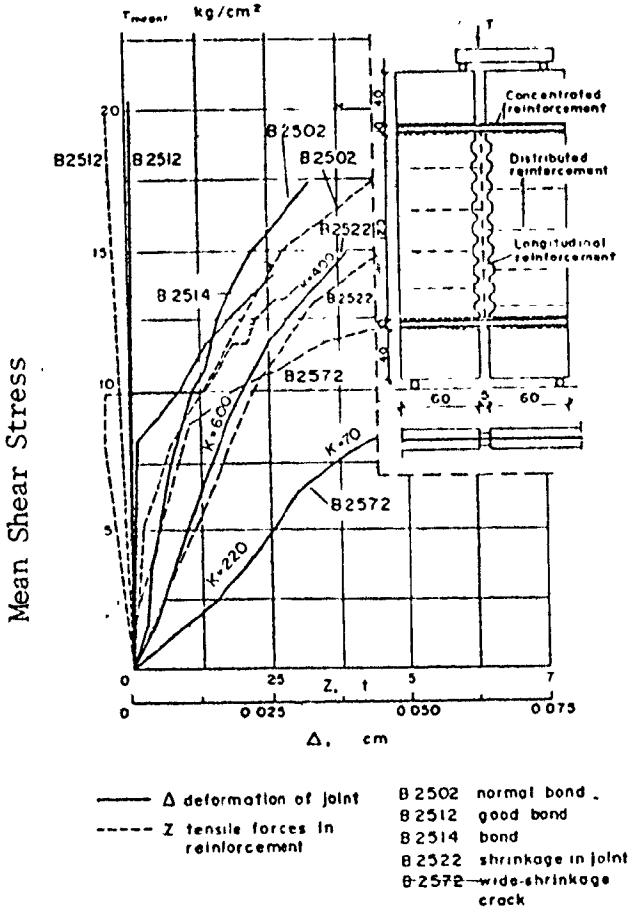

Fig. A.7 Mean Shear Stress (τ_{mean}) Versus Deformation (Δ) Curves by Hansen and Olesen[12]

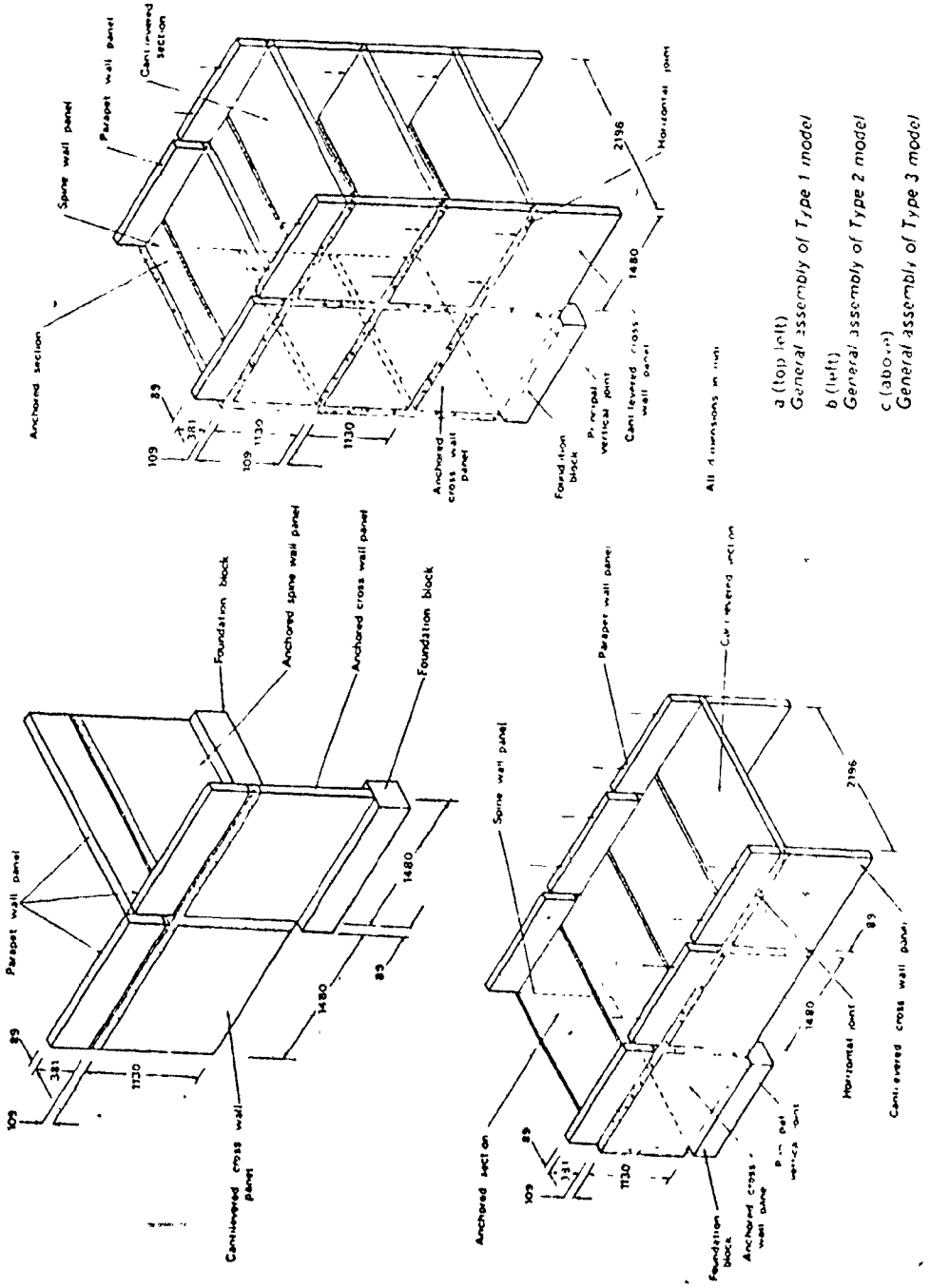

Fig. A.8 Armer and Kumar's Cantilever Test Assemblies(2)

panels were joined to their neighbours either by placing steel bars in the horizontal joints, or by incorporating loops and a dowel bar in the vertical connections. Twenty-four models of type 1 were tested with different amounts of steel in vertical and horizontal (peripheral) joints. The graphs of failure load versus the number of loops for various cases are illustrated in Fig. A.9.

Three models of the type 2 assembly were tested. The first model had an unreinforced principal vertical joint and a staggered floor slab. The second model had 3-6 mm loop in the principal vertical joint and staggered floor joints. The third model had unreinforced vertical joints and aligned floor and wall joints. All models had peripheral tie steel in the horizontal joints.

Only one model of the type 3 assembly was tested. Vertical joints were unreinforced and steel ties were provided only at the level of the floor slabs.

It is very important to note that the primary mode of failure in all the single panel tests (type 1) was simple bending with the cantilevered panel rotating about the lower corner at the support. In some tests, a secondary shear failure occurred after considerable rotation, but this did not affect the ultimate load.

The primary mode of failure in all test models of type 2 was also bending. However, there was no indication of a secondary shear failure.

The mode of failure in type 3 assembly was pure shear in the vertical joint and the load-deformation

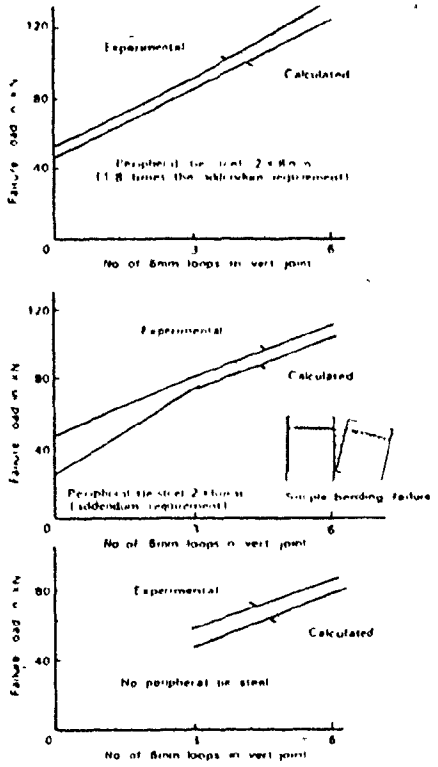

Fig. A.9 Comparison of Calculated and Experimental Failure Loads for Single Panel Cantilevers Armer-Kumar[2]

curve had the characteristic brittle form. Careful observation of the joints during the test indicated no bending cracks.

The author's finite element simulation of vertical joints for the combined action of bending and shear (Chapter 4), is in agreement with Armer-Kumar test results for single panel cantilevers. The bending action becomes a major consideration when horizontal joints are unreinforced and/or shrinkage has partially or completely destroyed the bond between the wall panel and the joint in-fill concrete.

A.2 A Summary of Progressive Collapse Studies

Since the partial collapse of the Ronan Point flats in May, 1968, considerable attention has been paid to the design of panel buildings and reducing the risk of progressive collapse. This form of failure was defined by Armer and Kumar[2] as "collapse triggered off by local damage due to accidental loading, e.g. an explosion or impact, which then propagates throughout the structure giving rise to severe damage which is not in proportion with the initial cause".

Among documents published for the purpose of providing guidance for designers of panel buildings, the CEB Recommendations[29] are worthy of special attention. Most building codes (Addendum No. 1 (1970) to BS Code of Practice 116[1]) follow the principles incorporated in the CEB Recommendations.

Short and Miles[56] in a comprehensive review of a member of documents relating to progressive collapse studies summarized the possible design techniques to resist progressive collapse as follows:

1. The Alternative Path Method which requires the transmission of loads to the foundation along an "Alternative Path" for each combination of unserviceable panels. The difficulty lies in specifying the likely combination of panels which may become simultaneously unserviceable.
2. The Over-all Strength Method in which the structure is shown to be able to withstand a given internal pressure. In this case it is quite difficult to specify the pressure which depends on both the nature of the explosion and the degree of venting provided. The CP116 addendum specifically permits a design method based on venting. Venting means provision of strengthened strips of wall and floor so that in the event of an explosion these strips remain effective even after the removal of the weaker sections. As long as the strips are capable of supporting the structure on their own, the requirements for prevention of progressive collapse are satisfied.
3. The Empirical Method in which calculations are omitted in favour of providing a specified amount of tying steel (determined on the basis of tests, experience and good judgement) which is assumed

to ensure adequate strength and ductility.

In a report on tests conducted on half scale assemblies of cantilevered panels Armer and Kumar[2] summarized the aims of the various design methods by simply stating that "the building should have a good plan form, and adequate continuity and tying steel should be provided between various elements of the structure".

The tests mentioned in the previous paragraph were designed with two objectives. Firstly, to investigate the effect of the new recommendations (Addendum No. 1 to BS Code of Practice 116) on the behaviour of assemblies of precast panels, and secondly to investigate the effect of group size on the number of panels in an assembly on the performance of the joints. A brief summary of these tests are presented in A.1(f) and will not be elaborated upon further here.

The theoretical sequence of failures in precast concrete wall panels resulting from lateral load action was investigated by Stafford Smith and Rahman[60]. Actually, this did not constitute a progressive collapse investigation, since no panels were suddenly removed. The stresses in the wall due to vertical and horizontal loads were analysed by the finite element method and compared with the joint strengths to determine the most imminent mode of failure. Five different modes of failure were considered. These were tensile and shear failures in each of the horizontal and the vertical joints and a compressive failure which was assumed to be similar for both types of

joints. The joint strengths were assumed to be accumulated as equivalent strengths at the corners of the panels. The essence of the method was to compare the corner stresses with the joint strengths for the whole assembly and to determine the minimum wind load which would cause a certain node to fail. The process was repeated for successive failures until the wall collapsed. The validity of the assumption that joint strengths could be concentrated at the corners of the panels was not investigated. This is one of the problems which is investigated in Chapter 3 of this thesis.

A.3 Summary of Stability Investigations

The static stability of panel type buildings was investigated by Stafford Smith and Lau[59]. Conventional precast concrete panel buildings consist of orthogonal assemblies of continuous vertical load-bearing walls and horizontal floor panels. This type of structure is analogous to the conventional beam-column system and can be shown to be stable for loading in any direction. Like frame structures, stable arrangements other than vertically continuous walls can be designed. The authors proposed a method of assessing the static stability of hinged-connected panel buildings based on the formulation of a 'restraint matrix', comprised of overlapping 6 x 2 submatrices, each of which represented the stability of an individual panel. The systematic approach made the method suitable for computer use and thus allowed

the stability of complicated structures to be assessed quickly and efficiently.

The above is the only stability study which has come to the attention of the author to date. The problem of configurational stability of panel buildings, or for that matter, progressive collapse studies, are outside the scope of this thesis which deals strictly with the problem of lateral loads in panel buildings and the development of a realistic model for the purpose of estimating the ultimate strength of complex cantilevers. Appendix A was therefore designed only as a guide to the related topics in the field of Large-panel buildings and in order to provide the interested reader with a summary of the available information in this general area.

APPENDIX B

METHOD OF CONDENSATION OF INTERNAL NODES

When an assembly of elastic elements is subjected to a set of gradually applied loads, the strain energy U in the assembly is given (in matrix notation) by

$$U = \frac{1}{2} \{u\}^T \{R\} = \frac{1}{2} \{R\}^T \{u\} \qquad (B.1)$$

where $\{R\}$ = external load vector , and

$\{u\}$ = assembly nodal displacement vector.

Substituting $[K][u]$ for $\{R\}$ in equation (B.1) yields

$$U = \frac{1}{2} \{u\}^T [K] \{u\} \qquad (B.2)$$

where $[K]$ is the stiffness matrix of the whole assembly.

The strain energy of the assembly can also be represented as the sum of strain energies of the individual components (elements) of the assembly,

$$U = \sum_{m=1}^{n} U_m = \frac{1}{2} \sum_{m=1}^{n} \{q\}_m^T [\bar{K}]_m \{q\}_m = \frac{1}{2} \{q\}^T [\bar{K}] \{q\} \qquad (B.3)$$

in which

$$\left\{q\right\} = \begin{Bmatrix} q_1 \\ \hline q_2 \\ \hline \vdots \\ \hline q_n \end{Bmatrix} \quad \text{and} \quad \left[\bar{K}\right] = \begin{bmatrix} \left[\bar{K}\right]_1 & & & \\ & \left[\bar{K}\right]_2 & & \\ & & \ddots & \\ & & & \left[\bar{K}\right]_n \end{bmatrix}$$

Subvectors $\{q_1\}$, $\{q_2\}$, ..., $\{q_n\}$ and submatrices $[\bar{K}]_1$, $[\bar{K}]_2$, ..., $[\bar{K}]_n$ are respectively the nodal displacement vectors and stiffness matrices of the component elements. Moreover, vectors $\{u\}$ and $\{\delta\}$ may be related through the matrix relationship,

$$\{q\} = [\beta]\{u\} \tag{B.4a}$$

The transposed relationship is

$$\{q\}^T = \{u\}^T [\beta]^T \tag{B.4b}$$

Matrix $[\beta]$ is entirely dependent on the arrangement of nodes being condensed. For the combination of elements shown on Fig. B.1(a), the formulation of matrix $[\beta]$ is derived as follows. To generate any column j of $[\beta]$ a unit displacement is applied at the system coordinate j only and corresponding compatible component displacements q_i are determined. These displacements form column j of $[\beta]$. Thus, equation (B.4a) for the system shown in Fig. B.1(a) has the form indicated in Fig. B.2.

Substituting for $\{q\}$ in equation (B.3) and equating to equation (B.2)

$$\{u\}^T[K]\{u\} = \{u\}^T[\beta]^T[\bar{K}][\beta]\{u\}$$

thus

$$[K] = [\beta]^T[\bar{K}][\beta] \tag{B.5}$$

If the symbol $\{u\}^o$ is used to identify the displacements corresponding to the degrees of freedom associated with zero applied forces, the displacements corresponding to those degrees of freedom for which loads $\{R\}^*$ are not zero, may be denoted by $\{u\}^*$.

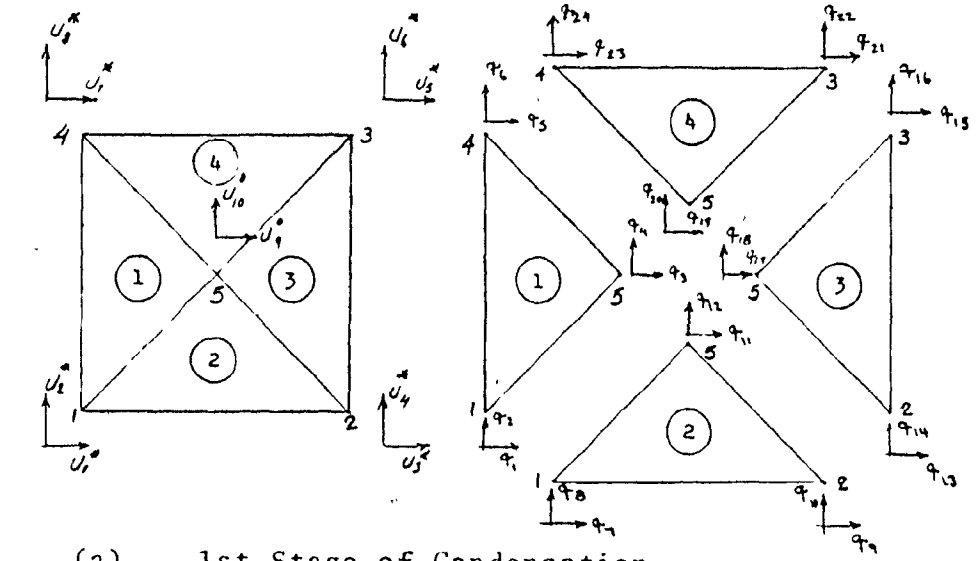

(a) 1st Stage of Condensation

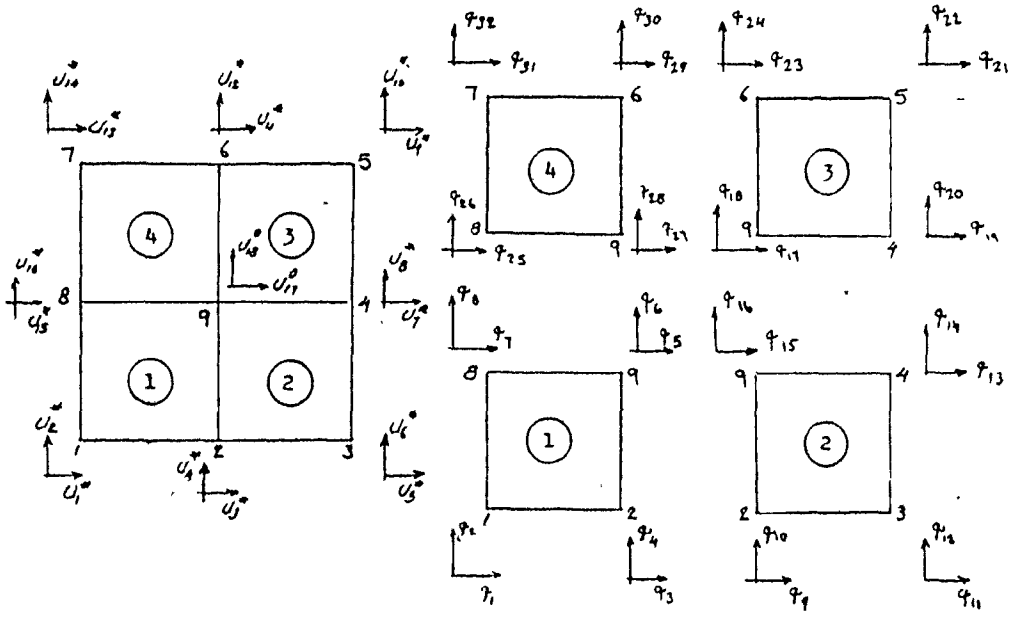

(b) 2nd Stage of Condensation

Fig. B.1 Condensation of Internal Nodes

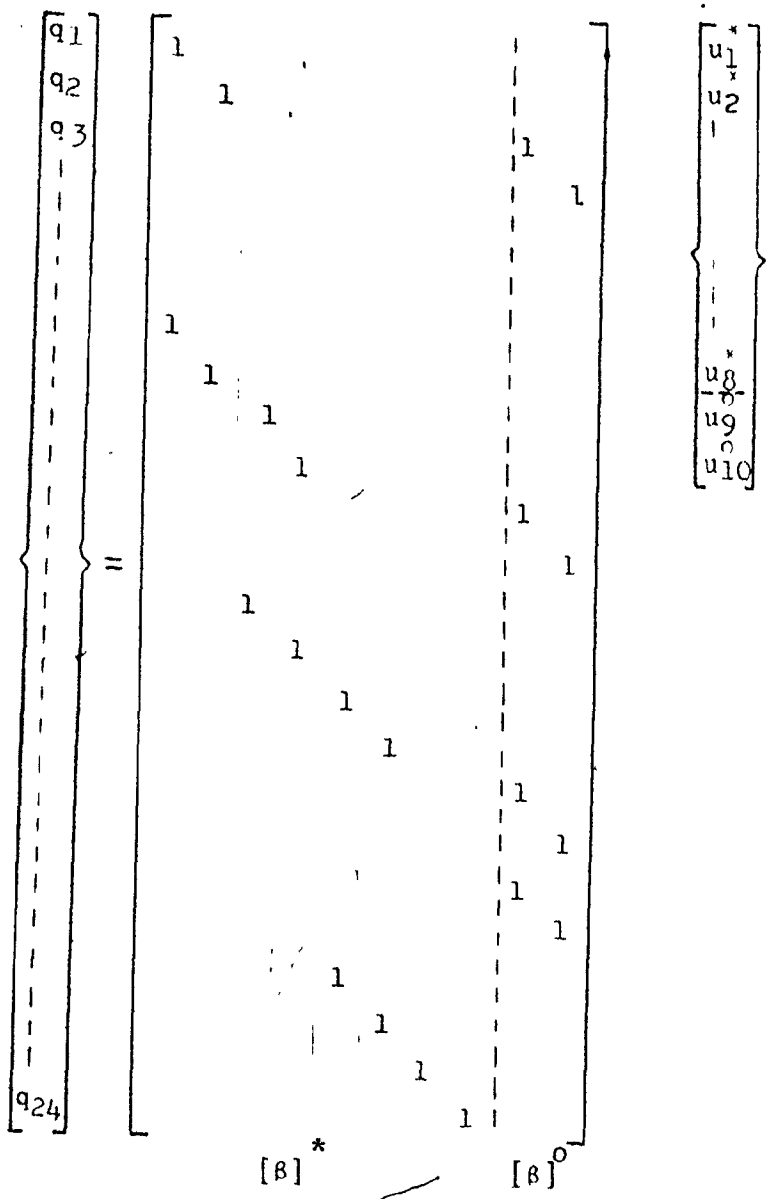

Fig. B.2 Equation (B.4a) in Expanded Form For the System Shown in Fig. B.1(a)†

Equation (B.4 and (B.5) can therefore be partitioned as follows:

$$\{q\} = [[\beta]^* ; [\beta]^0] \left\{\begin{matrix}\{u\}^* \\ \hline \{u\}^0\end{matrix}\right\} = [\beta]^*\{u\}^* + [\beta]^0\{u\}^0 \qquad (B.4c)$$

---

†Note that unspecified elements of matrix [β] shown above are zero.

and

$$[K] = [\beta]^T[\bar{K}][\beta] = \begin{matrix} * \\ o \end{matrix}\left[\begin{array}{cc} \overset{*}{[K]}_{11} & \overset{o}{[K]}_{12} \\ [K]_{21} & [K]_{22} \end{array}\right] = \left[\begin{array}{c} [\beta]^{*T} \\ \hline [\beta]^{oT} \end{array}\right][\bar{K}]\left[[\beta]^{*} \;\; [\beta]^{o}\right] \quad \text{(B.5a)}$$

Expanding equation (B.5a)

$$\begin{aligned} [K]_{11} &= [\beta]^{*T}[\bar{K}][\beta]^{*} \\ [K]_{12} &= [\beta]^{*T}[\bar{K}][\beta]^{o} \\ [K]_{21} &= [\beta]^{oT}[\bar{K}][\beta]^{*} \\ [K]_{22} &= [\beta]^{oT}[\bar{K}][\beta]^{o} \end{aligned} \quad \text{(B.6)}$$

The stiffness matrix of the condensed element can now be found.

The equilibrium equation for the assembly of elements shown on the left portion of Fig. B.1(a) is partitioned as

$$\begin{matrix} * \\ o \end{matrix}\left[\begin{array}{cc} \overset{*}{[K]}_{11} & \overset{o}{[K]}_{12} \\ [K]_{21} & [K]_{22} \end{array}\right]\left\{\begin{array}{c} \{u\}^{*} \\ \hline \{u\}^{o} \end{array}\right\} = \left\{\begin{array}{c} \{R\}^{*} \\ \hline \{R\}^{o} \end{array}\right\} \quad \text{(B.7)}$$

Since $\{R\}^o = 0$ (no loads are applied to the internal nodes)

$$\begin{aligned} \{R\}^{*} &= [K]_{11}\{u\}^{*} + [K]_{12}\{u\}^{o} \\ \{o\} &= [K]_{21}\{u\}^{*} + [K]_{22}\{u\}^{o} \end{aligned} \quad \text{(B.8)}$$

The second equation is solved for $\{u\}^o$

where $$\{u\}^{o} = -[K]_{22}^{-1}[K]_{21}\{u\}^{*} \quad \text{(B.9)}$$

$\{u\}^o$ is then substituted in the first of equations (B.8)

$$\{R\}^{*} = [K]_{11}\{u\}^{*} - [K]_{12}[K]_{22}^{-1}[K]_{21}\{u\}^{*} = [K]^{*}\{u\}^{*} \quad \text{(B.10)}$$

where $[K]^*$ is the stiffness matrix of the condensed element, and is given by

$$[K]^* = [K]_{11} - [K]_{12}\,[K]_{22}^{-1}\,[K]_{21} \qquad (B.11)$$

Once $\{u\}^*$ has been determined, using equations (B.9) and (B.4c), vector $\{q\}$ and the internal force vector $\{p\}$ can be determined. That is

$$\{q\} = ([\beta]^* - [\beta]^o[K]_{22}^{-1}[K]_{21})\,\{u\}^* \qquad (B.12)$$

and

$$\{p\} = [\bar{K}]([\beta]^* - [\beta]^o[K]_{22}^{-1}[K]_{21})\,\{u\}^* \qquad (B.13)$$

The internal node of the assembly of elements shown on the left portion of Fig. B.1(b) may also be eliminated using the procedure outlined above. This, if required, constitutes the second stage in the process of condensation of nodes. Each of the elements shown in Fig. B.1(b) may itself be composed of 4 triangular elements of the type shown in Fig. B.1(a). However, matrix $[\beta]$ is no longer the same and must be redefined.

Equation (B.4a) written in the expanded form for the arrangement of elements shown in Fig. B.1(b) is given on the following page.

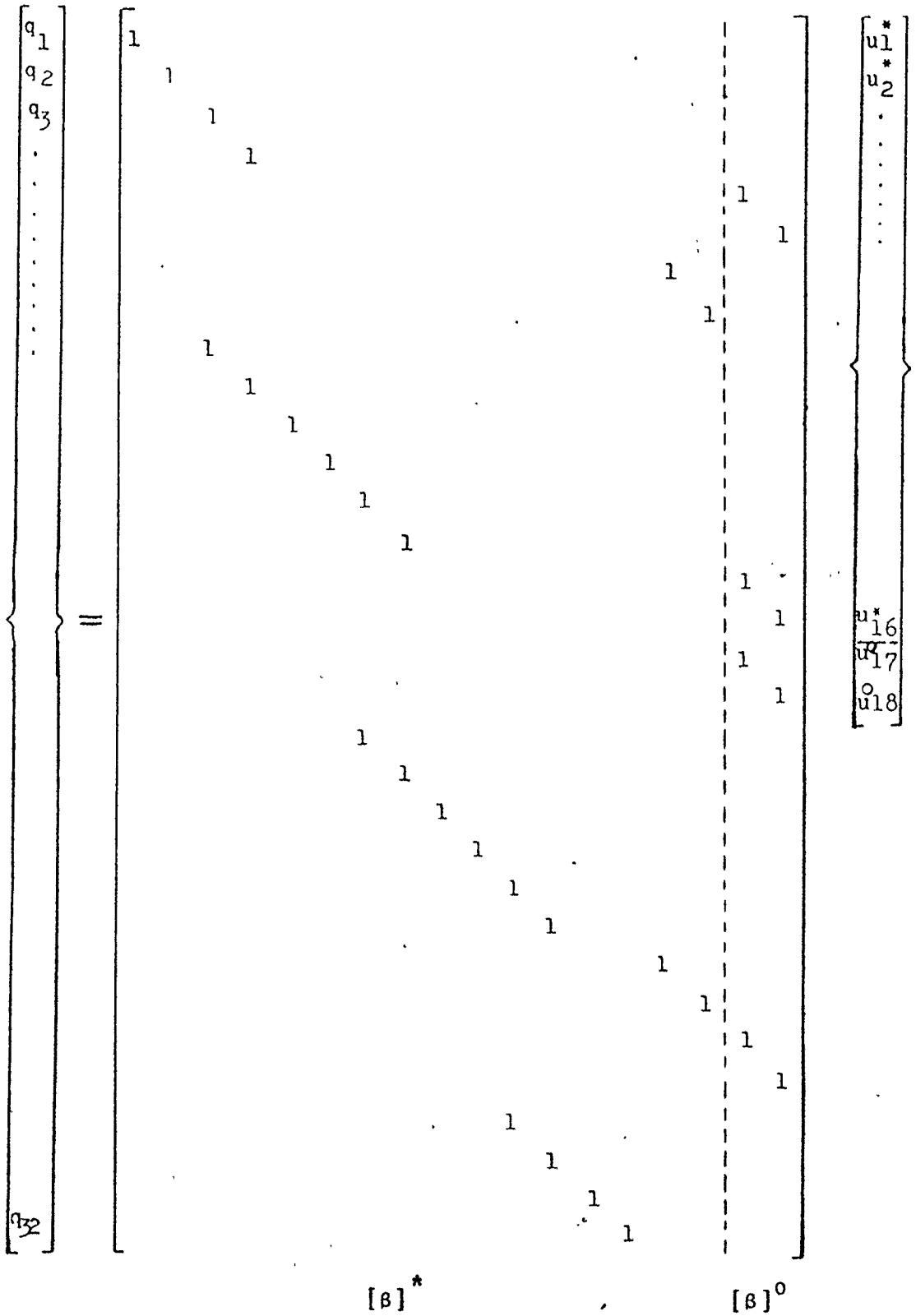

Note that the unspecified elements of $[\beta]$ are zero

APPENDIX C

COMPUTER PROGRAM

C.1 Computing Facilities

Location: Senior Sciences Building, McMaster University, Hamilton, Ontario.

Computer: CDC-6400 with a core capacity of 124K (Oct.).

Coding: FORTRAN IV

C.2 Subroutines

(1) Subroutine ACCUM

Purpose: To accumulate vertical joint concrete element stresses as joint passes from phase I to Transition stage to phase II.

Call & Argument List: CALL ACCUM (ST6C, NET6, INN, AUX, INI, STRSS6, NVJ, NCB, IJ, NEWL)

ST6C is a 2-dim. real array storing concrete element stresses (cumulative).

NET6 is an integer variable denoting the no. of vertical joint elements (type 6).

INN is a 1-dim. integer array whose elements may assume values of zero or one only. They are all zero to start with. Subsequent values are determined automatically.

AUX is a 2-dim. auxillary real array.

INI is a 1-dim. integer array whose elements may assume

values of zero or one only. They are all zero to start with. Subsequent values are determined automatically.

STRSS6 is a 2-dim. real array denoting concrete element stresses.

NVJ is an integer variable indicating the no. of vertical joints.

NCB is a 2-dim. integer array. The 1st element in each row indicates the vertical joint number. Other elements indicate the joint elem. numbers associated with that particular vert. joint.

IJ is an integer variable. It's value is dictated by a DO loop in the main program.

NEWL is an integer variable assuming values of zero or one only. Zero indicates no load increase. One indicates the opposite.

Subroutine Listing:

```
      SUBROUTINE ACCUM(ST6C,NET6,INN,AUX,INI,STRSS6,NVJ,NCB,IJ,NEWL)
      DIMENSION ST6C(NET6,2),AUX(NET6,2),STRSS6(NET6,2),INN(NVJ),
     1    INI(NVJ),NCB(NVJ,4)
      IF(INN(IJ).EQ. 0) GO TO 99
      IF(INI(IJ).EQ. 1) GO TO 10
      DO 20 I=2,4

      KK=NCB(IJ,I)
      ST6C(KK,1)=STRSS6(KK,1)
      ST6C(KK,2)=STRSS6(KK,2)
      AUX(KK,1)=STRSS6(KK,1)
      AUX(KK,2)=STRSS6(KK,2)
   20 CONTINUE
      INI(IJ)=1
      GO TO 99
   10 DO 30 I=2,4
      KK=NCB(IJ,I)
      IF(NEWL.EQ. 1) GO TO 40
      GO TO 30
   40 ST6C(KK,1)=STRSS6(KK,1)+AUX(KK,1)
      ST6C(KK,2)=STRSS6(KK,2)+AUX(KK,2)
   30 CONTINUE
   99 CONTINUE
      RETURN
      END
```

(2) Subroutine ADJK3

Purpose: To successively modify horiz. joint element stiffnesses when 3-element simplification is used.

Call & Argument List: CALL ADJK3 (WREL, T2S, N, A, T2S0, NET2S)

WREL is a 2-dimen. real array storing relative horiz. and vertical joint (horizontal) deformations.

T2S is a 2-dim. real array denoting the joint element stiffnesses.

N is an integer variable. Its value is dictated by a DO loop in the main program.

A is a constant supplied by the main program .

T2S0 is a variable indicating the unmodified joint element spring (horiz.) stiffness.

NET2S is an integer giving the number of horiz. joint elements.

Subroutine Listing:

```
SUBROUTINE ADJK3 (WREL,T2S,N,A,T2S0,NET2S)
DIMENSION WREL(NET2S,2),T2S(NET2S,2)
T2V=2.5E8
B1=0.106
B3=0.09
I1=N*3-2
I2=N*3-1
I3=N*3
Y1=WREL(I1,2)
Y2=WREL(I2,2)
Y3=WREL(I3,2)
IF(Y1.GT.0.0 .AND. Y2.GT. 0.0 .AND. Y3.GT. 0.0 )GO TO 99
IF(Y1.LE.0.0 .AND. Y3 .LE. 0.0) GO TO 10
IF (Y1 .GT. 0.0 ) GO TO 20
C=1.0-(ABS(Y1)-ABS(Y2))*A/ABS(Y1)
D=-0.50+1.50*C
IF (Y2.GT. 0.0) GO TO 70
IF(T2S(I2,1).LT. 1.0) GO TO 100
B42=-0.0557+0.3073*C
B43=0.1999-0.0472A*C
T2S(I2,1)=T2S0*C*B42*2.
```

(cont.)

Subroutine ADJK3 (cont.)

```
      T2S(I1,1)=T2SO*C*B4
      T2S(I1,2)=T2V*C*D
      GO TO 99
  100 IF(T2S(I1,1).LT. 1.0) GO TO 99
      B5=0.60307-0.88911*C
      T2S(I1,1)=T2SO*C*B5
      T2S(I1,2)=T2V*C*D
      GO TO 99
   70 IF(T2S(I1,1).LT. 1.0) GO TO 99
      C=(1.0-A)-(ABS(Y2)*(1.0-A)/(ABS(Y2)+ABS(Y1)))
      T2S(I1,1)=T2SO*C*B3
      T2S(I1,2)=T2V*C*D
      GO TO 99
   10 IF (ABS(Y1).L. .ABS(Y3)) GO TO 30
      C=1.0-(ABS(Y1)-ABS(Y2))*A/ABS(Y1)
      D=-0.50+1.50*C
      IF (T2S(I2,1) .LT. 1.0) GO TO 25
   55 T2S(I1,1)=T2SO*C*B1
      T2S(I2,1)=T2SO*C*B1*2.
      T2S(I3,1)=T2SO*C*B1
      T2S(I1,2)=T2V*C*D
      T2S(I3,2)=T2V*C*D
      T2S(I2,2)=T2V*C*D*2.
      GO TO 99
   25 B2=0.6944-1.0*(C**2)
      IF(T2S(I2,1) .LT. 1.0) GO TO 45
      T2S(I2,1)=T2SO*C*B2*2.
   45 T2S(I1,1)=T2SO*C*B2
      T2S(I1,2)=T2V*C*D
      T2S(I2,2)=T2V*C*D*2.
      GO TO 99
   30 C=1.0-(ABS(Y3)-ABS(Y2))*A/ABS(Y3)
      D=-0.50+1.50*C
      IF(T2S(I1,1).LT. 1.0) GO TO 35
      GO TO 65
   35 B2=0.6944-1.0*(C**2)
      IF(T2S(I2,1) .LT. 1.0) GO TO 65
      T2S(I2,1)=T2SO*C*B2*2.
   65 T2S(I3,1)=T2SO*C*B2
      T2S(I3,2)=T2V*C*D
      T2S(I2,2)=T2V*C*D*2.
      GO TO 99
   20 C=1.0-(ABS(Y3)-ABS(Y2))*A/ABS(Y3)
      D=-0.50+1.50*C
      IF (Y2.GT. 0.0) GO TO 50
      IF(T2S(I2,1).LT. 1.0) GO TO 110
      B42=-0.05534+0.3073*C
      B43=0.1999-0.0472*C
      T2S(I2,1)=T2SO*C*B42*2.
      T2S(I3,1)=T2SO*C*B43
      T2S(I3,2)=T2V*C*D
      GO TO 99
  110 IF(T2S(I3,1) .LT. 1.0) GO TO 99
      B5=0.60307-0.88911*C
      T2S(I3,1)=T2SO*C*B5
      T2S(I3,2)=T2V*C*D
      GO TO 99
   50 IF(T2S(I3,1).LT. 1.0) GO TO 99
      C=(1.0-A)-(ABS(Y2)*(1.0-A)/(ABS(Y2)+ABS(Y3)))
      T2S(I3,1)=T2SO*C*B3
      T2S(I3,2)=T2V*C*D
   99 CONTINUE
      RETURN
      END
```

(3) Subroutine BETA

Purpose: To generate 'Beta' matrix used for condensation purposes.

Call & Argument List: CALL BETA (BB, IB, M, N, K)

BB is a 2-dim. real array in which 'beta' is stored.

IB is a 2-dim. real array in which in-put data to generate Beta is stores.

M is the 1st dimension of BB.

N is the 2nd dimension of BB.

K is the 1st dimension of IB.

Subroutine Listing:

```
      SUBROUTINE BETA (BB,IB,M,N,K)
      DIMENSION BB(M,N),IB(K,2)
      DO 5 I=1,M
      DO 7 J=1,N
      BB(I,J)=0.0
    7 CONTINUE
    5 CONTINUE
      DO 10 I=1,K
      II=IB(I,1)
      JJ=IB(I,2)
      BB(II,JJ)=1.0
   10 CONTINUE
      RETURN
      END
```

(4) Subroutine BNDBPG

Purpose: To solve a system of simultaneous equation with an unsymmetrically banded coefficient matrix. The method used is Gaussian elimination followed by back substitution.

Call & Argument List: CALL BNDBPG (A, X, NB, ND, N, TEST, IND)

A is a 2-dim. real array storing the banded matrix.

X is a 1-dim. real array initially containing the external load vector, and finally the vector of nodal displacements.

NB is the 1st parameter in the dimension statement for A.

ND is the number of non-zero diagonals above and below the main diagonal.

N is the length of vector X.

TEST is a small number approximating zero.

IND is an integer variable assuming values of 0 or 1 only. One indicates singularity.

Subroutine Listing:

```
      SUBROUTINE BNDBPG(A,X,NB,ND,N,TEST,IND)
      DIMENSION A(NB,1),X(1)
      IND=0
      ND1=ND+1
      ND2=ND1+1
      ND3=ND+ND1
      NDN=N+ND1
      DO 10 J=2,N
      L=MAX0(1,ND2-J)
      JJ=J-ND1
      DO 11 K=L,ND
      M=K+JJ
      IF(ABS(A(ND1,M)).LE.TEST)GO TO 22
      Z=-A(K,J)/A(ND1,M)
      A(K,J)=0.
      IF(Z.EQ.0.)GO TO 11
      LL=MIN0(ND3,NDN-M)
      KL=K
      DO 12 KK=ND2,LL
      KL=KL+1
   12 A(KL,J)=A(KL,J)+Z*A(KK,M)
      X(J)=X(J)+Z*X(M)
   11 CONTINUE
   10 CONTINUE
      DO 20 J=1,N
      JJ=N+1-J
      IF(J.EQ.1) GO TO 20
      L=MIN0(ND3,ND+J)
```

Subroutine BNDBPG (cont.)

```
      MM=JJ-NC1
      DO 21 K=ND2,L
      M=K+MM
21    X(JJ)=X(JJ)-A(K,JJ)*X(M)
20    X(JJ)=X(JJ)/A(ND1,JJ)
      GO TO 23
22    IND=1
23    CONTINUE
      RETURN
      END
```

(5) Subroutine CKYC

Purpose: To determine panel element principle stresses.

Call & Argument List: CALL CKYC (SIGMA, S1, S2, S0, NC, NY)

SIGMA is a 1-dim. real array in which element stresses are stored.

S1 is a variable signifying the max. principal stress.

S2 is a variable signifying the min. principal stress.

S0 is a variable signifying the failure condition.

NC and NY are integer variables signifying the type of failure i.e. NC = 1 indicate tension failure whereas NY = 1 signifies failure by yielding.

Subroutine Listing:

```
      SUBROUTINE CKYC (SIGMA,S1,S2,S0,NC,NY)
      DIMENSION SIGMA(3,1)
      NC=0
      NY=0


      Z1=SIGMA(1,1)
      Z2=SIGMA(2,1)
      S=SIGMA(3,1)
      SOD=5.E3**2
      S1=((Z1+Z2)/2.)+SQRT((((Z1-Z2)/2.)**2)+(S**2))
      S2=((Z1+Z2)/2.)-SQRT((((Z1-Z2)/2.)**2)+(S**2))
      S0=(S1**2)-(S1*S2)+(S2**2)
      IF(S0.GT.SOD) NY=1
      IF(S1.LT. 0.0) GO TO 99
      IF(S1.GT. 660) NC=1
   99 CONTINUE
      RETURN
      END
```

(6) Subroutine DATA

Purpose: To generate a matrix containing the coordinates of general finite element from the input data.

Call & Argument List: CALL DATA (J, C, NE, NEJ1, NJ, NDFJ, NEJ, IJK, DAX, LAX1)

J is a 2-dim. integer array. The 1st element in each row indicate the element number. Other elements denote the corresponding nodal numbers.

C is a 2-dim. real array denoting the coordinates of the nodes.

NE is an integer variable indicating the number of elements.

NEJ1 is given by NEJ + 1

NJ is an integer variable indicating the number of nodes.

NDFJ is the number of degrees of freedom per node.

NEJ is the number of nodes associated with an element.

IJK is an integer variable dictated by a DO loop in the main program.

DAX is a 2-dim. array containing the coordinates of the element's nodal points.

LAX1 is a 1-dim. array containing the nodal numbers.

Subroutine Listing:

```
      SUBROUTINE DATA (J,C,NE,NEJ1,NJ,NDFJ,NEJ,IJK,DAX,LAX1)
      DIMENSION J(NE,NEJ1),C(NJ,NDFJ),LAX1(NEJ),DAX(NEJ,NDFJ)
      DO 40 I=1,NEJ
      LAX1(I)=0
   40 CONTINUE
      DO 10 I=2,NEJ1
      K=I-1
      LAX1(K)=J(IJK,I)
   10 CONTINUE
      DO 20 I=1,NEJ
      L=LAX1(I)
      DO 30 K=1,NDFJ
      DAX(I,K)=C(L,K)
   30 CONTINUE
   20 CONTINUE
      RETURN
      END
```

(7) Subroutine DBK

Purpose: To modify the stiffnesses of horizontal joint reinforcement elements.

Call & Argument List: CALL DBK (P, T4, NET4, BFL, N, IND4, FORS, FRST, SNDK)

P is a 1-dim. array in which element forces are stored.

T4 is a 2-dim. array in which element stiffnesses are stored.

NET4 is an integer variable denoting the number of elements.

DFL is a variable denoting the dowel force limit.

BFL is a variable denoting the bond force limit.

N is an integer variable the value of which is assinged automatically in a DO-loop in the main program.

IND4 is an integer variable indicating the occurrence of element stiffness modification.

FORS is a 1-dim. array in which element forces are stored.

FRST is a variable indicating the force at which stiffness must be modified.

SNDK is a variable denoting the modified stiffness.

Subroutine Listing:

```
      SUBROUTINE DBK (P,T4,NET4,DFL,BFL,N,IND4,FORS,FRST,SNDK)
      DIMENSION P(2,1),T4(NET4,2),FORS(4)
      RFD=1.0-(P(1,1)/DFL)
      RFB=1.0-(P(2,1)/BFL)
      B=BFL*RFD
      D=DFL*RFB
      IND4=0
      DO 40 I=1,4
      FORS(I)=0.0
   40 CONTINUE
```

(cont.)

Subroutine DBK (cont.)

```
      IF (P(2,1) .LE. 0.0) GO TO 10
      IF (P(2,1).GT.FRST) GO TO 7
      GO TO 5
    7 T4(N,2)=SNDK
    5 IF(ABS(P(1,1)).GT. 0 .OR. ABS(P(2,1)).GT. 0) GO TO 30
      GO TO 99
   30 T4(N,1)=0.0
      T4(N,2)=0.0
      IND4=2
      IF (ABS(P(1,1)).GT. 0) GO TO 50
      FORS(2)=B
      FORS(4)=-B
      IF (P(1,1).GT. 0.0) GO TO 60
      FORS(1)=-P(1,1)
      FORS(3)=P(1,1)
      GO TO 99
   60 FORS(1)=P(1,1)
      FORS(3)=-P(1,1)
      GO TO 99
   50 FORS(2)=P(2,1)
      FORS(4)=-P(2,1)
      IF (P(1,1) .GT. 0.0) GO TO 70
      FORS(1)=-0
      FORS(3)=0
      GO TO 99
   70 FORS(1)=0
      FORS(3)=-0
      GO TO 99
   10 IF (ABS(P(1,1)).GT. 0 ) GO TO 20
      GO TO 99
   20 T4(N,1)=0.0
      T4(N,2)=0.0
      IND4=1
      FORS(2)=-P(2,1)
      FORS(4)=P(2,1)
      IF (P(1,1).GT. 0.0) GO TO 80
      FORS(1)=-0
      FORS(3)=0
   80 FORS(1)=0
      FORS(3)=-0
   99 CONTINUE
      RETURN
      END
```

(8) Subroutine DBK2

Purpose: To modify the stiffness of tie-beam link elements.

Call & Argument List: CALL DBK2 (P, T5, NET5, DFL, BFL, N, IND4, FORS)

P is a 1-dim. array in which element forces are stored.

T5 is a 2-dim. array in which element stiffnesses are stored.

NET5 is an integer variable denoting the number of elements.

DFL is a variable denoting dowel force limit.

BFL is a variable denoting bond force limit.

N is an integer variable the value of which is assigned automatically in a DO-loop in the main program.

IND4 is an integer variable indicating the occurrence of joint element stiffness modification.

FORS is a 1-dim. array in which element forces are stored.

Subroutine Listing:

```
      SUBROUTINE DBK2(P,T5,NET5,DFL,BFL,N,IND4,FORS)
      DIMENSION P(2,1),T5(NET5,2),FORS(4)
      IND4=0
      RFB=1.0-(P(1,1)/BFL)
      RFD=1.0-(P(2,1)/DFL)
      D=DFL*RFB
      C=BFL*RFD
      DO 5 I=1,4
      FORS(I)=0.0
    5 CONTINUE
      IF(ABS(P(1,1)).GT. C.OR. ABS(P(2,1)) .GT.\D) GO TO 10
      GO TO 99
   10 T5(N,1)=0.0
      T5(N,2)=0.0
      IND4=1
      A=P(2,1)/ABS(P(2,1))
      B=P(1,1)/ABS(P(1,1))
      IF (ABS(P(1,1)) .GT. C) GO TO 20
      FORS(2)=C*A
      FORS(4)=-D*A
      FORS(1)=P(1,1)*B
      FORS(3)= -P(1,1)*B
```

(cont.)

Subroutine DBK2 (cont.)

```
      GO TO 99
20    FORS(2)=P(2,1)*A
      FORS(4)=-P(2,1)*A
      FORS(1)=C*B
      FORS(3)=-C*B
99    CONTINUE
      RETURN
      END
```

(9) Subroutine EDISPC

Purpose: To isolate the nodal displacements of individual condensed elements.

Call & Argument List: CALL EDISPC (W1, NDF, EDC, IJK, JF, NJ, NDFJ1, JC, NETC)

W1 is a 1-dim. array denoting the vector of nodal displacements.

NDF is an integer variable denoting the number of degrees of freedom.

EDC is a 1-dim. array in which the nodal displacements of individual elements are stored.

IJK is an integer variable the value of which is automatically assigned in a DO-loop.

JF is a 2-dim. integer array in which the degrees of freedom associated with each node is recorded.

NJ is an integer variable denoting the number of nodes.

NDFJ1 is an integer variable denoting the number of degrees of freedom per node plus one.

JC is a 2-dim. integer array denoting the nodal numbers of the elements.

NETC is an integer variable denoting the number of condensed elements.

Subroutine Listing:

```
      SUBROUTINE EDISPC(W1,NDF,EDC,IJK,JF,NJ,NDFJ1,JC,NETC)
      DIMENSION W1(NDF),EDC(16,1),JF(NJ,NDFJ1),JC(NETC,9)
      DO 10 I=1,16
      EDC(I,1)=0.0
   10 CONTINUE
      DO 20 I=1,8
      K=I+1
      NP=JC(IJK,K)
      I1=2*I-1
      I2=2*I
```

(cont.)

Subroutine EDISPC (cont.)

```
      N1=JF(NP,2)
      N2=JF(NP,3)
      IF(N1.EQ. 0 .AND. N2 .EQ. 0) GO TO 20
      IF (N1.EQ. 0) GO TO 30
      IF(N2.EQ. 0) GO TO 40
      EDC(I1,1)=W1(N1)
      EDC(I2,1)=W1(N2)
      GO TO 20
   30 EDC(I2,1)=W1(N2)
      GO TO 20
   40 EDC(I1,1) =W1(N1)
   20 CONTINUE
      RETURN
      END
```

(10) Subroutine EDSP2S

Purpose: To isolate nodal displacements of individual horizontal joint elements.

Call & Argument List: CALL EDSP2S (W1, NDF, ED2, IJK, JF, NJ, NDFJ1, J2, NET2)

W1 is a 1-dim. array denoting the vector of nodal displacements.

NDF is an integer variable denoting the number of degrees of freedom.

ED2 is a 1-dim. array in which nodal displacements of individual elements are stored.

IJK is an integer variable the value of which is automatically assigned in a DO-loop.

JF is a 2-dim. integer array in which the degrees of freedom associated with each node is recorded.

NJ is an integer variable denoting the number of nodes.

NDFJ1 is an integer variable denoting the number of degrees of freedom per node plus one.

J2 is a 2-dim. integer array denoting the nodal numbers of the elements.

NET2 is an integer variable denoting the number of horizontal joint elements.

Subroutine Listing:

```
      SUBROUTINE EDSP2S(W1,NDF,ED2,IJK,JF,NJ,NDFJ1,J2,NET2)
      DIMENSION W1(NDF), ED2(4), JF(NJ,NDFJ1),J2(NET2,3)
      DO 10 I=1,4
      ED2(I)=0.0
   10 CONTINUE
      DO 20 I=1,2
      K=I+1
      NP=J2(IJK,K)
```

(cont.)

Subroutine EDSP2S (cont.)

```
      I1=2*I-1
      I2=2*I
      N1=JF(NP,2)
      N2=JF(NP,3)
      IF (N1 .EQ. 0 .AND. N2 .EQ. 0) GO TO 20
      IF (N1 .EQ. 0) GO TO 30
      IF (N2 .EQ. 0) GO TO 40
      ED2(I1) =W1(N1)
      ED2(I2)=W1(N2)
      GO TO 20
30    ED2(I2)=W1(N2)
      GO TO 20
40    ED2(I1)=W1(N1)
20    CONTINUE
      RETURN
      END
```

(11) Subroutine FORM1

Purpose: To construct the stiffness matrix of a triangular finite element.

Call & Argument List: CALL FORM1 (DAX, E, V, T, AK, DB, ITEST, G)

DAX is a 2-dim. array used to store the coordinates of the element's nodal points.

E is the modulus of elasticity.

V is the Poisson's ratio

AK is a 2-dim. array in which the element's stiffness matrix is stored.

DB is a 2-dim. auxillary array.

ITEST is an integer variable to which a very small number is assigned.

G is the shear modulus.

Subroutine Listing:

```
      SUBROUTINE FORM1(DAX,E,V,T,AK,DB,ITEST,G)
      DIMENSION AK(6,6),A(6,6),C1(3,6),B(3,6),D(3,3),P(6,3),
     1    W(6,3),DB(3,6),N1(6),AUX(6,6) ,DAX(3,2)
      DO 10 I=1,6
      DO 20 J=1,6
      A(I,J)=0.0
      AK(I,J)=0.0
      AUX(I,J)=0.0


   20 CONTINUE
   10 CONTINUE
      A(1,1)=1.0
      A(1,2)=DAX(1,1)
      A(1,3)=DAX(1,2)
      A(2,4)=1.0
      A(2,5)=DAX(1,1)
      A(2,6)=DAX(1,2)
      A(3,1)=1.0
      A(3,2)=DAX(2,1)
      A(3,3)=DAX(2,2)
      A(4,4)=1.0
      A(4,5)=DAX(2,1)
      A(4,6)=DAX(2,2)
      A(5,1)=1.0
      A(5,2)=DAX(3,1)
```

(cont.)

Subroutine FORM1 (cont.)

```
      A(5,3)=DAX(3,2)
      A(6,4)=1.0
      A(6,5)=DAX(3,1)
      A(6,6)=DAX(3,2)
      ZERO=1.E-7
      CALL INVMAT (A,6,6,ZERO,IERR,N1)
      ITEST =IERR
      IF(ITEST.NE. 0) GO TO 50
      DO 30 I=1,3
      DO 40 J=1,6
      C10(I,J)=0.0
      B(I,J)=0.0
      DB(I,J)=0.0
   40 CONTINUE
   30 CONTINUE
      C10(1,2)=1.0
      C10(2,6)=1.0
      C10(3,4)=1.0
      C10(3,5)=1.0
      CALL MPRD (C10,A,B,3,6,0,0,6)
      COE=E/(1-(V**2))
      D(1,1)=COE
      D(1,2)=V*COE
      D(1,3)=0.0
      D(2,1)=D(1,2)
      D(2,2)=COE
      D(2,3)=0.0
      D(3,1)=0.0
      D(3,2)=0.0
      D(3,3)=G
      CALL MPRD(B,D,3,6,0)
      A1=DAX(1,1)
      A2=DAX(1,2)
      B1=DAX(2,1)
      B2=DAX(2,2)
      C1=DAX(3,1)
      C2=DAX(3,2)
      DEL2=((B1*C2)+(A1*B2)+(A2*C1)-(A1*C2)-(B2*C1)-(A2*B1))/2.0
      CALL MPRD(R,D,W,6,3,0,0,3)
      CALL MPRD (W,B,AUX,6,3,0,0,6)
      CALLMPRD(D,B,DD,3,3,0,0,6)
      VOL=DEL2*T
      CALL SMPY (AUX,VOL,AK,6,6,0)
   50 CONTINUE
      RETURN
      END
```

(12) Subroutine FORM2S

Purpose: To construct the stiffness matrix of a horizontal joint element.

Call & Argument List: CALL FORM2S (T2, NET2, J2, AK2, BK2, IJK, SI2, LX3, NEJ21, RESK, COEF)

T2 is a 2-dim. array in which element stiffnesses are recorded.

NET2 is an integer variable denoting the number of elements.

J2 is a 2-dim. integer array denoting the nodal numbers of the elements.

AK2 is a 2-dim. auxillary array.

BK2 is a 2-dim. array denoting the element stiffness matrix.

IJK is an integer variable the value of which is automatically assigned in a DO-loop.

SI2 is a variable denoting the orientation of the element with respect to structure coordinate system.

LX3 is a 1-dim. auxillary integer array.

NEJ21 is an integer variable denoting the number of nodes per element plus one.

RESK is a variable denoting a very small number.

COEF is a variable denoting the value of the coefficient of friction.

Subroutine Listing:

```
      SUBROUTINE FORM2S (T2,NET2,J2,AK2,RK2,IJK,SI2,LX3,NEJ21,RESK,COEF)
      DIMENSION T2(NET2,2),J2(NET2,NEJ21),AK2(4,4),RK2(4,4),A1(4,4)
     1    , A2(4,4),AUX(4,4),LX3(2)
      DO 10 I=1,4
      DO 20 J=1,4
      A1(I,J)=0.0
      AK2(I,J)=0.0
   20 CONTINUE
   10 CONTINUE
      A1(1,1)=COS(SI2)
      A1(1,2)=SIN(SI2)
      A1(2,1)=-A1(1,2)
      A1(2,2)=A1(1,1)
      A1(3,3)=A1(1,1)
      A1(3,4)=A1(1,2)
      A1(4,3)=A1(2,1)
      A1(4,4)=A1(1,1)
      CALL MTRA (A1,A2,4,4,0)
      IF(T2(IJK,1) .EQ. RESK ) GO TO 30
      AK2(1,1)=T2(IJK,1)
      AK2(1,3)=-AK2(1,1)
      AK2(2,2)=T2(IJK,2)
      AK2(2,4)=-AK2(2,2)
      AK2(3,1)= -AK2(1,1)
      AK2(3,3)=AK2(1,1)
      AK2(4,2)= -AK2(2,2)
      AK2(4,4)= AK2(2,2)
      GO TO 40
   30 AK2(1,1)= T2(IJK,1)
      AK2(1,2)=- COEF*T2(IJK,2)
      AK2(1,3)=-AK2(1,1)
      AK2(1,4)=-AK2(1,2)
      AK2(2,2)=T2(IJK,2)
      AK2(2,4)= -AK2(2,2)
      AK2(3,1)= -AK2(1,1)
      AK2(3,2)= -AK2(1,2)
      AK2(3,3)=AK2(1,1)
      AK2(3,4)=AK2(1,2)
      AK2(4,2)= -AK2(2,2)
      AK2(4,4)= AK2(2,2)
   40 CALL MPPD( A2,AK2,AUX,4,4,0,0,4)
      CALL MPPD(AUX,A1,RK2,4,4,0,0,4)
      DO 50 I=2,3
      K=I-1
      LX3(K)=J2(IJK,I)
   50 CONTINUE
      RETURN
      END
```

(13) Subroutine FORM3

Purpose: To construct the stiffness matrix of a bar element .

Call & Argument List: CALL FORM3 (J3, NET3, NEJ31, C, NJ, NDFJ, ES, AREA, IJK, LX5, AK3, BK3, A1)

J3 is a 2-dim. integer array denoting the element nodal numbers.

NET3 is an integer variable denoting the number of bor elements.

NEJ31 is an integer variable denoting the number of nodes per element plus one.

C is a 2-dim. array denoting the coordinates of the nodes .

NJ is an integer variable denoting the number of joints.

NDFJ is an integer variable denoting the number of degrees of freedom per joint.

ES is a variable denoting the modulus of elasticity.

AREA is a variable denoting the cross sectional area of the element.

IJK is an integer variable the value of which is automatically assigned in a DO-loop.

LX5 is a 1-dim. integer auxillary array.

AK3 is a 2-dim. auxillary array.

BK3 is a 2-dim. array denoting the element stiffness matrix.

A1 is a 2-dim. auxillary array.

Subroutine Listing:

```
      SUBROUTINE FORM3 (J3,NET3,NEJ31,C,NJ,NDFJ,ES,AREA,IJK,LX5,AK3,
     1    BK3,A1)
      DIMENSION J3(NET3,NEJ31),C(NJ,NDFJ),LX5(2),A1(4,4),A2(4,4),
     1    AK3(4,4),BK3(4,4),AUX3(4,4)
      DO 10  I=2,3
      K=I-1
      LX5(K)=J3(IJK,I)
   10 CONTINUE
      I1=J3(IJK,2)
      I2=J3(IJK,3)


      X1=C(I1,1)
      Y1=C(I1,2)
      X2=C(I2,1)
      Y2=C(I2,2)
      AL=SQRT(((X2-X1)**2)+((Y2-Y1)**2))
      COSINE=(X2-X1)/AL
      SINE=(Y2-Y1)/AL
      DO 20  I=1,4
      DO 30  J=1,4
      A1(I,J)=0.0
      AK3(I,J)=0.0
   30 CONTINUE
   20 CONTINUE
      A1(1,1)=COSINE
      A1(1,2)=SINE
      A1(2,1)=-A1(1,2)
      A1(2,2)=A1(1,1)
      A1(3,3)=A1(1,1)
      A1(3,4)=A1(1,2)
      A1(4,3)=A1(2,1)
      A1(4,4)=A1(1,1)
      CALL MTRA (A1,A2,4,4,0)
      FIG=ES*AREA/AL
      AK3(1,1)=FIG
      AK3(1,3)=-FIG
      AK3(3,1)=-FIG
      AK3(3,3)=FIG
      CALL MPRD (A2,AK3,AUX3,4,4,0,0,4)
      CALL MPRD (AUX3,A1,BK3,4,4,0,0,4)
      RETURN
      END
```

(14) Subroutine FORM4

Purpose: To construct the stiffness matrix of a horizontal joint reinforcement element.

Call & Argument List: (T4, NET4, AK4, BK4, J4, NEJ41, SI, LX7, IJK)

T4 is a 2-dimensional array in which element stiffness are recorded.

NET4 is an integer variable denoting the number of elements.

AK4 is a 2-dim. auxillary array.

BK4 is a 2-dim. array denoting the element stiffness matrix.

J4 is a 2-dim. integer array denoting the nodal numbers of the elements.

NEJ41 is an integer variable denoting the number of nodes per element plus one.

SI is a variable denoting the orientation of the element with respect to structures coordinate system.

LX7 is a 1-dim. integer auxillary array.

IJK is an integer variable the value of which is automatically assigned in a DO-loop.

Subroutine Listing:

```
      SUBROUTINE FORM4 (T4,NET4,AK4,BK4,J4,NEJ41,SI,LX7,IJK)
      DIMENSION   T4(NET4,2),AK4(4,4),J4(NET4,NEJ41),LX7(2),
     1    A1(4,4),A2(4,4),AUX4(4,4),BK4(4,4)
      DO 10 I=2,3
      K=I-1
      LX7(K)=J4(IJK,I)
   10 CONTINUE
      DO 20 I=1,4
      DO 30 J=1,4
      A1(I,J)=0.0
      AK4(I,J)=0.0
```

(cont.)

Subroutine FORM4 (cont.)

```
30  CONTINUE
20  CONTINUE
    A1(1,1)=COS(SI)
    A1(1,2)=SIN(SI)
    A1(2,1)=-A1(1,2)
    A1(2,2)=A1(1,1)
    A1(3,3)=A1(1,1)
    A1(3,4)=A1(1,2)
    A1(4,3)=A1(2,1)
    A1(4,4)=A1(1,1)
    CALL MTPA (A1,A2,4,4,0)
    AK4(1,1)=T4(IJK,2)
    AK4(1,3)=-AK4(1,1)
    AK4(2,2)=T4(IJK,1)
    AK4(2,4)=-AK4(2,2)
    AK4(3,1)=AK4(1,3)
    AK4(3,3)=AK4(1,1)
    AK4(4,2)=AK4(2,4)
    AK4(4,4)=AK4(2,2)
    CALL MPRO (A2,AK4,AUX4,4,4,0,0,4)
    CALL MPRO (AUX4,A1,BK4,4,4,0,0,4)
    RETURN
    END
```

(15) Subroutine FORM41

Purpose: To construct the stiffness matrix of a vertical joint element.

Call & Argument List: CALL FORM41 (T4, NET4, AK4, BK4, J4, NEJ41, SI, LX7, IJK, NR, NC, AV, INI, II, NVJ)

T4 is a 2-dim. array in which element stiffnesses are recorded.

NET4 is an integer variable denoting the number of vertical joint elements.

AK4 is a 2-dim. auxillary array.

BK4 is a 2-dim. array denoting the element stiffness matrix.

J4 is a 2-dim. integer array denoting the elements' nodal numbers.

NEJ41 is an integer array indicating the number of nodes per element plus one.

SI is a variable denoting the orientation of the element with respect to structure coordinate system.

LX7 is a 1-dim. auxillary integer array.

IJK is an integer variable the value of which is automatically assigned in a DO-loop.

NR is a 1-dim. integer array denoting the activation of horizontal joint reinforcement.

NC is an integer variable identifying the slip surface 1 or 2.

AV is a 1-dim. array in which the contributory area of the vertical joint elements are recorded.

INI is a 1-dim. array the elements of which may assume

values of zero or 1 only. They are all zero to begin with. Subsequent values are determined automatically.

II is an integer variable the value of which is automatically assigned in a DO-loop.

NVJ is an integer variable signifying the number of vertical joints.

Subroutine Listing:

```
      SUBROUTINE FORM41 (T4,NET4,AK4,PK4,J4,NEJ41,SI,LX7,IJK,NR,NC,AV,
     1    INI,II,NVJ)
      DIMENSION   T4(NET4,2),AK4(4,4),J4(NET4,NEJ41),LX7(2),
     1    A1(4,4),A2(4,4),AUX4(4,4),PK4(4,4),NR(NET4),AV(NET4),INI(NVJ)
      NNN=0
      RR=1.0
      PP=0.59
      IF (NC.EQ. 1) GO TO 130
      IF(INI(II).EQ. 1 .OR. NNN.EQ.1) GO TO 100
      XX=3.255*PP
      YY=6.198
      IF(NR(IJK).EQ.2 .AND.NNN.EQ.1)YY=2.04E3
      GO TO 120
  100 XX=6.30E3
      YY=2.04E3
  120 PP=XX*AV(IJK)
      T4(IJK,1)=AV(IJK)*YY
  130 CONTINUE
      IF(NC.EQ.2 .AND. NR(IJK) .EQ. 2) GO TO 140
      GO TO 145
  140 PP=0.0
      T4(IJK,1)=0.0
  145 CONTINUE
      IF(NNN.EQ.1)PP=0.0
      COEF=1.82
      DO 10 I=2,3
      K=I-1
      LX7(K)=J4(IJK,I)
   10 CONTINUE
      DO 20 I=1,4


      DO 30 J=1,4
      A1(I,J)=0.0
      AK4(I,J)=0.0
   30 CONTINUE
   20 CONTINUE
      A1(1,1)=COS(SI)
      A1(1,2)=SIN(SI)
      A1(2,1)=-A1(1,2)
      A1(2,2)=A1(1,1)
      A1(3,3)=A1(1,1)
      A1(3,4)=A1(1,2)
      A1(4,3)=A1(2,1)
      A1(4,4)=A1(1,1)
      CALL MTRA (A1,A2,4,4,0)
      IF(NR(IJK).EQ. 0.AND. NC.EQ. 2) GO TO 40
      AK4(1,1)=T4(IJK,1)
      AK4(1,3)=-AK4(1,1)
      AK4(2,2)=T4(IJK,2)
```

(cont.)

Subroutine FORM41 (cont.)

```
      AK4(2,4)=-AK4(2,2)
      AK4(3,1)=AK4(1,3)
      AK4(3,3)=AK4(1,1)
      AK4(4,2)=AK4(2,4)
      AK4(4,4)=AK4(2,2)
      IF(NP(IJK).EQ. 0) GO TO 40
      IF(NC.EQ. 1) GO TO 50
      AK4(1,2)=+PP/COEF
      AK4(1,4)=-AK4(1,2)
      AK4(3,2)=-AK4(1,2)
      AK4(3,4)=+AK4(1,2)
      GO TO 40
50    AK4(1,2)=-T4(IJK,2)/COEF
      AK4(1,4)=+AK4(1,2)
      AK4(3,2)=-AK4(1,2)
      AK4(3,4)=+AK4(1,2)
      AK4(2,1)=-COEF*T4(IJK,1)
      AK4(2,3)=-AK4(2,1)
      AK4(4,1)=-AK4(2,1)
      AK4(4,3)=AK4(2,1)
40    CONTINUE
      CALL MPPD (A2,AK4,AUX4,4,4,0,0,4)
      CALL MPPD (AUX4,A1,BK4,4,4,0,0,4)
      RETURN
      END
```

(16) Subroutine HJK

Purpose: To modify horizontal joint element stiffnesses on slip surface 1.

Call & Argument List: CALL HJK (P, T2S, AC2S, NET2S, N, IND2S, FCP, RESK, NO, NR, NDAT, NET4)

P is a 1-dim. array denoting the forces acting on horizontal joint elements.

T2S is a 2-dim. array in which element stiffnesses are recorded.

AC2S is a 2-dim. array in which horizontal joint properties i.e. the contributory areas and the coefficients of friction, are recorded.

NET2S is an integer variable denoting the number of elements.

N is an integer variable the value of which is automatically assigned in a DO-loop.

IND2S is an integer variable indicating whether joint stiffnesses have been modified or not.

FCP is a variable denoting the ultimate compressive strength of horizontal joints.

RESK is a variable denoting a very small number.

NO is an integer variable denoting the type failure occurring in a horizontal joint.

NR is a 1-dim. integer array denoting the activation of horizontal joint reinforcement.

NDAT is a 1-dim. integer array in which the horizontal joint reinf. element numbers are recorded in corresponding locations. Non-corresponding elements are assigned zero values.

NET4 is an integer variable denoting the number of horizontal joint reinforcement elements.

Subroutine Listing:

```
      SUBROUTINE HJK (P,T2S,AC2S,NET2S,N,IND2S,FCP,RESK,NC,NR,NDAT,NET4)
      DIMENSION P(2,1),T2S(NET2S,2),AC2S(NET2S,2),NR(NET4),NDAT(NET2S)
      PN=P(2,1)/AC2S(N,1)
      PS=P(1,1)/AC2S(N,1)
      IND2S=0
      NO=0
      FTP=460.0
      IF (PN.GT. 0.0) GO TO 10
      S1=SQRT(((PN/2.0)**2)+(PS**2))+(PN/2.0)
      IF(ABS(PN).GT. (FCP*0.8)) GO TO 20
      IF (ABS(S1) .GT. FTP) GO TO 30
      SH =(AC2S(N,2)*ABS(PN)) +0.01
      IF(ABS (PS).GT. SH) GO TO 40
      GO TO 99
10    T2S(N,1)=0.0
      T2S(N,2)=0.0
      IND2S=1
      NO=1
      IF(NDAT(N).EQ. 0) GO TO 99
      II=NDAT(N)
      NR(II)=1
      GO TO 99
20    T2S(N,1)=0.0
      T2S(N,2)=0.0
      IND2S=1
      NO=2
      GO TO 99
30    AC2S(N,2)=0.25


      T2S(N,1)=RESK
      IND2S=1
      NO=3
      GO TO 99
40    T2S(N,1)=RESK
      IND2S=1
      NO=4
99    CONTINUE
      RETURN
      END
```

(17) Subroutine HJK2

Purpose: To modify horizontal joint element stiffnesses on slip surface 2.

Call & Argument List: CALL HJK2 (P, T2S, AC2S, NET2S, N, IND2S, FCP, RESK, NO, NR, NDAT, NET4)

P is a 1 dim. array denoting the forces acting on horizontal joint elements.

T2S is a 2-dim. array in which element stiffnesses are recorded.

AC2S is a 2 dim. array in which horizontal joint properties i.e. the contributory areas and the coefficients of friction, are recorded.

NET2S is an integer variable denoting the number of elements.

N is an integer variable the value of which is automatically assigned in a DO-loop.

IND2S is an integer variable indicating whether joint stiffnesses have been modified or not.

FCP is a variable denoting the ultimate compressive strength of horizontal joints.

RESK is a variable denoting a very small number.

NO is an integer variable denoting the type of failure occurring in a horizontal joint.

NR is a 1-dim. integer array denoting the activation of horizontal joint reinforcement.

NDAT is a 1-dim. integer array denoting the horizontal joint element numbers corresponding to those of joint reinforcement element numbers.

NET4 is an integer variable denoting the number of horizontal joint reinforcement elements.

Subroutine Listing:

```
      SUBROUTINE HJK2(P,T2S,AC2S,NET2S,N,IND2S,FCP,RESK,NO,NR,NDAT,NET4)
      DIMENSION P(2,1),T2S(NET2S,2),AC2S(NET2S,2),NR(NET4),NDAT(NET2S)
      PN=P(2,1)/AC2S(N,1)
      PS=P(1,1)/AC2S(N,1)
      IND2S=0
      NO=0
      A=8.0
      B=4.0
      FTP=400.0
      IF(PN .GT. 0.0 ) GO TO 10
      S1=SQRT(((PN/2.0)**2)+(PS**2))+(PN/2.0)
      IF(ABS(PN).GT. (FCP*0.8)) GO TO 30
      IF (AC2S(N,2) .NE. 0.8) GO TO 99
      IF(ABS(PS).LE.AC2S(N,2)*ABS(PN)) GO TO 40
      PSB=(A*ABS(PS)-(A-B)*AC2S(N,2)*ABS(PN))/B
      S1=SQRT(((PN/2.0)**2)+(PSB**2))+(PN/2.0)
      IF(ABS(S1) .GT.FTP) GO TO 60
      GO TO 99
10    PNP=PN*A/B
      PSP=PS*A/B
      S1=SQRT(((PNP/2.0)**2)+(PSP**2))+(PNP/2.0)
      IF(ABS(PNP) .GT.      FTP .OR. S1 .GT. FTP) GO TO 20
      GO TO 99
20    T2S(N,1)=0.0
      T2S(N,2)=0.0
      IND2S=1
      NO=1
      IF(NDAT(N).EQ. 0) GO TO 99
      II=NDAT(N)
      NR(II)=1
      GO TO 99
30    T2S(N,1)=0.0
      T2S(N,2)=0.0
      IND2S=1
      NO=2
      GO TO 99
40    S1=SQRT(((PN/2.0)**2)+(PS**2))+(PN/2.0)
      IF(ABS(S1).GT. FTP) GO TO 50
      GO TO 99
50    AC2S(N,2)=0.25
      T2S(N,1)=RESK
      IND2S=1
      NO=3
      GO TO 99
60    AC2S(N,2)=(1.0*B+0.8*(A-B))/A
      T2S(N,1)=RESK
      IND2S=1
      NO=4
99    CONTINUE
      RETURN
      END
```

(18) Subroutine LOAD

Purpose: To apply cumulative loads to specific nodal points of a structural assembly.

Call & Argument List: CALL LOAD (WI, WIP, NDF, AW, NW, SAC, NJVL, AC2S, NET2S, II, JJ, EXTL)

WI is a 1-dim. array in which external loads are recorded.

WIP is a 1-dim. auxillary array in which external loads are recorded.

NDI is an integer variable denoting the number of degrees of freedom.

AW is a variable denoting the load increment.

NW is a 1-dim. integer array in which the numbers identifying the degrees of freedom of nodes with variable loads are recorded.

SAC is a 1-dim. array in which appropriate multiples of incremental load for various nodes are recorded.

NJVL is an integer variable indicating the number of nodes with variable loads.

AC2S is a 1-dim. auxillary array.

II is an integer variable the value of which is either one or zero depending on the need for additional incremental loads.

JJ is an integer variable the value of which is either zero or one depending on the need for halving the incremental load.

EXTL is a 1-dim. array in which variable external loads are recorded,

Subroutine Listing:

```
      SUBROUTINE LOAD (W1,W1P,NDF,AW,NW,SAC,NJVL,AC2S,NET2S,II,JJ,EXTL)
      DIMENSION W1(NDF),W1P(NDF),NW(NJVL),AC2S(NET2S),SAC(NJVL)
      DIMENSION EXTL(NJVL)
      DO 10 I=1,NDF
      W1(I)=W1P(I)
   10 CONTINUE
      IF(II) 20,30,40
   20 IF(JJ .NE. 0) AW=AW/2.0
      DO 50 I=1,NJVL
      J=NW(I)
      W1(J)=W1(J)-AW*SAC(I)
      EXTL(I)=EXTL(I)-AW*SAC(I)
   50 CONTINUE
      GO TO 80
   30 CONTINUE
      GO TO 80
   40 IF(JJ .NE. 0) AW=AW/2.0
      DO 70 I=1,NJVL
      J=NW(I)
      W1(J)=W1(J)+AW*SAC(I)
      EXTL(I)=EXTL(I)+AW*SAC(I)
   70 CONTINUE
   80 DO 90 I=1,NDF
      W1P(I)=W1(I)
   90 CONTINUE
      RETURN
      END
```

(19) Subroutine MEMST2

Purpose: To determine forces in spring-type elements.

Call & Argument List: CALL MEMST2 (ED4, T4, NET4, SI, IJK, P)

ED4 is a 1-dim. array in which nodal displacements of joint elements are stored.

T4 is a 2-dim. array in which element stiffnesses are stored.

NET4 is an integer variable denoting the number of elements.

SI is a variable denoting the orientation of the element with respect to structure coordinate system.

IJK is an integer variable the value of which is automatically assigned in a DO-loop in the main program.

P is a 1-dim. array in which element forces are recorded.

Subroutine Listing:

```
      SUBROUTINE MEMST2 (ED4,T4,NET4,SI,IJK,P)
      DIMENSION ED4(4),T4(NET4,2),D(2,4),WR(2,1),A1(4,4),
     1    ED4M(4),DK(2,2),P(2,1)
      DO 10 I=1,2
      DO 20 J=1,4
      D(I,J)=0.0
   20 CONTINUE
   10 CONTINUE
      D(1,1)=-1.0
      D(1,3)=1.0
      D(2,2)=-1.0
      D(2,4)=1.0
      DO 30 I=1,4
      DO 40 J=1,4
      A1(I,J)=0.0
   40 CONTINUE
   30 CONTINUE
      A1(1,1)=COS(SI)
      A1(1,2)=SIN(SI)
      A1(2,1)=-A1(1,2)
      A1(2,2)=A1(1,1)
      A1(3,3)=A1(1,1)
      A1(3,4)=A1(1,2)
      A1(4,3)=A1(2,1)
      A1(4,4)=A1(1,1)
      DO 50 I=1,4
      ED4M(I)=0.0
      DO 60 J=1,4
      ED4M(I)=ED4M(I)+A1(I,J)*ED4(J)
```

(cont.)

Subroutine MEMST2 (cont.)

```
60 CONTINUE
50 CONTINUE
   DO 70 I=1,2
   WR(I,1)=0.0
   DO 80 J=1,4
   WR(I,1)=WR(I,1)+D(I,J)*EM4M(J)
80 CONTINUE
70 CONTINUE
   IF(ABS(WR (2,1)).LE. 1.E-10) WR(2,1)=0.0
   DK(1,1)=T4(IJK,1)
   DK(2,2)=T4(IJK,2)
   DK(1,2)=0.0
   DK(2,1)=0.0
   CALL MPPD (DK,WR,P,2,2,0,0,1)
   RETURN
   END
```

(20) Subroutine MEMST3

Purpose: To determine forces in vertical joint elements.

Call & Argument List: CALL MEMST3 (ED4, T4, NET4, SI, IJK, P, NR, AK4, NC, AV, INI, II, NVJ)

ED4 is a 1-dim. array in which nodal displacements of vertical joint elements are stored.

T4 is a 2-dim. array in which element stiffness are recorded.

NET4 is an integer variable denoting the number of elements.

SI is a variable denoting the orientation of the element with respect to structure coordinate system.

IJK is an integer variable the value of which is automatically assigned in a DO-loop in the main program.

P is a 1-dim. array in which element forces are recorded.

NR is a 1-dim. integer array denoting the activation of vertical joint reinforcement element.

AK4 is a 2-dim. array in which the element's stiffness matrix is stored.

NC is an integer variable identifying the slip surface 1 or 2.

AV is a 1-dim. array in which elements' contributory areas are stored.

INI is a 1-dim. array the elements of which may assume values of zero or 1 only. They are all zero to begin with. Subsequent values are determined automatically.

II is an integer variable the value of which is automatically assigned in a DO-loop.

NVJ is an integer variable denoting the number of vertical joints.

Subroutine Listing:

```
      SUBROUTINE MEMST3 (ED4,T4,NET4,SI,IJK,P,NP,AK4,NC,AV,INI ,II,NVJ)
      DIMENSION ED4(4),T4(NET4,2),D(2,4),WP(2,1),A1(4,4),
     1    ED4M(4),DK(2,2),P(2,1),NP(NET4),P2(4,1),AK4(4,4)
      DIMENSION AV(NET4),INI(NVJ)
      NNN=0
      COEF=1.82
      RR=1.0
      RP=0.89
      IF(INI(II).EQ. 1 .OR. NNN.EQ. 1) GO TO 100
      XX=3.2505*RP
      GO TO 120
  100 XX=6.3053
  120 PP=XX*AV(IJK)
      IF(NC.EQ.2 .AND. NP(IJK) .EQ. 2) GO TO 140
      GO TO 145
  140 PP=0.0
      T4(IJK,1)=0.0
  145 CONTINUE
      IF(NNN.EQ.1) PP=0.0
      DO 10 I=1,2
      DO 20 J=1,4
      D(I,J)=0.0
   20 CONTINUE
   10 CONTINUE
      D(1,1)=-1.0
      D(1,3)=1.0
      D(2,2)=-1.0
      D(2,4)=1.0
      DO 30 I=1,4
      DO 40 J=1,4
      A1(I,J)=0.0
   40 CONTINUE
   30 CONTINUE
      A1(1,1)=COS(SI)
      A1(1,2)=SIN(SI)
      A1(2,1)=-A1(1,2)
      A1(2,2)=A1(1,1)
      A1(3,3)=A1(1,1)
      A1(3,4)=A1(1,2)
      A1(4,3)=A1(2,1)
      A1(4,4)=A1(1,1)
      DO 50 I=1,4
      ED4M(I)=0.0
      DO 60 J=1,4
      ED4M(I)=ED4M(I)+A1(I,J)*ET4(J)
   60 CONTINUE
   50 CONTINUE


      DO 70 I=1,2
      WP(I,1)=0.0
      DO 80 J=1,4
      WP(I,1)=WP(I,1)+D(I,J)*ED4M(J)
   80 CONTINUE
   70 CONTINUE
      IF(NC.EQ. 2) GO TO 90
      IF(NP(IJK).GT. 0) GO TO 95
      DK(1,2)=0.0
      DK(1,1)=T4(IJK,1)
      DK(2,2)=T4(IJK,2)
      DK(2,1)=0.0
      CALL MPPO (DK,WP,P,2,2,0,0,1)
```

(cont.)

Subroutine MEMST3 (cont.)

```
      GO TO 99
   95 DK(1,1)=T4(IJK,1)
      DK(2,2)=T4(IJK,2)
      DK(1,2)=-T4(IJK,2)/COEF
      DK(2,1)=-T4(IJK,1)*COEF
      CALL MPPC(DK,WR,P,2,2,0,0,1)
      GO TO 99
   90 IF(NP(IJK) .EQ. 0) GO TO 98
      DK(1,1)=T4(IJK,1)
      DK(2,2)=T4(IJK,2)
      DK(2,1)=0.0
      DK(1,2)=EP/COEF
      GO TO 97
   98 DK(1,1)=0.0
      DK(1,2)=0.0
      DK(2,1)=0.0
      DK(2,2)=0.0
   97 CONTINUE
      CALL MPPC(DK,WR,P,2,2,0,0,1)
   99 CONTINUE
      RETURN
      END
```

(21) Subroutine MULT

Purpose: To multiply a submatrix of a matrix [A] by a submatrix of another matrix [B] and recording the result in the upper left hand corner of a yet another matrix [C].

Call & Argument List: CALL MULT (A, B, C, M1, N1,M2,N2,M3, N3, I1, J1, I2, J2, L1, L2, L3, IT)

Artument List is defined in the following diagram

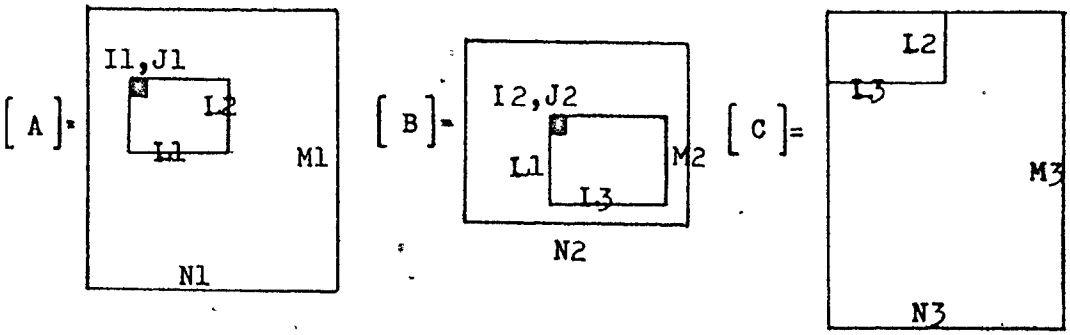

IT is an integer variable assuming a value of either zero or one. If its value is one, the 1st submatrix is transposed before multiplication.

Subroutine Listing:

```
      SUBROUTINE MULT (A,B,C,M1,N1,M2,N2,M3,N3,I1,J1,I2,J2,L1,L2,L3,IT)
      DIMENSION A(M1,N1),B(M2,N2),C(M3,N3)
      IF(IT. NE. 0) GO TO 10
      DO 20  I=1,L2
      DO 30  J=1,L3
      II=I+I1-1
      JJ=J+J2-1
      C(I,J)=0.0
      DO 40  K=1,L1
      K1=K+J1-1
      K2=K+I2-1
      C(I,J)=C(I,J)+A(II,K1)*B(K2,JJ)
   40 CONTINUE
   30 CONTINUE
   20 CONTINUE
      GO TO 99
   10 DO 50  I=1,L2
      DO 60  J=1,L3
      JJ=I+J1-1
      K1=J+J2-1
      C(I,J)=0.0
      DO 70  K=1,L1
```

(cont.)

Subroutine MULT (cont.)

```
      II=I1+K-1
      K2=I2+K-1
      C(I,J)=C(I,J)+A(II,JJ)*B(K2,K1)
70    CONTINUE
60    CONTINUE
50    CONTINUE
99    CONTINUE
      RETURN
      END
```

(22) Subroutine NODFSP

Purpose: To determine nodal forces in spring-type elements.

Call & Argument List: CALL NODFSP (W1P, NDF, J4, NET4, JF, NJ, IND4, N, FORS)

W1P is a 1-dim. auxillary array in which external loads are recorded.

NDF is an integer variable denoting the number of degrees of freedom.

J4 is a 2-dim. integer array in which the element's nodal numbers are recorded.

NET4 is an integer variable denoting the number of elements.

JF is a 2-dim. integer array in which the elements' nodal numbers are recorded.

NJ is an integer variable denoting the number of nodes.

IND4 is an integer variable indicating the occurrence and joint element stiffness modification.

N is an integer variable the value of which is automatically assigned in a DO-loop in the main program.

FORS is a 1-dim. array in which element forces are recorded.

Subroutine Listing:

```
SUBROUTINE NODFSP (W1P,NDF,J4,NET4,JF,NJ,IND4,N,FORS)
DIMENSION W1P(NDF),J4(NET4,3),JF(NJ,3),FORS(4),L(4)
IF (IND4.EQ. 0) GO TO 99
I1=J4(N,2)
I2=J4(N,3)
```

(cont.)

Subroutine NODFSP (cont.)

```
      L(1)=JF(I1,2)
      L(2)=JF(I1,3)
      L(3)=JF(I2,2)
      L(4)=JF(I2,3)
      DO 10 I=1,4
      IF(L(I) .EQ. 0) GO TO 10
      II=L(I)
      W1P(II)=FORS(I)
   10 CONTINUE
   99 CONTINUE
      RETURN


      END
```

(23) Subroutine NODF1

Purpose: To account for splitting or yield forces in external load vector.

Call & Argument List: CALL NODF1 (WIP, NDF, J4, NET4, JF, NJ, IND4, N, FORS, EXTL, NJVL, NW)

WIP is a 1-dim. auxillary array in which external loads are recorded.

NDF is an integer variable denoting the number of degrees of freedom.

J4 is an integer array in which the elements' nodal numbers are recorded.

NET4 is an integer variable denoting the number of elements.

JF is a 2-dim. integer array in which the degrees of freedom associated with each node is recorded.

NJ is an integer variable denoting the number of nodes.

IND4 is an integer variable indicating the occurrence of joint element stiffness modification.

N is an integer variable the value of which is automatically assigned in a DO-loop in the main program.

FORS is a 1-dim. array in which element yield forces are recorded.

EXTL is a 1-dim. array in which variable external loads are recorded.

NJVL is an integer variable denoting the number of node with variable loads.

NW is a 1-dim. integer array in which the degrees of freedom of nodes with variable loads are recorded.

Subroutine Listing:

```
      SUBROUTINE NODE1 (W1P,NDF,J4,NET4,JF,NJ,IN04,N,FORS,EXTL,NJVL,NW)
      DIMENSION EXTL(NJVL),NW(NJVL)
      DIMENSION W1P(NDF),J4(NET4,3),JF(NJ,3),FORS(4),L(4)
      IF (IN04.EQ. 0) GO TO 99
      I1=J4(N,2)
      I2=J4(N,3)
      L(1)=JF(I1,2)
      L(2)=JF(I1,3)
      L(3)=JF(I2,2)
      L(4)=JF(I2,3)
      DO 10 I=1,4
      IF(L(I) .EQ. 0) GO TO 10
      II=L(I)
      DO 20 J=1,NJVL
      IF(NW(J).EQ.II)GO TO 30
      W1P(II)=FORS(I)
      GO TO 20
   30 W1P(II)=EXTL(J)+FORS(I)
      GO TO 10
   20 CONTINUE
   10 CONTINUE
   99 CONTINUE
      RETURN
      END
```

(24) Subroutine PLANT2

Purpose: To plant the stiffness matrix of an element in a larger matrix denoting the stiffness matrix of the whole structure.

Call & Argument List: CALL PLANT2 (SK1, EK, NB, NDF, NEK, JF, NJ, NDEJ1, J, NE, NEJ1, NEJ, LAX1, LAX2)

SK1 is a 2-dim. array denoting the structure stiffness matrix.

EK is a 2-dim. array denoting the element stiffness matrix.

NB is an integer variable denoting the band width.

NDF is an integer variable indicating the number of degrees of freedom.

NEK is an integer variable denoting the number of rows or columns of the element stiffness matrix.

JF is a 2-dim. integer array in which the degrees of freedom associated with each node is recorded.

NJ is an integer variable denoting the number of joints.

NDEJ1 is an integer variable denoting the number of degrees of freedom per joint plus one.

J is a 2-dim. integer array the dimensions of which are defined by NE and NEJ1.

NE is an integer variable denoting the number of elements.

NEJ1 is an integer variable denoting the number of nodes per element plus one.

NEJ is an integer variable denoting the number of nodes per element.

LAX1 is a 1-dim. auxillary integer array.

LAX2 is a 1-dim. auxillary integer array.

Subroutine Listing:

```
      SUBROUTINE PLANT2 (SK1,EK,NR,NDF,NEK,JF,NJ,NDFJ1,J,NE,NEJ1,
     1        NEJ,LAX1,LAX2)
      DIMENSION SK1(NR,NDF),EK(NEK,NEK),JF(NJ,NDFJ1),J(NE,NEJ1),
     1    LAX1(NEJ),LAX2(NEK)
      ND=(NR-1)/2
      DO 20 I=1,NEK
      LAX2(I)=0
   20 CONTINUE
      L=0
      DO 40 I=1,NEJ
      K1=LAX1(I)
      DO 50 K=2,NDFJ1
      L=L+1
      LAX2(L)=JF(K1,K)
   50 CONTINUE
   40 CONTINUE
      DO 60 I=1,NEK
      IF(LAX2(I).EQ. 0) GO TO 60
      MM=LAX2(I)
      DO 70 K=1,NEK
      IF (LAX2(K).EQ. 0) GO TO 70
      NN=LAX2(K)
      K2=ND+1+NN-MM
      SK1(K2,MM)=SK1(K2,MM)+EK(I,K)
   70 CONTINUE
   60 CONTINUE
      RETURN
      END
```

(25) Subroutine RLTVD

Purpose: To determine the relative displaces of the nodal points of a spring-type element.

Call & Argument List: (ED6, WREL, NET6, N)

ED6 is a 1-dim. array in which nodal displacements of joint elements are recorded.

WREL is a 2-dim. array in which relative nodal displacements are recorded.

NET6 is an integer variable denoting the number of elements.

N is an integer variable the value of which is automatically designed in a DO-loop in the main program.

Subroutine Listing:

```
SUBROUTINE RLTVD (ED6,WREL,NET6,N)
DIMENSION ED6(4),WREL(NET6,2)
WRX=ED6(3)-ED6(1)
WRY=ED6(4)-ED6(2)
WREL(N,1)=WRX
WREL(N,2)=WRY
RETURN
END
```

(26) Subroutine SELECT

Purpose: To determine the element nodal displacements of the component elements of a condensed element.

Call and Argument List: CALL SELECT (A, M, N, N1, B, M1, I, J)

A is a 2-dim. array used in the determination of the nodal displacements of component elements.

M is an integer variable denoting the number of rows in matrix [A].

N1 is an integer variable the value of which is determined automatically in a DO-loop.

B is a 1-dim. array in which nodal displacements of component elements are recorded.

I and J are integer variables denoting the reference element of matrix [A].

Subroutine Listing:

```
      SUBROUTINE SELECT (A,M,N,N1,B,M1,I,J)
      DIMENSION A(M,N),B(M1)
      K2=I+(N1*M1)-1
      K1=K2-M1+1
      DO 10 N2=1,M1
      N3=K1+N2-1
      B(N2)=A(N3,J)
   10 CONTINUE
      RETURN
      END
```

(27) Subroutine SPSTRS

Purpose: To determine stresses in horizontal joint elements.

Call & Argument List: CALL SPSTRS (ED2, SI2, T2, RESK, COEF, P, NET2, IJK)

ED2 is a 1-dim. array in which nodal displacements of horizontal joint elements are stored.

SI2 is a variable denoting the orientation of the element with respect to structure coordinate system.

T2 is a 2-dim. array in which element stiffness are recorded.

RESK is a variable denoting a very small number.

COEF is a variable denoting the value of the coefficient of friction.

P is a 1-dim. array in which element stresses are recorded.

NET2 is an integer variable denoting the number of elements.

IJK is an integer variable the value of which is automatically assigned in a DO-loop.

Subroutine Listing:

```
      SUBROUTINE SPSTRS(ED2,SI2,T2,RESK,COEF,P,NET2,IJK)
      DIMENSION ED2(4),A1(4,4),ED2P(4),WP(2,1),C(2,4),DK(2,2),
     1   T2(NET2,2),P(2,1)
      DO 10 I=1,4
      DO 20 J=1,4
      A1(I,J)=0.0
   20 CONTINUE
   10 CONTINUE
      A1(1,1)=COS(SI2)
      A1(1,2)=SIN(SI2)


      A1(2,1)=-A1(1,2)
      A1(2,2)=A1(1,1)
      A1(3,3)=A1(1,1)
      A1(3,4)=A1(1,2)
```

(cont.)

Subroutine SPSTRS (cont.)

```
      A1(4,3)=A1(2,1)
      A1(4,4)=A1(1,1)
      DO 30 I=1,4
      ED2M(I)=0.0
      DO 40 J=1,4
      ED2M(I)=ED2M(I)+A1(I,J)*ED2(J)
   40 CONTINUE
   30 CONTINUE
      DO 70 I=1,2
      DO 80 J=1,4
      D(I,J)=0.0
   80 CONTINUE
   70 CONTINUE
      D(1,1)=-1.0
      D(1,3)=1.0
      D(2,2)=-1.0
      D(2,4)=1.0
      DO 50 I=1,2
      WR(I,1)=0.0
      DO 60 J=1,4
      WR(I,1)=WR(I,1)+D(I,J)*ED2M(J)
   60 CONTINUE
   50 CONTINUE
      IF(T2(IJK,1).EQ.RESK) GO TO 90
      DK(1,2)=0.0
      GO TO 100
   90 DK(1,2)=-COEF*T2(IJK,2)
  100 DK(2,1)=0.0
      DK(1,1)=T2(IJK,1)
      DK(2,2)=T2(IJK,2)
      CALL MPPD(DK,WR,P,2,2,0,0,1)
      RETURN
      END
```

(28) Subroutine SUB

Purpose: To subtract a submatrix of a matrix [B] from a submatrix of a matrix [A] and record the result in the same location in matrix [B].

Call & Argument List: CALL SUB (A, B, M1, N1, M2, N2, I1, J1, I2, J2, L1, L2)

Argument List is defined in the following diagram.

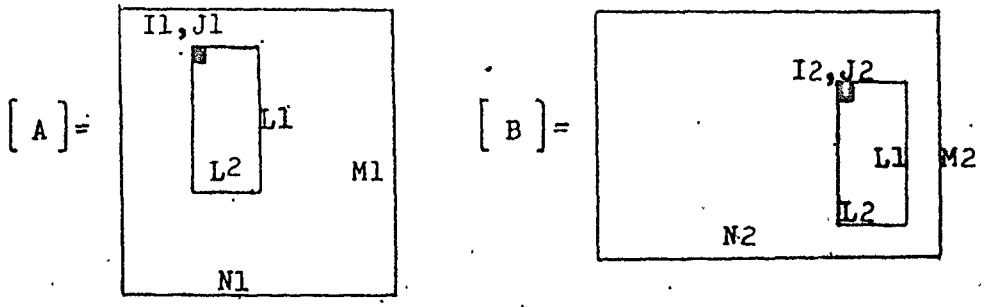

Subroutine Listing:

```
      SUBROUTINE SUB (A,B,M1,N1,M2,N2,I1,J1,I2,J2,L1,L2)
      DIMENSION A(M1,N1) ,B(M2,N2)
      DO 10  I=1,L1
      K1=I1+I-1
      K3=I2+I-1
      DO 20  J=1,L2
      K2=J1+J-1
      K4=J2+J-1
      B(K3,K4)=A(K1,K2)-B(K3,K4)
   20 CONTINUE
   10 CONTINUE
      RETURN
      END
```

(29) Subroutine TBL

Purpose: To modify the stiffnesses of tie-beam link elements.

Call & Argument List: CALL TBL (P, A5, N, IBAR, DSK, BSK, N5, IND5, NET5, T5)

P is a 1-dim. array in which element forces are stored.

A5 is a variable indicating the area of the element.

N is an integer variable the value of which is assigned in a DO-loop in the main program.

IBAR is an integer variable indicating the existance of reinforcing bars in the tie-beam elements.

DSK is a variable indicating the stiffness of dowel spring.

BSK is a variable indicating the stiffness of bond spring.

N5 is a 1-dim. integer array indicating the occurrence of cracks in tie-beam elements.

IND5 is an integer variable indicating the occurrence of joint element stiffness modification.

NET5 is an integer variable indicating the number of elements.

T5 is a 2-dim. array in which element stiffnesses are recorded.

Subroutine Listing:

```
      SUBROUTINE TBL (P,A5,N,IRAP,DSK,BSK,N5,IND5,NET5,T5)
      DIMENSION P(2,1),N5(NET5),T5(NET5,2)
      IF (N5(N).EQ. 1) GO TO 99
      PH=P(1,1)/A5
      PV=P(2,1)/A5
      FTP=460.0
      S1=SQRT(((PH/2.0)**2)+(PV**2))+(PH/2.0)
      IF (ABS(S1).GT. FTP) GO TO 10
      GO TO 99
   10 IF(IRAP.EQ.1) GO TO 20
      T5(N,1)=0.0
      T5(N,2)=0.0
      GO TO 99
   20 N5(N)=1
      T5(N,1)=BSK
      T5(N,2)=DSK
      IND5=1
   99 CONTINUE
      RETURN
      END
```

(30) Subroutine TRANS

Purpose: To transfer the stiffness matrices of component elements of a substructure to their appropriate locations in the stiffness matrix of the substructure.

Call & Argument List: CALL TRANS (A, B, M, N, I, II, J, JJ, K, L)

A is a 2-dim. array denoting the substructure stiffness matrix.

B is a 2-dim. array denoting the element stiffness matrix.

M is an integer variable indicating the number of rows or columns in matrix A.

N is an integer variable indicating the number of rows or columns in matrix B.

I, II, J, JJ, K & L are integer variables determining the location of the elements of the component stiffness matrices within the stiffness matrix of the substructure.

Subroutine Listing:

```
      SUBROUTINE TRANS (A,B,M,N,I,II,J,JJ,K,L)
      DIMENSION A(M,M),B(N,N)
      I1=I


      J1=J
      KK=K+II-I1
      LL=L+JJ-J1
      DO 10 MM=K,KK
      DO 20 NN=L,LL
      A(MM,NN)=A(MM,NN)+B(I1,J1)
      J1=J1+1
   20 CONTINUE
      I1=I1+1
      J1=J
   10 CONTINUE
      RETURN
      END
```

(31) Subroutine VJK

Purpose: To modify vertical joint stiffnesses.

Call & Argument List: CALL VJK (P, NET6, AFT, T6, NR, AV, VK1, IND6, N, FORS, AUX, STEEL, AUXS, T6D)

P is a 1-dim. array in which element forces are recorded.

NET6 is an integer variable denoting the number of vertical joint elements.

AFT is a 1-dim. array in which the value of max. principal stresses are recorded.

T6 is a 2-dim. array in which element stiffnesses are stored.

NR is a 1-dim. integer array indicating the activation of vertical joint reinforcement element.

AV is a 1-dim. array in which the contributory areas of vertical joint elements are stored..

VK1 is a variable indicating the unit shear stiffness of vertical joint elements in phase II.

IND6 is an integer variable indicating the occurrence of joint element stiffness modification.

N is an integer variable the value of which is automatically assigned in a DO-loop.

FORS is a 1-dim. array in which element yield forces are recorded.

AUX is a 2-dim. auxillary array.

STEEL is a 2-dim. array in which element reinforcement forces are recorded.

AUXS is a 2-dim. auxillary array.

T6D is a 2-dim. auxillary array.

Subroutine Listing:

```
      SUBROUTINE VJK(P,NET6,AFT,T6,NP,AV,VK1,INC6,N,FORS,AUX,
     1    STEEL,AUXS,T6D)
      DIMENSION P(2,1),AFT(NET6),T6(NET6,2),NP(NET6),AV(NET6),
     1    FORS(4),AUX (NET6,2)
      DIMENSION STEEL(NET6,2),AUXS(NET6,2),T6D(NET6,2)
      NN=1
      NNN=0
      CF=1.82
      P1=276.
      R=0.64
      RP=0.59
      IND6=0
      PN=P(1,1)/AV(N)
      PS=P(2,1)/AV(N)
      AFT(N)=0.0
      FTP=250.*P
      DO 90 I=1,4
      FORS(I)=0.0
   90 CONTINUE
      IF(NP(N).GT. 0) GO TO 10
      GO TO 20
   10 IF(NP(N).EQ. 1) GO TO 30


      GO TO 99
   30 PNP=PN+AUX (N,1)
      PSP=PS+AUX (N,2)
      FTT=SQRT(((PNP/2.)**2)+(PSP**2))+(PNP/2.)
      IF(FTT.GT. 250.) GO TO 40
      GO TO 99
   40 NP(N)=2
      T6(N,1)=0.0
      T6(N,2)=0.0
      IND6=1
      IF(NN.EQ. 0) GO TO 99
      AA=PSP/ABS(PSP)
      FORS(2)=276. *AV(N)*AA
      FORS(4)=-FORS(2)
      FORS(1)=0.0
      FORS(3)=-FORS(1)
      T6D(N,1)=0.0
      GO TO 99
   20 FT=SQRT(((PN/2.)**2)+(PS**2))+(PN/2.0)
      AFT(N)=FT
      IF(ABS(FT).GT. FTP) GO TO 60
      GO TO 99
   60 IND6=1
      NP(N)=1
      IF (PN.GT. 0.0) GO TO 70
      GO TO 80
   70 IF(NNN.EQ. 1) GO TO 100
      GO TO 80
  100 T6(N,1)=0.0
      T6(N,2)=0.0
      NP(N)=2
      GO TO 99
   80 T6(N,1)=T6(N,1)*0.140*RP
      T6(N,2)=T6(N,2)*RP
   99 CONTINUE
      RETURN
      END
```

(32) Subroutine VJK2

Purpose: To successively modify vertical joint stiffnesses.

Call & Argument List: CALL VJK2 (NR, NET6, T6, STRSS6, AV, INN, FORS, WIP, NDF, J6, JF, NJ, VK1, STEEL, EXTL, NJVL, NW, NVJ, IK, NCB)

NR is a 1-dim. integer array denoting the activation of vertical joint reinforcement element.

NET6 is an integer variable denoting the number of vertical joint elements.

T6 is a 2-dim. array in which element stiffnesses are recorded.

STRSS6 is a 2-dim. array in which vertical joint element stresses are recorded.

AV is a 1-dim. array in which vertical joints contributory areas are recorded.

INN is a 1-dim. array the elements of which may assume values of zero or one only. All elements are zero to start with. 1 indicates that joint stiffnesses are modified to conform to stiffnesses of phase II.

FORS is a 1-dim. array in which element forces are recorded.

WIP is a 1-dim. auxillary array in which external loads are recorded.

NDF is an integer variable denoting the number of degrees of freedom.

J6 is a 2-dim. integer array denoting the elements' nodal numbers.

JF is a 2-dim. integer array in which the degrees of freedom associated with each node is recorded.

NJ is an integer variable denoting the number of nodes.

VK1 is a variable indicating the unit shear stiffness of vertical joint elements in phase II.

STEEL is a 2-dim. array in which element reinforcement forces are recorded.

EXTL is a 1-dim. array in which variable external loads are recorded.

NJVL is an integer variable denoting the number of nodes with variable loads.

NW is a 1-dim. integer array in which the degrees of freedom of nodes with variable loads are recorded.

NVJ is an integer variable denoting the number of vertical joints.

IK is an integer variable the value of which is automatically assigned by a DO-loop in the main program.

NCB is a 2-dim. integer array. The 1st element in each row indicates the vertical joint number. Other elements indicate the joint element numbers associated with that particular vertical joint.

Subroutine Listing:

```
      SUBROUTINE VJK2(NR,NET6,T6,STRSS6,AV,INN,FORS,W1P,NDF,J6,JF,NJ,
     1    VK1,STEEL,EXTL,NJVL,NW,NVJ,IK,NCB)
      DIMENSION STEEL(NET6,2),EXTL(NJVL),NW(NJVL),NP(NET6),T6(NET6,2),
     1    STRSS6(NET6,2),AV(NET6),FORS(4),W1P(NDF),J6(NET6,3),
     1    JF(NJ,3),NCB(NVJ,4),INN(NVJ)
      NNN=0
      NCC=0
      IF(NNN.EQ.1) GO TO 99
```

(cont.)

Subroutine VJK2 (cont.)

```
      DO 10 K=2,4
      KK=NCR(IK,K)
      N=NF(KK)
      IF(N.GT. 0) GO TO 20
      GO TO 10
   20 NCC=NCC+1
   10 CONTINUE
      IF(NCC.EQ. 3) GO TO 30
      GO TO 99
   30 DO 40 K=2,4
      KK=NCR(IK,K)
      IJ=NF(KK)
      IF(IJ.EQ. 1) GO TO 50
      GO TO 40
   50 DO 60 II=1,4
      FORS(II)=0.0
   60 CONTINUE
      AA=STRSS6(KK,2)/ABS(STRSS6(KK,2))
      FORS(2)=AA*ABS(STRSS6(KK,2))*AV(KK)
      FORS(4)=-FORS(2)
      FORS(1)=0.0
      FORS(3)=-FORS(1)
      CALL NCDF1(W1P,NDF,J6,NET6,JF,NJ,1,KK,FORS,FXTL,NJVL,NW)
      T6(KK,1)=AV(KK)*2.04E3
      T6(KK,2)=AV(KK)*VK1
   40 CONTINUE
      INN(IK)=1
   99 CONTINUE
      RETURN
      END
```

(33) Subroutine VJK3

Purpose: To successively modify vertical joint stiffnesses.

Call & Argument List: CALL VJK3 (INDC, NET6, NR, T6, NVJ, IJ, NCB)

INDC is an integer variable indicating the occurrence of joint element stiffness modification.

NET6 is an integer variable indicating the number of vertical joint elements.

NR is a 1-dim. integer array denoting the activation of vertical joint reinforcement element.

T6 is a 2-dim. array in which element stiffnesses are recorded.

NVJ is an integer variable denoting the number of vertical joints.

IJ is an integer variable the value of which is automatically assigned by a DO-loop in the main program.

NCB has the same meaning as in subroutine VJK2.

Subroutine Listing:

```
      SUBROUTINE VJK3(INDC,NET6,NR,T6,NVJ,IJ,NCB)
      DIMENSION NR(NET6),T6(NET6,2),NCB(NVJ,4),INDC(NVJ)
      NNN=0
      RR=0.59
      NCLC=1
      IF(NCLC.EQ. 1) GO TO 99
      IF(NNN.EQ. 1 .OR. INDC(IJ) .EQ. 1) GO TO 99
      DO 10 K=2,4
      KK=NCB(IJ,K)
      IF (NR(KK).EQ. 1) INDC(IJ) =1
   10 CONTINUE
      IF(INDC(IJ).EQ. 0) GO TO 99
      DO 20 K=2,4
      KK=NCB( IJ,K)
      IF(NR(KK).EQ. 1) GO TO 20
      NR(KK)=1
      T6(KK,1) =T6(KK,1)*RR* 0.140
      T6(KK,2)= T6(KK,2) *RR
   20 CONTINUE
   99 CONTINUE
      RETURN
      END
```

(34) Subroutine ZERO

Purpose: To reduce elements of a matrix to zero.

Call & Argument List: CALL ZERO (A, M, N)

A is a 2-dim. array of M rows and N columns.

M is an integer variable indicating the no. rows.

N is an integer variable indicating the no. of columns.

Subroutine Listing:

```
      SUBROUTINE ZERO (A,M,N)
      DIMENSION A(M,N)
      DO 10 I=1,M
      DO 20 J=1,N
      A(I,J)=0.0
   20 CONTINUE
   10 CONTINUE
      RETURN
      END
```

C.3 List of Variables

In the following list the letters R,C and N noted in brackets after the explanation for the variables indicate respectively the number of rows, the number of columns and number of elements (in 1 - dimensional arrays).

The variable listed below, must be re-evaluated when dealing with a new problem.

AC25 is a 2-dim. real array in which the properties (contributory areas and coefficients of friction) for horizontal joint elements are recorded. (R=NET25, C=2)

AFT is a 1-dim. real array in which the values of max. principal stresses for vertical joint elements are recorded. (N=NET6).

AREA is a real variable indicating the area of bar elements.

AUX is a 2-dim. real auxillary array (R=NET6, C=2)

AUXS is a 2-dim. real auxillary array. (R=NET6, C=2)

AV is a 1-dim. real array in which contributory areas of vertical joint elements are stored (N=NET6)

AW is a real variable indicating the load increment.

A5 is a real variable indicating the area of tie-beam link element

BFL is a real variable denoting the bond force limit.

BSK is a real variable indicating the stiffness of bond spring.

C is a 2-dim. real array in which the coordinates of all the nodal points of the entire structure are recorded (R=NJ, C=2).

C11 is a 2-dim. real array in which coordinates of 4 triangulor elements which are required to be condensed into 1 rectangulor element are stored. (R=5, C=2).

DFL is a real variable indicating the dowel force limit.

DSK is a real variable indicating the stiffness of dowel spring.

ES is a real variable indicating the modulus of elasticity of bar elements.

EXTL is a 1-dim. real array in which variable external loads are recorded (N=NJVL)

FCP is a real variable indicating the ultimate compressive strength of horiz. joints.

FOR is a 2-dim. real array in which nodal forces for all vertical joint elements are stored (R=NET6, C=4)

FRST is a real variable indicating the force at which reinforcement element stiffness must be modified.

IBAR is an integer variable indicating the existance of reinforcing bars in the beam elements.

INDC is a 1-dim. integer auxillary array (N=NVJ)

INI is a 1-dim. integer array the elements of which may assume values of zero or one only. They are all zero to begin with. Subsequent values are determinded automatically. (N=NVJ)

INN is a 1-dim. integer auxillary array. (N=NVJ).

ISI is a 1-dim. integer auxillary array. (N=NVJ).

JC is a 2-dim. integer array in which the element numbers and the element node number for condensed element is recorded in the same fashion as described for J11. (R=NETC, C=9).

JF is a 2-dim. integer array in which the nodal numbers and the degrees of freedom associated with each node for the entire structure is recorded (R=NJ, C=3).

JX is a 2-dim. integer array in which element numbers of corresponding pairs of elements on slip surfaces 1 and 2 belonging to the same horizontal joint are stores. (R= Total number of pairs of horiz. joint elements belonging to joints consisting of both slip surface, C=2)

J2S is a 2-dim. real array in which the element numbers and the element node numbers for horizontal joint elements are recorded in the same fashion as described for J 11 (R-NET2S, C=3).

J2SZ is a 1-dim. integer array identifying the location of horiz. joint elements on slip surfaces (1 if located on slip surface 1 and 2 if located on slip surface 2). (N=NET6)

J3 is a 2-dim. integer array in which the element numbers and the element node numbers for bar elements are recorded in the same fashion as described for J 11 (R=NET3, C=3).

J4 is a 2-dim. integer array in which the element numbers and the element node numbers for horizontal joint reinforcement elements are recorded as described for J 11 (R=NET4, C=3).

J5 is a 2-dim. integer array in which the element numbers and the element node numbers for tie-beam link elements are recorded as described for J 11. (N=NET5, C=3).

J6 is a 2-dim. real array in which the element numbers and the element node numbers for vertical joint elements are recorded in the same manner as described for J 11 (R=NET6, C=3).

J11 is a 2-dim. integer array in which the element numbers and the node numbers of 4 triangular elements being condensed into 1 rectangular element are recorded. The 1st element in each row indicates the element No. other elements indicate the corresponding nodal numbers (R=4, C=4).

NB is a integer variable denoting the band width.

NCB is a 2-dim. integer array. The 1st element in each row indicates the vertical joint number. Other elements indicate the joint element numbers associated with that particular vertical joint. (R=NVJ, C=4).

NDAT is a 1-dim. integer array in which the horiz. joint reinforcement element numbers are recorded in corresponding location. Non-corresponding elements are assigned zero values.

NDF is an integer variable denoting the number of degrees of freedom.

NDOW is an integer variable which may assume a value of zero indicate no horizontal joint reinforcement. 1 indicates the reverse.

NETC is an integer variable denoting the number of condensed elements

NET25 is an integer variable denoting the number of horiz. joint elements.

NET252 is an integer variable the value of which determines the number of rows in matrix JX.

NET3 is an integer variable denoting the number of bar elements

NET4 is an integer variable denoting the number of horiz. joint reinforcement elements.

NET5 is an integer variable denoting the number of tie-beam link elements.

NET6 is an integer variable denoting the number of vertical joint elements.

NJ is an integer variable denoting the number of nodes.

NJVL is an integer variable denoting the number of nodes with variable loads.

NR is a 1-dim. integer array denoting the activation of horiz. joint reinforcement elements. Zero indicates no activation. 1 indicates activation. (N=NET4).

NR1 is a 1-dim. real array denoting the activation of vertical joint reinforcement elements similar to NR. (N=NET6).

NVJ is an integer variable denoting the number of vertical joints.

NW is a 1-dim. integer array in which the numbers identifying the degrees of freedom of nodes with variable loads are recorded. (N=NJVL).

NS is a 1-dim. integer array indicating the occurrence of cracks in tie-beam elements. Zero indicates no cracks. 1 indicates cracking. (N=NET5).

SEC is a 1-dim. integer array in which appropriate multiples of incremental load for various nodes are recorded. (N=NJVL).

SKI is a 2-dim. real array denoting the stiffness matrix of the entire structure (R=NB, C=NDE).

SNDK is a real variable denoting the modified stiffness.

STEEL is a 2-dim. real array in which vertical element reinforcement forces are recorded (R=NET6, C=2).

STRSS6 is a 2-dim. real array in which element stresses for vertical joint elements are recorded. (R=NET6, C=2).

STRS25 is a 2-dim. real array in which horiz. and vert. stresses for horiz. joint elements are stored. (R=NET6, C=2).

ST6C is a 2-dim. real array in which stresses for vertical joint elements are stored. (R=NET6, C=2).

T2S is a 2-dim. real array in which the horizontal joint stiffnesses are recorded (R=NET25, C=2).

T2S0 is a real variable indicating the modified joint element spring (horiz.) stiffness.

T4 is a 2-dim. real array in which the stiffnesses of the horizontal joint reinforcement elements are recorded (R=NET4, C=2).

T5 is a 2-dim. real array in which the tie-beam link element stiffnesses are recorded (R=NET5, C=2).

T6 is a 2-dim. real array in which the vertical joint stiffnesses are recorded (R=NET6, C=2).

T6D is a 2-dim. real auxillary array. (R=NET6, C=2).

VK1 is a real variable denoting the unit shear stiffness of vertical joint elements in phase II.

WL is a 2-dim. real array in which nodal displacements of all horiz. joint elements are recorded (R=NET6, C=4).

WREL is a 2-dim. real array in which relative displacements of all horizontal joint elements are stored. (R=NET6, C=2).

WREL6 is a 2-dim. real array in which relative displacements of the ends of vertical join elements are stored. (R=NET6, C=2).

W1 is a 1-dim. real array in which external loads are recorded (N=NDF).

WIP is a 1-dim. real auxillary array in which external loads are stored (N=NDF).

C.4 Program Listing

```
      PROGRAM TST (INPUT,OUTPUT,TAPE5=INPUT,TAPE6=OUTPUT)
      COMMON    AUX(15,2),AUXS(15,2),EXTL(15),FOR(15,4),ST6C(15,2),
     1   J2S(60,3),T6(15,2),J6(15,3),J3(20,3),T4(40,2),J4(40,3),T5(5,2),
     1   J5(5,3),W1(220),W1S(220),STPS2S(60,2),J2S7(60),WL(60,4),
     1   STPSSE(15,2),NR(40),AFT(15),WPEL6(15,2),NS(5),NW(15),SAC(15),
     1   INN(5),  NCR(5,4),T6D(15,2),AV(15),NR1(15),INI(5),STEEL(15,2),
     1   J11(4,4),C(115,2),JF(115,3),JC(10,9),ACCS(60,2),T2S(60,2),
     1   WPEL(60,2),C11(5,2),SK1(51,220),JX(24,2),INDC(5),ISI(5),NDAT(
     1   NDAT(60)
      DATA  NVJ/5/,NDOW/1/,NET2S2/24/,NJ/115/,NETC/10/,NBX51/,NDF/220/,
     1    NET2S/60/,NET6/15/,NET3/20/,NET4/40/,NET5/5/,VK17/.3E3/,
     1    RFL/47400./,DFL/20480./,IDAP/1/,A5/55.0/,DSK/6.48E6/,
     1   BSK/1.86E6/,SNDK/6.4E5/,FPST/11050./,AW/300.0    /,NJVL/15/,
     1    T2S0/1.08E8/,FCP/2800./,ES/7.5E5/,AREA/55./,NEJC/8/
      COMMON    IB1(24,2),IB2(32,2),KL1(4),KL2(4),SK(32,32),BB(32,18),
     1   P1(16,32),P2(32,16),P3(32,2),P4(24,8),P5(24,1),B11(16,16),
     1   B12(16,2),P21(2,16),P22(2,2),S0(16,16),S91(8,8),EDC(8,1),
     1   EDC2(16,1),LX3C(8),LX4C(16),ED1(6),SIGMA(3,1),STRSS1(4,3),
     1   TK1(4),FM(4),PP(4),G(4),N1(2),DAXT3,2),LX1(3),EK(6,6),DB(3,6),
     1   LX3(4),LX4(8),AK2S(4,4),BK2S(4,4),LX3S(2),LX4S(4),ED2S(4),
     1   A1(4,4),P(2,1),FORS(4),FORSV(4)
      DATA  NET11/4/,NDFS/72/,NEJ/5/,NJ11/5/,NET12/4/,NEJ1/3/,NDFJ/2/,
     1    NEJ2S/2/,RESK/1.E-9/
      TEST=1.E-3
      A=0.55
      NN=0
      NEWL=1
      DO 17 I=1,15
      EXTL(I)=0.0
   17 CONTINUE
      DO 3 I=1,NVJ
      INDC(I)=0
      INI(I)=0
      INN(I)=0
      ISI(I)=0
    3 CONTINUE
      DO 2 I=1,NET6
      DO 4 J=1,2
      ST6C(I,J)=0.0
      AUX(I,J)=0.0
      STEEL(I,J)=0.0
      AUXS(I,J)=0.0
    4 CONTINUE
    2 CONTINUE
      DO 7 I=1,NET6
      DO 9 J=1,4
      FOR(I,J)=0.0
    9 CONTINUE
    7 CONTINUE
      CALL ZERO (WPEL,NET2S,2)
      READ(5,10) (NDAT(I),I=1,NET2S)
      READ(5,5) ((NCR(I,J),J=1,4),I=1,NVJ)
      READ (5,5) ((J11(I,J),J=1,4),I=1,NET11)
    5 FORMAT (16I5)
      READ(5,10)((JC(I,J),J=1,9),I=1,NETC)
      READ (5,10)((J2S(I,J),J=1,3),I=1,NET2S)
   10 FORMAT (15I5)
      READ (5,10) ((J6(I,J),J=1,3),I=1,NET6)
      READ(5,10) ((J3(I,J),J=1,3),I=1,NET3)
      READ (5,10) ((J4(I,J),J=1,3),I=1,NET4)
      READ (5,10) ((J5(I,J),J=1,3),I=1,NET5)
      READ (5,5) (J2S7(I),I=1,NET2S)
      READ (5,5) ((JX(I,J),J=1,2),I=1,NET2S2)
      READ (5,15) ((C(I,J),J=1,2),I=1,NJ)
   15 FORMAT (8F10.2)
```

```
      READ (5,15) ((C11(I,J),J=1,2),I=1,NJ11)
      READ (5,25) (W1(I),I=1,NDF)
   25 FORMAT (6(F4.0,F9.0))
      READ (5,35) (NW(I),I=1,NJVL)
   35 FORMAT (10I8)
      READ (5,40) (SAC(I),I=1,NJVL)
   40 FORMAT (10F8.2)
      READ (5,5)((IB1(I,J),J=1,2),I=1,24)
      READ (5,5) ((IB2(I,J),J=1,2),I=1,32)
      READ (5,5)(KL1(I),I=1,4)
      READ (5,5)(KL2(I),I=1,4)
      READ(5,52)((AC2S(I,J),J=1,2),I=1,NET2S)
      READ(5,52)(AV(I),I=1,NET6)
   52 FORMAT(16F5.1)
      READ (5,54)((T2S(I,J),J=1,2),I=1,NET2S)
      READ(5,54)((T6(I,J),J=1,2),I=1,NET6)
   54 FORMAT (6E10.0)
      READ (5,54) ((T60(I,J),J=1,2),I=1,NET6T
      DO 70 I=1,NFJ
      JF(I,1)=I
      JF(I,2)=0
      JF(I,3)=0
   70 CONTINUE
      NFJ1=NFJ+1
      DO 75 I=NFJ1,NJ
      JF(I,1)=I
      L2=I*2-NFJ*2
      L1=L2-1
      JF(I,2)=L1
      JF(I,3)=L2
   75 CONTINUE
      DO 32 I=1,NET4
      T4(I,1)=8.65E5
      T4(I,2)=6.9E5
   32 CONTINUE
      DO 33 I=1,NET5
      T5(I,1)=4.50E7
      T5(I,2)=1.95E7
   33 CONTINUE
      DO 34 I=1,NET4
      NP(I)=0
   34 CONTINUE
      DO 36 I=1,NET6
      NP1(I)=0
   36 CONTINUE
      DO 50 I=1,NET11
      EM(I)=4.655
      G(I)=2.0156
      PR(I)=0.1455
      TK1(I)=8.0
   50 CONTINUE
      WRITE (6,105)
  105 FORMAT (1H1)
      WRITE (6,110)
  110 FORMAT (25X,*++++++++++++++++++++++++++++++++++++++++++++++++*)
      WRITE (6,107) ((NCR(I,J),J=1,4),I=1,NVJ)
  107 FORMAT (5X,4I10)
      WRITE (6,110)
      WRITE (6,115)((J11(I,J),J=1,4),I=1,NET11)
  115 FORMAT (5X,4I10,10X,4I10)
      WRITE (6,110)
  120 FORMAT (5X,9I10)
      WRITE (6,120) ((JC(I,J),J=1,9),I=1,NETC )
      WRITE (6,110)
      WRITE (6,125) ((J2S(I,J),J=1,3),I=1,NET2S)
```

```
  125 FORMAT (5X,3I10,10X,3I10,10X,3I10)
      WRITE (6,110)
      WRITE (6,125) ((J6(I,J),J=1,3),I=1,NET6)
      WRITE (6,110)
      WRITE (6,125)((J3(I,J),J=1,3),I=1,NET3)
      WRITE (6,110)
      WRITE (6,125) ((J4(I,J),J=1,3),I=1,NET4)
      WRITE (6,110)
      WRITE (6,125) ((J5(I,J),J=1,3),I=1,NET5)
      WRITE (6,110)
      WRITE (6,130) (J2S7(I),I=1,NET2S)
  130 FORMAT (5X,12I8)
      WRITE (6,110)
      WRITE (6,135)((JX(I,J),J=1,2),I=1,NET2S2)
  135 FORMAT (5X,2I10,10X,2I10,10X,2I10,10X,2I10)
      WRITE (6,110)
      WRITE (6,140) ((C11(I,J),J=1,2),I=1,NJ11)
  140 FORMAT (5X,12F10.1)
      WRITE (6,110)
      WRITE (6,125) ((JF(I,J),J=1,3),I=1,NJ)
      WRITE (6,110)
      WRITE (6,140) (W1(I),I=1,NDF)
      WRITE (6,110)
      WRITE (6,155) ((T2S(I,J),J=1,2),I=1,NET2S)
  155 FORMAT (5X,2E18.7,5X,2E18.7,5X,2E18.7)
      WRITE (6,110)
      WRITE(6,155) ((T6(I,J),J=1,2),I=1,NET6)
      WRITE (6,110)
      WRITE (6,155) ((T4(I,J),J=1,2),I=1,NET4)
      WRITE (6,110)
      WRITE (6,155) ((T5(I,J),J=1,2),I=1,NET5)
      WRITE (6,110)
      WRITE (6,160) (NW(I),I=1,NJVL)
  160 FORMAT (10X,10I8)
      WRITE (6,110)
      WRITE (6,165) (SAC(I),I=1,NJVL)
  165 FORMAT (10X,10F8.2)
      WRITE (6,110)
      WRITE (6,170) ((AC2S(I,J),J=1,2),I=1,NET2S)
  170 FORMAT (5X,2F15.2,5X,2F15.2,5X,2F15.2)
      WRITE (6,110)
      WRITE (6,175)(TK1(I),I=1,NET11)
  175 FORMAT (5X,8F12.1)
      WRITE (6,110)
      CALL ZERO (SK,NDFS,NDFS)
      DO 210 I=1,NDF
      W1P(I)=W1(I)
  210 CONTINUE
      NEJ11=NEJ1+1
      NEKC=NEJC*NDFJ
      NDFJ1=NDFJ+1
      NEJC1=NEJC+1
      NEJ2S1=NEJ2S+1
      NEK2S=NEJ2S*NDFJ
      DO 65 I=1,NET5
      N5(I)=0
   65 CONTINUE
  225 CALL ZERO (SK1,ND,NDF)
      NUMB=0
      IF (NN.NE. 0) GO TO 301
C  FORM CONDENSED MATRIX (TYPE C ELEM.)
      DO 300 N=1,NET11
      T=TK1(N)
      E=EM(N)
      V=PR(N)
```

```
      GP=G(N)
      CALL DATA (J11,C11,NET11,NEJ11,NJ11,NDFJ,NEJ1,N,DAX,LX1)
      CALL FORM1(DAX,E,V,T,EK,DD,ITEST,GP)
      IF (ITEST.NE. 0) GO TO 999
      K=KL1(N)
      L=K
      CALL TRANS(SK,EK,NDFS,6,1,6,1,6,K,L)
  300 CONTINUE
      CALL BETA (BB,IB1,32,18,24)
      CALL MULT(BB,SK,B1,32,18,32,32,16,32,1,1,1,1,24,A,2,1)
      CALL MULT(B1,BB,B11,16,32,32,18,16,16,1,1,1,1,24,A,A,0)
      CALL MULT(B1,BB,B12,16,32,32,18,16,2,1,1,1,9,24,A,2,0)
      CALL ZERO(B1,16,32)
      CALL MULT(BB,SK,B1,32,18,32,32,16,32,1,9,1,1,24,2,24,1)
      CALL MULT(B1,BB,B21,16,32,32,18,2,16,1,1,1,1,24,2,A,0)
      CALL MULT( B1,BB,B22,16,32,32,18,2,2,1,1,1,9,24,2,2,0)
      Z=1.E-7
      CALL INVMAT (B22,2,2,Z,IERR,N1)
      IF(IERR.NE. 0) GO TO 999
      CALL ZERO(B1,16,32)
      CALL MULT(B12,B22,B1,16,2,2,2,  16,32,1,1,1,1,2,A,2,0)
      CALL MULT (B1,B21,SB1,16,32,2,16,A,A,1,1,1,1,2,A,A,0)
      CALL SUB(B11,SB1,16,16,A,A,1,1,1,1,1,A)
      CALL MULT(BB,B22,B3,32,18,2,2,32,2,1,9,1,1,0,24,2,0)
      CALL MULT(B3,B21,B4,32,2,2,16,24,A,1,1,1,1,2,24,A,0)
      CALL SUB(BB,B4,32,18,24,A,1,1,1,1,24,A)
      CALL ZERO(SK,32,32)
      DO 162 N=1,NET12
      K=KL2(N)
      L=K
      CALL TRANS(SK,SB1,32,A,1,A,1,A,K,L)
  162 CONTINUE
      CALL ZERO(B1,16,32)
      CALL BETA(BB,IB2,32,18,32)
      CALL MULT(BB,SK,B1,32,18,32,32,16,32,1,1,1,1,32,16,32,1)
      CALL MULT(B1,BB,B11,16,32,32,18,16,16,1,1,1,1,32,16,16,0)
      CALL MULT(B1,BB,B12,16,32,32,18,16,2,1,1,1,17,32,16,2,0)
      CALL ZERO(B1,16,32)
      CALL MULT(BB,SK,B1,32,18,32,32,16,32,1,17,1,1,32,2,32,1)
      CALL MULT(B1,BB,B21,16,32,32,18,2,16,1,1,1,1,32,2,16,0)
      CALL MULT(B1,BB,B22,16,32,32,18,2,2,1,1,1,17,32,2,2,0)
      CALL INVMAT (B22,2,2,Z,IERR,N1)
      IF(IERR.NE. 0) GO TO 999
      CALL ZERO (B1,16,32)
      CALL MULT(B12,B22,B1,16,2,2,2,16,32,1,1,1,1,2,16,2,0)
      CALL MULT (B1,B21,SB,16,32,2,16,16,16,1,1,1,1,2,16,16,0)
      CALL SUB(B11,SB,16,16,16,16,1,1,1,1,16,16)
      CALL MULT(BB,B22,B3,32,18,2,2,32,2,1,17,1,1,2,32,2,0)
      CALL MULT(B3,B21,B2,32,2,2,16,32,16,1,1,1,1,2,32,16,0)
      CALL SUB(BB,B2,32,18,32,16,1,1,1,1,32,16)
  905 CONTINUE
      NN=NN+1
  301 CONTINUE
C  PLANT STIFFNESS MATRICES OF TYPE C ELEMENTS
      DO 305 N=1,NETC
      DO 310 M=1,NEJC
      L=M+1
      LX3C(M)=JC(N,L)
  310 CONTINUE
      CALL PLANT2(SK1,SB,NB,NDF,NEKC,JF,NJ,NDFJ1,JC,NETC,NEJC1,NEJC,
     1    LX3C,LX4C)
  305 CONTINUE
C  FORM AND PLANT STIFFNESS MATRICS OF HJ ELEMENTS(TYPE 2S ELEM.)
      S2S=0.0
      DO 315 N=1,NET2S
```

```
      COEF=AC2S(N,2)
      CALL FORM2S(T2S,NET2S,J2S,AK2S,BK2S,N,S2S,LX2S,NEJ2S1,BESK,COEF)
      CALL PLANT2( SK1,BK2S,NB,NDF,NEK2S,JF,NJ,NDFJ1,J2S,NET2S,NEJ2S1,
     1    NEJ2S,LX3S,LX4S)
  315 CONTINUE
C  FORM AND PLANT STIFFNESS MATRICES OF VJ ELEMENTS(TYPE 6 ELEM.)
      S6=0.0
      DO 320 II=1,NVJ
      DO 322 NNJ=2,4
      N=NCB(II,NNJ)
      CALL FORM41 (T6,NET6,AK2S,BK2S,J6,NEJ2S1,S6,LX2S,N,NN1,1,AV,
     1    INI,II,NVJ)
      CALL PLANT2(SK1,BK2S,NB,NDF,NEK2S,JF,NJ,NDFJ1,JF,NET6,NEJ2S1,
     1    NEJ2S,LX3S,LX4S)
  322 CONTINUE
  320 CONTINUE
      DO 324 II=1,NVJ
      DO 326 NNJ=2,4
      N=NCB(II,NNJ)
      CALL FORM41 (T6D,NET6,AK2S,BK2S,J6,NEJ2S1,S6,LX2S,N,NN1,2,AV,
     1    INI,II,NVJ)
      CALL PLANT2(SK1,BK2S,NB,NDF,NEK2S,JF,NJ,NDFJ1,J6,NET6,NEJ2S1,
     1    NEJ2S,LX3S,LX4S)
  326 CONTINUE
  324 CONTINUE
C  FORM AND PLANT STIFFNESS MATRICES OF BAR ELEMENTS(TYPE 3 ELEM.)
      DO 325 N=1,NET3
      CALL FORM3( J3,NET3,NEJ2S1,C,NJ,NDFJ,ES,AREA,N,LX2S,AK2S,BK2S,A1)
      CALL PLANT2 (SK1,BK2S,NB,NDF,NEK2S,JF,NJ,NDFJ1,J3,NET3,NEJ2S1,
     1    NEJ2S,LX3S,LX4S)
  325 CONTINUE
      IF (NDOW .EQ. 0)GO TO 331
C  FORM AND PLANT STIFFNESS MATRICES OF DOWEL-BEND ELEM. (TYPE - ELEM.)
      S4=0.0
      DO 330 N=1,NET4
      IF (NP(N).EQ. 0) GO TO 330
      CALL FORM4 (T4,NET4,AK2S,BK2S,J4,NEJ2S1,S4,LX2S,N)
      CALL PLANT2(SK1,BK2S,NB,NDF,NEK2S,JF,NJ,NDFJ1,J4,NET4,NEJ2S1,
     1    NEJ2S,LX3S,LX4S)
  330 CONTINUE
  331 CONTINUE
C  FORM AND PLANT STIFFNESS MATRICES OF TIE-BEAM LINKS(TYPE 5 ELEM.)
      S5=0.0
      DO 335 N=1,NET5
      CALL FORM4 (T5,NET5,AK2S,BK2S,J5,NEJ2S1,S5,LX2S,N)
      CALL PLANT2 (SK1,BK2S,NB,NDF,NEK2S,JF,NJ,NDFJ1,J5,NET5,NEJ2S1,
     1    NEJ2S,LX3S,LX4S)
  335 CONTINUE
C  SOLVE LINEAR SIMULTANEOUS EQNS.
      ND=(NB-1)/2
      CALL BANDRG(SK1,W1,NB,ND,NDF,TEST,IND)
      IF (IND.NE. 0) GO TO 1010
      WRITE (6,501)
  501 FORMAT (5X,*VECTOR OF NODAL DISPLACEMENT*)
      WRITE(6,340) (W1(I),I=1,NDF)
  340 FORMAT (5X,8E15.7)
      WRITE (6,110)
      WRITE (6,602)
  602 FORMAT (5X,*STRESSES IN X AND Y DIRECTIONS AND SHEAR STRESSES
     1    IN TYPE C ELEMENTS*)
      DO 907 N=1,NETC
      CALL EDISP(W1,NDF,EDC,N,JF,NJ,NDFJ1,JC,NETC)
      CALL MULT(R2,EDC2,R3,32,16,16,1,32,2,1,1,1,1,16,32,1,0)
      DO 909 N9=1,NET12
      CALL SELECT(R3,32,2,N9,EDC,8,1,1)
```

```
      CALL MULT(R4,EDC,R5,24,8,8,1,24,1,1,1,1,1,8,24,1,C)
      DO 921 NP=1,NET11
      CALL SELECT (R5,24,1,NP,ED1,6,1,1)
      T=TK1(NP)
      E=EM(NP)
      V=PR(NP)
      GR=G(NP)
      CALL DATA (J11,C11,NET11,NPJ11,NJ11,NDFJ,NEJ1,NP,CAX,LX1)
      CALL FORM1(DAX,E,V,T,EK,DR,ITEST,GR)
      IF(ITEST.NE. 0) GO TO 909
      CALL MPRD(DR,ED1,SIGMA,3,6,0,0,1)
      STRSS1(NP,1)=SIGMA(1,1)
      STRSS1(NP,2)=SIGMA(2,1)
      STRSS1(NP,3)=SIGMA(3,1)
      IF(N.NE.2) GO TO 921
      WRITE (6,910) (SIGMA(I),I=1,3)
  910 FORMAT(5X,3F15.2)
      CALL CKYC(SIGMA,S1,S2,S0,AC,AY)
      WRITE(6,915) S1,S2,S0,AC,AY
  915 FORMAT (5X,3F15.2,10X,2I5)
  921 CONTINUE
  909 CONTINUE
  907 CONTINUE
C  DETERMINE STRESSES AND MODIFY STIFFNESS COEF.OF TYPE 2S ELEMENTS
      DO 345 N=1,NET2S
      COEF=AC2S(N,2)
      CALL FDSF2S(W1,NDF,ED2S,N,JF,NJ,NDFJ1,J2S,NET2S)
      DO 350 I=1,6
      WL(N,I)=ED2S(I)
  350 CONTINUE
      CALL SPSTRS(ED2S,S2S,T2S,FESK,COEF,P,NET2S,N)
      STRS2S(N,1)=P(1,1)/AC2S(N,1)
      STRS2S(N,2)=P(2,1)/AC2S(N,1)
      IF (J2S7(N) .EQ.2) GO TO 345
      CALL HJK(P,T2S,AC2S,NET2S,N,IND2S,FCP,FESK,NO,NR,NCAT,NET4)
      IF(IND2S.NE.0) GO TO 355
      GO TO 365
  355 WRITE (6,360) N,IND2S,NO
  360 FORMAT (5X,*SLIP ZONE 1,VIOLATION*,5X,*ELEM.NUMBER=*,I4,7X,*
     1  IND2S=*,I2,7X,*NO=*,I2)
      NUMB=NUMB+1
  365 WREL(N,1)=ED2S(3)-ED2S(1)
      WREL(N,2)=ED2S(4)-ED2S(2)
  345 CONTINUE
      IF (NUMB .NE. 0) GO TO 375
      DO 390 N=1,NET2S
      IF (J2S7(N).EQ. 1) GO TO 380
      COEF=AC2S(N,2)
      CALL FDSF2S(W1,NDF,ED2S,N,JF,NJ,NDFJ1,J2S,NET2S)
      CALL SPSTRS(ED2S,S2S,T2S,FESK,COEF,P,NET2S,N)
      CALL HJK2(P,T2S,AC2S,NET2S,N,IND2S,FCP,FESK,NO,NR,NCAT,NET4)
      IF (IND2S.NE. 0) GO TO 385
      GO TO 390
  385 WRITE (6,505) N,IND2S,NO
  505 FORMAT (5X,*SLIP ZONE 2,VIOLATION*,5X,*ELEM.NUMBER=*,I4,7X,*
     1  IND2S=*,I2,7X,*NO=*,I2)
      NUMB=NUMB+1
  390 WREL(N,1)=ED2S(3)-ED2S(1)
      WREL(N,2)=ED2S(4)-ED2S(2)
  380 CONTINUE
  375 CONTINUE
      IF (NUMB.NE. 0) GO TO 379
      N22=NET2S/3
      DO 376 N=1,N22
      CALL ADJK3(WREL,T2S,N,A,T2SD,NET2S)
```

```
  376 CONTINUE
  379 CONTINUE
      WRITE (6,509)
  509 FORMAT (5X,*RELATIVE END DISP. OF TYPE 2S ELEM. (WREL)*)
      WRITE (6,386) ((WREL(I,J),J=1,2),I=1,NET2S)
  386 FORMAT (5X,8E15.7)
      WRITE (6,110)
      WRITE (6,511)
  511 FORMAT (5X,*RELATIVE TOTAL DISP. ACROSS MCRIZ. JOINTS(WX AND WY)*)
      DO 392 N=1,NET2S2
      I1=JX(N,1)
      I2=JX(N,2)
      WX=WL(I2,3)-WL(I1,1)
      WY=WL(I2,4)-WL(I1,2)
      WRITE (6,397) WX,WY
  397 FORMAT (25X,2E15.7)
  392 CONTINUE
      WRITE (6,110)
      WRITE (6,514)
  514 FORMAT (5X,*SHEAR AND NORMAL STRESSES IN TYPE 2S ELEM.*)
      WRITE (6,386) ((STRS2S(I,J),J=1,2),I=1,NET2S)
      WRITE (6,110)
C  DETERMINE STRESSES AND MODIFY STIFF. COEF. OF TYPE 6 ELEM.
      DO 400 II=1,NVJ
      DO 401 NNJ=2,4
      N=NCO(II,NNJ)
      CALL ECSR2S(W1,NDF,ED2S,N,JF,NJ,NDF1,J6,NET6)
      CALL FORM41(T60,NET6,AK2S,RK2S,J6,NEJ2S1,S6,LX3X,N,NR1,2,AV,
     1     INI,II,NVJ)
      CALL MEMST3 (ED2S,T60,NET6,S6,N,P,NR1,AK2S,2,AV,INI,II,NVJ)
      WRITE(6,601) P(1,1),P(2,1)
  601 FORMAT (5X,2E15.7)
      STEEL(N,1)=P(1,1)
      STEEL(N,2)=P(2,1)
  401 CONTINUE
  400 CONTINUE
      WRITE (6,110)
      DO 607 II=1,NVJ
      NU=0
      DO 607 NNJ=2,4
      N=NCO(II,NNJ)
      CALL ECSR2S(W1,NDF,ED2S,N,JF,NJ,NDF1,J6,NET6)
      CALL FORM41 (T6,NET6,AK2S,RK2S,J6,NEJ2S1,S6,LX3S,N,NR1,1,AV,
     1     INI,II,NVJ)
      CALL MEMST3(ED2S,T6,NET6,S6,N,P,NR1,AK2S,1,AV,INI,II,NVJ)
      STRSS6(N,1)=P(1,1)/AV(N)
      STRSS6(N,2)=P(2,1)/AV(N)
      CALL VJK(P,NET6,AFT,T6,NR1,AV,VK1,IND6,N,FORSV,AUX,STEEL,AUXS,
     1     T60)
      CALL NODF1(W1P,NDF,J6,NET6,JF,NJ,IND6,N,FORSV,EXTL,NJVL,NK)
      IF(NR1(N).EQ. 2 .AND. IND6.EQ. 1) GO TO 604
      GO TO 606
  604 DO 655 IJ=1,4
      FOR(N,IJ)=FORSV(IJ)
  655 CONTINUE
  606 CONTINUE
      IF(IND6 .NE. 0) GO TO 611
      GO TO 612
  611 NUMB=NUMB+1
      NU=NU+1
  612 CONTINUE
      CALL RLTVD(ED2S,WREL6,NET6,N)
  607 CONTINUE
      CALL VJK3(INDC,NET6,NR1,T6,NVJ,II,NCO)
      IF(NU.EQ. 0.AND. IMN(II) .EQ. 0) GO TO 609
```

```
      GO TO 610
  609 CALL VJK2(NP1,NET6,TA,STRSS6,AV,INN,FORS,W1P,NDF,JS,JF,NJ,VK1,
     1     STEEL,EXTL,NJVL,NW,NVJ,II,NCB)
  610 CONTINUE
      CALL ACCUM(ST6C,NET6,INN,AUY,INI,STRSS6,NVJ,NCB,IT,NEWL)
      IF(INI(II) .EQ. 1 .AND. ISI(II) .EQ. 0) GO TO 614
      GO TO 615
  614 DO 616,I=2,4
      N=NCB(II,I)
      AUXS(N,1)=STEEL(N,1)
      AUXS(N,2)=STEEL(N,2)
  616 CONTINUE
      ISI(IT)=1
  615 CONTINUE
  607 CONTINUE
      WRITE(6,620)
  620 FORMAT(5X,*STEEL AUXIL. FORCES*)
      WRITE (6,622) ((AUXS(I,J),J=1,2),I=1,NET6)
  622 FORMAT (5X,2E14.7,10X,2E14.7,10X,2E14.7)
      WRITE(6,110)
      WRITE(6,628)
  628 FORMAT (5X,* CRACK CONDITION *)
      WRITE(6,630) (NP1(I),I=1,NET6)
  630 FORMAT (5X,10I8)
      WRITE(6,110)
      WRITE(6,632)
  632 FORMAT (5X,*RELATIVE HORIZ. AND VERT. DISP. ACROSS VERT. J. *)
      WRITE(6,634) ((NPEL6(I,J),J=1,2),I=1,NET6)
  634 FORMAT (5X,2E15.7,10X,2E15.7)
      WRITE(6,110)
      WRITE(6,636)
  636 FORMAT (5X,*HORIZ. AND VERT. STRESSES ACROSS VERT. JOINTS*)
      WRITE (6,638) ((STRSS6(I,J),J=1,2),I=1,NET6)
  638 FORMAT(5X,2E15.7,10X,2E15.7)
      WRITE(6,110)
      WRITE (6,640)
  640 FORMAT (5X,*ACCUM. HORIZ. AND VERT. STRESSES*)
      WRITE(6,642) ((ST6C(I,J),J=1,2),I=1,NET6)
  642 FORMAT (5X,2E15.7,10X,2E15.7)
      WRITE (6,110)
      WRITE (6,644)
  644 FORMAT (5X,*MAX.PRINCIPAL STRESSES VERT. JOINTS*)
      WRITE(6,646) (AFT(I),I=1,NET6)
  646 FORMAT (5X,8E15.7)
      WRITE(6,110)
      WRITE (6,648)
  648 FORMAT (5X,*STIFFNESSES OF VERT. JOINT ELEM.*)
      WRITE (6,650) ((T6(I,J),J=1,2),I=1,NET6)
  650 FORMAT (5X,2E15.7,10X,2E15.7)
      WRITE(6,110)
      IF (NDOW.EQ. 0) GO TO 431
C  DETERMINE FORCES AND MODIFY STIFF. COEF. OF TYPE 4 ELEM.
      WRITE (6,521)
  521 FORMAT (5X,*DOWEL AND POND FORCES (ELEM. TYPE 4)*)
      DO 425 N=1,NET4
      IF(NR(N).EQ. 0) GO TO 425
      CALL EQSE2S(W1,NDF,EQ2S,N,JF,NJ,NDFJ1,NET4,NET4)
      CALL MEMST2(EQ2S,T4,NET4,S4,N,P)
      CALL ORK(P,T4,NET4,DEL,REL,N,IND4,FORS,FRST,SNOK)
      CALL NODFSP(W1P,NDF,J4,NET4,JF,NJ,IND4,N,FORS)
      WRITE (6,430) P(1,1),P(2,1)
  430 FORMAT (20X,2F15.2)
      IF(IND4.NE. 0) GO TO 435
      GO TO 425
  435 WRITE (6,445) N,IND4
```

```
  445 FORMAT (5X,*DOWEL-DOWC RESTRICTION IS VIOLATED,ELEM. NO.=*,I4,
     1   5X,*INDICATOR=*,I2)
  425 CONTINUE
      WRITE (6,110)
  431 CONTINUE
C  DETERMINE FORCES AND MODIFY STIFF. COEF. OF TYPE 5 ELEM.
      WRITE (6,523)
  523 FORMAT (5X,*HORIZ. AND VERT. FORCES ACROSS TIE BEAM (LINK*)
      DO 450 N=1,NET5
      CALL EDSP2S( W1,NDF,ED2S,N,JF,NJ,NDFJ1,J5,NET5)
      CALL MEMST2(ED2S,T5,NET5,S5,N,P)
      WRITE (6,430) P(1,1),P(2,1)
      CALL TRL(P,A5,N,IBAR,CSK,SSK,N5,IND5,NET5,T5)
      IF (IBAR .EQ. 0) GO TO 450
      IF (IND5 .EQ. 1) GO TO 455
      CALL DBK2(P,T5,NET5,DEL,BEL,N,IND4,FORS)
      CALL NODFSP(W1P,NDF,J5,NET5,JF,NJ,IND4,N,FORS)
      GO TO 450
  455 NUMB=NUMB+1
  450 CONTINUE
      WRITE (6,110)
      WRITE(6,460) NUMB
  460 FORMAT (20X,*NUMB=*,I10//)
      WRITE (6,110)
      WRITE (6,110)
      NEWL=0
      IF(NUMB.EQ. 0) GO TO 465
      IIP=0
      GO TO 470
  465 IIP=1
      NEWL=1
  470 CALL LOAD (W1,W1P,NDF,AW,AW,SAC,NJVL,AC2S,NET2S,IIP,C,EXTL)
      WRITE(6,472)W1(197)
  472 FORMAT (5X,*EXTERNAL LATERAL LOAD AT EACH NODE=*,F15.1)
      WRITE (6,110)
      GO TO 225
  999 WRITE (6,1000)
 1000 FORMAT (25X,*PROCESS OF INVERSION FAILS *//)
      GO TO 1020
 1010 WRITE (6,1030)
 1030 FORMAT (25X,*STIFFNESS MATRIX IS SINGULAR *)
 1020 CONTINUE
      STOP
      END
```

REFERENCES

1. Addendum No. 1 (1970) to B.S. Code of Practice CP 116 (1965) and CP116 Part 2 (1969), "Large Panel Structures and Structural Connections in Precast Concrete", BSI 1970.

2. Armer, G.S.T. and Kumars, S., "Tests on Assemblies of Large Precast Concrete Panels", Building Research Station, CP20/72, Dec. 1972.

3. Barnard, P., Role of Ontario Housing Corporation in System Buildings, Queen's Printer, Ontario, 1970.

4. Barnard, P., "Notes on Building Systems", McMaster University, Hamilton, Ontario, 1972.

5. Bate, E.H., "Some Experiments with Concrete", Reinforced Concrete Review, Vol. 4, No. 7, Sept. 1957, pp 421-447.

6. Birkeland, P.W. and Birkeland, H. W., "Connections in Precast Concrete Construction", ACI Journal, Vol. 63, No. 3, March 1966, pp 345-368.

7. "Building Research and Documentation", CIB, Elsevier, 1959.

8. Burhouse, P., "Connexions (Joints) in Structural Concrete", Building Research Station, Engineering papers 46, Dec. 1967.

9. Burnett, E.F.P. and Rajendra, R.C.S., "Influence of Joints in Panelized Structural Systems", J. of Stru. Div., Proc. ASCE, Sept. 1972, pp 1943-1955.

10. "Canadian Construction Outlook", Conference Board (Canada), 1970.

11. Cervenka, V., "Inelastic Finite Element Analysis of Reinforced Concrete Panels Under In-plan Loads", Ph.D. Thesis, University of Colorado, 1970.

12. Cholewicki, A., "Load bearing Capacity and Deformability of Vertical Joints in Structural Walls of Large Panel Buildings", Building Science, Vol. 6, pp 163-184, Pergamon Press, 1971.

13. "Collapse of Flats at Ronan Point", Ministry of Housing and Local Government, London, HMSO, 1968.

14. "The Comprehensive Industrialized Building Systems Annual", 1970.

15. Davey, N., "Construction Joints in Concrete: Bonding New Concrete to Old", Department of Scientific and Industrial Research, Building Research Special Report No. 16.

16. Desai, C.S. and Abel, J.F., Introduction to the Finite Element Method, Van Nostrand Reinhold Co., 1972.

17. "Design of Precast Concrete Wall Panels", Reported by ACI Committee 533, ACI Journal, July, 1971, pp 504-513.

18. Diamant, R.M.F., Industrialized Buildings - International Methods, Iliffe, 1965.

19. Dickson, M.G.T. and Nilson, A.H., "Analysis of Cellular Buildings for Lateral Loads", ACI Journal, Dec. 1970, pp 963-970.

20. "Economics of Construction Industry", Conference Board (Canada), Business Economics, No. 111, 1969.

21. Eden, J.F., and Seymour-Walker, K., "Joints in the Context of an Assembly Process", Building Research Station, CP1/71, Jan. 1971.

22. Eriksson, O., "Some Engineering Problems of Multistorey Construction", Paper to Prestressed Concrete Development Group, London, October 1962.

23. Halasz, R. and Tantow, G., "Schubfestigkeit der Vertical-fugen and Verticlung der Horizontalkrafter in Grosstafelban", Berichte aus der Bauforschung, 45, Berlin, 1966.

24. Hanson, N., "Precast-Prestressed Concrete Bridges: (2) Horizontal Shear Connections", Journal of PCA Research and Development Laboratories, Vol. 2, No. 2, pp 38-58, 1960.

25. "Housing from the Factory", Cement and Concrete Association, 1962.

26. "Industrialized Building Exposition & Congress Inco"., (Digest of Seminars), Cohners, 1972.

27. "Industrialized Buildings and the Structural Engineer", Inst. of Structural Engineers, 1966.

28. "Innovation in Buildings", CIB Elsevier, 1962.

29. International Recommendations for the Design and Construction of Large-Panel Structures. C and CA Translation No. 137 of CEB Bulletin d'Information No. 60, Paris, 1967.

30. Konez, T., Manual of Precast Concrete Construction, Banverlag Gmbh, Berlin, 1970.

31. Lau, P.C.M., "The Structural Behaviour of Panel Buildings", Ph.D. Thesis, University of Southampton, Nov. 1972.

32. Lewicki, B., Buildings with Large Prefabricants, Elsevier 1966.

33. Levy, M.P., and Varga, I.S., "High-rise Panel Structures", J. of Stru. Div., Proc. ASCE, May 1972, pp 975-985.

34. Lutz, L.A., "The Mechanics of Bond and Slip of Deformed Reinforcing Bars in Concrete", Research Report No. 324, Department of Structural Engineering, Cornell University, 1966.

35. Lutz, L.A. and Gergely, P., "Mechanics of Bond and Slip of Deformed Bars in Concrete", Journal of ACI, Vol. 64, No. 11, pp 711-721.

36. Mains, R.M., "Measurement of the Distribution of Tensile Stresses Along Reinforcing Bars", Journal of ACI, Vol. 23, No. 3, Nov. 1951, pp 225-252.

37. Marin, J. and Sauer, J.A., Strength of Materials, MacMillan Co., 1960.

38. Mast, R.F., "Auxiliary Reinforcement in Concrete Connections", Proceedings ASCE, Vol. 94, ST6, June 1968, pp 1485-1504.

39. Mathey, R.G. and Watstein, D., "Investigation of Bond in Beam and Pull-out Specimens with High-Yield-Strength Deformed Bars", Journal of ACI, March 1961, pp 1071-1090.

40. Mattock, A.H., Hofbeck, J.A. and Ibrahim, I.D., "Shear Transfer in Reinforced Concrete", Journal of ACI, Vol. 66, No. 2, Feb. 1969, pp 119-128.

41. Melhorn, G. and Schwing, H., "A Contribution to the Calculation of Precast Shear Walls", International Council of Building Research Studies, Commission W23A (Loadbearing Walls), Brussels, October 1972.

42. Melhorn, G. and Schwing, H., "Overall Behaviour of Large Panel Shear Walls", International Council for Building Research Studies and Documentation, Working Commission 23A (Bearing Walls), Copenhagen, September 1973.

43. Melhorn, G. and Schwing, H., "Joint Characteristics", International Council for Building Research Studies and Documentation, Working Commission 23A (Bearing Walls, Copenhagen, September 1973.

44. Neville, A.M., Properties of Concrete, Sir Isasc Pitman & Son Ltd., 1968.

45. Nilson, A.H., "Bond Stress-slip Relations in Reinforced Concrete", Department of Structural Engineering, Cornell University, Report No. 345, December 1971.

46. Nilson, A.H., "Internal Measurement of Bond-Slip", Journal of ACI, July 1972.

47. Nilson, A.H., "Non-Linear Analysis of Reinforced Concrete by the Finite Element", Journal of ACI, September 1968.

48. Ngo, D. and Scordelis, A.C., "Finite Element Analysis of Reinforced Concrete Beams", Journal of ACI, March 1967.

49. Paulay, T., "Some Aspects of Shear Wall Design", Bulletin of New Zealand Society for Earthquake Engineering, Vol. 5, No. 3, Sept. 1972.

50. Paulay, T., "The Shear Strength of Shear Walls", Bulletin of New Zealand Society for Earthquake Engineering, Vol. 3, No. 4, 1970.

51. Paulay, T. and Hitchings, A.J., Private Communication, Sept. 1975.

52. Phillips, M.N., "Horizontal Construction Joints in Cast-in-Place Concrete", M.Sc. Thesis, University of Canterbury, Christchurch, New Zealand, Feb. 1972.

53. Rubinstein, M.F., Matrix Computer Analysis of Structures, Prentice-Hall, 1966.

54. Scmid, T. and Testa, C., "Systems Building-an International Survey of Methods", 1969.

55. Sebastyen, G., Large Panel Buildings, Budapest, 1965.

56. Short, A. and Miles, J.R., "Large Panel Structures", Notes on Draft Addendum 1 to CP116 (1965), Building Research Station, August 1969.

57. Somerville, G., "Behaviour of Mortar Joints in Compression", Cement and Concrete Association, 42.476, Nov. 1972.

58. Somerville, G. and Burhouse, P., "Tests on Joints Between Precast Concrete Members", Building Research Station, Engineering papers 45, August 1967.

59. Stafford Smith, B. and Lau, P.C.M., "A Method of Assessing the Static Stability of Panel Type Buildings", Proc. Instn. Civ. Engrs., 1972, 53 (June), pp 77-86.

60. Stafford Smith, B. and Rahman, K.M.K., "A Theoretical Study of the Sequence of Failures in Precast Panel Walls", Proc. Instn. Civ. Engrs., 1973, 55 (Sept.), pp 581-592.

61. Stamato, M.C. and Stafford Smith, B., "An Approximate Method for Three Dimensional Analysis of Tall Buildings", Proc. Instn. Civ. Engrs., 1969, 43 (July), pp 361-379.

62. "Structural Stability and the Prevention of Progressive Collapse", Inst. of Stru. Engrs., RP/68/01, Dec. 1968.

63. "Towards Industrialized Building", CIB, Elsevier, 1965.

64. Troxell, G.E. and Davis, H.E., Composition and Properties of Concrete, McGraw-Hill, 1965.

65. Valliappan, S. and Doolan, T.F., "Nonlinear Stress Analysis of Reinforced Concrete", J. of Stru. Div., Proc. ASCE, April 1972.

66. Waters, T., "A Study of Tensile Strength of Concrete Across Construction Joints", Magazine of Concrete Research, Vol. 6, No. 18, Dec. 1954, pp 151-153.

67. Watstein, D., "Bond Stress in Concrete Pull-out Specimens", Journal of ACI, Vol. 13, No. 1, Sept. 1941, pp 37-50.

68. Watstein, D., "Distribution of Bond Stresses in Concrete Pull-out Specimens", Journal of ACI, Vol. 18, No. 7, May 1947, pp 225-252.

69. Zienkiewicz, O.C., The Finite Element Method in Engineering Science, McGraw-Hill, 1971.

70. Zienkiewicz, O.C., Parekh, C.J. and Teply, B., "Three-Dimensional Analysis of Buildings Composed of Floor and Wall Panels", Proc. Instn. Civ. Engrs., July 1971, pp 319-332.